Huminstoffe und organische Modellliganden und ihre Wechselwirkungen mit Metallionen und polyzyklischen aromatischen Kohlenwasserstoffen

Habilitationsschrift

Zur Erlangung des akademischen Grades doctor rerum naturalium habilitatus
(Dr. rer. nat. habil.)
in der Wissenschaftsdisziplin Physikalische Chemie

eingereicht an der
Mathematisch-Naturwissenschaftlichen Fakultät
der Universität Potsdam

von
Dr. Michael U. Kumke
geboren am 21.09.1963 in Braunschweig

Potsdam-Golm, im Januar 2005

Für Netti und Josy

Danksagung

Herrn Prof. Hans-Gerd Löhmannsröben danke ich für die Aufnahme in seine Arbeitsgruppe, das in mich gesetzte Vertrauen, die unzähligen fachlichen Diskussionen und die Entfaltungsfreiheit. Für den Rückhalt und die vielen Anstöße, die meinen bisherigen wissenschaftlichen Werdegang entscheidend geprägt haben, bin ich Hans-Gerd tief verbunden. An der Mentalität, kleinen Niederlagen das Positive abzugewinnen und in „große Siege“ zu verwandeln, nach dem Motto „jetzt erst recht“ - daran werde ich weiter arbeiten.
Herrn Prof. Fritz H. Frimmel gebührt mein Dank für die Aufnahme in eines der größten „Huminstoffzentren der Welt“, in dem ich Zugang zu nahezu unerschöpflichen Ressourcen an Huminstoffen hatte und in die „Tiefen“ der Huminstoffforschung vordringen konnte.
Der Arbeitsgruppe Löhmannsröben bin ich dankbar für das gute Arbeitsklima im Labor und im „G 0.01“. Neben den intensiven fachlichen Diskussionen, sind es besonders die „Freitagsgespräche“, die die Woche komplettieren. Jeannette, Wolfgang und Matthias danke ich für die Durchsicht der Arbeit und die hilfreichen Kommentare, Carsten für sein Drehen an der „Magic Screw“ sowie Oli und Niko für das „erfrischende Auslaufen“ nach getaner Arbeit.
Viele meiner praktischen Arbeiten am Institut für Chemie (Universität Potsdam) wurden durch technische Angestellte, Auszubildende und studentische Hilfskräfte unterstützt. Mein besonderer Dank gilt hier Melanie Hans, Franziska Luschtinetz, Noreen Splies, Marita Steffen, Stefanie Zilm, Sascha Eidner, Roman Flehr, Tobias Krüger und Sascha Prenzel, die mir viele von den lästigen kleinen Arbeiten im Labor abgenommen und „mal eben“ erledigt haben. Besonders möchte ich mich bei Herrn Tobias Krüger bedanken, dessen „Kondition“ echt bemerkenswert ist.
Meinen Amsterdamer Kollegen Freek Ariese, Arjen Bader und Cees Gooijer danke ich für Ihre Unterstützung - auch zu ziemlich späten Stunden - bei den Tieftemperaturmessungen. Freek danke ich im speziellen für die lehrreichen Einführungen in die Vielfalt einiger „belgischer Traditionen“.
Meinen ehemaligen Karlsruher Kollegen Daniel Schmitt, Christian Specht, Gerd Ohlenbusch, Tusnelda Doll, Michael Herrenbauer, Andreas Wolf und Axel Heidt bin ich für die zahlreichen fachlichen Diskussionen unter „Ingenieuren“ dankbar. Mit Gerd und Andreas haben viele gemeinsame Kilometer in den Karlsruher Wäldern nicht nur die Ausdauer, sondern auch die Laune immer wieder erheblich gesteigert.
Für die offene Aufnahme, die zahlreichen Diskussionen und die gemeinsamen Forschungsinteressen, die wir in vielen Seminaren kleinerer und größerer Natur vertieft haben, möchte ich mich bei Reiner Klenze, Jean-Marc Monsalier und Gunnar Buckau vom Forschungszentrum Karlsruhe (Institut für Nukleare Entsorgung) bedanken.
Mit Carmen Tiseanu (National Institute for Laser, Plasma and Radiation Physics, Bucharest-Magurele, Romania) und Gregory Korshin (Department of Civil and Environmental Engineering, University of Washington, Seattle, USA) verbindet mich eine fachliche Freundschaft, die sich in vielen Kooperationen aufgebaut hat und auch zukünftig sicher noch das eine oder andere Projekt initiieren wird.

Vorwort

In der vorliegenden Habilitationsschrift werden die Ergebnisse der Forschungsarbeiten seit 1995 anhand der neunzehn wichtigsten eigenen Veröffentlichungen zum Thema dargestellt. Die Arbeiten sind thematisch in drei Unterkapitel gegliedert, in denen die Beiträge zur spektroskopischen Charakterisierung der Huminstoffe (2.1, sieben Publikationen), Untersuchung der Wechselwirkungen mit hydrophoben Xenobiotika (2.2, vier Publikationen) und den Wechselwirkungen mit Metallkationen (2.3, drei Publikationen) zusammengefasst sind. Jedem Unterkapitel ist eine kurze Zusammenfassung der aktuellen Literatur (für die Jahre 2000 bis 2004) vorangestellt, um einerseits die Relevanz aber auch das fortbestehende Interesse an den Forschungsthemen zu dokumentieren. Die ältere Literatur ist bereits in den einzelnen Veröffentlichungen berücksichtigt.
Im Anschluss daran werden in Kapitel 3 Ergebnisse laufender Forschungsarbeiten präsentiert. Diese sind eine Fortsetzung der in den vorhergehenden Kapiteln dargestellten Forschungsarbeiten an Huminstoffen und ihrer Rolle als Reaktionspartner für Xenobiotika in der Umwelt, wobei besonders die Reaktivität gegenüber Metallkationen in den Mittelpunkt des Interesses gerückt ist. Durch die Verwendung von Lanthaniden[1] (Ln^{3+}) als molekulare Lumineszenzsonden wird die Komplexierung von Metallen durch Huminstoffe mit stationären und zeitaufgelösten Fluoreszenztechniken untersucht. Zum besseren Verständnis der Sondeneigenschaften der Ln^{3+} sind die relevanten (spektroskopischen) Eigenschaften der Lanthanide sowie ihrer Komplexe kurz in Abschnitt 3.1 zusammengefasst. Von den bislang erzielten Ergebnisse werden u.a. die aktuellen Resultate der Untersuchung der Energietransferprozesse in Huminstoff-Lanthanid-Komplexen diskutiert. Besonders die Bestimmung der mittleren Abstände von Metallbindungsplätzen in Huminstoffen über die Messung eines Interlanthanid-Energietransfers eröffnet neue Möglichkeiten, Phänomene wie die der Huminstoffassoziation auf Größenskalen von wenigen Nanometern zu untersuchen.
Die Darstellung in Kapitel 3 konzentriert sich vor allem auf die Diskussion der Ergebnisse, Informationen zu experimentellen Details (z.B. zu den verwendeten Geräten) und zu allgemeineren theoretischen Grundlagen finden sich in den Anhängen A und C.

[1] In der neueren Literatur wird auch häufig der Begriff Lanthanoide verwendet.

Inhaltsverzeichnis

Abbildungsverzeichnis

Tabellenverzeichnis

Kapitel 1

Einleitung

Huminstoffe (HS) entstehen aus pflanzlichen und tierischen Material durch chemische und biologische Ab- und Umbauprozesse. Wahrscheinlich liegen verschiedene Entstehungswege vor, die je nach lokalen Bedingungen (Klima, Pflanzenbewuchs, Mikroorganismen usw.) verschieden stark zum Gesamtentstehungsprozess beitragen. Als bekannteste Hypothesen für die HS-Genese sind die Lignin-Theorie und die Polyphenol-Theorie zu nennen, desweiteren ist die Kondensation von Polysacchariden und Aminoverbindungen in Betracht zu ziehen [1–4]. HS sind ubiquitär und stellen den wohl größten verfügbaren Kohlenstoffpool dar, er übertrifft selbst die in Pflanzen und Tieren gebundene Menge. Dennoch gehören HS zu einer Substanzklasse, die immer noch nicht vollständig verstanden ist in Bezug auf ihre Reaktivität in der Umwelt. Für die Jahre 2000 bis 2004 können im *Web of Science* 2075 Einträge zum Stichwort *humic substances* gefunden werden. Neben den eher traditionellen Themenschwerpunkten (s.u.), die sich mit den verschiedenen Effekten von HS auf die Speziation, Bioverfügbarkeit und veränderte Toxizität von Xenobiotika befassen, werden die Bedeutung der HS für die Nahrungskette (vor allem in aquatischen Lebensräumen) untersucht. Zusätzlich zu den eigentlichen physiologischen Effekten, die u.a. die Rolle von HS in Elektronen-Donor-Akzeptor-Zyklen in Verbindung mit Mikroorganismen untersuchen, ist vor allem die Wirkung von HS als Mediator beim Abbau bzw. in der Wasseraufbereitung bei der Bildung von halogenierten Verbindungen von Interesse. Durch Veränderungen im Klima, den steigenden Eintrag von anthropogenen Substanzen in die Umwelt und durch die sich stetig wandelnde Nutzung von Landflächen und Gewässern (z.B. durch Landwirtschaft) wird auch die Qualität und die Quantität der HS verändert. So verursacht der zunehmende Gehalt an HS in Oberflächengewässern bei der Trinkwasseraufbereitung stetig steigende Kosten in der Größenordnung von einigen 100 Mio. Euro. Wesentliche Kostenfaktoren sind die Entfernung von HS durch Flockungsprozesse, die Biofilmbildung in Wasserleitungssystemen und in Filteranlagen sowie die Bildung von gesundheitsschädlichen Substanzen im Zusammenhang mit Desinfektions- und Oxidationsschritten während der Wasseraufbereitung. Da HS zu ca. 50 bis 60% aus Kohlenstoff bestehen, ist ein Verständnis der Kohlenstoffdynamik in Zusammenhang mit HS auch für die Dynamik des Treibhausgases CO_2 bedeutsam (s. DFG Schwerpunktprogramm „Böden als

Quelle und Senke für CO_2-Mechanismen und Regulation der Stabilisierung organischer Substanz in Böden“).
HS können als Biopolymere aufgefasst werden, die sich neben ihrer außergewöhnlich großen Heterogenität durch eine große Zahl verschiedenster Funktionalitäten auszeichnen (z.B. aromatische Strukturen oder basische und saure Gruppen). Dementsprechend ist ihre Reaktivität gegenüber Xenobiotika in der Umwelt mannigfaltig. Säure-Base-Gruppierungen bestimmen die Komplexierung von Metallkationen, hydrophobe bzw. hydrophile Eigenschaften beeinflussen die Wechselwirkung mit organischen Xenobiotika. Die Wechselwirkung mit Xenobiotika kann entweder zu einer Immobilisierung oder zu einer erhöhten Mobilisierung dieser führen und aufgrund der veränderten Bioverfügbarkeit wird die Toxizität der Xenobiotika beeinflusst [1,5–10]. Durch die Anwesenheit von Chromophoren wird in natürlichen Wässern die Eindringtiefe der Sonnenstrahlung durch HS bestimmt. Variationen im HS-Gehalt können so einen bedeutsamen Effekt auf die Flora und Fauna von aquatischen Ökosystemen haben.
Für Untersuchungen der Reaktivität von HS werden Referenz- und Standard-HS benötigt. Von verschiedenen Arbeitsgruppen und der *International Humic Substances Society* (IHSS) werden Standardroutinen zur Isolierung von HS vorgeschlagen [1, 4, 11, 12]. So wird z.B. für die Isolierung von aquatischen HS die Adsorption bei pH-Werten < 2 an nicht-ionischen Polymeren (XAD-2 oder XAD-8) und die anschließende Desorption bei pH-Werten > 12 als Methode favorisiert. Dadurch wird eine operational-definierte Auftrennung der HS in hydrophile und hydrophobe Fraktionen erreicht. HS werden weiter unterteilt in Fulvinsäuren (FA, *fulvic acids*) und Huminsäuren (HA, *humic acids*). Diese Unterscheidung ist rein operational-definiert und basiert auf Unterschieden in der Löslichkeit und Adsorbierbarkeit von FA- und HA-Fraktion. So werden z.B. FA und HA durch die unterschiedliche Löslichkeit bei pH-Werten < 2 definiert - FA sind löslich, während HA ausgefällt werden. FA sind ionisch-hydrophil, HA ionisch-hydrophob. Daneben fallen bei der Isolierung noch die Fraktion der nicht an XAD-Harze adsorbierbaren Verbindungen sowie die Fraktion der irreversibel an die XAD-Harze gebundenen Verbindungen an. Letztere können nur durch Extraktion mit organischen Lösungsmitteln wieder von der Festphase entfernt werden. Zur Isolierung von bodenbürtigen HS wird der Boden z.B. mit einer alkalischen Lösung extrahiert und im Anschluss daran in die operational-definierten Fraktionen FA und HA aufgetrennt.
Bedingt durch die unterschiedlichen Ausgangsmaterialien in der Genese von HS (begründet in der unterschiedlichen Flora und Fauna in Kombination mit den jeweiligen klimatischen Bedingungen), ist eine Angabe einer generellen Struktur nicht möglich. Zur Beschreibung der Reaktivität von HS werden besser Bausteine (*building blocks*) bzw. funktionelle Gruppen identifiziert (s.u.). Hydroxid-, Amid-, Amin-, Carboxyl- sowie Carbonyl-, Phenol- und Quinon-Gruppen sind häufige funktionelle Gruppen in HS [1, 2, 4, 13–15]. Darüberhinaus müssen auch noch schwefelhaltige Gruppen in die Betrachtung einbezogen werden. Eine weitere Schwierigkeit beim Umgang mit HS ist die im Verlauf der Humifizierung auftretende ständige Veränderung der HS, wodurch das Isolieren und Bereitstellen von Standards und Referenzmaterialien erschwert

wird. Mit zunehmendem Alter der HS werden die beobachtbaren Veränderungen geringer und die HS können dann als refraktär bezeichnet werden [1]. Eine Isolierung von HS bedeutet aber auch immer einen Eingriff in das *Gesamtsystem HS*. So sind z.B. in HS Metallkationen Me^{n+} (z.B. Fe(II), Fe(III)) gebunden, deren Gehalt durch die Isolierung verändert werden kann. Die Anwesenheit der Me^{n+} kann z.B. das Redoxverhalten der HS beeinflussen [16]. Außerdem übernehmen Me^{n+} möglicherweise wichtige Funktionen bei der Ausbildung von Überstrukturen. HS können Aggregate bilden und bestimmte HS-Eigenschaften werden erst durch diese Überstrukturen definiert. Das hat wichtige Konsequenzen für die Definition von HS-Bausteinen zur Beschreibung der Reaktivität von HS, da so die makromolekularen Eigenschaften nicht mit erfasst werden.
HS sind von interdisziplinärem Interesse für Bio-, Geo- und Umweltwissenschaften. Vor dem Hintergrund der enormen Komplexität der HS ist die (Weiter)Entwicklung von analytischen Techniken zur Untersuchung der Wechselwirkungen bzw. der Wechselwirkungsmechanismen zwischen HS und Xenobiotika zwingend erforderlich. Erst die Anwendung von fundamentalen physiko-chemischen Konzepten, wie es z.B. der Resonanzenergietransfer darstellt, wird die Möglichkeit eröffnet, tragfähige Konzepte zur Beschreibung der Wechselwirkungen von HS in der Umwelt zu erarbeiten, die über die auf empirische Daten beruhenden hinausgehen.
Spektroskopische Methoden - vor allem die Fluoreszenzspektroskopie mit ihrer einzigartigen Multidimensionalität - sind als nicht-invasive Techniken besonders geeignet die Wechselwirkungen von HS mit Xenobiotika zu untersuchen. Ein Nachteil, den es bei der Anwendung von Fluoreszenztechniken zu überwinden gilt, ist das lückenhafte Verständnis der photophysikalischen Prozesse in Zusammenhang mit HS und zwar sowohl bezogen auf die intrinsische Fluoreszenz der HS als auch auf die von extrinsischen Lumineszenzsonden. In Kapitel 2 sind Veröffentlichungen zu Ergebnissen der spektroskopischen Untersuchungen von HS und ihren Wechselwirkungen mit organischen und anorganischen Verbindungen zusammengefasst. In diesen wurden fundamentale photophysikalische Prozesse in HS und von mit HS wechselwirkenden Lumineszenzsonden systematisch erforscht. Neben dem Einsatz von leistungsstarken spektroskopischen Verfahren, die in Einzelfällen eine spektrale Auflösung besser 0.1 nm haben (Tieftemperaturfluoreszenzexperimente) und in der Zeitdomäne, Prozesse im Pikosekundenbereich aufzulösen vermögen (Messungen mit Streak-Kamera), wurden auf chemischer Seite zusätzlich Modellverbindungen und gezielt-modifizierte HS untersucht. Die Auswahl der Modellverbindungen wurde an bekannten Struktureinheiten von HS-Vorläufersubstanzen (z.B. Lignin) orientiert.
Zunächst werden die Resultate der spektroskopischen Charakterisierung der HS selbst dargestellt (s. 2.1). Neben der Untersuchung der isolierten HS in Form von HA- und FA-Fraktionen wurden auch die lediglich 0.45 μm-filtrierten Huminstofflösungen spektroskopisch untersucht. Um die außergewöhnliche Komplexität der HS in den Experimenten zu reduzieren, wurden die HS-Proben chemischen und physikalischen Behandlungen (z.B. Oxidation durch O_3 oder Chlorung) unterzogen, um so definierte Reaktionen in den HS zu induzieren und aus deren Auswirkungen auf die photophysikalischen Parameter, Rückschlüsse auf die Photophysik der HS zu zie-

hen. In den Kapiteln 2.2 und 2.3 sind die gewonnenen qualitativen und quantitativen Erkenntnisse der Wechelwirkungen von HS mit organischen und anorganischen Verbindungen dargestellt. In Kapitel 2.2 werden polyzyklische aromatische Kohlenwasserstoffe (PAK) als Fluoreszenzsonden zur Untersuchung der Wechselwirkung von hydrophoben Xenobiotika mit HS eingesetzt. Insbesondere der Vergleich der Ergebnisse der nicht-invasiven Fluoreszenzmessungen mit Ergebnissen der Mikrofestphasenextraktion (SPME) lieferte wichtige Erkenntnisse zu den Wechselwirkungen von hydrophoben Xenobiotika mit HS. In den durchgeführten Tieftemperaturmessungen konnten erstmals hochaufgelöste Fluoreszenzspektren von HS-Pyrenkomplexen erhalten werden. In Kapitel 2.3 sind schließlich Veröffentlichungen, in denen die Wechselwirkungen von HS mit Metallionen - z.B. Eu^{3+} - untersucht worden sind, dargestellt. Die durch die Metallkomplexierung induzierten Veränderungen der photophysikalischen Parameter der HS wurden vor allem durch zeitaufgelöste Fluoreszenztechniken charakterisiert. Zur Auswertung der komplexen Abklingkinetiken werden speziell Lebenszeitverteilungen herangezogen.
Die im Kapitel 2 vorgestellten Arbeiten waren ein Teil folgender Forschungsvorhaben, welche im Zeitraum September 1995 bis Juni 2000 am Engler-Bunte-Institut, Bereich Wasserchemie der Universität Karlsruhe durchgeführt worden sind:

- Charakterisierung komplexer Stoffstrukturen in der Umwelt mit Hilfe hochauflösender Analysenverfahren
  (Forschungsschwerpunktprogramm Baden-Württemberg)

- Refraktäre organische Säuren im Gewässer
  (DFG-Schwerpunktprogramm)

- Einfluss von Oxidationsreaktionen auf die Wechselwirkungen zwischen natürlichen organischen Wasserinhaltsstoffen (NOM) und Metallionen
  (DFG-Forschungsvorhaben)

Die vorgestellten Ergebnisse finden z.T. ihre Fortsetzung in aktuell laufende Forschungsvorhaben am Institut für Chemie der Universität Potsdam:

- Laserspektroskopische Untersuchungen der Struktur-Wirkungsbeziehungen in Metall-Siderophor-Komplexen
  (DFG-Forschungsvorhaben)

- Spektroskopische Bestimmung von thermodynamischen und kinetischen Kenngrößen zur Beschreibung der Huminstoff-Metall-Komplexierung
  (Verbundvorhaben des BMWA)

- Fundamental Processes of Radionuclide Migration
  (Integriertes Projekt im 6. EU-Rahmenprogramm)

Ausgewählte Beispiele von bislang in diesen Forschungsvorhaben erzielten Ergebnissen sind abschließend in Kapitel 3 beschrieben.

Kapitel 2

Eigene Arbeiten - von 1995 bis 2000

Neben den Co-Autoren haben weitere Studenten in Studien- und Diplomarbeiten bei der Durchführung der Forschungsprojekte mitgewirkt und damit auch den Fortgang der in Kapitel 2 dargestellten Ergebnisse unterstützt.

Mein Dank gilt besonders:

Clemens Barth (*Modellversuche zur Mobilisierung von Schadstoffen durch Huminstoffe am Beispiel von Polyzyklischen aromatischen Kohlenwasserstoffen*),
Seema Chauhan (*Characterization of metal ion complexation by liposomes*),
Babak Ebrahimi (*Einfluss der Wasserhärte auf die Mobilisierung von PAK durch natürliche organische Wasserinhaltsstoffe (NOM)*),
Sabine Flaskämper (*Fluoreszenzspektroskopie an Proben mit hoher optischer Dichte: Bestimmung von Geometrieparametern zur Korrektur des Filtereffektes bei Fluoreszenzmessungen*),
Helga Gleißner (*Infrarotspektroskopische Charakterisierung von Huminstoffen in wässriger Lösung*),
Ralf Porkert (*Wechselwirkung von polyzyklischen aromatischen Kohlenwasserstoffen (PAK) mit natürlichen organischen Wasserinhaltsstoffen (NOM) - Vergleich zweier analytischer Methoden*),
Daniel Schmitt (*Einfluss gelöster organischer Bodenbestandteile auf den Transport von polyzyklischen aromatische Kohlenwasserstoffen (PAK) in Modellböden*)
und Thomas Weber (*Einfluss von oxidativen Wasseraufbereitungsverfahren auf die HS-Metallkomplexierung*).

2.1 Spektroskopische Charakterisierung von Huminstoffen

In der spektroskopischen Charakterisierung der HS wurde systematisch die stationäre und zeitaufgelöste intrinsische Fluoreszenz von HS untersucht. Durch die Multidimensionalität der Fluoreszenz (mit den Observablen Intensität I_F, Anregungswellenlänge λ_{ex}, Emissionswellenlänge λ_{em} und Fluoreszenzabklingzeit τ_F) und die gezielte chemische Modifikation von HS ist es in diesen Untersuchungen gelungen

- die Beteiligung von intra- und intermolekularen Energietransferprozessen sowie konformativen Reorganisationsprozessen an der elektronischen Desaktivierung von HS nachzuweisen,
- einfache Bausteine (*building blocks*) als fluoreszierende Strukturelemente von HS zu identifizieren,
- den Einfluss von Ursprungsort und Fortschreiten der Humifizierung zu untersuchen.

Die folgenden Veröffentlichungen beschreiben detailliert die spektroskopische Charakterisierung von HS verschiedener Ursprungsorte und sind in 2.1.1 bis 2.1.7 dargestellt:

1. C. Zwiener, M.U. Kumke, G. Abbt-Braun, F.H. Frimmel
   Acta Hydrochim. Hydrobiol., 1999, **27**, 208 - 213.
   Adsorbed and bound residues in fulvic acid fractions of a contaminated groundwater: Isolation, chromatographic and spectroscopic characterization.
2. M.U. Kumke, C. Zwiener, G. Abbt-Braun, F.H. Frimmel
   Acta Hydrochim. Hydrobiol., 2000, **27**, 409 - 415.
   Spectroscopic characterization of fulvic acid fractions of a contaminated groundwater.
3. G.V. Korshin, M.U. Kumke, C.-W. Li, M.M. Benjamin, F.H. Frimmel
   Environ. Sci. Technol., 1999, **33**, S. 1207 - 1212.
   Influence of chlorination on chromophores and fluorophores in humic substances.
4. M.U. Kumke, C.H. Specht, T. Brinkmann, F.H. Frimmel
   Chemosphere, 2001, **45**, 1023 - 1031.
   Alkaline hydrolysis of humic substances - Spectroscopic and chromatographic investigations.
5. M.U. Kumke, G. Abbt-Braun, F.H. Frimmel
   Acta Hydrochem. Hydrobiol., 1998, **26**, 73 - 81.
   Time-resolved fluorescence measurements of aquatic natural organic matter (NOM).
6. F.H. Frimmel, M.U. Kumke
   in: Humic Substances: structure, properties, and uses, G. Davies and E. Ghabbour (eds.), Royal Society of Chemistry, Cambridge 1998, 113 - 122.
   Fluorescence decay of humic substances (HS) - A comparative study.
7. M.U. Kumke, F.H. Frimmel
   in: Refractory organic substances in the Environment, F.H. Frimmel, G. Abbt-Braun (eds), Wiley-VCH, Weinheim 2002, 215 - 231.
   Stationary and time-resolved fluorescence for refractory organic substances characterization.

Bezug zur aktuellen Literatur Neben Weiterentwicklungen im Bereich der NMR-Spektroskopie und Massenspektrometrie in Kombination mit hochentwickelten Auswerteverfahren, der Standardisierung von Isolierungsprozeduren für HS zur Bereitstellung von Referenzmaterialien und der Anwendung von chromatographischen Verfahren mit multidimensionaler Detektion, ist es der Ausbau der stationären und zeitaufgelösten Fluoreszenztechniken, der einen großen Beitrag zur Charakterisierung von HS und deren Reaktionen geleistet hat [1,17–19]. Durch die Kombination analytischer Methoden werden für komplexe Proben wie HS verschiedene physikochemische Parameter zugänglich. Wilkinson et al. konnten durch die Kombination von Fluoreszenz-Korrelationsspektroskopie mit chromatographischen Verfahren für verschiedene HS und HS-Fraktionen Diffusionskoeffizienten bestimmen [20–24]. Besonders die Multidimensionalität der Fluoreszenztechniken hat zu einer breiten Anwendung in der Charakterisierung von HS und HS-Fraktionen geführt. Durch die instrumentellen Weiterentwicklungen wurden totale Lumineszenzspektren (TLS) von HS gekoppelt mit chromatographischen Trennverfahren gemessen [25–27]. In der steigenden Anwendung von TLS zur Charakterisierung setzt sich die Erkenntnis durch, dass einfache 2D-Fluoreszenzspektren nicht geeignet sind, da für ein komplexes Stoffgemisch wie HS ein starker Einfluss der gewählten Anregungs- und Emissionswellenlängen auf die gemessenen Spektren beobachtet wird. Mit der Messung der TLS können geeignetere experimentelle Parameter bestimmt werden, wie sie z.B. in der chromatographischen Analyse organischer Wasserinhaltsstoffe gebraucht werden [28]. Durch die Kombination mit Messungen von TLS verschiedener Referenzverbindungen ist eine Klassifizierung nach Ursprungsorten und Vorläufermaterialien möglich [28, 29]. So wurden große Unterschiede in der Fluoreszenz zwischen terrestrischen, aquatischen und marinen HS beobachtet [30]. Durch die Aufnahme von TLS und die zusätzliche Einteilung in spezifische spektrale Regionen können Ursprungsort, Humifizierungsgrad usw. verlässlicher beschrieben werden [31] (s. dazu auch 2.1.7).

In Kombination mit Absorptionsspektroskopie wird die Messung der Fluoreszenz zur einfachen und schnellen Bestimmung des Gehalts an HS in natürlichen Wässern angewandt [32] (s. auch Anhang D, Veröffentlichung Nr. 22). Als Methode, die nur geringe oder keine Probenaufbereitung benötigt, kann die Fluoreszenzspektroskopie auch als schnelle Vor-Ort-Methode eingesetzt werden, um z.B. das Ausbreitungsverhalten in Böden oder Gewässern zu untersuchen. Durch Messen der intrinsischen HS-Fluoreszenz können so Transportwege, der Eintrag von Verunreinigungen durch bestimmte Industrien (wie z.B. die Papierindustrie) oder der Zustand von Deponierenaturierungen verfolgt und charakterisiert werden [30, 33–36] (s. dazu auch 2.1.1, 2.1.2 und 2.1.3). Durch Untersuchungen der intrinsischen Fluoreszenz von Sickerwasserproben wurde der Grad der Humifizierung bestimmt. Dieser ist ein wichtiger Parameter zur Beurteilung einer Deponie z.B. mit Hinblick auf die Mobilität von Schadstoffen aus der Deponie [35]. Das Einleiten von Abwassern der Papierherstellung führt zu signifikanten Veränderungen in den TLS bzw. synchronen Fluoreszenzspektren von Flusswasserproben [37, 38]. Ausbreitung von Grundwasser und Eintrag von Stoffen wurden durch die Messung der intrinsischen Fluoreszenz von

HS unter verschiedenen experimentellen Bedingungen untersucht [39]. Für Küstenregionen wird versucht, anhand von Fluoreszenzmessungen von Wasserproben das Auftreten von Algenblüten und das Einleiten von anthropogenen Stoffen zu überwachen [40]. Durch Kontrolle der Qualität des gelösten organischen Kohlenstoffs in natürlichen Gewässern (von denen ein großer Anteil die HS sind) und im Auslauf von Kläranlagen wird den Betreibern der Anlagen ein Parameter an die Hand gegeben, der ein schnelles steuerndes Eingreifen ermöglicht [28, 34, 41, 42]. Aus den spektroskopischen Eigenschaften natürlicher Wässer werden Rückschlüsse auf die Reaktivität der gelösten organischen Stoffe gezogen [36, 43]. Dies ist u.a. bedeutsam im Falle einer Chlorung von Trinkwässern und der potentiellen Bildung von gesundheitsschädlichen chlorierten Reaktionsprodukten, einer in den USA weitverbreiteten Problematik (s. dazu 2.1.3). Basierend auf Fluoreszenzmessungen sind verschiedene Indizes entwickelt worden, die den Humifizierungsgrad, den Gehalt an aromatischen Strukturen oder die Herkunft der HS einzuordnen gestatten [33, 34, 44–50].
Aus vergleichenden Untersuchungen geht hervor, dass die relative Fluoreszenz der FA-Fraktion größer ist als die der dazugehörigen HA-Fraktion [25, 29]. Dass die Fraktionen mit den kleinen und mittleren molaren Größen besser fluoreszieren, konnte auch durch Kombination von Größenausschlusschromatographie (*size exclusion chromatography*, SEC) und Fluoreszenzdetektion gezeigt werden [28]. In Fraktionen mit hoher molekularer Größe scheint der Anteil an Polysacchariden dominant. In der Kopplung von TLS-Detektion und Hochdruck-SEC konnte ferner gezeigt werden, dass die kleinen, polaren Anteile der HS am stärksten fluoreszieren und sich auch in der Lage des Emissionsmaximums deutlich von den größeren unterscheiden [26] (s. dazu 2.1.3, 2.1.4 und 2.1.5). Die Fluoreszenz von partikulären, kolloidalen und gelösten HS scheint große Ähnlichkeit zu besitzen. Für HS isoliert aus dem Amazonas ließen sich zwei charakteristische Fluoreszenzanregungsbanden identifizieren, aus deren Quotienten ein linearer Zusammenhang für die pH-Abhängigkeit der HS-Fluoreszenz gefunden wurde [51]. In anderen Fällen zeigen auch mittels unterschiedlicher Festphasen isolierte HS gute Übereinstimmung in ihren Fluoreszenzeigenschaften, was auf sehr ähnliche Strukturen (bzw. Fluorophore) in den isolierten Fraktionen hinweist [52]. Dass die kleinen Größenfraktionen der HS neben der stärksten Fluoreszenz auch das größte photochemische Sensibilisierungspotential besitzen, konnten in photochemischen Abbauexperimenten mit 2,4,6-Trimethylphenol und dem Herbizid Fenuron gezeigt werden [53]. Allerdings scheint diese Sensibilisierung des photochemischen Abbaus durch HS von den abzubauenden Stoffen beeinflusst zu werden. In Photoabbauexperimenten mit polyzyklischen aromatische Kohlenwasserstoffen (PAK) konnte durch die Gegenwart von Suwannee River FA kein beschleunigter Photoabbau der PAK gefunden werden [54].
Neben der phänomenologischen Anwendung von Fluoreszenzmethoden zur Charakterisierung des Ursprungsorts oder des Eintrags von Verunreinigungen, gibt es mechanistische Untersuchungen, die das Ziel einer Identifizierung von Fluorophoren in HS haben. Es wurden verschiedene Modellsysteme diskutiert, die im Gegensatz zu früheren Meinungen nicht mehr von nahezu unendlich vielen Fluorophoren ausgehen, sondern eine begrenzte Anzahl von Fluorophoren annehmen. Vorangetrieben wurden

diese Überlegungen besonders durch Ergebnisse aus massenspektrometrischen Untersuchungen [18]. Fraktionierung in polyphenol-reiche und carbohydrat-reiche Anteile zeigten, dass die polyphenol-reiche Fraktion deutlich besser fluoresziert [55,56]. Der Vergleich von HS verschiedener Ursprungsorte in Bezug auf ihr spektroskopisches Verhalten im Temperaturbereich von -160°C bis +300°C legte nahe, dass es nur eine kleine begrenzte Anzahl von fluoreszierenden Strukturen gibt [25, 57] (s. dazu auch Kap. 2.1.1 bis 2.1.4). In anderen Studien wird vor allem die Anwesenheit von chinoiden Strukturen als fluoreszierendes Strukturelement favorisiert. Diese stützen sich u.a. auf ESR-Untersuchungen und vergleichende Betrachtungen mit Chinon-Hydrochinon-Modellsystemen [49,58]. Der Gehalt an Chinon-Hydrochinon-Strukturen bestimmt das Redoxverhalten der HS. Aus einem Vergleich der Fluoreszenzeigenschaften mit den Elektronenakzeptor-Eigenschaften verschiedener HS (gemessen durch Reduktion von Fe(III) zu Fe(II)) zeigte sich aber nur eine mäßige Korrelation [59]. In Absorptions- und Fluoreszenzmessungen in Kombination mit laserinduzierten Ausbleichexperimenten wurde versucht, selektiv bestimmte Chromophore bzw. Fluorophore anzuregen und photochemisch abzubauen. Aus den gewonnenen Ergebnissen wird auf eine intramolekulare Energie- und Landungstransfer-Kaskade geschlossen - ähnliche wie in 2.1.6 beschrieben - so dass nur eine begrenzte Anzahl von gekoppelten Fluorophoren für die beobachtete komplexe Fluoreszenz verantwortlich sind [60].

2.1.1 Adsorbed and bound residues in fulvic acid fractions of a contaminated groundwater: Isolation, chromatographic and spectroscopic characterization

C. Zwiener, M.U. Kumke, G. Abbt-Braun, F.H. Frimmel
Acta Hydrochim. Hydrobiol., 1999, **27**, 208 - 213.

In dieser und der in 2.1.2 angeführten Publikation wurden aus Grundwasserproben eines ehemaligen Gaswerksgeländes isolierte HS untersucht. Zunächst erfolgte die Charakterisierung vornehmlich über chromatographische Verfahren in Kombination mit UV/Vis- und Fluoreszenzspektroskopie.
Es zeigten sich in Abhängigkeit vom Probenahmeort deutliche Unterschiede zwischen den isolierten Huminstoffen, speziell den FA-Fraktionen. Während die Probe aus dem Abstrombereich in ihren untersuchten Werten sehr gut mit dem aus anderen natürlichen Gewässern isolierten HS übereinstimmte, zeigte die aus der Schadstoffahne gewonnene HS-Probe ein spezifisch-abweichendes Verhalten. Für letztere deuteten die Chromatogramme sowie die Absorptions- und Fluoreszenzspektren darauf hin, dass mit den HS assoziierte organische Verbindungen vorhanden waren, die noch nicht vollständig abgebaut bzw. noch nicht in die HS-Matrix integriert waren. Durch Extraktion mit unpolaren organischen Lösungsmitteln konnten teilweise organische Verbindungen extrahiert werden, wodurch das Vorliegen von an HS physisorbierte Rückstände weiter unterstrichen wurde. Aus Vergleich mit Einzelsubstanzen wurden Salicylsäure und verwandte Derivate als eine mögliche Verbindungsklasse identifiziert.

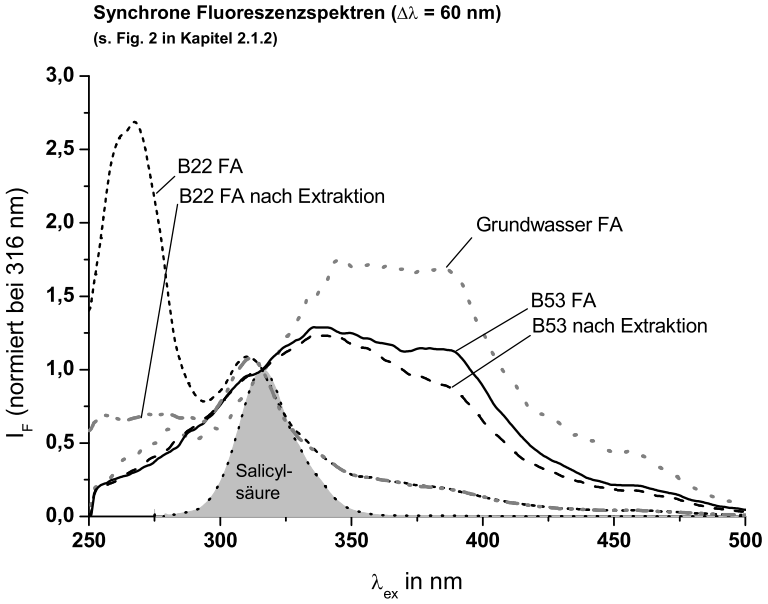

Adsorbed and Bound Residues in Fulvic Acid Fractions of a Contaminated Groundwater – Isolation, Chromatographic and Spectroscopic Characterization

Adsorbierte und gebundene Rückstände in den Fulvinsäurefraktionen eines kontaminierten Grundwassers – Isolierung, chromatographische und spektroskopische Charakterisierung

C. Zwiener, M. U. Kumke, G. Abbt-Braun, and F. H. Frimmel*

Keywords: Humic Substances, Fulvic Acids, Bound Residues, Gas Facility, XAD Adsorption, Size-exclusion Chromatography, Hydrophobic Interaction Chromatography

Summary: Humic substances (HS) were isolated from two contaminated groundwater samples (B22 and B53) from a site of a former gas facility. The isolation yielded almost only the fulvic acid fractions (FA). For characterization spectroscopic (UV, fluorescence) and chromatographic techniques (hydrophobic interaction chromatography – HIC as well as size-exclusion chromatography – SEC) were applied. The sample designated B22 FA was collected from the contamination plume whereas the sample B53 FA was collected downstream. Distinct differences were exhibited by these samples. The UV and fluorescence spectra as well as the HIC and SEC chromatograms of the B53 FA sample resemble those of the FA fraction obtained from natural water (groundwater, bog). The HIC and SEC chromatograms reveal the presence of organic compounds in B22 FA which can be derived from coal tar contaminants or their metabolites. Some of the compounds can be extracted from the FA fraction with non-polar organic solvents indicating adsorptive forces between the contaminants and the FA fraction.

Schlagwörter: Huminstoffe, Fulvinsäuren, gebundene Rückstände, Gaswerksgelände, XAD-Adsorption, Größenausschlußchromatographie, Umkehrphasenchromatographie

Zusammenfassung: Von den zwei kontaminierten Grundwasserproben B22 und B53 eines ehemaligen Gaswerksgeländes wurden Huminstoffe (HS) isoliert. Dabei wurde jeweils vorwiegend die Fulvinsäurefraktion (FA) erhalten. Zur Charakterisierung der FA-Fraktionen wurden spektroskopische (UV, Fluoreszenz) und chromatographische Methoden (hydrophobe Wechselwirkungschromatographie HIC auf Umkehrphasen und Größenausschlußchromatographie SEC) angewandt. Die Proben zeigen deutliche Unterschiede, wobei B22 FA direkt aus der Schadstoffahne und B53 FA aus dem Abstrombereich stammt. Berücksichtigt man die UV- und Fluoreszenzspektren sowie die Chromatogramme der HIC- und SEC-Trennung, so ist B53 FA sehr gut mit FA-Fraktionen natürlicher Gewässer (Grund- bzw. Braunwasser) vergleichbar. Die Anwesenheit von organischen Verbindungen in der Probe B22 FA wird besonders in den Chromatogrammen nach HIC- und SEC-Trennung deutlich. Diese Verbindungen können auf Kohleteerrückstände oder deren Metaboliten zurückgeführt werden. Ein Teil der organischen Verbindungen läßt sich mit unpolaren organischen Lösemitteln aus der FA-Fraktion extrahieren, was auf Sorptionswechselwirkungen zwischen den Kontaminanten und der FA-Fraktion hinweist.

1 Introduction

Gas production facilities were common in Germany at the beginning of the 19th century. Although almost all gas production was terminated in the 1970's, highly contaminated sites have remained. Groundwater samples taken from these sites often contain a variety of polyaromatic (PAH) and N-, O-, S-heterocyclic compounds as well as their metabolites [1–4].

* Dr. Christian Zwiener, Dr. Michael U. Kumke, Dr. Gudrun Abbt-Braun, Prof. Dr. Fritz H. Frimmel, Engler-Bunte-Institut, Bereich Wasserchemie, Universität Karlsruhe (TH), Engler-Bunte-Ring 1, D-76131 Karlsruhe, Germany

Correspondence to F. H. Frimmel
E-mail: fritz.frimmel@ciw.uni-karlsruhe.de

The transport, fate, and bioavailability of contaminants in aquatic environments is highly dependent largely on the partitioning of the pollutant between water, soil or sediment and natural organic matter (NOM, dissolved and adsorbed on soil or sediment) [5–7]. A main part of the NOM are usually humic substances (HS). The interaction between aquatic HS and organic pollutants can be attributed to van der Waals forces, charge-transfer mechanism, as well as hydrogen bond formation, ion exchange, and even covalent binding [8, 9]. The specific kind of interaction depends on the physico-chemical properties of both the HS and the organic pollutant.

The objective of this work was to investigate adsorbed or bound organic residues in the isolated fractions of aquatic HS. For that purpose aquatic HS were isolated from a contaminated site and characterized by different methods.

  0323-4320/99/0407-0208 $ 17.50+.50/0

2 Experimental

Sampling site

Aquatic samples were taken at the contaminated site of a former gas facility in southern Germany. Pollution at this site originated from gasification and gas purification processes due to leakage from storage facilities and water leaching of coal and tar dumping-grounds. Groundwater samples taken from these sites contain a variety of aromatic and heterocyclic compounds [10] and possibly their metabolites [4]. Different wells were installed to investigate the contaminated field and the groundwater below. The tubes installed were made of polyvinyl chloride and high density polyethylene, and their diameters were 125 mm and 150 mm, respectively. The well B22 was located within the contamination plume, i.e. in the primary source of contamination with a high contamination level. The well B53 was located downstream of the contamination plume with a low contamination level. More details were provided elsewhere [10].

Sampling procedure

Groundwater samples were collected from the aquifer at about 5.5 m below ground level with a submersible pump from the two wells (differing in their pollution burden). Two 100 L samples were collected into 50 L polyethylene containers from the wells B22 and B53, cooled immediately, and stored at 4 °C in the dark.

Isolation of humic substances

One hundred L water samples from wells B22 and B53 were filtered (0.45 µm, filter cartridge made from polypropylene and cellulose acetate, Sartorius) and then acidified to pH 2 with HCl prior to the isolation. The isolation of HS was performed by adsorption/desorption on a polystyrene-resin (XAD-8, Merck) as described by Mantoura and Riley [11] and varied by Abbt-Braun et al. [12]. The isolation of HS with XAD resin has been achieved by employing the following two steps: I The adsorption of organic matter on XAD-8 resin at pH 2; and II The desorption of adsorbed HS with NaOH (Fig. 1). The resulting solutions of fulvic acids (FA) and humic acids (HA) were used for further investigations, respectively the freeze-dried samples.

In addition, the FA fractions of a bog lake HO10 (Lake Hohloh, Black Forest) and of a natural groundwater FG1 (Fuhrberg) from the major research program ROSIG (Refrakäre organische Säuren in Gewässern) were used as reference materials [13]. The fractions had been isolated from 1 000 L samples with the above described method of XAD-adsorption. To investigate the organic contaminant content of the FA fractions 10 mL samples were extracted three times with 4 mL *n*-hexane (pro analysi, Merck) and subsequently three times with 4 mL dichloromethane (pro analysi, Merck).

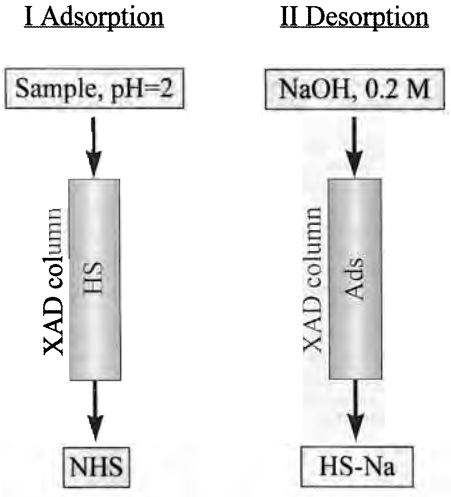

Fig. 1: Scheme of the first two steps of the adsorptive XAD isolation of humic substances. NHS: non adsorbable carbon fraction at pH 2; Ads: with NaOH (0.2 M) non desorbable carbon fraction.

Schema der ersten beiden Schritte der Adsorptionsanreicherung von Huminstoffen an XAD. NHS: bei pH = 2 nicht adsorbierbarer Anteil; Ads: mit NaOH (0.2molar) nicht desorbierbarer Anteil.

Analyses

Dissolved organic carbon (DOC) content was determined on 10 mL samples acidified with 0.1 mL concentrated phosphoric acid and purged with nitrogen, prior to analysis with a Dohrmann Carbon Analyzer DC 80 (Schmidlin, Mutlangen).

Copper complexation capacity (CCC) was measured by differential pulse polarography at pH 6.9 and a DOC content of the sample of 1 mg/L according to Frimmel and Geywitz [14], using a polarograph with a mercury hanging-drop electrode (646/647 VA, Metrohm). UV spectra were recorded on a spectrophotometer with a data station (Spectronic 1201, Milton Roy) in 10 mm quartz glass cuvettes (Hellma).

For the fluorescence experiments the samples were diluted with deionized water to a final DOC concentration of 10 mg/L. For the steady state fluorescence measurements a Perkin Elmer LS 5B was used with a spectral bandpass of 5 nm for both excitation and emission. Liquid chromatographic analyses were performed using a HP 1090 liquid chromatograph with HP ChemStation (Hewlett Packard), diode array and fluorescence detection [15]. Two methods were employed for size-exclusion and hydrophobic interaction chromatography (Table 1).

3 Results and Discussion

The carbon balance for the two steps of HS isolation (the adsorption of organic matter on XAD resin at pH 2, and the desorption of adsorbed HS with NaOH, cf. Figure 1) is shown in Figure 2 for the samples B22 and B53 in comparison to the bog lake sample HO10 representing a typical result for natural surface and groundwater. The samples B22 and B53 from the gas facility area exhibited a smaller amount of adsorbable organic substances (step I), compared with the HO10 sample.

More distinct differences are observed for the desorbed fraction (step II). For the sample HO10 the total amount of adsorbed organic carbon could be desorbed, for B53 85 % and finally for B22 only 49 %. This observation can be explained by the high contamination level of the sample B22 with organic compounds of coal tar residues and their metabolites (e.g. BTEX, indan, naphthalene, and other PAH). Representatives of these compound classes are not desorbed from the XAD resin with aqueous eluents at high pH value (NaOH), but they could be finally extracted with methanol in a soxhlet apparatus. In the methanol extract only a few compounds could be identified by HPLC/DAD and GC/MS: e.g. naphthalene, benzothiophen, methyl derivatives of phenol, phenanthridinone. Obviously, the DOC content of this fraction cannot be measured.

Table 1: HPLC parameters for gel and hydrophobic interaction (HI) chromatography.

Parameter für die HPLC-Messung der Gelchromatographie und der hydrophoben Wechselwirkungschromatographie.

	Method (gel chromatography)	Method II (HI chromatography)
Column	Progel-TSK, G2000SW$_{XL}$ (Supelco) 300 mm × 7.8 mm, 5 µm particle	ODS Hypersil (Hewlett Packard) 125 mm × 4 mm, 5 µm particle
Eluent	Phosphate buffer, c = 2.5 mmol/L, pH = 7	A: aqueous acetic acid (0.01 %) B: acetonitrile
Gradient		99 % A at 0 min, 70 % A at 2 min, 15 % A at 16 min, 15 % A at 20 min
Flow	1 mL/min	0.6 mL/min
Injection	50 µL by autosampler	50 µL by autosampler
Detection	UV absorption at 220 nm, 254 nm, 436 nm, spectra from 210...400 nm Fluorescence: excitation at 314 nm, emission at 430 nm	UV absorption at 220 nm, 254 nm, 436 nm, spectra from 210...400 nm Fluorescence: excitation at 314 nm, emission at 430 nm
Sample parameters	pH = 11.5...12, electrical conductivity 1...5 mS/cm, β(DOC) = 95...250 mg/L	pH = 11.5...12, electrical conductivity 83...98 mS/cm, β(DOC) = 95...250 mg/L

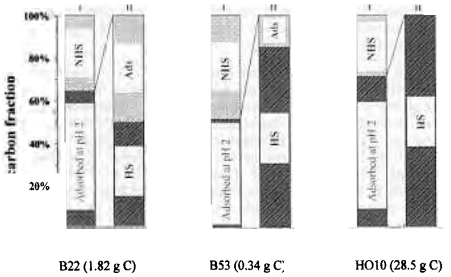

Fig. 2: Carbon balance during the XAD-8 isolation. Comparison of two samples of the gas facility site (B22, B53) with a sample of a natural bog lake (HO10). Adsorption steps: I adsorption on XAD-8 at pH 2; II desorption of the preloaded XAD resin with NaOH (0.2 M); NHS and Ads according to Figure 1; HS: humic substances.

Kohlenstoffbilanz der Adsorptionsanreicherung auf XAD-8. Vergleich für zwei Proben aus dem Gaswerksgelände (B22, B53) mit einem natürlichen Braunwasser (HO10). Anreicherungsschritte: I Adsorption bei pH = 2; II Elution mit NaOH (0.2molar); NHS und Ads entsprechend Bild 1; HS: Huminstoffe.

The yields of the FA and HA fractions for the whole isolation procedure are shown in Table 2. Mainly FA fractions were obtained from the aqueous samples according to the amount of carbon in the original water sample. The losses can be attributed to further steps of fractionation like precipitation, washing, repeated adsorption, and ion exchange separation.

The FA fractions were characterized by determining the pH-dependent specific absorption and the copper(II) complexing capacity (CCC). The FA fractions of B22 and B53 showed lower specific absorbance at 254 nm and 436 nm compared to the FA fraction of HO10 (Table 3). This indicates a lower content of UV light absorbing, unsaturated, or aromatic structures and of visible light absorbing chromophores (the wavelength 436 nm serves as measure for the yellow color) in the FA of the gas facility. The FA fraction from the contaminated sample B22 exhibited the lowest values.

Table 2: Yields of isolated FA and HA after the isolation with XAD-8 and further purification with ion-exchange columns.

Ausbeuten für FA- und HA-Fraktionen nach Isolierung mit XAD-8 und nachfolgenden Reinigungsschritten mit Ionenaustauschersäulen.

Carbon portion	B53		B22	
	mass in mg	fraction in %	mass in mg	fraction in %
Total	341	100	1 817	100
FA	62	18	257	14
HA			27	2
Loss during fractionation	113	33	876	48

Compared to HO10 the specific UV absorbance at 254 nm of the sample B22 exhibited less and that of B53 even lesser dependence on the pH value. It can be deduced, that the FA fractions from the gas facility site contain less phenolic or acidic groups attributed to UV absorbing moieties, than the FA fraction of HO10.

The copper(II) complexing capacity (CCC) was found to be 1.1 µmol/mg for the B22 FA, 1.4 µmol/mg for the B53 FA, and 2.2 µmol/mg for the HO10 FA. These measurements were carried out at a DOC concentration of 1 mg/L. The results are in good agreement with the above mentioned measurements.

The UV spectrum of the FA fraction of B53 (Fig. 3 a) is comparable to that of the FA fractions from natural origin. However, in the UV spectrum of the FA fraction of B22 an additional absorption band is noticeable in the wavelength range of 260 nm to 280 nm (Fig. 3 b). This band is suspected to be derived from organic contaminants which are associated with the FA or specific moieties of the FA. Due to their interaction the organic compounds are isolated together with the FA fraction.

Table 3: pH-value dependent absorbance of different FA samples normalized to the DOC content; pH adjusted with HCl and NaOH.
pH-Wert-abhängige, auf den DOC normierte Absorption verschiedener FA-Proben; pH-Wert-Einstellung mit HCl und NaOH.

pH value	a_{254nm}/β(DOC) L/(cm g)			a_{436nm}/β(DOC) L/(cm g)		
	B22 FA	B53 FA	HO10 FA	B22 FA	B53 FA	HO10 FA
11	28.3	33.1	51.5	1.1	1.6	5.8
7	25.8	31.6	48.5	0.8	1.1	3.8
5	24.8	32.2	–	0.6	0.9	–
2	24.8	32.0	39.3	0.6	0.8	2.3

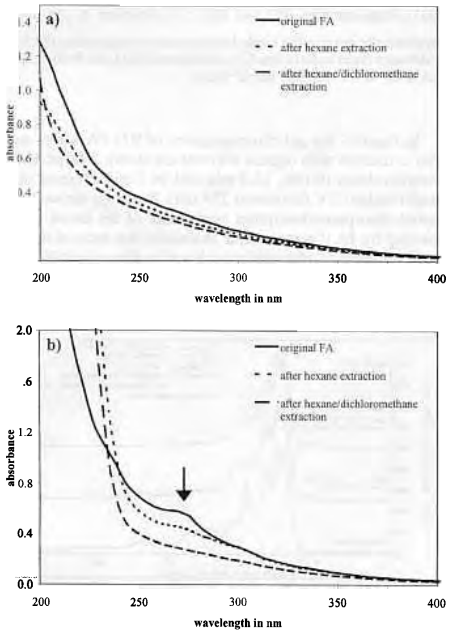

Fig. 3: UV spectrum of the original fulvic acid fraction (FA), that of the FA after hexane extraction, and that of the FA after hexane and subsequent dichloromethane extraction. The arrow indicates an absorption band attributed to organic contaminants. a) B53; b) B22.

UV-Spektren der originalen Fulvinsäurefraktion (FA), der FA nach Hexanextraktion und der FA nach Hexan- sowie Dichlormethanextraktion. Der Pfeil markiert eine Absorptionsbande, die organischen Kontaminanten zugeordnet wird. a) B53; b) B22.

To check whether only weak intermolecular forces prevail between the organic molecules and the FA (e.g. van der Waals or dipole-dipole forces), the FA solutions were subjected to liquid-liquid extraction with hexane, followed by dichloromethane. Organic solvents are expected to overcompensate weak intermolecular forces. Only little or no influence can be expected for the ionic interactions or specific bonds between reactive moieties of the organic compounds and FA. As a result of the extraction the above mentioned additional absorption band in the UV spectrum of B22 FA disappeared (see Fig. 3 b). This implies, that the organic contaminants causing the additional UV absorption band are associated by weak forces to the FA and can therefore be removed from the complex by organic solvents. The liquid-liquid extraction of B53 FA shows almost no influence on the shape of the UV spectrum in the wavelength range between 250 nm and 400 nm. Hexane extraction removes about 10 %, hexane/dichloromethane extraction about 20 % of the UV absorbing portion of the FA. These values were calculated for the wavelengths 250 nm and 280 nm.

The normalized fluorescence emission spectra of the samples B22 and B53 in water before and after extraction with hexane and dichloromethane is shown in Figure 4. Under the experimental conditions employed the fluorescence intensity of the sample B22 was five times the intensity of the sample B53. Due to the extraction procedure no change in the shape of the fluorescence spectra was observed and the relative fluorescence intensities before and after extraction with the organic solvents decreased only slightly. In Figure 4 the fluorescence spectra of a groundwater FA (FG1 FA) and of salicylic acid are shown as well. It is interesting to note that the fluorescence spectra of the sample B22 and of salicylic acid are quite similar in shape. Only in the wavelength range higher than 425 nm minor deviations were found. Salicylic acid can be considered as model compound for possibly occurring metabolites of the original coal tar contaminants in the sample B22. However, salicylic acid is not extractable with organic solvents at neutral pH.

On the other hand the fluorescence spectrum of the FG1 FA isolated from a non-contaminated groundwater resembles that of the sample B53 FA. However, the spectrum of the ground water FA was slightly shifted to longer wavelengths.

For the dichloromethane extracts of B22 FA and B53 FA the observed fluorescence spectra were identical. Compared to the spectra monitored in water the fluorescence maximum was shifted to 350 nm. For the sample B53 FA only a very weak fluorescence signal could be detected in the dichloromethane extract indicating that only minor amounts were extracted. The amount of non-polar, by organic solvents extractable fluorescent compounds in B53 FA was therefore smaller when compared with B22 FA.

Size-exclusion (SEC) and the hydrophobic interaction chromatography (HIC) allow a more detailed consideration of the FA fractions. The normalized gel chromatograms of the FA fractions of the samples B22, B53 and FG1 as detected at λ = 254 nm are shown in Figure 5. Once more, the chromatogram of the sample B53 is quite similar compared to that of the

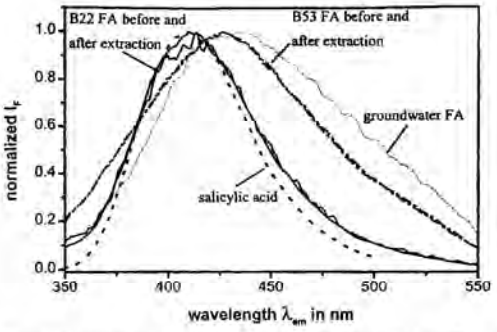

Fig. 4: Comparison of the steady-state fluorescence spectra (λ_{ex} = 314 nm) of salicylic acid and of the fulvic acid fractions of B22, B53 (before and after extraction), and of a natural groundwater (FG1 FA).

Vergleich der Steady-State-Fluoreszenzspektren (λ_{ex} = 314 nm) von Salicylsäure und den Fulvinsäurefraktionen von B22, B53 (vor und nach Extraktion mit organischen Lösemitteln) und eines natürlichen Grundwassers (FG1 FA).

natural groundwater (FG1). However, the chromatogram of the sample B22 shows additional peaks in the retention time range of the FA fraction (6 min to 11 min) and above. Due to their UV spectra the peaks can be attributed to organic compounds, which differ from those typical for the FA fraction.

The SEC results can be confirmed by hydrophobic interaction chromatography (HIC) with UV detection (Fig. 6). The complex sample composition of B22 FA is separated to a greater extent by HIC compared to SEC. No positive match could be obtained for a tentative identification of the peaks on the basis of known compounds and their UV spectra. Moreover, the shape of the FA elution band is strongly dependent on sample parameters such as pH or salt concentration and was not reproducible in the hydrophobic interaction chromatogram.

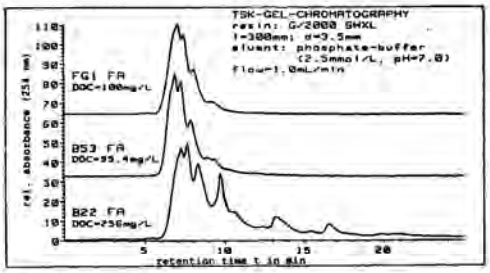

Fig. 5: Comparison of the normalized gel chromatograms of the FA fractions from a natural groundwater (FG1), from samples B53 and B22; UV detection at 254 nm.

Vergleich der normierten Gelchromatogramme der FA-Fraktionen eines natürlichen Grundwassers (FG1), der Proben B53 und B22; UV-Detektion bei 254 nm.

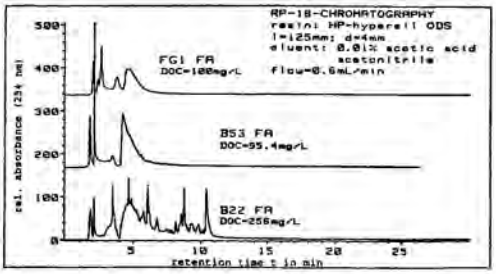

Fig. 6: Comparison of the normalized hydrophobic interaction chromatograms of the FA fractions from a natural groundwater (FG1), from samples B53 and B22; UV detection at 254 nm.

Vergleich der normierten Umkehrphasenchromatogramme der FA-Fraktionen eines natürlichen Grundwassers (FG1), der Proben B53 und B22; UV-Detektion bei 254 nm.

In Figure 7 the gel chromatograms of B22 FA before and after extraction with organic solvents are shown. The peaks at retention times 10 min, 13.5 min and 16.5 min decrease to a small residue (UV detector at 254 nm). Based on the well accepted adsorption/desorption mechanism of the initial isolation step for FA it is reasonable to assume that most of the organic compounds interacted via adsorptive forces with FA and they can be desorbed with organic solvents.

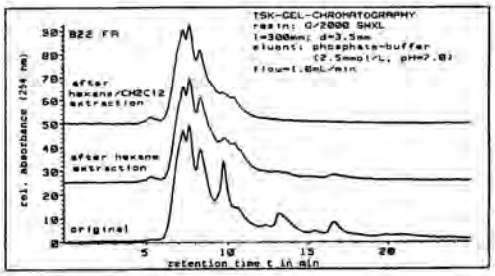

Fig. 7: Comparison of the normalized gel chromatograms of the FA fraction of B22 before and after solvent extraction; UV detection at 254 nm.

Vergleich der normierten Gelchromatogramme der FA-Fraktionen von B22 vor und nach Extraktion mit Lösemitteln; UV-Detektion bei 254 nm.

The gel chromatograms with fluorescence detection are shown in Figure 8 for the samples B22 FA and B53 FA after solvent extraction. Fluorescence allows a more selective and sensitive detection than UV. In the chromatogram of B22 FA a peak at 11 min with a striking fluorescence intensity can be recognized even after solvent extraction. On the basis of the retention times in SEC and HIC compared to a standard the peak can be tentatively attributed to salicylic acid. The tentative identification could be confirmed by further investigations applying synchronous fluorescence spectroscopy [16]. Since, it is obvious that the peak is only reduced in size by solvent extraction at neutral pH and salicylic acid should be associated with the FA by weak intermolecular forces, too.

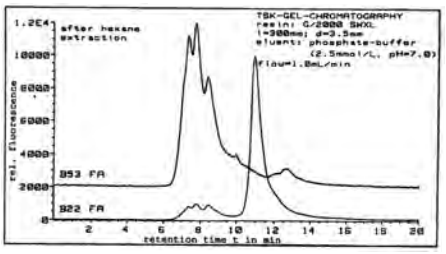

Fig. 8: Comparison of the normalized gel chromatograms of the FA fractions of B53 and B22 after hexane extraction; fluorescence detection (λ_{ex} = 314 nm; λ_{em} = 430 nm).

Vergleich der normierten Gelchromatogramme der FA-Fraktionen von B53 und B22 nach Hexanextraktion; Fluoreszenzdetektion (λ_{ex} = 314 nm; λ_{em} = 430 nm).

4 Conclusions

The samples B22 FA and B53 FA isolated from two wells with different pollution burden are quite different. The characteristics of B53 FA resemble those of the FA fractions of natural surface and groundwater. However, B22 FA is characterized by the content of some organic compounds, which is evident when comparing the UV and fluorescence spectra as well as the SEC and HIC chromatograms of the samples. The organic compounds are suspected to be associated with the FA or specific moieties of the FA. The different compound classes or different interaction forces between the organic contaminants and the FA fraction can be deduced from solvent extraction experiments. For instance, in the SEC chromatogram some UV absorbing compounds can be extracted with non-polar solvents indicating non-polar organic compounds. On the other hand, an abundant peak in the SEC chromatogram with fluorescence detection was not eliminated after solvent extraction of the sample indicating a more polar or ionic compound at neutral pH or even a strongly FA-bound pollutant. Compared to the retention behavior of standard compounds in SEC and HIC the peak could be tentatively identified as salicylic acid. Synchronous and time-resolved fluorescence measurements are promising approaches to further investigate these interactions and to confirm these results and interpret the fluorescing compounds. Results will be given in another paper [16].

With the above mentioned experimental methods only adsorbed or loosely-bound contaminants can be detected in the FA fractions. Nevertheless, also covalently bound contaminants (bound residues) are of interest, especially to judge the FA fraction of B53 downstream of the contamination plume by their pollution content. It is attractive to assume that the sample B53 FA contains bound residues as a result of chemical and biochemical processes. In such cases chemical or hydrolytic treatment of the FA fraction prior to analysis would be necessary to set free and further identify the bound residues.

Acknowledgement

This project was partially supported by funding provided by Deutsche Forschungsgemeinschaft (DFG), project number FR 536/17, as a part of the Priority Program "Geochemical processes with long-term effects in anthropogenically-influenced seepage- and groundwater". We also thank A. Heidt for the isolation of the samples, E. Karle for the HPLC analyses, M. Bissen for the CCC measurements, and J. Vollet for technical assistance.

References

[1] *Pellizzari, E. D., Castillo, N. P, Willis, S., Smith, D., Bursey, J. T.:* Identification of organic components in aqueous effluents from energy-related processes. In: *Van Hall, C. E.* (Ed.): Measurement of organic pollutants in water and wastewater. ASTM special technical publication 686. American Society for Testing and Materials, Philadelphia, 1978.

[2] *Novotny, M., Strand, J. W., Smith, S. L., Wiesler D., Schwende, F. J.:* Compositional studies of coal tar by capillary gas chromatography/mass spectrometry. Fuel *60*, 213–220 (1981).

[3] *Stuermer, D., Ng, D. J., Morris, C. J.:* Organic contaminants in groundwater near an underground coal gasification site in northwestern Wyoming. Environ. Sci. Technol. *16*, 582–587 (1982).

[4] *Edler, B., Zwiener, C., Frimmel, F. H.:* Particle beam LC/MS investigations of polar compounds in contaminated ground water samples from a former gas works. Fresenius J. Anal. Chem. *359*, 288–292 (1997).

[5] *Schwarzenbach, R. P., Gschwend, P. M., Imboden, D. M.:* Environmental organic chemistry. Wiley, New York, 1993.

[6] *Frimmel, F. H., Abbt-Braun, G., Hambsch, B., Huber, S., Scheck, C., Schmiedel, U.:* Behaviour and functions of freshwater humic substances - some biological, physical and chemical aspects. In: *Senesi, M., Miano, T. M.* (Eds.): Humic substances in the global environment and implications on human health. Elsevier, Amsterdam, 1994.

[7] *Bollag, J., Minard, R. D., Liu, S.:* Cross-linkage between anilines and phenolic humus constituents. Environ. Sci. Technol. *17*, 72–80 (1983).

[8] *Senesi, N.:* Binding mechanisms of pesticides to soil humic substances. Sci. Total Environ. *123/124*, 63–76 (1992).

[9] *Klaus, U., Oesterreich, T., Volk, M., Spiteller, M.:* Interaction of aquatic dissolved organic matter (DOM) with amitrole: The nature of the bound residues. Acta Hydrochim. Hydrobiol. *26*, 311–317 (1998).

[10] *Zwiener, C., Frimmel, F. H.:* Application of headspace GC/MS screening and general parameters for the analysis of polycyclic aromatic hydrocarbons in groundwater samples. Fresenius J. Anal. Chem. *360*, 820–823 (1998).

[11] *Mantoura, R. F. C., Riley, J. P.:* The analytical concentration of humic substances from natural waters. Anal. Chim. Acta *76*, 97–106 (1975).

[12] *Abbt-Braun, G., Frimmel, F. H., Lipp, P.:* Isolation of organic substances from the aquatic and terrestrial systems – Comparison of some methods. Z. Wasser-Abwasser-Forsch. *24*, 285–292 (1991).

[13] *Abbt-Braun, G., Frimmel, F. H.:* Basic characterization of reference NOM from central Europe – similarities and differences. Environ. Int. *25*, 191–207 (1999).

[14] *Frimmel, F. H., Geywitz, J.:* Zur koordinativen Bindung von Metallionen an Gewässerhuminstoffe. Fresenius Z. Anal. Chem. *316*, 582–588 (1983).

[15] *Gremm, T., Abbt-Braun, G., Frimmel, F. H.:* Einfluß verschiedener Parameter auf die HPLC-Charakterisierung organischer Säuren. Vom Wasser *77*, 231–241 (1991).

[16] *Kumke, M. U., Zwiener, C., Abbt-Braun, G., Frimmel, F. H.:* Spectroscopic characterization of fulvic acid fractions of a contaminated groundwater. Acta Hydrochim. Hydrobiol. *27* (6) (1999), in press.

received 23 October 1998
accepted 5 May 1999

2.1.2 Spectroscopic characterization of fulvic acid fractions of a contaminated groundwater

M.U. Kumke, C. Zwiener, G. Abbt-Braun, F.H. Frimmel
Acta Hydrochim. Hydrobiol., 2000, **27**, 409 - 415.

FA-Fraktionen, die aus Grundwasserproben eines ehemaligen Gaswerkgeländes isoliert worden waren, wurden mit synchroner und zeitaufgelöster Fluoreszenzspektroskopie eingehend untersucht (s. auch 2.1.1). Die dem unkontaminierten Grundwasser entnommene Probe entsprach im spektroskopischen Verhalten dem refraktären Stoffpool, wie er in anderen natürlichen Grundwässern gefunden wird. Hingegen hatte die aus dem kontaminierten Abstrombereich gewonnene HS-Probe deutlich veränderte spektroskopische Eigenschaften. Wie die Untersuchungen zeigten, bestimmte in dieser Probe eine eng definierte Stoffklasse die spektroskopischen Eigenschaften. Als eine repräsentative Verbindung konnte Salicylsäure identifiziert werden. Besonders deutlich trat dies in den zeitaufgelösten Fluoreszenzmessungen hervor. Die Auswertung lieferte für die aus kontaminiertem Grundwasser isolierten HS sehr enge Fluoreszenzlebenszeitverteilungen, woraus auf das Vorliegen von sehr ähnlichen fluoreszierenden Verbindungen geschlossen wurde. Dagegen zeigten HS, die aus nicht-kontaminierten Wässern isoliert worden waren, breite multi-modale Verteilungen, die u.a. in der Heterogenität der Probe und der Präsenz von Reaktionen im elektronisch-angeregten Zustand begründet sind.

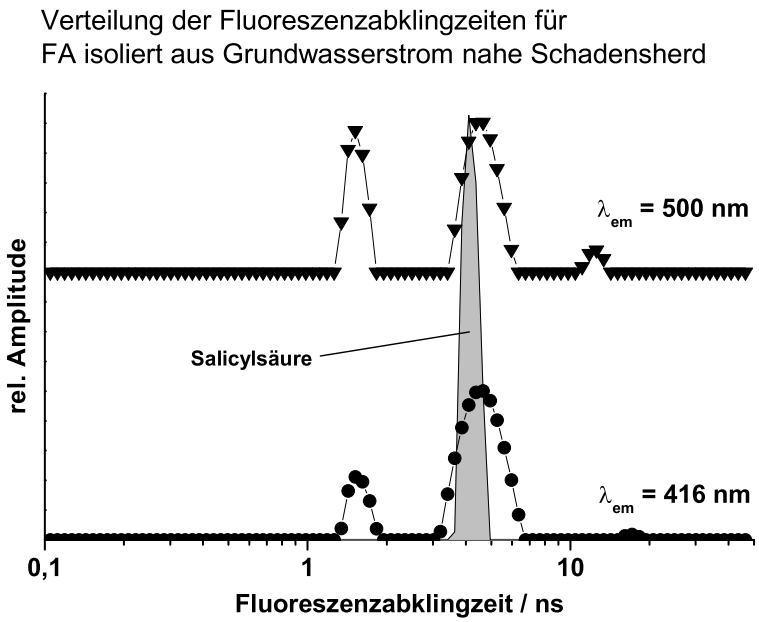

Research Papers

Spectroscopic Characterization of Fulvic Acid Fractions of a Contaminated Groundwater

Spektroskopische Charakterisierung der Fulvinsäurefraktionen eines kontaminierten Grundwassers

M. U. Kumke, C. Zwiener, G. Abbt-Braun, and F. H. Frimmel*

Keywords: Humic Substances, Fulvic Acids, Steady-state Fluorescence, Time-resolved Fluorescence

Summary: Two fulvic acid (FA) samples taken from a former gas production facility in the Southwest of Germany were characterized using advanced fluorescence techniques. Steady-state fluorescence (fluorescence excitation, synchronous fluorescence) as well as time-resolved fluorescence were applied. Distinct differences between the sample B22 FA taken within the contamination plume and the sample B53 FA taken downstream were found. Comparison with a model compound for metabolites and humic substances revealed that due to the downstream passage the characteristics of the dissolved organic matter became more humic-like. The assignment of single classes of compounds in the sample B22 FA is discussed in terms of their synchronous fluorescence spectra and fluorescence decay time distribution.

Schlagwörter: Huminstoffe, Fulvinsäuren, statische Fluoreszenz, zeitaufgelöste Fluoreszenz

Zusammenfassung: Eine ausführliche Untersuchung der Fulvinsäure-Fraktionen zweier wäßriger Proben eines Gaswerksgeländes wurde mit Hilfe fluoreszenzspektroskopischer Methoden durchgeführt. Dabei wurden sowohl verschiedene steady-state-Techniken (Fluoreszenzanregungsspektren, synchrone Fluoreszenzspektren) als auch zeitaufgelöste Fluoreszenzmessungen eingesetzt. Es zeigten sich große Unterschiede in den spektroskopischen Eigenschaften der untersuchten Proben. Von diesen wurde die Probe B22 FA direkt innerhalb des kontaminierten Bereichs in der gesättigten Grundwasserzone genommen, während die Probe B53 FA im Abstrom des Grundwassers gesammelt wurde. Es zeigte sich, daß die im Abstrom entnommene Probe in ihren Fluoreszenz-Eigenschaften schon sehr ähnlich dem refraktären Stoffpool aus unkontaminiertem Grundwasser war, während die Probe B22 FA von einer einzelnen Verbindungsklasse dominiert wurde.

1 Introduction

The interactions of contaminants with natural organic matter (NOM) highly determines their fate, transport, and bioavailability in the aquatic environment [1]. The main part in NOM can be attributed to humic substances (HS) which are divided into fulvic acids (FA) and humic acids (HA) on an operationally-defined basis [2, 3]. Different mechanisms for the interaction between NOM and organic contaminants ranging from weak van der Waals forces to covalent binding of the contaminant to the NOM matrix were reported [4–6]. Fluorescence spectroscopy is a multidimensional technique with three main independent variables: excitation wavelength λ_{ex}, emission wavelength λ_{em}, and fluorescence decay time τ_f. In principle, fluorescence spectroscopy is capable to investigate the interaction between NOM and fluorescing contaminants without pre-separation and pre-concentration which would disturb the equilibrium between NOM and contaminant. The combination of time-resolved and steady-state fluorescence techniques makes it possible to distinguish between dynamic interactions and static interactions like complex formation between the contaminant and the NOM matrix [7–10]. In case of sites of former gas production facilities the pool of substances that is involved in the building of NOM contains a considerable amount of contaminants, e.g., polycyclic aromatic hydrocarbons (PAH) found in coal tar. These substances are altered by physical, chemical, and microbiological processes. Within these different stages of alteration and degradation NOM can become a reaction partner.

The objective of the work was to investigate the possible incorporation of PAH into NOM in terms of alteration of the NOM found in the groundwater at different distances from the contamination plume. We were especially interested how the presence of PAH was changing the fluorescence properties of NOM formed over distance (and over time as well). The work discussed is highly important for the protection of groundwater resources and drinking water supplies.

* Dr. Michael U. Kumke, Dr. Christian Zwiener, Dr. Gudrun Abbt-Braun, Prof. Dr. Fritz H. Frimmel, Engler-Bunte-Institut, Bereich Wasserchemie, Universität Karlsruhe (TH), Engler-Bunte-Ring 1, D-76131 Karlsruhe, Germany

Correspondence to F. H. Frimmel
E-mail: fritz.frimmel@ciw.uni-karlsruhe.de

2 Experimental

The samples were taken from a former gas production facility in the southern part of Germany. Due to leakage from storage facilities of gas production and purification processes the groundwater is contaminated with a variety of organic compounds [11]. The

  0323–4320/99/0611–0409 $ 17.50+.50/0

sample site and the sampling procedure are described in detail elsewhere [11, 12]. Two wells were probed. Well B22 is located within the contamination plume whereas well B53 is situated downstream of the groundwater flow. The FA fractions of the two samples B22 and B53 were isolated using XAD-8 resin according to a modified method of Mantoura and Riley [2, 3]. The solutions of the samples B22 FA and B53 FA were diluted to similar concentrations of dissolved organic carbon using de-ionized water. In order to investigate the interactions between contaminants and natural organic matter in more detail the samples B22 FA and B53 FA were extracted using *n*-hexane (p.a., Merck) and dichloromethane (p.a., Merck).

The fulvic acid FG1 FA was isolated from an uncontaminated groundwater using XAD-8 resin as well and serves as a reference material in the multidisciplinary research program ROSIG (Fr 536/17) of the Deutsche Forschungsgemeinschaft. A detailed description of the sample is given in Frimmel and Abbt-Braun [13]. PAKA2 FA was isolated from the soil suspension of a microbial degradation of PAH using XAD-2 resin and was used as a reference FA as well [14].

For the fluorescence experiments the final concentration of the FA used in dissolved organic carbon (DOC) was adjusted to 10 mg/L. The model compound salicylic acid was of p.a. quality and used as received (Aldrich).

For the steady-state fluorescence measurements a Perkin Elmer LS 5B was used with a spectral bandpass of 5 nm in excitation and emission. The time-resolved fluorescence experiments were performed with a FL900 lifetime spectrometer (Edinburgh Instruments, Edinburgh, UK) in the time-correlated single photon counting (TCSPC) mode. The TCSPC set up is described in detail elsewhere [15, 16]. For the decay time measurements the emission monochromators were set to a spectral bandpass of 9 nm. In the steady-state and the time-resolved fluorescence experiments an excitation wavelength λ_{ex} = 314 nm was used. The steady-state emission spectra were recorded in the wavelength range of 350 nm < λ_{em} < 550 nm, the excitation spectra were monitored in the range between 250 nm < λ_{ex} < 440 nm with an emission wavelength set to λ_{em} = 450 nm. In addition, synchronous fluorescence spectra were recorded with set wavelength differences of $\Delta\lambda$ = 20 nm, 60 nm, and 100 nm, respectively. In the time-resolved measurements the fluorescence was detected at λ_{em} = 375 nm, 416 nm, 430 nm, and 500 nm.

Data analysis in the time-resolved fluorescence measurements

The fluorescence decay curves were evaluated with different data analysis approaches. In the first approach the experimental data were analyzed with a sum of three exponential decay functions (discrete component approach, DCA). Further, a global analysis using three exponential decay functions with linked fluorescence decay times was used. In both data evaluation approaches a discrete number of decay terms was applied. In addition a different approach using a distribution analysis with no initial guess on the number of decay times was used. The data analysis is described in detail elsewhere [15–18].

3 Results and Discussion

3.1 Steady-state Fluorescence Spectra

Under the experimental conditions applied the fluorescence intensity of the B22 FA sample was five times the intensity of the B53 FA sample. Due to the extraction procedure no change in the shape of the fluorescence emission spectra was found [12]. In Figure 1 the normalized fluorescence excitation spectra of the samples B22 FA and B53 FA are shown for three different emission wavelengths. It is obvious that for the B22 FA sample the excitation spectra are dominated by a single band located at λ_{ex} = 295 nm. No influence on the detection wavelength λ_{em} was observed. For λ_{em} = 500 nm an additional

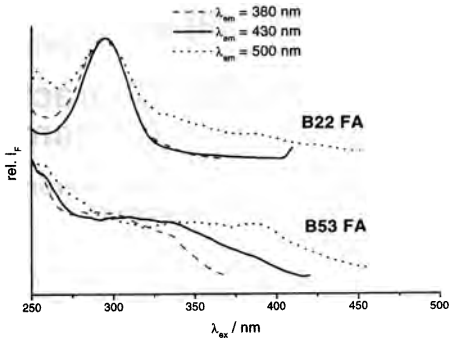

Fig. 1: Fluorescence excitation spectra of B22 FA and B53 FA at three different emission wavelengths λ_{em}. The spectra were normalized at λ_{ex} = 295 nm.

Fluoreszenzanregungsspektren der Proben B22 FA und B53 FA bei drei Detektionswellenlängen λ_{em}. Die Spektren sind bei λ_{ex} = 295 nm normiert.

poorly structured fluorescence contribution was detected in the wavelength range between 300 nm and 400 nm which resembled the spectral shape of sample B53 FA (see below). For B53 FA a clear dependence of the observed fluorescence excitation spectra on the detection wavelength λ_{em} was found. Moreover, no clear indication of a band located around 295 nm could be observed rather than broad non-structured excitation spectra. For the detection wavelength λ_{em} = 380 nm a slight maximum around 300 nm could be found. A dependence of the fluorescence excitation spectra has to be expected for mixture of fluorescing compounds and reflects for the sample B53 FA the increased heterogeneity. It indicates that during the downstream passage physically, chemically, and microbiologically induced processes altered the organic substances in the groundwater.

3.2 Synchronous Fluorescence Spectra

The application of the synchronous scanning mode in fluorescence spectroscopy is especially useful for mixtures of fluorophores because the wavelength difference $\Delta\lambda$ offers an additional parameter in selectivity. In principle, by scanning the mixtures with different $\Delta\lambda$ a complex steady-state fluorescence spectrum can be further resolved and single substance can be identified [19].

In Figure 2 the synchronous fluorescence spectra ($\Delta\lambda$ = 60 nm) of B22 FA, B53 FA in the aqueous phase (before and after organic solvent extraction with hexane and CH_2Cl_2), salicylic acid, and a groundwater FA (FG1 FA) are compared. The spectra are normalized at λ_{ex} = 316 nm which is equal to the emission maximum in the synchronous fluorescence spectrum of salicylic acid (grey area).

In the synchronous spectra of B53 FA no major influence of the extraction with the organic solvents was found, except in the long wavelength range. Here, the fluorescence was decreased compared to the B53 FA sample prior to extraction. The spectral shape of the B53 FA samples resembles the spectrum found for a groundwater FA. These trends were also

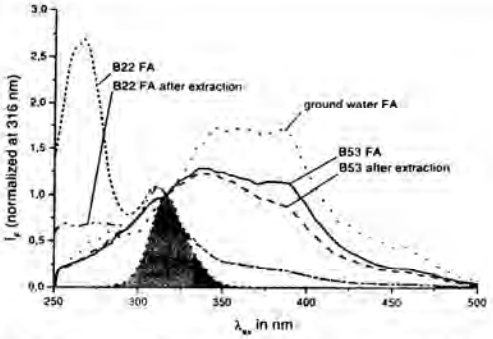

Fig. 2: Synchronous fluorescence spectra of the aqueous solution of B22 FA and B53 FA (before and after extraction with *n*-hexane and CH_2Cl_2). Comparison with salicylic acid and a groundwater FA (FG1 FA). The difference between excitation and emission wavelength was set to $\Delta\lambda$ = 60 nm.

Einfluß der Extraktion mit organischen Lösungsmitteln auf die synchronen Fluoreszenzspektren der wäßrigen Lösungen von B22 FA und B53 FA ($\Delta\lambda$ = 60 nm). Zum Vergleich sind die synchronen Fluoreszenzspektren von Salicylsäure und einer Grundwasser-FA (FG1 FA) gezeigt.

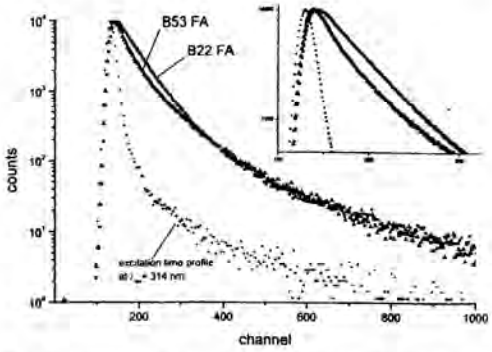

Fig. 3: Fluorescence decay curves of B22 FA and B53 FA at λ_{em} = 416 nm (λ_{ex} = 314 nm, time calibration 0.095 ns/channel). The inset shows the portion of the decay curves between channel 100 and channel 325 in order to visualize the clear difference in the fluorescence decay behavior of B22 FA and B53 FA.

Fluoreszenzabklingkurven der Proben B22 FA und B53 FA (λ_{em} = 416 nm, λ_{ex} = 314 nm, Zeitkalibrierung 0.095 ns/channel). Im Inset ist der Zeitbereich zwischen Kanal 100 und 325 vergrößert dargestellt, um die Unterschiede im Fluoreszenzabklingverhalten der Proben B22 FA und B53 FA klar hervorzuheben.

observed in the fluorescence emission spectra. However, for the B22 FA samples a major difference between the sample before and after solvent extraction was detected for excitation wavelength smaller than approx. 300 nm. Due to the extraction with *n*-hexane and CH_2Cl_2 the strong fluorescence band at λ_{max} = 268 nm vanished. In this emission range alkyl-substituted benzene derivatives can be expected to show fluorescence. For excitation wavelengths recorded above 290 nm the obtained spectrum after organic solvent extraction was unchanged.

In the synchronous fluorescence spectrum of salicylic acid (λ_{max} = 316 nm) the emission maximum occurred closely to the one of the spectra of the B22 FA samples (λ_{max} = 310 nm). The results confirm the observation made for the fluorescence emission spectra which showed that the fluorescence spectrum of the sample B22 FA closely resembles the fluorescence spectrum of salicylic acid [12]. Schmitt et al. [20] reported the occurrence of salicylic acid in the process of biodegradation of polycyclic aromatic hydrocarbons [21–25].

The fact that part of the fluorescing molecules was extractable by less-polar organic solvents indicates that no or only a weak interaction between these substances and the FA matrix was present. Moreover, it also indicates that this fraction of molecules was only of low polarity. Medium and strong organic acids, e.g., molecules of the salicylic acid type, are not likely to be extracted by the non-polar organic solvents used [12].

3.3 Time-resolved Fluorescence Emission Measurements

Figure 3 shows typical fluorescence decay curves obtained for the B22 FA and B53 FA sample. The fluorescence decay of B22 FA is strongly dominated by a single component, whereas for the B53 FA sample a more complex fluorescence decay was found. The linear decrease found in the first 30 ns of the fluorescence decay of the B22 FA sample was not present in the B53 FA fluorescence decay. The fluorescence decay of B53 FA was more comparable to the fluorescence decay found for natural organic matter samples of different origin [15, 16].

The results of the time-resolved fluorescence measurements are summarized in Table 1 and 2. Table 1 shows the results for the samples B22 FA and B53 FA prior to the extraction obtained with the DCA and the global analysis approach, respectively. In Table 2 the results of the decay time distribution analysis of the samples (in water) before and after extraction are shown.

In the DCA and the global analysis three exponential decay terms yielded a reasonable fit of the experimental data (judged by the χ^2-values and the randomness of the residuals). For both samples similar fluorescence decay times were recovered in the analysis. However, the relative fractional contributions were highly different for B22 FA and B53 FA at the investigated emission wavelength of λ_{em} = 416 nm and 500 nm. Whereas the fluorescence decay of B22 FA was dominated by τ_2 = 4.4 ns with a relative fractional intensity A_2 of about 80 % (73 % for 500 nm, respectively) at λ_{em} = 416 nm, the fluorescence decay of B53 FA was more complex and the relative contribution of τ_2 was only about 50 % at both emission wavelength investigated. This confirms the results of the steady-state fluorescence measurements which showed that the fluorescence of B22 FA was dominated by a single class of fluorophores.

In the DCA and global analysis a pre-assumed number of fluorescence decay terms is introduced into the data analysis. Especially for a presumable heterogeneous mixture of unknown compounds this method is prone to errors and the relation between the obtained parameter set is not straight forward. Therefore, the parameter set has to be treated as operationally-defined [15, 16]. In the decay time distribution analysis (exponential series method, ESM) no pre-assumed model is introduced and the analysis starts with a flat distribution of a large number (here 100) of exponential decay terms. Although both data evaluations were highly different the results obtained

Table 1: Fluorescence decay times τ and their relative amplitudes A of the B22 FA and B53 FA samples prior to extraction (σ: standard deviation, χ^2: goodness of the fit). The experimental data were analyzed using the DCA and the global analysis, respectively. In the global analysis the fluorescence decay times of B22 FA and B53 FA were linked. The fluorescence decay time of salicylic acid was measured for emission wavelengths 350 nm < λ_{em} < 450 nm and found to be constant within the experimental resolution.

Fluoreszenzabklingzeiten der Proben B22 FA und B53 FA bei λ_{ex} = 314 nm. Gezeigt sind die Ergebnisse einer globalen Analyse, in der die Abklingzeiten für die gesamten Datensätze gemeinsam optimiert wurden, wie auch der DCA-Methode. Die Fluoreszenzlebenszeit der Salicylsäure wurde im Spektralbereich 350 nm < λ_{em} < 450 nm gemessen und zeigte sich unabhängig von der Emissionswellenlänge.

	τ_1 (σ) ns	A_1 %	τ_2 (σ) ns	A_2 %	τ_3 (σ) ns	A_3 %	χ^2
λ_{em} = 416 nm							
B22 FA	1.4 (0.4)	8.2	4.4 (0.2)	84.9	14.5 (1.9)	7	1.09
B53 FA	1.4 (0.3)	34.1	4.8 (0.3)	52.9	14.1 (1.7)	13	1.095
λ_{em} = 500 nm							
B22 FA	1.5 (0.4)	17.8	4.7 (0.3)	71.6	15.6 (1.8)	10.6	1.07
B53 FA	1.3 (0.2)	29	4.9 (0.4)	54.9	14.5 (1.3)	16.1	1.27
			global analysis				
λ_{em} = 500 nm							
B22 FA	.2 (0.1)	13.6	4.4 (0.2)	73.3	13.8 (1)	13.2	1.17
B53 FA		25.1		56.2		18.7	1.35
salicylic acid			4.1				1.1

Table 2: Fluorescence decay time distribution analysis results (λ_{ex} = 314 nm, 100 decay times equally spaced in the range 0.1...50 ns). Shown are the mean fluorescence decay times τ for the samples B22 FA and B53 FA solved in water before and after (*) organic solvent extraction. For comparison the results are given for a non-contaminated groundwater FA (FG1 FA, λ_{em} = 410 nm) and for a FA isolated from a microbial degradation of PAH (PAKA2 FA, λ_{em} = 450 nm).

Mittlere Fluoreszenzabklingzeiten der ESM-Analyse der Proben B22 FA und B53 FA in Wasser, wobei die mit * markierten Zeilen den Ergebnissen nach Extraktion mit organischen Lösungsmitteln entsprechen. Zum Vergleich sind die Ergebnisse der ESM-Analyse für eine Grundwasser-FA (FG1 FA, λ_{em} = 410 nm) und für FA, die aus den Rückständen eines mikrobiellen PAK-Abbaus isoliert wurden (PAKA2 FA, λ_{em} = 450 nm), angegeben.

	τ_1 (σ) ns	A_1 %	τ_2 (σ) ns	A_2 %	τ_3 (σ) ns	A_3 %	χ^2
λ_{em} = 416 nm							
B22 FA	1.5 (0.1)	7.2	4.4 (0.5)	86.7	14.8 (0.6)	6.2	1.034
B22 FA*	1.5 (0.1)	6.3	4.5 (0.7)	90	10.8 (0.8)	3.7	1.047
B53 FA	1.1 (0.3)	27.1	4.2 (1.23)	59.9	12.4 (1.9)	13.8	1.053
B53 FA*	1 (0.3)	26.4	3.8 (1.2)	57.8	10.9 (1.7)	15.8	1.137
λ_{em} = 500 nm							
B22 FA			3.9 (1.75)	95.2	22.6 (2.8)	4.8	1.017
B22 FA*	1.5 (0.1)	13.5	4.5 (0.5)	73.3	12.2 (0.7)	13.2	1.059
B53 FA			2.6 (2.38)	96.1	21.3 (2.6)	3.9	1.096
B53 FA*	1.2 (0.3)	22.1	4.3 (1.2)	59.4	12.9 (2.1)	18.6	1.059
PAKA2 FA	1.1 (0.4)	18.7	5 (2)	65.7	15.4 (2.2)	15.6	1.125
FG1 FA	0.8 (0.6)	35	4.5 (1.7)	58.6	24 (3.8)	6.4	1.04

were strikingly similar as can be seen from the comparison of the data in Table 1 and Table 2. The fluorescence decay of B22 FA was found to be dominated by a mean decay time τ_2 of around 4 ns. The relative fractional contribution A_2 was calculated to be greater than 80 %. For B53 FA the relative contribution of the decay at τ_2 was only about 50 %. The results were in excellent agreement with the DCA and global analysis.

The results of the ESM analysis are shown in Figures 4A and 4B. They show a decay time pattern with well separated peaks for B22 FA and less separated peaks for B53 FA. At the emission wavelength λ_{em} = 416 nm for the B22 FA sample the solvent extraction yielded no further improvement in the resolution of the decay time distribution, whereas at λ_{em} = 500 nm the resolution of the decay time peaks was significantly better. Here, the obtained decay time pattern became equal to the pattern calculated for λ_{em} = 416 nm. On the other hand for the B53 FA sample broader peaks were calculated in the ESM analysis for which the relative fractional contributions were quite different compared with sample B22 FA (see Table 2 as well). Again, the extraction with organic solvents leads to an improvement in the resolution of the decay time distribution pattern (at λ_{em} = 416 nm). A similar decay time distribution as found for sample B53 FA was obtained for a number of HS of different origins. Considering the great similarity of the

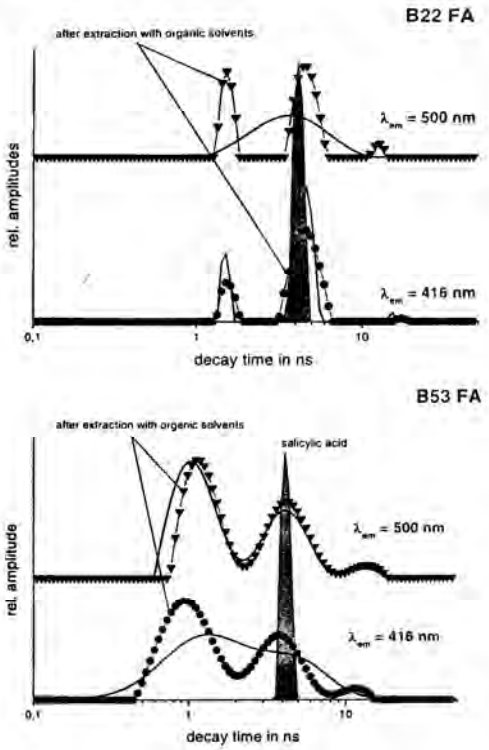

Fig. 4: Distribution of fluorescence decay times for B22 FA (top) and B53 FA (bottom) at two different emission wavelengths (λ_{em} = 416 nm and 500 nm with λ_{ex} = 314 nm). Compared are the aqueous solutions before and after extraction with organic solvents. The analysis was performed using the exponential series method with 100 decay times equally spaced in the time range between 0.1 and 50 ns.

Verteilung der Fluoreszenzabklingzeiten für B22 FA (oben) und B53 FA (unten) bei zwei Emissionswellenlängen (λ_{em} = 416 nm and 500 nm mit λ_{ex} = 314 nm). Zum Vergleich des Einflusses der Extraktion mit organischen Lösungsmitteln sind die Daten der wäßrigen Phasen vor und nach der Extraktion gegenübergestellt. Die Datenanalyse wurde mit Hilfe der Exponential Series Method (ESM) durchgeführt. Dabei wurden 100 Abklingzeiten, die gleichmäßig im Zeitbereich zwischen 0.1 ns und 50 ns verteilt waren, verwendet.

steady-state fluorescence emission spectra for B53 FA and a FA from non-contaminated groundwater the time-resolved fluorescence measurements confirmed that the sample B53 FA was similar to groundwater HS [12].

In Figure 4A and 4B the fluorescence decay time pattern obtained for salicylic acid at λ_{em} = 420 nm is shown as well. For the emission wavelength range between 350 nm and 450 nm (measured every 10 nm) a fluorescence decay time of 4.1 ns was found for salicylic acid (at medium pH) which is almost identical to τ_2 of B22 FA and B53 FA. Especially for B22 FA the results of the time-resolved fluorescence measurements are in excellent agreement with results found in the steady-state fluorescence experiments.

In order to relate the observed tendencies the fluorescence decays of a non-contaminated groundwater FA (FG1 FA) and a FA isolated from the slurry of a microbial degradation of a mixture of PAH (PAKA2 FA) were analyzed. These two reference FA represent the extremes of a natural FA and a FA that is built during microbial degradation of PAH. The emission wavelengths chosen were as close as possible to the emission wavelengths used in the time-resolved fluorescence measurements for B22 FA and B52 FA. The results are shown in Table 2 and in Figure 5. A gradual decrease in resolution of the decay time peaks was found for B22 FA, B53 FA, PAKA2 FA, and FG1 FA, respectively.

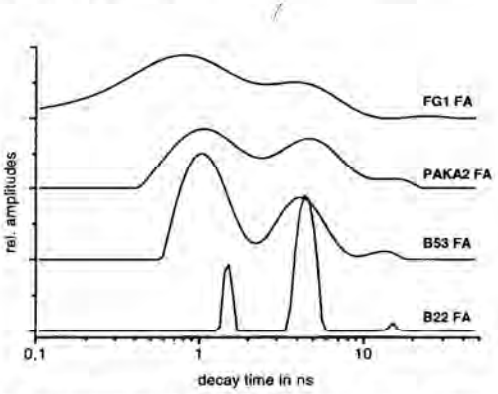

Fig. 5: Comparison of the observed fluorescence decay time distributions for λ_{ex} = 314 nm of B22 FA (λ_{em} = 416 nm), B53 FA (λ_{em} = 416 nm), PAKA2 FA (λ_{em} = 450 nm), and FG1 FA (λ_{em} = 410 nm), respectively. Experimental data were analyzed using ESM with 100 decay times in the decay time range between 0.1 and 50 ns. Only the contours of the calculated decay time distributions are shown.

Vergleich der Fluoreszenzabklingzeiten-Verteilungen bei λ_{ex} = 314 nm von B22 FA (λ_{em} = 416 nm), B53 FA (λ_{em} = 416 nm), PAKA2 FA (λ_{em} = 450 nm) und FG1 FA (λ_{em} = 410 nm). Zur Datenanalyse wurde die ESM verwendet (100 Abklingzeiten, verteilt im Zeitbereich zwischen 0.1 und 50 ns). Es sind die Einhüllenden der berechneten Fluoreszenzabklingzeiten-Verteilungen dargestellt.

The tendencies shown in Figure 5 make it attractive to assume that due to the progress in the degradation and the 'rebuilding' of the DOC the FA from the contaminated site became more similar to the FA isolated from non-contaminated groundwater.

4 Conclusions

In both modes of fluorescence measurements, steady-state and time-resolved, the samples B22 FA and B53 FA showed great differences in the results obtained. While the sample B22 FA resembled fluorescence properties of a mixture that was dominated by one class of compounds, the fluorescence spectra and the fluorescence decays observed for B53 FA were more closely related to groundwater HS. The observed tendency was confirmed by the investigation of a FA derived from a microbial degradation of a PAH mixture (PAKA2 FA, see Fig. 5). It was also indicated in size exclusion chromatography (SEC) using fluorescence detection [12]. Here, a very strong

fluorescence signal was observed in the lower molecular weight range for the sample B22 FA, whereas for the sample B53 FA a chromatogram similar to HS was obtained. While for the sample B22 FA the contribution of DOC originating from incoming groundwater can be considered small, the contribution of B22 FA itself is apparently decreased within the groundwater downstream. The transformation was also shown in the portion of total desorbed organic carbon during the XAD isolation [12]. For the sample B22 only 49 % of the adsorbed carbon could be desorbed because of the less polar character, while for the sample B53 85 % could be desorbed with water (pH 12) indicating an increase in the polarity of the sample and probably an increase in the heterogeneity of the sample as well.

Salicylic acid was chosen as a model compound to represent the class of substituted benzoic acids. A comparison of fluorescence decays of differently substituted benzoic acid and humic substances was presented elsewhere [26]. The results presented make it attractive to assume that for B22 FA the fluorescence properties are determined by compounds of the salicylic acid type. This assumption is supported by the steady-state as well as the time-resolved fluorescence measurements of B22 FA when compared to salicylic acid alone. Although for B53 FA in the analysis of the time-resolved fluorescence data a fluorescence decay time of approx. 4 ns was the main contribution, in the fluorescence emission and fluorescence excitation spectra the similarities to salicylic acid vanished or were covered by other fluorescence. Although only a single compound like salicylic acid was compared to a supposedly heterogeneous mixture of compounds the similarities found for B22 FA are quite striking. Considering the results of the SEC and hydrophobic interaction chromatography (HIC) presented by Zwiener et al. the advanced fluorescence measurements confirmed the dominance of a single class of low-molecular weight fluorescing compounds in sample B22 FA [12].

Due to the solvent extraction in the synchronous fluorescence spectrum of B22 FA the band at approx. 260 nm was lost, this went along with results obtained in the SEC experiments. The considerably long retention times in the SEC and the range of the fluorescence signals make the assumption of small, not or only weakly bound organic molecules with a relative low polarity attractive, e.g., metabolites of tar coal compounds. The results obtained in the fluorescence experiments indicate that due to the extraction procedure for the sample B22 FA a more homogeneous solution of closely related compounds (e.g. hydroxy-substituted benzoic acids) was obtained. Especially, the better resolved fluorescence decay time distributions supported this conclusion. From our results it can be deduced further that during the downstream passage the dissolved organic matter was transformed into more refractory material (hence, more similar to humic substances). While in the sample B22 FA a great portion of the dissolved organic material could be attributed to low-molecular weight compounds that were partly loosely bound by weak interactions to refractory fractions (HS fraction), this fraction was no longer identified in the B53 FA sample. This is supported by the separation experiments performed by Zwiener et al. [12]. To explain the observations two possible reasons have to be considered responsible. One could be a further biodegradation of the compounds and second, due to chemical and biochemical processes these compounds became more strongly bound to the matrix of humic substances, e.g. due to the formation of covalent bounds. In such a case the spectroscopic identity of the smaller molecules would be lost and they would no longer be detectable in the time-resolved fluorescence measurements. The fluorescence decay would become more and more complex which is indicated by the samples B22 FA and B53 FA. A major part of the fluorescence decay of B53 FA is still determined by fluorescence processes with a decay time of approx. 4 ns. However, compared to the model compound salicylic acid and to B22 FA the distribution peak is reasonably broader, probably due to the fact that because of the incorporation the site heterogeneity is increased. This increase in the heterogeneity of the chemical environment is then reflected in a broadening of the fluorescence decay time distributions.

Acknowledgements

The authors are grateful to the Deutsche Forschungsgemeinschaft (DFG) for supporting part of the work financially (project number FR 536/17 in the priority program "Geochemical processes with long-term effects in anthropogenically-influenced seepage and groundwaters"). They are also thankful to Axel Heidt for the isolation of the samples and the performance of the solvent extractions.

References

[1] *Senesi, N., Miano, T. M.* (Eds.): Humic Substances in the Global Environment and Implications on Human Health. Elsevier, Amsterdam, 1994.

[2] *Mantoura, R. F. C., Riley, J. P.:* The analytical concentration of humic substances for natural waters. Anal. Chim. Acta *76*, 97–106 (1975).

[3] *Abbt-Braun G., Frimmel, F. H., Lipp, P.:* Isolation of organic substances from aquatic and terrestrial systems – comparison of some methods. Z. Wasser-Abwasser-Forsch. *24*, 285–292 (1991).

[4] *Senesi, N.:* Binding mechanisms of pesticides to soil humic substances. Sci. Total Environ. *123/124*, 63–76 (1992).

[5] *Richnow, H. H., Seifert, R., Hefter, J., Link, M., Francke, W., Schaefer, G., Michaelis, W.:* Organic pollutants associated with macromolecular soil organic matter: Mode of binding. Org. Geochem. *26*, 745–758 (1997).

[6] *Dankwardt, A., Hock, B., Simon, R., Freitag, D., Kettrup, A.:* Determination of Non-extractable Triazine Residues by Enzyme Immunoassay: Investigation of Model Compounds and Soil Fulvic and Humic Acids. Environ. Sci. Technol. *30*, 3493–3500 (1996).

[7] *Kumke, M. U., Löhmannsröben, H.-G., Roch, Th.:* Fluorescence quenching of polynuclear aromatic compounds by humic acid. Analyst *119*, 997–1001 (1994).

[8] *McCarthy, J. F., Jimenez, B. D.:* Interactions between polycyclic aromatic hydrocarbons and dissolved humic material: binding and dissociation. Environ. Sci. Technol. *19*, 1072–1076 (1985).

[9] *Puchalski, M. M., Morra, M. J., von Wandruszka, R.:* Fluorescence quenching of synthetic organic compounds by humic materials. Environ. Sci. Technol. *26*, 1787–1792 (1992).

[10] *Zimmermann, U., Löhmannsröben, H.-G., Skrivanek, T.:* Absorption and fluorescence spectroscopic investigations of PAH/humic substance-interactions in water. In: *Cecchi, G., Lamp, T., Reuter, R., Weber, K.* (Eds.): Remote Sensing of Vegetation and Water, and Standardization of Remote Sensing Methods. SPIE *3107*, 239–249 (1997).

[11] *Zwiener, C., Frimmel, F. H.:* Application of headspace GC/MS screening and general parameters for the analysis of polycyclic aromatic hydrocarbons in groundwater samples. Fresenius J. Anal. Chem. *360*, 820–823 (1998).

[12] *Zwiener, C., Kumke, M. U., Abbt-Braun, G., Frimmel, F. H.:* Adsorbed and bound residues in fulvic acid fractions of contaminated groundwater - Isolation, chromatographic and spectroscopic characterization. Acta Hydrochim. Hydrobiol. *27*, 208–213 (1999).

[13] *Frimmel, F. H., Abbt-Braun, G.:* Basic characterization of reference NOM from Central Europe – Similarities and difference. Environ. Internat. *25*, 191–207 (1998).
[14] *Stieber, M.:* Untersuchungen zum mikrobiellen Abbau von polyzyklischen aromatischen Kohlenwasserstoffen – Monitoring, limitierende Faktoren, Ökotoxizität. Dissertation, Technische Universität Dresden, 1995.
[15] *Kumke, M. U., Abbt-Braun, G., Frimmel, F. H.:* Time-resolved Fluorescence Measurements of Aquatic Natural Organic Matter. Acta Hydrochim. Hydrobiol. *26*, 73–81 (1998).
[16] *Tiseanu, C., Kumke, M. U., Frimmel, F. H., Klenze, R., Kim, J. I.:* Time-Resolved Spectroscopy of Fulvic Acid and Fulvic Acid Complexed with Eu^{3+} – A Comparative Study. J. Photochem. Photobiol. *117*, 175–184 (1998).
[17] *Gamsky, D. M., Goldin, A. A., Petrov, E. P., Rubinov, A. N.:* Fluorescence decay time distribution for polar dye solutions with time-dependent fluorescence shift. Biophys. Chem. *44*, 47–60 (1992).
[18] *Siemiarczuk, A., Wagner, B. D., Ware, W. R.:* Comparison of the Maximum Entropy and Exponential Series Methods for the Recovery of Distributions of Lifetimes from Fluorescence Lifetime Data. J. Phys. Chem. *94*, 1661–1666 (1990).
[19] *Kumke, M. U., Löhmannsröben, H.-G., Roch, Th.:* Fluorescence spectroscopy of polynuclear aromatic compounds in environmental monitoring. J. Fluorescence *5*, 139–153 (1995).
[20] *Schmitt, R., Langgath, H. R., Pittmann, W., Rohus, H. P., Eckert, P., Schubert, J.:* Biodegradation of aromatic hydrocarbons under anoxic conditions in a shallow sand and gravel aquifer of the Lower Rhine Valley, Germany. Org. Geochem. *25*, 41–50 (1996).
[21] *Jeffrey, A. M., Yeh, H. J. C., Jerina, D. M., Patel, T. R., Davey, J. F., Gibson, D. T.:* Initial reactions in the oxidation of naphthalene by *Pseudomonas putida*. Biochemistry *14*, 575–584 (1975).
[22] *Cerniglia, C. E.:* Microbial metabolism of polycyclic aromatic hydrocarbons. Adv. Appl. Microbiol. *30*, 31–71 (1984).
[23] *Beyer, M., Klein, J.:* Mikrobiologischer Abbau von Teeröl-Aromaten. BioTech-Forum *6*, 254–260 (1989).
[24] *Kahle-Anders, G., Hanert, H. H.:* Mikrobiologischer Abbau von Teeröl in Wasser und Boden. Wasser – Abwasser *131*, 245–250 (1990).
[25] *Herbes, S. E., Schwall, L. R.:* Microbial transformation of polycyclic aromatic hydrocarbons in pristine and petroleum-contaminated sediments. Appl. Environ. Microbiol. *35*, 306–316 (1978).
[26] *Frimmel, F. H., Kumke, M. U.:* Fluorescence decay of humic substances. A comparative study. In: *Davies, G., Ghabbour, E. A.* (Eds.): Humic substances – Structures, Properties and Uses. RCS, Cambridge, 1998, pp. 113–122.

received 23 October 1998
accepted 4 May 1999

2.1.3 Influence of chlorination on chromophores and fluorophores in humic substances

G.V. Korshin, M.U. Kumke, C.-W. Li, M.M. Benjamin, F.H. Frimmel
Environ. Sci. Technol., 1999, 33, S. 1207 - 1212.

Die Veränderungen von HS (Suwannee River HS) durch Chlorung wurden absorptions- und fluoreszenzspektroskopisch untersucht. Dabei wurden die Auswirkungen der Chlorung auf die Halbwertsbreite der Elektronentransferbande im UV/Vis-Absorptionsspektrum, auf die Fluoreszenzintensität und auf die relativen Anteile von operational-definierten Fluoreszenzabklingzeiten als Parameter verfolgt und mit Veränderungen der Aromatizität sowie der Größe der HS korreliert. Durch die Chlorung schrumpfte die Halbwertsbreite der Fluoreszenzbande bei einer gleichzeitigen Zunahme der Fluoreszenzintensität. Die spektrale Lage der Fluoreszenz zeigte eine hypsochrome Verschiebung und die relativen Anteile der operational-definierten Fluoreszenzabklingzeiten änderten sich. Gleichzeitig nahm in den Absorptionsspektren die Extinktion (E_{254nm}) selbst ab und die Halbwertsbreite der Elektronentransferbande verringerte sich. Als Schlußfolgerung ergibt sich, dass die Chlorung von HS eine Abnahme der Aromatizität sowie eine Abnahme der mittleren Größe der HS-Moleküle bewirkt.

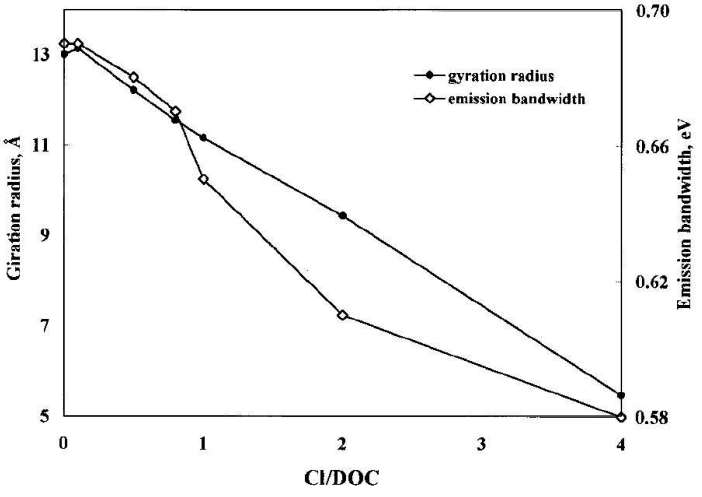

Environ. Sci. Technol. **1999**, *33*, 1207–1212

Influence of Chlorination on Chromophores and Fluorophores in Humic Substances

GREGORY V. KORSHIN,*,† MICHAEL U. KUMKE,‡ CHI-WANG LI,† AND FRITZ H. FRIMMEL‡

Department of Civil and Environmental Engineering, University of Washington, Box 352700, Seattle, Washington 98195-2700, and Engler-Bunte-Institute, Water Chemistry Division, University of Karlsruhe, Richard-Wiltstätter-Allee 5, Karlsruhe 76131, Germany

Three types of fluorophores (decay times 1.2, 4.3, and 10.7 ns, respectively) participate in the fluorescence of Suwannee River hydrophobic acid (HPOA). The emission of the fast-decaying fluorophores (FDF) is red-shifted compared with that of longer-decaying groups. Upon chlorination, the FDF contribution (I_{FDF}) to the emission declines, the specific absorbance at 254 nm ($SUVA_{254}$) decreases, and the electron-transfer absorbance band in the UV spectra of HPOA contracts. On the basis of the literature data and experimental evidence, the width of the electron-transfer absorbance band (Δ_{ET}) is found to be proportional to the gyration radii (R_g) of the humic molecules. The R_g values of chlorinated HPOA are also well-correlated with the energy of the emission band maximum (E_{max}) and emission bandwidth (Δ_{em}). These consistent changes reflect the destruction of aromatic halogen attack sites accompanied by the breakdown of the humic molecules into smaller fragments.

Introduction

Natural organic matter (NOM) is typically dominated by humic substances (HS), an operationally defined class of organic oligomers or polymers with molecular weights ranging from <1000 to >100000 Da (*1, 2, 3*). HS contain substantial amounts of hydroxy-, carboxy-, and methoxy-substituted aromatic units (*4, 5*) which are collectively referred to as polyhydroxyaromatic (PHA) or phenolic moieties. PHA is thought to constitute the substrate for halogenation reactions, and "masked" aromatic β-diketones (e.g., resorcinol, 3,5-dihydroxybezoic acids, and some flavonoids) are likely to be very important in the generation of trihalomethanes and possibly haloacetic acids (*6–9*).

The importance of activated aromatic, especially β-diketone, sites in the generation of trihalomethanes has been supported by experiments with model compounds (*7, 8, 10, 11*). However, efforts to probe the nature of the reaction sites in HS using structure-sensitive methods (notably, ^{13}C CP-MAS NMR), although successful (*12–14*), have had a limited scope. More insight into the nature of the reactive sites in NOM may be gained via in situ methods that use NOM concentrations typical for potable water (<10 mg/L of dissolved organic carbon, DOC), are structure-sensitive, provide information about the intermediates, and can be employed for a wide range of NOM types, pHs, and other reaction parameters.

UV absorbance and fluorescence of NOM meet several of these requirements, being simple, being sensitive to the presence of NOM, and possessing intrinsic, albeit complex, correlation with the internal structure of HS (*15–20*). Their use for NOM halogenation studies is attractive since the chromophores and fluorophores in NOM are activated aromatic units in PHA, and their involvement in halogenation may be tracked by both UV absorbance and fluorescence. Recent studies have shown a good correlation between the changes of UV absorbance spectra of NOM and formation of disinfection byproducts (*17, 21, 22*). The goal of this paper is to compare the effects of halogenation on the UV and fluorescence spectra of NOM and to explore their implications for understanding the halogenation mechanisms.

Materials and Methods

The hydrophobic acids fraction (HPOA) from Suwannee River natural organic matter was used in all experiments. The samples were obtained by Jerry Leenheer at the U.S. Geological Survey Laboratory in Boulder, CO using the XAD-8 adsorption procedure (*23*) and contained <0.7% nitrogen and <0.3% sulfur. On the basis of ^{13}C CP-MAS NMR analysis (using a Chemagnetics CMX 200 MHz spectrometer at a spinning rate of 5000 Hz) aromatic and carboxylic groups accounted for approximately 26% and 22%, respectively, of the total carbon in the sample.

The experiments were conducted with samples containing 5.0 mg/L (as carbon) HPOA and 0.01 M $NaClO_4$. The dissolved organic carbon concentration was measured using an OI 700 carbon analyzer (OI Corp., College Station, TX). Chlorination was carried out at pH 7.0 and 25 °C, using Cl/DOC ratios from 0.1 to 4.0 mg/mg (with Cl expressed as Cl_2). Free chlorine was measured using the standard DPD-FAS titrimetric method (*24*). The reaction time was 7 days. No residual chlorine was present at the end of the exposure time. UV spectra were recorded with a Perkin-Elmer Lambda-18 dual-beam spectrophotometer. Instantaneous emission spectra were recorded with a Perkin-Elmer LS-50B fluorescence spectrometer using an excitation wavelength of 320 nm. Emission spectra were recorded from 360 to 560 nm at an angle of 90° versus the position of the excitation beam. The bandwidth of the slits was 5 nm. The fluorescence emission spectra were corrected for inner filter effect (*25*).

Time-resolved fluorescence measurements were performed using a FL900CDT fluorescence decay time spectrometer (Edinburgh Analytical Instruments) in the time-correlated single-photon counting mode. The instrument was set up in a T-geometry with two analyzing detection channels. A Hamamatsu R1527 photomultiplier tube (PMT) with a rise time of 2.2 ns was used for light detection. A nF900 nitrogen-filled nanosecond flash lamp (Edinburgh Analytical Instruments) operated at 40 kHz was used as the excitation light source. A Norland 5000 multichannel analyzer (MCA) (Viking Instruments Inc.) with a 4096-channels memory was operated in the pulse height analysis mode; 1024 channels of the MCA memory were attributed to each detection channel in a typical experiment. The stability of the excitation pulse profile was controlled throughout each fluorescence decay experiment. To obtain a sufficient number of counts in a wide dynamic range of the emitted light intensity, the measurements were done in cycles of 5000 counts. The counts from 10 cycles were summed to yield a

* Corresponding author: phone (206) 543-2394, fax: (206) 685-9185, e-mail: korshin@u.washington.edu.
† University of Washington.
‡ University of Karlsruhe.

10.1021/es980787h CCC: $18.00
Published on Web 03/04/1999

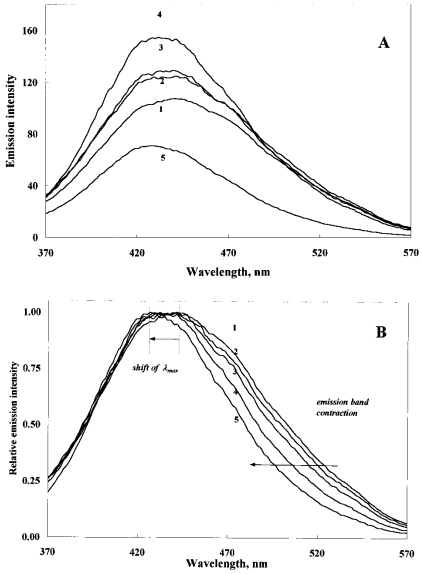

FIGURE 1. Comparison of fluorescence emission spectra of chlorinated HPOA. Varying Cl/DOC ratios. DOC 5 mg/L. (1) 0 (initial sample); (2) 0.5; (3) 1.0; (4) 2.0; (5) 4.0. (A) Absolute intensities. (B) Normalized spectra.

total of 50000 counts per emission decay profile in the maximum channel. The experiments were typically run at a time base of 100 ns with a 5 ns delay of the stop photomultiplier tube. The time calibration was 0.095 ns/channel. The excitation wavelength was 314 nm. The emitted light was monitored at 410 nm using a spectral bandwidth of 9 nm. To prevent counting artifacts caused by excessively high-photon loads, the counting rate was typically <1%, so pile-up problems in the decay time analysis were very unlikely. The instrument's software provided multiexponential data fitting, decay time distribution analysis, and global analysis. The experimental decay data were analyzed with nonlinear least-squares algorithms based on the Marquardt method. The results of the data-fitting procedures were evaluated using the χ^2-values and the randomness of the weighed residuals. Only the fluorescence decay observed within the first 85 ns after the excitation flash was taken into account in the data fitting, and no shift term was introduced into the data analysis. The performance of our fluorescence decay time spectrometer was tested with a number of model compounds with known fluorescence decay times as described in ref *26*.

Results

The fluorescence spectra of HPOA dosed with chlorine are shown in Figure 1A. The first 0.5 mg/L of chlorine had virtually no effect on the emission spectrum (data not shown), but subsequent Cl doses up to 10 mg/L caused the emission intensity to increase substantially.

When the spectra shown in Figure 1A are normalized by their respective maximum emission intensities, two trends are evident (Figure 1B): the position of the emission maximum (λ_{max}) exhibits a blue shift and the emission band contracts with increasing chlorine dose. To compare the shapes of the normalized spectra, the emission intensity was replotted as a function of the energy of the emitted light quanta ($E = 1240/\lambda$, where E is the energy in eV and λ is the wavelength in nm). The emission spectra were then fit using the Gaussian function (*27*):

$$I(E) = I_0 \exp\left[-\frac{4\ln(2)\,(E - E_{max})^2}{\Delta_{em}^{\ 2}}\right] \quad (1)$$

where I_0 and E_{max} are the emission intensity ($I_0 = 1$ for normalized spectra) and the energy corresponding to the wavelength of maximum emission, respectively, and Δ_{em} is the width of the emission band measured at 50% of the maximum intensity.

TABLE 1. Gauss Fitting Parameters for Emission Spectra of Chlorinated HPOA

Cl/DOC dose	E_{max}, eV	λ_{max}, nm	Δ_{em}, eV
0	2.82	440	0.69
0.1	2.82	440	0.69
0.5	2.83	438	0.68
0.8	2.84	437	0.67
1.0	2.85	435	0.65
2.0	2.86	434	0.61
4.0	2.89	429	0.58

The best-fit parameters and other data relevant for characterizing these samples according to eq 1 are given in Table 1. At Cl/DOC ≥ 0.5, halogenation affected both the position and the width of the Gauss band modeling the emission of HPOA. The emission bandwidth decreased from 0.69 eV in unchlorinated HPOA to 0.58 eV as the Cl/DOC ratio was increased to 4.0.

The Gauss function may be thought to describe the distribution of identical fluorophores in slightly different chemical environments associated with instantaneous conformational variations of polymeric/oligometic molecules of HS. The literature, however, indicates that HS contain more than one fluorophore-type (*28*−*32*) and the approximation of the emission or absorbance spectra using one Gauss band is not per se a proof of a one-fluorophore or one-chromophore model but a convenient way to quantify the influence of halogenation on the spectral bands. Manifestations of dissimilar fluorophores in the emission may also be detected using evolving factor analysis, by mathematical analysis of the spectra and by time-resolved spectroscopy that unambiguously evaluates the contribution of fluorophores with unequal decay times. The two latter approaches were used in this study.

The intrinsic structure of the emission spectra of HPOA and its chlorinated analogues was examined using the first-order derivatives of the normalized emission spectra (Figure 2A,B). The derivatives of all these spectra have structures that deviate from the one-band Gauss band model. These features were most evident for unaltered HPOA (Figure 2A). Their intensity substantially exceeded that of artifacts caused by high-frequency numerical noise in the spectra. Numerical processing using varying differentiation intervals (*27*) always resulted in the same features in the derivatives. These features (denoted as α, β, γ, and δ in Figure 2B) appear to indicate the presence of dissimilar chromophores.

The intersection of the derivatives with the abscissa shifts toward higher energy with increasing chlorine dose. This corresponds to the blue shift of the maximum of the emission spectra seen in the first-order emission data (e.g., Figure 1B). The intensity of feature γ located at 2.61 eV is not affected by chlorination while that of feature δ steadily increases with the chlorine dose. In contrast, structures α and β located at

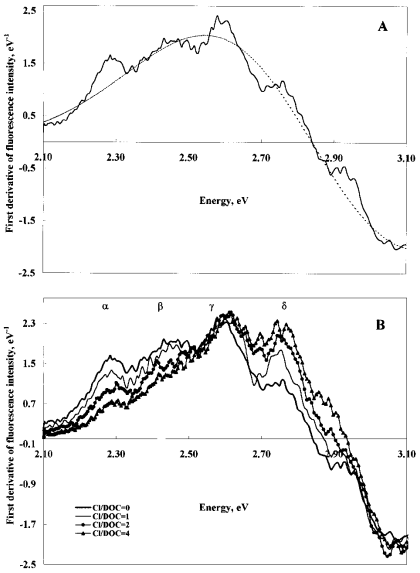

FIGURE 2. First derivatives of selected normalized fluorescence emission spectra. (A) Comparison of the single-band Gauss fit with the experimental spectrum for unaltered HPOA and effects of minor bands. (B) First derivatives for varying chlorine/DOC ratios.

2.29 and 2.45 eV become progressively weaker with the increase of the Cl/DOC ratio.

Time-resolved fluorescence confirmed the existence of dissimilar fluorophores in HPOA. The discrete component approach (DCA) which employs the smallest number of exponential terms to fit the observed decay was used to process the data. DCA analysis of the HPOA emission established that the emission decay profiles could be fitted using at least three exponential terms. To confirm the validity of the DCA approach, the fluorescence decay of HPOA was additionally evaluated using the distribution analysis, which does not introduce any a priori model of the fluorescence decay lifetimes distribution. These two methods of the evaluation of the fluorescence decay times are compared in more detail in refs *26, 33, 34*. It was found that the mean fluorescence decay times obtained using the distribution analysis mode were comparable to those calculated in the DCA mode. The trends observed for halogenated HPOA using either approach were identical. Therefore, only the DCA results will be discussed here. However, it needs to be recognized that the three fluorophores presumed to exist within the DCA approach are operationally defined and do not necessarily correspond to distinct chemical entities.

The contribution of the three components in the emission was evaluated presuming that the decay times of the three components were constant for all samples and only their relative contributions were affected by chlorination. The decay times were extracted having the goal of maximizing the global goodness-of-fit considering all the experimental data. The best-fit decay times (1.2, 4.3, and 10.7 ns) and the contributions of the respective fluorophores to the emission of chlorinated HPOA are shown in Table 2. The decay times shown are comparable with those reported for other HS

TABLE 2. Fluorescence Decay Times Obtained for Chlorinated HPOA Samples; Emission Wavelength 410 nm

Cl/DOC dose	τ_1 (σ), ns	A_1, %	τ_2 (σ), ns	A_2, %	τ_3 (σ), ns	A_3, %	ξ^2
			Three Linked Exponential Terms				
0	1.2 (0.1)	34.6	4.3 (0.3)	45.9	10.7 (0.7)	19.5	1.382
0.1		36.8		40.1		23.1	1.388
0.8		29.6		41.2		29.2	1.480
2.0		29.5		44.6		25.9	1.352
4.0		23.9		51.0		25.2	1.228

TABLE 3. Parameters of UV Absorbance Spectra of Chlorinated HPOA

Cl/DOC dose	$SUVA_{254}$, L/(mg·m)	A_{350}/A_{280}	Δ_{ET}, eV
0	5.01	0.413	2.31
0.1	4.90	0.416	2.32
0.5	4.54	0.393	2.25
0.8	4.19	0.377	2.20
1.0	4.07	0.366	2.17
2.0	3.21	0.319	2.04
4.0	1.85	0.208	1.74

samples (*28*−*32*). The respective fluorophores will be operationally referred to as the fast-, medium-, and slow-decaying fluorophores (FDF, MDF, and SDF, respectively).

The contribution of these fluorophores to the emission was affected by chlorination. For the unaltered sample, FDF, MDF, and SDF fluorophores contributed 35%, 46%, and 19% of the emission output, respectively. The lowest chlorine dose (Cl/DOC = 0.1) caused a marginal increase of the FDF and SDF contributions while that of MDF decreased correspondingly. A further increase of the chlorine dose reversed this trend. As the Cl/DOC ratio reached 4.0, the FDF contribution declined from 37% to 24% while those of the MDF and SFD increased from 40% to 51% and from 23% to 25%, respectively. Thus, the FDF sites are selectively eliminated by chlorination while the MDF and SDF contributions increase with the Cl dose.

Simultaneously with the changes in fluorescence, considerable effects in UV absorbance of HPOA were detected. Chlorination caused a substantial decrease of UV absorbance. Visually, the UV spectra of chlorinated HPOA were similar to those reported in refs *17, 21, 22*. The influence of chlorination on UV absorbance of HPOA was quantified based on the specific UV absorbance at 254 nm ($SUVA_{254}$), the ratio of absorbances at 280 and 350 nm (A_{350}/A_{280}), and the width of the electron-transfer band (Δ_{ET}) (*17, 35*). The value of Δ_{ET} was calculated using the ratio of absorbances at 350 and 280 nm (A_{350}/A_{280}). Assuming that the Gaussian function (eq 1) can describe the shape of the ET band for $\lambda > 250$ nm and the maximum of the band is located in the range 252−254 nm (~4.90 eV) (*17, 35*), the following formula for Δ_{ET} was derived:

$$\Delta_{ET} = 2.18\left(\ln\left(\frac{A_{280}}{A_{350}}\right)\right)^{-1/2} \quad (2)$$

The parameters of the UV spectra are compiled in Table 3. $SUVA_{254}$ has been reported to be proportional to the aromaticity of HS (*9, 16,* 36, 37) although it may also be affected by nonaromatic conjugated double bonds. Accepting the position that $SUVA_{254}$ is mainly determined by the activated aromatic groups, its decrease from 5.01 to 1.85 L/(mg·m) seen in chlorinated HPOA supports the assumption that chlorine specifically targets these aromatic sites. The less anticipated effect is that the width of the ET band Δ_{ET}

decreases from 2.31 to 1.74 eV as the Cl/DOC ratio increases. A possible meaning of Δ_{ET} for the chemistry of HS is discussed in the next section.

Discussion

The trends in fluorescence and UV absorption spectra of chlorinated HPOA are summarized as follows:

(1) Chlorination causes the emission band to contract and shift toward lower λ (higher quanta energies).

(2) The FDF contribution (I_{FDF}) to the fluorescence decreases with chlorine dose while that of MDF and SDF increases. This occurs simultaneously with the weakening of α and β features and enhancement of the δ structure in the first derivatives of the emission spectra of HPOA.

(3) The intensity of fluorescence emission increases for a Cl/DOC ratio < 2.

(4) $SUVA_{254}$ and Δ_{ET} decrease.

We interpret these trends with the major premise that halogenation decreases the aromaticity of HPOA and causes its molecules to break down into smaller fragments. The literature establishes unambiguously that a decrease in the average molecular weight (AMW) of HS is associated with an increase of the fluorescence intensity (observed for Cl/DOC ratios < 2 in this work) (*38*−*41*). The reported time-resolved fluorescence data also indicate that the contribution of "medium" ($2 < \tau < 10$ ns) and "slow" ($\tau > 10$ ns) fluorophores increases with the decrease of AMW. This is accompanied by a decrease of the FDF contribution ($\tau < 2$ ns). For instance, HS with molecular weights 3−50 kDa have I_{FDF} of 17% while for MW ranging from 50 to 100 kDa I_{FDF} was 28% (*30, 42*). The AMWs of aqueous HS are lower compared with that of soil HS, and the contribution of "medium" fluorophores in them is considerably higher (*43*).

We attempt to use the results of UV and fluorescence spectroscopy to probe the influence of halogenation on the size (deemed to be proportional to the AMW) of the HPOA molecules. We hypothesize that the width of the ET band may be indicative of the AMW of HS. The rationale for this assumption is that the chromophores in an HS molecule are more likely to interact each with other as the size of the molecule increases because of the increasing degree of conformational degrees of freedom. These interchromophore interactions may generate additional absorbance bands located at wavelengths longer than the ET bands of individual, noninteracting chromophores (*44, 45*). If these bands are present, the single Gauss function employed for modeling the UV absorbance at $\lambda > 250$ nm should be viewed as a composite representation for a more complex system of overlapping bands. Because of their contribution, Δ_{ET} will increase with the AMW of HS.

The literature data allow testing this hypothesis. To do so, we used the published absorbance data at 254 and 400 nm for several humic and fulvic acids (*46*). This data set also contains the average sizes (giration radii, R_g) determined for the HS samples by low-angle X-ray diffraction. We calculated the corresponding Δ_{ET} for these samples and compared them to the reported radii. The Δ_{ET} values were calculated using a formula similar to formula 2 and presuming that the maximum of the ET band was located at 254 nm and the contribution of absorbance bands other than the ET band was negligible. The results are shown in Figure 3. A modest correlation between the radius of HS and Δ_{ET} was found for the series of 10 samples ($R^2 = 0.66$). The relationship between Δ_{ET} and R_g was as follows:

$$R_E = 13.2\Delta_{ET} - 17.5 \qquad (3)$$

where the giration radius is measured in Å and the width of the ET band is in eV. When one outlier was excluded, the correlation was much stronger ($R^2 = 0.78$). By contrast, the correlation between R_g and $SUVA_{254}$ was weak ($R^2 = 0.33$). On the basis of these data, it was presumed that the changes of the giration radii of HPOA caused by halogenation might be semiquantitatively estimated using the R_g versus Δ_{ET} correlation obtained for independent samples of HS. The giration radii of HPOA and its analogues calculated using formula 3 are estimates that need to be confirmed through independent experiments. It is nevertheless believed that the R_g data so obtained allow evaluating the trends associated with HPOA halogenation.

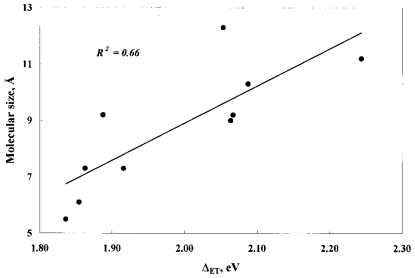

FIGURE 3. Correlation between the giration radii and width of the electron-transfer band in HS. Data published in ref *46* are used for calculations.

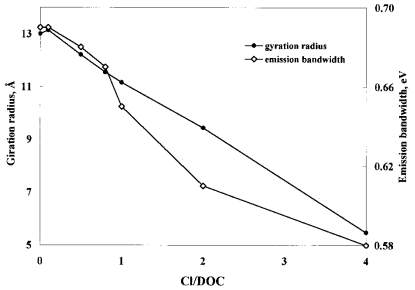

FIGURE 4. Relationship between Cl/DOC dose and the giration radii and the width of emission of band of chlorinated HPOA.

A good dose-property correlation between the Cl/DOC dose, the estimated giration radii of chlorinated HPOA, and the width of the emission band was found (Figure 4). For Cl/DOC > 0.1, the size of HPOA molecules decreases in parallel to the contraction of the fluorescence emission band. The giration radius of HPOA is also correlated with the position of the maximum in the emission spectra and with I_{FDF}. The correlation coefficients for these data sets are 0.89 and 0.97, respectively (Figure 5). The blue shift of the emission band and of the decrease of I_{FDF} associated with the decrease of the molecular size demonstrated here corroborates the trends described qualitatively in the literature (*30, 31, 42*).

It has also been proposed that the fluorescence decay characteristics of HS may be affected by the energy transfer inside the polymeric molecules (*47*). In large HS molecules, intrafluorophore energy transfer shortens the apparent decay lifetimes of the fluorophores. In smaller molecules, this channel of the excitation energy dissipation may be weakened and the lifetimes of the fluorophores increase. Since chlorination decreases the size of the HPOA molecules and destroys some of the aromatic chromophores involved in

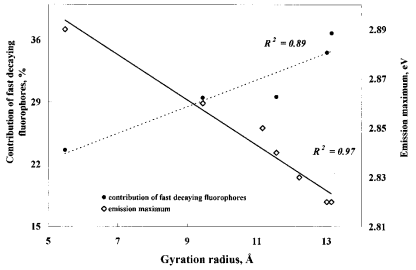

FIGURE 5. Relationship between the estimated giration radii of halogenated HPOA, contribution of fast-decaying fluorophores (τ = 1.2 ns) into the emission, and the position of maximum in the instantaneous emission spectra.

the energy transfer, the decrease of I_{FDF} in chlorinated HPOA correlates well with this hypothesis.

The blue shift of the emission associated with the depletion of FDF signifies that their contribution is more notable in the red part of the fluorescence spectra of HPOA. This is also demonstrated by the weakening of structures α and β (located at 2.28 and 2.45 eV, respectively) in the derivatized emission spectra (Figure 2B). This indicates that the FDF emission band is likely to be located in the range of energy quanta from <2.5 to 2.6 eV (λ > 480 nm). This location of emission spectra has been associated with high-AMW samples (e.g., humic acids extracted from soils and water sources (*19, 20, 41*)). The increase of the intensity of feature δ in chlorinated HPOA signifies that the emission of MDF and SDF is likely to be blue-shifted compared with that of FDF.

Acknowledgments

The authors express their appreciation to Prof. Mark Benjamin (University of Washington, Seattle, WA) for his valuable critique. The authors thank Dr. Jerry Leenheer (U.S. Geological Survey, Denver, CO) who participated in the discussion of the results, provided, and characterized humic substances from Suwannee River, GA. This work was partly funded by the American Water Works Research Foundation (Project # 159-94). Support from HDR Engineering (Omaha, NE) is also greatly appreciated.

Nomenclature

AMW	average molecular weight
Cl/DOC	chlorine to DOC mass ratio
DCA	discrete component approach in the analysis of fluorescence decay
Δ_{ET}	width of the electron-transfer band in UV spectra, eV
Δ_{em}	width of the emission band in fluorescence spectra, eV
DOC	dissolved organic carbon, mg/L as carbon
E_{max}	position of maximum in the emission spectra, eV
ET	electron transfer
eV	electron volt
FDF	fast-decaying fluorophores
HPOA	fraction of hydrophobic acids
HS	humic substances
I_{FDF}	intensity of emission of fast-decaying fluorophores
MDF	medium-decaying fluorophores
NOM	natural organic matter
PHA	polyhydroxyaromatic moiety
R_g	gyration radius
SDF	slow-decaying fluorophores
$SUVA_{254}$	"specific" absorbance at 254 nm (A_{254}/DOC)

Literature Cited

(1) Thurman, E. M. *Organic Geochemistry of Natural Waters*; Nijhoff/Junk: Dordrecht, The Netherlands, 1985.
(2) Marinsky, J. A.; Reddy, M. M. *Chim. Acta* **1990**, *232*, 123−130.
(3) McIntyre, C.; Batts, B. D.; Jardine, D. R. *J. Mass Spectrom.* **1997**, *32*, 328−330.
(4) Stevenson, F. J. *Humus Chemistry, Genesis, Composition, Reactions, Spectroscopic Approaches*; Hayes, M. H. B., MacCarthy, P., Malcolm, R. L., Swift, R. L., Eds.; J. Wiley and Sons: New York, 1982; Chapter 11, pp 264−284.
(5) Christman, R. F.; Norwood, D. L.; Seo, Y.; Frimmel, F. H. Oxidative Degradation of Humic Substances from Freshwater Environments. In *Humic Substances II*; John Wiley & Sons: New York, 1989.
(6) Larson, R. A.; Weber, E. J. *Reaction Mechanisms in Environmental Organic Chemistry*; Lewis Publishers: Boca Raton, FL, 1994.
(7) Rook, J. J. *Environ. Sci. Technol.* **1977**, *11*, 478−482.
(8) Boyce, S. D.; Hornig, J. F. *Environ. Sci. Technol.* **1983**, *17*, 202−211.
(9) Reckhow, D. A.; Singer, P. C.; Malcolm, R. L. *Environ. Sci. Technol.* **1990**, *24*, 478−482.
(10) Topidurti, K. V.; Haas, C. N. *J. AWWA* **1991**, *83* (May), 62−66.
(11) Howard, A. G.; Pizzie, R. A.; Whitehouse, J. W. *Water Res.* **1985**, *19*, 241−248.
(12) Hanna, J. V.; Johnson, W. D.; Quezada, R. A.; Wilson, M. A.; Xia-Qiao, L. *Environ. Sci. Technol.* **1991**, *25*, 1160−1164.
(13) Thorn, K. A.; Arterburn, J. B.; Mikita, M. A. *Environ. Sci. Technol.* **1992**, *26*, 107−116.
(14) Ginwalla, A. S.; Mikita, M. A. *Environ. Sci. Technol.* **1992**, *26*, 1148−1150.
(15) Bloom, P. B.; Leenheer, J. A. Vibrational, Electronic and High-Energy Spectroscopic Methods for Characterizing Humic Substances. In *Humic Substances II*; Hayes, M. H. B., MacCarthy, P., Malcolm, R. L., Swift, R. L., Eds.; John Wiley & Sons: New York, 1989; pp 409−446.
(16) Chin, Y. P.; Aiken, G.; O'Loughlin, E. *Environ. Sci. Technol.* **1994**, *28*, 1853−1858.
(17) Korshin, G. V.; Li, C.-W.; Benjamin, M. M. *Water Res.* **1997**, *31*, 1787−1795.
(18) MacCarthy, P.; Rice, J. A. Spectroscopic Methods (Other than NMR) for Determining Functionality in Humic substances. In *Humic Substances in Soil, Sediment and Water*; Aiken, G. R., et al., Eds., John Wiley & Sons: New York, 1985.
(19) Senesi, N.; Miano, T.; Provenzano, M. R.; Brunetti, G. *Soil Sci.* **1991**, *152*, 259−271.
(20) Senesi, N. *Anal. Chim. Acta* **1990**, *232*, 77−106.
(21) Korshin, G. V.; Li, C.-W.; Benjamin, M. M. *Water Res.* **1997**, *34*, 946−949.
(22) Li, C.-W.; Korshin, G. V.; Benjamin, M. M. *J. AWWA* **1998**, *90* (Aug) 80−92.
(23) Leenheer, J. A. *Environ. Sci. Technol.* **1981**, *15*, 578−587.
(24) *Standard Methods for the Examination of Water and Wastewater*, 18th ed.; American Public Health Association, American Water Works Association, Water Pollution Control Federation: Washington, D. C., 1995.
(25) Puchalski, M. M.; Morra, M. J.; von Vandruska, R. *Fresenius J. Anal. Chem.* **1991**, *340*, 341−344.
(26) Frimmel, F. H.; Kumke, M. U. In *Humic Substances: Structure, Properties, and Uses*; Davies, G., Ghabbour, E., Eds.; Royal Society of Chemistry: Cambridge, 1998; pp 113−122.
(27) Pelikán, P.; Ceppan, M.; Liška, M. *Application of Numerical Methods in Molecular Spectroscopy*; CRC Press: Boca Raton, FL, 1994.
(28) Goldberg, M. C.; Negomir, P. M. Characterization of Aquatic Humic Acid Fractions by Fluorescence Depolarization Spectroscopy. In *Luminescence Applications in Biological, Chemical, Environmental and Hydrological Sciences*; Goldberg, M. C., Ed.; ACS Symposium Series 383; American Chemical Society: Washington, D. C., 1989, pp 180−205.

(29) Gauthier, T. D.; Shane, E. C.; Guerin, W. F.; Seitz, W. R. *Environ. Sci. Technol.* **1986**, *20*, 1162−1166.
(30) Jones, G.; Indig, G. L. *New J. Chem.* **1996**, *20*, 221−232.
(31) Cook, R. L.; Lanford, C. H. *Anal. Chem.* **1995**, *67*, 174−180.
(32) McGown, L. B.; Hemmingsen, S. L.; Shaver, J. M.; Geng, L. *Appl. Spectrosc.* **1995**, *49*, 60−66.
(33) Tiseanu, C.; Kumke, M. U.; Frimmel, F. H.; Klenze, R.; Kim, J. I. *J. Photochem. Photobiol. A* **1998**, *117*, 175−184.
(34) Kumke, M. U.; Tiseanu, C.; Abbt-Braun, G.; Frimmel, F. H. *J. Fluoresc.* **1998**, *8*, 309−318.
(35) Korshin, G. V.; Li, C.-W.; Benjamin, M. M. Use of UV Spectroscopy to Study Chlorination of Natural Organic Matter. In *Water Disinfection and Natural Organic Matter*; Minear, R. A., Amy, G., Eds.; American Chemical Society: Washington, D.C., 1996.
(36) Traina, S. J.; Novak, J.; Smeck, N. E.; *J. Environ. Qual.* **1990**, *19*, 151−153.
(37) Edzwald, J. K.; Becker, W. C.; Wattier, K. L. *J. AWWA* **1985**, *77* (April), 122−132.
(38) Levesque, M. *Soil Sci.* **1972**, *113*, 346−353.
(39) Smart, P. L.; Finlayson, B. L.; Rylands, W. C.; Ball, C. M. *Water Res.* **1976**, *10*, 805−811.
(40) Stewart, A. J.; Wetzel, R. G. *Limnol. Oceanogr.* **1980**, *25*, 559−564.
(41) Hayase, K.; Tsubota, H. *Geochim. Cosmochim. Acta* **1985**, *49*, 159−163.
(42) Lochmueller, C. H.; Saavedra, S. S. *Anal. Chem.* **1986**, *58*, 1978−1981.
(43) Kumke, M. U.; Frimmel, F. H. *Proceedings of the 8th Meeting of the IHSS 8*, Wroclaw, Poland, Sept 9−14, 1996; Drozd, J., Gonet, S. S.; Senesi, N., Weber, J., Ed.; PTSH: Wroclaw, 1997; pp 525−531.
(44) Jaffe, H. H.; Orchin, M. *Theory and Applications of Ultraviolet Spectroscopy*; John Wiley and Sons: New York, 1962.
(45) Scott, A. I. *Interpretation of the Ultraviolet Spectra of Natural Products*. Pergamon Press: New York, 1964.
(46) Reckhow, D. A.; Singer, P. C.; Malcolm, R. L. *Environ. Sci. Technol.* **1990**, *24*, 1655−1664.
(47) Kumke, M. U.; Abbt-Braun, G.; Frimmel, F. H. *Acta Hydrochem. Hydrobiol.* **1998**, 73−81.

Received for review July 31, 1998. Revised manuscript received January 13, 1999. Accepted January 19, 1999.

ES980787H

2.1.4 Alkaline hydrolysis of humic substances - Spectroscopic and chromatographic investigations

M.U. Kumke, C.H. Specht, T. Brinkmann, F.H. Frimmel
Chemosphere, 2001, **45**, 1023 - 1031.

Optische Spektroskopie und Größenausschluss-Chromatographie wurden als analytische Methoden zur Detektion der Veränderungen in HS, induziert durch alkalische Hydrolyse, verwendet. Ähnlich zu den durch Chlorung (s. auch 2.1.3) induzierten Veränderungen wurde bei der alkalischen Hydrolyse insgesamt eine Spaltung der HS in kleinere Fragmente beobachtet. In den Absorptionsspektren nahm die Extinktion ab, während die Fluoreszenzintensität insgesamt zunahm, begleitet von einer hypsochromen Verschiebung des Fluoreszenzmaximums. Die deutliche Zunahme der Fluoreszenz von HS nach erfolgter Hydrolyse ist auch ein Indiz für die Wirksamkeit von intramolekularen Löschprozessen in HS. Der Vergleich der Hydrolysate mit verschiedenen aromatischen Carbonsäuren, wie z.B. Gallussäure, 4-Hydroxybenzoesäure oder Acetylsalicylsäure, zeigte bemerkenswerte Übereinstimmungen in den spektroskopischen und chromatographischen Eigenschaften. Die einfachen aromatischen Carbonsäuren können als - in erster Näherung und mit aller gebotenen Vorsicht, die solch starke Vereinfachungen gebieten - gute Modellstrukturen von fluoreszierenden Einheiten in HS angesehen werden.

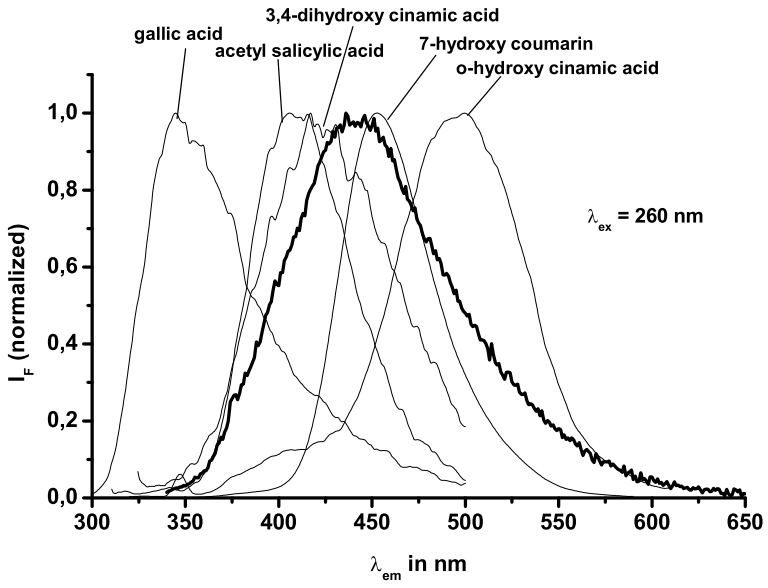

PERGAMON

Chemosphere 45 (2001) 1023–1031

CHEMOSPHERE

www.elsevier.com/locate/chemosphere

Alkaline hydrolysis of humic substances – spectroscopic and chromatographic investigations

Michael U. Kumke, Christian H. Specht, Thomas Brinkmann, Fritz H. Frimmel *

Division of Water Chemistry, Engler-Bunte-Institut, University of Karlsruhe, Engler-Bunte-Ring 1, D-76131 Karlsruhe, Germany

Received 26 July 2000; accepted 5 December 2000

Abstract

To find out more on the structure of humic substances (HS), isolated dissolved organic carbon (DOC) samples from a brown water lake and a wastewater effluent were fractionated and subjected to alkaline hydrolysis. UV/Vis and fluorescence spectroscopy, as well as size-exclusion chromatography with on-line detection of UV absorption, fluorescence and DOC concentration were used to investigate the structural changes caused by the hydrolysis reaction. Following hydrolysis, the fluorescence intensity increased considerably despite a decrease in the UV absorption. The UV absorption and the DOC data from the SEC experiments revealed a strong shift to smaller molecular sizes after hydrolysis. The spectra of the hydrolysed samples, as well as the size-exclusion chromatograms, were compared to spectra of hydroxybenzoic acids and hydroxycinnamic acids. From this comparison, it can be concluded that the hydrolysis products have a structure similar to these organic acids.

Keywords: Humic substances; Alkaline hydrolysis; Fluorescence; Size-exclusion chromatography; Model compounds

1. Introduction

Humic substances (HS) account for a major part of the dissolved organic carbon (DOC) in all aquatic ecosystems. Although it is impossible to describe an exact formation pathway, two general conceptual models have been discussed in the literature. The first one assumes HS to be formed from the tissues of plant material by their partial breakdown and oxidation due to extracellular enzymes and abiotic processes. The second concept states a polymerization of simple compounds like quinones that are derived from degraded plant material. Aquatic HS can be derived from both external sources like plants/soils (allochthonous) and from sources produced within the aquatic ecosystem like algae/bacteria (autochthonous) (Mc Knight and Aiken, 1998).

Due to the enormous number of different precursor materials, an exact structure of HS is impossible to define. More useful is the identification of structural building blocks and their relation to the reactivity of HS. Due to the vast heterogeneity of HS, an in situ characterization of structural elements is very difficult. A promising experimental approach is to reverse the formation of HS and to release structural sub-units under defined experimental conditions. Hydrolysis reactions have been successfully applied in the past to release amino acids, carbohydrates, aliphatic and aromatic carboxylic acids, as well as phenols from HS (Liao et al., 1982; Parsons, 1989; Hautala et al., 1997; Jahnel et al., 1998; Frimmel et al., 1998; Hautala et al., 1998).

The objectives of the presented work were to investigate the effect of alkaline hydrolysis on the properties of HS, especially on their size and their spectroscopic properties. Differences and similarities were evaluated for HS of different origin. The ultimate goal is to identify

* Corresponding author. Tel.: +49-721-608-2580; fax +49-721-699-154.

E-mail address: fritz.frimmel@ciw.uni-karlsruhe.de (F.H. Frimmel).

0045-6535/01/$ - see front matter
PII: S0045-6535(01)00006-6

substructures in HS that define their spectroscopic and chromatographic properties and to use them for a classification of HS in terms of their reactivity with xenobiotics.

2. Experimental details

2.1. Materials, samples and sample treatment

Ultrapure water (18.2 MΩ cm, Milli-Q PLUS, Millipore) was used in all experiments. A sodium hydroxide solution ($c = 1$ mol/l) was prepared by diluting a commercially available concentrate (50–52% (w/w), Fluka, puriss. p. a.).

The HS samples investigated were collected from a brown water lake (Hohlohsee, Northern Black Forest, Germany; HO14) and wastewater effluent (water treatment plant, Neureut, Germany; ABV3). While the brown water was of natural origin and its precursors can be considered to be mainly plant remains, the wastewater effluent had a strong contribution from anthropogenic activities. The original samples were freeze-dried (Orig) or separated into fulvic acids (FA), humic acids (HA) and non-humic substances (NHS) by using an XAD-8 (polymethylmethacrylate) resin according to a modified method of Mantoura and Riley (Mantoura and Riley, 1975; Abbt-Braun et al., 1991). Basic sample parameters are described in detail elsewhere (Frimmel and Abbt-Braun, 1999). The concentration of dissolved organic carbon was measured using a Shimadzu 5000 TOC analyzer, calibrated with potassium hydrogenphthalate standards.

Sample solutions were prepared by adding 10 ml of water to approximately 2.5 mg of freeze-dried material. The resulting mixtures were sonified for 15 min and subsequently filtered (0.45 μm, polyvinylidenefluoride). For the hydrolysis 0.75 ml of sodium hydroxide ($c = 1$ mol/l) solution was added to 2.25 ml of sample solution. The resulting solution was heated under nitrogen in a sealed glass vial for 48 h at 100°C. Subsequently, 25 ml of water was added, then the solution was filtered using a 0.45 μm polyvinylidenefluoride filter. A styrene-based cation exchange resin cartridge (OnGuard-H, Dionex) was used to neutralize the solutions. After discarding the first 4 ml, the solutions obtained were used in the further spectroscopic and chromatographic measurements.

Different benzene carboxylic acids were investigated for their spectroscopic properties. The compounds are listed in Table 1. All compounds were purchased from Aldrich (grade > 97%) and used as received. The UV/Vis absorption measurements and the fluorescence measurements were carried out at pH values of 2, 7, and 11, respectively. To adjust the pH, aqueous HCl and NaOH were added to the solutions. In case of pH = 7, a phosphate buffer was used. For the fluorescence measurements, the optical density of the samples was adjusted to 0.1 at 265 nm in order to measure all samples under the same excitation conditions.

2.2. UV/Vis and fluorescence

For the UV/Vis measurements, a Cary50 spectrometer (Varian) was used. The absorption spectra were recorded in the range of 200 nm $< \lambda_{abs} <$ 500 nm. All spectra were background corrected.

The fluorescence spectra were recorded using a CDT900 fluorescence spectrometer (Edinburgh Analytical Instruments). The instrument was equipped with a 450 W Xenon lamp and a red-sensitive photomultiplier tube, which was operated in the single photon counting mode. The instrument is described in detail elsewhere (Kumke et al., 1998; Frimmel and Kumke, 1999). Fluorescence emission spectra and fluorescence excitation spectra were recorded. The fluorescence emission spectra were measured for three different excitation wavelengths of $\lambda_{ex} = 260$, 270, and 330 nm, in the wavelength range of 265 nm $< \lambda_{em} <$ 650 nm, respectively. For the fluores-

Table 1
Spectroscopic properties of the benzoic acids investigated[a]

	UV absorption maximum[b] (in nm)	Fluorescence maximum[c] (in nm)
Gallic acid	262	349
4-Hydroxycinnamic acid	288	401
2-Hydroxycinnamic acid	271 (314)	498 ($408_{shoulder}$)
3,4-Dihydroxycinnamic acid	288 (314)	426
4-Hydroxybenzoic acid	248	–
Acetylsalicylic acid	(266)	411
Coniferyl alcohol	263 ($300_{shoulder}$)	340
Ferulic acid	265 (310)	442
7-hydroxycoumarin	325	453

[a] The data were collected from solution at pH 7.
[b] Given are the wavelengths for the absorption maximum. In case of two maxima, the second is given in parentheses.
[c] The excitation wavelengths were chosen according to the UV absorption maxima.

cence excitation spectra, two different detection wavelengths ($\lambda_{em} = 310$ and 450 nm) were chosen, and the spectra were measured in the wavelength range of 225 nm $< \lambda_{ex} <$ 440 nm. The spectra were recorded with a spectral bandpass of 1.8 nm in the excitation as well as in the emission monochromator. The dwell time of the measurements was set to 0.5 s and data points were taken every nanometer.

2.3. Size-exclusion chromatography

The experimental set-up for the size-exclusion chromatography (SEC) measurements is described in detail elsewhere (Specht et al., 2000). Three different on-line detection methods were used: UV-absorption at $\lambda_{abs} =$ 254 nm, fluorescence at $\lambda_{ex,1} = 260$ nm, $\lambda_{em,1} = 310$ nm and at $\lambda_{ex,2} = 330$ nm, $\lambda_{em,2} = 450$ nm and DOC. A TSK-50 HW (S) column was used with a phosphate buffer as the mobile phase (28 mmol/l, pH 6.8). The exclusion volume (19 ml) and the permeation volume (47 ml) were determined using dextrane blue and water, respectively. The injection volume of the samples was 2 ml and the DOC concentration of the samples was in the range of 2–10 mg/l.

3. Results and discussion

3.1. UV/Vis spectroscopy

The UV/Vis spectra were recorded in the range of 200 nm $< \lambda_{abs} <$ 500 nm. For the humic substances ABV3 isolated from the wastewater effluent, a decrease in the UV/Vis absorption was observed after hydrolysis only for the HA fraction. For the absorption spectra of ABV3 FA and ABV3 NHS no significant changes were found. More conclusive results were obtained for the brown water HO14 and its isolated fractions. Here, a decrease in the absorption was found for all fractions investigated. While the brown water samples HO14 before hydrolysis showed featureless absorption spectra, the hydrolysis caused a significant change in the related absorption spectra (e.g., Fig. 1 for HO14 FA before and after hydrolysis). This was observed for the HA fraction of the wastewater effluent ABV3 as well. Due to hydrolysis, a well-pronounced absorption band around $\lambda_{abs} = 265$ nm appeared in the spectra (Fig. 1). It was strongest for the FA and HA fraction and least pronounced for the NHS fraction of the brown water HO14.

To compare the influence of the hydrolysis on the different HS fractions investigated, the UV/Vis spectral data were normalized to the concentration of DOC. The absorption $\lambda_{abs} = 254$ nm and $\lambda_{abs} = 436$ nm is frequently used to characterize the properties of HS solutions. These wavelengths were formerly used to estimate the aromaticity and the content of quinones in HS samples (Stevenson, 1982). Korshin et al. (1997) suggested the use of the absorption at $\lambda_{abs} = 203$ nm and at $\lambda_{abs} = 253$ nm for an estimation of the degree of functionality of the aromatic ring. Benzenoid compounds usually show an absorption band at 203 nm, which is often referred to as the benzenoid band (Bz). An absorption around 253 nm can be attributed to a charge-transfer transition (CT). While the strength of the Bz band stays relatively unchanged upon changes in the functionality of the aromatic ring, the CT band is strongly altered. Therefore, a change in the ratio of these wavelengths should be indicative of alterations in the functionality of the aromatic system.

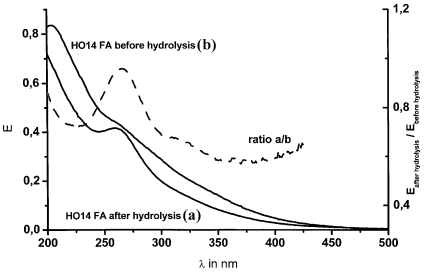

Fig. 1. UV/Vis spectra (not normalized) of HO14 FA before and after hydrolysis. The ratio of the two spectra is shown as well as the spectra of the pure medium before (a) and after hydrolysis (b).

In Fig. 2 the ratio of the UV/Vis absorption at 254 nm to that at 203 nm is shown (later referred to as

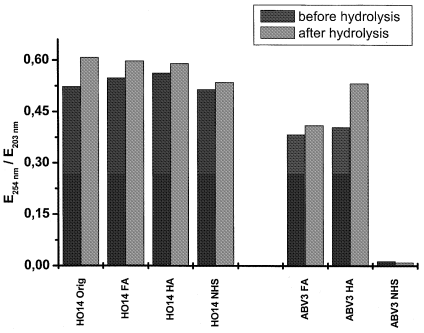

Fig. 2. Comparison of the absorption ratio $\lambda_{254\ nm}/\lambda_{203\ nm}$ for the HS samples before and after alkaline hydrolysis. The pH was adjusted to 4.

ratio I). For the HS fractions investigated, an increase in ratio I was observed after hydrolysis, which indicates an increase in the degree of *effective* functionality of the benzoic rings. Because a direct attack of hydroxide ions on the aromatic moieties is improbable under the reaction conditions applied (Fyfe, 1971), side chain alterations like ester and amide hydrolyses, retro-aldol reactions, benzil-benzilic rearrangements, α– and β–ether cleavages as well as β–γ–C–C cleavages may be responsible for the increase (Wallis, 1971; Parsons, 1989; Beyer, 1998).

3.2. Fluorescence spectroscopy

In Fig. 3, the influence of hydrolysis on the steady-state fluorescence of the brown water samples HO14 is shown.

For comparison, the fluorescence intensities were normalized to the concentration of dissolved organic carbon. As a general trend , the fluorescence of the NOM samples investigated was increased upon hydrolysis. However, the observed increase was much stronger for the brown water samples and within the fractions decreasing in the order HO14 Orig > HO14 FA > HO14 HA > HO14 NHS. For the wastewater effluent, ABV3 FA and ABV3 NHS showed a small increase.

To quantify the alteration in the fluorescence intensity, the fluorescence spectra recorded at different excitation wavelengths were integrated and the relative change upon hydrolysis was calculated. The calculated overall change in the fluorescence intensity of the HS samples is shown in Fig. 4 for two different excitation wavelengths. Independent of the excitation wavelength, the fluorescence intensity of the wastewater effluent fractions was only slightly changed upon hydrolysis, indicated by a relative change in fluorescence intensity close to one (see Fig. 4(b)). On the other hand, for the brown water and its fractions, a strong increase in the overall fluorescence intensity was observed (for HO14 Orig a 2.5-fold increase was observed for $\lambda_{ex} = 260$ nm; see Fig. 4(a)). Moreover, the observed increase caused by hydrolysis was dependent on the excitation wavelength. For $\lambda_{ex} = 330$ nm, the increase of the overall fluorescence intensity was smaller. Here, an increase less than 2-fold was measured for all brown water samples HO14.

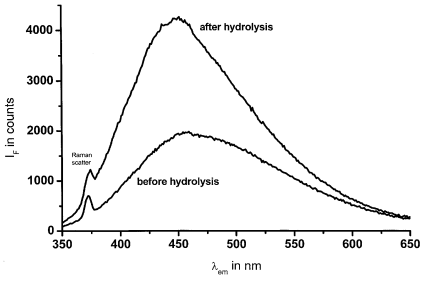

Fig. 3. Steady-state fluorescence spectra ($\lambda_{ex} = 330$ nm, pH 4) of brown water HO14 Orig before and after alkaline hydrolysis of the sample.

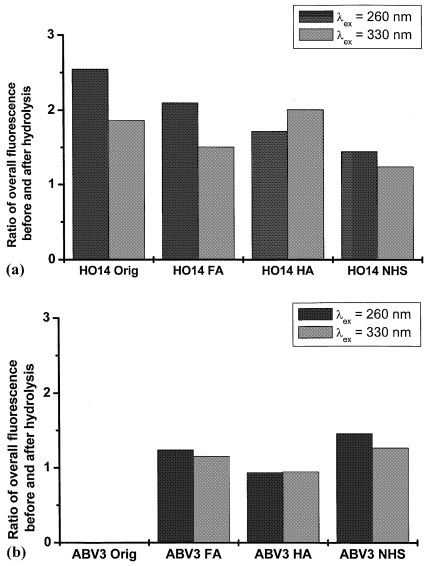

Fig. 4. Relative change of the overall fluorescence intensity of the NOM samples due to hydrolysis at different excitation wavelengths. Shown are the ratios of the integrated fluorescence intensity before hydrolysis and after hydrolysis ((a) brown water HS and (b) wastewater effluent HS).

The completely different behaviour of the wastewater samples ABV3 might be attributed to their young age. On the other hand, the brown water samples HO14 are much older which means, that they have been subjected to numerous alterations like enzymatic or light-induced oxidations. These alterations seem to favour the spectroscopic changes induced by alkaline treatment. As the hydroxide ions preferently attack aliphatic moieties with oxygen-containing functional groups (Wallis, 1971; Parsons, 1989; Beyer, 1998), the results show the importance of these structural parts for the spectroscopic properties of HS.

The effect of increasing fluorescence intensity has also been observed after chlorination, ozonation and UV

irradiation of HS (Korshin et al., 1999; Win et al., 2000). Under these different conditions HS are supposed to be cleaved to smaller molecules. These might have higher fluorescence quantum yields than the original macromolecular substances. Another possibility is, that upon degradation, fluorescence quenching of small molecules by their interaction with HS (Morra et al., 1990; Doll et al., 1999) is reduced. The two explanations were further examined by size-exclusion chromatography and are discussed later in the paper.

It is interesting to note that the observed increase in the fluorescence intensity was not uniform in the spectral range of the fluorescence spectrum which becomes obvious from the calculation of the difference of fluorescence intensity before and after hydrolysis (see Fig. 5). The maximum increase of the fluorescence intensity was found in the wavelength range between 415 nm $< \lambda_{em} <$ 440 nm. In Fig. 5, the calculated spectra (for $\lambda_{ex} = 330$ nm) of the brown water samples are shown.

In Fig. 5(b), the fluorescence excitation spectra of the brown water HO14 FA fraction before and after hydrolysis are compared. The ratio of the two spectra is shown as well. For a simple homogeneous solution of a fluorescent compound, it can be expected that the observed fluorescence excitation spectrum and the corresponding UV/Vis absorption spectrum are identical (assuming that the intensity distribution of the excitation lamp was considered properly). In general, for HS the measured fluorescence excitation spectrum and the UV/Vis absorption spectrum are not identical. While the absorption spectrum is (almost) featureless with an increasing absorption toward the UV region, in the fluorescence excitation spectrum, a relatively well-resolved band is observed in the spectral region around 310 nm $< \lambda_{ex} <$ 370 nm. These differences indicate that only a part of the light-absorbing chromophores present in HS is fluorescent. Based on the fluorescence excitation spectra, a connection between the observed fluorescence increase and the related change in the absorption spectra can be drawn. The comparison of the ratio of the fluorescence excitation spectra and the difference in the absorption spectra (see Fig. 1) reveals striking similarities and it also gives one explanation for the observed dependence on the fluorescence excitation wavelength of the fluorescence increase upon hydrolysis. The compounds built (or released) by the hydrolysis of the HS showed a strong absorption around $\lambda_{abs} = 265$ nm. The larger increase in the fluorescence intensity, with $\lambda_{ex} = 260$ nm, can be attributed to that fact. The number of compounds (or subunits) released from HS participating in light absorption was found to be larger for $\lambda = 260$ nm, and therefore, the observed overall increase in the fluorescence intensity with that particular excitation wavelength can also be expected to be higher when compared to an excitation wavelength of lower energy (e.g., $\lambda_{ex} = 330$ nm).

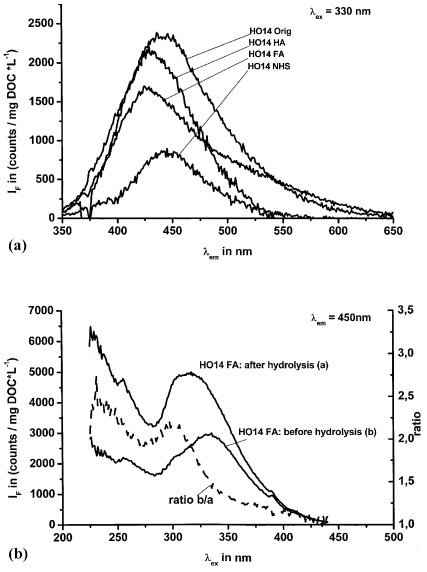

Fig. 5. (a) Calculated differences of the steady-state fluorescence spectra of the brown water and its HS fractions upon alkaline hydrolysis ($\lambda_{ex} = 330$ nm). (b) Comparison of the fluorescence excitation spectra of HO14 FA before and after hydrolysis (not corrected for lamp profile). The ratio of both spectra is shown as well ($\lambda_{em} = 450$ nm).

3.3. Comparison of the spectral character of benzoic acid and the changes induced by hydrolysis in fluorescence and UV/Vis absorption

In a comparative approach, the UV/Vis absorption spectra and the fluorescence spectra of different benzoic acids and related compounds were measured and compared with spectra of the HS and the calculated differences observed upon hydrolysis. Table 1 summarizes the relevant spectroscopic properties of the compounds investigated. All benzoic acid derivatives show absorption maxima between 250 nm $< \lambda_{abs,max} <$ 330 nm. A strong overlap was found compared to the UV/Vis absorption spectra calculated from the measurements before and after hydrolysis of HS. This was also valid for the steady-state fluorescence excitation spectra of the benzoic acids. In Fig. 6, the calculated fluorescence spectra of the hydrolysis products of the brown water HO14 Orig is compared with the fluorescence spectra of various benzene carboxylic acids.

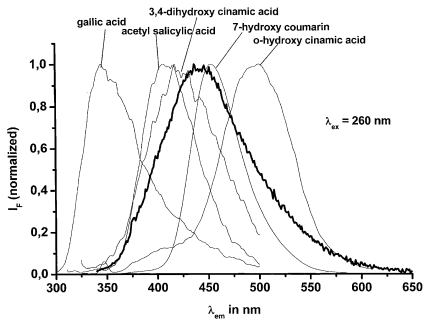

Fig. 6. Comparison of the fluorescence spectra of several benzoic acids with the calculated difference spectrum of HO14 Orig upon hydrolysis ($\lambda_{ex} = 260$ nm, pH 7).

Assuming that some of the building processes of HS are reversed due to the alkaline treatment, a release of lignin-derived moieties like *p*-coumaryl, sinapyl and coniferyl alcohol-like structures can be expected. This is strongly supported by the striking agreement between the UV/Vis absorption spectra, as well as the steady-state fluorescence spectra of those simple model compounds and the calculated changes upon hydrolysis in the spectra of the HS. Furthermore, the results are in qualitative accordance with analytical pyrolysis data of lake Hohloh samples, where 16–22% of the volatile matter were assigned to phenols, lignin monomers and dimers (Schulten and Gleixner, 1999). A significant contribution of allochthonous, soil-derived precursors to lake Hohloh HS seems to be reasonable, since it is a nutrient-poor bog lake, that will slowly become overgrown by detrital plant material.

3.4. Size-exclusion chromatography

The data from the size-exclusion chromatography confirmed the findings from the UV/Vis and fluorescence measurements. The chromatograms of the wastewater samples were only slightly altered by hydrolysis. Whereas the DOC and UV-absorption traces of the FA and NHS sample showed virtually no changes, the fluorescence trace of the FA sample revealed an increase of fluorescence intensity. This increase was not attributable to single fractions and occurred at both sets of excitation and emission wavelengths. Both, the DOC and the UV absorption trace of the HA sample showed a shift to higher elution volumes. In size-exclusion chromatography, several non-ideal interactions between the gel and sample such as ion exclusion, ion exchange and adsorption can occur (Johansson and Gustavsson, 1988; Potschka, 1988). These interactions are superimposed to the separation of the molecules due to their size. Under the reaction conditions applied, the most likely reactions are ester and ether cleavages (Wallis, 1971), which lead to an increase in carboxyl and hydroxyl group content. As a result, the gel–sample interactions, which may lead to a retardation, are decreased (Specht and Frimmel, 2000). Because of this, the shift to higher elution volumes can most likely be attributed to smaller molecules rather than to an increase in the attractive interactions between gel and sample.

The influence of hydrolysis on the brown water sample was much more pronounced in comparison to the wastewater samples. For all brown water samples (original, FA, HA, and NHS) the fluorescence intensity increased whereas the UV absorption decreased. In connection with a shift to higher elution volumes, this is another indication for breakdown of larger molecules due to hydrolysis. Large molecules have the ability to release the energy from an absorbed photon via processes which do not involve the emission of light. For smaller molecules, this is often not the case. Because of this, the fluorescence increases even if the UV absorption decreases, i.e., the fluorescence yield increases. Due to the chromatographic separation quenching of the smaller fluorescent entities by larger NOM molecules is suppressed even for the non-hydrolysed sample. Therefore, the increase of fluorescence is more likely caused by an increase of the fluorescence yield and the number of fluorescent entities rather than by a decrease of the quenching effect of NOM. In contrast to the wastewater sample, the increase of fluorescence intensity can be attributed to several fractions.

Fig. 7 depicts the chromatograms obtained with DOC-, UV absorption-, and the fluorescence detection of the brown water sample HO14 Orig before and after hydrolysis. The DOC and UV absorption chromatograms show a considerable shift to higher elution volumes, i.e., lower molecular mass. This shift cannot be found in the fluorescence trace. From these results one can conclude, that the higher molecular mass fractions of natural organic matter contain structures which are potentially capable of fluorescence. These structures are unveiled by the hydrolysis reaction and lead to an increase in fluorescence intensity. This holds for all brown water samples investigated in this work. The highest increase in fluorescence intensity (by a factor of 3.8) was found for $\lambda_{ex,1} = 260$ nm and $\lambda_{em,1} = 310$ nm. At $\lambda_{ex,2} = 330$ nm, $\lambda_{em,2} = 450$ nm, fluorescence intensity increased by a factor of 2.7. This increase is higher than the increase in overall fluorescence intensity, which was found for the non-separated sample. In the non-separated sample, fluorescence quenching can occur through intermolecular energy transfer from smaller to larger molecules, which is not possible after separation in the SEC column. As the total area of the DOC chromato-

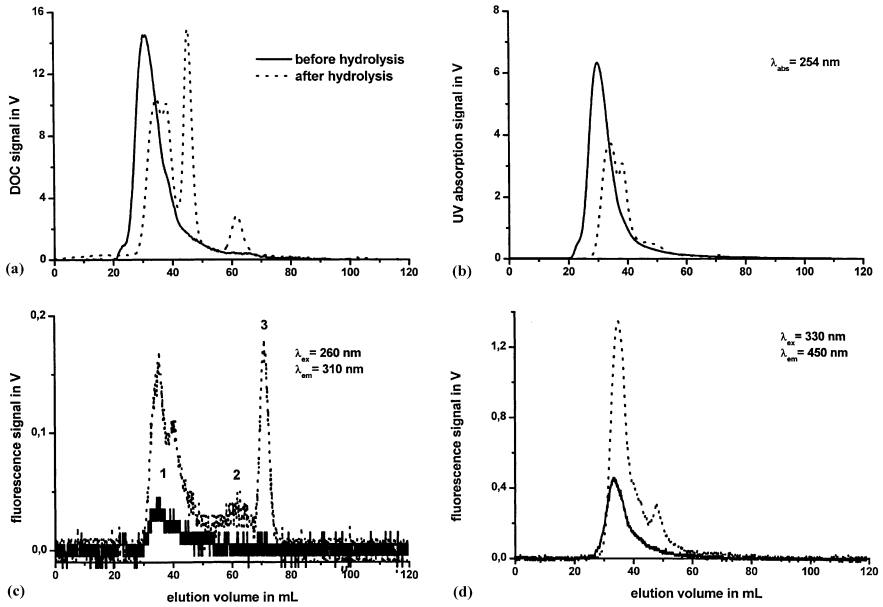

Fig. 7. SEC chromatograms of brown water HO14 Orig before and after hydrolysis obtained with DOC, UV absorbance, and fluorescence detection.

grams does not decrease, no degradation of organic matter to CO_2 took place due to hydrolysis. On the other hand, the total area of the UV signal decreases by 16%. Because of the cleavage of side groups, conjugated systems might be destroyed, resulting in a lower UV absorption. In addition to the shift, the chromatograms of the samples after hydrolysis show fractions which were set free from the original sample. No major differences can be found between the different natural organic matter fractions in the DOC and UV absorption chromatograms. In contrast, it was possible to detect significant differences between the samples in the fluorescence signal. Fig. 7(c) shows the chromatogram of the fluorescence detector with $\lambda_{ex,1} = 260$ nm and $\lambda_{em,1} = 310$ nm. Whereas fractions 2 and 3 could be found in the original sample as well as in the FA sample, fraction 2 was absent in the HA sample and fraction 3 could not be found in the NHS sample. Also, the HA showed no fluorescence at the chosen set of excitation and emission wavelengths before hydrolysis. The chromatograms of the fluorescence signal at $\lambda_{ex,2} = 330$ nm, $\lambda_{em,2} = 450$ nm showed only minor changes in shape. Since humic substances show a strong fluorescence signal at this set of excitation and emission wavelengths, the increase in intensity is probably caused by a decrease in the self-quenching effect of humic substances.

To determine the structures of the substances which make up fractions 2 and 3 found in the fluorescence chromatograms, SEC experiments with the compounds listed in Table 1 were carried out under the same conditions used for the natural organic matter samples, i.e., the same UV absorption and fluorescence excitation and emission wavelengths were used. The data showed, that benzoic acid derivatives like gallic acid and 4-hydroxybenzoic acid had a strong fluorescence signal at $\lambda_{ex,1} = 260$ nm, $\lambda_{em,1} = 310$ nm, but hardly any signal at $\lambda_{ex,2} = 330$ nm, $\lambda_{em,2} = 450$ nm. The derivatives of cinnamic acid on the other hand showed a strong signal at $\lambda_{ex,2} = 330$ nm, $\lambda_{em,2} = 450$ nm, but only a weak signal at $\lambda_{ex,1} = 260$ nm, $\lambda_{em,1} = 310$ nm. In addition, the elution volume of the benzoic acid derivatives coincides with the elution volume of fraction 3. From this, one may conclude, that the fractions 2 and 3 consist of substances with a structure similar to hydroxybenzoic acids rather than hydroxycinnamic acid.

4. Conclusions

Hydrolysis reactions have been used quite extensively to obtain information on the structure of the building blocks of humic matter. In combination with spectroscopy in the UV/Vis range, hydrolysis gives information not only on the aromatic and unsaturated areas of the molecules with main absorbances around $\lambda = 260$ nm, but also on the molecular size. Especially fluorescence spectra give insight into the stability of the molecular structure in aqueous solution. The significant increase in the fluorescence after hydrolysis makes it attractive to assume the presence of quenching mechanisms in the original dissolved macromolecule which are lost in the smaller hydrolysed products. The identification of the building blocks still remains troublesome. Poor resolution of chromatographic fractionation based on water as the mobile phase and lack of powerful identification methods are the main reasons. A way out of this dilemma seems to be the use of reasonable model compounds. Their properties in mixtures can be compared with the integrated character of the complex samples to be investigated. The best fit is a good basis for structural assumptions. The application of that strategy to the hydrolysis products of HS makes the substituted representatives of salicylic acid, cinnamic acid, and 7-hydroxy-coumarin to appear as attractive building blocks of the complex organic matter in brown water.

Acknowledgements

The work was funded by the Deutsche Forschungsgemeinschaft in the ROSIG research program and in the research project MetalOM (Grant Fr 536/21-1). The authors wish to thank Dr. Gudrun Abbt-Braun and Axel Heidt for preparing and supplying the HS samples.

References

Abbt-Braun, G., Frimmel, F.H., Lipp, P., 1991. Isolation of organic substances from aquatic and terrestrial systems – comparison of some methods. Z. Wasser-Abwasser-Forsch 24, 285–292.

Beyer, H., 1998. Lehrbuch der Organischen Chemie. Hirzel, Stuttgart.

Doll, T.E., Frimmel, F.H., Kumke, M.U., Ohlenbusch, G., 1999. Interaction between natural organic matter (NOM) and polycyclic aromatic compounds (PAC) – comparison of fluorescence quenching and solid phase micro extraction (SPME). Fresenius J. Anal. Chem. 364, 313–319.

Frimmel, F.H., Jahnel, J., Hesse, S., 1998. Characterization of biogenic organic matter (BOM). Water Sci. Technol. 37, 97–103.

Frimmel, F.H., Abbt-Braun, G., 1999. Basic characterization of reference NOM from central Europe – similarities and differences. Environ. Int. 25, 191–207.

Frimmel, F.H., Kumke, M.U., 1999. Optische Parameter zur Stoffcharakterisierung vom Trinkwasser bis zum Abwasser. Wien. Mitt. 156, 1–24.

Fyfe, C.A., 1971. Nucleophilic attack by hydroxide and alkoxide ions. In: Patai, S. (Ed.). The Chemistry of the Hydroxyl Group – Part 1. The Chemistry of Functional Groups. Interscience, London, pp. 52–131.

Hautala, K., Peuravuori, J., Pihlaja, K., 1997. Estimation of origin of lignin in humic DOM by CuO-oxidation. Chemosphere 35, 809–817.

Hautala, K., Peuravuori, J., Pihlaja, K., 1998. Organic compounds formed by chemical degradation of lake aquatic humic matter. Environ. Int. 24, 527–536.

Jahnel, J.B., Ilieva, P., Abbt-Braun, G., Frimmel, F.H., 1998. Aminosäuren und Kohlenhydrate als Strukturbestandteile von refraktären organischen Säuren. Vom Wasser 90, 205–216.

Johansson, B.-L., Gustavsson, J., 1988. Elution behavior of some proteins on fresh, acid- or base-treated sephacryl S-200 HR. J. Chromatogr. 457, 205–215.

Korshin, G.V., Li, C.-W., Benjamin, M.M., 1997. Monitoring the properties of natural organic matter through UV spectroscopy: a consistent theory. Water Res. 31, 1787–1795.

Korshin, G.V., Kumke, M.U., Li, C.W., Frimmel, F.H., 1999. Influence of chlorination on chromophores and fluorophores in humic substances. Environ. Sci. Technol. 33, 1207–1212.

Kumke, M.U., Abbt-Braun, G., Frimmel, F.H., 1998. Time-resolved fluorescence measurements of aquatic natural organic matter (NOM). Acta Hydrochim. Hydrobiol. 26, 73–81.

Liao, W., Christman, R.F., Johnson, J.D., Millington, D.S., 1982. Structural characterization of aquatic humic material. Environ. Sci. Technol. 16, 403–410.

Mantoura, R.F.C., Riley, J.P., 1975. The analytical concentration of humic substances from natural waters. Anal. Chim. Acta 76, 97–106.

Mc Knight, D.M., Aiken, G.R., 1998. Sources and age of aqutic humus. In: Hessen, D.O., Tranvik, I.J. (Eds.), Aquatic Humic Substances – Ecology and Biogeochemistry. Springer, Berlin, pp. 9–39.

Morra, M.J., Corapcioglu, M.O., von Wandruszka, R.M.A., Marshall, D.B., Topper, K., 1990. Fluorescence quenching and polarization studies of naphthalene and 1-naphthol interaction with humic acid. Soil Sci. Soc. Am. J. 54, 1283–1289.

Parsons, J.W., 1989. Hydrolytic degradations of humic substances. In: Hayes, M.H.B., MacCarthy, P., Malcolm, R.L., Swift, R.S. (Eds.), Humic Substances II – in Search of Structure. Wiley, Chichester, pp. 99–120.

Potschka, M., 1988. Size-exclusion chromatography of polyelectrolytes, experimental evidence for a general mechanism. J. Chromatogr. 441, 239–260.

Schulten, H.-R., Gleixner, G., 1999. Analytical pyrolysis of humic substances and dissolved organic matter in aquatic systems: structure and origin. Water Res. 33, 2489–2498.

Specht, C.H., Frimmel, F.H., 2000. Specific interactions of organic substances in size-exclusion chromatography. Environ. Sci. Technol. 34, 2361–2366.

Specht, C.H., Kumke, M.U., Frimmel, F.H., 2000. Characterization of NOM adsorption to clay minerals by size exclusion chromatography. Water Res. 34, 4063–4069.

Stevenson, F.J., 1982. Humus Chemistry, Genesis, Composition, Reactions. Wiley, New York.

Wallis, A.F.A., 1971. Solvolysis by acids and bases. In: Sarkanen, K.V., Ludwig, C.H. (Eds.), Lignins, Occurrence, Formation, Structure and Reactions. Wiley–Interscience, New York, pp. 345–372.

Win, Y.Y., Kumke, M.U., Specht, C.H., Schindelin, A.J., Kolliopoulos, G., Ohlenbusch, G., Kleiser, G., Hesse, S., Frimmel, F.H., 2000. Influence of oxidation of dissolved organic matter (DOM) on subsequent water treatment processes. Water Res. 34, 2098–2104.

2.1.5 Time-resolved fluorescence measurements of aquatic natural organic matter (NOM)

M.U. Kumke, G. Abbt-Braun, F.H. Frimmel
Acta Hydrochem. Hydrobiol., 1998, **26**, 73 - 81.

Das Fluoreszenzabklingverhalten von FA- und HA-Fraktionen verschiedener Ursprungsorte wurde untersucht und mit unterschiedlichen Auswertemethoden analysiert. Sowohl die Annahme von diskreten Fluoreszenzkomponenten als auch die Auswertung mittels Verteilungsfunktionen zeigten die Unterschiede bzw. Gemeinsamkeiten im Fluoreszenzabklingverhalten der verschiedenen HS. Die aus der Annahme von diskreten Fluoreszenzkomponenten resultierende Anzahl an Fluorophoren ist rein operational-definiert. Eine bessere Beschreibung wird durch die Anwendung von Verteilungsanalysen (*maximum entropy method* (MEM) oder *exponential series method* (ESM)) erreicht. Neben den Unterschieden in den Ursprungsorten spiegelt sich im Fluoreszenzabklingverhalten auch der Einfluss von Oxidationsreaktionen wider, ein Indiz für den Einfluss der HS-Gesamtstruktur auf die spektroskopischen Eigenschaften von HS.

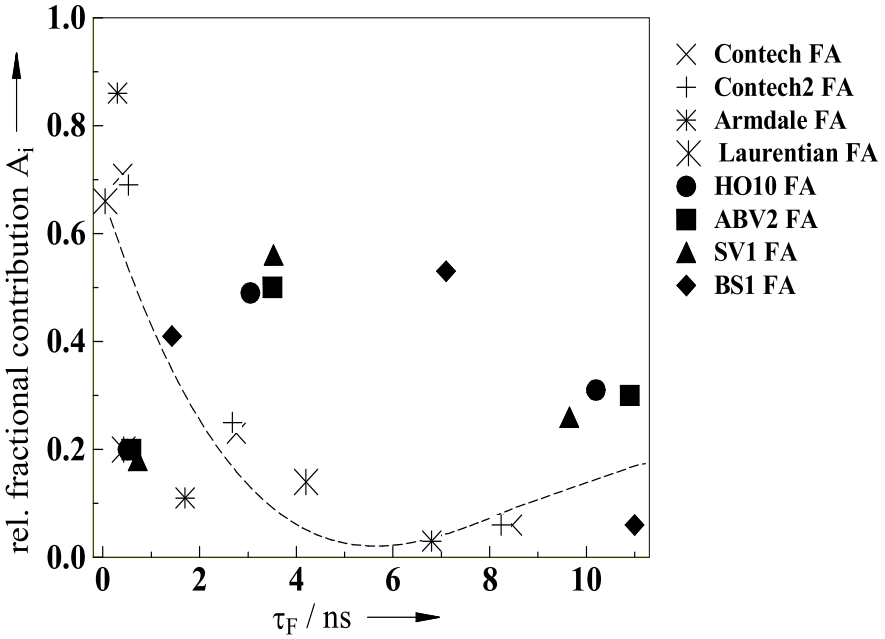

Research Papers

Time-resolved Fluorescence Measurements of Aquatic Natural Organic Matter (NOM)*

Zeitaufgelöste fluoreszenzspektroskopische Untersuchungen natürlicher organischer Wasserinhaltsstoffe (NOM)

M. U. Kumke, G. Abbt-Braun, and F. H. Frimmel**

Keywords: Time-resolved Fluorescence, Natural Organic Matter, Humic Substances, Ozonation

Summary: The fluorescence decay of aquatic natural organic matter (NOM) samples was investigated using the time-correlated single photon counting technique (TCSPC). Two different approaches for the data analysis are presented: the discrete component approach (DCA) and the exponential series method (ESM). The parameter set obtained in the DCA is discussed in terms of characterization for NOM of different origins. However, the obtained parameter set can only be interpreted as operationally defined. Using the ESM for a fluorescence decay time distribution analysis no a priori assumption about the number of fluorescing components was introduced into the data analysis. The interpretation of fluorescence decay time data for samples before and after ozonation is in good agreement with results of other analytical methods.

Schlagwörter: Zeitaufgelöste Fluoreszenzspektroskopie, natürliche Wasserinhaltsstoffe, Huminstoffe, Ozonung

Zusammenfassung: Das Fluoreszenzabklingverhalten von natürlichen organischen Wasserinhaltsstoffen (NOM) wurde mittels der zeitkorrelierten Einzelphotonenzählung untersucht. Zur Auswertung der Abklingkurven wurden zwei unterschiedliche Analyseverfahren verwendet: Ansatz diskreter Komponenten (DCA) und Fluoreszenzabklingzeitenverteilung (ESM). Die in der DCA erhaltenen Parameter können nur zur Charakterisierung der NOM verwendet werden und sind rein operational definiert. In der ESM-Analyse wurde a priori kein Modell angenommen.

1 Introduction

During the last decades substantial effort has been directed towards the characterization of natural organic matter (NOM). The application of elemental analysis, chromatographic, spectroscopic, and pyrolysis techniques yielded valuable results for a general characterization of NOM [1–7]. The combination of pyrolysis results with data obtained from NMR, IR, and titration experiments revealed the presence of a variety of structural elements like aromatic carboxylic acids, phenolic groups, and aliphatic moieties [8, 9]. However, the results obtained so far were only successful in describing these basic features of NOM, whereas the understanding of the relationship between the structure of NOM and its interaction with xenobiotics is still poor [10-14]. The main disadvantages of the techniques commonly used for characterization purposes are their destructive character, the high concentrations of samples needed, and the neglect of conformational dynamics of NOM.

In general, spectroscopic techniques are powerful and non-destructive. They have been successfully applied for the identification and characterization of a great variety of compounds even in diluted aqueous samples. Steady state fluorescence spectroscopy has proven to be a highly sensitive technique which has been already successfully applied in the characterization of NOM [3, 5–8]. Recently, a few attempts have been made to approach the characterization of NOM and its dynamics by time-resolved fluorescence spectroscopy [15–18].

In the present contribution we show results of time-resolved fluorescence decay measurements of aquatic NOM of different origin. The data are discussed using two different approaches for the data analysis. Results for the original NOM and the fulvic and humic acid fractions are presented as well as those for chemically modified NOM due to ozonation.

2 Experimental

2.1 Spectrometry

Time-resolved fluorescence measurements were performed using a FL900CDT fluorescence lifetime spectrometer (Edinburgh Analytical Instruments, Research Park, Riccarton, Currie, Edinburgh EH14 4AP, UK) in the time-correlated single photon counting mode. The instrument was set up in a T-geometry format with two analyzing detection channels. The focal length of the monochromators in the excitation and emis-

* This contribution was presented as a lecture during the annual meeting of the Water Chemistry Division in the German Chemical Society (Fachgruppe Wasserchemie in der GDCh), Lindau, May 1997.

** Dr. Michael U. Kumke, Dr. Gudrun Abbt-Braun, Prof. Dr. Fritz H. Frimmel, Engler-Bunte-Institut, Bereich Wasserchemie, Universität Karlsruhe (TH), Richard-Willstätter-Allee 5, D-76131 Karlsruhe, Germany

Correspondence to F. H. Frimmel
E-mail: fritz.frimmel@ciw.uni-karlsruhe.de

sion channels was 300 mm with an aperture of f/4.2 (optical configuration: symmetrical Czerny-Turner). The grating of the excitation monochromator was blazed at 250 nm and the gratings of the emission monochromators were blazed at 500 nm for optimal performance. The linear dispersion of the monochromators was 1.8 nm/mm which determines together with the slit width the spectral bandpass of the fluorescence measurements. For the detection a photomultiplier tube (PMT) R1527 (Hamamatsu) with a rise time of 2.2 ns was used.

A nF900 nanosecond flash lamp (Edinburgh Analytical Instruments) filled with nitrogen gas (1 bar, 6.6 kV, 0.3 mm electrode separation, operated at 40 kHz) was used for the excitation of the samples. The multichannel analyzer (MCA) Norland 5000 (Viking Instruments Inc., 128 Owen Road, Madison, WI 53716, USA) was used in the pulse height analysis mode. The memory of the MCA Norland 5000 consists of 4 096 channels. In the typical T-geometry format experiment 1 024 channels of the MCA were attributed to each detection channel.

For the data analysis the commercial software package of Edinburgh Instruments was used. In addition to the standard software features (discrete multi-exponential approach), the level 2 software was used for the decay time distribution analysis.

For a reliable data evaluation of complex fluorescence kinetics the acquisition rate (reported as the count rate at peak maximum) is a crucial parameter. Experiments at different count levels (10^3...10^6 counts at peak maximum, CPM) were performed and the influence on fitting results was monitored. In order to get reliable results in an acceptable period of time the experiments were performed at a count level of 3...5 · 10^4 CPM. The measurement time was usually below 4 hours, and the stability of the time profile of the excitation pulse was controlled by monitoring the fluorescence decay of the NOM samples and the excitation pulse in cycles of 5 000 CPM per cycle. The excitation wavelengths in the time-resolved fluorescence measurements were 314 nm, 337 nm, and 357 nm. The experiments were typically run at a time base of 100 ns with 5 ns delay of the stop PMT. The fluorescence emission was detected between λ_{em} = 400 nm and λ_{em} = 530 nm with a slit width of 9 nm. For the comparison of NOM samples λ_{em} = 450 nm was used in terms of a standard emission wavelength which was different from the fluorescence emission maximum for some of the NOM samples. In general, the counting rate was less than 1 % for the natural organic matter samples under investigation and therefore pile up problems in the lifetime data analysis were not likely to occur. The experimental data were analyzed with non-linear least square (NLLS) algorithms based on the method of Marquardt. The results of the data fitting procedures was judged by the χ^2-value and the randomness of the weighted residuals. In general, the fit was made starting with the rising edge of the experimental data.

The steady state fluorescence measurements were performed with a Perkin Elmer LS 5B spectrofluorometer. In the standard steady state experiment a spectral bandwidth of 10 nm for excitation and emission was used. Excitation wavelengths of λ_{ex} = 330 nm or λ_{ex} = 314 nm were applied, and the spectra were recorded in the range of 350 nm < λ_{em} < 550 nm. The spectra were background corrected and for comparison purposes correlated with the dissolved organic carbon concentration (DOC, in mg/L). The steady state fluorescence spectra were not quantum-corrected. The Raman signal of pure water was used as internal standard for correction of day-to-day fluctuations of the excitation intensity.

2.2 Samples and Sample Treatment

In the fluorescence experiments a dissolved organic carbon (DOC) concentration of 2...5 mg/L was used. Unless otherwise noted the samples were dissolved in deionized water (MilliQ water purification system) at a pH of 6...7. The fluorescence measurements were performed with air-saturated samples. In preliminary experiments with air-saturated and nitrogen-saturated samples only a minor influence of oxygen on the observed fluorescence decay was monitored. This is subject to further investigations.

The samples of NOM were of different origin. Table 1 summarizes the samples investigated.

Table 1: Notation and origin of the NOM samples investigated. FA: fulvic acid, HA: humic acid

Herkunft und Notation der untersuchten NOM-Substanzen. FA: Fulvinsäure, HA: Huminsäure

Assignment (fraction)	Origin
FG1 (FA, HA)	groundwater (Fuhrberg)
SV1 (FA, HA)	production effluent from brown coal (Schwelvollertsee)
BS1 (FA, HA)	soil seepage water (Bayreuth)
ABV2 (FA, HA)	wastewater effluent (Karlsruhe)
HO10 (FA, HA)	bog lake (Hohlohsee, Black Forest)
BM7 (FA)	bog lake (Brunnsee, Seeon)
BM12 (FA)	bog lake (Brunnsee, Seeon)
BR2B (FA)	soil seepage water
MEX1 (FA)	Mexican soil
WIN1 (FA)	bog lake

The isolation procedure was based on the XAD-method of Mantoura and Riley and was described by Abbt-Braun et al. [19]. All NOM samples were of aquatic origin with the exception of the MEX1 FA and WIN1 HA samples which were isolated from soil.

2.3 Ozonation

The ozonation of the NOM samples was performed in a vessel (height: 0.35 m, diameter: 0.065 m) stirred by a magnetic stirrer. For the dispersion of the ozone the reactor was equipped with a porous glass frit. The ozone concentration in the gaseous phase was measured before and after passing the reactor using two UV-detectors at a detection wavelength of 254 nm.

In the experiments the ozonation was stopped after 5 min and the absorbed mass of ozone was determined in a mass balance of the gas phase of the reactor. The experimental setup is described in more details by Wolf and Frimmel [20].

3 Theory/Data Evaluation

3.1 Data Analysis Using a Small Set of Exponential Functions

The experimental data were evaluated with a sum of up to 4 exponential decay terms (Eq. (1), *discrete component approach*, DCA).

$$I(t) = \sum_{i=1}^{4} B_i \cdot e^{-\frac{t}{\tau_i}} \qquad (1)$$

Here, $I(t)$ is the fluorescence intensity of the sample dependent on the time t after the excitation pulse, τ_i is the fluorescence decay time and B_i is the related fractional intensity. The relative fractional contributions A_i of each component to the total fluorescence decay is given with:

$$A_i = \frac{B_i \cdot \tau_i}{B_1 \cdot \tau_1 + B_2 \cdot \tau_2 + B_3 \cdot \tau_3 + B_4 \cdot \tau_4} \qquad (2)$$

with $i = 1, 2, 3, 4$

Using the DCA a pre-assumed model for the fluorescence decay of NOM was introduced into the data analysis. The obtained parameter set characterizes the experimental fluorescence decay data by *operationally defined fluorescence decay times* (τ_i) and *operationally defined relative fractional intensities* (A_i), respectively. This approach was used in the past for the evaluation of the fluorescence decay of NOM. For comparison purposes with literature data the experimental data were evaluated using the DCA. However, it has to be stressed that at this point of knowledge the obtained parameter set is only *operationally defined* and it should not be mistaken for *real physical fluorophores* present in NOM.

3.2 Exponential Series Method

In a different approach no initial model for the fluorescence decay was introduced into the data analysis. Using the exponential series method (ESM) no assumption was initially made about the number of fluorophores responsible for the fluorescence decay rather than starting with a flat distribution of exponential decays evenly spaced on a logarithmic scale [21–24]. The number of exponential terms could be up to one hundred distributed over several decades of nanoseconds. In this kind of data analysis the fluorescence decay times were fixed to certain values depending on the time interval and number of decay times chosen. The fractional contribution a_i of each lifetime was varied during the fitting procedure.

To avoid bias, the fitting was performed with different numbers of decay times and different time intervals in terms of lower and upper limits of the flat starting distribution of fluorescence decay times. For artificial lifetime components introduced due to noise in the experimental data it is expected that these components are influenced by the different fitting start conditions. Real decay time components should be independent of the start parameters.

In general, a number of 100 fluorescence decay times was chosen with the lower limit at 0.1 ns and the upper limit at 50 ns. It should be kept in mind that without further evidence from other experiments the obtained parameter set of the ESM analysis is also still not identical to real physical fluorophores. However, the parameter set was derived without a pre-assumption of a number of components. Only a range for the fitting was pre-set. Because the experimental data showed that the initial fluorescence intensity had decayed to almost zero within 90 ns after the excitation flash, it seemed reasonable to consider 50 ns as the upper limit in the ESM analysis.

4 Results and Discussion

Figure 1 shows a typical data set obtained in a single photon counting experiment for the NOM sample HO10. The fluorescence decay and the corresponding excitation lamp pulse are presented on a logarithmic scale. It is obvious that no simple monoexponential fluorescence decay is observed and a more sophisticated approach is required for the data evaluation.

The measurement was performed under standard conditions described above with an excitation wavelength at $\lambda_{ex} = 337$ nm and the emission was monitored at $\lambda_{em} = 450$ nm. In a first visual inspection of the experimental fluorescence decay data short-lived components in the first part (channel <200) of the decay can be recognized as well as longer living contributions by slowly decaying components. This was typical for the observed fluorescence decays of all NOM samples investigated.

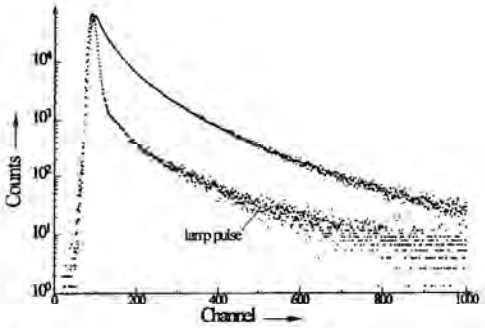

Fig. 1: Fluorescence decay of NOM derived from a bog lake (original water after 0.45-µm filtration, Hohlohsee, Black Forest: HO10). Shown are the excitation pulse time profile at $\lambda_{ex} = 337$ nm and the fluorescence decay of the NOM sample at $\lambda_{em} = 450$ nm. The time calibration was 0.095 ns per channel

Fluoreszenzabklingkurve der natürlichen organischen Wasserinhaltsstoffe eines Moorwassersees (Originalwasser nach 0.45-µm-Filtration, Hohlohsee, Schwarzwald: HO10). Dargestellt sind sowohl das Zeitprofil des Lampenanregungspulses ($\lambda_{ex} = 337$ nm) als auch das Fluoreszenzabklingen der NOM ($\lambda_{em} = 450$ nm). Zeitkalibrierung: 0.095 ns pro Kanal

4.1 Data Evaluation Using the Discrete Component Approach

In recent literature the reported fluorescence decays of NOM were evaluated using the DCA. To compare the fluorescence decay of the NOM samples used with the reported results of NOM fluorescence decay measurements the experimental data were evaluated using a sum of three or four exponential decay terms (Eq. (1)). An interpretation in terms of real physical components is not intended and seems not to be reasonable at this point.

The fitting results were judged by the χ^2-value and the randomness of the residuals. Under our experimental conditions the χ^2-value of each fit was better than 1.2, and the visual inspection of the residuals revealed no deviation from randomness of the weighted residuals. In general, the χ^2-value of a four-exponential fit was better, especially at higher count rates ($> 5 \cdot 10^5$ counts at peak maximum). Here, deviations in the short time region (< 1 ns) from a random distribution of the residuals occurred for a three-exponential fit. In general, the standard deviations of the fluorescence decay times calculated in the DCA were smaller than 5 %, only for the longest living fluorescence decay components (around 10 ns) the calculated standard deviations were in some cases up to 10 %.

In Figures 2A and 2B the results of the fits using the DCA with four exponential decay terms are shown for the fulvic acid fraction (FA) and the humic acid fraction (HA) of the NOM samples investigated. The data shown were derived for an excitation wavelength of λ_{ex} = 337 nm and an emission wavelength of λ_{em} = 450 nm. Figure 2A shows the operationally defined fluorescence decay times and the related fractional contributions of the NOM FA fractions which are operationally defined as well. In Figure 2B the corresponding results for the HA fractions of the NOM samples are given. The χ^2-values of the fitting results were better than 1.2, and the residuals were distributed randomly around zero. In Figure 2A and 2B the calculated fluorescence decay times are plotted versus the related fractional intensity on a logarithmic time scale.

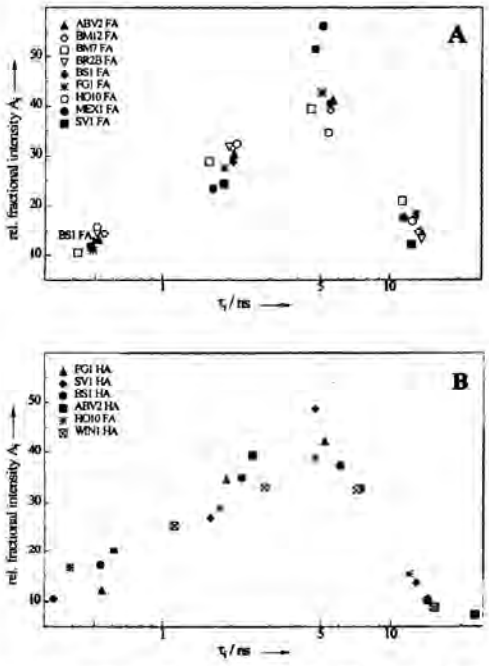

Fig. 2: Comparison of the *operationally defined* fluorescence decay parameters of the investigated NOM fractions. Shown are the *operationally defined fluorescence decay times* vs. the related *operationally defined fractional intensities*.
A: FA fractions **B**: HA fractions

Vergleich der *operational definierten* Fluoreszenzabklingparameter der untersuchten NOM-Fraktionen. Dargestellt sind die *operational definierten Fluoreszenzabklingzeiten* und die zugehörigen *relativen Intensitäten*.
A: Fulvinsäuren (FA) **B**: Huminsäuren (HA)

The comparison of Figure 2A and Figure 2B reveals a remarkable difference between the FA and HA fractions in the time-resolved fluorescence data. For all FA fractions the fluorescence decay times were clustered for each of the four operationally defined components, whereas for the HA fractions no such pronounced clustering could be observed. The operationally defined fluorescence decay data of the FA samples could be divided into the four main time regions around 0.5 ns, 2 ns, 5 ns and 12 ns. An exception was the soil derived MEX1 FA sample for which the fastest decaying component had a fluorescence decay time of 1.7 ns. In general, there were only small variations in the operationally defined fluorescence decay times, especially for the fast decaying component τ_1 which was calculated around 0.5 ns for the FA samples investigated. For all NOM samples analyzed using the DCA the mainly contributing components were found to belong to τ_2 and τ_3.

However, differences in the fractional intensities were more pronounced for the NOM FA fractions. NOM samples closely related to each other because of their origin were more similar in the fractional contributions A_i of the fluorescence decay times τ_1 through τ_4. For example, all NOM FA samples were of aquatic origin except the MEX1 FA sample which was isolated from a Mexican soil. This sample had obviously no fluorescence decay contribution below 1 ns and had a fractional contribution A_2 of 56 % with its τ_2 component which was rather high compared to the other NOM samples in that time range (typically around 40 %). On the other hand the results of the DCA for the aquatic FA fractions were fairly similar. Only the A_3 value of the SV1 FA sample differed when compared with the A_3 values of the other FA samples. This might be attributed to its specific origin which is presumably responsible for a higher content of aromatic structures.

For the HA fractions of the NOM samples a higher variation in the calculated fluorescence decay times as well as in the related fractional intensities was observed (see Fig. 2B). It is interesting to note that τ_4, for the slowest decaying component, was found to increase when the HA sample is compared to the corresponding FA sample. In general, longer fluorescence decay times τ_4 were found for the HA fraction, but the fractional contribution of these components was found to be attenuated, and the second operationally defined fluorescence lifetime became more comparable to the third one in terms of the fractional intensities. The NOM sample WIN1 HA showed the most pronounced differences in the fluorescence decay times, which might be due to the fact that it is soil-derived.

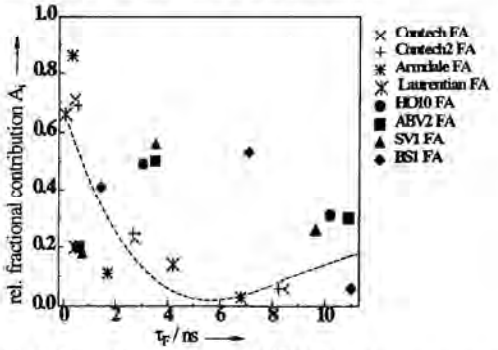

Fig. 3: Comparison of soil-derived NOM FA fractions and aquatic NOM FA fractions. The data for the soil-derived NOM samples were taken from the literature. The dotted line was introduced for visualization purposes only of the trend in the fluorescence decay times and the related fractional intensities of the soil-derived NOM samples, no model was used for the calculation.

Vergleich von bodenbürtigen Fulvinsäuren (Literaturdaten) und aquatischen Fulvinsäuren. Die gebrochene Linie dient zur Veranschaulichung des Trends und basiert auf keinem Modell.

In the recent literature only a few applications of time-resolved fluorescence measurements on NOM samples can be found. Milne et al. used a simple single exponential approach in the data evaluation [25]. For NOM of different marine origin they reported fluorescence decay times of approximately 1 ns. In more sophisticated approaches Lochmüller et al. and Langford et al. used three exponential decay terms in the data evaluation [15–17]. In these investigations only NOM samples isolated from soils were used.

For comparison with the few results reported in the literature we analyzed some of the experimental data also by fitting with a sum of three exponential decay terms (see Fig. 3). The dotted line shown in Figure 3 visualizes the observed trend of the literature data (and was not calculated by a model). For the soil-derived samples the fastest decaying part of the total fluorescence decay had the strongest contribution whereas for the aquatic NOM samples the main contribution in the fluorescence decay is due to operationally defined components with a fluorescence decay time of 3 to 4 ns. It is interesting to note that for the soil seepage NOM sample BS1 FA the fastest decaying component is pronounced compared to the other aquatic NOM samples. This soil seepage NOM sample is closest related to the soil derived NOM samples reported in the literature.

4.2 Data Evaluation Using the Exponential Series Method

Because of the large heterogeneity of NOM the assumption in the DCA analysis of the presence of a small number of well-defined fluorophores is of low probability. In a different approach the experimental data were evaluated using the exponential series method. Here, no initial guess about the number of contributing fluorescence components in the observed fluorescence decay has to be made. Only the lower and upper limit of the decay time range had to be introduced into the analysis. The shortest reliable fluorescence decay time that can be determined with the used setup was approximately 0.1 ns and was therefore set for the lower decay time limit in the ESM analysis. For the upper limit a value of 50 ns was chosen. In the fluorescence decay measurements the time range of the MCA was set to 100 ns. In the experiments at this point of time the initial fluorescence intensity already decayed to less than 0.1 % of its initial value, which suggests that an upper limit of 50 ns is a reasonable assumption.

In the ESM approach the heterogeneity of fluorophores as well as the heterogeneity of different environments of the fluorophores is considered. However, these two kinds of heterogeneity cannot be distinguished, the obtained fluorescence lifetime distributions are a sophisticated data representation for heterogeneous systems, especially for samples, in which the actual shape of the fluorescence spectra is changing during the fluorescence decay because of intramolecular energy transfer processes or intramolecular motions. The time dependence of the shape of the fluorescence spectra was proven in time-resolved fluorescence emission spectra (TRES) measurements and will be reported in detail elsewhere. Briefly, the TRES measurements revealed that the fluorescence maximum is shifted to longer wavelengths during the lifetime of the excited state, e.g., due to intramolecular reorientation of the fluorophore's environments.

In Figure 4 a typical result for NOM samples isolated from different origins is shown (see Table 1). The relative contributions versus fluorescence lifetimes in the considered time window are given. The number of lifetimes is limited to 100, and these are logarithmically spaced in the considered time range. The results are summarized in Table 2. For the results shown the shift term in the data analysis was fixed to 0.1 channels for all NOM samples analyzed. The data shown were obtained with an excitation wavelength λ_{ex} = 337 nm and an emission wavelength λ_{em} = 450 nm. For all samples investigated no significant contributions of fluorescence lifetimes longer than 20 ns were obtained, and the main contribution in the observed fluorescence decay was in the time range between 2 ns and 4.5 ns. The fluorescence lifetime distributions can be represented by mean fluorescence decay times and the width of the calculated distribution given by a standard deviation in Table 2. For most of the NOM samples the ESM approach revealed more than one local maximum.

The calculated fluorescence decay time distributions were different according to the origin of the NOM samples. When the FA and HA fractions of one NOM sample were compared the HA fractions showed a general tendency towards longer fluorescence decay times. Normally, a higher aromatic content and a more rigid structure can be attributed to the HA fractions. This would go along with the tendency of longer fluorescence decay times. The actual fluorescence decay time pattern for some NOM samples are quite similar, but further experiments and the comparison with the results of other analytical methods, like LC-DOC analysis, are needed for a detailed interpretation.

4.3 Chemical Modification of the NOM Structure by Ozonation

The capabilities of the ESM approach were tested for the characterization of NOM samples treated with ozone. In the ozonation process structural units containing low valent nitrogen and sulfur or double bounds are preferentially oxidized. Due to the oxidation the molecular structure of the NOM is changed. Gel chromatography measurements of the NOM samples before and after ozonation revealed an enhanced contribution of low molecular weight structures after the NOM sample reacted with ozone.

In Figure 5 the results of the ESM analysis for NOM samples of two different wastewaters (originals) are shown. In general, for both NOM samples after ozonation the contribution of long fluorescence decay times is decreased and the relative amount of short-lived fluorescence components is enhanced. The extent of the decrease in long fluorescence lifetimes and the relative enhancement of the short decaying fluorescence fraction corresponds well to the degree of ozone absorption by the NOM sample. The wastewater effluents were rich in sulfur- and nitrogen-containing groups as well as carbon double bonds. These samples showed a strong absorption of ozone compared to a NOM sample of higher refractory character, like that of a bog water. The content of sulfur- and nitrogen-containing groups in a bog water is much lower compared to the brown coal derived production effluent (SV1). The smaller degree in the refractory character was reflected in the calculated fluorescence decay time distributions before and after ozonation [26]. The contribution of the long fluorescence decay components is decreased due to the ozonation for both wastewater effluents and was found to a smaller extent for the bog lake NOM sample.

It is interesting to note that the shape of the calculated fluorescence decay time distributions of the bog lake NOM and the NOM from a brown coal derived production effluent became more similar after ozonation. This may be an indication for the

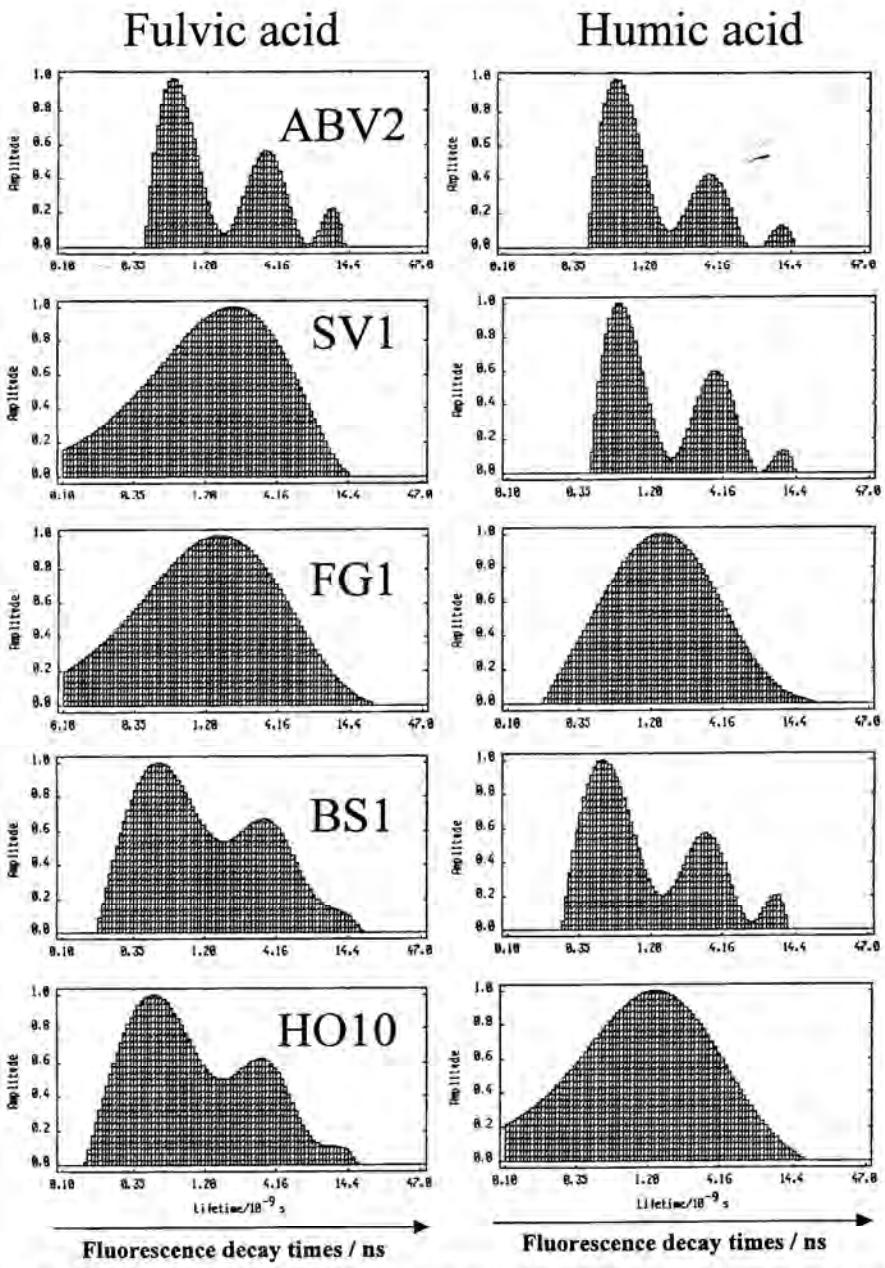

Fig. 4: Comparison of the ESM results for the fulvic and humic acid fraction of NOM samples of different origins (λ_{ex} = 337 nm, λ_{em} = 450 nm, shift fixed to 0.1 channels, 100 decay times in the time range between 0.1 ns and 50 ns)

Vergleich der ESM-Anpassung für Huminstoffe (Fulvin- und Huminsäurefraktionen) unterschiedlichen Ursprungs (λ_{ex} = 337 nm, λ_{em} = 450 nm, shift-Parameter fix: 0.1 Kanäle, 100 Fluoreszenzabklingzeiten im Bereich zwischen 0.1 ns and 50 ns)

Table 2: Results for the ESM data analysis of the NOM samples investigated: 100 decay times in the time range between 0.1 ns and 50 ns with a fixed shift at 0.1 channels. In the time-resolved fluorescence experiments the excitation wavelength was 337 nm and the emission wavelength was set to 450 nm with a bandwidth of 18 nm in the emission. Shown are the calculated mean fluorescence decay times τ_i and the corresponding fractional intensities a_i of the distribution analysis.

Ergebnisse der ESM-Analyse der untersuchten NOM-Proben (100 Fluoreszenzabklingzeiten zwischen 0.1 ns und 50 ns; shift-Term fix: 0.1 Kanäle; λ_{ex} = 337 nm, λ_{em} = 450 nm mit einer spektralen Bandbreite von 18 nm). Aufgeführt sind die in der Verteilungsanalyse gefundenen mittleren Fluoreszenzabklingzeiten τ_i und die entsprechenden relativen Intensitäten a_i.

	τ_1/ns	a_1/%	τ_2/ns	a_2/%	τ_3/ns	a_3/%
HO10 FA	0.6 ± 0.3	21.8	3.6 ± 1.8	65.2	12.5 ± 1.8	13
BS1 FA	0.7 ± 0.4	19.7	4.5 ± 2.9	80.4		
FG1 FA			2.2 ± 2.6	100		
ABV2 FA	0.8 ± 0.2	20.2	3.5 ± 1.0	51.9	10.3 ± 1.4	27.9
SV1 FA			2.2 ± 2.2	100		
	τ_1/ns	a_1/%	τ_2/ns	a_2/%	τ_3/ns	a_3/%
HO10 HA			2.0 ± 2.3	100		
BS1 HA	0.6 ± 0.3	21.5	3.1 ± 1.1	52.8	9.8 ± 1.5	25.7
FG1 HA			2.2 ± 2.2	100		
ABV2 HA	0.8 ± 0.3	28.4	3.6 ± 1	50.9	12.2 ± 1.4	20.9
SV1 HA	0.8 ± 0.2	21.8	3.7 ± 1.1	61.8	11.3 ± 1.3	16.4

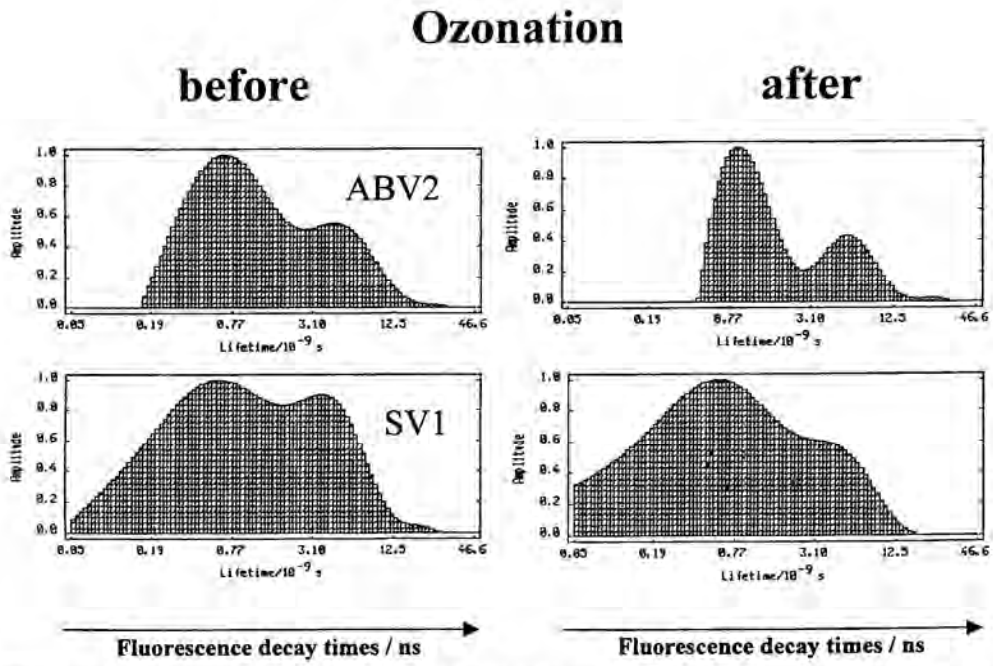

Fig. 5: Comparison of the ESM results of two wastewater effluents, before and after ozone treatment (λ_{ex} = 314 nm, λ_{em} = 450 nm, shift fixed to 0.1 channels, 100 lifetimes in the time range between 0.1 ns and 50 ns)

Vergleich der ESM-Analyse von NOM zweier Abwässer vor und nach Ozonbehandlung (λ_{ex} = 314 nm, λ_{em} = 450 nm, shift-Term fix: 0.1 Kanäle, 100 Fluoreszenzabklingzeiten im Bereich zwischen 0.1 ns und 50 ns)

presence of similar fluorophores including their molecular framework after both NOM samples were oxidized by ozone. This is subject of further investigations.

5 Conclusions

Because of the heterogeneity of original NOM samples in the composition of fluorophores as well as in the molecular environment for one particular fluorophore, the fluorescence decay of NOM is of highly complex nature. The data analysis using a discrete component approach yielded excellent data representation in terms of fit parameter like randomness of the residuals and χ^2-values. However, the calculated set of four fluorescence decay times and the related fractional intensities can only be understood in terms of *operationally defined* parameters and the interpretation in terms of real physical fluorophores is crucial. Even though the obtained operationally defined parameter sets seem to be able to characterize the fluorescence decay of NOM when NOM samples of different origin are compared with one another. It is interesting to note that closely related samples became very similar, e.g., due to their comparable genesis like samples isolated from bog waters. They showed highly similar fluorescence decay times and fractional intensities as revealed in the DCA. This could be an indication of the presence of molecular similarities in the fluorescing structures.

Even though the DCA yielded excellent results in the representation of the NOM fluorescence decay data, the a priori introduction of a limited number of fluorescent components is most probably an over-simplification of the fluorescence decay processes inside the NOM samples. Therefore, the representation of the fluorescence decay data by fluorescence decay time distributions is a promising approach. The obtained fluorescence decay time distributions of the NOM samples investigated turned out to be different according to their origin and chemical history. Using the ESM approach for the analysis of fluorescence decay data of NOM samples, e.g., before and after ozonation, revealed a shift in the observed fluorescence decay time distribution towards shorter decay times for the ozonated samples. That goes along with the observation of an increase of the low-molecular size fractions in the LC-DOC analysis. It is attractive to assume that the observed shorter fluorescence decay time contributions are due to fractions of low molecular size. The time-resolved fluorescence measurement of model compounds for the fluorescent building blocks of NOM revealed that all of the model compounds investigated (quinones, aromatic hydroxylic acids) showed fluorescence lifetimes shorter than 1 ns. This work is still in progress and indicates that interactions between fluorescing structures (through bonds or space) might be responsible for the observed complex fluorescent decay. Intramolecular energy transfer processes, self quenching, or formation of excited dimers may be involved in these processes.

Further investigations are needed for a more detailed interpretation of the results obtained so far. The introduction of external fluorescence quenchers and fluorescence probes seems to be a very promising tool for these experiments. The usefulness of the obtained parameter sets in DCA and ESM for NOM characterization purposes is subject to further investigations. Investigations of further NOM samples under variation of experimental parameters like temperature, pH, ionic strength, emission and excitation wavelength will challenge the presented data analysis.

Acknowledgement

The authors wish to thank Dipl.-Ing. Andreas Wolf for performing the ozonation of the NOM samples and Dipl.-Ing. Sebastian Hesse for the LC-DOC measurements. The Deutsche Forschungsgemeinschaft (DFG) supported part of the work in the ROSIG program.

References

[1] *Abbt-Braun, G., Schmiedel, U., Frimmel, F. H.:* Elementaranalytische Untersuchungen isolierter Fulvinsäuren unterschiedlichen Ursprungs. Vom Wasser *75*, 59–73 (1990).

[2] *Schulten, H.-R., Abbt-Braun, G., Frimmel, F. H.:* Time-Resolved Pyrolysis Field Ionization Mass Spectrometry of Humic Material Isolated from Freshwater. Environ. Sci. Technol. *21*, 349–357 (1987).

[3] *Liao, W., Christman, R. F., Johnson, J. D., Millington, D. S., Hass, J. R.:* Structural Characterization of Aquatic Humic Material. Environ. Sci. Technol. *16*, 403–409 (1982).

[4] *Frimmel, F. H., Gremm, T., Huber, S.:* Liquid chromatographic characterization of refractory organic acids. Sci. Total Environ. *117/118*, 197–206 (1992).

[5] *Huber, S., Gremm, T., Frimmel, F. H.:* Chromatographische Trennung natürlicher organischer Wasserinhaltsstoffe mit UV-, Fluoreszenz- und DOC/TOC-Detektion ohne Probenvoranreicherung: Auswahl geeigneter Trennsysteme. Vom Wasser *75*, 331–342 (1990).

[6] *Miano, T. M., Sposito, G., Martin, J. P.:* Fluorescence spectroscopy of humic substances. Soil Sci. Soc. Am. J. *52*, 1016–1019 (1988).

[7] *Mobed, J. J., Hemmingsen, S. L., Autry, J. L., McGown, L. B.:* Fluorescence Characterization of IHSS Humic Substances: Total Luminescence Spectra with Absorbance Correction. Environ. Sci. Technol. *30*, 3061–3065 (1996).

[8] *Abbt-Braun, G., Frimmel, F. H.:* Spektroskopische Strukturaufklärung aquatischer Huminstoffe. Vom Wasser *77*, 291–302 (1991).

[9] *Abbt-Braun, G., Frimmel, F. H., Schulten, H.-R.:* Strukturelle Charakterisierung isolierter aquatischer Huminstoffe – Anwendbarkeit, Grenzen und Vergleich ausgewählter Methoden. Vom Wasser *74*, 325–338 (1990).

[10] *Zepp, G. R., Schlotzhauer, P. F., Sink, R. M.:* Photosensitized tranformations involving electronic energy transfer in natural waters: role of humic substances. Environ. Sci. Technol. *19*, 74–81 (1985).

[11] *Puchalski, M. M., Morra, M. J., von Wandruszka, R.:* Fluorescence quenching of synthetic organic compounds by humic materials. Environ. Sci. Technol. *26*, 1787–1792 (1992).

[12] *Chen, S., Inskeep, W. P., Williams, S. A., Callis, P. R.:* Complexation of 1-naphthol by humic and fulvic acids. Soil Sci. Soc. Am. J. *56*, 67–73 (1992).

[13] *Chen, S., Inskeep, W. P., Williams, S. A., Callis, P. R.:* Fluorescence lifetime measurements of fluoranthene, 1-naphthol, and napropamide in the presence of dissolved humic acid. Environ. Sci. Technol. *28*, 1582–1588 (1994).

[14] *Kumke, M. U., Löhmannsröben, H.-G., Roch, Th.:* Fluorescence quenching of polycyclic aromatic compounds by humic acid. Analyst *119*, 997–1001 (1994).

[15] *Lochmüller, C. H., Saavedra, S. S.:* Conformational changes in a soil fulvic acid measured by time-dependent fluorescence depolarization. Anal. Chem. *58*, 1978–1981 (1986).

[16] *Power, J. F., LeSage, R., Sharma, D. K., Langford, C. H.:* Fluorescence lifetimes of the well characterized humic substance, Armdale fulvic acid. Environ. Technol. Lett. *7*, 425–430 (1986).

[17] *Cook, R. L., Langford, C. H.:* Metal ion quenching of fulvic acid fluorescence intensities and lifetimes: nonlinearities and a possible three-component model. Anal. Chem. *67*, 174–180 (1995).

[18] *McGown, L. B., Hemmingsen, S. L., Shaver, J. M., Geng, L.:* Total lifetime distribution analysis for fluorescence fingerprinting and characterization. Appl. Spectrosc. *49*, 60–66 (1995).
[19] *Abbt-Braun, G., Frimmel, F. H., Lipp, P.:* Isolation of organic substances from aquatic and terrestrial systems – comparison of some methods. Z. Wasser-Abwasser-Forsch. *24*, 285–292 (1991).
[20] *Wolf, A., Frimmel, F. H.:* The ozone absorption index (OAI) – A fast screening method to determine the efficiency of ozonation processes. Proceedings of the 7th International Symposium: Chemical Oxidation Technology for the Nineties, Nashville, TN, USA, in press (1997).
[21] *Gamsky, D. M., Goldin, A. A., Petrov, E. P, Rubinov, A. N.:* Fluorescence decay time distribution for polar dye solutions with time-dependent fluorescence shift. Biophys. Chem. *44*, 47–60 (1992).
[22] *James, D. R., Ware, W. R.:* Recovery of underlying distributions of lifetimes from fluorescence decay data. Chem. Phys. Lett. *126*, 7–11 (1986).
[23] *Siemiarczuk, A., Wagner, B. D., Ware, W. R.:* Comparision of the Maximum Entropy and Exponential Series Methods for the Recovery of Distributions of Lifetimes from Fluorescence Lifetime Data. J. Phys. Chem. *94*, 1661–1666 (1990).
[24] *Brochon, J.-C., Livesey, A. K., Pouget, J., Valeur, B.:* Data analysis in frequency-domain fluorometry by the maximum entropy method – recovery of fluorescence lifetime distributions. Chem. Phys. Lett. *174*, 517–522 (1990).
[25] *Milne, P. J., Zika, R. G.:* Luminescence quenching of dissolved organic matter in seawater. Mar. Chem. *27*, 147–164 (1989).
[26] *Frimmel, F. H., Abbt-Braun, G.:* Refraktäre organische Säuren in Gewässern. In: Mitteilung XII der Senatskomission für Wasserforschung. VCH Verlagsgesellschaft, Weinheim, 1993.

received 7 July 1997
accepted 5 November 1997

2.1.6 Fluorescence decay of humic substances (HS) - A comparative study

F.H. Frimmel, M.U. Kumke
in: Humic Substances: structure, properties, and uses, G. Davies and E. Ghabbour (eds.), Royal Society of Chemistry, Cambridge 1998, p. 113 - 122.

Die intra- und intermolekularen Prozesse der strahlenden und strahlungslosen Desaktivierung von HS nach erfolgter elektronischer Anregung wurden mittels zeitaufgelöster Fluoreszenzspektroskopie untersucht.
HS zeigen ein höchst komplexes Fluoreszenzabklingverhalten. Die experimentellen Daten wurden sowohl mittels operational-definierten Einzelkomponenten als auch mit Lebenszeitverteilungen ausgewertet (s. auch 2.1.5) und anschließend mit einfachen Modellverbindungen verglichen. Aus Untersuchungen des Fluoreszenzabklingverhaltens in Abhängigkeit von der Emissionswellenlänge wurde ein Modell zur Beschreibung der intramolekularen Desaktivierungsprozesse in HS entwickelt, nachdem insbesondere Energietransferprozesse zwischen verschiedenen HS-Chromophoren die Fluoreszenzabklingkinetik bestimmen.

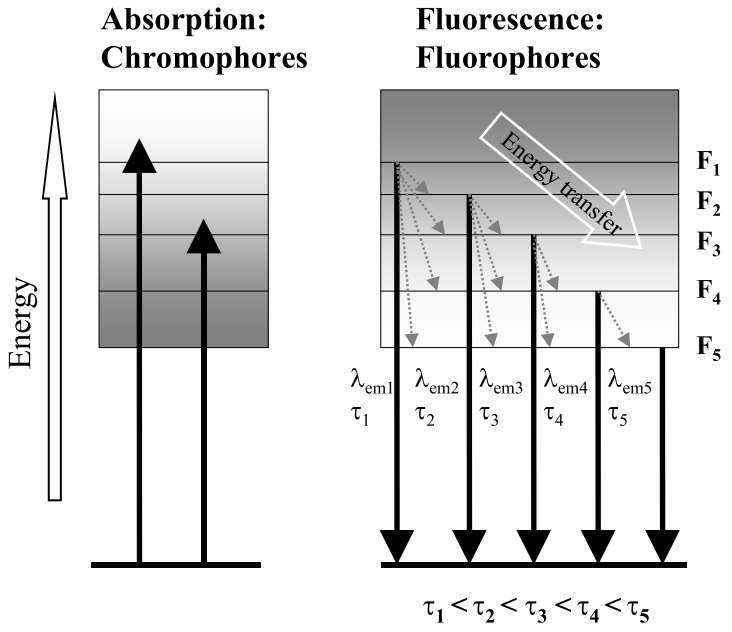

FLUORESCENCE DECAY OF HUMIC SUBSTANCES (HS) – A COMPARATIVE STUDY

Fritz H. Frimmel and Michael U. Kumke

Engler-Bunte-Institute, Division of Water Chemistry, University of Karlsruhe, Richard-Willstätter-Allee 5, 76131 Karlsruhe, Germany

1 INTRODUCTION

The fluorescence of aquatic humic substances (HS) is commonly found in the wavelength region between 275 nm and 600 nm. Up until now mainly steady-state fluorescence techniques including emission, excitation, and synchronous fluorescence spectroscopy were used for the investigation of HS. These techniques were successfully applied in the characterization of HS of different origin and in the investigation of molecular interactions between HS and Xenobiotics. Steady-state fluorescence techniques were applied to characterize HS of different origin, e.g. aquatic and soil-derived HS were distinguished[1-3]. Fluorescence anisotropy techniques were used to monitor association processes of HS[4]. In order to get more specific information on fluorophores present in HS chemometric data evaluation approaches, e.g. rank analysis, were introduced[5]. Using fluorescence techniques conditional binding constants for the interaction of metal ions and HS were determined. Here, especially fluorescence quenching has proven to be a valuable tool[6,7]. The synchronous scan fluorescence technique was applied to investigate the competitive binding of different metal ions and HS[9]. A combination of steady-state fluorescence techniques and chemometric data analysis, e.g. rank analysis, evolving factor analysis, yielded a deeper understanding of the acid-base properties and the metal binding sites of HS[9-13]. The fluorescence quenching approach was further used for the determination of interaction constants of PAH and

HS[14-16]. Here, the extrinsic fluorescence of the probe (PAH) was detected and HS served as a quencher. Based on results obtained in fluorescence quenching experiments models on the micro-organization of HS were proposed[17].

Recently, time-resolved fluorescence techniques were applied for the investigation of the fluorescence decay of HS and of the dynamics of interaction processes between HS and environmental contaminants. The combination of steady-state fluorescence quenching and time-resolved fluorescence quenching experiments has proven that the observed interaction of PAH and HS was due to a static ground state interaction[15,16]. Time-resolved laser-induced fluorescence spectroscopy was applied in the characterization of the complexation processes of actinide and lanthanide ions with HS. The method was used for the speciation of different ion/HS-complexes with hydroxide and carbonate. The great sensitivity and selectivity allowed the distinction between individual carbonato complexes, e.g. $M(CO_3)^+$, $M(CO_3)_2^-$,and $M(CO_3)_3^{3-}$, respectively[18-21]. In these experiments the extrinsic fluorescence of the metal ions was used for the analysis. Only very few results on the investigation of the fluorescence decay of HS itself are published. Time-resolved fluorescence anisotropy measurements of HS were performed in order to monitor changes in size and shape of HS in solution with variation of pH, ionic strength and HS concentration[22]. Langford and Cook investigated the fluorescence of HS quenched upon metal ion complexation[23]. For all HS investigated highly complex fluorescence decay kinetics were found. In Order to account for the high complexity three exponential decay terms were introduced. Although this could only be a rough approximation the approach was successful in describing conformational changes of the HS. Based on the results a three-component model for the binding of metal ions was suggested[23]. The introduction of a small limited number of exponential terms in the analysis a priori assumes that the number of participating fluorescing sites is known. Considering the heterogeneity of HS this has to be considered very carefully. In a more sophisticated approach no initially pre-assumed number of decay terms is introduced in the analysis of the fluorescence decay of HS rather than a large number (i approx. 100). Here, the Maximum Entropy Method (MEM) and the Exponential Series Method (ESM) were used for the analysis of the HS fluorescence decay[24,25]. In both approaches for the fluorescence decay of the HS investigated a tri-modal fluorescence decay time distribution was found.

The scope of the present work was to further evaluate the capabilities of time-resolved fluorescence techniques and of ESM for the characterization of intra- and intermolecular interaction dynamics of HS. In order to achieve the set objective a) a characterization of fluorescing sites inside the HS of different origin is necessary. and b) a deeper understanding of the intramolecular processes involved in the fluorescence decay of HS is inevitable

2 EXPERIMENTAL DETAILS

In the fluorescence experiments the HS samples investigated were of aquatic origin and the concentration of dissolved organic carbon (DOC) was 10 mg/L unless otherwise stated. In the investigation of original waters the samples were filtered (0.45 μm). The isolation procedure for the FA samples was based on the XAD-method of Mantoura and Riley and was described by Abbt-Braun et al.[26]. The concentrations of the model compounds were in the range of 10^{-4} – 10^{-5} M for the benzoic acid derivatives. The lignin sulfonic acid was used at a DOC concentration of 10 mg/L. All model compounds were of analytical purity and used as received. Table 1 summarizes basic experimental parameters of the samples investigated.

Table 1 *Model compounds investigated.*

Name	λ_{ex} *(in nm)*	λ_{em} *(in nm)*	*pH*	*conc.*
Salicylic acid	314	360 - 480	4, 6	10^{-5} M
Benzoic acid	314	400, 450	4, 11	10^{-5} M
Methoxy benzoic acid	314	400, 420	4, 11	10^{-5} M
3,5 Dihydroxy benzoic a	337	400, 420	4, 11	$5 * 10^{-4}$ M
Lignin sulfonic acid	314	370 - 540	7	10 mg/L

In the steady-state experiments a spectral bandwidth of 10 nm and of 9 nm in the time-resolved measurements was applied, respectively. (Perkin Elmer LS 5B Luminescence Spectrometer). A wavelength of 314 nm was chosen for the excitation of the samples in the steady-state experiments as well as in the time-resolved experiments. The steady-state emission spectra were recorded between 330 nm and 550 nm, respectively.

The experimental set-up of the time-resolved fluorescence experiments is described in detail elsewhere[25]. Briefly, a lifetime spectrometer FL 900 (Edinburgh Instruments) was set up in the single photon counting mode. A nitrogen filled flash lamp was used as excitation light source (1 bar, 40 kHz). The experiments were performed with a final count number in the decay peak maximum of $5*10^4$ counts (CPM). In order to control the performance of the instrument such as the stability of the excitation light pulse, the experimental data were collected in five cycles of $1*10^4$ CPM. All fluorescence decay curves were deconvoluted with the time profile of the excitation light flash. The fluorescence measurements were performed with air-saturated samples.

1.1 Data Treatment

The fluorescence decay curves of the HS samples were analyzed by two different approaches using a small number of exponential terms (i max. 4; discrete component approach, DCA) and a large number of exponential decay terms (i max. 100, distribution analysis)[25,27]. The later approach was considered to be superior because no initial assumption about the number of fluorophores had be made and the heterogeneity of the HS samples could be taken into account best. For the distribution analysis an exponential series method (ESM) was applied (commercial software package Edinburgh Instruments, Level 2 software). In the ESM analysis no shift term was applied and a decay time range between 0.1 ns through 50 ns was introduced.

The overall mean fluorescence decay time τ_{mean} of the distribution was calculated following equation (1):

$$\tau_{mean} = \frac{\sum_i A_i \cdot \tau_i}{\sum_i A_i} \qquad (1)$$

3 RESULTS AND DISCUSSION

3.1 General Aspects on the Fluorescence Decay of HS

In figure 1 the fluorescence decays of salicylic acid and a brown water HS are compared. The data evaluation of the fluorescence decay of salicylic acid yielded a fluorescence lifetime of 4.1 ns for all emission wavelength investigated (380 nm < λ_{em} < 480 nm, step width 10 nm) using ESM and DCA, respectively. Contrary to the mono-exponential fluorescence decay of salicylic acid which can be found for most solutions of a single fluorophore the fluorescence decay of HS was highly complex as shown in figure 1. In order to represent the experimental data a number of at least 3 exponential decay terms were necessary (DCA). The disadvantage of analyzing the fluorescence decay data of HS with a small limited number of exponential decay terms is the introduction of a a priori model. Because of the large heterogeneity of HS a self-modeling distribution analysis (ESM) of the fluorescence decay without a pre-assumed number of fluorescence decay terms was preferred in the data evaluation. Starting with a flat distribution of decay times the ESM analysis optimized the amplitudes of each decay time which were evenly spaced in the considered decay time range. In figure 2 the results of the ESM analysis for a brown water FA, lignin sulfonic acid and some benzoic acids derivatives are summarized.

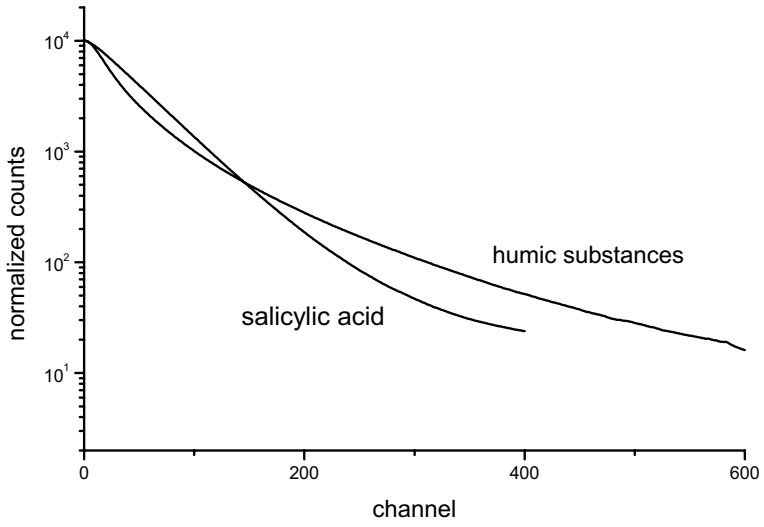

Figure 1 *Comparison of fluorescence decay curves of salicylic acid (λ_{ex}= 314 nm, λ_{em}= 425 nm, pH 6, τ_f = 4.1 ns) and a brown water HS (λ_{ex}= 314 nm, λ_{em}= 420 nm, pH 6.5). The time calibration of the measurement was 0.095 ns /channel.*

The benzoic acid derivatives were chosen because structures related to the compounds are considered as models for fluorophores present in HS[2]. For a homogenous solution of a single compound well resolved narrow peaks were found in the ESM. The mean fluorescence decay time of these peaks agreed with results obtained in a standard analysis fitting a single exponential decay (DCA). For lignin sulfonic acid and for HS in general less resolved broad fluorescence decay time distributions were found in the ESM analysis. Commonly, for HS bi- or tri-modal fluorescence distributions are calculated with mean decay times centered around approximately 1 ns, 4 ns, and 10 ns, respectively[25,28]. There are several reasons possible causing the broad poorly resolved decay time distribution found for HS. Apparent reasons could be the heterogeneity of the HS and the limited capability of ESM to resolve closely located decay times with small fractional intensities (or small differences in their fractional intensities)[27]. Due to the heterogeneity of the HS a large number of different fluorophores in different molecular environments has to be considered. Furthermore, possible intra- and inter-molecular interaction processes, e.g., energy transfer processes have to be

taken into account. For the model compounds which are assumed to be 'fluorecing structures' of HS sharp narrow peaks were calculated.

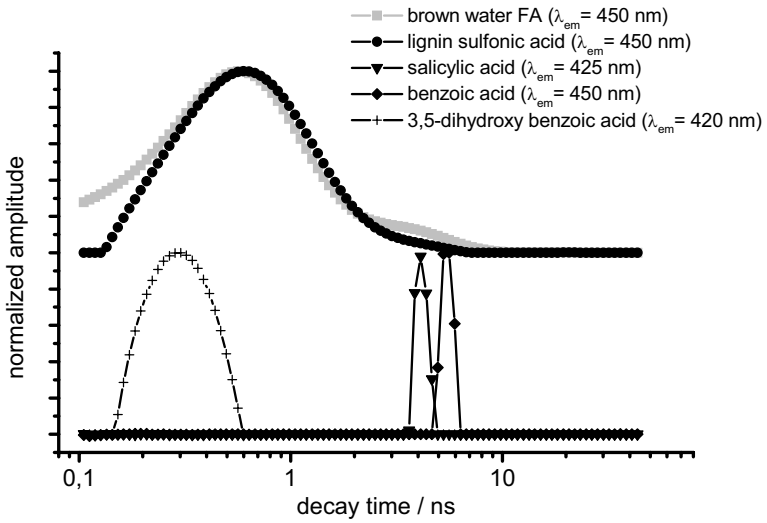

Figure 2 *Shown are the result of an ESM analysis for benzoic acid (pH 4), 3,5-dihydroxy benzoic acid (pH 4), salicylic acid (pH 4), lignin sulfonic acid (pH 7), and brown water FA (pH 7), respectively. For the benzoic acid and its derivatives mean fluorescence decay times of 5.4 ns, 4.1 ns, and 0.2 ns were calculated.*

The found decay times were located within the decay time distribution range found for HS. However, for HS no such sharp peaks were found. This makes the assumption attractive that the fluorophores present in HS are interacting and non-isolated structures. Figure 2 shows the obtained fluorescence decay time distribution of lignin sulfonic acid as well. The found distribution agrees well in the first broad peak centered around 0.7 ns. But no contributions of longer decay times were found. Here, the fluorescence decay time distribution of HS differed significant. The brown water FA was mainly built from plant material. This makes it tempting to relate part of the observed fluorescence decay of the brown water HS to fluorescing structures originating from lignin.

3.2 Fluorescence Decay of HS of Different Origin

In figure 3 the fluorescence decays of HS of different aquatic origin are compared. The brown water and the soil seepage water are dominated by HS derived from plant tissues. For these HS the observed fluorescence decays are quite similar. However, for HS from the River Rhine and from a waste water effluent different fluorescence decay curves were observed. In addition to the plant tissues for the later two HS contributions of bacterial and animal tissue, and of anthropogenic substances like detergens, optical brighteners and other classes of chemical compounds have to be considered as well.

The fluorescence decay observed for HS of the River Rhine resembles at short times (channel < 100) the fluorescence decay of brown water HS and of soil seepage water HS. For longer times the fluorescence decay starts to differ and approaches the decay curve observed for a waste water effluent. It is tempting the attribute the observed time-dependence of the River Rhine fluorescence to a combination of HS structures originating

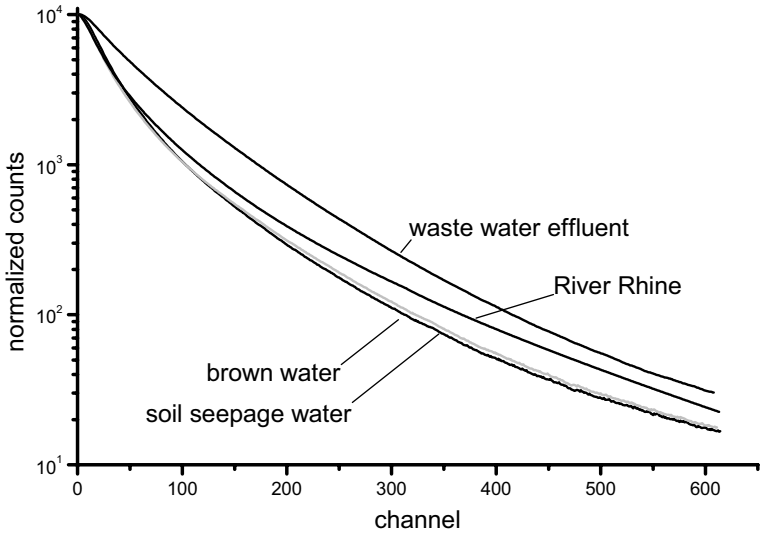

Figure 3 *Fluorescence decay curves of HS of different origin (λ_{ex}= 314 nm, λ_{em}= 450 nm, time calibration: 0.095 ns / channel).*

from (natural) plant tissue and from anthropogenic compounds. The later ones could be considered to influence the fluorescence properties of the waste water HS more strongly.

In order to investigate intramolecular processes involved in the fluorescence decay of HS the influence of the emission wavelength was monitored. In the ESM distribution analysis an increase of the contribution of longer fluorescence decay times was found when the fluorescence emission wavelength was shifted to lower energy. To summarize the observed tendencies for different HS a mean fluorescence decay time τ_{mean} was calculated according to eq.(1). In figure 4 the dependence of τ_{mean} on the emission wavelength is shown. Similar to the difference for the single decay curves monitored at λ_{em}= 450 nm (see figure 3) the observed emission wavelength dependence of τ_{mean} was related to the origin of the HS. For all HS samples investigated τ_{mean} increased with increasing emission wavelength. For the brown water FA and the waste water the mean fluorescence decay time showed an increase up to approx. 470 nm. For higher emission wavelength, however, τ_{mean} decreased slightly again. For the ground water FA the increase of τ_{mean} was found for all emission wavelength investigated.

In order to prove the contribution of lignin-like structures to the fluorescence of HS the dependence of τ_{mean} on the emission wavelength was monitored for a range of 370 nm < λ_{em} < 540 nm. Again, the decay time distribution found in an ESM analysis was shifted with decreasing energy of λ_{em} towards longer decay times. This emphasizes the role of plant-derived materials in the origin of the HS samples investigated.

The comparison with model compounds proved the capabilities of the ESM analysis and showed that the calculated broad decay time distribution pattern are caused by the properties of the HS. Especially, the comparison of the fluorescence decay pattern of lignin sulfonic acid and HS samples showed a close relationship indicating that for the samples investigated lignin-like structures were retained during the origin of the HS. This indicates further that for HS derived form plant materials lignin-related structures still determine the fluorescence of the HS. It is tempting to attribute the observed high complexity of the fluorescence decay of HS to the heterogeneity of the HS structure as well as to intra- and intermolecular interaction processes. Attractive to assume are interaction processes like intra- and intermolecular energy transfer processes the HS matrix. The observed dependence of the ESM decay time pattern on the emission wavelength could be based on such processes. In HS fluorophores with different energy levels are present. Fluorophores with high energy levels can among other deactivation processes either fluoresce or transfer the energy to a fluorophore in the molecular neighborhood which possess suitable acceptor levels. To allow a successful energy transfer several limiting conditions have to be satisfied like overlap of the donor-acceptor orbital, proximity of donor and acceptor etc.

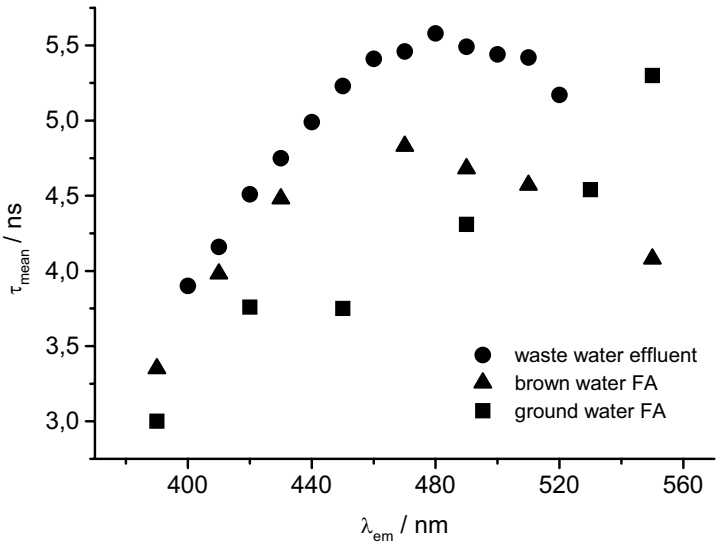

Figure 4 *Dependence of τ_{mean} on the emission wavelength λ_{em}. τ_{mean} was calculated according to eq.(1).*

In case of an energy transfer the decay time of the energy donor would be quenched. For the acceptor a longer decay time could be expected because it is 'excited' by the excitation light flash and by the donor fluorophore which could be considered as a kind of second 'light source'. Because of the great heterogeneity of HS and limiting experimental conditions it was up to now impossible to monitor a build-up kinetic of an acceptor fluorophore. Because of the heterogeneity of HS it is tempting to assume a high density of energy levels of fluorophores. In HS at short emission wavelengths (equal to high energy) a tendency of short decay times was found whereas at longer emission wavelength (equal to lower energy) the mean fluorescence decay time was increased and finally leveled off indicating that at very long emission wavelength (λ_{em} > 480 nm) energy transfer does no longer occur because of the low energy of the fluorophores. More experiments are necessary to prove the suggested model summarized in figure 5.Experiments with chemical modified HS are in progress. Due to oxidation the chemical structure of HS is modified. In case of energy transfer processes present these should be altered by such treatment of the HS. Moreover, the complexation with metal ions and the effect on the observed fluorescence decay of HS is investigated as well and will give a further understanding of the dynamic processes of HS.

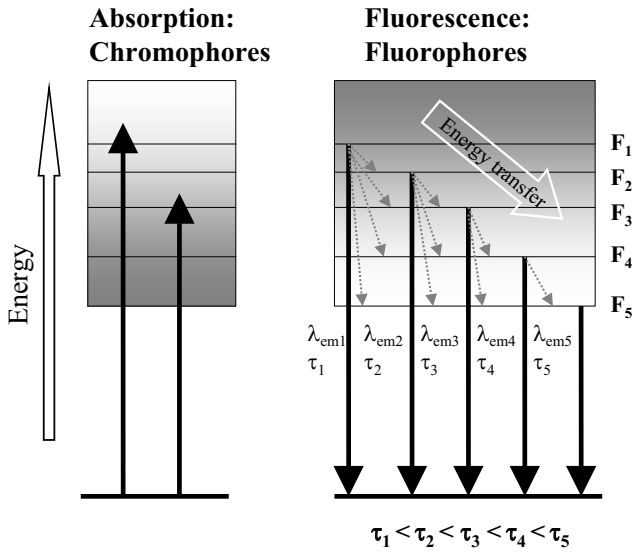

Figure 5 *Schematic representation of the proposed energy transfer interactions inside a HS matrix*.

4 ACKNOWLEDGEMENTS

The German Research Association funded part of the work presented in the ROSIG program. The authors wish to thank Dr. Gudrun Abbt-Braun for the supply of HS samples. They further appreciate the support of the staff of the Engler-Bunte-Institute, Division of Water Chemistry.

5 REFERENCES

1. K.M. Spark, R.S. Swift, *Humic Substances in the Global Environment and Implications on Human Health,* Elesevier, Amsterdam, N. Senesi, T.M. Miano (eds), 1994, 153.
2. N. Senesi, T.M. Miano, M.R. Provenzano, *Humic Substances in the Aquatic and Terrestrial Environment*, B. Allard, H. Boren, A. Grimwall (eds.), *Lecture Notes in Earth Sciences*, Springer Verlag, 1991, **33**, 63.
3. J.J. Mobed, S.L. Hemmingsen, J.L. Autry, L.B. McGown, *Environ. Sci. Technol.*, 1996, **30**, 3061.

4. R.R. Engebretson, T. Amos, R. von Wandruszka*, Environ. Sci. Technol*., 1996, **30**, 990.
5. M.J. Pullin, S.E. Cabaniss, *Environ. Sci. Technol.*, 1995, **29**, 1460.
6. F.H. Frimmel, W. Hopp, Fresenius *Z. Anal. Chem*., 1986, **325**, 68.
7. C.F. Scheck, F.H. Frimmel, A.M. Braun, *Z. Naturforsch.,* 1992, **47b**, 399.
8. S.E. Cabaniss, *Environ. Sci. Technol.,* 1992, **26**, 1133.
9. J.C.G.E. da Silva, M.A. Ferreira, A.A.S.C. Machado, *Talanta*, 1994, **41**, 2095.
10. E. Casassas, I.M.R. Tauler, *Anal. Chim. Acta*, 1995, **310**, 473.
11. J.C.G.E. da Silva, A.A.S.C. Machado, C.S.P.C.O. Silva, *Anal. Chim. Acta,* 1996, **318**, 365.
12. J.C.G.E. da Silva, M.A. Ferreira, A.A.S.C. Machado, F. Rey, *Anal. Chim. Acta,* 1996, **333**, 71.
13. J.C.G.E. da Silva, M.A. Ferreira, A.A.S.C. Machado, *Analyst*, 1997, **122**, 1299.
14 T.D. Gauthier, E.C. Shane, W.F. Guerin, W.R. Seitz, C.L. Grant, *Environ. Sci. Technol.*, 1986, **20**, 1162.
15. M.U. Kumke, H.-G. Löhmannsröben, Th. Roch, *Analyst*, 1994, **119**, 997.
16. U. Zimmermann, H.G. Löhmannsröben, T. Skrivanek, *Remote Sensing of Vegetation and Water, and Standardization of Remote Sensing Methods*, SPIE, G. Cecchi, T. Lamp, R. Reuter, K. Weber (eds.), 1997, **3107**, 239.
17. R.R. Engebretson, R. von Wandruszka, *Environ. Sci. Technol.,* 1994, **28**, 1934.
18. H. Wimmer, J.I. Kim, R. Klenze, *Radiochim. Acta*, 1992, **58/59**, 165.
19. J.I. Kim, R. Klenze, H. Wimmer, W. Runde, W. Hauser, *J. Alloys Comp.*, 1994, **213/214**, 333.
20. P. Panak, R. Klenze, J.I. Kim, *Radiochim. Acta*, 1996, **74**, 141.
21. G. Bidoglio, I. Grenthe, P.Qi, P. Robouch, N. Omenetto, *Talanta*, 1991, **38**, 999.
22. C.H. Lochmüller, S.S. Saavedra, *Anal. Chem.,* 1986, **58**, 1978.
23. R.L. Cook, C.H. Langford, *Anal. Chem.,* 1995, **67**, 174.
24. L.B. McGown, S.L. Hemmingson, J.M. Shaver, L. Geng, *Appl. Spec.,* 1995, **49**, 60.
25. M.U. Kumke, G. Abbt-Braun, F.H. Frimmel, *Acta Hydrochim. Hydrobiol.,* 1998, **26**, 73.
26. G. Abbt-Braun, F.H. Frimmel, P. Lipp *Z. Wasser - Abwasser-Forsch*., 1991, **24**, 285.
27. D.M. Gakamsky, A.A. Godin, E.P. Petrov, A.N. Rubinov, *Biophys. Chem*., 1992, **44**, 47.
28. M.U. Kumke, C.D. Tiseanu, G. Abbt-Braun, F.H. Frimmel, *J. Fluorescence*, 1998, submitted for publication.

2.1.7 Stationary and time-resolved fluorescence for refractory organic substances characterization

M.U. Kumke, F.H. Frimmel
in: Refractory organic substances in the Environment, F.H. Frimmel, G. Abbt-Braun (eds), Wiley-VCH, Weinheim 2002, p. 215 - 231.

Stationäre und zeitaufgelöste Fluoreszenzuntersuchungen wurden mit FA- und HA-Fraktionen von HS unterschiedlicher Ursprungsorte durchgeführt. Als experimentelle Parameter wurden die relative Fluoreszenzeffizienz, die Fluoreszenzabklingzeiten, das globale Emissionsmaximum und die Breite der Emissionsbanden für die verschiedenen HS-Proben bestimmt. Das globale Emissionsmaximum wurde aus Messungen des Totalen Lumineszenz Spektrums (TLS) der jeweiligen HS ermittelt. Die spektroskopischen Daten der FA- und HA-Fraktionen wurden korreliert und es konnte gezeigt werden, dass diese Parameter für FA- und HA-Fraktionen bemerkenswerte Unterschiede zeigen. Die Messungen der TLS unterstrichen die Bedeutung der experimentellen Geräteparameter bei der Aufnahme der HS-Fluoreszenzspektren, da diese im Gegensatz zu Einzelsubstanzen, einen deutlichen Einfluss der gewählten Anregungswellenlängen zeigen so wie weiterhin einem starken Einfluss von Inner-Filter-Effekten (erster und zweiter Ordnung) unterliegen. Die Verwendung von Modellverbindungen, die aus Abbauexperimenten und aus möglichen Vorläuferverbindungen von HS (z.B. Lignine) abgeleitet wurden, lieferte nützliche Informationen zum Verständnis der komplexen Fluoreszenzprozesse in HS. Die Untersuchungen zeigten abermals deutlich, dass in HS verschiedene Fluorophore nebeneinander vorliegen und dass Energietransfer- sowie Protonentransferreaktionen Hauptdesaktivierungskanäle sind und in den Betrachtungen berücksichtigt werden müssen.

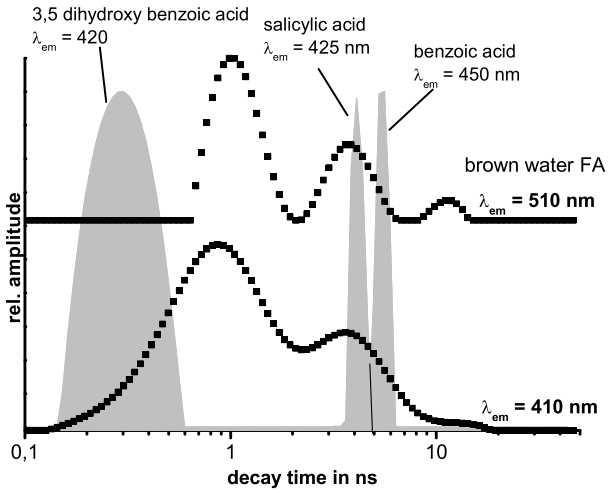

2.11
Stationary and Time-resolved Fluorescence for Refractory Organic Substances Characterization

M. U. Kumke and F. H. Frimmel

Steady-state and time-resolved fluorescence methods were applied to investigate the fluorescence properties of refractory organic substances (ROS) of different origins. Using standard 2D emission and total luminescence spectra, fluorescence maxima, the width of the fluorescence band and a relative fluorescence quantum efficiency were determined. Different trends for fulvic and humic acids were observed indicating differences in the heterogeneity of the sample fractions. The complexity of the fluorescence decay of ROS is discussed and compared to simple model compounds. The effect of oxidation of ROS on their fluorescence properties is discussed as well.

2.11.1
Introduction

The importance of understanding the interaction mechanism between refractory organic substances (ROS; or humic substances (HS)) and xenobiotics has already been pointed out. The ultimate goal is to use fast and simple measurements for an identification of HS (or ROS) and an estimation of their interaction with different xenobiotics in order to predict fate and transport of these chemicals for a fast and reliable risk assessment. Together with other analytical techniques, spectroscopic approaches have been widely used for the investigation of HS and their environmentally relevant reactions. In particular, fluorescence spectroscopy has been applied for the characterization of HS because of its high selectivity and outstanding sensitivity. The non-invasive character of the experiments and the capabilities to monitor reactions on a sub-nanosecond time-scale make it highly attractive for the investigation of HS and reactions of HS with xenobiotics. In the priority program ROSIG, a joined effort was made to deepen the understanding of those reactions. The scope of the work presented here was a thorough investigation of the intrinsic fluorescence properties of HS. A part of the work is closely related to results presented in other chapters of this textbook, particularly to the contributions of Kopinke et al. and Löhmannsröben et al. (Chapters 4.6 and 4.7).

HS are a complex, heterogeneous mixture of compounds originating from degradation of plant and animal tissues. The question of existence and the search of a general structure of HS seem therefore somewhat ill-defined. Although a general structure of HS can not be proposed, a classification scheme of HS and of their reactions with xenobiotics is within reach. This scheme can be based on the information on the precursor materials, on the origin of HS and on their characteristic properties. However, a major drawback in HS research results from the extreme heterogeneity of the samples and the information on HS gained by analytical techniques suffers strongly from this fact. The application of fluorescence spectroscopy as analytical technique can overcome several of the limitations and yield useful information on structure and reactivity of HS. In fluorescence spectroscopy, multidimensional measurements including variations of the excitation wavelength λ_{ex}, emission wavelength λ_{em}, fluorescence lifetime τ_f and fluorescence anisotropy ρ, can be used to gain specific information on complex mixtures like HS. To reach this aim, one has to understand the processes connected with the intrinsic fluorescence properties of HS and has to identify the most important fluorescence parameters needed to address the issues under investigation.

Based on considerations of precursor materials and on degradation experiments, common structural features of HS have been suggested (Liao et al. 1982; Schulten et al. 1987; Senesi et al. 1991; Langvik et al. 1994; Leenheer et al. 1995a, b; Schulten 1995). The importance of specific substructures as potential reaction sites for metal ion complexation and in the formation of hazardous compounds (e. g. disinfection by-products) has also been discussed. The role of aromatic moieties in the formation of mutagenic substances (e. g. MX) during water disinfection was investigated (Langvik et al. 1994). However, experimental approaches using pyrolysis or other intrusive techniques are prone to artifacts. The application of non-invasive techniques such as fluorescence that have already been used for the determination of metal binding to HS or the determination of acid–base properties of HS, seems much more promising (Da Silva and Machado 1994; Casassas and Tauler 1995; Da Silva et al. 1996). Recently, fluorescence spectroscopy, in particular synchronous fluorescence and total luminescence, have been successfully used to distinguish between HS isolated from soil and aquatic origins (Senesi et al. 1989; Patterson et al. 1992; Pullin and Cabaniss 1995; Mobed et al. 1996; Da Silva and Machado 1997) or to determine the concentration of HS in natural fresh waters (Mittenzwey et al. 1996; Hautala et al. 2000). Fluorescence spectroscopy and especially fluorescence quenching have also been applied as powerful tools for the investigation of interactions and transformations of organic xenobiotics in the presence of HS (Kumke et al. 1994; Zimmermann et al. 1997; Doll et al. 1999; Illenseer et al. 1999; Kumke et al. 1999, 2000). A more detailed discussion of these issues is beyond the scope of the work discussed here and is presented in detail in other contributions of this textbook (Chapter 4).

The time course of the fluorescence of HS following pulsed excitation has been investigated using time-resolved fluorescence techniques both in the time and in the frequency domains (Power et al. 1986; Cook and Langford 1995; McGown et al. 1995; Zimmermann et al. 1997). A highly complex fluorescence decay was

reported for the HS investigated. In the data evaluation different models were applied, however only little effort has been spent in a detailed interpretation of the obtained data.

Although, some limitations caused by the heterogeneous character of HS have to be accepted, the outstanding sensitivity and selectivity make fluorescence a method of choice for the investigation of HS and their reactions. However, further knowledge is required for a thorough understanding of the intra- and intermolecular processes relevant to the fluorescence of HS. Therefore, the objectives of the work were to gain deeper insight in the intrinsic processes connected to the fluorescence of HS and to identify suitable parameters for a meaningful interpretation of these phenomena on the molecular level. Ultimately, based on these parameters, it was to develop a classification scheme for HS applicable for the prediction of environmentally relevant reactions. Therefore, the first step is to elucidate the processes directly and indirectly influencing the intrinsic HS fluorescence.

2.11.2 Experimental Details

In this study the fulvic acid (FA) fractions and humic acid (HA) fractions of a brown water (HOx, x = 10, 13, 14), of a soil seepage water (BS1), of a ground water (FG1), of a waste water effluent (ABVx, x = 2, 3), and of a production effluent from brown coal industry (SV1) were investigated. The isolation procedure and basic characterization data for these samples are described in detail elsewhere (Frimmel and Abbt-Braun 1999, and Chapter 1.1). FA and HA stock solutions were diluted to a final concentration of 10 mg/L. For the determination of the fluorescence efficiencies, the optical densities of the samples and of the salicylic acid reference were adjusted to 0.1 to achieve equal absorption conditions and to minimize inner filter effects (IFE). The pH value of the samples was adjusted to seven using a standard phosphate buffer. The ionic strength of the samples was approx. 0.02 M.

The fluorescence experiments were carried out using a FL/FS900CDT combined fluorescence lifetime spectrometer (Edinburgh Analytical Instruments, UK). The instrument was equipped with a 450-W Xenon arc lamp (steady-state operation), a pulsed nitrogen flash lamp (time-resolved mode), and red-sensitive photomultiplier tubes which were operated in the single photon counting mode. The instrument is described in detail elsewhere (Kumke et al. 1998a, b). Because of the extremely heterogeneous character of the HS samples an absolute determination of fluorescence quantum yields could not be done in a straightforward manner. Therefore, the quantum efficiencies relative to the fluorescence of salicylic acid were determined and are further referred to as relative fluorescence quantum efficiencies (RFQE). For the determination of the quantum efficiencies, the fluorescence spectra of the HS samples were recorded in the wavelength range of 300 nm $< \lambda_{em} <$ 600 nm using an excitation wavelength λ_{ex} = 295 nm. The spectra were corrected for the spectral response of the detector.

The total luminescence was determined in the wavelength range of 275 nm $< \lambda_{ex} <$ 401 nm ($\Delta\lambda$ = 3 nm) and 281 nm $< \lambda_{em} <$ 545 nm ($\Delta\lambda$ = 1 nm). The spectra were recorded using a spectral band-pass of 1.8 nm both for the excitation and the emission monochromators. All fluorescence spectra were corrected for instrumental response functions (e. g. quantum efficiency of the photomultiplier tube) using a calibration function provided by Edinburgh Instruments. For the determination of the relative fluorescence quantum efficiencies (RFQE) spectral band-passes of 1 nm were used in the excitation and emission path. The dwell time of the measurements was set to 0.5 s.

2.11.3 Results and Discussion

2.11.3.1 Steady-state Fluorescence of Humic Substances

In general, the fluorescence of HS is measured as a featureless, broad-banded spectrum with emission maxima approx. between 420 nm $< \lambda_{em,\,max} <$ 480 nm. Unlike the absorption spectra, which show a continuous increase from low absorbance in the NIR to high absorption in the UV, the fluorescence excitation spectra exhibit a

Tab. 2.11-1. Comparison of the fluorescence maxima and width of emission bands for different FA and HA.

HS*	RFQE† (%)	Emission maximum‡ (cm^{-1})	Width of emission band‡ (cm^{-1})
ABV2 FA	4.7	22800	7801
ABV2 HA	2.8	22889	9104
ABV3 HA	5.1	22225	8407
SV1 FA	1.8	22760	7409
SV1 HA	2.8	23880	7576
FG1 FA	9.4	21948	6918
FG1 HA	6.4	20942	7499
BS1 FA	3.0	21920	6609
BS1 HA	2.1	22177	7429
HO10 FA	3.0	21513	6929
HO10 HA	1.6	21275	7900
HO13 FA	3	21981	6748
HO14 FA	1.9	21879	6902

* The fluorescence measurements were performed with an excitation wavelength λ_{ex} = 295 nm and an optical density at λ_{ex} of 0.1.

† Relative fluorescence quantum efficiency (RFQE) determined relative to the fluorescence of salicylic acid which was set to 100 %

‡ Determined by a Gaussian fit of the emission spectrum

maximum between 315 nm $< \lambda_{ex} <$ 370 nm. However, it has to be emphasized that the fluorescence intensity and the shape of the fluorescence spectrum of humic substances are strongly dependent on experimental parameters. Due to the presence of a continuous absorption spectrum with gradually increasing absorbance to the UV region the induced inner filter effects are wavelength-dependent. This applies both to the excitation and the emission wavelengths used. Furthermore, the fluorescence efficiency and the shape of the fluorescence spectrum are strongly dependent on the excitation wavelength, and also on characteristics of the solution of those. The pH is probably the most important one to be considered.

In Tab. 2.11-1 the results for the fluorescence maxima and the width of the emission band are compared. After converting the spectra from the wavelength scale to the wavenumber scale, it was found that all spectra were almost perfectly Gaussian shaped. A data analysis using a mono modal Gaussian distribution function yielded fits with correlation coefficients $r^2 > 0.98$. The band width of the emission spectra of HA fractions was broader than that of the related FA fraction. Although HA are considered of larger size and a higher content of aromatic structures the location of the emission maxima for HA and FA are similar in the steady-state spectra.

While the location of $\nu_{em,max}$ of the FA exhibited small differences, the $\nu_{em,max}$ of HA showed larger variations (Tab. 2.11-1). To reduce the number of factors that influence the fluorescence spectrum, the total luminescence (TL) spectra were recorded.

In Fig. 2.11-1 the TL spectrum of a brown water FA (HO14 FA) is shown. In the upper part of the figure the 3D representation is shown and in the bottom part a 2D projection in the form of a contour plot of the same spectrum is given. The increase in the color intensity corresponds to the increase of the fluorescence intensity. In the TL spectrum, the influence of the excitation wavelength on the observed fluorescence can be seen. This can be used as an additional selection parameter (Mobed et al. 1996). Since the excitation wavelength was changed during the experiment and the absorption spectra of the HS samples were different, the adjustment to a constant pre-selected optical density was not applicable. Instead, the concentration of dissolved organic carbon (DOC) was adjusted to 10 mg/L for all samples and the pH was set to 7. From the obtained TL spectra excitation/emission pairs were obtained for maximum fluorescence intensity. For all samples investigated the $\lambda_{ex,max}/\lambda_{em,max}$ data pairs determined are shown in Fig. 2.11-2.

Similar to the data already discussed with the 2D spectra, in the TL measurements of the HA fractions a relatively large variation in the position of the wavelength pair corresponding to the maximum fluorescence intensity was observed, while on the other hand, only a very small variation was found for the FA fractions. For all the FA investigated the $\lambda_{ex,max}/\lambda_{em,max}$ data pairs were located in a small wavelength range of $\Delta\lambda_{ex} \approx 15$ nm and $\Delta\lambda_{em} \approx 15$ nm (the gray area in Fig. 2.11-2).

The fluorescence quantum yield is also a useful parameter for the identification of substances and for the characterization of interactions with its molecular environment. For HS in general a determination of a quantum yield is ill-defined due to the heterogeneous character of the material. However, a relative quantum

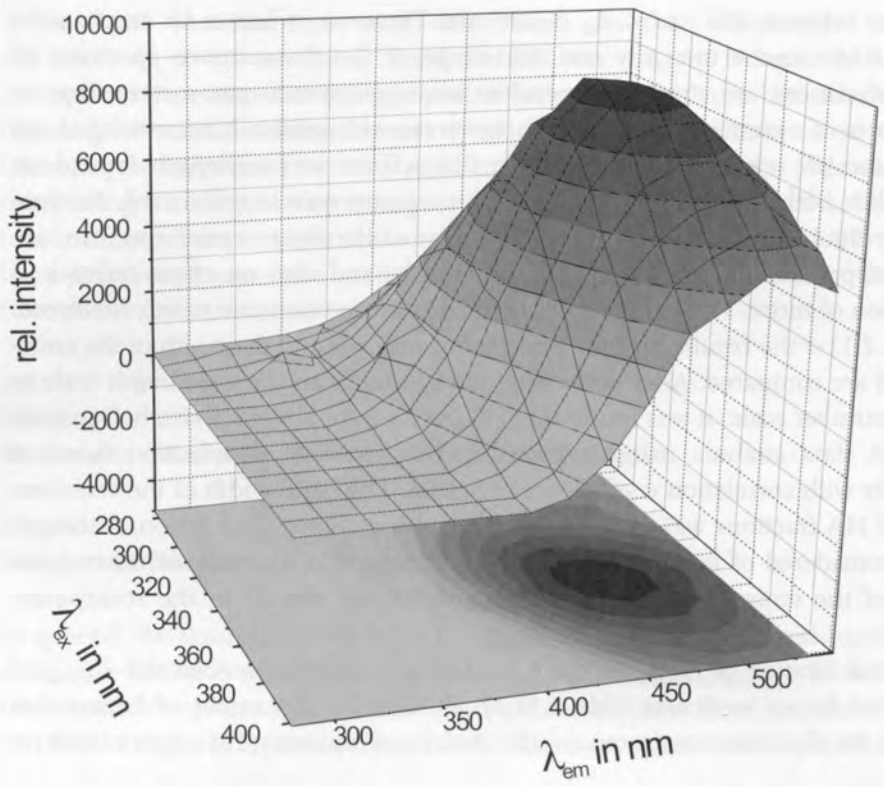

Fig. 2.11-1. Total luminescence spectrum of brown water HO14 FA (10 mg/L DOC; pH 7).

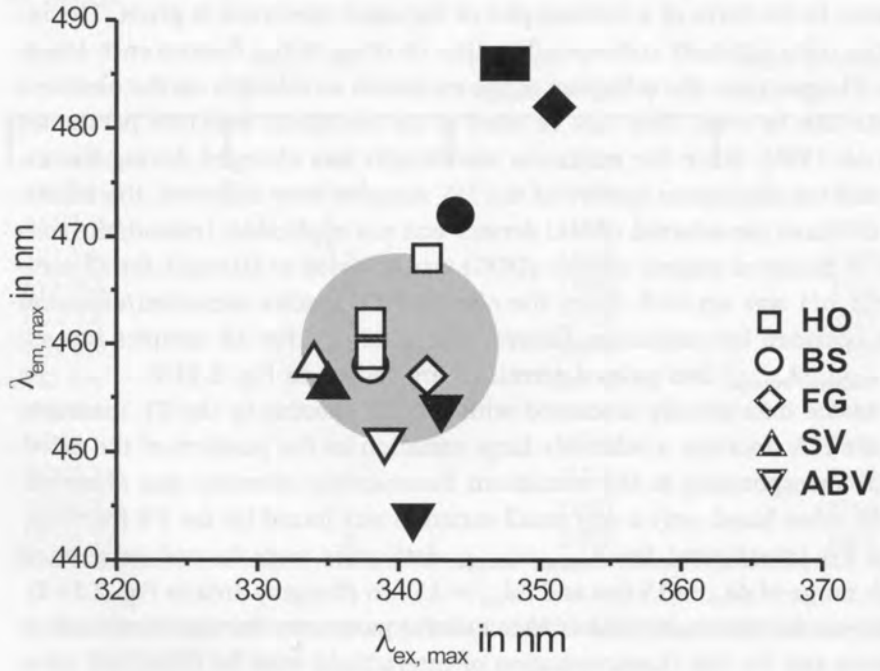

Fig. 2.11-2. Wavelength pairs of $\lambda_{ex,max}$ and $\lambda_{em,max}$ for HA (filled symbols) and FA (open symbols) fractions determined from the corresponding TL spectra (10 mg/L DOC; pH 7).

efficiency under well-defined experimental conditions can be obtained and used for the comparison of different HS. The determination of a relative fluorescence quantum efficiency (RFQE) has the advantage that it is independent of the instrument used and therefore, data acquired in different laboratories could be easily compared. To circumvent the tedious calibration with fluorescence standards a simple relative measurement with salicylic acid used as a reference compound was performed. The optical density of all samples was adjusted to 0.1 at $\lambda = 295$ nm and the quantum efficiency was determined relative to salicylic acid which was set as 100 %. In Tab. 2.11-1 the RFQE of the HA and FA investigated are compared. Compared to that of salicylic acid, the fluorescence quantum efficiencies of all HS samples were quite low with an average value of approx. 3 %. Significantly higher values were found for the ground water samples FG1 FA and FG1 HA. As a general trend, it was found that the FA had a slightly higher RFQE compared to the related HA.

According to Korshin et al. (1997) the absorption at 203 nm and at 254 nm can be ascribed to the benzenoid (Bz) and electron transfer (ET) bands of aromatic compounds. It was proposed that due to the presence of polar functional groups (e. g. carbonyl, carboxyl, and ester groups) attached to the aromatic units the intensity of the ET band can be affected to a large extent while the intensity of the Bz band is much less sensitive. On the other hand, non-polar groups were not presumed to affect the ET band. In HS the vast majority of groups active in fluorescence can be considered of benzenoid character (Senesi et al. 1991). The fluorescence of benzene is weak, but it can be enhanced in the presence of attached functional groups, like hydroxyl or carboxyl groups. Hence, a correlation of the fluorescence change and the degree of substitution with functional groups obtained from absorption experiments was investigated. In Fig. 2.11-3 a correlation of the observed location of the fluorescence maximum ($\lambda_{ex} = 295$ nm) with the ratio of the Bz and ET bands is shown.

For the majority of HS investigated a reasonable correlation between the fluorescence maximum and ratio of Bz/ET bands is found, this holds especially for the FA fractions. The correlation with the RFQE was less successful when all data points are considered (Fig. 2.11-4). However, the FG1 sample had originally a high iron content which made the sample very unstable and caused precipitation over time. Therefore, it is possible that the fraction of the HS which remained in solution had a relative higher fluorescence capability causing an overestimation of the RFQE. This could explain the observed large RFQE compared to the other FA and HA investigated.

2.11.3.2
Time-resolved Fluorescence of Humic Substances

In addition to the steady-state fluorescence measurements time-resolved experiments were performed and the fluorescence decay of different HS was measured. These results are described in detail elsewhere and will be only summarized here (Kumke and Frimmel 1996; Frimmel and Kumke 1998; Kumke et al. 1998a, b; Kor-

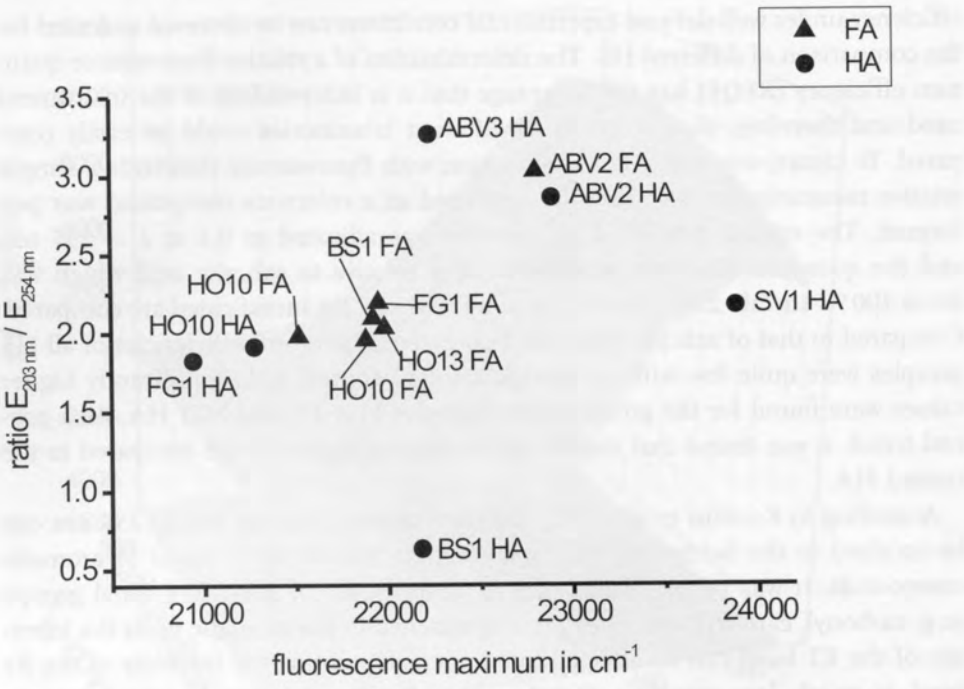

Fig. 2.11-3. Correlation of the fluorescence emission maximum $\nu_{em,max}$ (with $\lambda_{ex} = 295$ nm) with the ratio of the absorption at $\lambda = 254$ nm and $\lambda = 203$ nm.

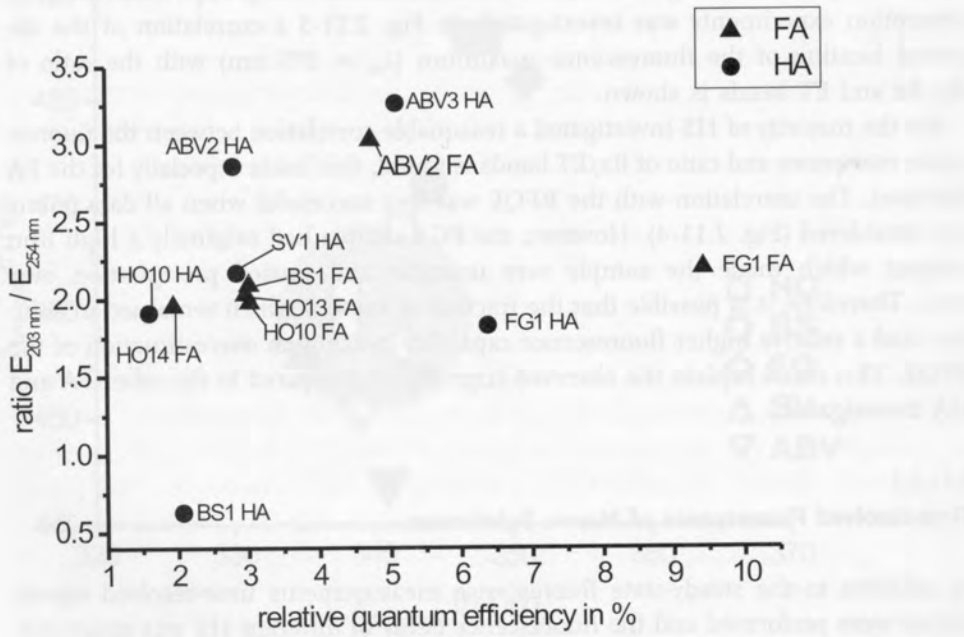

Fig. 2.11-4. Correlation of the RFQE (with $\lambda_{ex} = 295$ nm) with the ratio of the UV–visible absorption at $\lambda = 254$ nm and $\lambda = 203$ nm for FA fractions (triangles) and HA fractions (circles).

shin et al. 1999). In general, for all samples a highly complex decay kinetic was found. Hence, sophisticated data analysis was absolutely required for an adequate data processing. The applicability of simplified approaches in which only a single decay time was used for the characterization of HS is very limited and a part of the information contained in the fluorescence decay data of HS is lost (Zimmermann et al. 1997; Illenseer 1999). Therefore, two different approaches were pursued in the decay data analysis. In the discrete component approach (DCA) a pre-set number of exponential decay terms was used. However, due to the heterogeneous character of HS the correct estimation of the pre-set number of decay components is crucial. Therefore, an alternative data analysis approach was used, in which no presumed number of decay components was introduced. In this case, the fluorescence decays were evaluated with decay time distributions using the exponential series method (ESM) and the maximum entropy method (MEM).

In Fig. 2.11-5 a typical fluorescence decay of HS investigated is shown. Two features are immediately obvious from Fig. 2.11-5. First, the fluorescence decay is of higher order and second, the decay processes involved occur on a nanosecond time-scale (approx. < 50 ns).

In general, two main reasons have to be considered to explain the observed complexity of the fluorescence decay of HS:

(1) HS are a complex, heterogeneous mixture of compounds; and
(2) various excited-state processes including conformational re-orientation as well as intra- and intermolecular proton transfer reactions.

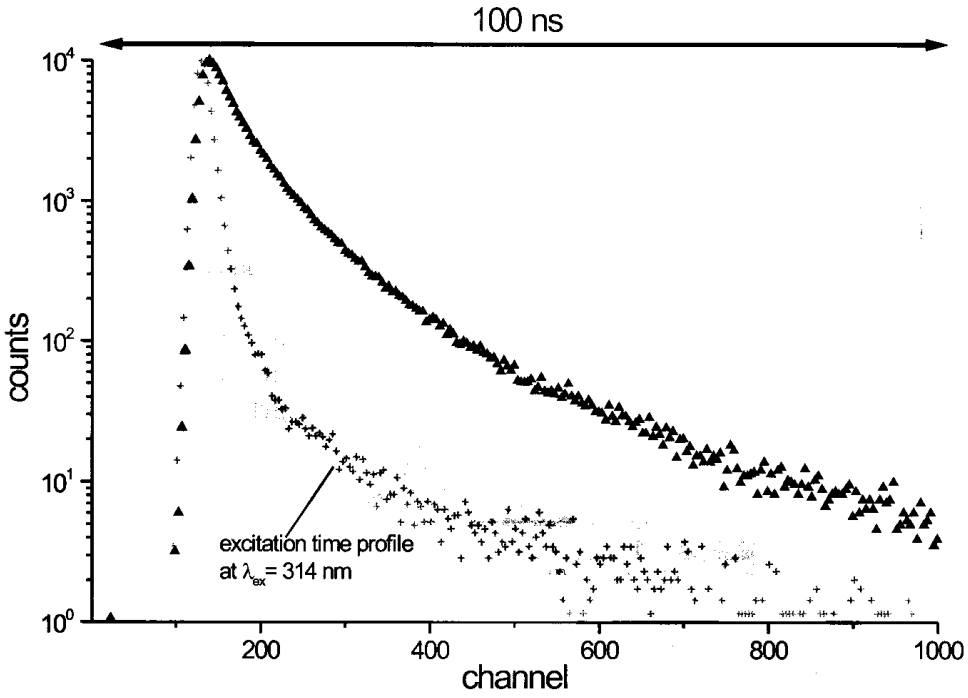

Fig. 2.11-5. Fluorescence decay of soil seepage water BS1 FA (λ_{ex} = 314 nm, λ_{em} = 450 nm).

To account for the complexity in the DCA at least 3 exponential terms were necessary to obtain a reasonable data fit in terms of χ^2 and the randomness of the residuals. In the DCA mean decay times in the range of $\tau_1 = 1$ ns $\pm$ 0.5 ns, $\tau_2 = 4$ ns $\pm$ 1 ns, and $\tau_3 = 10$ ns $\pm$ 5 ns with the largest contribution of τ_2 were found for all HS investigated. It was already emphasized that the calculated decay times can not be readily ascribed to real chemical entities or substructures in the HS, and therefore, are operationally-defined (Kumke et al. 1998a). In the decay time distribution analysis, the starting point was a flat distribution of 100 decay times (Kumke et al 1998a, b). The use of the distribution analysis was preferred since the heterogeneity of the sample could be better taken into account and thus, was less biased. It is interesting to note that in the decay time distribution analysis (ESM and MEM) a three-modal distribution of decay times was found as well. The mean decay times of each distribution peak were very similar to the decay times found in the DCA. In addition to decay times the width of the distribution peaks was obtained as well. It is tempting to relate the obtained peak width of the decay time distributions with the heterogeneity of the sample under investigation. For example, for some samples, (e. g. the waste water effluent ABV2 and ABV3 fractions), narrower peaks were found. It is tempting to assume for those samples a different stage of humification compared to the brown water or soil seepage water samples which are in an advanced humification stage.

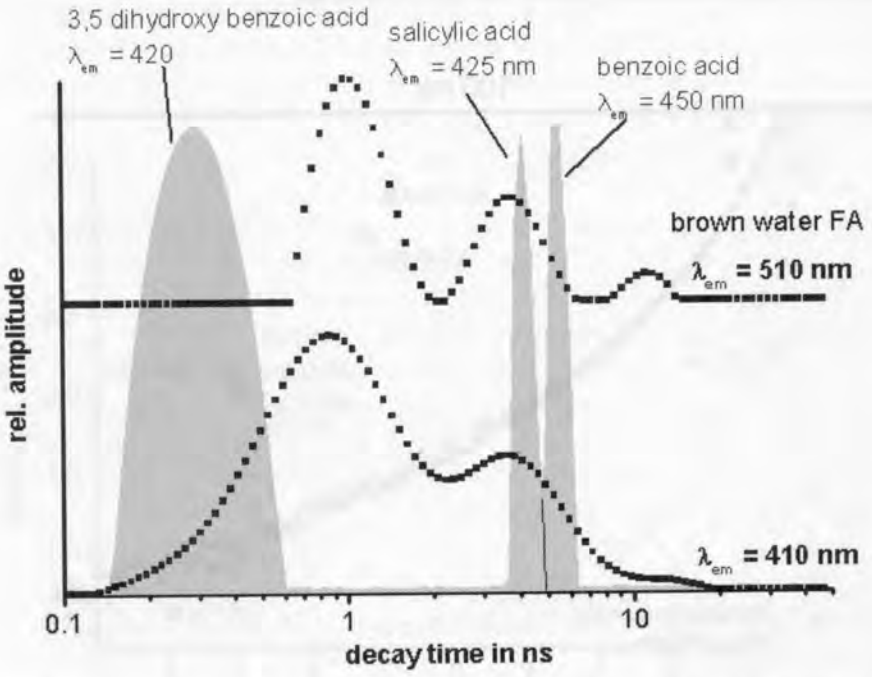

Fig. 2.11-6. Fluorescence decay distribution of brown water HO10 FA ($\lambda_{ex} = 314$ nm). Compared are the obtained fluorescence decay times of simple aromatic carboxylic acids. For all data evaluations the analysis was started with a flat distribution of 100 decay times in the time range between 0.1 ns $< \tau_i <$ 50 ns.

The complexity of the fluorescence of HS is further reflected in the strong dependence of the fluorescence decay on λ_{ex} and λ_{em}. For the relative contribution of the mean decay time $\tau_2 = 4.3$ ns values between 40 % and 75 % were determined in the wavelength range of 400 nm $< \lambda_{em} <$ 520 nm for SV1 FA (Kumke et al. 1998b). On the other hand, HO10 FA showed for $\tau_2 = 4.1$ ns in the same emission wavelength range a much smaller variation.

Individual compounds (e. g. salicylic acid), measured and analyzed under the same conditions, showed in distribution analyses sharp and mono modal distributions (Fig. 2.11-6). Using simple compounds as reference compounds, which are also assumed to be similar to precursors or building blocks for HS (e. g. aromatic carboxylic acids containing additional hydroxyl groups), a strong overlap with the second peak (around 4 ns) of the decay time distribution of HS was found (Fig. 2.11-6) (Frimmel and Kumke 1998).

2.11.3.3

Fluorescence of Chemically Altered Humic Substances

Different HS altered by ozone, combined UV/H_2O_2, or by chlorination have also been investigated with spectroscopic methods (Korshin et al. 1998; Win et al. 2000). Under mild oxidation conditions (e. g. low ozone dose) an enhancement of the fluorescence intensity as well as a hypsochromic shift of the fluorescence maximum were observed. Furthermore, an overall shift from shorter to longer fluorescence decay times was observed in the distribution analysis of time-resolved fluorescence data. In combination with size-exclusion chromatography the results were discussed in terms of an apparent breakdown of larger HS molecules into smaller fragments (Korshin et al. 1998).

In Fig. 2.11-7 the ratio of the TL spectra before and after chlorination of a brown water FA (HO10 FA) is shown. In the wavelength range marked by the light gray area (with a maximum around $\lambda_{ex} = 300$ nm and $\lambda_{em} = 410$ nm) a strong increase of the fluorescence intensity was observed since decreasing color corresponds to an increase in fluorescence enhancement. With an initial concentration of 5 mg/L DOC the fluorescence intensity was increased by more than a factor of two. It is interesting to note that the wavelength range, in which the increase of the fluorescence intensity was observed, was almost independent of the oxidation process applied. Similar results were found in treatments of HS with low ozone doses (Win et al. 2000). In Fig. 2.11-7 the spectral location of the TL spectrum of a simple aromatic acid (salicylic acid) is shown as well (black lines). The emission maximum of salicylic acid falls well within the spectral range of the fluorescence increase caused by the oxidation treatment. For HS isolated from natural waters (e. g. bog water or soil seepage water) the observed fluorescence increase upon oxidation was strong while for HS isolated from a waste water effluent only a minor increase was observed. Very similar results were obtained for HS hydrolyzed under controlled experimental conditions. In case of HS, which was closely related to plant material precursors in the first place (e. g. brown water), a well pronounced fluorescence increase was observed in the same spectral regions of the TL spec-

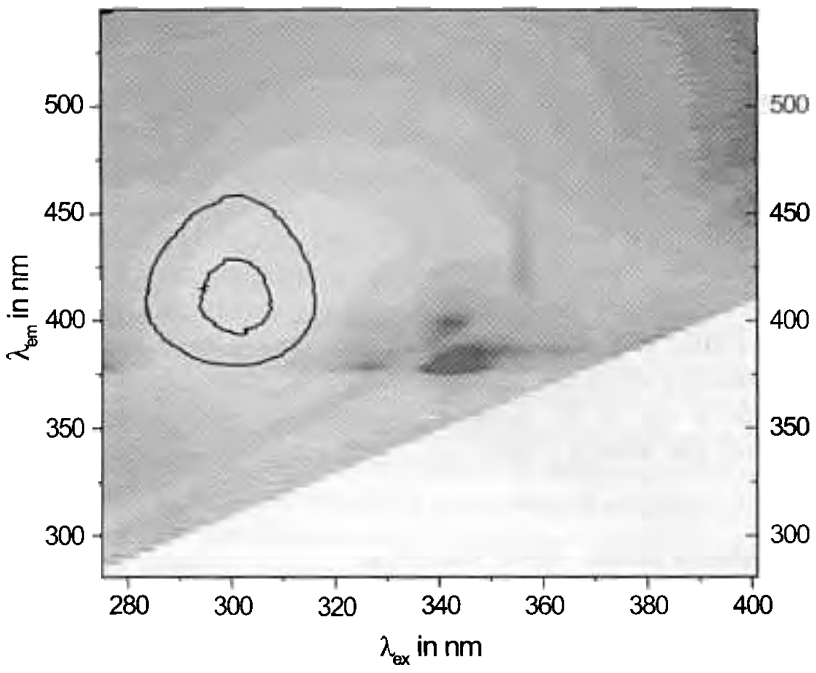

Fig. 2.11-7. Ratio of the total luminescence spectra of HO10 FA before and after chlorination (at a molar ratio of 5:10 (DOC/Cl)). Compared is the TL spectrum of salicylic acid (black contour lines). Because of the chlorination a fluorescence increase was observed (light area).

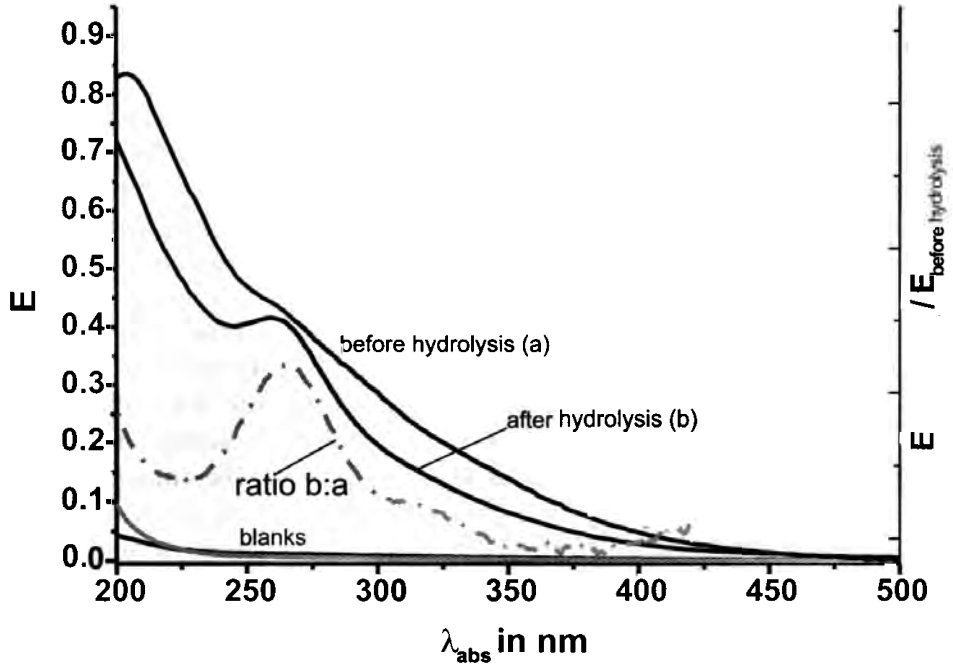

Fig. 2.11-8. UV-visible absorbance spectra of brown water HO14 FA before and after hydrolysis (6 M NaOH at 100 °C; 5 mg/L DOC; pH of the solution was adjusted to pH 7 using an ion exchange resin).

trum. HS samples isolated from a waste water showed almost no change in the fluorescence properties upon hydrolysis. For those HS samples the UV-visible spectrum stayed unchanged as well (Kumke et al. 2001).

On the other hand, for samples with a possible strong contribution of plant material precursors (e. g. HS of brown water or soil seepage water), the unresolved absorbance spectrum was noticeably altered and a distinct peak appeared. In Fig. 2.11-8 the absorbance spectra of a brown water FA before and after hydrolysis are shown together with the ratio of both spectra. Due to the hydrolysis new spectral features evolve from the unstructured background. The new absorption band at $\lambda = 265$ nm and a shoulder at $\lambda = 315$ nm appear to be correlated with the observed increase in fluorescence intensity. This is indicated by the comparison of fluorescence excitation spectra with a detection wavelength around 410 nm, which corresponds to the maximum of the observed fluorescence increase (Kumke et al. 2000b).

2.11.4 Conclusions

The simplest fluorescence approach used in HS studies is the measurement of standard 2D emission and excitation spectra. However, simple fluorescence intensity measurements of HS suffer from several limitations associated with the issues of comparability among different experimental conditions (concentration, pH, and chosen λ_{ex}) and the proper consideration of inner filter effects (Mobed et al. 1996; Illenseer et al. 1999). The latter limitation can be overcome without complex correction methods by using diluted solutions of HS. With the introduction of an external standard the dependence on experimental parameters can be minimized and the determination of a relative quantum efficiency becomes feasible. The usage of simple aromatic acids and their derivatives (e. g. salicylic acid, benzoic acid) appears justified because the substances can be considered as precursors in the generation processes or, alternatively, as degradation products in the breakdown of HS. It is therefore reasonable to assume these entities in HS as significant contributors in HS fluorescence and the use as reference fluorophores seems to be clearly justified. Compared to salicylic acid, the fluorescence quantum efficiencies of the aquatic HS were found to be small (between 1 % and 5 % for the majority of HS investigated). Only for the FA and HA isolated from a ground water (FG1) higher values were obtained. There may be two main reasons for the low fluorescence intensities of HS:

1. Only a small number of chromophores, which are present in a reasonable high percentage since the color of HS is intense, are actively participating in fluorescence, or
2. the fluorescence is reduced due to effective radiationless deactivation processes.

The fluorescence spectra were strongly dependent on the excitation wavelength. This supports the assumption that more than one type of fluorophore contributes

to the emission. Depending on the excitation wavelength, at least two groups of fluorophores have to be considered. One group is excited in the UV region (group I: 225 nm $< \lambda_{ex} <$ 300 nm) and the second group of fluorophores is excited at longer wavelengths (group II). At excitation wavelengths $\lambda_{ex} <$ 300 nm both, group I and group II were excited. For group I, a relative weak fluorescence emission in the wavelength range 300 nm $< \lambda_{em} <$ 370 nm was observed. Of course, within each group further heterogeneity due to slightly different chemical environments is present and this leads also to a spectral broadening. In the TL measurements the complete steady-state fluorescence characteristics of HS (of group II fluorophores in the first place) was obtained. It was found that although the HS were isolated from different aquatic sources with quite different histories, the location of the emission and excitation maxima of the fluorescence spectra were very similar. This is especially valid for the FA fractions of the HS investigated which indicates that similar fluorophores are involved (at least for group II). The width of the emission band should be indicative for the chemical (or environmental in terms of different functional groups) heterogeneity of the fluorescing sites. It is interesting to note that for the FA fractions very similar band widths were found while the HA fractions showed a larger variation in this parameter. It is tempting to attribute those effects to differences in molecular size and to a narrower distribution of fluorescing sites in smaller molecules. The observed Stokes shift between excitation maximum and emission maximum was huge. For all HS investigated, a Stokes shift >100 nm was found (see Fig. 2.11-2). Again, for the FA fractions only a small variation was observed for this parameter. The large Stokes shift is a further indication that the fluorescence of HS is influenced (or determined) by the presence of intra- and intermolecular reactions in the excited state. An interpretation of the observed fluorescence of HS as only a sum of fluorophores is therefore definitely an oversimplification.

The strong involvement of intra- and intermolecular reactions in the fluorescence properties of HS is further supported by the results of the time-resolved fluorescence measurements. The experiments showed a highly complex fluorescence decay. The results obtained under variation of experimental conditions and after chemical modification of the HS support the interpretation in terms of intra- and intermolecular processes (e. g. proton transfer, conformational reorientation) (Frimmel and Kumke 1998; Kumke et al. 1998 b; Illenseer et al. 1999).

The fluorescence intensity was significantly increased upon chemical reactions (e. g. oxidation, hydrolysis). In combination with size-exclusion experiments (SEC) it was shown that due to the chemical treatment the apparent molecular size was decreased. It is tempting to connect the observed increase in fluorescence intensity with a decrease in the structural disorder due to the reduction in molecular size. There are two aspects of structural disorder that have to be considered: disorder due to heterogeneity of compounds and disorder due to the flexibility of each HS molecule. Upon degradation into smaller fragments, the overall flexibility of the fluorophores is reduced and because of the presence of less vibrational and rotational degrees of freedom the fluorescence is increased. Furthermore, the introduction of hydroxyl and carboxyl groups in the aromatic fluorophores could lead to

an increase as well. Recently, the absorption spectra of HS were discussed in terms of the Urbach theory (Mullins et al. 1992; Mullins and Zhu 1992; Illenseer et al. 1999). The results reported here add further evidence that HS have to be considered as highly structure-disordered systems.

Acknowledgments

The authors would like to thank Dr. G. Abbt-Braun for her marvelous work on the isolation and basic characterization of the humic substances used. They are further thankful to Axel Heidt for his engagement in the sampling campaigns. The financial support by the Deutsche Forschungsgemeinschaft within the ROSIG priority research program is greatly appreciated.

References

Casassas, E., Marques, I., Tauler, R. (1995) Study of acid–base properties of fulvic acids using fluorescence spectrometry and multivariate curve resolution methods. Anal. Chim. Acta **310**, 473–484.

Cook R. L., Langford C. H. (1995) Metal ion quenching of fulvic acid fluorescence intensities and lifetimes: nonlinearities and a possible three-component model. Anal. Chem. **67**, 174–180.

Da Silva, J. C. G. E., Machado, A. A. S. C. (1994) A combination of synchronous fluorescence spectroscopy with chemometric treatment and internal standards in non-aqueous potentiometric titrations of fulvic acids. Talanta **41**, 2095–2104.

Da Silva, J. C. G. E., Machado, A. A. S. C., Silva, C. S. P. C. O. (1996) Simultaneous use of evolving factor analysis of fluorescence spectral data and analysis of pH titration data for comparison of the acid–base properties of fulvic acids. Anal. Chim. Acta **318**, 365–372.

Da Silva, J. C. G. E., Machado, A. A. S. C. (1997) Procedure for the classification of fulvic acids and similar substances based on the variation with pH of their synchronous fluorescence spectra. Analyst **122**, 1299–1305.

* Doll, T. E., Frimmel, F. H., Kumke. M. U., Ohlenbusch, G. (1999) Interaction between natural organic matter (NOM) and polycyclic aromatic compounds (PAC) – comparison of fluorescence quenching and solid phase micro extraction (SPME). Fresenius J. Anal. Chem., **364**, 313–319.

* Frimmel, F. H., Kumke, M. U. (1998) Fluorescence decay of humic substances (HS) – A comparative study. In: Davies, G., Ghabbour, E. (Eds.) Humic Substances: Structure, Properties, and Uses. Royal Society of Chemistry, Cambridge, pp. 113–122.

Frimmel, F. H., Abbt-Braun, G. (1999) Basic characterization of reference NOM from central Europe – similarities and differences. Environ. Int. **25**, 191–207.

Hautala, K., Peuravuori, J., Pihlaja, K. (2000) Measurement of aquatic humus content by spectroscopic analyses. Water Res. **34**, 2246–258.

Illenseer, C., Löhmannsröben, H.-G., Skrivanek, Th., Zimmermann, U. (1999) Laser spectroscopy of humic substances. In: Davies, G., Ghabbour, E. (Eds.) Understanding Humic Substances – Advanced Methods, Properties and Applications. Royal Society of Chemistry, Cambridge, pp. 129–145.

Korshin, G. V., Li, C.-W., Benjamin, M. M. (1997) Monitoring the properties of natural organic matter through UV spectroscopy: a consistent theory. Water Res. **31**, 1787–1795.

Korshin, G.V., Kumke, M.U., Li, C.-W., Benjamin, M.M., Frimmel, F.H. (1999) Influence of chlorination on chromophores and fluorophores in humic substances Environ. Sci. Technol. **33**, 1207–1212.

* Kumke, M.U., Löhmannsröben, H.-G., Roch, T. (1994) Fluorescence quenching of polynuclear aromatic compounds by humic acid. Analyst **119**, 997–1001.

* Kumke, M.U., Frimmel, F.H. (1996) NOM – Experienced by time-resolved spectroscopy. In: Drozd, J., Gonet, S.S., Senesi, N., Weber, J. (Eds.) The Role of Humic Substances in the Ecosystems and in Environmental Protection, Proceedings of the 8th Meeting of the IHSS 8, Wroclaw, Poland, September 9–14, 1996, PTSH, Wroclaw, 1997, pp. 525–531.

* Kumke, M.U., Abbt-Braun, G., Frimmel, F.H. (1998a) Time-resolved fluorescence measurements of aquatic natural organic matter. Acta Hydrochim. Hydrobiol. **26**, 73–81.

Kumke, M.U, Tiseanu, C., Abbt-Braun, G., Frimmel, F.H. (1998b) Fluorescence decay of natural organic matter (NOM) – Influence of fractionation, oxidation, and metal ion complexation. J. Fluorescence. **8**, 309–318.

* Kumke, M.U., Zwiener, C., Abbt-Braun, G., Frimmel, F.H. (1999) Spectroscopic characterization of fulvic acid fractions of a contaminated groundwater. Acta Hydrochim. Hydrobiol. **27**, 409–415.

* Kumke, M.U., Frimmel, F.H., Ariese, F., Gooijer, C. (2000) Fluorescence of humic acids (HA) and pyrene–HA complexes at ultra-low temperature. Environ. Sci. Technol. **34**, 3818–3823.

Kumke, M.U., Specht, C.H., Brinkmann, T., Frimmel, F.H. (2001) Alkaline hydrolysis of humic substances – Spetroscopic and chromatographic investigations. Chemosphere **45**, 1023–1031.

Langvik, V.-A., Akerback, N., Holmbom, B. (1994) Characterization of aromatic structures in humic and fulvic acids. Environ. Int. **20**, 61–65.

Leenheer, J.A., Wershaw, R.L., Reddy, M.M. (1995a) Strong-acid, carboxyl-group structures in fulvic acid form the Suwannee River, Georgia. 1. Minor structures. Environ. Sci. Technol. **29**, 393–398.

Leenheer, J.A., Wershaw, R.L., Reddy, M.M. (1995b) Strong-acid, carboxyl-group structures in fulvic acid form the Suwannee River, Georgia. 2. Major structures. Environ. Sci. Technol. **29**, 399–405.

Liao, W., Christman, R.F., Johnson, J.D., Millington, D.S. (1982) Structural characterization of aquatic humic material. Environ. Sci. Technol. **16**, 403–410.

McGown L.B., Hemmingsen S.L., Shaver J.M., Geng L. (1995) Total lifetime distribution analysis for fluorescence fingerprinting and characterization. Appl. Spectrosc. **49**, 60–66.

Mittenzwey, K.-H., Reuter, R., Gitelson, A. (1996) Analysis of dissolved humic substances in eutrophic waters using the fluorescence of natural samples: calculations and experiments. Int. Revue ges. Hydrobiol. **81**, 1–12.

Mobed, J.J., Hemmingsen, S.L., Autry, J.L., McGown, L.B. (1996) Fluorescence characterization of IHSS humic substances: total luminescence spectra with absorbance correction. Environ. Sci. Technol. **30**, 3061–3065.

Mullins, C.O., Mitra-Kirtley, S., Yifu, Z. (1992) The electronic absorption edge of petroleum. Appl. Spectrosc. **46**, 1405–1411.

Mullins, C.O., Yifu, Z. (1992) First observation of the Urbach tail in a multicomponent organic system. Appl. Spectrosc. **46**, 354–356.

Patterson, H.H., Cronan, C.S., Lakshman, S., Plankey, B.J., Taylor, T.A. (1992) Comparison of soil fulvic acids using synchronous scan fluorescence spectroscopy, FTIR, titration and metal complexation kinetics. Sci. Tot. Environ. **113**, 179–196.

Power J.F., LeSage R., Sharma D.K., Langford C.H. (1986) Fluorescence lifetimes of the well characterized humic substance, Armdale fulvic acid. Environ. Technol. Lett. **7**, 425–430.

Pullin, M.J., Cabaniss, S.E. (1995) Rank analysis of the pH-dependent synchronous fluorescence spectra of six standard humic substances. Environ. Sci. Technol. **29**, 1460–1467.

Schulten, H.-R. (1995) The three-dimensional structure of humic substances and soil organic matter studied by computational analytical chemistry. Fresenius J. Anal. Chem. **351**, 62–73.

Schulten, H.-R., Abbt-Braun, G., Frimmel, F.H. (1987) Time-resolved pyrolysis field ionization mass spectrometry of humic

material isolated from freshwater. Environ. Sci. Technol. **21**, 349–357.

Senesi, N., Miano, T. M., Provenzano, M. R., Brunetti, G. (1989) Spectroscopic and compositional comparative characterization of I. H. S. S. reference and standard fulvic and humic acids of various origin. Sci. Tot. Environ. **81/82**, 143–156.

Senesi, N., Miano, T. M., Provenzano, M. R. (1991) Fluorescence spectroscopy as a means of distinguishing fulvic and humic acids from dissolved and sedimentary aquatic sources and terrestrial sources. In: Allard, B., Boren, H., Grimvall (Eds.) Humic Substances in the Aquatic and Terrestrial Environment. Lectures Notes in Earth Science, pp. 63–73.

Tiseanu, C, Kumke, M. U., Frimmel, F. H., Klenze, R., Kim, J. I. (1998) Time-resolved spectroscopy of fulvic acid and fulvic acid complexed with Eu^{3+} – a comparative study. J. Photochem. Photobiol. A, **117**, 175–184.

Win, Y. Y., Kumke, M. U., Specht, C. H., Schindelin, A. J., Kolliopoulos, G., Ohlenbusch, G., Kleiser, G., Hesse, S., Frimmel, F. H. (2000) Influence of oxidation of dissolved organic matter (DOM) on subsequent water treatment processes. Water Res. **34**, 2098–2104.

Zimmermann, U., Löhmannsröben, H.-G., Skrivanek, Th. (1997) Absorption and fluorescence spectroscopic investigations of PAC/humic substance-interactions in water. In: Cecchi, G., Lamp, T., Reuter, R., Weber, K. (Eds.) Remote Sensing of Vegetation and Water, and Standardization on Remote Sensing Methods. Proc. SPIE **3107**, pp. 239–249.

* Denotes work carried out as part of the DFG priority programme.

2.2 Wechselwirkungen von Huminstoffen mit polyzyklischen aromatischen Kohlenwasserstoffen (PAK)

Organische Xenobiotika, wie z.B. Pestizide, stellen aufgrund der Persistenz vieler dieser Verbindungen eine wachsende Gefährdung der Umwelt dar. Deshalb sind Untersuchungen zur Mobilität und Bioverfügbarkeit dieser Verbindungen von großem Interesse, um Gefährdungspotentiale einzuordnen, Renaturierungen von kontaminierten Standorten zu überwachen und um leistungsstarke Modelle für deren Verhalten in der Umwelt zu entwickeln. In natürlichen Gewässern und im Boden stellen HS einen Hauptreaktionspartner für hydrophobe Xenobiotika dar. Durch Sorption an HS werden Mobilität und Bioverfügbarkeit dieser maßgeblich verändert. PAK gehören zur Gruppe der hydrophoben Xenobiotika und besitzen aufgrund ihrer mutagenen und krebserregenden Wirkung ein großes Gefährdungspotential. Sie werden bei unvollständigen Verbrennungsprozessen (z.B. Hausbrand oder KFZ-Betrieb) gebildet und sind inzwischen ubiquitär. Andererseits besitzen PAK ausgezeichnete Fluoreszenzeigenschaften, die sie als molekuare Fluoreszenzsonde zur Untersuchung der Wechselwirkungen zwischen HS und hydrophoben Xenobiotika wertvoll machen. In den eigenen Arbeiten wurden durch die Anwendung von stationären und zeitaufgelösten Fluoreszenzmethoden einerseits und der Mikrofestphasenextraktion andererseits die Wechselwirkungen zwischen hydrophoben Xenobiotika und HS charakterisiert. Es zeigte sich, dass

- eine Unterscheidung von konzentrationsbezogenen und aktivitätsbezogenen Effekten bei der Bindung von hydrophoben Xenobiotika an HS gemacht werden sollte,
- neben den im wesentlichen durch hydrophob / hydrophil bestimmten Wechselwirkungen auch zusätzlich noch spezifische in Betracht gezogen werden müssen, sofern die Xenobiotika funktionelle Gruppen enthalten,
- durch die Kombination von Fluoreszenzmethoden und Mikrofestphasenextraktion zwei in ihrer Stärke verschiedene Wechselwirkungen unterschieden werden können,
- für den Fall der schwachen Wechselwirkung die molekulare Umgebung der Xenobiotika in ihrer Polarität der von niederen Alkoholen entspricht.

Die folgenden Veröffentlichungen beschreiben Untersuchungen der Wechselwirkungen zwischen HS und hydrophoben Xenobiotika und sind in 2.2.1 bis 2.2.4 dargestellt:

8. K. Mackenzie, A. Georgi, M.U. Kumke, F.-D. Kopinke
   Environ. Sci. Technol., 2002, **36**, 4403 - 4409.
   Sorption of pyrene to dissolved humic substances and related model polymers. 2. SPME and FQT as analytical methods.

9. G. Ohlenbusch, M.U. Kumke, F.H. Frimmel
Sci. Tot. Environ., 2000, **253**, 63 - 74.
Sorption of phenols to dissolved organic matter investigated by solid phase microextraction.

10. M.U. Kumke, F.H. Frimmel, F. Ariese, C. Gooijer
Environ. Sci. Technol., 2000, **34**, 3818 - 3823.
Fluorescence of humic acids (HA) and pyrene-HA complexes at ultralow temperature.

11. T.E. Doll, F.H. Frimmel, M.U. Kumke, G. Ohlenbusch
Fres. J. Anal. Chem., 1999, **364**, 313 - 319.
Interaction between natural organic matter (NOM) and polycyclic aromatic compounds (PAC) - comparison of fluorescence quenching and solid phase micro extraction (SPME).

Bezug zur aktuellen Literatur Die wirksamen Mechanismen und Modelle zur Beschreibung sind in den vergangenen Jahren kontinuierlich weiterentwickelt worden. So konnte durch direkte Messung der laser-induzierten Fluoreszenz von Pyren gezeigt werden, dass Pyren im fettreichen Gewebe von Nematoden akkumuliert wird. Durch die Anwesenheit von HS wird die Bioakkumulation reduziert [61]. Mittels quantitativen Struktur-Wirkungsbeziehungen (*quantitative structure activity relationship*, QSAR) wurden verschiedene Eigenschaften von HS mit ihrer Wirksamkeit in Bezug auf eine verringerte Bioakkumulation untersucht [62] (s. 2.2.2). Vor allem zwischen dem aromatischen Charakter der HS und der Bioverfügbarkeit von PAK ergaben sich bemerkenswert gute Korrelationen. So konnte die Abnahme der Toxizität verschiedener PAK gegenüber *Daphnia Magna* durch die Anwesenheit von HS mit dem aromatischen Charakter der HS korreliert werden [63]. Eine verringerte Bioverfügbarkeit von hydrophoben Xenobiotika resultiert zusätzlich durch die starke Sorption an an Oberflächen gebundenen HS. Die Sorption von hydrophoben Xenobiotika an adsorbierte HS war im Vergleich zu gelösten HS erhöht. So wurde durch die Adorption von HS an Kaolinit die Sorption von Pyren deutlich vergrößert und entsprechend die Mobilität der hydrophoben Xenobiotika verringert [64].
Neben dem aromatischen Charakter, der für die hydrophoben Wechselwirkungen mit PAK dominierend zu sein scheint, müssen für den Fall, dass die Xenobiotika funktionelle Gruppe enthalten, spezifische Wechselwirkungen in Betracht gezogen werden (s. 2.2.2). Für 1-Naphthol wurden gute Übereinstimmung zwischen Resultaten aus Fluoreszenzlöschexperimenten und Dialyse-Methoden für die Sorption an HS gefunden [65]. Für Chinolin und Naphthalin ergaben beide Methoden allerdings etwas unterschiedliche Ergebnisse, besonders wenn der Einfluss von Solventsbedingungen, wie z.B. pH-Wert oder Ionenstärke, betrachtet wurde [66, 67]. Gründe für die beobachtete Abhängigkeit von Solventsparametern können Konformationsänderungen der HS, Aggregation der HS und Aussalzen des Analyten sein [67]. Die Beiträge von spezifischen Wechselwirkungen sind mögliche Gründe für die teilweise beobachtete Nichtlinearität der Adsorptionsisothermen von hydrophoben Xenobiotika an HS [68]. Die Anwendung der Fluoreszenzlöschung zur Bestimmung von Wechselwirkungskonstanten wird weiterhin kontrovers diskutiert (s. 2.2.1). Die Einflüsse von Innerfiltereffekten (erster und zweiter Ordnung), die Kombination von statischen und dynamischen Löschprozessen sowie die vollständige Fluoreszenzlöschung im Falle einer

Grundzustandskomplexbildung zwischen HS und Fluorophor (statischer Löschmechanismus, Bildung eines *dark complex*) müssen weiter aufgeklärt werden (s. 2.2.3) [69–71]. Die Bestimmung der Wechselwirkungskonstanten zwischen PAK und HS aus Fluoreszenzlöschexperimenten hat den Vorteil, dass keine Auftrennung der Reaktionspartner notwendig ist und somit auch keine Störung des Sorptionsgleichgewichtes induziert wird. Die Fluoreszenzlöschmethode ist experimentell schnell und direkt anwendbar und darüber hinaus ist die Sensitivität für Untersuchungen im Ultraspurenbereich bestens geeignet [72, 73]. Dies ist besonders für Vor-Ort-Untersuchungen wichtig.
Auch für mechanistische Untersuchungen sind analytische Methoden zu bevorzugen, die die zu untersuchenden Gleichgewichte möglichst wenig verändern. Spektroskopische Methoden, aber auch einige Extraktionsmethoden wie z.B. die Mikrofestphasenextraktion (*Solid Phase Microextraction*, SPME) sind geeignete Untersuchungsmethoden. Die PAK sind eine Verbindungsklasse, die sowohl repräsentativ für hydrophobe Xenobiotika ist und gleichzeitig hervorragende Fluoreszenzeigenschaften besitzt, womit sie bevorzugt als Fluoreszenzsonden in mechanistischen Untersuchungen der Wechselwirkungen zwischen hydrophoben Xenobiotika und HS eingesetzt werden können (s. 2.2.1 bis 2.2.4) [69, 74, 75].

2.2.1 Sorption of pyrene to dissolved humic substances and related model polymers. 2. SPME and FQT as analytical methods

K. Mackenzie, A. Georgi, M.U. Kumke, F.-D. Kopinke
Environ. Sci. Technol., 2002, **36**, 4403 - 4409.

Die Sorption von Pyren als Modellsubstanz für unpolare Xenobiotika an HS und an Polyacrylsäureester wurde qualitativ und quantitativ mittels Mikrofestphasenextraktion (SPME) und Fluoreszenzlöschung (FQT) charakterisiert. In den Fluoreszenzexperimenten wurde die intrinsische Fluoreszenz des Pyrens als Sonde zur Beschreibung der wirksamen Wechselwirkungen eingesetzt. Für den Fall der Sorption von Pyren an Polyacrylsäureester konnte durch die Veränderung der Intensitätsverteilung im Pyrenfluoreszenzspektrum auf die Polarität der molekularen Umgebung des Pyrens geschlossen werden.
Der Vergleich von SPME und FQT verdeutlichte, dass die mit verschiedenen Methoden erhaltenen Sorptionskoeffizienten nicht einfach verglichen werden können. So ist es bei dem Vergleich von SPME und FQT wichtig zu beachten, dass mit der SPME erhaltenen Resultate proportional zur Aktivität eines Analyten, die mit der FQT gewonnenen aber proportional zur Konzentration des Analyten sind.

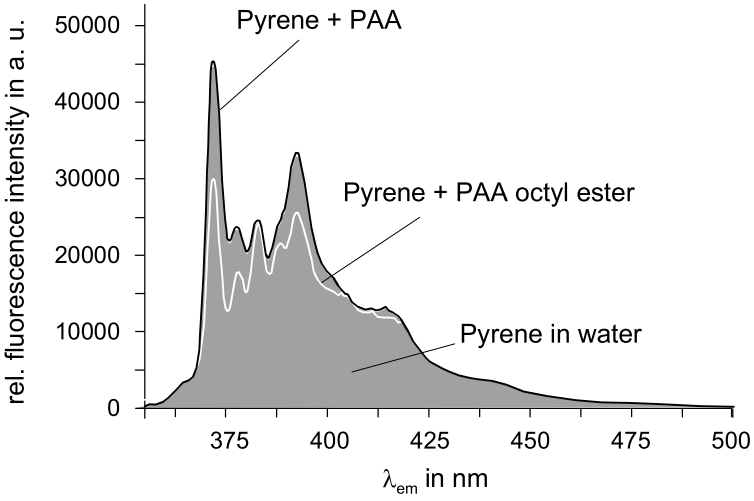

nach:
F.-D. Kopinke, A. Georgi, K. Mackenzie, M.U. Kumke
in: Refactory Organic Substances in the Environment; F.H. Frimmel, G. Abbt-Braun (eds), Wiley 2002.
Sorption and chemical reactions of PAHs with dissolved humic substances and related model polymers

Environ. Sci. Technol. **2002**, *36*, 4403−4409

Sorption of Pyrene to Dissolved Humic Substances and Related Model Polymers. 2. Solid-Phase Microextraction (SPME) and Fluorescence Quenching Technique (FQT) as Analytical Methods

KATRIN MACKENZIE,† ANETT GEORGI,† MICHAEL KUMKE,‡ AND FRANK-DIETER KOPINKE*,†

Department of Remediation Research, UFZ-Center for Environmental Research Leipzig-Halle, Permoserstrasse 15, D-04318 Leipzig, Germany, and Department of Physical and Theoretical Chemistry, Potsdam University, Karl-Liebknecht-Strasse 24−25, D-14476 Golm, Germany

Sorption coefficients for pyrene on dissolved humic substances and on poly(acrylic acid) esters as well-defined model polymers were determined using solid-phase microextraction (SPME) and the fluorescence quenching technique (FQT). The results of both analytical methods were compared and theoretically evaluated, which led to the conclusion that the sorption coefficients measured by SPME and FQT are inevitably different: SPME measures activity-based and FQT concentration-based sorption coefficients. The environmental relevance of the two types of sorption coefficients is discussed. FQT is inappropriate to measure sorption coefficients for pyrene with the synthetic sorbents. Inspection of the vibrational structure of the fluorescence spectra of those solutions indicates a highly hydrophobic microenvironment of pyrene. This can be explained by an intra- or intermolecular agglomeration of hydrophobic moieties forming a favorable host for hydrophobic solutes.

Introduction

Retardation and mobilization of hydrophobic organic compounds (HOCs), caused by sorption or complexation to particulate and dissolved organic matter respectively, determine the fate of many pollutants in the environment. Therefore, sorption processes have been the subject of numerous scientific studies (*1*, *2*). When sorption of HOCs from the aqueous phase to particulate sorbents is measured, simple phase-separation techniques (such as centrifugation) have proved to be sufficient. For dissolved sorbents, such a phase separation is more complicated and may affect the sorption equilibrium. Therefore, when one is measuring interactions of solutes with dissolved sorbents, it is necessary to evaluate carefully the experimental methods to be applied. The predominant customary techniques are the fluorescence quenching technique (FQT) (*3*, *4*), the fast solid-phase extraction (SPE) or reversed phase (RP) method (*5*, *6*), flocculation (*7*, *8*), solubility enhancement (*9*−*12*), dialysis (*13*,*14*), and the gas-purging or headspace-partitioning method (*15*, *16*).

FQT is the most frequently used method for studying sorption phenomena. FQT is a true in-situ method, based on the quenching of the fluorescence of a fluorophore [e.g., polycyclic aromatic hydrocarbons (PAHs)] interacting with dissolved polymers. The fluorescence intensity is considered to be a measure of the concentration of the freely dissolved fluorophore. Problems may result from the absorption of excitation and fluorescence light by the polymer (the inner filter effect), which has to be corrected for. Furthermore, the applicability of the method is limited to fluorescence-active compounds, it is a single-component method (i.e., mixtures of analytes in a sample cannot be measured), and the assumption of the formation of a "dark complex" between fluorophore and dissolved humic substances (DHS) is not undisputed (*17*). On the other hand, the method is very sensitive and can be used for time-resolved measurements, which may be useful for studying sorption kinetics.

Laor and Rebhun (*7*, *8*) proposed a simple complexation−flocculation method to determine binding coefficients of organic compounds to DHS. The method is based on the precipitation of the humic substances by adding a coagulant, for example, aluminum sulfate. After the flocculation is complete, the fraction of the analyte remaining in the clarified supernatant can be determined by conventional methods. The authors claim that the DHS−HOC complexes are sufficiently stable to survive the flocculation procedure. Nevertheless, it may strongly affect the DHS conformation and charge. It is well-known from many previous studies that changing the pH value or the ionic strength in the aqueous solution may result in significant changes of the binding coefficients (*4*, *18*). Therefore, it must be taken into account that flocculation may disturb the original complexation equilibrium.

The fast SPE technique uses the selective adsorption of freely dissolved HOCs on a reversed-phase column, whereas the more hydrophilic DHS−HOC complex passes through the column. Again, the separation step is a significant interference with the sorption equilibrium. The removal of the freely dissolved analyte fraction causes an equilibrium shift toward desorption. If the desorption kinetics is in the time scale of the column passage (some minutes), then it gives rise to an underestimation of the sorption coefficients.

Most of the techniques available have various shortcomings, and none of the methods listed is able to meet all of the demands simultaneously. We decided to use solid-phase microextraction (SPME), a relatively new technique, primarily for the reason that it does not interfere with the original sorption equilibrium. The application of SPME for measuring sorption coefficients on DHS was first described in 1995 by Kopinke et al. (*19*) and further developed by the same working group (*20*−*23*).

The monograph edited by Pawliszyn (*23*) presents an up-to-date overview of various SPME applications. The two possible sampling modes, headspace sampling and the direct solution sampling, produced identical results in our studies. Headspace sampling is the mode of choice for solutions containing dissolved organic matter (DOM), such as humic substances or other dissolved polymers, because it avoids any direct contact between the fiber coating and the sample (*22*) and, therefore, any fouling of the SPME fiber.

When we chose the method to determine the sorption coefficients for dissolved sorbents, we attached great importance to avoiding interference with the sorption equi-

* Corresponding author phone: ++49 (0)341 235 3264; fax: ++49 (0)341 235 2492; e-mail: kopinke@san.ufz.de.
† UFZ-Center for Environmental Research Leipzig-Halle.
‡ Potsdam University.

10.1021/es010310x CCC: $22.00
Published on Web 09/07/2002

librium and therefore decided to use SPME and FQT and compare the results obtained with these two methods. It is known from the literature that sorption coefficients measured by different analytical methods can differ markedly (*24*, *25*). This paper is meant as a continuation of part 1 already published in this journal (*26*), which dealt with the structure−property correlation of humic substances and soluble model polymers. In this continuation we concentrate on the comparison of the analytical methods, their theoretical evaluation, and their applicability in studying sorption processes in the presence of DOM.

Materials and Methods

Solvents, poly(acrylic acid) (PAA) samples (2, 8, 250, and 450 kDa), and pyrene (99+%) were purchased from Aldrich Chemicals. PAA esters −$(CH_2CH[COOH])_n(CH_2CH[COOR])$− bearing 5−15% aliphatic or aromatic ester substituents (R) were prepared by acidic esterification of the dry PAA sample using the corresponding alcohol or phenol. The preparation and workup procedures are described in detail in ref *26*. The humic substances investigated were a commercially available, coal-derived humic acid (HA) from Roth Ltd. (Germany) (Com-HA) and an aquatic HA (BW-HA) from the brown-water lake Hohlohsee in Germany (*26*).

SPME. For sorption experiments, the analyte was spiked as an ethanolic solution into the various aqueous solutions containing dissolved organic matter (in our case humic acids or PAA esters) (c_{DOM} = 50−1000 mg L^{-1}; pH 2−7; 0.004 M NaN_3; IS = 0.01 M NaN_3 + NaCl). The final pyrene concentration in SPME experiments was 15 μg L^{-1} in reference solutions and 30 μg L^{-1} in solutions containing DOM. DOM solutions containing pyrene were prepared by dissolving the solid polymer in diluted NaOH, followed by further dilution with deionized water, pH adjustment, and NaN_3 addition. When PAA esters with aromatic substituents (phenyl, naphthyl) were dissolved, hydrolysis was observed starting at pH >9; hydrolysis of aliphatic PAA esters was negligible. Therefore, the aromatic PAA esters were dissolved under conditions where they were not subjected to hydrolysis reactions: minimum dissolution time at pH ≤9. After purging with N_2, the solutions were spiked with the ethanolic solution of the analyte (final ethanol concentration <0.2 vol %). The SPME was performed either in the direct solution extraction mode or in the headspace mode (*22*, *23*). For the direct mode, the fiber was equilibrated with the DOM/pyrene solution for 6 h; for the headspace mode, the fiber was placed above the solution (sampling time = 18 h). Conditions were chosen where the depletion of the analytes from the sample and their gaseous fractions was insignificant: a 7 μm PDMS fiber from Supelco and 80−100 mL sample volume. After equilibration, the loaded fiber was transferred for pyrene desorption into a gas chromatographic (GC) injector (splitless injection at 290 °C for 3 min). For quantitative analyses, either a DANI 8610.10HT gas chromatograph with an FID or a Shimadzu QP5000 GC/MS was used.

FQT. The standard steady-state fluorescence experiments were carried out using a Perkin-Elmer LS 5B fluorescence spectrometer. The scan rate was set to 60 nm/min with an excitation wavelength λ_{ex} = 333 nm, excitation spectral band-pass set to 10 nm, and the emission spectral band-pass set to 2.5 nm. In addition, high-resolution fluorescence spectra were recorded on an FS900CDT fluorescence spectrometer (Edinburgh Analytical Instruments) using a spectral band-pass of 0.9 nm for the slits in the excitation and the emission channel and an excitation wavelength of 330 nm. The emission was recorded in the range of 350 nm < λ_{em} < 500 nm. In control experiments, the emission was monitored up to 600 nm. No indications for the presence of excimer emission were observed. In addition to the steady-state fluorescence investigations, time-resolved fluorescence experiments were carried out. For measuring the fluorescence lifetime, an FL900CDT spectrometer (also from Edinburgh Analytical Instruments) was set up in a T-geometry and the fluorescence decay of pyrene was monitored at λ_{em} = 373 nm and λ_{em} = 393 nm simultaneously, applying an excitation wavelength of λ_{ex} = 314 nm. The instrument was operated in the single-photon counting mode.

For the sample preparation, an O_2-free stock solution of pyrene in water was prepared with a final pyrene concentration of 100 μg L^{-1}. This stock solution was further diluted by mixing with the O_2-free sorbent stock solution prepared in a phosphate buffer (pH 7). The final pyrene concentration was in the range of 20−50 ppb. PAA ester concentrations between 10 and 1000 mg L^{-1} and HA concentrations between 10 and 50 mg L^{-1} for Com-HA and between 10 and 100 mg L^{-1} for BW-HA were chosen. In general, the samples were measured after being equilibrated overnight. All solutions were carefully purged for 2 min with N_2 (10 mL mL^{-1}) prior to fluorescence measurements. To minimize losses due to the sorption of pyrene to the glass walls, the cuvettes used were first equilibrated three times with the solution under investigation; the solutions were then removed and substituted by a fresh volume of the same sample solution. The measured fluorescence intensities were corrected for the inner filter effect according to the method of Lakowicz (*27*)

$$\log(FI_{corrected}/FI_{measured}) = (a_{ex}L_{ex} + a_{em}L_{em})/2 \quad (1)$$

where FI are fluorescence intensities, a spectral absorptions, and L path lengths in the fluorescence cuvette, each for the excitation and the emission light. All sorption experiments were performed at ambient temperature (23 ± 2 °C).

Results and Discussion

Recently, Doll et al. (*24*) compared sorption coefficients obtained with SPME and with the FQT. Both techniques were applied to the same set of solutes (PAHs) and DOM samples. The binding constants calculated from FQT measurements ($K_{Stern-Volmer}$) were up to an order of magnitude higher than those from SPME (K_{SPME}). Burkhard's statistical comparison of literature data (*23*) also revealed higher K_{DOC} values for Aldrich HA and natural humic and fulvic acids when measured with FQT compared to SPME-derived K_{DOC} values. Doll et al. (*24*) interpret the method-dependent deviations in the sorption coefficients in terms of different types of interactions: they postulate an "outer sphere" and an "inner sphere" of DOM, which are responsible for weak and strong binding of solutes, respectively. FQT detects both types of interactions, because they both give rise to fluorescence quenching, whereas SPME possibly does not acknowledge the weak binding to the DOM outer sphere. If the number of high-affinity sorption sites is small compared to the sorbate loading, nonlinear sorption isotherms would result over extended concentration ranges. However, we have shown that the sorption isotherm of pyrene on a commercial HA, measured by means of SPME, is completely linear in the concentration range of 5−2000 mg_{DOC} L^{-1} (*26*). The same holds true for various noncommercial DHS, which were measured in a narrower concentration range (50−250 mg_{DOC} L^{-1}) (*22*). Furthermore, we also compared SPME and FQT data for the interaction of pyrene exemplarily with two HAs under identical solution conditions. Interfering effects of dissolved oxygen were carefully excluded in our FQT experiments; the results are presented in Table 1.

The difference between the corresponding K_{DOC} values is a factor of 4. The same tendency is observed for phenanthrene [log K_{DOC} = 4.29 with SPME versus 4.73 with FQT using Com-HA (*22*)]. Thus, the principal findings of Doll et al. (*24*) are confirmed by our data.

TABLE 1. log K_{DOC} Values[a] Determined by SPME and FQT

humic acid	SPME	FQT
commercial HA (Roth)	4.93[b]	5.54 (373 nm)[d]
	4.96[c]	5.53 (393 nm)
BW-HA	4.21[c]	4.93 (373 nm)
		4.87 (393 nm)

[a] RSD = ± 0.05, c_{HA} = 10−100 mg L^{-1}, c_{pyrene} = 35 μg L^{-1}, pH 7, IS = 0.02 M NaCl. [b] This study. [c] Reference *21*. [d] Emission wavelength used for calculation of K_{DOC}.

Concentration-Based versus Activity-Based Sorption Coefficients. At this point it is necessary to discuss the definition and the environmental importance of sorption coefficients. Usually, the carbon-normalized sorption coefficient K_{DOC} is defined in terms of concentration ratios according to

$$K_{DOC} = \frac{c_{sorbed}}{c_{freely\ dissolved}} = \frac{n_{sorbed}}{n_{freely\ dissolved}} \times \frac{1}{c_{DOC}}\ [mL \cdot g_{DOC}^{-1}] \quad (2)$$

where c_{sorbed} and $c_{freely\ dissolved}$ are the concentrations of the sorbed and the freely dissolved solute fractions [g of sorbed solute per g of DOC (dissolved organic carbon) and g of freely dissolved solute per mL of water, respectively], c_{DOC} is the concentration of the dissolved sorbent (g of DOC per mL of water), and n_{sorbed} and $n_{freely\ dissolved}$ are the amounts of the corresponding solute fractions in arbitrary units. Equation 2 does not define the type or strength of interaction which classifies a solute as being "sorbed" or "freely dissolved". Alternatively, instead of concentration ratios, the activities a of the solute can be considered. This is a more rigorous treatment from the thermodynamic point of view. Generally, SPME gives signals (GC peak areas) that are proportional to the activities of analytes in solution, but not a priori to their concentrations. For example, the addition of a cosolvent or a salt to an aqueous solution may change the activity of a hydrophobic solute (and consequently its SPME signal), without significantly changing its concentration. If one compares two solutions, which differ only in their DOM content, SPME measures the change in the solute activity caused by its interaction with DOM:

$$\frac{\text{SPME-signal}_{\text{without DOM}}}{\text{SPME-signal}_{\text{with DOM}}} = \frac{a_{\text{solute without DOM}}}{a_{\text{solute with DOM}}} = 1 + K_{DOC}^{SPME} c_{DOC} \quad (3)$$

One can show that under certain circumstances ($c_{freely\ dissolved} \ll c_{total}$), the SPME-derived sorption coefficient K_{DOC}^{SPME} is equal to the activity-based sorption coefficient K_{DOC}^{*} and is correlated with the concentration-based sorption coefficient K_{DOC} simply through division by the activity coefficient γ_i of the freely dissolved solute i in the DOM-containing aqueous phase (*23*):

$$K_{DOC}^{SPME} \approx K_{DOC}^{*} = \frac{c_{sorbed}}{a_{freely\ dissolved}} = \frac{K_{DOC}}{\gamma_i} \quad (4)$$

The convention for the activity coefficient is $\gamma_i = 1$ for an infinitely diluted solution (lim $x_{water} \rightarrow 1$, Henry's law convention). Provided that these conditions are complied with, one would expect to measure identical sorption coefficients with activity-based and concentration-based methods. It is worthy of mention that a has different definitions in eqs 3 and 4: in eq 3, a stands for the activity of the total amount of solutes, whereas in eq 4 it stands for the activity of the freely dissolved fraction. The different meanings are indicated by the appropriate indices.

The following example illustrates the importance of γ_i in eq 4. We assume two DOM-containing samples: sample A with a high salinity and sample B with a low salinity. Both are spiked with a hydrophobic organic compound (HOC) in order to measure the DOM sorption coefficients. First, let us consider the scenario that the DOM properties (charge, conformation, degree of aggregation, etc.) are not affected by the ionic strength of the solution. In this case, we can expect $K_{DOC,sample\ A} > K_{DOC,sample\ B}$, because the activity of the HOC is higher in sample A and will, therefore, cause a higher degree of sorption ($c_{HOC,sorbed}$). However, $K_{DOC,sample\ A}^{*} = K_{DOC,sample\ B}^{*}$, because the higher degree of sorption in sample A is compensated for by the higher activity coefficient $\gamma_{HOC,sample\ A}$ in eq 4. The situation can be illustrated for SPME as follows: a change in the thermodynamic activity of the analyte caused by a change in the solution chemistry (e.g., ionic strength) affects both processes—the extraction by the SPME fiber and the sorption on DOM—to the same extent. Each affects the size of the SPME signal in the opposite direction, and they totally compensate for each other in the special case of DOM-containing solutions:

$$\text{SPME-signal}_{\text{with DOM}} \sim a_{\text{solute with DOM}} = c_{freely\ dissolved}\gamma_i = \frac{c_{sorbed}\gamma_i}{K_{DOM}^{*}\gamma_i} = \frac{c_{sorbed}}{K_{DOM}^{*}} \quad (5)$$

According to eq 5, the SPME signal (GC peak area) does not depend on the activity coefficient of the freely dissolved solute; that is, it does not reflect changes in the solution chemistry. The entire measurement can be attributed to the change in the DOM properties. The sorption coefficient determined in this manner is therefore a true DOM parameter. Strictly interpreted, this holds only for high degrees of sorption ($c_{freely\ dissolved} \ll c_{total}$, i.e., $c_{sorbed} \approx c_{total}$). The reference solutions for samples A and B are pure water with neither DOM nor salts. In this scenario, K_{DOC} represents the overall sorption, determined by the DOM affinity *and* the salinity of the solution, whereas K_{DOC}^{*} reflects only the first term. In other words, K_{DOC}^{*} is a "DOM property", whereas K_{DOC} is "sample property".

In a more realistic scenario, the sorption properties of any kind of DOM will also be affected by the ionic strength of the solution. Thus, $K_{DOC,sample\ A}^{*} \neq K_{DOC,sample\ B}^{*}$. The difference between the two activity-based sorption coefficients reflects exclusively the salt effect on the sorption affinity of the DOM. This may be a more definitive piece of information than the superposition of various effects in terms of K_{DOC}. The same conclusion can be drawn for other features of solution chemistry, such as pH value, cosolvents, and "matrix effects" of real environmental samples (*28*).

Equation 3 can be developed further to eq 6, which clearly defines what is considered to be a "sorbed" solute: the sorbed fraction x_{sorbed} is equal to the amount of solute that corresponds to the decrease in its thermodynamic activity.

$$x_{sorbed} = \frac{n_{sorbed}}{n_{total}} = \frac{a_{\text{solute without DOM}} - a_{\text{solute with DOM}}}{a_{\text{solute without DOM}}} = \frac{K_{DOC}^{SPME} c_{DOC}}{1 + K_{DOC}^{SPME} c_{DOC}} \quad (6)$$

In other words, all effects that contribute to this decrease are classified as "sorption" or "sorptive interaction", regardless of the interaction mechanism, strength, or lifetime of binding between sorbent and sorbate (eq 6).

In contrast to SPME, it may be of interest to determine which type of sorption coefficient is measured by FQT. FQT measures a concentration-based K_{DOC} value, because the freely dissolved fraction of the solute is detected by a

concentration-proportional signal—the fluorescence intensity. Moreover, FQT also includes in the sorbed fraction all solute molecules which are sufficiently close to the sorbent that their fluorescence signal is quenched. Clearly, this is significantly different from the SPME-derived definition above.

For dissolved humic substances, a static rather than a dynamic quenching mechanism is usually assumed (*18*, *29*–*31*). Considering $K_{\text{Stern-Volmer}} \approx 4 \times K_{\text{DOC}}^{\text{SPME}}$ for pyrene (Table 1), the majority of interacting pyrene molecules can be expected to be located in the outer sphere of the dissolved colloid. In this outer sphere, pyrene interactions with DOM are such that on the one hand fluorescence quenching occurs, but on the other hand the interactions are sufficiently loose that the pyrene molecules retain a significant proportion of their thermodynamic activity. These two features of interactions can be expressed by the equations

$$a_{\text{total}} = c_{\text{total}} (\gamma_{\text{freely dissolved}} x_{\text{freely dissolved}} + \gamma_{\text{loosely bound}} x_{\text{loosely bound}} + \gamma_{\text{strongly bound}} x_{\text{strongly bound}}) \quad (7)$$

$$\text{FI}_{\text{total}} \sim \phi_{\text{freely dissolved}} x_{\text{freely dissolved}} + \phi_{\text{loosely bound}} x_{\text{loosely bound}} + \phi_{\text{strongly bound}} x_{\text{strongly bound}} \quad (8)$$

where $\gamma_{\text{loosely bound}} \approx \gamma_{\text{freely dissolved}}$ for the activity coefficients of the analyte fractions, but $\phi_{\text{loosely bound}} \ll \phi_{\text{freely dissolved}}$ for the corresponding fluorescence quantum yields.

Compared to the lifetime of the excited state (10^{-7} s), the exchange of pyrene molecules between the outer sphere and the water bulk phase is slow. Otherwise, FQT would detect a dynamic rather than a static quenching. However, time-resolved and stationary fluorescence measurements showed unambiguously that in the presence of DHS static quenching strongly dominates in the quenching of pyrene fluorescence (*4*) ($\tau_{H_2O}{}^0/\tau_{\text{DHS}} = 1$, with the fluorescence lifetimes $\tau_{H_2O}{}^0$, τ_{DHS} of pyrene in absence and presence of DHS).

There is a lot of debate in the literature about the validity of FQT for determining sorption coefficients (e.g., refs *32* and *33*). Nevertheless, FQT is still the most frequently used experimental method for this purpose (*18*). To the best of our knowledge, there are very few papers that compare different methods under identical conditions. Other activity-based methods, such as the solubility enhancement method, gas purging, or the dialysis method, should also produce sorption coefficients that are different in an analogous way from the concentration-based FQT data. Methods based on the same physical value should ideally produce identical sorption coefficients. Laor and Rebhun (*7*) compared FQT with a complexation−flocculation method, where they measured the same samples using the two methods in turn. Flocculation is based on phase separation of the contaminant−OM complex and the water phase by adding a coagulant (e.g., Fe^{3+} or Al^{3+} ions). The data show that FQT yields somewhat higher sorption coefficients than flocculation. However, the differences vary considerably, depending on the solute and the source of the DOM. For pyrene and Aldrich-HA, the K_{DOC} values are almost identical (1.19×10^5 mL g^{-1} with FQT and 1.05×10^5 mL g^{-1} with flocculation). In a recent paper, significant differences between sorption coefficients determined with FQT and the complexation−flocculation method were observed by the same authors (*8*), for example, a factor of 3.5 for phenanthrene and Aldrich-HA. Kukkonen and Pellinen (*34*) found similar sorption coefficients ($\log K_{\text{DOC}} = 5.90$) for benzo[*a*]pyrene on dissolved chloroligning ($M_w > 12$ kDa) with FQT and the equilibrium dialysis method. Danielsen et al. (*32*) compared FQT with the solubility enhancement method for binding of pyrene to Suwannee River FA and HA. They found K_{DOC} values higher by factors of 2.7 and 1.6, respectively, with the FQT method and ascribed the differences to the interference of dissolved oxygen during fluorescence measurements. The differences in the K_{OM} values that Peuravuori (*12*) found for a variety of humic substances using FQT and the solubility enhancement method were even more pronounced. FQT produced 1.7−8.3 times higher K_{OM} values under anoxic conditions. The author pointed out that the Stern−Volmer plot already showed a significant curvature even with low concentrations of HS, whereas the corresponding isotherms obtained with the solubility enhancement method were linear. Equilibrium dialysis and solubility enhancement are both activity-based methods. Therefore, differences similar to those for the comparison between SPME and FQT are to be expected.

Haitzer et al. (*35*) compared the reduction in the bioavailability of [^{14}C]pyrene for nematodes in the presence of dissolved HS with FQT-based sorption coefficients. The results of these two different experimental methods agreed well, indicating that the fraction of pyrene determined as freely dissolved by FQT is comparable to the bioavailable fraction. However, if one takes into account that the pH value in FQT experiments was significantly higher than in the biological experiments (10 versus ~8, respectively), a tendency $K_{\text{FQT}} > K_{\text{bioavailability}}$ seems to be more realistic. In summary, these results make it difficult to present a consistent picture of the various experimental methods, but it seems that FQT-based sorption coefficients for DOM always show higher values than sorption coefficients measured with other methods.

Nevertheless, there are two practical conclusions of these methodical and theoretical considerations: First, we must distinguish between concentration-based and activity-based sorption coefficients. This enables us to separate different effects on the degree of interaction. Second, we have to answer the question, which definition of "sorbed state" is more relevant for prediction of the environmental behavior of chemicals? Some physical and chemical properties, such as water solubility and vapor pressure, are clearly correlated with the activity of the solute. In such cases, the activity-based sorption coefficient K_{DOC}^{*} is the appropriate parameter. On the other hand, the rate of chemical reactions is determined by the concentrations of the reaction partners. The concentration-based K_{DOC} should be applicable in this context. For other properties, such as bioavailability or colloid-supported transport, the answer is not that straightforward. More work is necessary in order to understand the nature of solute−DOM interactions as well as the consequences of these interactions for the environmental behavior of xenobiotics.

In part 1 of this series, a set of water-soluble aliphatic and aromatic PAA esters was used to correlate individual structural parameters such as molecular weight and aromaticity of the sorbent with its sorption potential toward hydrophobic substances (*26*). Using these model polymers, the validity of the SPME method to determine bound analyte fractions in the presence of dissolved polymers was examined by comparison with two other independent methods: FQT and a phase separation after flocculation of the ester, similar to the procedure described by Laor and Rebhun (*7*). A solution of 35 μg L^{-1} pyrene and 1 g L^{-1} PAA 2-phenylethyl ester (esterification degree = 5%) was analyzed with the SPME method in the usual manner, that is, by comparing the pyrene peak area with that from an aqueous solution free of DOM. We obtained a sorption coefficient of $\log K_{\text{DOC}} = 3.65$ [which corresponds to a sorption coefficient of $\log K_{\text{DOC(R)}} = 4.6$ normalized to the carbon fraction in the hydrophobic ester substituent (C_R) according to $K_{\text{DOC(R)}} = K_{\text{DOC}}(C_{\text{total}}/C_R)$]. After the SPME measurement, the PAA ester was flocculated by adding 0.5 g L^{-1} $Fe(NO_3)_3$ and removed by centrifugation. The DOM-free centrifugate was then analyzed once again by SPME. The pyrene activity in the centrifugate was almost identical with that in the presence of the dissolved PAA ester.

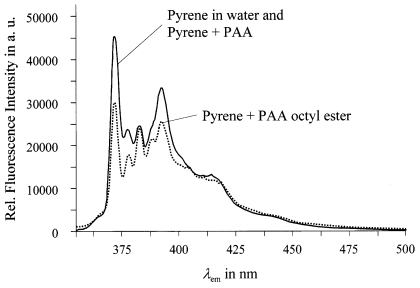

FIGURE 1. Fluorescence spectra of pyrene in pure water, with PAA, and with PAA *n*-octyl ester (M_w = 8 kDa, 5.5% degree of esterification, λ_{ex} = 330 nm, slits = 0.9 nm, c_{pyrene} = 50 μg L^{-1}, $c_{PAA} = c_{ester}$ = 500 mg L^{-1}, spectra normalized to peak intensity at 383 nm).

This proves that the decrease in the SPME signal can be attributed to a pyrene fraction, which is closely bound to the DOM. Apparently, the flocculation step did not significantly affect the sorption potential of the PAA ester.

Pyrene as a Fluorescence Probe for the Microenvironment of Sorbates. The fluorescence measurements revealed that the vibrational structure of the fluorescence spectrum of pyrene analyzed under standard conditions (λ_{ex} = 333 nm, λ_{em} = 373 and 393 nm) was altered in the presence of several PAA esters and that the fluorescence intensity varied in an irregular manner. In some cases we even found fluorescence amplification instead of the expected attenuation. Therefore, a data evaluation according to the Stern–Volmer relation was not applied (the assumption of the formation of a dark complex is not true for the PAA ester systems investigated). This behavior was pronounced with aliphatically substituted PAA esters. Figure 1 shows exemplarily the difference in the fluorescence spectra of pyrene in pure water, in the presence of PAA, and the octyl ester. In contrast, the addition of the PAA phenyl ester did not lead to any pronounced change in the vibrational structure of the pyrene spectrum.

Although the SPME method detects a significant decrease of the pyrene activity, its fluorescence is not—or is only partly—quenched in the presence of (mainly aliphatic) PAA esters. This observation does not necessarily indicate fundamentally different types of interaction between pyrene and the PAA esters compared with dissolved humic substances. It is plausible that sorbents with large aromatic moieties, such as humic substances, might quench the fluorescence more effectively than macromolecules with less electronic interactions. Therefore, this difference does not necessarily reflect the nonspecific "hydrophobic" interactions, which probably control the thermodynamic activity of the solute. On the other hand, there are indications that the complete fluorescence quenching to a dark complex is not the only interaction mechanism between organic matter and pyrene (*36*).

The observable changes in the fluorescence spectrum of pyrene offer an interesting tool for characterization of the molecular environment of sorbates. It is well-known from the literature that the fluorescence spectrum of pyrene is strongly affected by the polarity of its environment (*37*–*40*). This can be explained in terms of specific interactions between the excited singlet state of pyrene with solvent molecules or other surrounding components. The fluorescence spectrum of monomeric pyrene has five vibronic bands at 373, 379, 383, 389, and 393 nm. The intensity of the

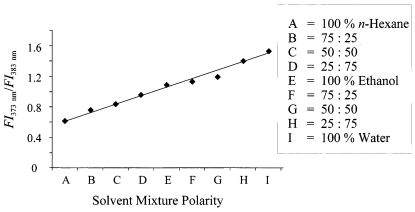

FIGURE 2. Dependence of the ratio of peak intensities FI_{373nm}/FI_{383nm} in the fluorescence spectrum of pyrene on the relative polarity of the solvent (λ_{ex} = 333 nm, spectral band-passes = 2 nm, c_{pyrene} = 50 μg L^{-1}); solvent composition was from 100% *n*-hexane through ethanol up to 100% water in 25% steps by volume.

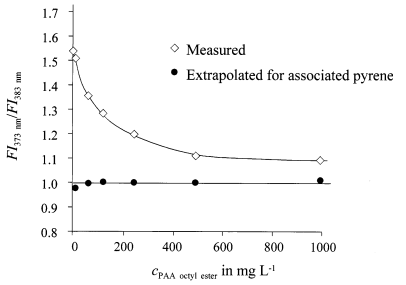

FIGURE 3. Dependence of the measured and extrapolated peak ratio FI_{373nm}/FI_{383nm} in the fluorescence spectrum of pyrene on the concentration of PAA *n*-octyl ester (λ_{ex} = 330 nm, slits = 0.9 nm, c_{pyrene} = 50 μg L^{-1}, extrapolation with log K_{DOC} = 4.15).

forbidden vibronic bands (e.g., the 0–0 band, peak 1) is enhanced with increasing polarity of the environment (*41*). Pyrene has therefore been used as a polarity probe in studies of solvents, micellar systems, membranes, proteins, and various polymers (*37*, *42*–*44*).

We measured the fluorescence spectrum of pyrene in binary solvent mixtures of increasing polarity, starting with pure *n*-hexane (ϵ_r = 1.9) through ethanol (ϵ_r = 25.3) up to pure water (ϵ_r = 74.6). The most sensitive peak ratio with respect to solvent polarity is FI_{373nm}/FI_{383nm}, which varies by a factor of 2.4 between the two extremes, *n*-hexane and water. Figure 2 shows the dependence of the peak ratio FI_{373nm}/FI_{383nm} on the polarity of the solvent mixture.

The intensities of the vibronic bands of the pyrene fluorescence spectrum in the presence of PAA are identical to those in pure water (Figure 1). This is in accordance with the SPME results, which indicate no significant interactions of pyrene with PAA. Comparing the pyrene spectra of all esters under study, the strongest effects with respect to the intensity and the vibronic structure of the spectra were observed with the PAA *n*-octyl ester (Figure 2); the dependence of the peak ratio on the ester concentration is plotted in Figure 3.

The peak ratios changed continuously over the whole range of the ester concentrations studied (12.5–1000 mg L^{-1}). There is no indication of a critical micelle concentration as a step in the curve, as is frequently observed for surfactants.

The most significant alterations in the vibrational intensities of the pyrene fluorescence spectrum are compiled in Table 2. The interaction of pyrene with the naphthyl esters could not be observed in the fluorescence spectra, because of their high self-fluorescence. Other aromatic esters (phenyl,

TABLE 2. Peak Ratios of Pyrene Fluorescence Spectra in the Presence of PAA Esters[a]

sorbents, PAA esters with substituents R in $-(CH_2CH[COOH])_n-(CH_2CH[COOR])-$	FI_{373nm}/FI_{393nm}[b]	FI_{373nm}/FI_{383nm}	x_{sorbed}[c]
none (pure water)	1.23	1.53	0
H (PAA)	1.22	1.54	<0.07
n-butyl (5.4%)[d]	1.16	1.43	0.47
2-phenylethyl (5.0%)	1.05	1.42	nd
n-octyl (5.5%)	0.94	1.11	0.41

[a] pH 7, $M_{w,ester}$ = 8 kDa, λ_{ex} = 330 nm, c_{ester} = 500 mg L^{-1}, c_{pyrene} = 50 μg L^{-1}. [b] Data are corrected for polymer fluorescence and inner filter effect. [c] According to K_{DOC} from SPME (*23*). [d] Degree of esterification in parentheses.

cyanophenyl, methoxyphenyl, and 2-phenylethyl) and the PAA ethyl ester show only minor effects. This is consistent with the hypothesis that longer hydrocarbon substituents, such as *n*-octyl, *n*-butyl, and ethoxyphenyl, tend to create hydrophobic domains in aqueous solution. It is remarkable, however, that the aromatic PAA esters behave similarly with respect to incomplete fluorescence quenching or even fluorescence enhancement at high ester concentrations. Apparently, an isolated benzene ring is not sufficient for an effective fluorescence quenching, irrespective of electron-pushing or -withdrawing substituents.

The observed peak ratios in Table 2 and Figure 3 are the result of a superposition of the fluorescence spectra of freely dissolved and ester-associated pyrene molecules after a sorption equilibrium has been reached. An extrapolation of the fluorescence spectrum of pyrene "completely associated" with the PAA octyl ester led to a peak ratio of $FI_{373nm}/FI_{383nm} \approx 1.0$. A reasonable fit between observed and calculated fluorescence spectra was achieved with $\log K_{DOC} = 4.15$, which is higher by a factor of 5 than the sorption coefficient determined with the SPME method (cf. Table 1, $\log K_{DOC} = 3.45$). This is in agreement with our conclusions drawn from results with dissolved humic substances: sorption coefficients derived from fluorescence measurements are always higher than those derived from activity measurements.

Comparing the extrapolated peak ratio with the qualitative solvent polarity scale in Figure 2, the chemical environment of associated pyrene can be characterized as being similar to a hexane−ethanol mixture rich in ethanol. This indicates a rather hydrophobic microenvironment of the associated pyrene, which can only be explained by an intra- or intermolecular aggregation of the hydrophobic ester substituent.

It is worthy of mention that no significant shift in the pyrene fluorescence spectrum was observed in the presence of dissolved HAs ($c_{HA} = 25-100$ mg L^{-1}, 50−90% fluorescence quenching). This is in agreement with the prevailing view that HA-associated fluorophores are quenched completely (*18*, *29*, and references cited therein), which makes pyrene (and probably also other fluorescence probes) inappropriate for characterizing the microenvironment of dissolved HS sorbates. However, approaches based on an incomplete fluorescence quenching of fluorophores in association with humic substances can also be found in the literature (*17*, *45*).

To summarize, the interaction of pyrene with mainly aliphatic PAA esters caused no or only minor fluorescence quenching, even though the SPME measurements showed that the thermodynamic activity of pyrene in the solution phase was significantly decreased. With DHS, on the other hand, FQT reports a higher fraction of sorbed pyrene than SPME. Obviously, the two methods differ markedly in their definition of the sorbed state. Generally, it must be distinguished between concentration-based and activity-based sorption coefficients, depending on the method used for their determination. For activity-based methods such as SPME, solubility enhancement, gas purging, or the dialysis method, all effects caused by DOM that contribute to a decrease in thermodynamic activity of the solute are considered as sorption, regardless of the mechanism, strength, or lifetime of the binding between sorbent and sorbate. For FQT, which in principle is a concentration-based method, the sorbed state appears to be rather method-defined. Other concentration-based methods, including the SPE or RP method and the flocculation method, can also show method-dependent artifacts. Further research is necessary to compare the various methods and to evaluate which definition of the sorbed state is more relevant with regard to the various effects of sorption on DOM for the environmental behavior of xenobiotics.

Acknowledgments

We thank the Deutsche Forschungsgemeinschaft (DFG) for financial support, which was granted within the research project "Refractory Organic Acids in Waters (ROSIG)".

Literature Cited

(1) Frimmel, F. H.; Christman, R. F. *Humic Substances and Their Role in the Environment*; Wiley: Chichester, U.K., 1988.
(2) Piccolo, A. *Humic Substances in Terrestrial Ecosystems*; Elsevier: Amsterdam, The Netherlands, 1996.
(3) Gauthier, T. D.; Shane, E. C.; Guerin, W. F.; Seitz, W. R.; Grant, C. L. *Environ. Sci. Technol.* **1986**, *20*, 1162.
(4) Kumke, M. U.; Loehmannsroeben, H.-G.; Roch, T. *Analyst* **1994**, *119*, 997.
(5) Landrum, P. F.; Nihart, S. R.; Eadie, B. J.; Gardner, W. S. *Environ. Sci. Technol.* **1984**, *18*, 187.
(6) Maxin, R.; Koegel-Knabner, I. *Eur. J. Soil Sci.* **1995**, *46*, 193.
(7) Laor, Y.; Rebhun, M. *Environ. Sci. Technol.* **1997**, *31*, 3558.
(8) Laor, Y.; Rebhun, M. *Environ. Sci. Technol.* **2002**, *36*, 955.
(9) Chiou, T.; Malcom, R. C.; Brinton, T. I.; Kile, D. E. *Environ. Sci. Technol.* **1986**, *20*, 502.
(10) Tanaka, S.; Oba, K.; Fukushima, M.; Nakayasu, K.; Hasebe, K. *Anal. Chim. Acta* **1997**, *337*, 351.
(11) Kopinke, F.-D.; Georgi, A.; Mackenzie, K. *Anal. Chim. Acta* **1997**, *355*, 101.
(12) Peuravuori, J. *Anal. Chim. Acta* **2001**, 429, 65.
(13) McCarthy, J. F.; Jimenez, B. D. *Environ. Sci. Technol.* **1985**, *19*, 1072.
(14) De Paolis, F.; Kukkonen, J. *Chemosphere* **1997**, *34*, 1693.
(15) Lueers, F.; ten Hulscher, T. E. M. *Chemosphere* **1996**, *33*, 643.
(16) Hassett, J. P.; Milicic, E. *Environ. Sci. Technol.* **1985**, *19*, 638.
(17) Ganaye, V. A.; Keiding, K.; Vogel, T. M.; Viriot, M.-L.; Block, J.-C. *Environ. Sci. Techol.* **1997**, *31*, 2701.
(18) Schlautman, M. A.; Morgan, J. J. *Environ. Sci. Technol.*, **1993**, *27*, 961.
(19) Kopinke, F.-D.; Poerschmann, J.; Remmler, M. *Naturwissenschaft* **1995**, *82*, 28.
(20) Poerschmann, J.; Zhang, Z.; Kopinke, F.-D.; Pawliszyn, J. *Anal. Chem.* **1997**, *69*, 597.
(21) Poerschmann, J.; Kopinke, F.-D.; Pawliszyn, J. *Environ. Sci. Technol.* **1997**, *31*, 3629.
(22) Georgi, A. Ph.D. Thesis, University of Leipzig, Germany, 1998.
(23) Kopinke, F.-D.; Poerschmann, J.; Georgi, A. In *Applications of SPME*; Pawliszyn, J., Ed.; RSC Chromatographic Monographs: Royal Society of Chemistry: London, U.K., 1999; pp 111−128.
(24) Doll, T. E.; Frimmel, F. H.; Kumke, M. U.; Ohlenbusch, G. *Fresenius' J. Anal. Chem.* **1999**, *364*, 313.
(25) Burkhard, L. P. *Environ. Sci. Technol.* **2000**, *22*, 4663.
(26) Kopinke, F.-D.; Georgi, A.; Mackenzie, K. *Environ. Sci. Technol.* **2001**, *35*, 2536.
(27) Lakowicz, J. R. *Principles of Fluorescence Spectroscopy*; Plenum Press: New York, 1983.
(28) Poerschmann, J.; Kopinke, F.-D.; Pawliszyn, J. *J. Chromatogr. A* **1998**, *816*, 159.
(29) Zimmermann, U. Ph.D. Thesis, University of Erlangen, Germany, 1999.
(30) Zimmermann, U.; Skrivanek, T.; Loemannsroeben, H.-G. *J. Environ. Monit.* **1999**, *1*, 525.
(31) Northcott G. L.; Jones, K. C. *Environ. Pollut.* **2000**, *108*, 19.

(32) Danielsen, K. M.; Chin, Y.-P., Buterbaugh, J. S.; Gustafson, T. L.; Traina, S. J. *Environ. Sci. Technol.* **1995**, *29*, 2162.
(33) Tiller, C. L.; Jones, K. D. *Environ. Sci. Technol.* **1997**, *31*, 424.
(34) Kukkonen, J.; Pellinen, J. *Sci. Total Environ.* **1994**, *152*, 19.
(35) Haitzer, M.; Loemannsroeben, H.-G.; Steinberg, C. E. W.; Zimmermann, U. *J. Environ. Monit.* **2000**, *2*, 145.
(36) Ganaye, V. A.; Keiding, K.; Vogel, T. M.; Viriot, M.-L.; Block, J. C. *Environ. Sci. Technol.* **1997**, *31*, 2701.
(37) Kalyanasundaram, K.; Thomas, J. K. *J. Am. Chem. Soc.* **1977**, *99*, 2039.
(38) Dong, D. C.; Winnik, M. A. *Photochem. Photobiol.* **1982**, *35*, 17.
(39) Kalyanasundaram, K. *Photochemistry in Microheterogeneous Systems*; Academic Press: London, U.K., 1987.
(40) Zhang, S.; Rusling, J. F. *J. Colloid Interface Sci.* **1996**, *182*, 558.
(41) Nakajima, A. *J. Luminscence* **1977**, *11*, 429.
(42) Glushko, V.; Thaler, M. S. R.; Karp, C. D. *Arch. Biochem.* **1981**, *210*, 33.
(43) Horiuchi, K.; Rharbi, Y.; Spiro, J. G.; Yekta, A.; Winnik, M. A.; Jenkins, R. D.; Bassett, D. R. *Langmuir* **1999**, *15*, 1644.
(44) de Oliveira, V. A.; Teira, M. J.; Gehlen, M. H.; Neumann, M. G. *Photochem. Photobiol.* **1996**, *63*, 779.
(45) Engebretson, R. R.; von Wandruszka, R. *Environ. Sci. Technol.* **1994**, *28*, 1934.

Received for review December 3, 2001. Revised manuscript received May 15, 2002. Accepted July 24, 2002.

ES010310X

2.2.2 Sorption of phenols to dissolved organic matter investigated by solid phase microextraction

G. Ohlenbusch, M.U. Kumke, F.H. Frimmel
Sci. Tot. Environ., 2000, **253**, 63 - 74.

Phenole und Chlorphenole werden aus verschiedensten Quellen in die Umwelt eingetragen. Sie entstehen als Nebenprodukte in der Papierherstellung, werden als Pestizide eingesetzt und dienen als Konservierungsmittel für Bekleidung. Ihr Vorkommen in der Umwelt ist äußerst bedenklich. Deshalb müssen Transportmechanismen und Verbleib dieser Verbindungsklasse gründlich untersucht werden.
Auch für die Untersuchung der Wechselwirkungen zwischen polaren Xenobiotika wie den Phenolen und HS erwies sich die SPME als leistungsstarke Methode. Die Wechselwirkungen verschiedener Phenole mit HS unterschiedlicher Ursprungsorte wurden durch Sorptionskonstanten quantitativ charakterisiert. Es zeigte sich, dass in Abhängigkeit vom Ursprungsort der HS erhebliche Unterschiede in den Sorptionskonstanten bestehen. Im Unterschied zu hydrophoben Xenobiotika, bei denen sich die Solvenskonditionen (wie z.B. der pH-Wert der Lösung) in erster Linie durch Veränderungen in den HS bemerkbar machen (z.B. Veränderung der Assoziation bzw. Konformation der HS), ist bei polaren Xenobiotika speziell der Einfluss von funktionellen Gruppen auf die Speziation der Xenobiotika zu berücksichtigen. Die daraus resultierenden spezifischen Wechselwirkungen, im Fall von Phenolen z.B. mit basischen Funktionalitäten der HS, können dann für die Stärke der effektiven Wechselwirkungen entscheidend sein .

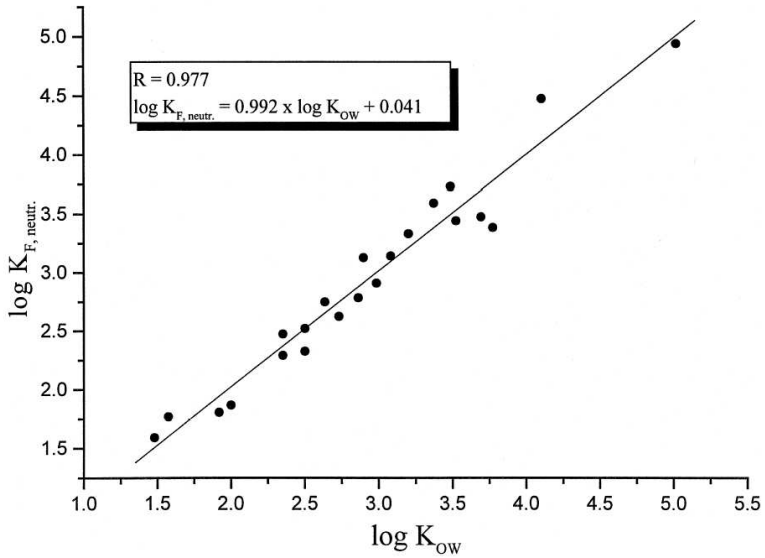

ELSEVIER

The Science of the Total Environment 253 (2000) 63–74

the Science of the Total Environment

www.elsevier.com/locate/scitotenv

Sorption of phenols to dissolved organic matter investigated by solid phase microextraction

Gerd Ohlenbusch, Michael U. Kumke, Fritz H. Frimmel*

Bereich Wasserchemie, Engler-Bunte-Institut, Universität Karlsruhe, Engler-Bunte-Ring 1, 76131 Karlsruhe, Germany

Received 9 October 1999; accepted 14 December 1999

Abstract

The sorption of phenol and different halogenated phenols to natural organic matter of a brown water lake (HO14), of a compost extract, of Aldrich humic acid (Aldrich-HA), and to the protein bovine serum albumin (BSA) was investigated using solid phase microextraction (SPME). The limit of determination for the SPME analysis was < 15 μg/l for all phenols investigated. The extraction coefficients K_F were calculated according to a first-order extraction kinetics. In general, the extraction equilibrium was established faster due to the presence of dissolved organic matter (DOM). The highest sorption capacity of phenols was observed for BSA with log K_{OC} values in the range between 2 and 6. For the compost extract and HO14 only a small sorption of the investigated phenols was determined. On the other hand, Aldrich humic acid showed a reasonable sorption of phenols with log K_{OC} values between 2 and 3. The sorption to DOM decreased when the pH of the solution was increased.

Keywords: Phenols; Solid phase microextraction; Dissolved organic matter; Sorption coefficients

1. Introduction

Dissolved organic matter (DOM) can be found in surface waters as well as in ground and pore waters (Stevenson, 1982; Frimmel and Christman, 1988; Rebhun et al., 1996). It is well known that sorption of xenobiotics to dissolved organic matter (DOM) changes the fate and transport of xenobiotics (McCarthy and Zachara, 1989; Huber et al., 1992; Klaus et al., 1998). Several authors have shown that the sorption process causes an alteration of bioavailability and toxicity (McCarthy, 1989; Lee et al., 1993; Steinberg et al.

* Corresponding author. Tel.: +49-721-608-2580; fax: +49-721-699154.
E-mail address: fritz.frimmel@ciw.uni-karlsruhe.de (F.H. Frimmel)

0048-9697/00/$ - see front matter
PII: S0048-9697(00)00376-4

1993; Kördel, 1997). Steinberg et al. (1992) observed that in the presence of DOM the toxicity of diazinon, 4-chloroanilin and 4-nitrophenol to the waterflea *Daphnia magna* was increased, whereas the toxicity of 2,4-dichlorophenol and 2,4,5-trichlorophenol was decreased.

Two general analytical approaches for the determination of sorption coefficients of xenobiotics to DOM can be distinguished: methods that include a separation step and techniques that analyze the samples directly. Of the two general analytical approaches for the determination of DOM-Xenobiotics sorption coefficients methods applying a separation step prior to the analysis will (strongly) influence the equilibrium between xenobiotics and DOM. Analytical methods like the reversed phase method (Landrum et al., 1984), the solvent extraction (Parris, 1980; Kopinke et al., 1995), the gas purging method (Hassett and Milicic, 1985; Lüers and Ten Hulscher, 1996), and the DOM-flocculation method (Gießl, 1999) are prone to disturbing the sorption equilibrium and hence, the sorption coefficients obtained have to be considered with care. Others like the dialysis method are difficult to handle, are time consuming, and can also lead to an underestimation of the sorption coefficients as a result of DOM diffusion through the dialysis membrane (Carter and Suffet, 1982; Chin and Weber, 1989; Paolis and Kukkonen, 1997). On the other hand, spectroscopic methods like fluorescence were applied in order to investigate sorption processes to DOM without a prior separation. However, those techniques are limited to certain groups of compounds and/or are only applicable under specific experimental conditions to avoid problems inherent to the method used. The fluorescence quenching approach was frequently applied to determine the sorption of polycyclic aromatic hydrocarbons (PAH) to DOM (Loar et al., 1998; Backhus and Gschwend, 1990; Schlautmann and Morgan, 1993; Kumke et al., 1994; Georgi, 1998). Due to inner filter effects caused by the DOM this technique yields only reliable results for low concentrations of DOM.

The solid phase microextraction proved to be an attractive alternative for sorption measurements. The amount of the analyte extracted is very small and therefore, it is reasonable to assume that no relevant disturbance of the sorption equilibrium is induced (Vaes et al., 1996; Poerschmann et al., 1997). The method is applicable to a broad variety of different analytes and is not limited to a certain concentration range of DOM. Moreover, in a mixture of xenobiotics sorption coefficients can be determined simultaneously in case of independent sorption processes.

Phenols are introduced into the environment by different sources. In paper mills, chlorophenols are produced as by-products in chloro-bleaching of pulp. As a result, high concentrations are found in paper mill effluents (Paasivirta et al., 1990). Some chlorophenols like pentachlorophenol are directly used as pesticides or are produced in the metabolism of common pesticides like (2,4-dichlorophenoxy)acetic acid. Another major source of chlorophenols in the environment can be attributed to their application as preservatives for wood, textiles, and leather. Although short degradation times of chlorophenols, especially for the lower chlorinated compounds, have been reported, the broad application of these compounds leads to a ubiquitous presence in the environment (Fingler et al., 1994; Quemerais et al., 1994; Jensen, 1996; Veningerova et al., 1996, Cardellicchio et al., 1997; Jobst, 1998; Schilling et al., 1998). Because of the highly harmful character of this group of compounds a broad understanding of the transport and transformation processes in environmental matrixes is indispensable (Smith et al., 1994; Kishino and Kobayashi, 1996a,b). While for hydrophobic substances (e.g. PAH) a large set of data is easily accessible, for polar compounds like phenols only a limited number of data characterizing the sorption to DOM is available.

The objective of the presented work was to investigate the interaction of different halogenated phenols with DOM of different origins. Sorption coefficients were determined in order to describe the environmental characteristics of phenols. Therefore, a SPME methology for the analysis of polar, dissociating compounds was developed. Due to the variation of the origin of DOM conclusions on the interaction mechanism are drawn.

2. Experimental details

The sorption of phenols to DOM can be described by the following equation, if the DOM is expressed by the DOC-concentration:

$$\mathrm{DOC} + \mathrm{Phe} \underset{k_2}{\overset{k_1}{\rightleftharpoons}} \mathrm{DOC}\cdots\mathrm{Phe} \quad (1)$$

where k_1 is the rate constant of the sorption process and k_2 is the rate constant of the desorption process.

In case of equilibrium, the sorption coefficient is expressed by the ratio of the rate constants

$$K_{OC} = \frac{k_1}{k_2} \quad (2)$$

where K_{OC} is the sorption coefficient in litres per kilogram (l/kg).

Sorption measurements should be done under the assumption that the sorption equilibrium is not disturbed by measuring the concentration of the free analyte.

In the linear part of the sorption isotherms, the sorption coefficient can be determined either by the Henry equation [Eq. (3)] or by an equation [Eq. (4)] that is similar to the Stern–Vollmer equation which is used in the fluorescence quenching method for determination of sorption coefficients. The Henry equation connects the loading q (in µg/kg DOC) of phenol on the DOM and the equilibrium concentration β (in µg/l) of the free phenol in the liquid phase.

$$q = K_{OC} \cdot \beta(\mathrm{Phe})_{eq} \quad (3)$$

where q is the loading in micrograms per kilogram (µg/kg) of DOC and $\beta(\mathrm{Phe})_{eq}$ is the equilibrium concentration of the phenol in micrograms per litter (µg/l).

In Eq. (4), the ratio of the signals (e.g. areas of the chromatographic peaks) in the absence and presence of DOC is calculated depending on the concentration of dissolved organic carbon (in kg/l).

$$\frac{\beta(\mathrm{Phe})_0}{\beta(\mathrm{Phe})_{eq}} = 1 + K_{OC} \cdot \beta(\mathrm{DOC}) \quad (4)$$

where $\beta(\mathrm{Phe})_0$ is the initial phenol concentration in µg/l and β(DOC) is the DOC concentration in kg/l.

It could be shown that K_{OC} values of the Henry equation [Eq. (3)] and Eq. (4) are describing the same sorption equilibrium (Doll et al., 1999).

In Appendix A the equations used for the calculation of the limit of detection (NG) and the limit of determination (BG) according to DIN 32645 (Norm, 1994) are given. A first-order kinetics was applied for the description of the extraction in the SPME analysis. Based on the first-order kinetics the amount of extracted phenol could be calculated (see Appendix A).

2.1. Sample preparation

Stock solutions of 22 phenols with a concentration of approximately 1 g/l of each phenol were prepared in methanol. All phenols were of analytical grade. Mix I contained phenol[a]; 4-fluorophenol[a]; 2,4-dimethylphenol[b]; 2,5-dichlorophenol[b]; 2,6-dichlorophenol[b]; 3-chlorophenol[c]; 3-methoxyphenol[b]; 4-bromophenol[b]; 2,4,6-trichlorophenol[b]; 4-chloro-3,5-dimethylphenol[b]; 4-iodophenol[b]; 3,4-dichlorophenol[b] and 2,3,4,6-tetrachlorophenol[d]. Mix II contained 4-fluorophenol[a]; 4-methylphenol[c]; 2,4-dichlorophenol[b]; 4-ethylphenol[c]; 4-chlorophenol[c]; 2,4,6-trimethylphenol[c]; 4-chloro-3-methylphenol[b]; 2,3,6-trichlorophenol[a]; 3,5-dichlorophenol[b]; 2,3,4,6-tetrachlorophenol[d] and pentachlorophenol[a] (purchased from [a]Fluka, [b]Aldrich, [c]Dr Ehrenstorfer, [d]Lancaster).

In the sorption experiments different DOM samples were used: a commercially available humic acid (Aldrich-HA, Aldrich), natural organic matter of a brown water lake (HO14, Lake Hohloh, Black Forest, Germany), a compost extract, and bovine serum albumin (BSA, Fluka). A stock solution of Aldrich-HA was prepared by

dissolving 8 g of Aldrich-HA in 1000 ml of demineralized water. The solution was sonicated for 30 min, shaken for 24 h, and finally centrifuged for 60 min at 5000 rev./min and filtered with a 0.45-μm cellulose acetate membrane filter. The final concentration was 1460 mg/l DOC. Water of the brown water lake was filtered by a 0.45-μm membrane filter, and the DOM was concentrated in a rotavapor at 30–40°C and 13 mbar. After additional membrane filtration (0.45 μm), the final DOC concentration was 425 mg/l. The compost extract was prepared by sieving green waste compost soil with a 2-mm sieve and extracting 350 g with 1000 ml of demineralized water by shaking for 24 h. Subsequently, the extract was decanted, centrifuged for 60 min at 5000 rev./min, and filtrated with a 0.45-μm membrane filter. Final concentration was 606 mg/l DOC. All DOC measurements were performed with a total organic carbon analyzer (TOC-5000, Shimadzu). A stock solution of BSA was prepared by dissolving 2 g of BSA in 500 ml of demineralized water. The final concentrations of Aldrich-HA and of BSA used in the SPME experiments were 507 mg/l DOC and 95 mg/l DOC, respectively. In order to investigate the influence of pH, the samples were prepared by adding 2 ml of a 0.4 M phosphate buffer with a pH value of pH 6, 7 or 8 to a solution of 98 ml. Final buffer concentrations were 8 mM and final pH values were 6.5, 7.3 and 8.3.

Polyacrylate coated fibers (Supelco, 85 μm) were used in the SPME-measurements which have a good affinity for phenols (Buchholz and Pawliszyn, 1993, 1994; Bartak and Cap, 1997). The sorption experiments were performed in teflon sealed 40-ml glass vials. Thirty microliters of DOM-solution or demineralized water containing 8 mM phosphate buffer (pH 7.3) and 0.005% of sodium azide were added to the vial. Different aliquots of phenol stock solutions were added and subsequently solutions were stirred with a 5-mm spin bar on a magnetic stirrer at 850 rev./min for 24 h to establish sorption equilibrium. To determine the sorption coefficients, four different phenol concentrations of 20, 40, 80, and 100 μg/l were used. The K_{OC} values were calculated by Eq. (4). All experiments were performed in duplicate. Prior to the first application, the SPME fiber was once conditioned for 3 h at 300°C in a helium stream.

All analysis were performed using a GCQ (Finnigan MAT) equipped with an Optic2000 injector (Axel Semrau/Germany), a 30 m × 0.32 mm fused silica column DB5.MS (J&W Scientific) with 0.30-μm film thickness. The injector was kept at 230°C and was used in the splitless mode for the first 3 min during which the desorption of the fiber was performed. The oven was kept at 40°C for the first 3 min, then temperature was increased to 130°C with 4°C/min, raised again up to 200°C with 10°C/min and finally increased to 250°C with 30°C/min. The MS detector was operated in the full scan mode. Quantification of the phenols was performed in the selected ion monitoring (SIM) mode.

For the calibration of the SPME extraction 10 standard solutions of the phenols, investigated in a concentration range of 5–150 μg/l, were prepared. The extraction time applied in the SPME was set to 30 min. All measurements were performed in duplicate.

For the kinetic measurements, 10 standard solutions of phenols with a concentration of 100 μg/l were prepared and extracted between 5 and 100 min. The concentration in the fiber coating was calculated by the extracted amount of phenol and the volume of the fiber coating. The extracted amount was evaluated by a calibration which was obtained by splitless injection of 1 and 2 μl of phenol standard in a concentration range between 0.5 and 40 mg/l. The volume of the fiber coating was 0.521 μl (outer radius 140 μm, inner radius 55 μm).

In order to investigate the influence of DOM on the extraction kinetics nine samples with a phenol concentration of 100 μg/l were prepared with and without DOM and extracted between 5 and 900 min.

For the determination of the limit of detection (NG) and limit of determination (BG) 10 standard samples in a concentration range from 1 to 10 μg/l were measured. NG and BG were calculated according to Eqs. (10) and (11) in Appendix A.

Table 1
Extraction coefficients (K_F), limits of detection (NG), limits of determination (BG), log K_{OC} values for the sorption by Aldrich-HA and BSA with standard deviation and log K_{OW} values for selected phenols

Substance	K_F	NG (µg/l)	BG (µg/l)	Log K_{OC} (Aldrich-HA)	Log K_{OC} (BSA)	Log K_{OW} [a]
Phenol	39	4.0	10.9	nm	nm	1.50
4-Fluorophenol	64	2.5	7.7	2.32 ± 0.16	3.23 ± 0.03	1.92
3-Chlorophenol	324	2.0	6.1	2.46 ± 0.23	2.57 ± 0.38	2.50
4-Chlorophenol	294	1.4	4.2	2.31 ± 0.39	2.64 ± 0.33	2.35
4-Bromophenol	556	1.3	4.1	2.34 ± 0.44	2.93 ± 0.38	2.63
4-Iodophenol	1333	1.6	4.8	2.69 ± 0.12	3.22 ± 0.26	2.90
2,4-Dichlorophenol	1103	1.9	5.7	2.50 ± 0.21	3.79 ± 0.16	3.08
2,5-Dichlorophenol	1332	1.4	4.9	2.58 ± 0.31	3.52 ± 0.14	3.20
2,6-Dichlorophenol	144	2.5	7.8	2.58 ± 0.18	3.90 ± 0.15	2.86
3,4-Dichlorophenol	3741	1.2	3.8	2.87 ± 0.14	3.47 ± 0.19	3.37
3,5-Dichlorophenol	2466	2.2	6.6	2.84 ± 0.15	4.55 ± 0.21	3.52
2,4,6-Trichlorophenol	178	2.4	7.4	2.69 ± 0.13	5.70 ± 0.09	3.69
2,3,6-Trichlorophenol	333	2.1	6.6	2.72 ± 0.15	4.97 ± 0.11	3.88
2,3,4,6-Tetrachloroph.	298	2.3	7.1	2.91 ± 0.24	5.80 ± 0.15	4.10
Pentachlorophenol	370	2.1	6.6	3.00 ± 0.21	5.92 ± 0.17	5.01
4-Methylphenol	74	2.6	8.1	2.11 ± 0.14	2.63 ± 0.17	1.96
4-Ethylphenol	212	2.1	6.3	nm	2.49 ± 0.29	2.50
2,4-Dimethylphenol	196	1.8	5.5	2.24 ± 0.36	2.56 ± 0.27	2.35
2,4,6-Trimethylphenol	422	0.9	2.7	2.29 ± 0.23	2.59 ± 0.18	2.73
4-Chloro-3-methylphenol	810	2.0	6.0	2.47 ± 0.08	2.65 ± 0.46	2.98
4-Chloro-3,5-dimethylph.	5384	1.1	3.5	2.83 ± 0.12	3.22 ± 0.18	3.48
3-Methoxyphenol	59	4.1	14.1	2.00 ± 0.17	2.31 ± 0.35	1.57

[a] Literature values (Smith et al., 1994; Luehrs et al., 1996). nm, not measurable.

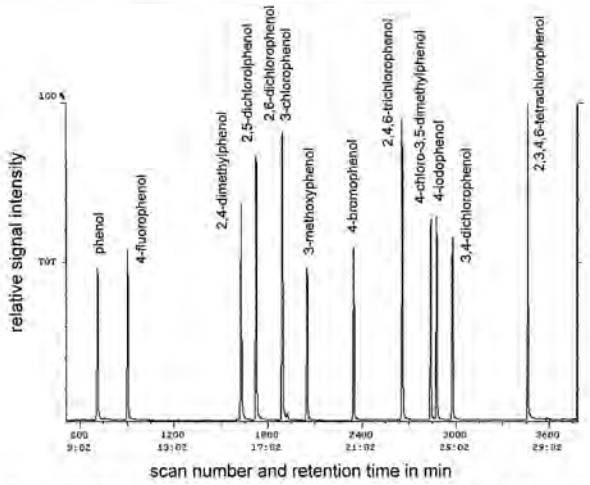

Fig. 1. Full scan GC/MS-chromatogram of phenol-mix I (1-µl splitless injection of a 20 mg/l solution).

3. Results and discussion

3.1. Adapting of SPME analysis for phenols

Figure 1 shows the GC-MS chromatogram of a mix I solution with a concentration of each phenol of 20 mg/l in acetone. It was performed by a splitless injection with an injection volume of 1 μl. A good separation of the underivated phenols was obtained by using the GC parameters described in the experimental section. Even though 2,6-dichlorophenol and 3-chlorophenol were not separated, all substances could be quantified because the quantification was performed in the SIM modus using the characteristic mass numbers of each phenol investigated.

A GC-MS chromatogram of the desorption of the SPME fiber after equilibration with an aqueous mix I solution is shown in Fig. 2. By comparing Fig. 1 and Fig. 2 it is obvious that the amounts extracted in the SPME were strongly dependent on the particular phenol. In general, for all phenols investigated in this work the amount extracted by the SPME fiber was below 1.5% of the total amount in the solution. The extraction amount can be expressed by the extraction coefficient K_F [Eq. (5), which is calculated by the rate constants of the extraction process using Eqs. (8) and (9) in Appendix A]. The values calculated for the phenols are listed in Table 1.

$$K_F = \frac{k_3}{k_4} \tag{5}$$

One would expect a correlation of K_F and octanol/water partition coefficient K_{OW} in case the extraction process of the phenols in the SPME is determined by hydrophobic interactions with the fiber.

In Table 1 the calculated K_F values are compared with log K_{OW}. No direct correlation of K_F and K_{OW} was found indicating the presence of additional processes determining the sorption to the SPME fiber. Since the phenols investigated are weak acids, under the experimental conditions used the neutral compound and the phenolate anion were present. Because it is reasonable to assume that the neutral compounds are extracted preferentially, the pK_a values of the phenols under investigation have to be taken into account. The fraction of the non-dissociated species was calculated using Eq. (6) and the ob-

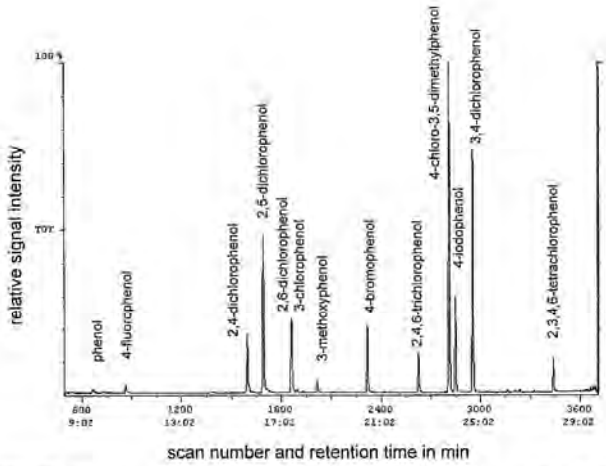

Fig. 2. Full scan GC/MS-chromatogram of phenol-mix I after SPME extraction (30-min extraction of a 40-μg/l solution).

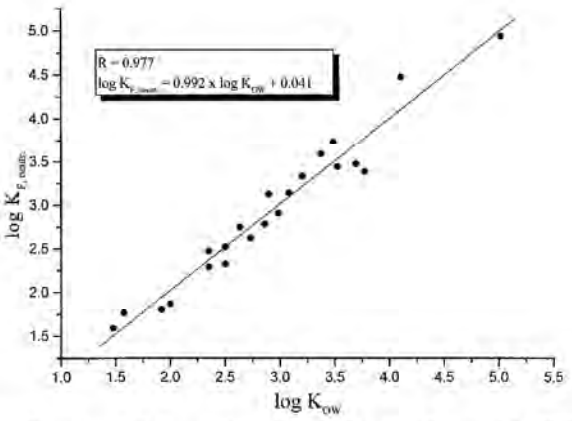

Fig. 3. Correlation of log K_{OW} values to the corrected extraction coefficient log $K_{F,neutr}$ of the SPME for selected phenols ($n = 22$).

tained extraction coefficients K_F were corrected according to Eq. (7) for the fraction of the neutral species that was extracted in the SPME.

$$\alpha = \frac{1}{1 + 10^{(pK_a - pH)}} \tag{6}$$

$$K_{F,neutr} = \frac{K_F}{\alpha} \tag{7}$$

When the $K_{F,neutr}$ values were used the correlation with log K_{OW} was highly improved yielding a correlation coefficient of 0.977 (see Fig. 3) and confirming the assumption that preferentially

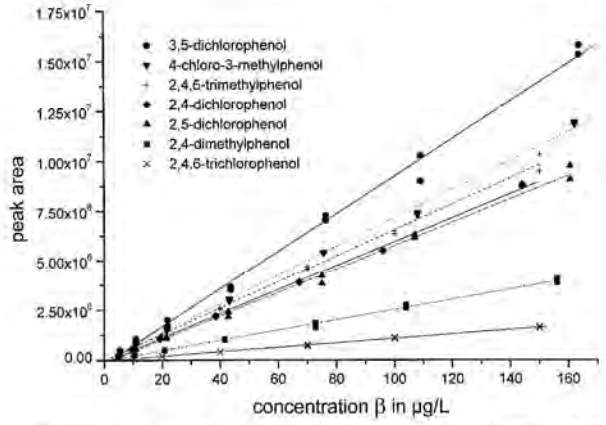

Fig. 4. Calibration curves for SPME analysis of selected phenols in a concentration range of 5–150 µg/l (30-min extraction time).

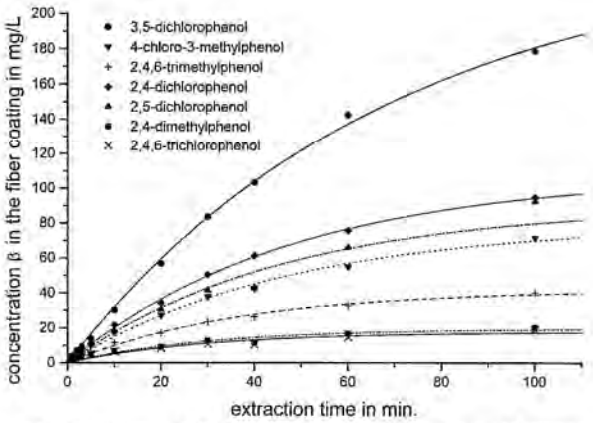

Fig. 5. Extraction kinetics of selected phenols for SPME analysis with a polyacrylate fiber (phenol concentration was 100 μg/l).

non-dissociated phenols were extracted by the SPME.

The calibration of the SPME analysis was performed for a concentration range of 5 μg/l < c_{Phenol} < 150 μg/l with an excellent linearity (correlation coefficient > 0.997). Examples of the calibration lines obtained are presented in Fig. 4. The limits of detection and determination for the investigated phenols were calculated by Eqs. (10) and (11) (see Appendix A) and were found to be below 4 μg/l and 15 μg/l, respectively (see Table 1).

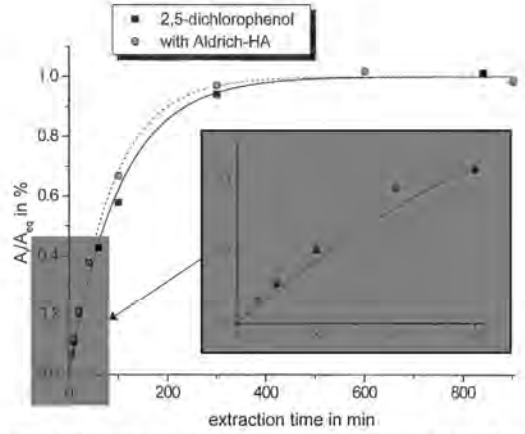

Fig. 6. Extraction kinetics for SPME analysis of 2,5-dichlorophenol in the presence and absence of Aldrich-HA (phenol concentration was 100 μg/l).

In order to determine the optimal extraction time, the time dependence of the SPME analysis was measured using an aqueous solution of mix I and mix II containing 100 μg/l of each phenol investigated.

As suggested by Vaes et al. (1996) first order formalism to describe the extraction kinetics was applied and the rate constants k_3 and k_4 of Eq. (8) (see Appendix A) were calculated accordingly. Fig. 5 shows the fitted curves of selected phenols. It was found that phenols with low K_F values reached their equilibrium faster than phenols with a higher affinity to the extraction fiber. This effect was attributed to mass-transfer limitations in case of phenols with high affinities to the SPME fiber. In order to work in a reasonable time frame the extraction time for further experiments was set to 30 min. This was long enough to avoid working in the high dynamic part of the extraction kinetics and short enough to allow several extractions per day.

3.2. Sorption of phenols to DOM

For the determination of the sorption isotherms the kinetics of the extraction in the presence and absence of DOM was measured. Fig. 6 shows the results of the measurements for 2,5-dichlorophenol. As can be seen there was a difference of up to 10% in the extraction kinetics at an extraction time between 50 and 400 min.

In order to consider the different extraction kinetics due to the presence of DOM in the calculation of the sorption isotherms, the extracted amounts of phenols were normalized to the amount extracted when the extraction equilibrium was established. A close inspection of the extraction kinetics showed two possible time windows for the SPME analysis. Either the extraction time is kept below 50 min or kept very long in order to have the extraction equilibrium established. Other extraction times would lead to an underestimation of the sorption constants for the sorption of phenols to DOM.

The isotherms obtained for the sorption of phenols to DOM showed a linear relationship between equilibrium concentration β and loading q according to the Henry equation. The sorption coefficients for the sorption of phenols to DOM were calculated by Eq. (4). The initial concentration $\beta(\mathrm{Phe})_0$ was determined by extracting a standard solution without DOM.

The sorption found in the SPME analysis were dependent on the origin of the DOM as well as on the particular phenol investigated. While the compost extract and HO14 showed only a small sorption of the investigated phenols, a more pronounced sorption to the commercial Aldrich-HA was observed. The log K_{OC} values varied between 2 and 3 (see Table 1). This stronger sorption behavior of the commercial Aldrich-HA compared to natural DOM has been recently reported in the literature and was attributed to the special origin of the material (Landrum et al., 1984; MacCarthy, 1989; Gremm, 1992; Loar et al., 1998).

For BSA the highest sorption of the phenols among the investigated DOM was observed. Here, the log K_{OC} values varied between 2 and 6 depending on the phenol under investigation.

The highest sorption of the phenols was determined for pentachlorophenol (PCP). With BSA and Aldrich-HA log K_{OC} values of 5.92 ± 0.17 and 3.00 ± 0.21, respectively, were calculated.

The observed sorption to the DOM was directly correlated with the hydrophobicity of the phenol. Compounds with small log K_{OW} values showed a small sorption to DOM, whereas the high log K_{OW} values usually resulted in a stronger sorption.

Upon raising the pH the observed sorption to DOM was decreased. For example 2,5-dichlorophenol showed with Aldrich-HA a log K_{OC} of 2.76 at pH 6.5. At pH 7.3 it decreased to 2.60 and at pH 8.3 to 1.66. The change of the pH caused a deprotonation of functional groups in the DOM as well as of the phenols. Hence, both effects have to be considered responsible for the decreased sorption. Due to the deprotonation of the phenols their hydrophobicity was decreased. On the other hand, the overall charge of the DOM molecules was increased with increasing pH which will also increase the repulsion between DOM and phenols. Furthermore, it is also attractive to consider a change of the confirmation of the

DOM with an overall loss of hydrophobic cavities for the sorption.

4. Conclusions

SPME proved to be an excellent tool for the investigation of the interaction of polar xenobiotics and DOM in solution. Because of the extremely small amount of analyte extracted from the solution a considerable influence on the sorption equilibrium is unlikely to occur and it can be applied to a broad variety of different groups of compounds simultaneously. However, the sorption kinetics in the presence and absence of DOM has to be evaluated very carefully. For the DOM investigated an accelerated sorption for phenols was observed. The same behavior was observed by Georgi (1998) for the extraction of PAH. The effect was explained by a carrier function of the DOM-molecules. In the absence of DOM, the extraction equilibrium is controlled by diffusion of the analyte alone. In the presence of DOM, an additional transport process of DOM-sorbed analytes to the fiber was assumed. Since the extracted amounts of compounds by the SPME fiber are very low and hence, an sorption of the DOM to the fiber is difficult to determine, an induced change of the sorption characteristics of the fiber due to sorbed DOM has also to be considered.

The sorption of xenobiotics to DOM is a complex combination of different interaction mechanisms. For non-polar xenobiotics (e.g. PAH) hydrophobic interactions have to be considered in the first place and the capability of the investigated DOM to form 'hydrophobic cavities' will determine the sorption. However, for polar xenobiotics containing functional groups (e.g. with acidic or basic character) specific interactions have to be taken into account. While for non-polar xenobiotics alterations of the interaction with DOM due to changes of the medium conditions (e.g. pH) can be attributed to altered DOM properties in the first place, for polar xenobiotics variations in their speciation have to be considered which will directly effect specific interactions to DOM.

The contribution of specific interactions to the overall sorption can vary to a great extent and is highly dependent on the xenobiotic and the DOM investigated. In our experiments, the highest sorption for phenol was observed for BSA which was the DOM sample with the highest molar weight and the highest content of basic functional groups. It is therefore attractive to attribute the observed strong sorption compared to the other DOM samples especially to the presence of functional groups (e.g. basic amino groups). Aldrich HA showed the highest sorption of the other natural DOM samples investigated. For those samples the apparent molar mass decreased in the order of Aldrich HA > HO14 > soil extract. It is reasonable to assume that with decreasing molar mass the capability of forming 'hydrophobic cavities' is decreased as well. Furthermore, the content of nitrogen in HO14 is rather low compared to other DOM samples (Frimmel and Abbt-Braun, 1999) and therefore, only a small degree of specific interactions can be expected.

It is intended to test the correlation of log K_{OC} values with molecular parameters like log K_{OW} and pK_a. Preliminary results made it tempting to look for a correlation in order to estimate K_{OC} values without time consuming measurements.

Acknowledgements

The work presented was financially supported by the Deutsche Forschungsgemeinschaft (grant Fr 536/20-1) which is greatly appreciated by the authors. Furthermore, the authors are grateful to Thomas Böhm for performing some sorption experiments.

Appendix A

In case the SPME extraction is described by a first-order kinetics

$$\frac{d\beta(Phe)_{SPME}}{dt} = k_3 \cdot \beta(Phe)_a - k_4 \cdot \beta(Phe)_{SPME} \quad (8)$$

where

- k_3 is the rate constant of the extraction process;
- k_4 is the rate constant of the desorption process;
- $\beta(Phe)_a$ is the phenol concentration in the aqueous phase in μg/l; and
- $\beta(Phe)_{SPME}$ is the phenol concentration in the fiber coating in μg/l.

the amount of phenol in the fiber coating at any time can be expressed by the following equation:

$$\beta(Phe)_{SPME,t} = \frac{k_3}{k_3(V_f/V_a) + k_4} \cdot \beta(Phe)_0 \times (1 - e^{-(k_3(V_f/V_a)+k_4)\cdot t}) \quad (9)$$

where

- $\beta(Phe)_{SPME,t}$ is the phenol concentration at time t in μg/l;
- V_f is the volume of the fiber coating; and
- V_a is the volume of the aqueous phase.

The limit of detection and limit of determination were calculated according to DIN 32645 (Norm, 1994) by the following formulas:

Limit of detection (NG):

$$NG = s_{x0} \cdot t_{n-2;1-\alpha} \cdot \sqrt{\frac{1}{n_1} + \frac{1}{n_2} + \frac{\bar{x}^2}{\sum(x_i - \bar{x})^2}} \quad (10)$$

where

- s_{x0} is the standard deviation;
- t is a student factor;
- n_1 is the number of sample measurements ($n_1 = 1$);
- n_2 is the number of calibration points ($n_2 = 10$);
- is the arithmetic mean of the x-values;
- x_i is the x-value; and
- α is the level of significance ($\alpha = 0.01$)

Limit of determination (BG):

$$BG = k \cdot s_{x0} \cdot t_{n-2;1-(\alpha/2)} \cdot \sqrt{\frac{1}{n_1} + \frac{1}{n_2} + \frac{(k \cdot NG - \bar{x})^2}{\sum(x_i - \bar{x})^2}} \quad (11)$$

where k is a factor of insecurity ($k = 3$).

References

Backhus DA, Gschwend PM. Fluorescent polycyclic aromatic hydrocarbons as probes for studying the impact of colloids on pollutant transport in groundwater. Environ Sci Technol 1990;24:1214–1223.

Bartak P, Cap L. Determination of phenols by solid-phase microextraction. J Chromatogr A 1997;767:171–175.

Buchholz KD, Pawliszyn J. Determination of phenols by solid-phase microextraction and gas chromatographic analysis. Environ Sci Technol 1993;27:2844–2848.

Buchholz KD, Pawliszyn J. Optimization of solid-phase microextraction conditions for determination of phenols. Anal Chem 1994;66:160–167.

Cardellicchio N, Cavalli S, Piangereli V, Giandomenico S, Ragone P. Determination of phenols in environmental samples by liquid chromatography–electrochemistry. Fresenius Anal Chem 1997;358:749–754.

Carter CW, Suffet IH. Binding of DDT to dissolved humic materials. Environ Sci Technol 1982;16:735–740.

Chin YP, Weber WJ. Estimating the effects of dispersed organic polymers on the sorption of contaminants by natural solids. Environ Sci Technol 1989;23:978–984.

Doll TE, Frimmel FH, Kumke MU, Ohlenbusch G. Interaction between natural organic matter (NOM) and polycylic aromatic compounds (PAC) — comparison of fluorescence quenching and solid phase micro extraction (SPME). Fresenius J Anal Chem 1999;364:313–319.

Fingler S, Tkalcevic B, Fröbe Z, Drevenkar V. Analysis of polychlorinated biphenyls, organochlorine pesticides and chlorophenols in rain and snow. Analyst 1994;119:1135–1140.

Frimmel FH, Abbt-Braun G. Basic characterization of reference NOM from central Europe — similarities and differences. Environ Int 1999;25:191–207.

Frimmel FH, Christman RF. Humic substances and their role in the environment. Chichester: Wiley, 1988.

Georgi A. Sorption von hydrophoben Verbindungen an gelösten Huminstoffen, UFZ-Umweltforschungszentrum: Leibzig-Halle GmbH, 1998.

Gießl H. DOM-flocculation: a suitable approach for separating free and DOM-bound herbicides? Environ Sci & Pollut Res 1999;6:77–82.

Gremm T. Zur Verteilung von polycyclischen aromatischen

Kohlenwasserstoffen und zinnorganischen Verbindungen in gewässerrelevanten Mehrphasensystemen. Dissertation, Karlsruhe, 1992.

Hassett JP, Milicic E. Determination of equilibrium and rate constants for binding of a polychlorinated biphenyl congener by dissolved humic substances. Environ Sci Technol 1985;19:638–643.

Huber SA, Scheunert I, Dörfler U, Frimmel FH. Zum Einfluß des gelösten organischen Kohlenstoffs (DOC) auf das Mobilitätsverhalten einiger Pestizide. Acta Hydrochim Hydrobiol 1992;20:74–81.

Jensen J. Chlorphenols in the terrestrial environment. Rev Environ Contam Toxicol 1996;146:25–52.

Jobst H. Chlorophenols and nonylphenols in sewage sludges. Part II: Did contents of pentachlorophenol and nonylphenol reduce. Acta Hydrochim Hydrobiol 1998;26:344–348.

Kishino T, Kobayashi K. Acute toxicity and structure–activity relationships of chlorophenols in fish. Water Res 1996a;30:387–392.

Kishino T, Kobayashi K. Studies on the mechanism of toxicity of chlorophenols found in fish through quantitative structure–activity relationships. Water Res 1996b;30:393–399.

Klaus U, Oesterreich T, Volk M, Spiteller M. Interaction of aquatic dissolved organic matter (DOM) with amitrole: the nature of the bound residues. Acta Hydrochim Hydrobiol 1998;26:311–317.

Kördel W. Fate and effects of contaminants in soils as influenced by natural organic materials — status of information. Chemosphere 1997;35:405–411.

Kopinke FD, Pörschmann J, Stottmeister U. Sorption of organic pollutants on anthropoganic humic matter. Environ Sci Technol 1995;29:941–950.

Kumke MU, Löhmannsröben HG, Roch T. Fluorescence quenching of polycyclic aromatic compounds by humic acids. Analyst 1994;119:997–1001.

Landrum PF, Nihart SR, Eadie BJ, Gardner WS. Reverse-phase separation method for determining pollutant binding to Aldrich humic acid and dissolved organic carbon of natural waters. Environ Sci Technol 1984;18:187–192.

Lee SK, Freitag D, Steinberg C, Kettrup A, Kim YH. Effects of dissolved humic materials on acute toxicity of some organic chemicals to aquatic organisms. Water Res 1993;27:199–2204.

Loar Y, Farmer WJ, Aochi Y, Strom PF. Phenanthrene binding and sorption to dissolved and to mineral-associated humic acid. Water Res 1998;32:1923–1931.

Lüers F, Ten Hulscher TEM. Temperature effect on the partitioning of polycyclic aromatic hydrocarbons between natural organic carbon and water. Chemosphere 1996; 4:643–657.

Luehrs DC, Hickey JP, Nilsen PE, Godbole KA, Rogers TN. Linear solvation energy relationship of the limiting partition coefficient of organic solutes between water and activated carbon. Environ Sci Technol 1996;30:143–152.

MacCarthy P. The nature of commercial humic acids. In: Suffet IH, McCarthy JF, editors. Aquatic humic substances. Washington DC: American Chemical Society, 1989:55–63.

McCarthy JF. 'Bioavailability and toxicity of metals and hydrophobic organic contaminants. In: Suffet IH, McCarthy JF, editors. Aquatic humic substances. Washington: American Chemical Society, 1989:263–277.

McCarthy JF, Zachara JM. Subsurface transport of contaminants. Environ Sci Technol 1989;23:496–502.

Norm DIN 32645 Nachweis-, Erfassungs- und Bestimmungsgrenze. Beuth Verlag GmbH, Berlin, 1994.

Paasivirta J, Hakala H, Knuutinen J et al. Organic chlorine compounds in lake sediments. III. Chlorohydrocarbons, free and chemically bound chlorophenols. Chemosphere 1990;21:1355–1370.

Paolis F De, Kukkonen J. Binding of organic pollutants to humic and fulvic acids: influence of pH and the structure of humic material. Chemosphere 1997;34:1693–1704.

Parris GE. Covalent binding of aromatic amines to humates. 1. Reactions with carbonyls and quinones. Environ Sci Technol 1980;14:1099–1106.

Poerschmann J, Zhang Z, Kopinke FD, Pawliszyn J. Solid phase microextraction for determining the distribution of chemicals in aqueous matrices. Anal Chem 1997;69: 597–600.

Quemerais B, Lemieux C, Lum KR. Distribution and fate of chlorophenols in the St. Lawrence river basin, Canada. Chemosphere 1994;28:1943–1960.

Rebhun M, de Smedt F, Rwetabula J. Dissolved humic substances for remediation of sites contaminated by organic pollutants. Binding-desorption model predictions. Water Res 1996;30:2027–2038.

Schilling R, Clarkson PJ, Cooke M. Enhanced recovery of chlorophenols from surface waters using polymer based extraction cartridges. Fresenius J Anal Chem 1998;360: 90–94.

Schlautmann MA, Morgan JJ. Effects of aqueous chemistry on binding of polycylic aromatic hydrocarbons by dissolved humic materials. Environ Sci Technol 1993;27:961–969.

Smith S, Furay VJ, Layiwola PJ, Menezes-Filho JA. Evaluation of the toxicity and quantitative structure–activity relationships (QSAR) of chlorophenols to the copepodid stage of a marine copepod (*Tisbe battaglini*) and two species of benthic flatfish, the flounder (*Platichthys flesus*) and sole (*Solea solea*). Chemosphere 1994;28:825–836.

Steinberg CEW, Sturm A, Kelbel J et al. Changes in acute toxicity of organic chemicals to *Daphnia magna* in the presence of dissolved humic material (DHM). Acta Hydrochim Hydrobiol 1992;20:326–332.

Steinberg CEW, Xu Y, Kyu Lee S, Freitag D, Kettrup A. Effects of dissolved humic material (DHM) on bioavailability of some organic xenobiotics to *Daphnia magna*. Chem Spec Bioavail 1993;5:1–9.

Stevenson FF. Humus chemistry — genesis, composition, reactions. New York: Wiley, 1982.

Vaes WHJ, Ramos EU, Verhaar HJM, Seinen W, Hermes JLM. Measurement of the free concentration using solid-phase microextraction. Anal Chem 1996;68:4463–4467.

Veningerova M, Uhnak J, Prachar V, Kovacicova J. Chlorinated phenols in human milk. Z Lebensm Unters Forsch 1996;2203;309–310.

2.2.3 Fluorescence of humic acids (HA) and pyrene-HA complexes at ultralow temperature

M.U. Kumke, F.H. Frimmel, F. Ariese, C. Gooijer
Environ. Sci. Technol., 2000, **34**, 3818 - 3823.

Die Verwendung von Fluoreszenzsonden zur Untersuchung von Wechselwirkungsmechanismen und molekularen Umgebungsparametern ist in biologischen und biochemischen Systemen, aber auch zur Untersuchung von heterogenen Systemen Handwerkszeug geworden. Oft eingesetzte Fluoreszenzsonden sind PAK und deren Derivate. Pyren zeichnet sich unter anderem durch eine Hypersensitivität gegenüber der Umgebungspolarität aus, d.h. die Schwingungsstruktur des Fluoreszenzspektrums ändert sich als Funktion der Polarität (s. 2.2.1 und Anhang D, Nr. 32). Die Verwendung von Pyren als Fluoreszenzsonde zur Untersuchung der Wechselwirkungen von hydrophoben Xenobiotika und HS war bislang nicht erfolgreich, da die Fluoreszenz des Pyrens durch HS gelöscht wird. In Untersuchungen bei Raumtemperatur konnten daher keine Veränderungen im Fluoreszenzspektrum des Pyrens gemessen werden (s. auch 2.2.1). In Tieftemperaturexperimenten bei 10 K konnten Variationen in der Schwingungsstruktur des Pyrenfluoreszenzspektrums beobachtet werden, da mittels *fluorescence line narrowing* extrem kleine spektrale Veränderungen noch auflösbar sind. Es konnte gezeigt werden, dass sich ein Teil des mit HS wechselwirkenden Pyrens in einer Umgebung befindet, die in ihrer Polarität vergleichbar mit einem kurzkettigen Alkohol wie Butanol ist. Weiterhin wurden auch die intrinsische Fluoreszenz von HS verschiedener Ursprungsorte bei 10 K mit Hilfe der *fluorescence line narrowing* Technik untersucht. Es konnte kein entsprechender Tieftemperatureffekt beobachtet werden, was ein Beleg für die Beteiligung von Energietransfer- und Protonentransferprozessen sowie konformativen Änderungen im elektronisch-angeregten Zustand ist (s. auch 2.1).

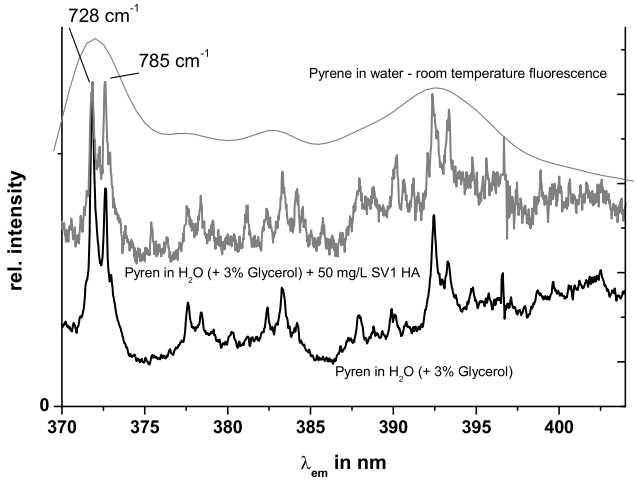

Environ. Sci. Technol. 2000, 34, 3818−3823

Fluorescence of Humic Acids (HA) and Pyrene-HA Complexes at Ultralow Temperature

M. U. KUMKE* AND F. H. FRIMMEL
Division of Water Chemistry, Engler-Bunte-Institut, TH Karlsruhe, Engler-Bunte-Ring 1, 76131 Karlsruhe, Germany

F. ARIESE AND C. GOOIJER
Department of Analytical Chemistry and Applied Spectroscopy, Vrije Universiteit, De Boelelaan 1083, 1081 HV Amsterdam, The Netherlands

The interaction of pyrene with humic acids of different origins was investigated using fluorescence line narrowing (FLN) spectroscopy at 10 K. FLN spectroscopy can be used to obtain vibrationally resolved fluorescence spectra from samples that under ordinary conditions suffer from extensive spectral broadening. Due to the presence of humic acid the site distribution and the relative intensities of the ground-state vibrations in the fluorescence spectrum (Ham-effect) of pyrene were changed. Both effects were related to the altered microenvironment of pyrene in the presence of humic acid. On the other hand, for humic acids no fluorescence line narrowing effect was observed indicating the occurrence of intra- and intermolecular processes.

Introduction

The interaction of hydrophobic organic compounds with humic substances is a subject of great importance for the evaluation of the transport and distribution of contaminants in the environment. The class of polycyclic aromatic compounds (PAC) is one of the most prominent. Because of their carcinogenic potential, PAC represent a potential risk to human health, and, therefore, their fate and transport is of high interest (*1*−*6*). In the past, different analytical approaches were used in order to characterize quantitatively and qualitatively the interactions between humic substances and contaminants (*7*−*14*). Here, two main types of analytical techniques can be distinguished: on the one side techniques using a separation step, like high-performance liquid chromatography (HPLC), prior to detection, and on the other side spectroscopic techniques that analyze the sample directly without a separation.

The fluorescence quenching approach is frequently used for the determination of the sorption of PAC by humic substances. Besides its high sensitivity, especially at low concentrations of humic substances, the noninvasive character makes the method highly attractive for the investigation of interactions between PAC and humic substances (*15*−*20*). Moreover, the multidimensional character of the fluorescence approach is especially beneficial for the characterization of the interaction processes. However, fluorescence techniques are prone to experimental limitations, and a careful consideration of inner filter effects and fluorescence quenching effects other than those induced by the humic substances is highly important for a correct interpretation of the observed effects (*17*−*19*). While the fluorescence data can readily be corrected for experimental artifacts, knowledge of the interaction mechanism is indispensable for the interpretation of the experimental results.

The combination of time-resolved fluorescence and steady-state fluorescence experiments was used to distinguish between static and dynamic interactions (*17, 21*). It was shown that for the investigated samples mainly a static interaction mechanism was dominant (*17, 21, 22*). To get a deeper insight into the interaction mechanism, e.g., whether the sorption is due to inclusion in micelle-like structures or sorption to hydrophobic subunits of the humic substances, further fluorescence techniques including fluorescence anisotropy were applied (*21, 23, 24*). In these experiments some indications for a micellar binding mechanism were observed. One of the basic assumptions often made in the interpretation of the steady-state fluorescence experiments is the complete quenching of the PAC fluorescence due to the interaction with humic substances. However, for some humic substances investigated, indications were found that not a total quenching of the fluorescence of the PAC was induced by the interaction, or the data evaluation revealed that the assumption of a purely static interaction might be an oversimplification (*16, 21, 22, 25*). Recently, the interactions of PAC and humic substances of different origins were investigated using fluorescence spectroscopy as well as solid-phase micro extraction (SPME) combined with gas chromatography/mass spectrometry (GC/MS) analysis (*20*). In both approaches a strong dependence of the observed interaction on the origin of the humic substances and on the water solubility of the PAC was observed. However, using the fluorescence approach a stronger interaction was found when compared to the SPME-GC/MS technique.

The objective of the present work was to further investigate the interaction mechanism between PAC and humic substances on a molecular level. Fluorescence line narrowing (FLN) spectroscopy is a technique that—to the best of our knowledge—has never been applied to study PAC-humic substance interactions. FLN spectroscopy can be used to obtain vibrationally resolved fluorescence spectra from samples that under ordinary conditions suffer from extensive spectral broadening. One of the major underlying causes for spectral broadening in solutions is solvent inhomogeneity. Chemically identical molecules are surrounded by different solvent environments or adopt different conformations, resulting in a Gaussian distribution of energy transitions. Under normal room-temperature conditions the corresponding fluorescence bands show a peak width of 300 cm^{-1} or more; thus blurring all underlying vibrational information. When lowering the temperature of such disordered solutions, one usually observes only a limited improvement in resolution. However, when a narrow-banded light source such as a laser is used for excitation only a selection of molecules, i.e., those molecules whose individual energy levels happen to match the photon energy of the laser, will be excited. In frozen solutions at temperatures of 4−20 K this selection is maintained during the lifetime of the excited state, and only this selection of energetically equivalent molecules ("isochromat") will fluoresce, resulting in a highly resolved emission spectrum. For a more detailed review on various applications of FLN spectroscopy for chemical analysis see Jankowiak and Small (*26, 27*). In this study, the environmental sensitivity of the pyrene fluorescence combined with the high spectral resolution of fluorescence line narrowing

* Corresponding author phone: ++49 721 608 6381; fax: ++49 721 608 7051; e-mail: Michael.Kumke@ciw.uni-karlsruhe.de.

10.1021/es9910457 CCC: $19.00
Published on Web 07/29/2000

spectroscopy was applied to probe the molecular environment of PAC in the presence of humic substances.

Experimental Section

The samples were filled in an in-lab built sample holder and mounted to a Cryodyne closed-cycle helium refrigerator (CTI Cryogenics, Waltham, MA, Model 21). For the FLN experiments, four samples at a time were cooled to 10 K. Fluorescence was collected in a front-face geometry and the sample thickness was only 0.5 mm. Therefore, inner filter effects, which are influencing standard room-temperature fluorescence measurements to a great extent, were insignificant in the FLN experiments.

Two different freezing procedures were tested. In the first one the sample was frozen within seconds by dipping the probe head together with the sample in liquid nitrogen. In the second approach the sample was cooled within 40 min with the close-cycle helium refrigerator starting at room temperature. Both cooling procedures yielded indistinguishable FLN spectra. The FLN experiments were carried out in triplicate.

The excitation wavelength was varied between 360 nm < λ_{ex} < 368 nm using a XeCl excimer laser (Lambda Physik LPX 110i, Göttingen Germany) pumping a dye laser (Lambda Physik LPD 3002). Fiber optics were used to transport the excitation light to the quartz window of the cryostat, the average output power at the end of the fiber optics used was 12 mW. The laser system was operated at 10 Hz; the pulse width was ca. 10 ns. The fluorescence was collected with a 9 cm F/1 quartz lens and focused on the entrance slit of a Spex 1877 triple monochromator (Edison, NJ). The spectral resolution was 0.1 nm. For the detection a Princeton Instrument (Trenton, NJ) intensified linear diode array type IRY 1024 BRG covering a spectral range of 36 nm was used.

In the FLN measurements the concentration of pyrene was < 10^{-6} M. The pyrene was first dissolved in ethanol yielding a concentration in the stock solution of 10^{-5} M. One milliliter of the stock solution was transferred into a glass vial and the organic solvent was evaporated. Ten milliliters of water or water/humic acid (HA) were added to the vial. The solution was equilibrated for at least 24 h. Pure water samples gave relatively poor FLN spectra, probably caused by solubility problems during the cooling procedure. To improve the quality of the FLN spectra a small amount of glycerol was added to the samples. Glycerol was chosen in order to avoid alterations of the solvent properties (e.g. polarity) and to keep the pyrene in solution during the cooling procedure. The polarity of the aqueous solution is only slightly altered by the addition of glycerol, but the viscosity of the solution is increased, improving the intensities of the FLN spectra. To minimize the effects of the added glycerol on the pyrene-HA equilibrium, glycerol was added right before the samples were transferred into the FLN sample holder. The glycerol concentration was varied between 1% and 10% in order to monitor the influence on the observed FLN spectra.

To measure selectively the pyrene fluorescence signal in the FLN experiments the detector was gated with a delay of ca. 30 ns, and the data were collected in a time window of 2.5 μs and integrated for 28 s. After 30 ns no emission of the HA was left, and the pyrene fluorescence was detected exclusively.

The HA samples were taken from different aquatic origins and were isolated using a XAD-8 resin according to a modified method of Mantoura and Riley (*28, 29*). The basic properties of the samples are well characterized (*30*). HO13 HA was isolated from a brown water lake (Lake Hohloh, Black Forest, Germany), FG1 HA from a groundwater (Fuhrberg, Hannover, Germany), and SV1 HA from a production effluent of brown coal industry (Halle/Leipzig, Germany). The pH of the HA solutions was adjusted to 4.3 since it is known from previous studies investigating the binding of hydrophobic organic compounds to humic substances that at low pH the observed interaction is maximized.

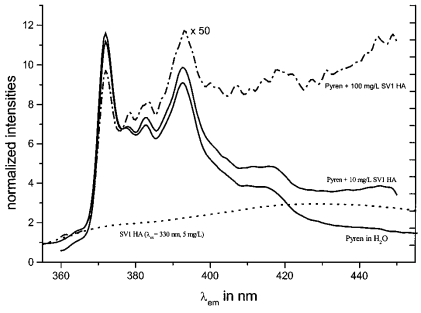

FIGURE 1. Normalized room-temperature fluorescence spectra of pyrene, SV1 HA and mixtures of both in water, for an excitation wavelength λ_{ex} = 330 nm.

Results and Discussion

The dependence of the vibronic features of the pyrene fluorescence emission spectra on the polarity of the solvent (the so-called Ham effect) has frequently been used in investigations probing the molecular environment of the pyrene (*31*). Moreover, pyrene was often used in experiments dealing with the interactions of PAC and humic substances. However, at room temperature, beside the "real" fluorescence quenching, the observed steady-state fluorescence spectra are also altered due to inner filter effects and the intrinsic fluorescence of the humic substances. Both drawbacks make it very difficult to use the environmental sensitivity of the pyrene fluorescence for investigations of the interaction with humic substances. In Figure 1 the drawbacks described are shown for pyrene and SV1 HA, as an example of the relevant optical properties of humic substances. Here, the room-temperature fluorescence spectra were normalized to visualize the influence of SV1 HA on the pyrene fluorescence due to inner filter effects and intrinsic fluorescence of SV1 HA.

Based on the room temperature fluorescence spectra it is not feasible to distinguish between different forms of pyrene in the presence of humic substances, e.g., free pyrene and pyrene trapped in a micellar-like environment inside the humic matrix (close proximity). This is especially the case when the trapped pyrene contributes only with an extremely low fluorescence quantum yield to the total observed fluorescence. Furthermore, due to the broadness of the fluorescence bands, subtle shift of a few tenths of a nanometer cannot be observed.

To circumvent these problems, the fluorescence of pyrene was investigated at ultralow temperatures using a fluorescence line narrowing approach. Fluorescence line narrowing (FLN) spectra are vibronically high-resolved fluorescence spectra that are sensitive to changes in the molecular environment of the probe (*26, 27, 32*). A similar approach was used by Suh et al. (*33*) to study subtle conformational changes of benzo[*a*]pyrene-DNA adducts as a function of base sequence. Due to the experimental set up, the influence of inner filter effects and intrinsic fluorescence of the humic substances were reduced to a minimum. Furthermore, the use of a pulsed laser and time-resolved detection allowed us to selectively monitor the pyrene fluorescence, without any interference from HA emission (the fluorescence lifetime of pyrene is several hundred nanoseconds, much longer than that of all humic acids tested).

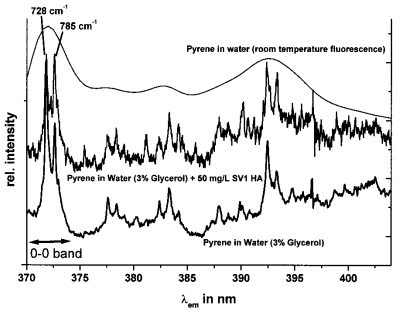

FIGURE 2. FLN spectrum of pyrene in water (bottom) and in the presence of 50 mg/L SV1 HA (λ_{ex}= 362 nm; middle). The room-temperature fluorescence spectrum of pyrene in water is shown on top. The wavenumbers given in the multiplet 0−0 band represent vibrational energies of the first electronically excited state ($\nu_{ex} - \nu_{0-0}$).

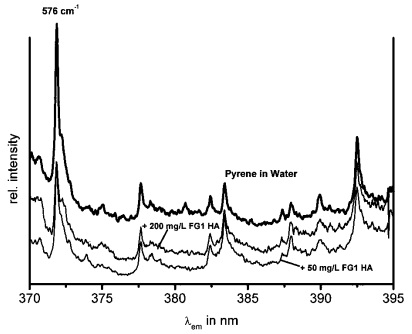

FIGURE 3. FLN spectrum of pyrene in water (top) and in the presence of different concentrations of FG1 HA (λ_{ex}= 364 nm).

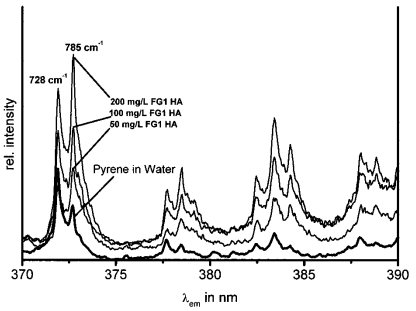

FIGURE 4. FLN spectrum of pyrene in water (bottom) and in the presence of different concentrations of FG1 HA (λ_{ex}= 362 nm). All samples were in aqueous solution with 3% glycerol.

Influence of Glycerol on the FLN Spectra of Pyrene. In preliminary FLN experiments with pyrene in pure water it was found that the signal intensity was dramatically decreased due to losses of dissolved pyrene during the freezing process. To keep the pyrene in solution and prevent it from crystallizing during the freezing procedure a small amount of glycerol was added. FLN measurements were taken at glycerol contents between 10% and 1%. Due to the addition of glycerol the overall signal intensity was significantly improved, and, more important, it was found that for this concentration range the glycerol showed no detectable effect on the vibronic features of the FLN spectra of pyrene. For further FLN experiments investigating the interaction of pyrene with humic acids (HA) the concentration of glycerol was adjusted to 3%. The glycerol was added immediately before the freezing procedure in order to minimize its influence on the interaction between HA and pyrene. Allowing the system to reequilibrate in the 3% glycerol environment would increase the risks of inadvertently altering the HA-pyrene binding modes.

FLN Spectra of Pyrene in the Presence of Humic Acids (HA). *(a) General Aspects: Effect of λ_{ex}.* Figure 2 shows typical FLN spectra obtained for pyrene in water with 3% glycerol in absence and presence of SV1 HA. For comparison, also the room temperature fluorescence spectrum of pyrene in water is shown, illustrating the typical improvement in spectral resolution that can be obtained with the FLN approach. In general, the observed fluorescence intensity of pyrene in the presence of HA was quenched, which agrees with results previously reported for fluorescence quenching experiments performed at room temperature (e.g., ref *17*). The laser was tuned to different regions of the $S_1 \leftarrow S_0$ absorption, each probing a different set of S_1 vibrations. For λ_{ex} = 362 nm two isochromates (sites) were excited, corresponding to two excited-state vibrations at ν_A = 728 cm^{-1} and ν_B = 785 cm^{-1} and resulting in the doublet structure of the FLN spectrum. In the presence of HA, the vibrational frequencies in the FLN spectra of pyrene were not altered, but the intensity of the 785 cm^{-1} band increased significantly relative to the 728 cm^{-1} band. These phenomena will be explained in more detail below.

While for λ_{ex} = 362 nm two different isochromates were excited and a doublet spectrum obtained (see Figure 2), for λ_{ex} = 364 nm only one isochromate (with an exited state vibration at 576 cm^{-1}) was excited (see Figure 3). Here, the laser wavelength matches only a single, predominant vibronic transition.

Interestingly, Figures 2−4 also present a clear illustration of the Ham-effect, i.e., the phenomenon that weakly allowed transitions show an intensity enhancement in polar solvents as a result of symmetry reduction (*34*). In the case of pyrene, the origin band is only weakly allowed; without strong interactions with the solvent the origin is often weak or of similar intensity as the vibronic transitions. In polar solvents, however, the relative intensity of the origin transition increases, and this effect has been used to probe the microenvironment of pyrene in different solvents and inside micelles (*31*).

As shown in Figures 2−4 the relative intensity of the origin band decreases in the presence of humic acids SV1 HA or FG1 HA, indicating that the micro-environment surrounding pyrene in these samples is of a less polar character than water. This can best be seen for λ_{ex} = 364 nm (Figure 3). At room temperature this change was also observed when the polarity of the solvent was changed (*31*) and is attributed to the so-called Ham effect. In Figure 3 it is especially obvious for the peaks at 372 and 383 nm, but it can also be seen in the other FLN spectra shown (Figures 2, 4, and 5). The ratio of the peak intensities at 383 and 372 nm in Figure 3 changes from 0.35 for pyrene in water to about 0.65 for pyrene in the presence of FG1 HA. This ratio was found to be independent from the concentrations of FG1 HA investigated, which could

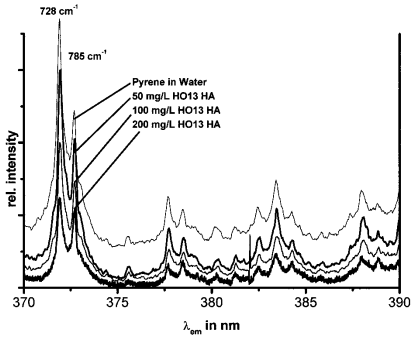

FIGURE 5. FLN spectrum of pyrene in water (top) and in the presence of different concentrations of HO13 HA (λ_{ex} = 362 nm).

mean that at the lowest concentration of HA the reaction with pyrene is already complete in terms of changing the molecular environment of the PAC. On the other hand, in the case of HO13 HA (see Figure 5), the FLN spectra show a red-shift similar to those of Figures 2−4, but the Ham effect is absent or very weak. Apparently, the microenvironment surrounding pyrene in this particular humic acid sample is of a relatively polar character, that is, not very different from water. It is interesting to note that the change in the intensity ratio points in the same direction found for pyrene at room temperature when going from water to less polar solvents. Kalyanasundaram and Thomas reported a change from 0.63 to 1.07 in the intensity ratio I_1/I_3 when changing the solvent from water to pentanol (*31*). Of course, these ratio changes refer to poorly resolved RT fluorescence spectra and can only be compared to the FLN spectra in a qualitative way.

(b) Influence of HA Concentration. The FLN experiments were performed at different concentrations of HA. Because of the small sample thickness, artifacts related to inner filter effects were negligible. In the experiments, HA concentrations of 50 mg/L, 100 mg/L, and 200 mg/L dissolved organic carbon (DOC) were used, and the obtained FLN spectra are compared. With increasing DOC concentration, the ratio of $\nu_{728\ cm}/\nu_{785\ cm}$ decreased (see Figures 4 and 5). Similar effects were found for other ground-state vibrational intensity ratios, as is also shown in Figures 4 and 5. Interestingly, the $\nu_{728\ cm}/\nu_{785\ cm}$ intensity ratios continued to change with increasing HA concentrations, while the maximum Ham-effect was already observed at the lowest HA concentrations.

(c) Influence of HA Origin. The magnitude of the vibrational intensity shifts in the FLN spectrum of pyrene was dependent on the origin of the HA used. In Figure 5 the observed FLN spectra in the presence of a brown water HA (HO13 HA) are shown at different concentrations. Again, the ratio of vibrational intensities (e.g., for site A at 728 cm^{-1} compared to site B at 785 cm^{-1}) was decreasing with increasing HA concentration. However, these changes were much less pronounced when compared with the FLN spectra measured in the presence of FG1 HA (see Figure 4) at similar HA concentrations.

In summary, two effects were observed in the FLN experiments with pyrene in the presence of HA: (a) a change in the site distribution when HA was added and (b) a change in the relative intensities of the ground-state vibrations (Ham-effect).

The former effect, i.e., the change in the site distributions upon the addition of HA, can be explained by means of an energy diagram as shown in Figure 6. Due to solvent inhomogeneity, the electronic transitions are broadened, indicated by Gaussian profiles. When irradiating the sample with 362.00 nm laser light, pyrene is excited into the vibronic region of the first electronically excited state, S_1. In this case, pyrene is excited through two major S_1 vibrations, $\nu_A \approx 728$ cm^{-1} and $\nu_B \approx 785$ cm^{-1}. In water (Figure 6a), the laser energy corresponds to the center of the ν_A distribution and overlaps only slightly with the low-energy edge of the ν_B distribution. Few pyrene molecules will therefore be excited through the ν_B vibronic transition, and as a result the corresponding origin band (marked site B in the insert) is relatively weak. In the

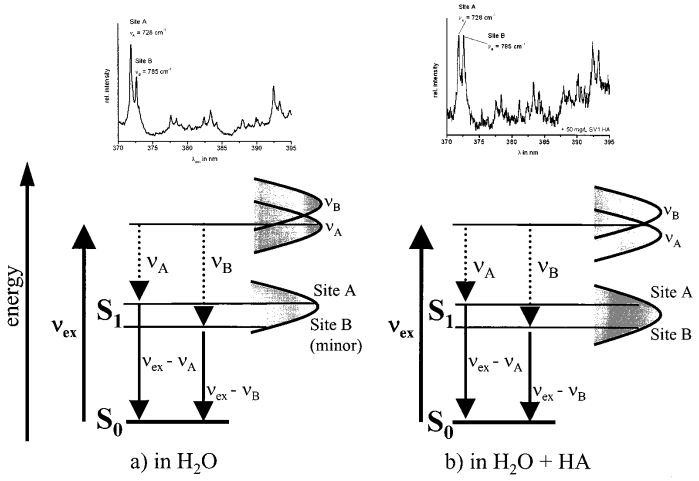

FIGURE 6. Illustration of the vibrational intensity shift of the 0−0 origin multiplet as a result of a decreasing S_0−S_1 energy gap. For explanation see text.

presence of HA (Figure 6b), the interactions cause a small shift of the S_1 level (and its corresponding vibrational levels) to lower energy. The excitation energy of the laser now shows comparable overlap with both the ν_A and the ν_B distributions, and as a result the corresponding origin bands are of approximately equal intensity. In other words, the FLN technique allows us to observe slight shifts in the average 0−0 transition energy that would go unnoticed under broadbanded, room-temperature conditions.

In a previous study differences between the apparent binding constant found in SPME and in fluorescence quenching were reported when the interaction of phenanthrene and amino-phenanthrene with humic acid was investigated (*20*). Under the simple assumption of a 1:1 reaction between HA and phenanthrene (or amino-phenanthrene), similar binding constants should have been observed with both methods. It was suggested that the observed differences were due to the fact that the fluorescence of the probe molecules is quenched already even in weakly bound states (equal to close proximity), while the SPME detects only the strongly bound fraction. The results of the present FLN experiments further support the suggested presence of probe molecules bound to humic acids at different binding stages. In the FLN experiments, using pyrene as a fluorescence probe, the overall fluorescence intensity was decreased when HA were present, which can be attributed to the strongly bound fraction of pyrene for which a complete quenching is assumed. Dynamic quenching can be excluded in the frozen matrices used in these experiments.

The fluorescence quantum yield and the fractional contribution of the weakly interacting pyrene molecules have not yet been determined and are subject to future work. Based on the results found at room temperature and at low temperature, it can be expected that the fluorescence quantum yield is rather small.

FLN Experiments with HA. Most humic substances show native fluorescence, and this emission (without addition of pyrene) was studied as well. In Figure 7a the room-temperature fluorescence emission and excitation spectra of SV1 HA are shown. In the FLN experiments an excitation range between 360 and 370 nm was probed. Based on the steady-state spectra this should have been a reasonable range for exciting fluorophores of humic acid molecules into a vibronic level of a corresponding S_1 state. However, under the experimental conditions applied no significant FLN effect was found for the investigated humic acids. A typical fluorescence emission found for humic acids at 10 K is shown in Figure 7b.

Since lignin and further plant material is considered as precursors of humic acids, it is reasonable to attribute the observed fluorescence to moieties such as quinones and aromatic hydroxy carboxylic acids (*35*−*38*). It is well-known that for this class of compounds often a large Stokes' shift is found in their steady-state emission spectra caused by a large change in dipole moment or by a proton exchange process. Moreover, humic acids are considered as fairly large polyelectrolytes, and, therefore, intramolecular motions due to electronic excitation are likely to occur as well. Strong indications that the processes described above occur and contribute to the observed fluorescence emission were also found in time-resolved fluorescence experiments with humic substances and their metal complexes (*39, 40*). The results reported here further support the previously presented data. Excited-state reactions, e.g., intramolecular proton transfer and/or charge transfer reactions, are likely to occur even at very low temperatures which could be an explanation (together with the heterogeneity of the HA) for the nonobservation of a clear FLN effect for the humic acids investigated. Differences in the interactions due to the origin of the HA call for a detailed investigation of the correlation with other characteristics such as functional groups and building blocks of the humics.

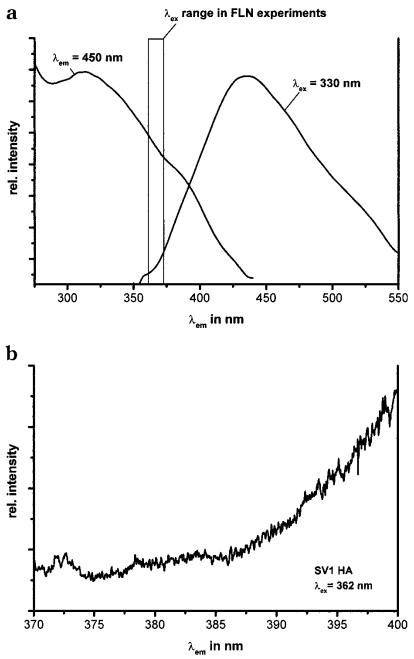

FIGURE 7. (a) FLN spectrum of SV1 HA in water (at 10 K). (b) Fluorescence excitation and emission spectra of HO13 HA in water (pH 7). Shown also is the excitation wavelength range used in the FLN experiments.

Acknowledgments

The authors are grateful to the Deutsche Forschungsgemeinschaft for supporting the work financially within the ROSIG program. They especially thank Dr. G. Abbt-Braun for the supply of the humic acid materials.

Literature Cited

(1) Rügner, H.; Kleinedam, S.; Grathwohl, P. *Environ. Sci. Technol.* **1999**, *33*, 1645−1651.
(2) Kleinedam, S.; Rügner, H.; Ligouis, B.; Grathwohl, P. *Environ. Sci. Technol.* **1999**, *33*, 1637−1644.
(3) Raber, B.; Kögel-Knabner, I. *Eur. J. Soil Sci.* **1997**, *48*, 443−455.
(4) Rebhun, M.; De Smedt, F.; Rwetabula, J. *Water Res.* **1996**, *30*, 2027−2038.
(5) Rav-Acha, C.; Rebhun, M. *Water Res.* **1992**, *26*, 1645−1654.
(6) Johnson, W. P.; Amy, G. L. *Environ. Sci. Technol.* **1995**, *29*, 807−817.
(7) Gauthier, T. D.; Seitz, W. R.; Grant, C. L. *Envrion. Sci. Technol.* **1987**, *21*, 243−248.
(8) Chiou, C. T.; Kile, D. E.; Malcolm, R. L. *Environ. Sci. Technol.* **1988**, *22*, 298−303.
(9) McCarthy; J. F., Roberson, L. E.; Burrus, L. W. *Chemosphere* **1989**, *19*, 1911−1920.
(10) Chin, Y.-P.; Weber, W. J.; Eadie, B. J *Environ. Sci. Technol.* **1990**, *24*, 837−842.
(11) Spark, K. M.; Swift, R. S. *Sci. Tot. Environ.* **1994**, *152*, 9−17.
(12) Kopinke, F.-D.; Pörschmann, J.; Stottmeister, U. *Environ. Sci. Technol.* **1995**, *29*, 941−950.

(13) Kumke, M. U.; Löhmannsröben, H.-G.; Roch, T. *J. Fluorescence* **1995**, *5*, S. 139−153.
(14) Laor, Y.; Farmer, W. J.; Aochi, Y.; Strom, P. F. *Wat. Res.*, **1998**, *32*, 1923− 1931.
(15) Gauthier, T. D.; Shane, E. C.; Guerin, W. F.; Seitz, W. R.; Grant, C. L. *Environ. Sci. Technol.* **1986**, *20*, 1162−1166.
(16) Schlautman, M. A.; Morgan, J. J. *Environ. Sci. Technol.* **1993**, *27*, 961−969.
(17) Kumke, M. U.; Löhmannsröben; H.-G., Roch, T. *Analyst* **1994**, *119*, S. 997−1001.
(18) Danielsen, K. M., Chin, Y.-P., Buterbaugh, J. S., Gustafson, T. L., Traina, S. J. *Environ. Sci. Technol.* **1995**, *29*, 2162−2165.
(19) Tiller, C. L.; Jones, K. D. *Environ. Sci. Technol.* **1997**, *31*, 424−429.
(20) Doll, T. E.; Frimmel, F. H.; Kumke, M. U.; Ohlenbusch, G. *Fresenius. J. Anal. Chem.* **1999**, *364*, 313−319.
(21) Morra, M. J.; Corapciolglu, M. O.; von Wandruszka, R. M. A.; Marshall, D. B.; Topper, K. *Soil Sci. Soc. Am. J.* **1990**, *54*, 1283−1289.
(22) Puchalski, M. M.; Morra, M. J.; von Wandruszka, R. *Environ. Sci. Technol.* **1992**, *26*, 1787−1792.
(23) Engebretson, R. R.; von Wandruszka R. *Environ. Sci. Technol.* **1994**, *28*, 1934−1941.
(24) Engebretson, R. R.; von Wandruszka, R. *Environ. Sci. Technol.* **1996**, *30*, 990−997.
(25) Backhus, D. A.; Gschwend, P. M. *Environ. Sci. Technol.* **1990**, *24*, 1214−1223.
(26) Jankowiak, R.; Small, G. J. *Anal. Chem.* **1989**, *61*, 1023A−1032A.
(27) Jankowiak, R.; Small, G. J. *Chem. Res. Toxicol.* **1991**, *4*, 256−269.
(28) Mantoura, R. F. C.; Riley, J. P. *Anal. Chim. Acta* **1975**, *76*, 97−106.
(29) Abbt-Braun, G.; Frimmel, F. H.; Lipp, P. *Z. Wasser-Abwasser-Forsch.* **1991**, *24*, 285−292.
(30) Frimmel, F. H.; Abbt-Braun, G. *Environ. Intern.* **1999,** *25*, 191−207.
(31) Kalyanasundaram, K.; Thomas, J. K. *J. Am. Chem. Soc.* **1977**, *99*, 2039−2044.
(32) Larsen, O. F. A.; Kozin, I. S.; Rijs, A. M.; Stroomberg, G. J.; de Knecht, J. A.; Velthorst, N. H.; Gooijer, C. *Anal. Chem.* **1998**, *70*, 1182−1185.
(33) Suh, M.; Jankowiak, R.; Ariese, F.; Mao, B.; Geacintov; N. E., Small, G. J. *Carinogenesis* **1994**, *15*, 2891−2898.
(34) Durocher, G.; Sandorfy, C. *J. Mol. Spectrosc.* **1966**, *20*, 410−424.
(35) Langvik, V.-A.; Akerback, N.; Holmborn, B. *Environ. Int.* **1994**, *20*, 61−65.
(36) Senesi, N.; Miano, T. M.; Provenzano, M. R. In *Humic substances in the aquatic and terrestrial environment*; Allard, E., Boren, H., Grimvall, Eds.; Springer-Verlag: Berlin, 1991; pp S 63−73.
(37) Liao, W.; Christman, R. F.; Johnson, J. D.; Millington, D. S. *Environ. Sci. Technol.* **1982**, *16*, 403−410.
(38) Leenheer, J. A.; Wershaw, R. L.; Reddy, M. M. *Environ. Sci. Technol.* **1995**, *29*, 399−405.
(39) Kumke, M. U.; C. Tiseanu, C. D.; Abbt-Braun, G.; Frimmel, F. H. *J. Fluorescence* **1998**, *8*, 309−318.
(40) Tiseanu, C. D.; Kumke, M. U.; Frimmel, F. H.; Klenze, R.; Kim J. I. *J. Photochem. Photobiol. A* **1998**, *117*, 175−184.

Received for review September 9, 1999. Revised manuscript received May 23, 2000. Accepted June 15, 2000.

ES9910457

2.2.4 Interaction between natural organic matter (NOM) and polycyclic aromatic compounds (PAC) - comparison of fluorescence quenching and solid phase micro extraction (SPME)

T.E. Doll, F.H. Frimmel, M.U. Kumke, G. Ohlenbusch
Fres. J. Anal. Chem., 1999, **364**, 313 - 319.

Die Wechselwirkungen von Phenanthren und 9-Aminophenanthren mit HS verschiedener Ursprungsorte wurden mittels SPME und Fluoreszenzspektroskopie untersucht. Die beim Vergleich der Ergebnisse beobachteten Differenzen wurden im Zusammenhang mit Unterschieden in der Art der durch die Methode detektierten Wechselwirkungen interpretiert. Es wurden zwei unterschiedliche Arten von Wechselwirkungen postuliert. In Fluoreszenzlöschexperimenten wird die Summe beider beobachtet und kann nicht differenziert werden, während in SPME-Experimenten nur einer der beiden Mechanismen zu beobachten ist. Damit wird der gefundene Unterschied in den durch die beiden Methoden gemessenen Sorptionskonstanten erklärbar. Während mit der SPME Aktivitäten der Analyten bestimmt werden, ist die Messung der Fluoreszenz konzentrationsbezogen (s. auch 2.2.1). Aus den SPME-Experimenten konnten desweiteren auch Hinweise zum Aggregationsverhalten von HS abgeleitet werden. Die Sorptionskonstanten K_H und K_{DOM} für c(PAK) = const. bzw. c(HS) = const. waren verschieden, da die Anzahl der qualitativ unterschiedlichen Bindungsplätze im Verhältnis zur Anzahl der PAK-Moleküle in beiden Ansätzen unterschiedlich variiert.

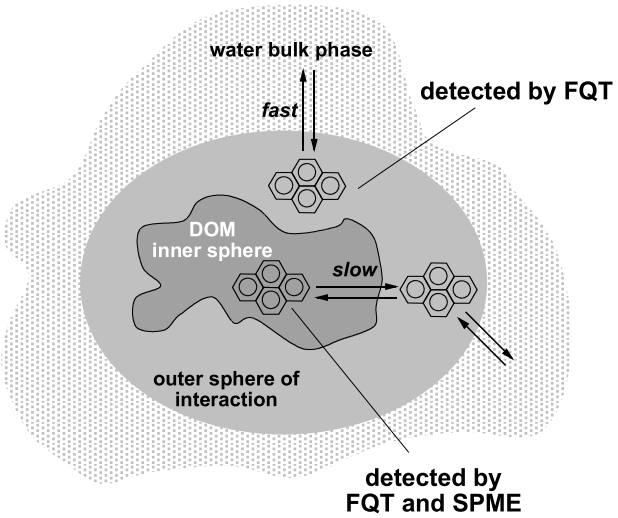

nach:
F.-D. Kopinke, A. Georgi, K. Mackenzie, M.U. Kumke
in: Refactory Organic Substances in the Environment; F.H. Frimmel, G. Abbt-Braun (eds), Wiley 2002.
Sorption and chemical reactions of PAHs with dissolved humic substances and related model polymers

M.U. Kumke

Fresenius J Anal Chem (1999) 364:313–319

ORIGINAL PAPER

T. E. Doll · F. H. Frimmel · M. U. Kumke
G. Ohlenbusch

Interaction between natural organic matter (NOM) and polycyclic aromatic compounds (PAC) – comparison of fluorescence quenching and solid phase micro extraction (SPME)

Received: 12 November 1998 / Revised: 22 December 1998 / Accepted: 30 December 1998

Abstract The interaction of phenanthrene and 9-aminophenanthrene with natural organic matter (NOM) of different origin was investigated using the fluorescence quenching approach and the solid phase micro extraction method. The results of both methods are compared in terms of the influence of the concentration of the polycyclic aromatic compounds (PAC) as well as the concentration of the NOM on the observed binding constant. Due to the combination of steady-state and time-resolved fluorescence techniques it could be concluded that the observed fluorescence quenching was caused by a static interaction like a complex formation. While for phenanthrene both analytical methods showed no long term effects and the reaction equilibrium between NOM and phenanthrene was established within the first hour, for 9-aminophenanthrene a slow reaction kinetics (within days) was found indicating specific interactions between NOM and the amino group.

Introduction

Natural organic matter (NOM) is present in surface, pore and ground waters [1–3]. It is well established that NOM determines the fate and transport of hydrophobic organic substances [3–8]. However, the interaction mechanism is still a matter of discussion. Often the interaction has been described as a non-specific sorption mechanism of the hydrophobic organic compound (HOC) to hydrophobic structures of NOM. The driving force for this reaction is considered to be an increase in the entropy of the system due to a release of water molecules of the hydrate shell of the HOC. Recently, specific binding sites were taken into account and in some cases micelle-like structures were assumed for the binding of HOC [9, 10].

The measurement of binding constants between organic contaminants and NOM is still crucial. Especially analytical methods using a separation approach like solid phase extraction or solvent extraction will influence the sorption equilibrium between NOM and contaminant [11–13]. Other experimental techniques less prone to this interference are limited in their application to fluorescing compounds (e.g., fluorescence quenching approach) or time consuming like the dialysis approach [12, 14–17]. The solid phase micro extraction (SPME) offers a promising solution for the determination of binding constants. It is not limited to fluorescing compounds and has the advantages of few experimental requirements and negligible disruption of the sorption equilibrium [18–20].

While the interaction of NOM and HOC was investigated extensively, little work has been presented on the interaction of slightly polar compounds like substituted polycyclic aromatic compounds (PAC). Due to the functional groups (e.g., hydroxy or amino) more specific binding via dipol-dipol interactions or even covalent binding could become important. Recently it was proposed that aromatic amines lead in a slow reaction pathway with quinone substructures of soil organic matter to covalently bound products [11, 21].

The objective of the work was to further elucidate the interaction between NOM and PAC. For the investigation of the interaction mechanism a non-invasive technique (fluorescence quenching method) and an invasive technique (solid phase micro extraction) were applied. The obtained binding constants K_{SV} (fluorescence quenching), K_H (SPME, variation of PAC concentration), and K_{POM} (SPME, variation of NOM concentration) are in particular discussed with respect to the influence of the concentration of the PAC and of the effect of functional groups which were used in order to probe specific and non-specific binding sites of NOM.

T. E. Doll · F. H. Frimmel (✉) · M. U. Kumke · G. Ohlenbusch
Division of Water Chemistry, Engler-Bunte-Institute,
University of Karlsruhe, Engler-Bunte-Ring 1,
D-76131 Karlsruhe, Germany
e-mail: fritz.frimmel@ciw.uni-karlsruhe.de

Experimental

The polycyclic aromatic compounds (PAC) were purchased from Aldrich and used as received. For the preparation of the aqueous stock solutions phenanthrene (Phen) and 9-aminophenanthrene (9-NH_2-Phen) were dissolved in acetone. 400 µl of the acetone stock solutions were transferred into a volumetric flask and the solvent was evaporated applying vacuum. The residue was dissolved in water by sonification for 30 min and shaking over night. Finally, the aqueous solutions were filtered using a 0.2 µm polycarbonate filter. The final concentrations of 9-NH_2-Phen and Phen were 1.4 mg/L and 0.7 mg/L, respectively. The solutions were kept in the dark.

In the experiments natural organic matter (NOM) samples of a brown water lake (HO13, Lake Hohloh, Black Forest, Germany) and a commercially available humic material (Al-HS, Aldrich) were used. The concentration of dissolved organic carbon (DOC) of the stock solutions was 210 mg/L (HO13) and 1732 mg/L (Al-HS). In order to obtain a high concentrated stock solution of HO13 the original water (DOC approx. 20 mg/L) was carefully pre-concentrated by evaporation (13 mbar, 30 °C). The samples were 0.45 µm filtered and kept refrigerated in the dark. For the experiments the pH of the solution was adjusted to 7.3 using a phosphate buffer solution.

The interaction between the PAC and NOM samples was investigated using the solid phase micro extraction (SPME) and the fluorescence quenching technique.

Fluorescence experiments

In the fluorescence experiments concentrations of DOC up to 30 mg/L were used, while in the SPME experiments concentrations up to 300 mg/L DOC were applied. The sorption experiments as well as the fluorescence quenching experiments were performed at 20 °C.

The steady-state fluorescence measurements were performed on a LS 5B luminescence spectrometer (Perkin Elmer). In the experiments a spectral bandpass of 5 nm in excitation and emission was used. The measurements were carried out at an excitation wavelength λ_{ex} = 314 nm and λ_{ex} = 275 nm for 9-aminophenanthrene (9-NH_2-Phen) and phenanthrene (Phen), respectively. The spectra were recorded in the emission wavelength range between 300 nm and 600 nm. The fluorescence measurements of the natural organic matter samples were performed under identical experimental conditions. In the fluorescence quenching experiments the inner filter effect of the NOM itself had to be considered. Therefore, the UV/Vis absorption of the sample solutions was determined at the excitation and emission wavelengths used. The data were corrected for the primary and secondary inner filter effect with an overall correction factor < 3 for the range of NOM concentrations investigated [14, 22]. For the determination of the binding constants K_{SV} the experimental data were analyzed according to Stern-Volmer [14, 22, 23]

The time-resolved fluorescence experiments were performed using a FL900CDT lifetime spectrometer (Edinburgh Analytical Instruments) operated in the time-correlated single counting mode (TCSPC). The experimental setup is described in detail elsewhere [24, 25]. In the time-resolved fluorescence experiments an excitation wavelength λ_{ex} = 314 nm was used for both PAC investigated. The fluorescence decay was detected at λ_{em} = 365 nm and 375 nm for Phen and at λ_{em} = 430 nm and 500 nm for 9-NH_2-Phen. The spectral bandpass in the detection channels was 9 nm. The fluorescence decay was recorded in a time window set to 200 ns.

Solid phase micro extraction (SPME)

In the SPME experiments a fused-silica fiber (Supelco) coated with polydimethylsiloxane (thickness 7 µm) was used. Prior to the first application the fiber was once conditioned for 3 h at 300 °C in a helium stream and after that at the beginning of the experiments the fiber was heated for 5 min at 250 °C in order to avoid contamination. The sample solutions were agitated for 24 h in the dark at room temperature to assure that equilibrium was established. For the sorption experiments the SPME fiber was introduced through a septum into 30 mL of sample solution. For the analysis the SPME fiber was directly injected into the injection port of a GC and the PAC were thermally desorbed for 5 min at 250 °C (Finnigan MAT, GCQ; GC capillary column DB-5.MS, J&W). The temperature program in the GC analysis started with an initial temperature of 40 °C for 5 min. The temperature was raised with 20 °C/min up to 250 °C and held constant for 4.5 min. Finally, the temperature was increased to 280 °C with a rate of 10 °C/min and kept at 280 °C for 7 min.

The determined retention times for Phen and 9-NH_2-Phen were 12:58 min and 15:04 min, respectively. For quantification the single ion monitoring mode was used and the mass peak pairs at 178/152 for Phen and at 193/165 for 9-NH_2-Phen were evaluated. For the SPME measurements typical standard deviations of 5.3% and 6.5% were found for Phen and 9-NH_2-Phen, respectively. In kinetic experiments the sorption on the SPME fiber was monitored for 50 min. Equilibrium between fiber and aqueous PAC solution was reached after approx. 20 min. The amount of PAC extracted by the SPME fiber at that point was smaller than 1% of the total PAC in the aqueous sample.

For Al-HS and HO13 the investigated concentration range was < 300 mg/L DOC. The concentration of Phen was < 0.07 mg/L, and the concentration of 9-NH_2-Phen was < 0.6 mg/L.

Results and discussion

Fluorescence quenching experiments

Steady state fluorescence spectra of the PAC were recorded at different NOM concentrations and the fluorescence intensities were evaluated according to the Stern-Volmer equation (1):

$$\frac{I_F^0}{I_F} = 1 + K_{SV} \cdot \beta(DOC) \qquad (1)$$

Here, I_F represents the corrected fluorescence intensity in the absence (0) and presence of NOM (in mg/L DOC) and K_{SV} the binding constant (in L/mg). For all PAC investigated the observed fluorescence intensity decreased in the presence of HO13 and Al-HS. Because of the inner filter effect due to absorption of emission and excitation light by the NOM, the observed decrease in the fluorescence intensity was corrected to obtain the real fluorescence quenching effect. The corrections are limited to correction factors < 3 according to Parker [26], therefore the concentration range of NOM investigated in the fluorescence quenching experiments was kept smaller than 30 mg/L DOC. For this concentration range a linear relationship between the fluorescence quenching and the concentration of DOC was found, for higher concentrations in DOC (> 30 mg/L) the data showed a positive deviation (upward curvature). Two possible reasons have to be considered: 1. the limited applicability of the correction of the inner filter effects and 2. the combination of static and dynamic quenching processes. The combination of a static quenching (e.g., complex formation) and dynamic quenching (e.g., collisional encounter) can be

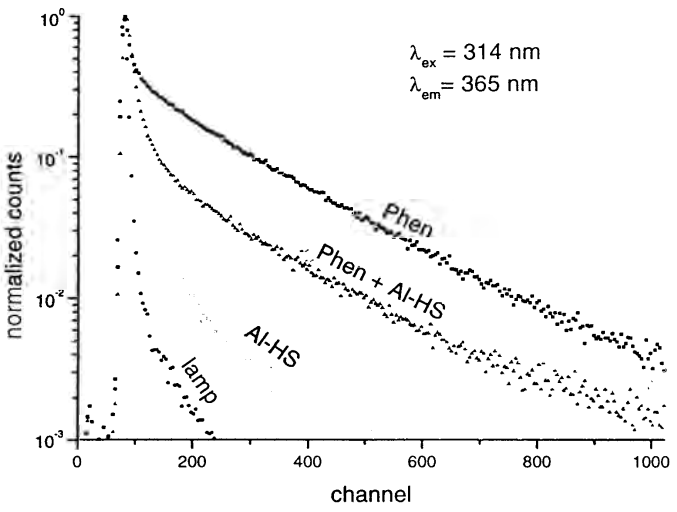

Fig. 1 Normalized fluorescence decays of Phen, Al-HS, and Phen + Al-HS in water (pH 7, λ_{ex} = 314 nm, λ_{em} = 365 nm, time calibration: 0.19 ns/channel, T = 20°C, band pass of detection = 9 nm). The time profile of the lamp excitation pulse is shown as well

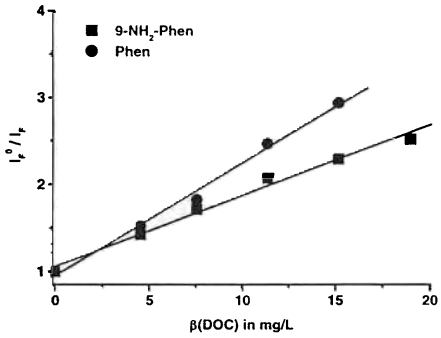

Fig. 2 Results of the Stern-Volmer analysis of fluorescence quenching experiments of Phen (circles) and 9-NH_2-Phen (squares) with Al-HS. The calculated binding constants K_{SV} for Phen and 9-NH_2-Phen were 0.13 ± 0.007 L/mg and 0.08 ± 0.003 L/mg, respectively

evaluated performing time-resolved fluorescence experiments.

In Fig. 1 the fluorescence decays of Phen, Al-HS, and Phen in the presence of Al-HS are shown. The fluorescence decays contained a fast component that was attributed to Raman scattering of the excitation light.

In the data analysis fluorescence decay times of 33.5 ± 0.2 ns and 13.5 ± 0.1 ns were found for Phen and 9-NH_2-Phen in water, respectively. In the presence of NOM the fluorescence lifetimes of the PAC were almost unchanged. Changes of a few hundred picoseconds were calculated in the analysis of the corresponding fluorescence decay data. These small alterations could be attributed to a small contribution of NOM fluorescence in the overall fluorescence decay of the samples (PAC + NOM). This was a confirmation of recently reported results that the interaction between PAC and NOM is of static nature [9, 22] and indicated further that a static interaction (e.g. complex formation, sorption) applies for PAC with functional groups as well. Therefore, the observed upward curvature in the Stern-Volmer data evaluation of the steady state experiments was most likely caused by the insufficient correction of the inner filter effects (primary and secondary) at high concentration of NOM (β(DOC) > 30 mg/L).

In Fig. 2 a Stern-Volmer data evaluation (Eq. 1) of the fluorescence quenching of Phen and 9-NH_2-Phen by Al-HS is shown.

In Fig. 3 and Table 1 the results of the fluorescence quenching experiments for Phen and 9-NH_2-Phen with Al-HS and HO13 are summarized. In the fluorescence quenching approach the binding constants K_{SV} were determined for different PAC concentrations and at different reaction times. For Phen the observed binding constant with Al-HS was twofold the binding constant found with HO13. The calculated K_{SV} of Al-HS was 0.13 ± 0.01 L/mg and agrees well with recently reported K_{SV} for the binding of Phen [22]. It is widely accepted that the influence of the origin of the NOM on the binding constant is connected to the content of hydrophobic (and aromatic) structures of the NOM. HO13 was of aquatic origin and had less hydrophobic structures compared to Al-HS which was isolated from soil. Hence, the observed tendency supported the proposed relationship between con-

316

Table 1 Binding constants for the interaction of PAC (phenanthrene, 9-amino-phenanthrene) and NOM (Aldrich-HS, brown water HS HO13). Compared are the calculated binding constants of the fluorescence quenching experiments (K_{SV}, according to Eq. 1) and of the SPME experiments (K_H and K_{DOM}, according to Eqs. 2 and 3)

	K_{SV}/[L/mg]; β_{PAC}/[mg/L]; reaction time	K_H/[L/mg]; β_{DOC}/[mg/L]; reaction time 24 h	K_{DOM}/[L/mg]; β_{PAC}/[mg/L]; reaction time 24 h
Phen + Al-HS	0.13 ± 0.01; 0.4; 4 h 0.129 ± 0.007; 0.4; 5 d 0.146 ± 0.008; 0.08; 4 h 0.12 ± 0.01; 0.02; 4 h	0.0097 ± 0.0009; 43	0.0104 ± 0.0007; 0.02
Phen + HO13	0.058 ± 0.002; 0.4; 4 h	0.0015 ± 0.0005; 70	0.012 ± 0.002;
9-NH_2-Phen + Al-HS	0.089 ± 0.005; 0.7; 4 h 0.131 ± 0.008; 0.7; 17 d 0.082 ± 0.003; 0.1; 4 h	0.014 ± 0.005; 43	0.015 ± 0.001;
9-NH_2-Phen + HO13	0.033 ± 0.001; 0.8; 4 h	0.006 ± 0.001; 68	0.012 ± 0.002;

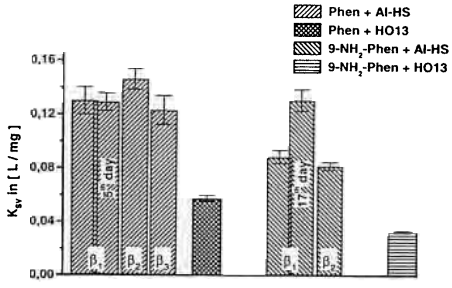

Fig. 3 Comparison of the binding constants K_{SV} for the interaction of the investigated NOM and PAC. Presented are the influence of PAC concentration (β_x = 0.4, 0.08, and 0.02 mg/L for Phen and β_x = 0.7 and 0.1 mg/L for 9-NH_2-Phen) as well as the influence of the reaction time

tent of hydrophobic structures of the NOM and binding behavior for hydrophobic organic compounds. A similar tendency was observed for 9-NH_2-Phen. However, the binding constants K_{SV} with the investigated NOM were found to be generally smaller which can be attributed to the increased water solubility of the PAC due to the NH_2-group.

In Fig. 3 the long-term time dependence of the observed binding constants K_{SV} are presented as well. For Phen no influence of the reaction time (up to 5 days) on the observed binding constant K_{SV} could be detected. It is interesting to note that 9-NH_2-Phen showed an increased fluorescence quenching when the sample solutions were aged for approx. two weeks. This indicates that in addition to a fast binding within the first few minutes (or seconds) of contact 9-NH_2-Phen reacted further on a much slower time-scale with Al-HS. It is attractive to assume that this slower interaction process is connected to the NH_2-group and its interactions with functional groups of the NOM. Due the slow reaction process the binding constant was increased by approx. 40%.

In order to further investigate the interaction mechanism, the influence of the PAC concentration on the observed binding constant K_{SV} was evaluated. The concentrations were 0.4, 0.08, 0.02 mg/L, and 0.8 and 0.1 mg/L for Phen and 9-NH_2-Phen. For the monitored concentration range no influence on the observed binding constant K_{SV} was detected. The obtained constants were identical within the error of determination (see Fig. 3).

Solid phase micro extraction (SPME) experiments

For the determination of the sorption constants two sets of isotherms were recorded varying the PAC concentration with data evaluation according to Henry's law (Eq. 2) and according to the mass action expression by variation of the concentration of the NOM (Eq. 3). Equation 2 connects the loading q of PAC on the NOM (in µg/kg) and the equilibrium concentration β (in mg/L) of the free PAC in the solution phase.

$$q = K_H \cdot \beta(PAC) \tag{2}$$

In Eq. 3 the ratio of the signals F (e.g., areas of the chromatographic peaks) in the absence and presence of NOM are evaluated depending on the concentration β of dissolved organic carbon (in mg/L).

$$\frac{F_0}{F} = 1 + K_{DOM} \cdot \beta(DOC) \tag{3}$$

Figures 4 and 5 show typical results obtained in the two experimental approaches for the interaction of Phen with Al-HS. Both data evaluation methods yielded linear isotherms in the investigated concentration ranges of PAC and NOM, respectively. It can be shown that theoretically $K_H = K_{DOM}$ (see appendix).

Figure 6 summarizes the results of the SPME experiments and compares the obtained K_H and K_{DOM} values of the investigated PAC and NOM.

The binding of the PAC was found to be stronger with Al-HS. This is in good agreement with the fluorescence quenching results. However, for 9-NH_2-Phen the calculated binding constants were larger compared to the bind-

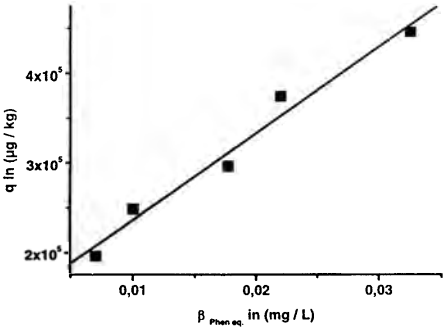

Fig. 4 SPME-determination of the binding constant K_H according to Eq. 2 for the interaction of Phen and Al-HS (K_H = 0.01 ± 0.0009 L/mg, β(DOC) = 43 mg/L)

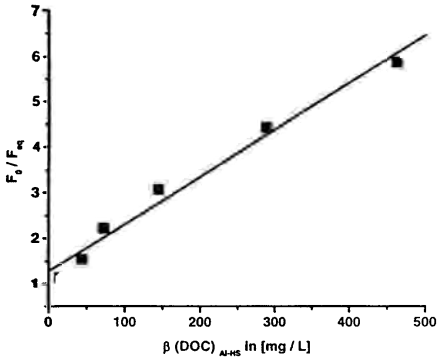

Fig. 5 SPME-determination of the binding constant K_{DOM} according to Eq. 3 for the interaction of Phen and Al-HS (K_{DOM} = 0.01 ± 0.0007 L/mg, β(DOC) = 43 mg/L)

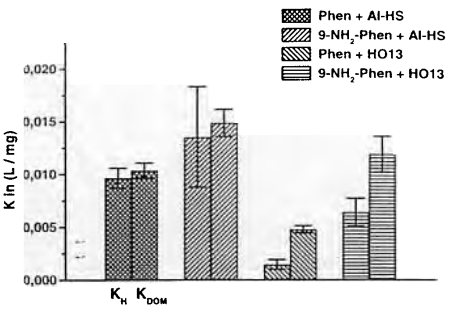

Fig. 6 Comparison of the in SPME experiments for the determination of binding constants K_H and K_{DOM} of Phen and 9-NH_2-Phen with Al-HS and HO13

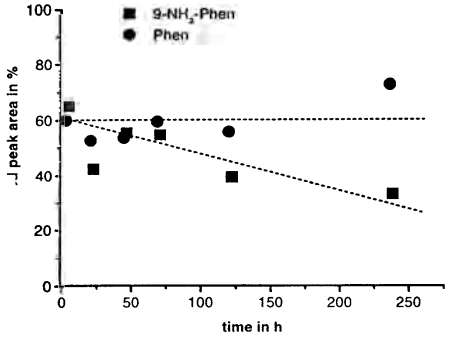

Fig. 7 Influence of reaction time on the observed binding of Phen and 9-NH_2-Phen to Al-HS

ing constants of Phen which was in contrast to the results of the fluorescence quenching experiments as well as to the expected influence of the water solubility of the PAC. The fiber coating which was designed for hydrophobic substances had a smaller affinity for the polar 9-NH_2-Phen. In this case the NOM could become more 'attractive' for 9-NH_2-Phen compared to Phen and therefore causing a relatively high binding constant.

For Al-HS almost no differences between K_H and K_{DOM} were detected for the investigated PAC. However, for HO13 the calculated binding constant K_H using Eq. 2 was smaller for both PAC when compared to K_{DOM} which could be attributed to the different origin of the two NOM materials.

The increase of binding due to a slow reaction of 9-NH_2-Phen was confirmed in the SPME experiments. Figure 7 shows the increased binding to Al-HS for the investigated PAC. Within the first 250 h the binding of 9-NH_2-Phen is increased by approx. 40% while for Phen no change of its binding interaction in time was detected.

From Table 1 it is obvious that the binding constants found in the fluorescence quenching experiments and in the SPME experiments were highly different. For both PAC the binding constants determined with the fluorescence quenching method were almost one order of magnitude larger compared to the SPME results. There are two possible method-related sources that could cause the observed differences: 1. an insufficient inner filter correction of the fluorescence quenching data and 2. an aging of the SPME fiber. An insufficient correction of the inner filter effects should lead to an upward curvature of the Stern-Volmer plots at higher NOM concentrations. In our fluorescence quenching experiments the NOM concentrations were limited to β(DOC) < 30 mg/L. No upward curvature was detectable for this concentration range. In general, the

linear correlation coefficients of the Stern-Volmer analysis were better than 0.98. Even considering that the correction of the inner filter effects was insufficient, it would hardly explain the large differences between SPME and fluorescence quenching approach. The aging of the fiber was checked in a separate set of experiments (data not shown). Here, no influence on the sorption capabilities of the fiber was found. However, the sorption kinetics of the PAC was changed in the presence of NOM. Due to the NOM the sorption was slower. In a set of experiments the extraction time was increased to 2 h. It was found that the binding constants for Phen to Al-HS was nearly doubled to K_{DOM} = 0.02 L/mg. In control experiments the binding of Phen to BSA (bovine serum albumin) was determined for 30 min and 2 h. Here, no influence on the calculated K_{DOM} was found, indicating that for NOM a very slow sorption kinetic was present.

Results for the binding between Phen and Al-HS reported in the literature showed differences of more than one order of magnitude. In particular, binding constants obtained with different analytical methods were highly different. In general the fluorescence quenching approach yielded higher binding constants (reported as K_{OC} which is normalized to the organic carbon content of the NOM, in mL/g) compared to other analytical methods. Laor et al. [17] and Kumke et al. [22] calculated a log K_{OC} of 5.11 and 5.04 using the fluorescence quenching approach. Backhus and Gschwend [15] and Landrum et al. [27] used a reversed phase approach for the same system and determined a log K_{OC} of 3.99 and 3.92, respectively. It is interesting to note that Backhus and Gschwend found a K_{OC} of 4.78 when they investigated the interaction using fluorescence spectroscopy. While the reported K_{OC} values determined by different groups with the same analytical method did agree quite well, the comparison of different methods is obviously crucial. This underlines the operationally defined character of the values.

In summary, both analytical methods yielded similar tendencies: a) in comparison to the Al-HS, NOM of aquatic origin bound less PAC; b) due to the NH_2-group a second slow reaction was revealed indicating specific interactions with NOM, and c) there was no influence of the concentration of the PAC on the observed fast binding and therefore, no limitation of binding sites for the fast interaction in the investigated PAC concentration range. However, the quantitative data on the interactions revealed by fluorescence quenching were clearly different from those obtained by SPME.

Conclusions

In theory the binding constants K_{SV}, K_H, and K_{DOM} describe the same equilibrium reaction and, therefore, should be the same for a single type of interaction. The differences in the binding constants obtained by different analytical approaches suggest the presence of several interaction processes, resulting in non-linear sorption isotherms of the PAC to the NOM. In the non-invasive fluorescence quenching approach all PAC molecules, even the ones weakly attached to the *outer sphere* of NOM, were quenched and hence detected as 'bound'. On the other hand, in SPME and the reversed phase approach the distribution of the PAC between NOM, analytical phase (fiber or chromatography column), and the aqueous phase are probed. PAC molecules loosely attached to the *outer sphere* of NOM could readily exchange with the aqueous phase imposing a higher PAC concentration in the aqueous phase and thus causing an underestimation of binding to NOM.

The assumption of a distribution of binding (sorption) sites for PAC in NOM would also explain the differences between K_H and K_{DOM} determined in the SPME experiments (see Fig. 6, especially for HO13). Due to the increase of the PAC concentration more and more weak binding sites (*outer sphere*) will be involved in the interaction process causing a shift of the experimentally determined apparent binding constant to lower values. In contrary, when the NOM concentration is increased the number of stronger binding sites is increased relative to the PAC concentration which remains constant. A higher value for the apparent PAC binding constant is determined. Moreover, the experimental data make it tempting to assume that with increasing NOM concentration aggregation phenomena became important for the sorption processes. This was indicated by a small negative deviation from linearity (Fig. 5). In case no aggregation would be present, the number of strong and weak binding sites (*inner and outer spheres*) would increase and enough strong binding sites would be available for the PAC. Here, a perfect linear relationship in the K_{DOM}-determination according to Eq. 3 would be obtained. As a matter of fact, in our experiments a slight deviation from linearity was observed. Assuming an aggregation of NOM this could be attributed to the decrease of the number of readily accessible strong binding sites. In this case more PAC molecules are forced to interact with the weaker binding sites in the NOM, causing the apparent overall decrease in bound PAC observed with the SPME approach.

These differences in binding strength may not be detected in the fluorescence quenching experiments if all PAK molecules bound to the NOM (*inner and outer sphere*) are assumed to be non-fluorescent. The differences between K_H and K_{DOM} were more pronounced for HO13. Because of its aquatic origin the number of strong binding sites (proportional to its hydrophobicity) were smaller.

The increase of the determined binding constant in the SPME experiments with increased sorption time could also be understood in terms of a limited number of readily accessible strong binding sites and slow reorganization processes of the NOM (e.g., its aggregates).

Due to results of the combination of fluorescence quenching and SPME it is attractive to assume for the sorption of PAC to NOM binding sites of different strength. Because of these differences in the overall probed binding sites, comparison of binding constants obtained with different analytical techniques has to be done with care. Fu-

ture research will investigate the observed differences between the calculated binding constants K_H, K_{DOM}, and K_{SV} to further distinguish binding sites.

Variations in the affinity of the SPME fiber with different PAC will prove the conclusions drawn and will help to further distinguish between different binding sites of NOM.

Acknowledgements The work presented was financially supported by the Deutschen Forschungsgemeinschaft which is greatly appreciated by the authors. Furthermore, the authors are grateful to Dipl.-Ing. Christian Specht for the pre-concentration of the sample HO13.

Appendix

$$q = K_H \cdot \beta(PAK)_{eq} \tag{A1}$$

$$q = \frac{\beta(PAK)_0 - \beta(PAK)_{eq}}{\beta(DOM)} \Rightarrow \frac{\beta(PAK)_0 - \beta(PAK)_{eq}}{\beta(DOM)} = K_H \cdot \beta(PAK)_{eq} \tag{A2}$$

$$K_H = \frac{\beta(PAK)_0 - \beta(PAK)_{eq}}{\beta(DOM) \cdot \beta(PAK)_{eq}} \tag{A3}$$

$$\beta(PAK)_0 - \beta(PAK)_{eq} = \beta(PAK \cdots DOM) \tag{A4}$$

The index *0* and *eq.* refer to the initial concentration and the concentration in equilibrium, respectively.

Substitution of Eq. (A4) into Eq. (A3) yields:

$$K_H = \frac{\beta(PAK \cdots DOM)}{\beta(DOM) \cdot \beta(PAK)_{eq}} = K_{DOM} \tag{A5}$$

References

1. Stevenson JF (1982) Humus chemistry – Genesis, composition, reactions. Wiley, New York
2. Frimmel FH, Christman RF (1988) Humic Substances and Their Role in the Environment. Wiley, Chichester
3. Rebhun M, de Smedt F, Rwetabula J (1996) Wat Res 30: 2027–2038
4. Schwarzenbach RP, Westall J (1981) Environ Sci Technol 15:1360–1367
5. Chiou CT, Porter PE, Schedding DW (1983) Environ Sci Technol 17:227–231
6. McCarthy JF, Jimenez BD (1985) Environ Sci Technol 19:1072–1076
7. Liu H, Amy G (1993) Environ Sci Technol 27:1553–1562
8. Johnson WP, Amy GL (1995) Environ Sci Technol 29:807–817
9. Engebretson RR, von Wandruszka R (1994) Environ Sci Technol 28:1934–1941
10. Schmitt P, Freitag D, Trapp I, Garrison AW, Schiavon M, Kettrup A (1997) Chemosphere 35:55–75
11. Parris GE (1980) Environ Scil Technol 14:1099–1106
12. Chin YP, Weber WJ (1990) Environ Sci Technol 24:837–842
13. Kopinke FD, Pörschmann J, Stottmeister U (1995) Environ Sci Technol 29:941–950
14. Gauthier TD, Shane EC, Guerin WF, Seitz WR, Grant CL (1986) Environ Sci Technol 20:1162–1166
15. Backhus DA, Gschwend PM (1990) Environ Sci Technol 24: 1214–1223
16. Schlautman MA, Morgan JJ (1993) Environ Sci Technol 27: 961–969
17. Laor Y, Farmer WJ, Aochi Y, Strom PF (1998) Wat Res 32:1923–1931
18. Vaes WHJ, Ramos EU, Verhaar HJM, Seinen W, Hermes JLM (1996) Anal Chem 68:4463–4467
19. Poerschmann J, Kopinke FD, Pawliszyn J (1997) Environ Sci Technol 31:3629–3636
20. Georgi A (1998) Sorption von hydrophoben organischen Verbindungen an gelösten Huminstoffen. Dissertation am Umweltforschungszentrum Leipzig-Halle GmbH
21. Weber EJ, Spidle DL, Thorn KA (1996) Environ Sci Technol 30:2755–2763
22. Kumke MU, Löhmannsröben HG, Roch T (1994) Analyst 119:997–1001
23. Lakowicz JR (1983) Principles of fluorescence spectroscopy. Plenum Press, New York
24. Kumke MU, Abbt-Braun G, Frimmel FH (1998) Acta Hydrochem Hydrobiol 26:73–81
25. Kumke MU, Tiseanu C, Abbt-Braun G, Frimmel FH (1998) J Fluorescence 8:309–318
26. Parker CA (1968) Photoluminescence of solutions. Elsevier, Amsterdam
27. Landrum PF, Nihart SR, Eadle BJ, Gardner WS (1984) Environ Sci Technol 18:187–192

2.3 Wechselwirkung von Huminstoffen (HS) mit Metallionen

Die Löschung der intrinsischen HS-Fluoreszenz durch Me^{n+} wurde systematisch mit stationären und zeitaufgelösten Fluoreszenztechniken untersucht. Es wurde vor allem der Mechanismus der Löschung hinterfragt. Dabei wurde gefunden, dass

- neben der Löschung durch die Komplexierung bestimmter Metallionen (z.B. Al^{3+} und Ga^{3+}) die HS-Fluoreszenz auch verstärkt werden kann,
- bestimmte Metallionen (z.B. Eu^{3+}) einen Einfluss auf die Fluoreszenzabklingkinetik der HS haben,
- durch die Komplexierung von Me^{n+} die HS einen Teil der konformativen Freiheiten verlieren,
- es in den Metall-HS-Komplexen durch Photoanregung zu Ligand-zu-Metall-Ladungstransfer-Prozessen kommt.

Qualitativ läßt sich die Löschung der intrinsischen Fluoreszenz durch Komplexierung von Metallionen als die Kombination aus äußerem Schweratomeffekt, Veränderung der konformativen Freiheit der HS und Ladungstransfer-Reaktionen verstehen. Besonders die Bedeutung von konformativen Veränderungen, wie sie etwa für eine Reihe von organischen Fluorophoren als TICT-Zustände (*twisted intramolecular charge transfer*) beschrieben sind, war bisher unterbewertet worden.
In den folgenden Veröffentlichungen wurden Effekte der Metallkomplexierung auf die Fluoreszenzeigenschaften - vor allem auf das Fluoreszenzabklingverhalten - von HS untersucht:

12. M.U. Kumke, C. Tiseanu, G. Abbt-Braun, F.H. Frimmel
J. Fluorescence, 1998, **8**, 309 - 318.
Fluorescence decay of natural organic matter (NOM) - Influence of fractionation, oxidation, and metal ion complexation.

13. C. Tiseanu, M.U. Kumke, F.H. Frimmel, R. Klenze, J.I. Kim
J. Photochem. Photobiol. A, 1998., **117**(3), 175 - 184.
Time-resolved fluorescence spectroscopy of fulvic acid and fulvic acid complexed with Eu^{3+} - A comparative study.

14. J.-M. Monsalier, F. Scherbaum, G. Buckau, J.I. Kim, M.U. Kumke, C.H. Specht, F.H. Frimmel
J. Photochem. Photobiol. A, 2001, **138**, 55 - 63.
Influence of photochemical reactions on the complexation of humic acid with europium(III).

Bezug zur aktuellen Literatur Auf die Literatur speziell im Zusammenhang mit der Komplexierung von Ln^{3+}-Ionen durch HS wird in Kapitel 3 eingegangen.
Die Speziation von Metallionen in natürlichen Systemen wird durch die Anwesenheit von Huminstoffen in diesen bestimmt. Für eine erfolgreiche Modellierung des

Transportverhaltens verschiedener Metallionen in der Umwelt ist daher das Verständnis der Metall-HS-Wechselwirkungen von entscheidender Bedeutung [76]. Erst dann können verlässliche Modelle erarbeitet werden, die eine qualitative und quantitative Beschreibung der relevanten Prozesse in der Umwelt erlauben. Diese sind z.B. für Langzeitsicherheitsanalysen bei der Planung von End- und Zwischenlagerstätten für radioaktive Abfälle oder andere schwermetallhaltige Abfälle bedeutsam, um Transport- und Mobilisierungsverhalten entsprechend den geogenen Bedingungen zu erfassen [76–80]. Zur Beschreibung der HS-Me^{n+} -Wechselwirkungen sind verschiedene Modelle entwickelt (bzw. weiterentwickelt) worden, von denen das bekannteste wohl das NICA-Donnan Modell ist, daneben sind weitere Modelle vorgestellt worden, die für spezielle Fragestellungen entsprechend den Anforderungen verfeinert sind [80–90].
Neben elektrochemischen Methoden sind spektroskopische Verfahren weit verbreitet zur Quantifizierung von verschiedensten Me^{3+}-Spezies. Atomabsorptionsspektroskopie (AAS) und Massenspektrometrie (MS) gekoppelt mit verschiedenen chromatographischen Verfahren sind gängige analytische Methoden, die zur Quantifizierung von Metallen verwendet werden und mehr oder weniger gut zur Speziation der Metallionen in Gegenwart von HS geeignet sind [91, 92]. Der Nachweis über die intrinsische HS-Fluoreszenz und/oder die intrinsische Ln^{3+}-Lumineszenz (bzw. Ac^{3+}-Lumineszenz) hat den Vorteil, dass eine direkte Untersuchung ohne eine vorhergehende chromatographische Trennung erfolgen kann, das System HS-Me^{n+} wird also nahezu ungestört untersucht. Es wurden einfache Emissionsspektren, synchrone Emissionsspektren und Totale Lumineszenzspektren (*excitation-emission matrices*, EEM) aufgenommen [93].
In den synchronen Fluoreszenzspektren der HS wurden bei Zugabe von Me^{n+} unterschiedliche Veränderungen in den verschiedenen Fluoreszenzpeaks beobachtet, woraus Rückschlüsse auf die Anzahl der beteiligten, unterschiedlichen Bindungsplätze für Me^{n+} in HS gezogen wurden [89, 94–97]. Ähnlich wurde in der Auswertung der EEM vorgegangen [98]. Die Auswertung und Bestimmung der Wechselwirkungskonstanten wurde oft mittels einer Stern-Volmer-Analyse gemacht oder nach modifizierten anderen Modellen, wie z.B. von Ryan und Weber [88, 94, 96, 99]. Aus diesen Messungen wurden häufig zwei bis drei verschiedene Bindungsplätze in den HS abgeleitet.
Neben der intrinsischen HS-Fluoreszenz wird die intrinsische Lumineszenz verschiedener Lanthanide und Actinide als Sonde genutzt, um die Wechselwirkung von Me^{n+} mit HS zur charakterisieren. Dabei werden zeitaufgelöste Fluoreszenzspektren (*time-resolved laser fluorescence spectroscopy*, TRLFS) gemessen, in denen Beiträge durch Hintergrundfluoreszenz ausgeblendet werden und so das reine Signal der Lanthanide bzw. Actinide detektiert werden kann. Da die Hintergrundfluoreszenz meist auf der Nanosekundenzeitskala, die Lumineszenz von Lanthaniden und Actiniden aber auf der Mikrosekundenzeitskala erfolgt, kann dies mit hoher Effizienz experimentell leicht durchgeführt werden. Die Hypersensitivität verschiedener Übergänge der Ln^{3+}- und Ac^{n+}-Ionen spielt hier bei der Speziation der Komplexe eine ganz wichtige Rolle (s. auch Kapitel 3). Bei den Lanthaniden wurde das Eu^{3+} häufig als Lumi-

neszenzsonde eingesetzt, bei den Actiniden waren es für die +III-Oxidationsstufe das Cm^{3+} und das Am^{3+} [100–103]. Neben den Wechselwirkungen mit HS wurden zunehmend auch ternäre Systeme betrachtet, in denen Kolloide bzw. feste Oberfläche in die Betrachtungen miteinbezogen wurden [102–105]. Außerdem wurde die Rolle von mikrobiologischen Prozessen auf die Mobilität von Metallen verstärkt untersucht [106]. Durch Hypersensitivität einzelner f-f-Übergänge konnten Komplexe mit Huminstoffen, OH^- sowie CO_3^{2-} unterschieden und die konditionellen Wechselwirkungskonstanten bestimmt werden [100]. Das Verhalten von Uran-Spezies in verschiedenen Umweltkompartimenten, insbesondere die Wechselwirkung mit HS, wurde mit verschiedenen Fluoreszenzmethoden charakterisiert, z.B. indem die Fluoreszenzlöschung im Zusammenhang mit verschiedenen HS-Fraktionen, die durch Gelpermeation erhalten wurden, quantifiziert wurde [107]. Weiterhin wurde die Speziation von U(VI) (meist das UO_2^{2+}) intensiv mittels TRLFS verfolgt [88, 108]. Parallel zu Untersuchungen von HS/UO_2^{2+}-Komplexen wurden auch Komplexe mit einfachen Modellliganden, wie z.B. Malonsäure und anderen aromatischen Carbonsäuren, qualitativ und quantitative mittels TRLFS charakterisiert [109–111].

2.3.1 Fluorescence decay of natural organic matter (NOM) - Influence of fractionation, oxidation, and metal ion complexation

M.U. Kumke, C. Tiseanu, G. Abbt-Braun, F.H. Frimmel
J. Fluorescence, 1998, **8**, 309 - 318.

Die Bestimmung der Komplexierungskonstanten von HS für verschiedene Metallionen wird häufig über eine Stern-Volmer-Auswertung der Löschung der intrinsischen Huminstofffluoreszenz durchgeführt. Das Problem hierbei ist, dass der Zusammenhang zwischen Metallbindungsplätzen der HS und den Fluorophoren unklar ist und dass der wirksame Löschmechanismus weitgehend ungeklärt ist. Durch detailierte Untersuchungen, vor allem in zeitaufgelösten Fluoreszenzexperimenten, wurden die wirksamen Löschmechanismen hinterfragt. Die Fluoreszenzabklingkinetiken von HS verschiedener Ursprungsorte wurden in An- und Abwesenheit von Cu^{2+}, Fe^{2+}, Al^{3+}, und Eu^{3+} gemessen und mittels Verteilungsfunktionen bzw. globaler Analyse ausgewertet. Zusätzlich wurden die HS gezielt durch Fraktionieren oder Oxidieren modifiziert. Es zeigten sich je nach betrachtetem Metallion unterschiedliche Einflüsse auf die Fluoreszenzabklingkinetiken. Für Kupfer wurde kein Einfluss beobachtet, während die übrigen Metallionen deutliche Veränderungen in den Fluoreszenzabklingkinetiken verursachten. Als mögliche Gründe hierfür sind die veränderte Konformation der HS durch die Einbindung von Metallionen zu nennen, die sich besonders bei Ionen mit großer Ladungsdichte (also z.B. Al^{3+}) bemerkbar macht oder der mögliche Energietransfer vom Liganden (hier: HS) auf das Metallion. Dies ist für die Lanthanide (besonders Eu^{3+} und Tb^{3+}) zu berücksichtigen.

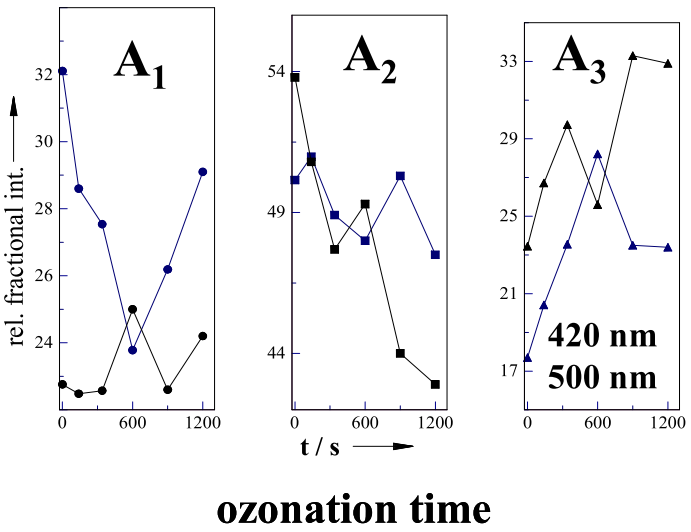

Journal of Fluorescence, Vol. 8, No. 4, 1998

Fluorescence Decay of Natural Organic Matter (NOM)—Influence of Fractionation, Oxidation, and Metal Ion Complexation

M. U. Kumke,[1] C. Tiseanu,[1] G. Abbt-Braun,[1] and F. H. Frimmel[1,2]

Received January 25, 1998; accepted August 12, 1998

Time-resolved fluorescence measurements of aquatic natural organic matter (NOM) derived from different origins were performed using the time-correlated single-photon counting technique. The obtained experimental data were analyzed with nonlinear least-squares (NLLS) algorithms. The results of a global analysis with three exponential decay terms were compared with the results obtained in a distribution analysis (exponential series method; ESM). Fulvic acid fractions from a bog lake water, from a brown coal production effluent, and from a soil seepage water as well as NOM from a municipal waste water were investigated. The influence of the emission wavelength on the NOM fluorescence decay was monitored. Furthermore, the influence of fractionation using size exclusion chromatography, of ozonation, and of metal ion complexation on the fluorescence decay of the NOM samples was investigated.

KEY WORDS: Natural organic matter; humic substances; time-resolved fluorescence; distribution analysis.

INTRODUCTION

In the aquatic environment the transport and transformation of organic and inorganic contaminants are closely related to the presence of natural organic matter (NOM). Therefore, the characterization of NOM and of its interaction processes with xenobiotics is indispensable.

Recently, efforts were concentrated in investigating NOM using time-independent techniques and neglecting the influence of molecular motions of NOM molecules. These *steady-state* methods yielded information on molecular weight distributions [1,2] and the content of structural components such as phenolic and carboxylic groups [3–6], and even some basic structures inside the NOM matrix responsible for light absorption and fluorescence were concluded [3,4,7]. Fluorescence spectroscopic techniques are powerful tools for the investigation of molecular processes and structures. During the last decades steady-state fluorescence techniques have been applied successfully in NOM research [8–12]. Especially, the synchronous fluorescence spectroscopy has proven to yield valuable results in the characterization of NOM [10,12–14]. Recently, the application of time-resolved fluorescence techniques was introduced into NOM research [15–20]. For all NOM samples investigated in time-resolved fluorescence measurements, a highly complex fluorescence decay has been reported [17–21]. Different approaches to data analysis have been applied: (a) a robust approach that selects the point of time the initial fluorescence intensity has decayed to $1/e$ (or $1/3e$) to characterize the fluorescence decay [22,23], (b) the use of a small number of exponential decay functions assuming a low number of fluorescence components (discrete component approach; DCA) [17,20,21], and (c) the assumption of a large number of decay functions ($i \approx 100$) resulting in a distribution of decay times [19,21]. The robust approach will not add substantial

[1] Water Chemistry Division, Engler-Bunte-Institute, University of Karlsruhe, Richard-Willstätter-Allee 5, 76131 Karlsruhe, Germany.
[2] To whom correspondence should be addressed.

1053-0509/98/1200-0309$15.00/0

information in the understanding of the NOM fluorescence decay, although it offers a simple way to obtain an additional characterization parameter for NOM [22,23]. Using the DCA at least three exponential decay terms were necessary for a satisfying data representation of the NOM fluorescence decay (judged on the χ^2 value and the randomness of the residuals) [17,20,21]. However, the interpretation of the parameters found is crucial because they were operationally defined and should not be mistaken for real fluorophores without further structural information of NOM. In the application of decay time distributions no preassumed number of fluorescence decay components is introduced. McGown *et al.* used the maximum entropy method (MEM) and found a trimodal distribution of decay times for different NOM samples [19]. Kumke *et al.* applied the exponential series method (ESM) in the analysis of NOM samples of different aquatic origin and found multimodal decay time distributions [21].

The high complexity of the NOM fluorescence decay could be caused by several intra- and intermolecular processes and structural features of the NOM matrix such as a large number of different fluorophores or a small number of fluorophores in many molecular environments. Possible intra- and intermolecular interactions are energy transfer between fluorophores and reorientation processes (e.g., proton transfer reactions).

The objective of the presented work was to investigate the fluorescence decay of natural organic matter (NOM) of different origins. By monitoring the influence of oxidation, of fractionation, and of metal ion complexation on the time-resolved fluorescence of NOM, the relationship between observed fluorescence and structure was further probed.

EXPERIMENTAL

Time-Resolved Fluorescence Measurements

Time-resolved fluorescence measurements were performed using a FL900CDT fluorescence spectrometer (Edinburgh Analytical Instruments, Research Park, Riccarton, Currie, Edinburgh UK) in the time-correlated single-photon counting mode. The instrument was set up in a T-geometry format with two analyzing detection channels. The focal length of the monochromators in the excitation and emission channels was 300 mm, with an aperture of f/4.2 (optical configuration: symmetrical Czerny–Turner). The grating of the excitation monochromator was blazed at 250 nm and the gratings of the emission monochromators were blazed at 500 nm for optimal performance. The linear dispersion of the monochromators was 1.8 nm/mm, which, together with the slit width, determines the spectral bandpass of the fluorescence measurements. For the detection a photomultiplier tube (PMT) R1527 (Hamamatsu) with a rise time of 2.2 ns was used. A nF900 nanosecond flash lamp (Edinburgh Analytical Instruments) filled with nitrogen gas (1 bar, 6.6 kV, 0.3-mm electrode separation, operated at 40 kHz) was used for the excitation of the samples. A multichannel analyzer (MCA) Norland 5000 (Viking Instruments Inc., 128 Owen Road, Madison, WI) was operated in the pulse height analysis mode. The memory of the MCA Norland 5000 consists of 4096 channels. In the typical T-geometry format experiment 1024 channels of the MCA were attributed to each detection channel.

For data analysis the commercial software of Edinburgh Instruments was used. In addition to the standard software features (multiexponential data fitting), level 2 software was chosen for the decay time distribution analysis and the global analysis.

In order to get reliable results in an acceptable period of time the experiments were performed at a count level of 5×10^4 cpm. The measurement time was usually below 4 h and the stability of the time profile of the excitation pulse was controlled by monitoring the fluorescence decay of the NOM samples and the excitation pulse in cycles of 5000 cpm per cycle.

The excitation wavelength in the time-resolved fluorescence experiments was 314 nm. The experiments were typically run at a time base of 100 ns, with 5 ns delay of the stop PMT. The NOM fluorescence was investigated between λ_{em} = 390 nm and λ_{em} = 590 nm. In the time-resolved fluorescence experiments the emission bandpass was 9 nm in both detection channels.

In general, the counting rate was less than 1% for the NOM samples under investigation, and therefore, pile-up problems in the decay time data analysis were not likely to occur. The experimental data were analyzed with nonlinear least-squares (NLLS) algorithms based on the method of Marquardt. The results of the data-fitting procedures were judged by the χ^2 value and the randomness of the weighted residuals. In the data fitting, only the fluorescence decay was taken into account. Therefore, it was not necessary to introduce a shift term into the data analysis.

Samples and Sample Treatment

In the fluorescence experiments a dissolved organic carbon (DOC) concentration of 5. . .10 mg/L was used. Unless noted otherwise the samples were dissolved in

Table I. Basic Parameters of the Aquatic NOM Samples [$Q = (a_{254\ nm}/a_{436\ nm})$], Where a Is the Specific Absorption Coefficient at Wavelength λ

	H/C	O/C	N/C	S/C	Q (pH 7)
Bog lake water FA	0.83	0.57	0.01	0.005	12.6
Municipal wastewater effluent	1.19	0.49	0.05	0.02	1.8
Effluent from brown coal production (FA)	1.04	0.50	0.03	0.07	9.8
Soil seepage water FA	0.82	0.59	0.01	0.002	13

deionized water (MilliQ water purification system) at a pH value of 6. . .7.

The NOM samples were of different aquatic origin, with the exception of the soil seepage water. Table I summarizes the samples investigated. The isolation procedure was based on the XAD method of Mantoura and Riley using XAD-8 resins and was described by Abbt-Braun *et al.* [24].

Fractionation

The FA isolated of a bog lake water and of a soil seepage water were further fractionated by size exclusion gel chromatography (TSK HW40S, Merck). The process was operationally defined by collecting fractions of the eluting NOM sample at preset times. The soil seepage water FA was divided into four and the bog lake water FA into three fractions, respectively. To obtain a sufficient amount of each fraction the procedure was repeated several times. The fluorescence results shown represent the average of the runs of fractionation. In the time-resolved fluorescence measurements an excitation wavelength λ_{ex} = 314 nm and an emission wavelength λ_{em} = 450 nm were used.

Ozonation

The ozonation of the NOM sample was performed in a vessel (height, 0.35 m; diameter, 0.065 m) stirred by a magnetic stirrer. For the dispersion of the ozone the reactor was equipped with a porous glass frit. The ozone concentration in the gaseous phase was measured before and after passing the reactor using two UV detectors at a detection wavelength of 254 nm [25]. The bog lake water (DOC = 15 mg/L) was filtered (0.45 μm) and ozonated for a maximum of 20 min. During this ozonation samples were taken at preset times.

DATA EVALUATION

Data Analysis Using a Small Set of Exponential Functions with Linked Decay Times (Global Analysis)

The experimental data were evaluated with a sum of three exponential terms [eq. (1)]:

$$I(t) = \sum_{i=1}^{3} B_i \cdot e - \frac{t}{\tau_i} \qquad (1)$$

Here, $I(t)$ is the fluorescence intensity of the sample dependent on time t after the excitation pulse, τ_i is the fluorescence decay time, and B_i is the related fractional intensity. The relative fractional intensity A_i of each component of the total fluorescence decay is given by Eq. (2):

$$A_i = \frac{B_i\tau_i}{B_1\tau_1 + B_2\tau_2 + B_3\tau_3} \quad \text{with} \quad i = 1,2,3 \qquad (2)$$

In the global analysis the three decay times were linked during the fitting process of a set of experimental data (e.g., for different emission wavelengths or different times of ozonation) to find the set of fluorescence decay times optimized for all decay data sets introduced, and only the fractional intensities were fitted independently for each decay data set.

Exponential Series Method (ESM)

In the ESM approach no initial model for the fluorescence decay was introduced into the data analysis. Using the exponential series method (ESM) no assumption was initially made about the number of fluorophores responsible for the fluorescence decay rather than starting with a flat distribution of exponential decays evenly spaced on a logarithmic scale [26–29]. The number of exponential terms could be up to 100 distributed over several decades of nanoseconds. The fractional intensities A_i of each decay time were varied during the fitting procedure. To avoid bias and to vary the decay times, the fitting was performed with different numbers of decay time and different time intervals in terms of lower and upper limits of the flat starting distribution of fluorescence decay times. For artificial decay time components introduced due to noise in the experimental data, it is expected that these components are influenced by the different start conditions for the fit. Real decay time components should be independent of the start parameters.

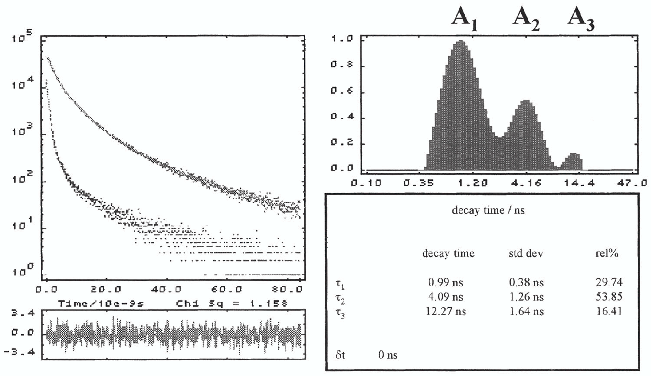

Fig. 1. ESM analysis of NOM derived of a municipal waste water. The experimental data, the fitted curve, and the corresponding residuals are shown at the left. Right: The obtained distribution of fluorescence decay times and the calculated mean decay times and related fractional intensities. For the fit 100 decay terms in a time range between 0.1 and 50 ns were used (λ_{ex} = 314 nm, λ_{em} = 420 nm, DOC = 10 mg/L, pH 6.5).

In general, for the data evaluation a number of 100 fluorescence decay times was chosen, with the lower limit at 0.1 ns and the upper limit at 50 ns.

RESULTS AND DISCUSSION

For all NOM samples investigated the observed fluorescence decay was highly complex. The experimental NOM fluorescence data were fitted in terms of a mathematical description by a sum of three exponential decay terms (DCA) and by a distribution of a large number of exponential decay terms (ESM). The fluorescence decay distribution analysis worked without a preassumed number of fluorescing components; only the time range was preset in the data analysis and should therefore be less biased.

In the data analysis a parameter set of fluorescence decay times τ_λ and related fractional intensities A_τ was obtained. These parameter sets were *operationally defined*. It should be stressed that their interpretation in terms of real physical fluorophores (or groups of fluorophores in case of the distribution analysis) has to be done very carefully.

Fluorescence Decay of NOM Samples of Different Aquatic Origins—Influence of the Emission Wavelength

In order to overcome the lack of reliable literature data on time-resolved fluorescence, measurements of NOM of different aquatic origin were performed. The obtained data were evaluated with three exponential decay terms (DCA; global analysis) as well as with a distribution of fluorescence decay times (ESM). The elemental composition and the spectral absorption of the NOM samples investigated are summarized in Table I.

Figure 1 shows data on the fluorescence decay of a municipal waste water and results of the distribution analysis. For all NOM samples investigated the distribution analysis yielded a trimodal distribution. The results presented are in good agreement with previously reported data [17,19,20]. McGown *et al.* applied a different distribution analysis (maximum entropy method; MEM) and found a trimodal distribution for the investigated humic substance as well.

The fluorescence decays of the NOM samples (a municipal wastewater effluent, a bog lake water FA, and a brown coal production effluent FA) were monitored in the emission wavelength range between λ_{em} = 390 nm and λ_{em} = 550 nm. For all fluorescence emission wavelengths the ESM analysis recovered a trimodal distribution and variations of the calculated mean fluorescence decay times of each peak were smaller than 10% for each NOM sample. It is interesting to note that the mean fluorescence decay times of the three NOM samples were quite similar (see Table II).

The mean fluorescence decay times reported by McGown *et al.* were found to be in the same time range ($\tau_1 < 1$ ns, $\tau_2 \sim 3$ ns, $\tau_3 \sim 10$ ns) using MEM analysis

Table II. Average Mean Fluorescence Decay Times of the Three NOM Samples Investigated in the Emission Wavelength Range Between λ_{em} = 390 and λ_{em} = 530 nm

	Global analysis (ns)			Distribution analysis (ns)		
Sample	τ_1	τ_2	τ_3	τ_1	τ_2	τ_3
Bog lake water FA	1.1 ± 0.1	4.1 ± 0.3	11.8 ± 0.9	1 ± 0.1	4.3 ± 0.3	14.6 ± 1.2
Municipal wastewater effluent	1.1 ± 0.2	4.4 ± 0.4	12.6 ± 1	1 ± 0.2	4.1 ± 0.2	12.8 ± 0.9
Effluent from brown coal production (FA)	1.2 ± 0.1	4.3 ± 0.2	12.4 ± 1.1	1.1 ± 0.2	4.1 ± 0.5	14.8 ± 2.7

[19]. Langford and Cook investigated NOM samples derived from soil organic matter. They applied a DCA with three-exponential decay functions in the data analysis. They reported decay times shorter compared to the decay times presented here and found by McGown *et al.*, probably due to the fact that the samples were of soil origin [20].

In contrast to the fluorescence decay times, the relative fractional intensities were found to be strongly dependent on the fluorescence emission wavelength for each of the NOM samples investigated in this study. Figure 2 shows the relative fractional intensities calculated in the distribution analysis for the three mean fluorescence decay times. These results are in good agreement with previously reported measurements of FA of different aquatic origins [21].

For further discussion the shortest decay time component is referred to as τ_1 and the related relative fractional intensity as A_1(τ_2, A_2 and τ_3, A_3, respectively). For τ_1 = 1.1 ns the relative fractional intensity decreased for all investigated NOM samples with increasing emission wavelength; for the FA of a brown coal production effluent it started to rise again for emission wavelengths above 440 nm. Overall, for this NOM sample the relative fractional intensity of τ_1 decreased from 47% at 390 nm to about 23% at 510 nm. At the same time its decay time τ_2 = 4.1 ns increased in its fractional intensity from 40% at 390 nm to almost 67% at 510 nm. The relative fractional intensity of the third fluorescence decay time (τ_3 = 14.8 ns) was almost unchanged over the whole investigated emission wavelength range. The bog lake water FA showed a comparable trend in the first fluorescence decay time, τ_1 = 1 ns. Its fractional intensity A_1 decreased but to a lesser extent. The fractional intensities of τ_2 as well as τ_3 changed with the fluorescence emission wavelength. Finally, the NOM of a municipal wastewater effluent showed a steady decrease in the fractional intensity of τ_1, no change for the fractional intensity of τ_2, and a steady increase for the fractional intensity of the third fluorescence decay time. Because

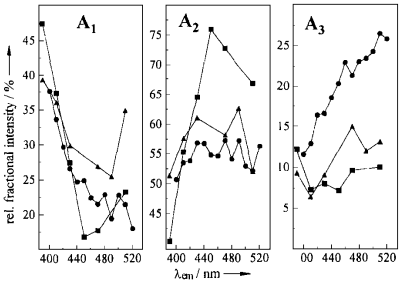

Fig. 2. Calculated relative fractional intensities of the three mean fluorescence decay times in the emission wavelength range investigated. The results for a bog lake water FA (triangle), a brown coal production effluent FA (squares), and a municipal wastewater effluent (circles) (λ_{ex} = 314 nm, DOC = 10 mg/L, pH 6.5) are shown.

the municipal waste water is relatively young in terms of genesis, its content of fulvic acid-like matter is high and therefore determined the observed fluorescence.

The experimental data were also evaluated using three exponential decay functions with the three fluorescence decay times linked in the fitting process (global analysis). For all three NOM samples investigated a global χ^2 value better than 1.2 was obtained in the data analysis. It is interesting to note that the results of the global analysis yielded the same trends in the emission wavelength dependence of the fractional intensities that were found in the distribution analysis. In Table II the calculated fluorescence decay times are compared with the results obtained in the distribution analysis. It can be seen that both data evaluation methods yielded the similar fluorescence decay times.

The elemental composition of the three samples was highly different regarding the content of heteroatoms (especially of sulfur and nitrogen; see Table I). The three investigated NOM samples had a relative content

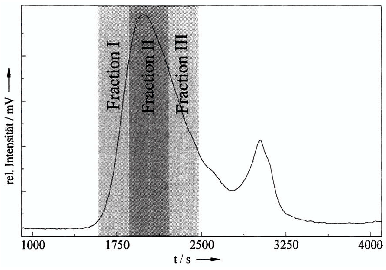

Fig. 3. Size exclusion chromatogram (SEC) of a bog lake water FA used in the fractionation experiments (TSK gel, DOC detection). Shown schematically are the operationally defined cutoff times for the fractionation.

of sulfur in the order of brown coal production effluent FA > municipal wastewater effluent > bog lake water FA. But in the case of the relative nitrogen content the order has to be changed to municipal wastewater effluent > brown coal production effluent FA > bog lake water FA. It is interesting to compare the observed differences in the fractional contributions A_1, A_2, and A_3 for the three NOM samples with their different heteroatom contents. For all NOM samples the trend of A_1 was quite similar, but the FA of the effluent of brown coal industry (highest sulfur content) showed the strongest dependence on the emission wavelength for A_2, and for the municipal wastewater effluent (highest nitrogen content) the most pronounced influence on A_3 was observed (refer to Table I and Fig. 2, respectively).

Fractionation of NOM

Figure 3 shows a size exclusion chromatogram of the bog lake water FA. Schematically shown are the cutoff times in the fractionation of the NOM sample. The time-resolved fluorescence measurements of the fractions revealed only a small difference in the fluorescence decay. The calculated fluorescence decay time pattern in the distribution analysis as well as the global analysis of the experimental data showed minor differences between each fraction. For the bog lake water FA the data analysis of the three fractions I, II, and III and the original FA yielded, within the error of the measurements, identical decay times and fractional intensities. The decay time distribution pattern showed a small change in the decay time regime between 2 and 15 ns, with an increase going from fraction I, with a higher mean nominal molar mass, to fraction III, with a lower mean nominal molar mass. These results were in agreement with data obtained for other properties of the NOM fractions I. . .III of the bog lake water (e.g., UV/vis, proton capacities), where only very small differences were detectable between the fractions.

For the soil seepage water FA and its fractions I. . .IV (see Table III), the differences were more pronounced. With increasing mean nominal molar mass, the contribution of the longer fluorescence decay times relative to the 1-ns peak was amplified (see Table III and Fig. 4). Judged by the fluorescence decay time distribution, fractions III and IV were most closely related to the original soil seepage water FA.

The two fractions with a nominal molar mass smaller than the original FA seemed to determine the fluorescence decay. For these two fractions the calculated fluorescence decay time pattern in the distribution analysis as well as the results of a global analysis was similar to the original FA. Fractions I and II showed a clear decrease in the contribution of longer decay times (see Fig. 4). Considering the relative contributions of each fraction to the total dissolved organic carbon of the original sample, fractions III and IV represent approx. 80% which has to be taken into account in the interpretation of the data (see Table III).

Ozonation of Bog Lake Water

In a previous paper the results of ozonation of NOM samples of different origins were reported [21]. In the distribution analysis it was found that due to the ozonation, the relative contributions of fluorescence decay times in the time range below 1.5 ns (''fast-decaying components'') and above 1.5 ns (''slow-decaying components'') were changed. The contribution of decay times shorter than 1.5 ns appeared to be increased relative to the longer fluorescence decay times. This was interpreted in terms of a decrease in the molar mass supported by the results of gel chromatography.

For further investigation we performed experiments with bog lake water under different times of exposure to O_3. The measurement of the dissolved organic carbon (DOC) concentration revealed no significant change during the ozonation ($\approx$15 mg/L). In steady-state fluorescence experiments the fluorescence intensity was increased within the first 5 min of ozonation and decreased with further ozonation, with only a slight spectral change. The initial increase in fluorescence intensity could be due to a decrease in the color of the sample solution, which would have resulted in a reduction of the ''inner-filter'' effect. The absorption of the bog lake

Table III. Fractionation of a Soil Seepage Water FA Using SEC (TSK Gel)[a]

Sample	Mean nominal molar mass (g/mol)	Relative portion of DOC (%)	A_1 (%) (τ_1 = 1 ± 0.1 ns)	A_2 (%) (τ_2 = 3.9 ± 0.4 ns)	A_3 (%) (τ_3 = 10.6 ± 0.7 ns)
Soil seepage water FA	857	100	22.8	46.4	30.8
Fraction I	969	6	39.8	42.1	18.04
Fraction II	850	11	33.3	42	24.7
Fraction III	716	45	23.3	48.5	28.2
Fraction IV	654	35	20.6	50.7	28.7

[a] The mean nominal molar mass was determined relative to a standard (polyethylenglycol oxide; PEO). In the time-resolved fluorescence measurements an excitation wavelength λ_{ex} = 314 nm was used in combination with a detection wavelength of 450 nm. In the measurements the spectral bandpass was set to 9 nm.

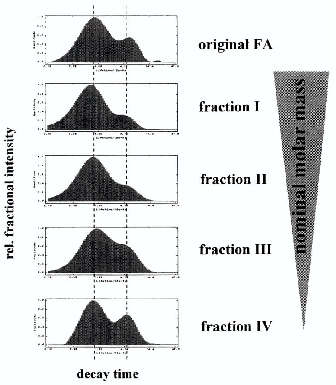

Fig. 4. Distribution analysis of a soil seepage water FA and its fractions I, II, III, and IV, with mean nominal molar masses of 857, 969, 850, 716, and 654 g/mol, respectively (λ_{ex} = 314 nm, λ_{em} = 450 nm, DOC = 10 mg/L, pH 5; PEO standard for the determination of the nominal masses in the SEC).

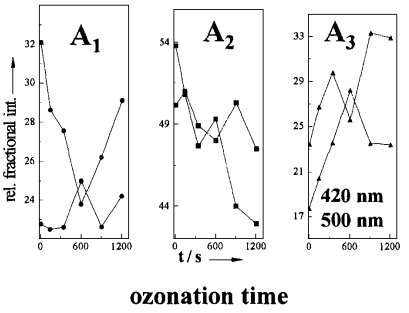

Fig. 5a. Ozonation of a bog lake water (DOC = 15 mg/L, pH 6, λ_{ex} = 314 nm) monitored at two emission wavelengths (λ_{em1} = 420 nm and λ_{em2} = 500 nm). The fractional intensities calculated in the global analysis approach with three linked fluorescence decay times (τ_1 = 0.8 ± 0.1 ns, τ_2 = 3.4 ± 0.3 ns, and τ_3 = 9.7 ± 0.7 ns) at different times of ozone treatment are shown.

water decreased from 0.06 before ozonation down to 0.02 after 20 min of ozone treatment. The absorbed ozone concentration of the reaction solution was approximately 10 mg/L at t = 20 min.

Time-resolved fluorescence measurements were performed at two emission wavelengths (420 and 500 nm). In the distribution analysis the recently described trend of a relative decrease in the longer fluorescence decay times in favor of the shorter time domain was confirmed [21]. During the time course of the ozonation this tendency became more pronounced. Furthermore, a dependence of the observed trend on the detection wavelength in the time-resolved fluorescence measurements was found. In Fig. 5a the results for the global analysis approach with three linked fluorescence decay times are presented. Shown are the fractional intensities of the three fluorescence decay times (τ_1 = 0.8 ± 0.1 ns, τ_2 = 3.4 ± 0.3 ns, and τ_3 = 9.7 ± 0.7 ns, respectively) in the course of the ozonation process.

In the distribution analysis the obtained fluorescence decay time pattern was changed due to the ozonation and the quite resolved three main fluorescence decay time maxima were lost, which went along with the observed changes of the gel chromatographic separation, in which the higher molar mass fraction was reduced and the contribution of organic compounds with a low molar mass (see Fig. 5b; "salt boundary") was increased. The observed changes in the fluorescence decay due to ozonation were dependent on the emission wavelength. The fractional intensities A_1, A_2, and A_3 showed a different influence of the ozonation process.

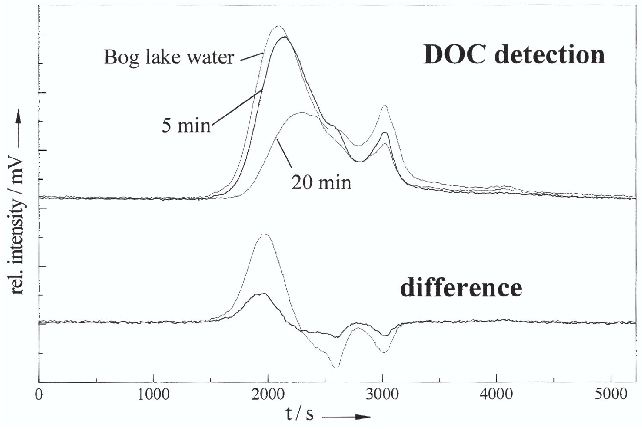

Fig. 5b. SEC of a bog lake water before and after ozonation (5- and 20-min ozone treatment).

A comparison on a relative base of the emission wavelength dependence for the influence of the ozonation process was made. In Fig. 5a the emission wavelength dependence of the ozonation for the calculated fractional intensities in the global analysis is summarized. Considering that different fluorescent structures were attacked to a different extent by the ozone, the observed dependence of the change in the fluorescence decay at the two emission wavelengths can be understood.

Effects of Metal Ion Complexation on the Observed Fluorescence Decay of NOM

For the fluorescence intensity of NOM, quenching was observed upon metal ion binding. The degree of fluorescence quenching was dependent on the metal ion. For copper and iron high fluorescence quenching efficiencies were reported, whereas manganese, lead, and cadmium were rather weak fluorescence quenchers [30,31]. Often the observed quenching of the NOM fluorescence intensity is used to determine binding constants for the metal ions. The mechanism of the fluorescence quenching process is only poorly understood. Neither has the reason for the different quenching efficiencies of different metal ions been fully investigated, nor is the connection between NOM binding sites and fluorophores clear. The application of time-resolved fluorescence methods is suitable to investigate the dynamic interaction processes between metal ions and NOM. Bidoglio *et al.* investigated the luminescence decay of terbium and europium in the presence of NOM, but because of the NOM fluorescence, no conclusions were made about an interaction mechanism [32].

Our preliminary results revealed no effects of copper on the fluorescence decay of a bog lake water FA, although the fluorescence intensity was strongly quenched. Experiments were performed for different emission wavelengths in the range between 400 and 550 nm as well as for two different excitation wavelengths (314 and 357 nm, respectively) at pH 5 with a DOC concentration of 10 mg/L. In the experiments no bulk precipitation was apparent. The formation of small particulates (e.g., colloids) could not be totally ruled out but was assumed to be very small as indicated by the only minor increase in the light scatter peak. The copper concentration was varied between 10^{-5} and 10^{-7} *M* without a detectable influence on the observed NOM fluorescence decay.

The first results of experiments with alumina and iron indicated that both metal ions influenced the NOM fluorescence decay. In the presence of iron(II) at pH 3 the fluorescence decay time distribution was shifted toward shorter decay times. The ratio of the three mean fluorescence decay times found in the distribution analysis without and with iron(II) present was the same ($\tau_x / \tau_x^{HS} \sim 1.2$, $x = 1,2,3$). The dynamic quenching of the

iron(II) was dependent on the emission wavelength and was increased at shorter emission wavelengths. The fact that iron(II) equally influenced all fluorescence decay times made an interpretation in terms of a nonspecific dynamic interaction process tempting.

Al^{3+} also effected the fluorescence decay of the bog lake water FA investigated. However, the observed dynamic quenching was smaller compared to iron(II), the three mean fluorescence decay times were altered to an different extent, and moreover, the obtained pattern in the decay time distribution seemed to change upon the complexation of Al^{3+}.

In further experiments the lanthanide ions europium and terbium were introduced. Here, the influence on the NOM fluorescence decay was monitored as well as the luminescence of the lanthanide ions themselves, indicating energy transfer from the NOM ligands to the lanthanide ions. In the time-resolved fluorescence measurements it was found that the observed change in the NOM fluorescence decay was dependent on the detection wavelength. For fluorescence emission wavelengths greater than 400 nm a quenching of the NOM fluorescence decay was found, whereas for shorter wavelengths the opposite effect was monitored. These results are describe in more detail in a separate paper [36]. Investigations of the interaction between metal ions and NOM are a subject of current research projects.

CONCLUSIONS

The application of global analysis with three exponential decay terms and the distribution analysis revealed similar tendencies for the fluorescence decay times and the related fractional intensities. Within the experimental uncertainty identical fluorescence decay times could indicate that similar fluorescence structures are present in the investigated NOM samples. Based on the results reported for the fluorescence decay of NOM, it is tempting to attribute a key position to the presence of heteroatoms. However, this conclusion has been based on a small number of NOM samples, and further investigations are needed. It is well proven that a great part of the nitrogen content of NOM can be attributed to bound amino acids [33]. Work is in progress to investigate the influence of enzymatic hydrolysis of the bound amino acids on the fluorescence of the municipal wastewater effluent and on the observed emission wavelength dependence of fractional intensities A_x.

Another parameter that should be related to the observed fluorescence of the investigated NOM sample is the metal ion content, especially that of paramagnetic metal ions. Paramagnetic metal ions show the strongest fluorescence intensity quenching. In our experiments with metal ions different effects on the fluorescence decay were indicated. Measurements to determine the content of metal ions in the used NOM samples are in progress. Preliminary results show that, especially, the iron content is considerablely high for all NOM samples investigated (several hundred micrograms per gram of DOC) [34]. The important role of the iron(III)/iron(II) balance in photochemical reactions in the presence of NOM in surface waters is well known [35], but its role for NOM fluorescence has to be elucidated. The application of lanthanide ions, especially europium and terbium, is promising because the metal ion luminescence offers an additional detection parameter. The fact that some of the energy level in the europium complexes is located below 400 nm might explain the observed wavelength dependence on the fluorescence decay. Experiments with other lanthanide ions with different energy levels are planed in order to investigate this influence to a deeper extent.

Based on these results of fractionation using size exclusion chromatography, it is tempting to assume a quite homogeneous distribution of fluorescence subunits inside the investigated FA, probably produced in the XAD isolation procedure or caused by the similarities in the educts from which the NOM samples were descended.

The suggested connection between nominal molar mass and observed fluorescence is supported by the investigations of the influence of the ozone on the NOM fluorescence decay. Experiments with NOM samples fractionated based on, e.g., hydrophobicity will further elucidate the effect of the molar mass on NOM fluorescence decay.

ACKNOWLEDGMENTS

The authors wish to thank the Deutsche Forschungsgemeinschaft (DFG) for funding great parts of the work in the ROSIG program. Further, they are grateful to A. Heidt for the isolation and fractionation of the fulvic acid fractions and to A. Wolf for ozonation of the NOM sample. They also wish to thank R. Klenze for supplying the Eu^{3+} solutions.

REFERENCES

1. P. J. Shaw, R. I. Jones, and H. DeHaan (1994) *Environ. Technol.* **15**, 765–774.

2. D. B. Wagoner, R. F. Christman, G. Couchon, and R. Paulson (1997) *Environ. Sci. Technol.* **31**, 937–941.
3. G. Abbt-Braun, U. Schmiedel, and F. H. Frimmel (1990) *Vom Wasser* **75**, 59–73.
4. H.-R. Schulten, G. Abbt-Braun, and F. H. Frimmel (1987) *Environ. Sci. Technol.* **21**, 349–357.
5. G. Abbt-Braun, F. H. Frimmel, and H.-R. Schulten (1990) *Vom Wasser* **74**, 325–338.
6. J. A. Leenheer, R. L. Wershaw, and M. M. Reddy (1995) *Environ. Sci. Technol.* **29**, 399–405.
7. W. Liao, R. F. Christman, J. D. Johnson, D. S. Millington, and J. R. Hass (1982) *Environ. Sci. Technol.* **16**, 403–409.
8. S. Huber, T. Gremm, and F. H. Frimmel (1990) *Vom Wasser* **75**, 331–342.
9. T. M. Miano, G. Sposito, and J. P. Martin (1988) *Soil Sci. Soc. Am. J.* **52**, 1016–1019.
10. J. J. Mobed, S. L. Hemmingsen, J. L. Autry, and L. B. McGown (1996) *Environ. Sci. Technol.* **30**, 3061–3065.
11. G. Abbt-Braun and F. H. Frimmel (1991) *Vom Wasser* **77**, 291–302.
12. R. R. Engebretson and R. von Wandruszka (1994) *Environ. Sci. Technol.* **28**, 1934–1941.
13. S. E. Cabaniss (1992) *Environ. Sci. Technol.* **26**, 1133–1139.
14. M. J. Pullin and S. E. Cabaniss (1995) *Environ. Sci. Technol.* **29**, 1460–1467.
15. S. Chen, W. P. Inskeep, S. A. Williams, and P. R. Callis (1994) *Environ. Sci. Technol.* **28**, 1582–1588.
16. M. U. Kumke, H.-G. Löhmannsröben, and Th. Roch (1994) *Analyst* **119**, 997–1001.
17. C. H. Lochmüller and S. S. Saavedra (1986) *Anal. Chem.* **58**, 1978–1981.
18. J. F. Power, R. LeSage, D. K. Sharma, and C. H. Langford (1986) *Environ. Technol. Lett.* **7**, 425–430.
19. L. B. McGown, S. L. Hemmingsen, J. M. Shaver, and L. Geng (1995) *Appl. Spectrosc.* **49**, 60–66.
20. R. L. Cook and C. H. Langford (1995) *Anal. Chem.* **67**, 174–180.
21. M. U. Kumke, G. Abbt-Braun, and F. H. Frimmel (1998) *Acta Hydrochim. Hydrobiol.* **26**, 73–81.
22. P. J. Milne and R. G. Zika (1989) *Marine Chem.* **27**, 147–164.
23. U. Zimmermann, H.-G. Löhmannsröben, and T. Skrivanek (1997). *Proceedings EUROPTO Series: Remote Sensing of Vegetation and Water, and Standardization of Remote Sensing Methods* Vol. 3107, pp. 239–249.
24. G. Abbt-Braun, F. H. Frimmel, and P. Lipp (1991) *Z. Wasser-Abwasser-Forsch.* **24**, 285–292.
25. A. Wolf and F. H. Frimmel (1997) *Proceedings of the 7th International Symposium: Chemical Oxidation Technology for the Nineties*, Nashville, TN (in press).
26. D. M. Gamsky, A. A. Goldin, E. P. Petrov, and A. N. Rubinov (1992) *Biophys. Chem.* **44**, 47–60.
27. D. R. James and W. R. Ware (1986) *Chem. Phys. Lett.* **126**, 7–11.
28. A. Siemiarczuk, B. D. Wagner, and W. R. Ware (1990) *J. Phys. Chem.* **94**, 1661–1666.
29. J.-C. Brochon, A. K. Livesey, J. Pouget, and B. Valeur (1990) *Chem. Phys. Lett.* **174**, 517–522.
30. C. F. Scheck, F. H. Frimmel, and A. M. Braun (1992) *Z. Naturforsch.* **47b**, 399–405.
31. F. H. Frimmel and W. Hopp (1986) *Fresenius Z. Anal. Chem.* **325**, 68–72.
32. G. Bidogilio, I. Grenthe, P. Qi, P. Robouch, and N. Omenetto (1991) *Talanta* **9**, 999–1008.
33. J. B. Jahnel and F. H. Frimmel (1995) *Acta Hydrochim. Hydrobiol.* **23**, 31–35.
34. G. Abbt-Braun (1997) Personal communication.
35. B. C. Faust and R. G. Zepp (1993) *Environ. Sci. Technol.* **27**, 2517–2522.
36. C. Tiseanu, M. U. Kumke, F. H. Frimmel, R. Klenze, and J. I. Kim (1998) *J. Photochem. Photobiol. A* (in press).

2.3.2 Time-resolved fluorescence spectroscopy of fulvic acid and fulvic acid complexed with Eu^{3+} - A comparative study

C. Tiseanu, M.U. Kumke, F.H. Frimmel, R. Klenze, J.I. Kim
J. Photochem. Photobiol. A, 1998., **117**(3), 175 - 184.

In zeitaufgelösten Fluoreszenzuntersuchungen wurden neben den Fluoreszenzabklingkinetiken bei verschiedenen Emissionswellenlängen die zeitaufgelösten Fluoreszenzspektren von aus Grundwasser isolierten HS gemessen und der Einfluss der Komplexierung von Eu^{3+} untersucht. Durch die Metallkomplexierung änderten sich die operational-definierten Fluoreszenzabklingzeiten nur wenig, allerdings änderten sich die relativen Anteile dieser deutlich. Es zeigte sich eine Abhängigkeit der Parameter von Anregungs- und Emissionswellenlänge. Die mittlere, gewichtete Fluoreszenzabklingzeit nahm mit zunehmender Emissionswellenlänge zu. In Gegenwart von Eu^{3+} war dieser Effekt reduziert. Noch deutlicher konnte der Effekt der Komplexierung von Eu^{3+} in den zeitaufgelösten Fluoreszenzspektren der untersuchten HS gezeigt werden. So wurde beispielsweise der Schwerpunkt im Fluoreszenzspektrum in Abhängigkeit von der Zeit nach Anregung betrachtet. In Abwesenheit von Eu^{3+} verschob sich der Schwerpunkt deutlich bathochrom, während diese durch die Komplexierung von Eu^{3+}-Ionen fast vollständig aufgehoben wurde. Als Gründe für die beobachten Veränderungen in der Fluoreszenzabklingkinetik können eine veränderte Konformation (oder Konformationsdynamik) und Energietransferprozesse in Betracht gezogen werden.

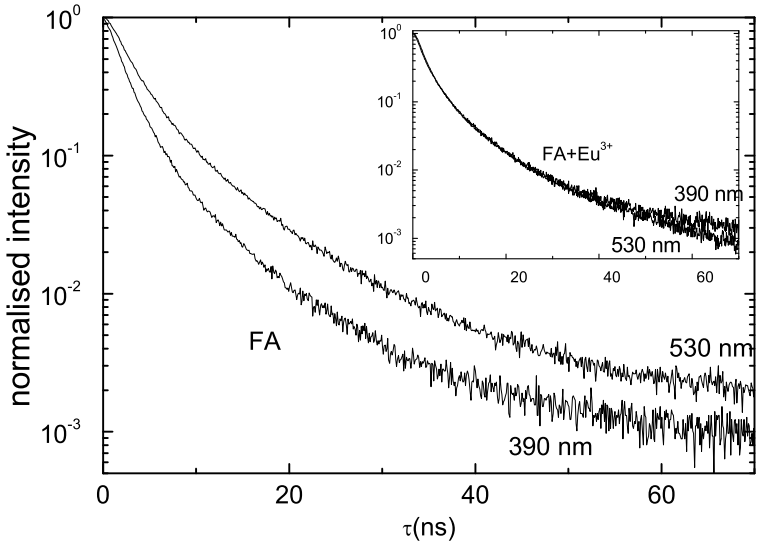

ELSEVIER

Journal of Photochemistry and Photobiology A: Chemistry 117 (1998) 175–184

Journal of Photochemistry and Photobiology A:Chemistry

Time-resolved fluorescence spectroscopy of fulvic acid and fulvic acid complexed with Eu^{3+} – a comparative study

C.-D. Tiseanu[1,a], M.U. Kumke[a], F.H. Frimmel[a,*], R. Klenze[b], J.I. Kim[b]

[a] *Engler-Bunte Institute, Division of Water Chemistry, Univerity of Karlsruhe, Richard-Willstätter-Allee 5, 76131 Karlsruhe, Germany*

[b] *Forschungszentrum Karlsruhe, Institut für Nukleare Entsorgungstechnik, 76126 Karlsruhe, Germany*

Received 30 March 1998; received in revised form 22 June 1998; accepted 24 June 1998

Abstract

In this work a systematic characterization of the fluorescence kinetics of fulvic acid by means of a single-photon time correlation technique is reported. The data were extracted from both single decay curves and time-resolved emission spectra and analyzed by the exponential series method. The results strongly suggest the existence of a tri-modal decay time distribution with peak decay time values centred around 0.7, 3 and 10 ns. The relative amplitudes of the decay time distributions were shown to depend on the emission wavelength, indicating a three-species mixture with slightly different emission maxima and widths. As sustained by time-resolved emission spectra the same species of fluorophores are responsible for the fluorescence kinetics behaviour of fulvic acid at all excitation wavelengths used in the experiments. For the first time these techniques and methods were applied in investigating the effects of the Eu^{3+} complexation upon fluorescence kinetics of the fulvic acid. Single decay analysis indicates that the peak decay time values are not affected by Eu^{3+} addition at all emission and excitation wavelengths used in the experiments. On the contrary, the dependency of relative amplitudes on emission wavelength was greatly reduced in comparison with the uncomplexed fulvic acid. This effect is further evidenced by analysing the barycenter transients of time-resolved emission spectra. Finally, it is also indicated that within the temporal resolution of the experimental set up used the singlet states play no role as donor states in intramolecular energy transfer from the organic fulvic acid ligands to the Eu^{3+} energy levels.

Keywords: Time-resolved fluorescence; Fulvic acid; Europium ion

1. Introduction

Humic substances (HS) – humic acids (HA) and fulvic acids (FA) – are macromolecular compounds with a very complex and heterogeneous structure that show polyfunctional, polyelectrolytic and conformationally related properties [1–4]. Consequently, the fluorescence of dissolved HS depends strongly on their origin, molecular weight, concentration, pH, ionic strength, temperature, redox potential of the medium and finally on the interactions with organic xenobiotics and anorganic constituents, e.g. metal ions [5,6].

During the last decade fluorescence spectroscopy has been successfully applied in extracting useful information on quantitative and qualitative aspects of HS. However, only little reliable data on the dynamic fluorescence behaviour of HS (e.g. fluorescence decay times, time-resolved fluorescence emission spectra (TRES)) have been reported in the literature.

Recently, the maximum entropy method (MEM) was used for the data analysis of FA fluorescence decays indicating a tri-modal fluorescence decay times distribution for the investigated FA [7]. The peak decay time values reported were around 1, 3 and 10 ns. In a more detailed study [8], HS from different aquatic origins were investigated by means of a different deconvolution algorithm (exponential series method, ESM), and again a tri-modal distribution with similar peak decay time values was found for the investigated HS as well. The study proved the applicability of time-resolved fluorescence measurements for the investigation of the molecular dynamics of humic substances. A suggestion to relate certain parts of the calculated fluorescence decay time distribution with structural subunits of the investigated humic substances was made.

The acidic functional groups of HS are an abundant source of metal binding sites in the natural environment. Studies of metal binding to HS are of great environmental interest because of the biological and physicochemical

*Corresponding author. E-mail: fritz.frimmel@ciw.uni-karlsruhe.de

[1]Present address: Institute of Atomic Physics, Solid State Quantum Electronics Laboratory, POB MG-36, R-76900 Bucharest, Romania.

1010-6030/98/$ – see front matter
PII: S1010-6030(98)00336-0

properties of metals which are often dramatically changed as a result of complexation by HS [9,10].

In order to understand how these heterogeneous organic macromolecules bind metals within a large range of binding energies, TRES has been used to study changes in the luminescence spectra of lanthanide metal ion when binding to HS. The study of sensitised fluorescence by energy transfer from the excited chromophores to the *f*-element ion may yield, among others, information about binding distance between the organic ligand and the metal ion. One of the metals most extensively studied is the Eu^{3+} ion. As reported by other authors, Eu binding to humic substances resulted in sensitised Eu^{3+} luminescence following the intramolecular energy transfer (IMET) from HS ligands to Eu excited levels [11–16]. The 'traditional' picture of IMET is based on the donor character of the triplet state of the organic ligands which transfers the excitation energy through a dipole–dipole interaction mechanism to the excited Eu^{3+} levels. For a recent review on IMET, see, for example, reference [17].

This assumption, however, lacks two important experimental evidences: (a) the impossibility of observing the phosphorescence of the donor (e.g. the triplet state of HS) at room temperature and in solution due to strong quenching processes. In other words, no experimental observations of the dynamic effect of energy transfer manifested as a fast initial drop in the luminescence kinetics of the HS donor could be extracted; (b) no effects of the energy transfer may be inferred from the acceptor (Eu^{3+}) luminescence as well, within the usual temporal resolution reported in such studies.

Our preliminary results obtained in a different series of TRES experiments (details will be published elsewhere) indicate that the rate of the energy transfer from FA to Eu^{3+} is faster than the temporal resolution of the instrumental set up (approx. 10 ns) e.g., larger than 10^{-7}–10^{-8} s^{-1}. In this case, quantitative estimations of the energy transfer from the acceptor (Eu^{3+}) luminescence kinetics were not possible, as no rise time in Eu^{3+}-sensitised luminescence was detected.

Moreover, the mechanism of IMET from the donor triplet state to most of the excited state levels of the lanthanide ions is a (super)exchange one as imposed by the Wigner–Pauli rule [17,18]. In this case, information on distances between ligand and metal ion commonly obtained within the Foerster–Dexter formalism is not straightforward to obtain [19]. However, this rule may be relaxed in case of the mixing of the triplet states with energetically closely situated singlet states.

To the difficulties one usually encounters in TRES studies concerning interactions between HS and Eu^{3+} ions (as well as other lanthanides and actinide ions), we must add the lack of reliable data concerning the effects induced by lanthanide ions on the fluorescence kinetics of humic substances.

There are three issues we investigate in this paper: (1) the kinetics of the FA fluorescence and its dependence on excitation wavelength, emission wavelength and FA concentration, (2) the effects induced by Eu^{3+} binding on the FA fluorescence kinetics, and (3) the possible role of FA singlet states as a donor state for an energy transfer from FA ligands to Eu^{3+}. The latter issue was imposed by (a) the dense scheme of excited energy levels presented by Eu^{3+} in the region of FA fluorescence (e.g. between 390 and 550 nm) [20] and (b) some earlier observations according to which in some of the lanthanide complexes, the IMET process seems to occur through a direct resonance energy transfer between a ligand singlet level and a lanthanide ion level [21]

2. Experimental details

The time-resolved fluorescence measurements were performed using a FL900CDT fluorescence decay time spectrometer (Edinburgh Analytical Instruments, UK) in the time-correlated single photon counting mode. The instrument was set up in a T-geometry format with two analyzing detection channels. The grating of the excitation monochromator was blazed at 250 nm and the grating of the emission monochromators was blazed at 500 nm for optimal performance. The linear dispersion of the monochromators was 1.8 nm/mm which determined together with the slit width the spectral bandpass of the fluorescence measurements. For the detection photomultiplier tubes (PMT) R1527 (Hamamatsu) with a typical rise time of 2.2 ns were used. A nF900 ns flash lamp (Edinburgh Analytical Instruments) filled with nitrogen gas was used for the excitation of the samples. The multichannel analyser (MCA) Norland 5000 (Viking Instruments, USA) was operated in the pulse height analysis mode. The memory of the MCA Norland 5000 consists of 4096 channels. In the typical T-geometry format experiment 1024 channels of the MCA were attributed to each detection channel.

For data analysis the commercial software package of Edinburgh Instruments was applied based on the ESM approach and on the discrete components approach (DCA). For a reliable data evaluation of complex fluorescence kinetics the acquisition rate (reported as the count rate at peak maximum) is a crucial parameter. Experiments at different levels of counts (10^3–10^5 counts at the peak maximum) were performed and the influence on fitting results was monitored.

The measurement time was usually below 4 h, and the stability of the time profile of the excitation pulse was controlled by monitoring the fluorescence decay of the NOM samples and the excitation pulse in cycles of 5000 counts per cycle. In general, the counting rate was less than 1% for the natural organic matter samples under investigation and therefore pile-up problems in decay time analysis were not likely to occur.

The excitation wavelengths in the time-resolved fluorescence experiments were 314, 357 and 379 nm. The experiments were typically run at a time base of 100 ns with

5 ns delay of the stop PMT. Fluorescence emission was detected between 380 and 580 nm with a spectral bandwidth of 9 nm.

Steady-state fluorescence measurements were performed with a Perkin–Elmer LS 5B spectrofluorometer. In the standard steady-state experiments a spectral bandwidth of 10 nm in excitation and emission was used. Excitation wavelengths of 314 nm were applied and the spectra were recorded in the range between 350 and 600 nm. The spectra were background corrected and for comparison purposes normalized to the dissolved organic carbon concentration (DOC, in mg/l). The Raman signal of pure water was used as internal standard for the correction of day-to-day fluctuations of excitation intensity. The fluorescence intensities were not corrected for the inner filter effects nor for the spectral difference of the PMT response because the spectra were evaluated on a relative base and no change in the shape of fulvic acid fluorescence was observed under experimental conditions.

The fulvic acid fraction under investigation was extracted from one of the deep ground waters in Gorleben area in northern Germany. Details of the extraction and purification as well as basic data can be found elsewhere [22]. Stock solutions of Eu^{3+} were prepared by dissolving Eu_2O_3 in 0.1 M $HClO_4$ and dilution with 0.1 M $NaClO_4$. The pH for pure and complexed FA samples was adjusted to approx. 6, and the concentration of Eu^{3+} was kept in all time-resolved fluorescence experiments at 10^{-4} M.

Fluorescence was monitored for a DOC in the range between 5 and 30 mg/l in steps of 5 mg/l. In general, the influence of Eu^{3+} on FA fluorescence decay was monitored for a DOC of 10 mg/l. All fluorescence measurements were performed at room temperature.

3. Results

The time dependence of the fluorescence intensity $I(t)$ was measured and the data were analyzed using three discrete exponential terms (DCA) and with a distributional analysis based on the ESM, [23,24].

$$I(t) = \int_0^\infty A(\tau)\exp(-t/\tau)\mathrm{d}\tau \quad (1)$$

In this approach up to 100 decay times ranging from 0.1 to 50 ns equally spaced in the logarithmic time scale were used. The amplitude distribution $A(\tau)$ recovered by the ESM represents the maximum probability of amplitudes among the decay time components. The quality of the exponential fit was determined from the randomness of the weighted residuals distribution at χ^2 close to unity. The parameters of fluorescence decay obtained by the ESM are defined as follows: (a) the distribution $A(\tau)$ is divided in as many peaks (or decay components) as can be clearly separated by two successive well-defined minima; (b) the peak decay time values, τ_i, represent the average position of the peak i in ns, calculated as:

$$\tau_i = \sum_j A_j\tau_j / \sum_j A_j \quad (2)$$

calculated over all decay times j included in the peak i; the relative amplitude A_i is the ratio of the peak surface $\sum A_j$ over the entire surface of the distribution. The ESM analysis also provides the distribution width parameters reflecting both the degree of inhomogeneity experienced by fluorescing species and noise effects. The experimental data consist of a convolved decay curve, and thus the ESM recovery curve, $I(t)$, is obtained by iterative re-convolution with the instrumental response function.

To obtain accurate fluorescence decay parameters, the following steps were used: the visual inspection of the experimental decay curves to establish the best fitting range; DCA fit and ESM analysis together with choosing between the optimum of the χ^2 values and the best images of the residuals.

3.1. Single decay curves analysis

3.1.1. Dependence of the fluorescence decay of FA and FA complexed with Eu^{3+} on the excitation wavelength

FA: The FA fluorescence was excited at three excitation wavelengths λ_{ex}=314, 357 and 379 nm, the first two wavelengths were chosen around the maximum of the fluorescence excitation spectrum of the FA and the third wavelength was selected at the red edge of the fluorescence excitation spectrum (see Fig. 1).

Within the experimental spectral resolution, the shape of FA excitation spectra were minimally changed upon complexation with Eu^{3+}: there were only second-order

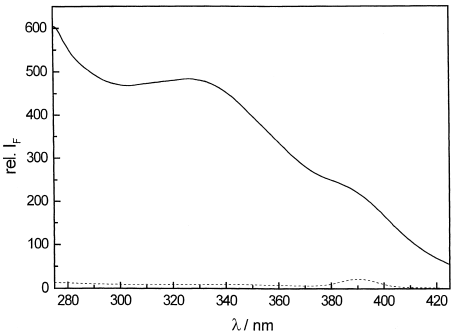

Fig. 1. Excitation spectrum of the FA at room temperature (emission wavelength is 450 nm). The excitation and the emission slit widths were 10 nm. The dotted line represents the background fluorescence spectrum of water.

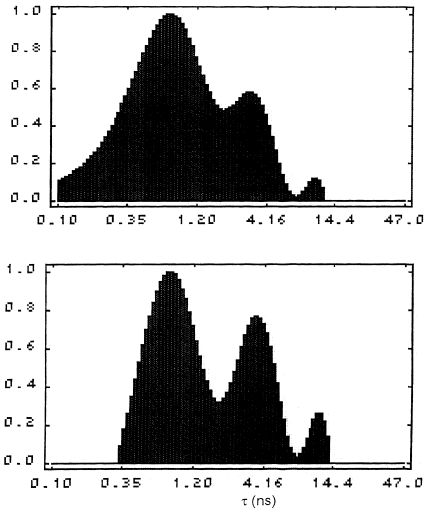

Fig. 2. The fluorescence lifetimes distribution of the FA recovered by ESM. Excitation wavelength: 314 nm (bandwidth 10 nm). Temperature 18°C. Above: λ_{em}=390 nm; 4×10^4 counts in the peak channel. The corresponding χ^2 value was 1.037. Below: λ_{em}=530 nm; 4×10^4 counts in the peak channel. The corresponding χ^2 value was 1.098. Fluorescence decay parameters values are listed in Table 1.

changes observed in the difference spectrum (figure not shown). These changes may involve increased intensities of certain modes but no changes in the eigenvalues of the FA states.

In most cases, the decay time distributions obtained with the ESM analysis had a three modes pattern with the corresponding peak decay times centred around the following values: 0.7–1; 3–3.6 and 8–10 ns with λ_{ex}=314 nm (Fig. 2) and three to four peak decay times centred around 0.7–0.9, 2.2–2.7, 5–6 ns and 15 ns with λ_{ex}=357 nm, respectively. At an excitation wavelength of 357 nm a fourth decay time component appeared that could not be neglected, as its relative amplitude was around 10% for emission wavelengths larger than 450 nm. At an excitation wavelength of 379 nm the decay parameters for the emission wavelengths λ_{em}=390 nm and λ_{em}=420 nm were comparable with those obtained with λ_{ex}=314 nm.

Table 1 summarises the fluorescence decay parameters found for the FA under different excitation wavelengths. The results for peak decay time values, the relative amplitudes and the mean decay times recovered by the ESM analysis are also shown. Within certain limits, these results witness the absence of a significant excitation wavelength dependence of the fluorescence decay time distribution. The ESM results are in satisfactory agreement with the results recovered by DCA (three-exponential fitting).

FA complexed with Eu^{3+}: In the time-resolved fluorescence experiments the concentration was 10^{-4} M. At this Eu^{3+} concentration all metal binding sites were saturated.

Similar with the case of FA, the ESM results concerning the fluorescence kinetics of FA complexed with Eu^{3+} did not reveal significant changes with the excitation wavelength. At each excitation wavelength a three-modes decay times distribution was calculated, the peak decay-times values being unchanged in comparison with the values obtained without Eu^{3+}. For illustration, in Table 2 the decay parameters obtained at λ_{ex}=314 nm are listed. The ESM results are also in satisfactory agreement with the results recovered by DCA (three-exponential fitting).

3.1.2. Dependence of the fluorescence decay of FA and FA complexed with Eu^{3+} on the emission wavelength

FA: All the measured fluorescence decays were highly non-exponential and showed a large variation as the emission wavelength λ_{em} was varied in the range between 390 and 550 nm. The mean decay times at λ_{ex}=314 and 357 nm increased up to 50% and 200%, respectively (see Table 1). At λ_{ex}=379 nm the fluorescence decay was measured at two emission wavelengths 390 and 420 nm. Therefore no trend of the mean decay time over the emission range could be inferred. Below, we resume the results obtained with λ_{ex}=314 nm, with the emphasis that these results could also be regarded representative for λ_{ex}=357 nm, and for λ_{ex}=379 nm: (a) all peak decay time values showed a slight shift in the same direction (towards larger values) with increasing emission wavelengths. However, due to experimental and method calculation errors this trend has to be judged very carefully. (b) there was a continuous redistribution of the relative amplitudes between the shortest and the longest decay time values, in a sense that the latter is favoured at longer emission wavelengths. The second decay constant represented the majority of the fluorescence decay components and it showed only a slight variation of its relative amplitude (about 45–55%) over the measured emission wavelength range. Therefore, variation of the FA fluorescence mean decay time across the emission spectrum could be related to changes in the relative amplitudes of the first and the third component of fluorescence decay. At λ_{ex}=357 nm and for emission wavelengths larger than 450 nm, the middle decay time components, centred around 2 and 6 ns, redistributed their relative amplitudes in the sense that the 6 ns decay time became favoured at longer emission wavelengths. (c) There was a significant contribution to the decay time distribution at short decay times (up to 35–40%) at the blue edge of the emission spectrum at λ_{ex}=314 nm and up to 30% at λ_{ex}=357 nm. This feature is typical of FA from different origins [8] and, as resulted from our data, this parameter did not vary with the concentration of the FA. (d) For the longest decay component obtained at λ_{ex}=314 nm there was a larger dispersion of its values between 6 and 10 ns, most probably due to the noise effects which imposed different final fitting range values in

Table 1
Dependence of the fluorescence decay parameters of FA on the emission wavelength recovered by ESM (excitation wavelengths λ_{ex}=314, 357 and 379 nm, temperature 18°C)

λ_{ex} (nm)	λ_{em} (nm)	Peak decay times, τ_i (ns) and relative A_i (%)				τ_{mean}[a] (ns)	χ^2
314	390	0.7±0.3	3.1±0.9	9±1.1		5.2	1.037
		36	51	13			
357	390	0.7±0.4	2.2±1	6.1±1.2		4.1	1.065
		31	46	21			
314	420	0.8±0.5	3.3±1.1	10±1.5		6.2	1.074
		27	56	17			
357	420	0.7±0.3	2.3±0.9	6±0.6	16±1.2	6.9	0.985
		21	46	28	5		
379	420	1±0.6	3.2±1.1	8.5±1.4		5	1.121
		39	47	14.5			
314	450	0.8±0.5	3±0.9	8±0.9		5.7	1.034
		25	49	26			
357	450	0.9±0.6	2.5±1.2	5.5±1	15±2.5	7.3	1.155
		23	35	34	8		
379	450	1±0.5	3.2±0.6	8±0.8		5.4	1.023
		27	48	22			
314	490	0.9±0.6	3.3±1.2	9±1.5		6.4	1.046
		22	51	27			
357	490	0.7±0.4	2.2±0.8	5.1±0.9	15	8.5	1.080
		13	34	39	10		
314	530	1±0.6	3.2±0.9	9±1.1		6.7	1.098
		18	52	30			
357	530	0.8±0.6	2.7±0.8	6.5±0.9	15±2.4	8.5	1.043
		13	40	35	12		
314	550	1±0.5	3.6±0.6	10±1.2		7.5	1.025
		16	51	33			
357	550	0.8±0.7	2.2±1.2	5.7±1.4	16±2.6	8.8	1.117
		14	32	43	10		

[a] τ_{mean} is calculated according to equation: $\tau_{mean} = \sum A_i\tau_i^2 / \sum A_i\tau_i$, which emphasises the long time component of the decay function.

each of the cases. (e) All values of relative amplitudes were positive over the whole emission range studied, i.e. no tendency to negative values for the third amplitude was observed, even for emission wavelengths longer than 500 nm. (f) The decay parameters were invariant with FA concentration in the range between 5 and 15 mg/l dissolved organic carbon (DOC).

FA complexed with Eu^{3+}: In contrast to the slight dependency of the decay parameters of FA complexed with Eu^{3+} on the excitation wavelength, the variation of the emission wavelength gave strong differences relative to the FA fluorescence mainly at the blue and the red edges of the emission spectra. To illustrate these changes, in Fig. 3 the decay curves of FA and FA complexed with Eu^{3+} are presented, measured at the spectral edges of the emission spectra at λ_{ex}=314 nm

As shown in Fig. 3, the effects of Eu^{3+} complexation on FA fluorescence kinetics can be resumed as follows: (1) at the blue edge (390 nm), the kinetics of FA in the presence of Eu^{3+} was slowed down in the first approx. 20 ns while for times longer than approx. 40 ns the kinetics was accelerated; (2) at the red edge of the emission spectra (530 nm), the opposite effect was observed and (3) the effect of Eu^{3+} on FA fluorescence kinetics was stronger with decreasing emission wavelengths (Tables 1 and 2, Fig. 3).

Upon the addition of Eu^{3+}, we found that the differences in FA fluorescence decay times between the extremes of the emission range investigated were strongly reduced; a surprising result if one takes into account the strong variation of FA fluorescence kinetics with emission wavelength. For comparison, in Fig. 4 the experimental decay curves of FA and FA complexed with Eu^{3+} are shown measured at λ_{em}=390 nm and 530 nm with λ_{ex}=314 nm.

As expected, the decay parameters for FA complexed with Eu^{3+} showed a only slight dependence on the emission

Table 2
Fluorescence decay parameters of FA complexed with Eu^{3+} at different emission wavelengths (excitation wavelength λ_{ex}=314 nm, temperature 18°C, ($(Eu^{3+})=10^{-4}$ M)

λ_{em}(nm)	Peak decay times, τ_i (ns) and relative A_i (%)			τ_{mean} (ns)	χ^2
390	0.7±0.5	3.2±0.7	11±0.8	6.9	1.037
	29	54	17		
420	0.7±0.6	3.1±0.9	11±1.1	7.2	1.074
	26	55	19		
450	0.75±0.5	3.2±0.8	10±1.1	7.7	1.034
	26	50	24		
530	0.8±0.5	3.2±1.1	11±1.4	7.7	1.098
	27	49	24		

τ_{mean} is calculated as shown in Table 1.

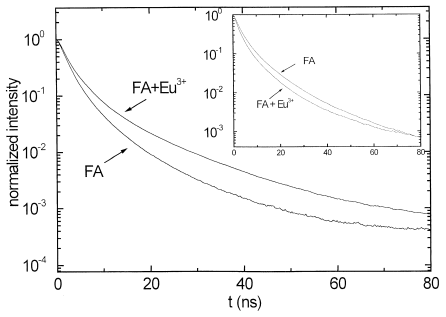

Fig. 3. The fluorescence kinetics of the FA and FA complexed with Eu^{3+} excited at 314 nm and measured at 390 nm. The insert shows the fluorescence kinetics of the FA and FA complexed with Eu^3 measured at 530 nm. ((Eu^{3+})=10^{-4} M). All curves represent the fits of the experimental fluorescence decays to a three-exponential function.

wavelength for the decay time distribution with the peak decay time values centred at 0.7, 3.1 and 11 ns, and the relative amplitudes of 27–29%, 49–54% and 17–24%, respectively (Table 2). Also, the mean decay times varied only slightly with emission wavelength: 10% in comparison with a 50% increase in the mean decay time of the FA over the same emission spectral range is measured at λ_{ex}=314 nm (Table 2).

3.2. Time-resolved emission spectra

TRES were reconstructed from 20–21 individual decays as a function of emission wavelength in the range between 390 and 580 nm (bandwidth 9 nm) with a 10 nm spectral step. Fluorescence was excited at 314, 357 and 379 nm and the decays were accumulated up to approx. 3×10^4 counts in the peak channel. Each decay curve was fitted with a three-exponential function by using an iterative reconvolution scheme to partially remove the effects of instrumental broadening.

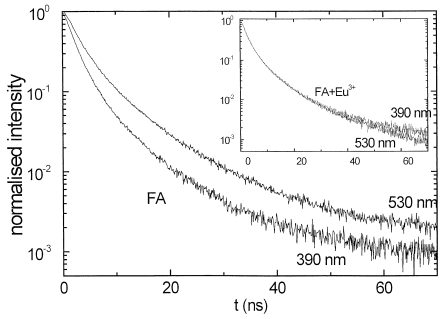

Fig. 4. The fluorescence kinetics of FA excited at 314 nm and measured at 390 and 530 nm emission wavelengths. Insert shows the fluorescence kinetics of FA complexed with Eu^{3+} measured at the same excitation and emission wavelengths. All curves represent the experimental fluorescence decays.

To describe quantitatively the evolution in time of the emission spectra, the experimental spectra were fitted at any time to a log-normal line shape [25]. Two parameters were used: (a) the *barycenter* in frequency, $B(t)$ was computed from the raw spectra and (b) emission maxima ν_{max} were determined from the log-normal line shape fitted spectra.

In contrast to the single-curve decay analysis, the construction of time-resolved emission spectra has the advantage that the full contour of the emission spectrum obtained from an analytical procedure may lead to a better visualisation of processes occurring in the excited state. This is especially important for the extraction of qualitative and to a less extent quantitative effects on FA fluorescence induced by Eu^{3+} complexation. The analysis of the TRES performed involved at least two steps of non-linear regression which were the fitting of the decay curves at each emission wavelength to a multi-exponential form (to a three-exponential function in our case) and a fitting of the emission spectra at each moment t to a log-normal gaussian line shape function. In more sophisticated approaches of dynamical relaxation, the transient of the spectral shift is also fitted to a multi-exponential form [26]. An error source imposed by our experimental set-up was the normalization of emission spectra [27] because the steady-state emission spectra and TRES were measured on different instruments.

In order to overcome these limitations, all TRES results were discussed only on a comparative basis: TRES were compared either at different excitation wavelengths for the FA, or at the same excitation wavelength for FA and FA complexed with Eu^{3+}.

The expression for the log-normal gaussian line shape used in TRES fitting is:

$$I_t(\nu) = \frac{I_0}{1+\beta\Delta\nu}\exp[-\alpha\ln^2(1+\beta\Delta\nu)] \quad (3)$$

with $\Delta\nu=\nu_{max}-\nu$ and $\nu=1/\lambda$ in units of cm^{-1}. There are four parameters in the fit: the amplitude at the peak I_0, the width and skewness parameters, α and β, and the frequency at the peak, ν_{max} (emission maxima). The log-normal distribution is a skewed gaussian distribution (it tends to a gaussian one as ($\beta\Delta\nu\rightarrow0$). Its area, a and full width at half height, w are given by:

$$a = I_0 = [\pi/(\alpha\beta^2)]^{1/2}$$
$$w = [\exp(\delta) - \exp(-\delta)]/[\beta\exp(2\alpha)^{-1}] \quad (4)$$
$$\delta^2 = (2\alpha)^{-2} + (\ln2)/\alpha$$

Due to spectral resolution, no variation in time of the full width at half height, w, could be measured at each of the

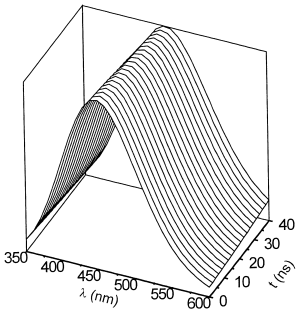

Fig. 5. Three-dimensional representation of a TRES experiment. The smooth curves shown in the graph are the fits of the FA experimental spectra (21 emission wavelengths) to a log-normal line shape function. λ_{ex}=314 nm and Δt=2 ns.

three excitation wavelengths. As a consequence, we limited our investigations to one parameter, e.g. the emission maxima, ν_{max} provided by means of a non-linear least squares routine.

Time dependence of the barycenter and of the emission maximum of the emission spectra: The variation of the fluorescence composition with the emission decay rate gave rise to time-evolving spectra shown in Fig. 5.

The curves in Fig. 5 are log-normal fits to the 21-point experimental data at times between 0 and 40 ns, at λ_{ex}=314 nm, using a temporal step of 2 ns. As can be seen, the fluorescence spectra shifted in time without any noticeable narrowing or changes in shape. A detailed analysis of the spectra, applying a deconvolution with three gaussians, revealed slight variations of line shape and width, nicely illustrated in Fig. 6. No similar behaviour was observed with FA complexed with Eu^{3+}, the emission spectra remaining constant in line shape, width and, within spectral resolution, in the position of the maximum intensity (results not shown in the graph).

Thus, the instantaneous emission spectrum was attributed as the envelope of three gaussians with different centres of gravity (υ_{0i}) and widths (σ_i):

$$I(\upsilon,t)=\sum_{i=1}^{3} I_{0i}\exp(-t/\tau_{0i})\times\frac{1}{\sqrt{2\pi\sigma_i}}\times\exp\left(-\frac{[\upsilon_i-\nu_{0i}]^2}{2\sigma_i^2}\right) \quad (5)$$

We must stress that the analysis based on multi-gaussian deconvolution needs to be proven with both a higher spectral and temporal resolution and it is the subject of current work.

FA: The evolution in time of the barycenters of the emission spectra at each excitation wavelength is shown in Fig. 7.

Several features of these curves deserve comments: (a) the emission spectra moved in the same sense, e.g., towards

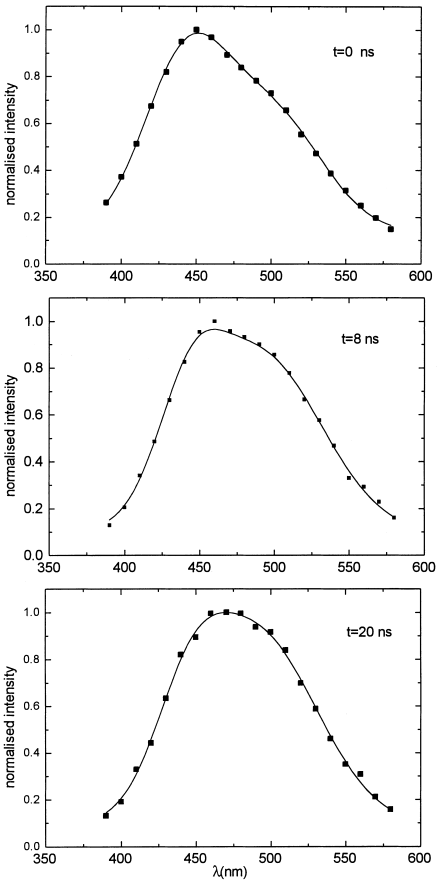

Fig. 6. Time-resolved emisson spectra measured at times of 0, 8 and 20 ns. The smooth curves shown in the graph are the fits of the FA experimental spectra to a three-gaussian line shape function. λ_{ex}=357 nm.

longer emission wavelengths; (b) the barycenter shifts were quite similar, and they were about 15–20 nm (approx. 600–1000 cm^{-1}). Accuracy in determining the emission maxima shifts could be regarded as satisfactory, as these shifts were larger than the spectral resolution (limited to 9 nm); (c) the time dependencies of the barycenters were rather similar for all excitation wavelengths used. There were still some differences: at λ_{ex}=314 nm, most part of the barycenter shift (more than 60%) was accomplished in the first 3–5 ns, while for the other two excitation wavelengths the same range shifted towards longer times (about 10 ns); (d) The plots of emission maxima and barycenter transients look

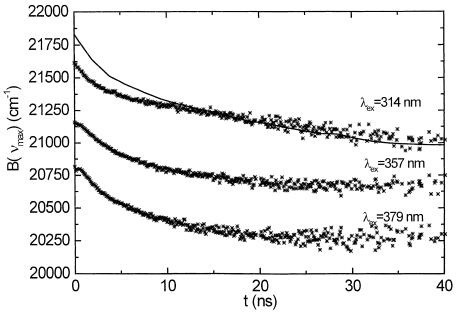

Fig. 7. Evolution with time of the FA emission spectra barycenters at 314, 357 and 379 nm (star curves). For comparison, the evolution with time of the maxima of emission spectra at 314 nm excitation wavelength (see text) is also represented (line curve).

qualitatively similar, suggesting that within our experimental resolution, the spectra did not change noticeably in time in their width and shape, independent of the excitation wavelength. For comparison, in Fig. 7 also the emission maxima transient obtained at λ_{ex}=314 nm is plotted.

FA complexed with Eu^{3+}: With the addition of Eu^{3+} the temporal behaviour of the maximum and of the barycenter of emission spectra changed significantly. Within our experimental resolution these changes are consistent with the single decay curve analysis, e.g., showing an almost constant value with time for these two parameters. However, judged on a comparative basis, the trends are clearly different for the TRES of FA and FA complexed with Eu^{3+}.

In Fig. 8 the evolution in time of the barycenters of emission spectra of FA and Eu^{3+}-bound FA in the first 40 ns after excitation are shown. For comparison purposes only, the B and ν_{max} measured for FA and Eu^{3+}-bound FA at time 0 were normalized.

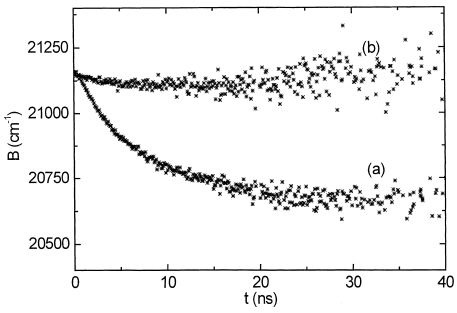

Fig. 8. Evolution with time of the barycenter of emission spectra at 357 nm excitation wavelength: (a) FA complexed with Eu^{3+} and (b) FA.

4. Discussion

FA: The kinetics behaviour of FA fluorescence showed a strong deviation from mono-exponentiality. Analysis of the multi-exponential decays was performed without restrictions on their number (up to 100 exponential terms were included in ESM analysis) and position. In the great majority of cases, we obtained a three-modal distribution with peak decay time values centred approximately at 0.7, 3 and 10 ns.

The FA fluorescence kinetics was strongly dependent on the emission wavelength, being different at the short and long wavelength sides of emission spectra. These differences were expressed mainly in changes of the relative amplitudes of the decay components while the values of peak decay time may be regarded as constant within experimental and method calculation errors (Table 1). In contrast with emission wavelength dependency, fluorescence kinetics changed only slightly with excitation wavelength (Table 1).

The study of the emission wavelength dependency of the decay curves indicated that a great part of fluorescence decay complexity was due to the inhomogeneous emission decay kinetics determined by ground state heterogeneity effects. Ground state heterogeneity can be expected due to complex mixture of different fluorophores which compose the FA structure on which are superimposed different distributions of environments experienced by each of the fluorophore species. The results indicate that the emission spectrum of FA may be regarded as the superposition of (at least) three broad spectral envelopes, with slightly different emission maxima and widths. It is tempting to attribute the shortest decay time component (approx. 0.7 ns) to the blue edge of the spectral range, where its amplitude was most pronounced. This feature may be regarded as typical for FA of different origins [8].

However, if ground state heterogeneity would be the only factor responsible for the trends in the TRES, one may expect that the amplitude of the short decay time component has a maximum value either at the blue or the red region, depending on the details of the FA structure. Also, fluorescence kinetics would depend more strongly on the excitation wavelength as this dependency is an indication of inhomogenous decay kinetics due to the static effects in the distribution of the excited state species within the initial ensemble of fluorophores. The expected effect would manifest in the enhancement of one of the relative amplitudes of the decay components to the detriment of the other. As shown in Table 1, this is not actually the case, as the value of the relative ratio $A_1/A_2/A_3$ is almost invariant with the excitation wavelength at least in the blue region of the emission range (390–460 nm). As a consequence of the above considerations, one could expect that other processes contribute to the temporal inhomogeneity of FA fluorescence decay as well. These processes may manifest during the excited states decay time of the FA, such as intramolecular and intermolecular rearrangements of the fluorophores

together with a reorganization of fluorophore-solvent hydrogen bonds.

The TRES are very sensitive to both changes of τ_i and A_i in the course of the relaxation processes [27]. Together with single decay analysis a deeper insight into FA fluorescence decay kinetics was achieved. The time shift of the TRES may be observed even in the case when negative amplitudes are absent (no excited state reactions) or in the absence of the dynamic relaxation process. As discussed in Section 3.1.2, no tendency towards negative values of the relative amplitudes (related to the longest peak decay time) was detected when measuring the kinetics at the red spectral edge. Also, the relaxation process takes place on a time scale much faster than our experimental resolution as the time of the reorientation of the water dipoles is the order of picoseconds, much too fast to be detected with the instrumental set-up used [26].

The TRES data sustain two important conclusions: (a) the fluorescence kinetics of FA depended rather weakly on the excitation wavelength and (b) there were the same fluorophores which contributed to the evolution in time of the emission spectra, whatever excitation wavelength was used. The last conclusion is based on the similar trends with time presented by the barycenters of the emission spectra of FA, at each of the excitation wavelengths (Fig. 7).

Fluorescence spectra shifted in time with slight narrowing and changes in shape (Fig. 6). These aspects of the dynamics may be not intuitive, especially when the ratio of the shortest and longest decay time components has a good contrast value, which is approx. 15 (see Table 1). Thus, one might expect instead that the heterogeneity effects would lead to a narrowing of the spectrum due to the preferential depletion of the short decay time component (situated more or less by coincidence, at the blue spectral edge). That this did not happen in the present case may be due to the fact that we have a superposition (at least) of three broad emission spectra, with closely spaced maxima and similar widths.

Eu^{3+} complexation effects upon FA fluorescence kinetics: In the presence of the Eu^{3+}, the dependency of the relative amplitudes of the fluorescence decay of the fulvic acid on the emission wavelength was greatly reduced (in comparison with the uncomplexed FA). (Tables 1 and 2 and also the insert in Fig. 4). As expected, for the FA in the presence of Eu^{3+} the mean decay time varied within only 10%, from 7 ns at λ_{em}=390 nm to 7.7 ns at λ_{em}=550 nm, whereas in the case of FA the mean decay time varied with almost 50% from 5.2 to 7.5 ns over the same spectral range (Tables 1 and 2).

These results are contrary with what was expected from a dynamic quenching effect, e.g. reduction of the peak decay time values of FA fluorescence in the presence of Eu^{3+}. The invariance of the decay time values of the FA fluorescence with Eu^{3+} addition indicates that the effects of Eu^{3+} complexation upon FA fluorescence were not related to energy or/and electron transfer between FA singlet states and the Eu^{3+} ion. Quenching of FA fluorescence induced by Eu^{3+} appeared only static in origin and may have as much to do with its paramagnetic properties as with its spectral properties. Quenching involving the so-called external heavy atom effect reflects efficient singlet–triplet intersystem crossing in FA brought up by an increase in spin-orbit coupling [28]. In our preliminary steady-state experiments the extent of static quenching, $\eta = 1 - I/I_0$ with I and I_0 being the fluorescence intensities of Eu^{3+}-bound FA and FA, respectively, was around 20% at λ_{ex}=314 nm.

TRES data confirmed the Eu^{3+} effect upon the relative amplitudes redistribution of FA decay time components. As illustrated in Fig. 8, the barycenter varied almost insignificantly in time, in comparison with the same evolution of FA. This small variation in time of the barycenter may be easily explained if one takes into account the constancy of the peak decay time values and the small variation with the emission wavelength of the corresponding relative amplitudes (Table 2).

In conclusion, single fluorescence decay curve analysis combined with the analysis of the time-resolved emission spectra has been proven to be a powerful method for the investigation of the complex temporal behaviour of FA fluorescence. Results indicated the presence of at least three species of FA fluorophores, each species experiencing its own distribution of chemical environments. The addition of Eu^{3+} induced besides static quenching of the FA fluorescence an invariance of the relative amplitudes of the decay components with the emission wavelength. The peak decay time values of the FA fluorescence in the presence of Eu^{3+} were almost unchanged at all emission and excitation wavelengths investigated. Thus, at this stage it seems to be reasonable to conclude that within the temporal resolution of the experimental set-up used the singlet levels of FA played no role as donor state in intramolecular energy transfer from FA ligands to the upper excited levels of Eu^{3+}. Future experiments which will include other quencher ions like Gd^{3+} Tb^{3+} and Sm^{3+} as well as a better correlation between the steady-state and time-resolved emission experiments will attempt to elucidate the specific role of spectroscopic properties of different lanthanide ions in quenching FA fluorescence.

Even though the results have been obtained on the FA fraction of only one NOM sample the spectroscopic approach proved that time-resolved fluorescence experiments can yield valuable information on the molecular dynamics of metal ion complexation by NOM. In future experiments with NOM of different origins and their FA fractions this approach will be further examined.

Acknowledgements

The authors are grateful to the German Research Foundation (Deutsche Forschungsgemeinschaft, DFG) for their financial support. They appreciate the funding by the German Federal Ministry for Education, Science, Research and Technology (Bundesminesterium fhr Bildung und Forschung, BMBF) as well.

References

[1] J. Buffle, Complexation Reactions in Aquatic Systems, An Analytical Approach, Ellis Horwood and Wiley, New York, 1988.

[2] R.R. Engebretson, R. Vonwandruska, The effect of molecular size on humic acid associations, Geochem. 26 (1997) 759–767.

[3] J.A. Leenheer, D.M. McKnight, E.M. Thurman, P. McCarthy, Humic substances in the Suwannee river, in: R.C. Averett, D.M. Leenheer, D.M. McKnight, K.A. Throne (Eds.), Georgia: Interaction, Properties and Proposed Structures, Open File Report 87-557, U.S. Geol. Surv., Denver, CO, 1989, p. 331.

[4] Byoung Ho Lee, Kun Ho Chung, Hyun Sang Shin, Yeong Jae Park, Hichung Moon, Europium(III) complexes of polyfunctional carboxylic acids: Luminescence probes of possible binding sites in fulvic acid, J. Colloid and Interface Sci. 188 (1997) 439–443.

[5] J. Buffle, Natural organic matter and metal–organic interactions in aquatic systems, in: H. Siegel (Ed.), Metal Ions in Biological Systems, vol. 18, Marcel Dekker, New York, 1984, pp. 165–221.

[6] M.U. Kumke, H.-G. Löhmannröben, Th. Roch, Fluorescence quenching of polynuclear aromatic compounds by humic acid, Analyst 119 (1994) 997–1001.

[7] Sherry L. Hemmingsen, Linda B. McGown, Phase-resolved fluorescence spectral and lifetime characterization of commercial humic substances, Appl. Spec. 51 (1997) 921–929.

[8] M.U. Kumke, C. Tiseanu, G. Abbt-Braun, F.H. Frimmel, 1998, Fluorescence decay of natural organic matter (NOM)-influence of fractionation, oxidation and metal ion complexation, J. Fluorescence, submitted for publication.

[9] B.J. Colston, J.T. Vanelteren, Z.I. Kolar, J.J.M. Degoeji, Kinetics in a Eu(III)-humic acid system by isotopic exchange with Eu(152)$^{3+}$ and size exclusion chromatography. A feasibility study, Radiochimica Acta 78 (1997) 111–115.

[10] F. Rey, E. Calle, J. Casado, Study of the effects of concentration and pH on the dissociation kinetics of Fe(II)-fulvic acid complexes, Int. J. Chem. Kinetics 30 (1998) 63–67.

[11] J.R. Lead, J. Hamilton-Taylor, M. Kelly, Artifacts in the determination of the binding of americium and europium to aquatic fulvic acid, Sci. Total Environ. 177 (1996) 221–224.

[12] J.I. Kim, R. Klenze, H. Wimmer, W. Runde, W. Hauser, A study of the carbonate complexation of Cm^{3+} and Eu^{3+} by time resolved later fluorescence spectroscopy, J. Alloys and Compounds 213/214, 333–340.

[13] E.K. Legin, Yu.I. Trifonov, M.L. Khokhlov, D.N. Suglobov, Solubilisation of europium fulvate in aqueous solutions containing complexing agents, Radiochemistry 37 (1996) 253–257.

[14] W.Susetyo Thomason, L.A. Carreira, Fluorescence studies of metal–humic complexes with the use of lanthanide ion probe spectroscopy, Appl. Spectr. 50 (1996) 401–408.

[15] M. Nordén, J.H. Ephraim, B. Allard, Europium complexation by an aquatic fulvic acid – effects of competing ions, Talanta 44 (1997) 781–786.

[16] G. Bidoglio, I. Grenthe, P. Qi, P. Robouch, N. Omenetto, Complexation of Eu and Tb ions with Fulvic Acids as Studied by time-resolved laser-induced fluorescence, Talanta 3 (1991) 999–1004.

[17] W.R. Kirk, W.S. Wessels, F.G. Prenergast, Lanthanides-dependent petubations of luminescence in indolylethylenediaminetrtraacetic acid-lanthanide chelate, J. Phys. Chem. 97 (1993) 10326–10340.

[18] S. Speiser, Photophysics and mechanisms of intramolecular electronic energy transfer in bichromophoric molecular systems: Solution and supersonic jet studies, Chem. Rev. 96 (1986) 1953–1976.

[19] T. Foerster, in: O. Sinanoglu (Ed), Modern Quantum Chemistry, Academic, New York, 1964.

[20] W.T. Carnall, The absorption and fluorescence spectra of rare earth ions in solution, in: K.A. Gschneider Jr., L. Eyring (Eds.) Handbook on the Physics and Chemistry of Rare Earths, North-Holland Publishing Company, 1979.

[21] See, for example, I.M. Alaoui, and the references cited herein – Nonparticipation of the ligand's first triplet state in intramolecular energy transfer in Eu^{3+} and Tb^{3+} Ruhemann's Purple complexes. J. Phys. Chem. 99 (1995) 13280–13282.

[22] J.I. Kim, G. Buckau, G.H. Li, H. Duschner, N. Psarros, Characterization of humic and fulvic acids from Gorleben groundwater. Fresenius J. Anal. Chem. 338 (1990) 245–252.

[23] W.R. Ware, Recovery of fluorescence lifetime distributions in heterogenous systems, in: V. Ramamamurthy (Ed.), Photochemistry in Organized and Constrained Media, VCH Publishers, New York, Chem. Phys. Lett. 126 (1991) 7–11.

[24] A. Semiarczuk, B.D. Wagner, W.R. Ware, Comparison of the maximum entropy method and exponential series method for the recovery of distributions of the lifetimes from fluorescence lifetime data, J. Phys. Chem. 94 (1990) 1661–1667.

[25] A. Ord Stuart, K.J. Kendall's, 1987. In Advanced Theory of Statistics, 5th ed., Oxford University Press, New York, vol. 1.

[26] M. Vincent, J. Gallay, A.P. Demchenko, Relaxation around the excited state of indole: Analysis of fluorescence lifetimes distributions and time-dependence spectral shifts, J. Phys. Chem. 99 (1995) 14931–14941.

[27] J.R. Lakowicz, Principles of Fluorescence Spectroscopy, Plenum Press, New York, 1983.

[28] A. Abragam, B. Bleaney, Electron paramagnetic resonance of transition ions, Oxford University, Oxford, 1970.

2.3.3 Influence of photochemical reactions on the complexation of humic acid with europium(III)

J.-M. Monsalier, F. Scherbaum, G. Buckau, J.I. Kim, M.U. Kumke, C.H. Specht, F.H. Frimmel
J. Photochem. Photobiol. A, 2001, **138**, 55 - 63.

Bei der Untersuchung der Komplexierung von Actiniden durch HS hat sich besonders die zeitaufgelöste Laserfluoreszenzspektroskopie (*time-resolved laser fluorescence spectroscopy*, TRLFS) als empfindliche Methode etabliert, da sie große Vorteile beim Umgang mit radioaktiven Materialien mit sich bringt - besonders hervorzuheben sind die hohe Empfindlichkeit, die große Selektivität und der nicht-invasive Charakter der Methode. In der Vergangenheit wurde aber der Einfluss auf HS von durch den Anregungslaser induzierten Photoreaktionen auf das Ergebnis der Speziationsuntersuchungen wenig untersucht. In dieser Studie wurde der photoinduzierte Abbau von HS und dessen Konsequenzen für die Bestimmung von Komplexbildungskonstanten mit TRLFS bestimmt. Dabei wurden zur Charakterisierung der Effekte eine Reihe verschiedener spektroskopischer und chromatographischer Methoden eingesetzt. Durch die Bestrahlung wurde bei großen eingetragenen Energien ein Abbau der HS induziert, der sich u.a. in einer Abnahme der mittleren molekularen Größe äußerte. Dadurch veränderte sich auch die Komplexbildungskonstante und nahm mit zunehmendem Abbau der HS ebenfalls ab. Der photoinduzierte Abbau der HS wurde durch die Gegenwart von Eu^{3+} verlangsamt. Die Ergebnisse machen deutlich, dass bei der Verwendung von TRLFS zur Bestimmung von Komplexbildungskonstanten die experimentellen Bedingungen, wie z.B. die eingetragene Laserenergie, unbedingt berücksichtigt werden müssen. Außerdem wurde für Europium festgestellt, dass nach Lichtabsorption bedingt durch HS eine Reduktion stattfindet und somit ein Wechsel der Oxidationsstufe von +III nach +II induziert wird, wodurch wiederum veränderte Komplexbildungskonstanten zu erwarten sind.

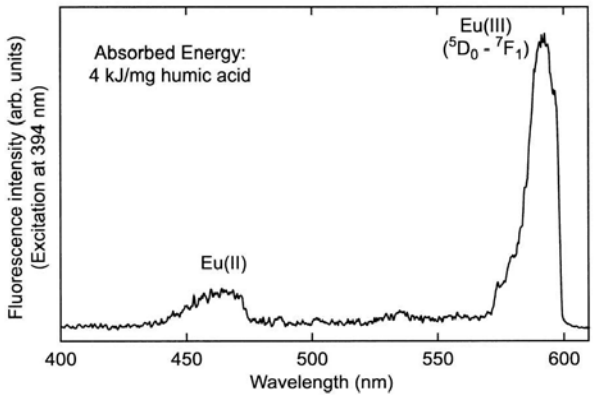

ELSEVIER

Journal of Photochemistry and Photobiology A: Chemistry 138 (2001) 55–63

Journal of Photochemistry and Photobiology A:Chemistry

www.elsevier.nl/locate/jphotochem

Influence of photochemical reactions on the complexation of humic acid with europium(III)

Jean-Marc Monsallier [a,*], Franz J. Scherbaum [a], Gunnar Buckau [a], Jae-Il Kim [a], Michael U. Kumke [b], Christian H. Specht [b], Fritz H. Frimmel [b]

[a] *Forschungszentrum Karlsruhe, Institut für Nukleare Entsorgung, PO Box 3640, 76021 Karlsruhe, Germany*

[b] *Division of Water Chemistry, Engler-Bunte-Institut, University of Karlsruhe, Engler-Bunte-Ring 1, 76131 Karlsruhe, Germany*

Received 5 July 2000; received in revised form 20 September 2000; accepted 21 September 2000

Abstract

Photochemical reactions in the Eu(III)–humic acid system are investigated by fluorescence spectroscopy. For comparison, humic acid without europium is also studied. Irradiation is performed by high energy laser beam and a low pressure mercury lamp. The impact of photodegradation on spectroscopic properties, size and decomposition of humic acid is monitored by steady state and time-resolved fluorescence spectroscopy, UV–Vis spectroscopy, gel permeation chromatography (GPC), dissolved organic carbon (DOC) analysis and ultrafiltration. The different indicators for photodegradation show different sensitivity. The decrease in DOC content with increasing irradiation dose is lower than the decrease in UV/Vis absorption. The highest impact is found for the fluorescence intensity. At 3 kJ/mg humic acid absorbed energy and in absence of europium, fluorescence diminishes by more than 90%. In the presence of Eu(III), however, fluorescent groups are partly stabilized in this range of absorbed energy. Results from GPC show changes in the chemical structure, especially generation of smaller entities. The photodegradation of the humic acid leads to a decrease of the europium–humate complexation constant. Furthermore, europium is reduced to the divalent state. The present study shows that for metal ion humic acid complexation studies by laser fluorescence spectroscopy, great care is needed to avoid significant experimental artifacts, such as photodegradation and metal ion redox reactions. © 2001 Published by Elsevier Science B.V.

Keywords: Humic acid; Europium; Complexation; Photodegradation; Laser spectroscopy

1. Introduction

All natural waters contain dissolved organic substances in concentrations ranging from approximately 0.1 up to more than 100 mg dissolved organic carbon (DOC) per liter [1,2] depending on the geochemical surrounding. Between 50 and 90% of DOC consist of humic substances [2] which are macromolecules with a complex and heterogeneous structure [3,4]. These acids have a high density of proton exchanging groups varying between 1.5 and 11.2 meq/g [5]. The high functional group content gives them their strong affinity for metal cations, leading to complexation with metal cations, especially of higher charge [6].

Numerous investigations have been performed on the complexation behavior of humic acid with actinide ions. Different methods have been used such as gel permeation chromatography (GPC) [7], solvent extraction [8,9], UV spectroscopy [10–16], ion exchange [17–19], laser induced photoacoustic spectroscopy (LPAS) [11], time-resolved laser fluorescence spectroscopy (TRLFS) [12,20–22], ultrafiltration [11,23,24] and dialysis [19,25]. Depending on the method, the results vary considerably. TRLFS has the advantage of direct speciation and allows measurements at the very low metal ion concentrations required for the low solubility of multivalent metal cations. Thereby, spectral information is obtained from excitation, emission and the lifetime of emission. When TRLFS is used to evaluate the metal ion complexation, it is generally assumed that no photodegradation accompanies the excitation of these multi-functional macromolecules. Such photodegradation, however, has been reported for excitation of the Eu– and Tb–humate at 308 and 394 nm using an excimer laser [21]. The objective of the present work is to evaluate photochemical reactions induced by UV and laser irradiation and their influence on complexation studies of the Eu(III)–humic acid system by fluorescence spectroscopy.

In this work, humic acid solution is irradiated with different light sources. For comparison between different sources

* Corresponding author. Tel.: +49-7247-82-2231; fax: +49-7247-82-4308.
E-mail address: monsallier@ine.fzk.de (J.-M. Monsallier).

1010-6030/01/$ – see front matter © 2001 Published by Elsevier Science B.V.
PII: S1010-6030(00)00380-4

and wavelengths, the irradiation is expressed in energy absorbed per unit weight humic acid (kJ/mgHA). The resulting photodegradation is measured at different absorbed energy by steady state and time-resolved fluorescence spectroscopy, UV–Vis absorption spectroscopy, DOC concentration and GPC. Furthermore, the influence of photodegradation of humic acid on the Eu(III)–humate complexation is determined by measuring the emission spectra of Eu with photodegraded humic acid. The complexation constant of Eu(III) with non-photodegraded and photodegraded humic acid is determined by means of ultrafiltration.

2. Experimental

2.1. Reagents

The humic acid investigated is Gohy-573(HA), which originates from a groundwater at 139 m depth of the Gorleben aquifer system located in Northern Germany. The purification and characterization of Gohy-573(HA) can be found elsewhere [26]. Its proton exchange capacity (PEC) determined by pH titration under Ar atmosphere is 5.38 ± 0.20 meq/g [26]. Stock solutions are prepared by dissolving a known amount of humic acid in 0.1 M NaOH rapidly followed by dilution with 0.1 M $NaClO_4$. The pH is adjusted to 6.0 by addition of $HClO_4$. With few exceptions, 10^{-3} M MES buffer (2-mospholine–ethane sulfonic acid) is used for stabilization of pH. The molar humic acid concentration is obtained by multiplying a given weight concentration (g/l) by the PEC (meq/l) divided by the charge of the metal ion under investigation (z). Thus, for europium(III), the humic acid concentration is expressed as [HA(III)] [27].

2.2. Hg/UV irradiation

In the Hg/UV irradiation experiment, a 14 W low pressure mercury lamp (Katadyn GmbH, Germany) is used at an irradiation wavelength of $\lambda = 254$ nm. The photon flux is determined to 9.91 μEinstein/s by actinometry (with $K_3Fe(C_2O_4)_3$) at a radiation power of 4.7 ± 0.5 W.

2.3. Laser induced fluorescence spectroscopy

The laser system used for irradiation of humic acid solution and for laser fluorescence spectroscopy of complexed and non-complexed europium is an excimer pumped dye laser system (Lambda Physics, Compex 205 and Scanmate II). Dye-laser pulse at 394 nm (dye: Qui), 1 mJ pulse energy and a pulse duration of 25 ns at FWHM is used for irradiation of the sample solution. The sample cell is a rectangular silica cell (HELLMA). The fluorescence emission light is monitored perpendicular to the laser pulse, spectrally resolved by a polychromator (Acton Research, Spectra Pro 275; entrance slit width: 0.5 mm; grating: 300 lines/mm) and detected by an intensified time gated diode array detector (Princeton Instruments, OSMA IRY 700 GR, 1024 linear arranged Si photo diodes). The experimental equipment operates in a spectral window of 210 nm width with a wavelength resolution of about 1.1 nm. Using a beam splitter, a small fraction of the laser pulse is reflected onto a pyroelectric detector connected to a powermeter (Newport 1835C) to monitor the pulse energy. Reading out and digitizing the data from the diode array detector is controlled by an SI180 camera controller (Spectroscopy Instruments). The system components are synchronized by a digital delay/pulse generator (Stanford Research Systems: DG535) as a master trigger unit. With the software POSMA (Spectroscopy Instruments), a PC is used to control the system and analyze the data. Final emission spectra obtained are the results of 10–25 averaged single spectra. The resulting emission spectra are normalized to the average pulse energy.

2.4. Flashlamp induced fluorescence lifetime determination

Time-resolved humic acid fluorescence measurement is performed using an FL900CDT fluorescence lifetime spectrometer (Edinburgh Analytical Instruments, UK) in the time-correlated single photon counting mode. The instrumental set up is described in detail elsewhere [28]. An F900 nitrogen-filled (1 bar, 6.6 kV, 0.3 mm electrode separation) nanosecond flash lamp (Edinburgh Analytical Instruments) operated at 40 kHz is used as excitation light source. The excitation wavelength in the time-resolved fluorescence experiments is $\lambda_{ex} = 314$ nm. The experiment is typically run at a time base of 100 ns with a 5 ns delay of the photomultiplier tube. The time calibration is 0.095 ns per channel. The emitted light is monitored at $\lambda_{em} = 400$ and 500 nm using a spectral bandwidth of 9 nm. To prevent counting artifacts caused by excessively high photon loads, the counting rate is typically <1%. The fluorescence decay is evaluated with a commercial software package of Edinburgh Analytical Instrument based on the Marquardt algorithm which is described elsewhere [29]. The same spectrometer is used for the steady state fluorescence experiments. The instrument is set up in a T-format with two detection channels and operated in the single photon counting mode. A 450 W Xenon arc lamp is used for the excitation of samples. The slit width is 1 μm in the excitation and emission path with a spectral resolution of 1.8 nm. The emission spectra are recorded for excitation wavelength range from 275 to 401 nm ($\Delta\lambda = 3$ nm) in the emission range from 281 to 545 nm ($\Delta\lambda = 1$ nm).

2.5. Ultrafiltration

Ultrafiltration is used to investigate the Eu complexation with photodegraded and non-photodegraded humic acid. This method allows the separation of the non-complexed

Eu ion from its humate complex by size fractionation [30]. The filtration system uses a membrane of nominal cut-off 1000 Da (Filtron, Microsep™ Microconcentrators). Europium concentrations in filtrates are quantified by ICP-MS. A correction is used for the partial retention of the non-complexed Eu ion, and possibly sorption on the membrane (at pH 6.0, 0.1 M $NaClO_4$, 75% of the non-complexed Eu^{3+} ion is found in the filtrate). The Eu species distribution is calculated by the total Eu concentration and the concentration in filtrate, applying the correction factor. Published results [30] show the validity of the method for non-photodegraded humic acid. Alteration of humic acid by photodegradation, including changes in size distribution, could introduce experimental artifacts. As shown in this work, however, this method can be applied also for photodegraded humic acid.

2.6. Gel permeation chromatography

The GPC is performed with on-line detection of fluorescence (λ_{ex} = 300 nm, λ_{em} = 400 nm), UV absorption at λ_{abs} = 254 nm and DOC detection [31]. The column, packed with TSK HW 50 S (Toyopearl), has a length of 25 cm and an inner diameter of 2 cm. The exclusion volume is 19 ml, (determined with dextran blue) and the total volume is 46 ml. Phosphate buffer with $c(K_2HPO_4{\cdot}2H_2O)$=1.25 g/l and $c(NaH_2PO_4{\cdot}2H_2O)$=2.5 g/l, pH = 6.8, is used as eluent at a flow rate of 1 ml/min. Samples are diluted with phosphate buffer ($c(K_2HPO_4{\cdot}2H_2O)$=2.5 g/l and $c(NaH_2PO_4{\cdot}2H_2O)$=5 g/l) the ratio of 1:1 to adjust the phosphate concentration of the sample and eluent. The system is integrated in an assembly for column experiments with additional detectors for electrical conductivity (LDM/S, WTW) and pH-value (Ingold).

The detection limit of the DOC detector (determined with potassium hydrogen phthalate according to DIN 32645 (calibration curve method)) is 0.2 mg C/l. The eluent passes an UV reactor before use in order to decrease the background concentration of DOC. The irradiation time is approximately 8.5 h. The samples are injected by an autosampler (Gilson Abimed, Model 231 BIO with Dilutor 401), whose injection volume can be set within the range from 0 to 2000 μl. In this work, 2 ml of sample is injected. To remove bicarbonate from the sample stream after passing through the column and before the DOC measurement, a continuous stream of diluted H_3PO_4 together with $K_2S_2O_8$ is added to lower the pH value to 1.5. Subsequently CO_2 is stripped with N_2. The sample is then pumped through a capillary UV reactor, where the organic substances react with $K_2S_2O_8$ and UV light to form CO_2. The retention time within the reactor is about 14 s. The CO_2 is stripped by a N_2 stream. The gas stream is passed through a cooling module to remove water vapor in order to improve the signal-to-noise ratio in the IR absorption detector (Ultramat 3, Siemens). The data collected from all detectors are recorded on a PC.

3. Results and discussion

Humic acid has a broad UV/Vis absorption, increasing strongly towards shorter wavelength without distinct features. It has broad excitation and emission bands and a complex fluorescence decay time dependency. Part of the complexity in fluorescence properties has been attributed to excited state processes (e.g., intramolecular energy transfer) [28,32]. Due to irradiation, a number of different photochemical processes can be induced, including breaking of bonds, change in functional groups and structures that may also change intramolecular interactions. Through examination of UV/Vis absorption and fluorescence, including comparison of fluorescence decay between irradiated and non-irradiated humic acid, information is obtained on structural changes induced by photodegradation. Additional information is obtained by GPC with different detection methods.

3.1. Humic acid solution without europium

Humic acid solution is irradiated at wavelengths of 254, 308 and 394 nm. Continuous irradiation at 254 nm is done by a mercury lamp light source. Discontinuous irradiation at 308 and 394 nm is made by the pulsed laser system; 308 nm is chosen because at this wavelength the highest dose rate is achieved and 394 nm is chosen because of its relevance for Eu–humate interaction studies. For comparison, an absorbed energy of 3.0 kJ/mg HA reflects the typical situation for measurement of the Eu fluorescence lifetime for speciation purposes under these conditions.

3.1.1. Influence on UV/Vis absorption

In Fig. 1, UV/Vis absorption spectra are shown for humic acid after irradiation at 308 nm with absorbed energy up

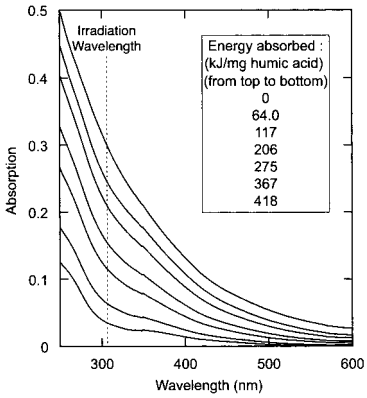

Fig. 1. UV/Vis absorption spectra of humic acid for different absorbed energy from pulsed laser irradiation at 308 nm.

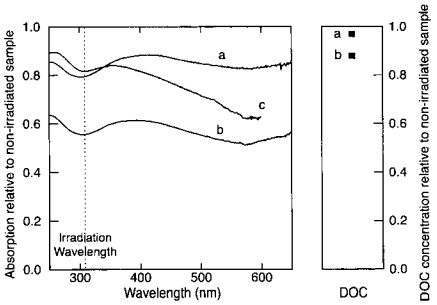

Fig. 2. UV/Vis absorption and DOC concentration relative to non-irradiated samples of humic acid for different absorbed energy from pulsed laser irradiation at 308 nm. Samples a and b are without MES buffer and 28.1 and 66.8 kJ/mg humic acid absorbed irradiation energy, respectively. Sample c is with 10^{-3} mol/l MES buffer and 64.0 kJ/mg humic acid absorbed irradiation energy.

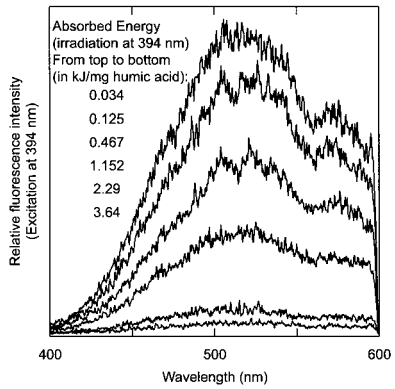

Fig. 3. Influence of irradiation by laser at 394 nm on the fluorescence of humic acid. Fluorescence spectra from excitation at 394 nm are shown for different absorbed irradiation energy.

to 418 kJ/mg humic acid. The UV/Vis absorption decreases over the entire wavelength range and for the highest dose the absorption decreases with almost 80%.

In Fig. 2, the absorption relative to non-irradiated samples is shown for irradiation doses of 28.1 and 66.8 kJ/mg humic acid, with and without presence of MES buffer. The decrease in absorption is higher around the irradiation wavelength than at shorter and longer wavelengths. Nevertheless the decrease in absorption is relatively uniform and also takes place at shorter wavelengths than that of irradiation. In the presence of MES buffer, the decrease in UV/Vis absorption is lowered compared to samples without the buffer. This indicates that the organic buffer acts as a scavenger for photochemically generated reactive species.

A key question is to which extent UV/Vis absorption can be used as an indicator for decomposition of humic substances. As seen in Fig. 2, the decrease in DOC concentration with increased absorbed irradiation dose is lower than the decrease in UV/Vis absorption. This shows that the decrease in UV/Vis absorption is the result of a variety of photochemical reactions including modification of the electronic structure and bond-breakage. As seen below, this includes the generation of smaller entities.

3.1.2. Influence on fluorescence spectrum

The decrease in fluorescence intensity with irradiation is much stronger than the decrease in UV/Vis absorption. In Fig. 3, the fluorescence spectra of humic acid are shown for irradiation at 394 nm. In Fig. 4, the fluorescence emission intensity at 500 nm is shown as a function of the absorbed energy. The fluorescence intensity decreases with increasing absorbed energy. At an absorbed energy of approximately 3.0 kJ/mg HA, the fluorescence intensity is decreased by approximately 95%, compared to an only marginal decrease in the UV/Vis absorption for the same irradiation dose (cf. Fig. 1).

3.1.3. Influence on fluorescence decay time

The fluorescence decay can be evaluated by different approaches. On the one extreme, the decay can be seen as a continuum with certain features. On the other hand, one may also represent the fluorescence decay by a limited number of operational components. The latter approach is guided

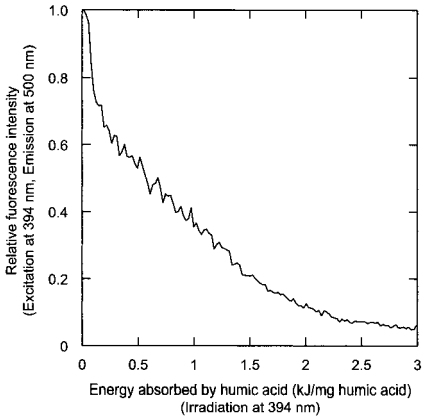

Fig. 4. Influence of irradiation by laser at 394 nm on the fluorescence of humic acid. Fluorescence at 500 nm from excitation at 394 nm is shown as a function of the absorbed irradiation energy.

Table 1
Selected results for fluorescence lifetime of humic acid, described by three individual components (excitation wavelength 314 nm)

Humic acid	Emission wavelength (nm)	Fluorescence lifetime (ns) of operational decay components		
		1	2	3[a]
Non-photodegraded	400	1.7	5.0	8
	500	1.6	4.8	12
Photodegraded	500	1.6	4.8	10

[a] The contribution of this component to the total fluorescence is approximately 15%. Due to the low contribution and low intensity at long delay time, the error of this component is larger than that of the other ones.

by the perception that different distinguishable fluorescent entities are present. It furthermore allows better visualization of the fluorescence decay process. Results show that the humic acid fluorescence decay can be well represented by three operationally defined individual decay components ([32], Table 1).

For the first two operationally defined fluorescence decay components, no significant difference is found for different degrees of photodegradation. The third component with the longest decay time represents only approximately 15% of the total fluorescence. Due to the delay and low intensity, the error in evaluation of this component is larger than for the other two. Also for this component, however, no major impact of photodegradation is seen.

3.1.4. Gel permeation chromatography of UV-irradiated HA

GPC in aquatic media separates substances according to their hydrodynamic size, charge and gel surface sorption properties. In Fig. 5, GPC chromatograms of humic acid are shown before and after irradiation at 254 nm with the low pressure mercury lamp. One main peak is observed by UV and fluorescence detection. Chromatograms from absorption detection at 254 nm fall mainly within the working range of the column (between dotted vertical lines), however, tailing beyond the total volume is also observed. For the fluorescence detection (excitation at 300 nm and emission at 400 nm), this tailing is more pronounced. With increasing irradiation dose the peak maximum is shifted to larger elution volume, indicative for a change in charge/surface sorption properties, but especially smaller size. The main part of non-irradiated humic acid is eluted between 22 and 38 ml. With increasing irradiation dose, the amount eluted in this region is decreased. Integration of the chromatograms, however, reveals that at 8.05 kJ/mg humic acid absorbed dose, the total area of the absorption chromatogram decreases only by 10%. This shows that the main effect at this dose is not oxidation to CO_2, but rather fragmentation of humic acid.

The gel permeation chromatograms with DOC detection (Fig. 5) are strongly influenced by the signal from the MES buffer. In addition to the large signal from the buffer, three peaks can be seen, at around 35, 70 and 80 ml elution volume. With increasing irradiation, the first peak decreases where this decrease is less pronounced for entities of larger apparent size. The peaks at 70 and 80 ml elution volume, i.e. beyond the total volume, are hardly visible in the original humic acid, but become more intense with increasing irradiation dose. These entities show no significant absorption or fluorescence signals.

In summary, the results from GPC verify findings discussed above (cf. Fig. 2). Photodegradation results in changes in the humic acid with emphasis on generation of smaller molecular size and small fragments with no measurable absorption and fluorescence.

3.2. Irradiation of a humic acid solution containing Eu

3.2.1. Influence on the emission spectrum of Eu and humic acid

When exciting a non-complexed Eu^{3+} ion solution at 394 nm, two main bands ($^5D_0$–$^7F_1$ and $^5D_0$–$^7F_2$, at 592 and

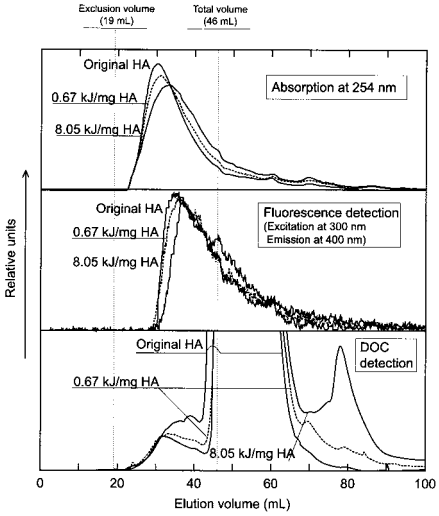

Fig. 5. GPC of original and photodegraded humic acid (HA) applying different detection methods, namely absorption at 254 nm, fluorescence (excitation at 300 nm, emission at 400 nm) and DOC.

617 nm, respectively) are observed. Another weak band can also be seen ($^5D_0$–$^7F_4$ at 697 nm), whereas the other transitions ($^5D_0$–$^7F_3$, $^5D_0$–$^7F_5$ and $^5D_0$–$^7F_6$) are very weak. For the non-complexed Eu^{3+} ion, the band at 592 nm is the most intense. Upon complexation, the peak positions do not change, but the relative intensity of the different bands change and for Eu(III)–humate, the $^5D_0$–$^7F_2$ (617 nm) band becomes the most intense.

Humic acid is complexed with europium at pH 6.0 (buffered with 10^{-3} mol/l MES) in 0.1 mol/l $NaClO_4$. The europium concentration equivalent to 20, 40 and 65% of the fraction of humic acid functional groups that can be complexed under these conditions (the loading capacity) [27]. This ensures that the concentrations of non-complexed europium are negligible in the starting solutions. The solutions are equilibrated for 48 hours prior to irradiation experiments. Fig. 6 shows the europium and humic acid fluorescence as a function of the absorbed energy at 40% europium loading. The irradiation energy is delivered by the laser source used for the fluorescence measurements (394 nm). The fluorescence intensities of both europium bands and that of humic acid decrease with increasing irradiation dose.

The ratio between the two bands at 592 and 617 nm for different absorbed energies is shown in Table 2. Irrespective of the absorbed energy, this ratio remains basically constant (2.36 ± 0.17). This observation suggests that during photodegradation, the ratio of free Eu/complexed Eu is not affected. However, the fluorescence intensity of free Eu being much smaller than that of Eu–humic acid complex, a small change in the free Eu concentration is difficult to observe by the Eu emission spectrum (cf. Fig. 9). Furthermore, to which extent the mode of complexation between humic acid and Eu(III) is affected by degradation of humic acid cannot be determined.

Table 2
Europium fluorescence intensity ratio of bands at 617–592 nm as a function of absorbed energy by laser irradiation at 394 nm[a]

Absorbed energy (kJ/mg HA)	Ratio FI 617 nm/ FI 592 nm
0.012	2.39
0.10	2.32
0.45	2.38
0.56	2.33
1.13	2.25
1.71	2.10
2.28	2.40
4.23	2.69
	2.36 ± 0.17[b]

[a] The europium concentration is equivalent to 40% of the loading capacity of humic acid; FI: fluorescence intensity.
[b] Mean value.

In Fig. 7, the relative fluorescence intensities of humic acid with and without europium as well as the two europium emission bands are shown. As shown in Table 2, the relative fluorescence intensity ratio of the two europium emission bands remains virtually constant with increasing irradiation dose. In absence of europium, the humic acid fluorescence diminishes rapidly and, as discussed above, decreases by approximately 95% at an absorbed irradiation dose of 3 kJ/mg humic acid (cf. Fig. 4). In the presence of europium, the humic acid fluorescence becomes stabilized for absorbed doses

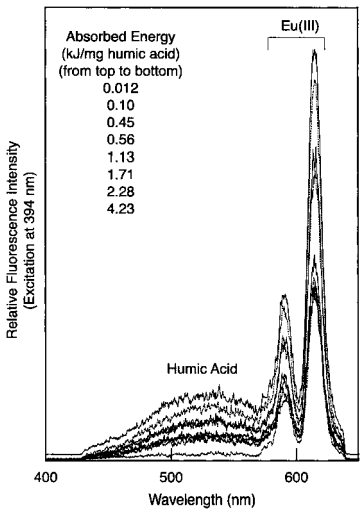

Fig. 6. Fluorescence of europium complexed with humic acid and that of humic acid (500 nm) as a function of absorbed irradiation energy by laser at 394 nm. The europium concentration is equivalent to occupation of 40% of the fraction of humate sites that can be complexed (loading capacity) under these conditions (pH 6.0, $I = 0.1$ ($NaClO_4$)).

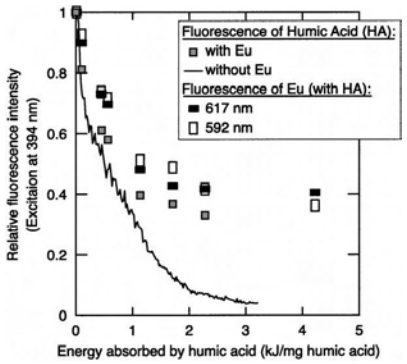

Fig. 7. Decrease in europium fluorescence bands (592 and 617 nm)) and humic acid fluorescence at 500 nm with and without europium as a function of absorbed irradiation dose (cf. Figs. 4 and 6).

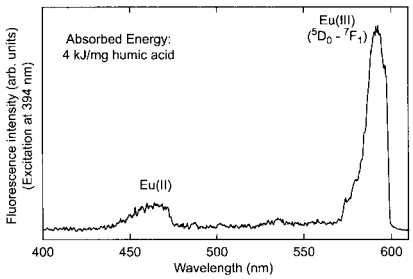

Fig. 8. Photolytic generation of Eu^{2+} in humic acid solution irradiated by laser at 394 nm (4 kJ/mg HA). The europium concentration is equivalent to 65% of the loading capacity of the humic acid.

above approximately 1 kJ/mg humic acid. The reason for the stabilization of humic acid fluorescence by europium in this range of absorbed energy is not yet clear.

3.2.2. Photolytic generation of Eu(II)

Irradiation with laser light at 394 nm not only leads to changes in the absorption, fluorescence, size distribution and functional group content of humic acid but also leads to the generation of divalent europium. In Fig. 8, the $^5D_0$–$^7F_1$ transition (592 nm) of Eu(III) is shown for photodegraded humic acid in the presence of europium. This spectrum is recorded for the highest europium concentration, i.e. 65% of the humic acid europium loading capacity and photodegradation by an absorbed energy of 4 kJ/mg humic acid. Around 460 nm a band corresponding to Eu(II) is observed.

3.2.3. Influence on the Eu–humate complexation

Stability constants of europium with non-photodegraded and photodegraded humic acid are determined by the ultrafiltration method at pH 6.0 and $I = 0.1$ M ($NaClO_4$). Degradation of humic acid is done by laser irradiation at 308 nm with an absorbed energy of 80 kJ/mg HA. After laser irradiation, europium is added in concentrations equivalent to 20 and 65% of the humic acid europium(III) loading capacity. The stability constants are evaluated by the charge neutralization model [27]. The results are shown in Table 3. For the investigation on the non-photodegraded humic acid, as expected, no influence of the loading is found. The overall average of the europium–humate stability constant is found to be 6.37 ± 0.10, which is in good agreement with values determined for different trivalent f-elements by ultrafiltration and spectroscopic methods ($\log \beta = 6.24 \pm 0.28$ [27]). For the photodegraded humic acid results are different. Again, no significant influence of the loading of humic with europium is found, however, the overall average of the stability constant is much lower, namely 5.19 ± 0.12.

The lower values for the stability constants found for photodegraded humic acid, could be the result of ultrafiltration artifacts. If humic acid entities decrease in size with photodegradation, the filter membrane could be partly

Table 3
Europium–humate complexation results at pH 6.0 ($I = 0.1$ M ($NaClO_4$))[a]

Total	[Eu] (μmol/l)		$[HA(III)]_{free}$ (μmol/l)	$\log \beta$ (l/mol)	$\log \beta$ (average)
	Non-complexed	Humate complex			
Non-photodegraded humic acid (20% europium loading)					
2.32	0.10	2.22	9.38	6.37	
2.32	0.13	2.19	9.41	6.25	6.31 ± 0.06
Photodegraded humic acid (20% europium loading)					
2.32	0.81	1.51	10.09	5.27	
2.32	0.90	1.42	10.18	5.19	
2.32	1.18	1.14	10.46	4.97	
2.32	1.04	1.28	10.32	5.08	5.13 ± 0.11[b]
Non-photodegraded humic acid (65% europium loading)					
7.54	0.55	6.99	4.61	6.44	
7.54	0.44	7.10	4.50	6.55	
7.54	0.72	6.82	4.78	6.30	
7.54	0.69	6.85	4.75	6.32	6.40 ± 0.10
Photodegraded humic acid (65% europium loading)					
7.54	3.24	4.30	7.30	5.26	
7.54	2.85	4.69	6.91	5.38	
7.54	3.53	4.01	7.59	5.18	
7.54	3.45	4.09	7.51	5.20	5.26 ± 0.08[b]

[a] The effective humic acid concentration equals 11.6 μmol/l, taking into account the loading capacity under these experimental conditions. Concentrations of the non-complexed europium ion and europium–humate are determined via species separation by ultrafiltration, taking into account partial retention of the non-complexed europium ion at this pore-size (1000 Da). Non-photodegraded and photodegraded humic acid is investigated for europium concentrations equivalent to 20 and 65% of the effective humic acid concentration.

[b] No correction is made for the impact of photodegradation on the functional group content.

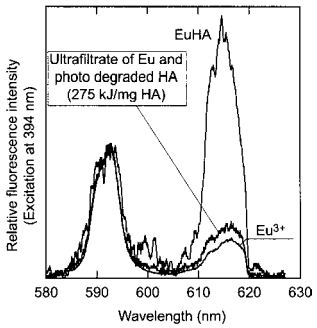

Fig. 9. Emission spectra of the Eu(III) ion in the non-complexed form as well as complexed with photodegraded and non-photodegraded humic acid (HA).

permeable for the europium complex. The composition of the filtrate was measured by taking an emission spectrum of this filtrate and comparing to the emission spectra of free Eu and complexed Eu. The $^5D_0$–$^7F_2$ transition for Eu (617 nm) is sensitive to the complexation by humic acid and would increase drastically if smaller size europium humic acid entities would pass through the filter. In a good approximation, it is possible to estimate the amount of complexed Eu going through the filter by normalizing the intensity of the $^5D_0$–$^7F_1$ (592 nm) transition for the different solutions and comparing directly the intensity of the $^5D_0$–$^7F_2$ transition (Fig. 9). By this method, less than 8% of Eu in the filtrate is found to be complexed. Taking this correction value into account, the stability constant of photodegraded humic acid does not change significantly ($\log \beta$ becomes 5.33 ± 0.08 instead of 5.26 ± 0.08 at 65% Eu loading of the humate ligand). Thus, the lowering of the stability constant by photodegradation is not a consequence of ultrafiltration artifacts.

Photodegradation leads to changes both in the functional group content of humic acid and decrease in molecular size. Investigations on different size fractions of humic acid show that with decreasing size the complexation strength decreases [33]. Comparison of the metal ion complexation with humic and with fulvic acid also shows lower complexation strength for the smaller fulvic acid [12]. Simultaneously, photodegradation results in modification of the functional group content. Delineation of the impacts from decrease in the molecular size and change in the functional group content, cannot be performed by the present data.

4. Summary and conclusions

The sensitivity of different properties of humic acid towards photodegradation varies strongly. Photodegradation leads to generation of smaller entities. The decrease in DOC is lower that the decrease in UV/Vis absorption. The decrease in fluorescence intensity, however, is much more pronounced that the former two decomposition indicators. Addition of europium leads to stabilization of humic acid towards photodegradation.

Application of laser induced fluorescence spectroscopy for studying the europium–humate interaction may be subject to considerable experimental artifacts through photochemically induced reactions. These artifacts are due to changes in functional group content and lowering in molecular size of humic acid. Simultaneously, photolytic reduction of europium from the trivalent to the divalent state takes place. Due to the relatively low fluorescence efficiency of europium, significant photolytic impact can occur. This is especially true for high absorbed irradiation doses, for example where europium lifetime measurements are conducted. Therefore, great care is needed to ensure that significant experimental artifacts are avoided where the europium humic acid system is studied.

References

[1] J.I. Kim, G. Buckau, Huminstoffuntersuchungen an Gorleben-Grundwässern, Report: RCM 01590, TU, München, Germany, 1990.
[2] R. Artinger, G. Buckau, J.I. Kim, S. Geyer, P. Fritz, M. Wolf, Characterization of groundwater humic substances: influence of sedimentary organic carbon, Appl. Geochem. 15 (1999) 81.
[3] J. Buffle, Complexation Reactions in Aquatic Systems. An Analytical Approach, Ellis Horwood, New York, 1988.
[4] J.A. Leenbeer, D.M. McKnight, E.M. Thurman, P. McCarthy, Humic substances in Suwannee river, in: R.C. Averett, D.M. Leenbeer, D.M. McKnight, K.A. Throne (Eds.), Interaction, Properties and Proposed Structures, Open File Report 87-557, US Geological Survey, Denver, CO, 1989, p. 331.
[5] M. Schnitzer, Recent findings on the characterization of humic substances extracted from soils from widely differing climatic zones, in: Proceedings of the Symposium on Soil Organic Matter Studies, Braunschweig, International Atomic Agency, Vienna, 1977, p. 117.
[6] G. Buckau, Komplexierung von Am(III) mit Huminstoffen in natürlichen Grundwässern, Dissertation, FU Berlin, 1991.
[7] V. Lesourd-Moulin, Les acides humiques et leurs interactions avec les elements metalliques Cu(II), Eu(III), Th(IV), U(VI), Dissertation, Universite Claude Bernard, Lyon, October 1985.
[8] R. Torres, G.R. Choppin, Europium(III) and americium(III) stability constants with humic acid, Radiochim. Acta 35 (1984) 143.
[9] K.L. Nash, G.R. Choppin, Interaction of humic and fulvic acids with Th(IV), J. Inorg. Nucl. Chem. 42 (1980) 1045.
[10] V. Moulin, P. Robouch, P. Vitorge, B. Allard, Spectrophotometric study of the interaction between Am(III) and humic materials, Inorg. Chim. Acta 140 (1987) 303.
[11] J.I. Kim, G. Buckau, E. Bryant, R. Klenze, Complexation of americium(III) with humic acid, Radiochim. Acta 48 (1989) 135.
[12] G. Buckau, J.I. Kim, R. Klenze, D.S. Rhee, H. Wimmer, A comparative study of the fulvate complexation of trivalent transuranic element ions, Radiochim. Acta 57 (1992) 105.
[13] J.I. Kim, D.S. Rhee, G. Buckau, Complexation of americium(III) with humic acids of different origin, Radiochim. Acta 52/53 (1991) 49.
[14] J.I. Kim, T. Sekine, Complexation of neptunium(V) with humic acid, Radiochim. Acta 55 (1991) 187.
[15] C.M. Marquardt, J.I. Kim, Complexation of Np(V) with humic acid: intercomparison of results from different laboratories, Radiochim. Acta 80 (1998) 129.

[16] J.I. Kim, C.M. Marquardt, Chemical reaction of Np(V) with humic colloids in groundwater: influence of purification on the complexation behaviour, Radiochim. Acta 87 (1999) 105.
[17] E.L. Bertha, G.R. Choppin, Interaction of humic and fulvic acids with Eu(III) and Am(III), J. Inorg. Nucl. Chem. 40 (1978) 655.
[18] A. Maes, J. De Brabandere, A. Cremers, A modified Schubert method for the measurement of the stability of europium humic acid, Radiochim. Acta. 44/45 (1988) 51.
[19] A. Diercks, A. Vancluysen, A. Maes, Contribution by KUL, in: J.I. Kim, G. Buckau (Eds.), Effects of Humic Substances on the Migration of Radionuclides: Complexation of Actinides with Humic Substances, Report RCM 00392, TU, München, Germany, 1992.
[20] J.I. Kim, H. Wimmer, R. Klenze, A study of curium(III) humate complexation by time resolved laser fluorescence spectroscopy, Radiochim. Acta 54 (1991) 35.
[21] G. Bidoglio, N. Omnetto, P. Robouch, Kinetic studies on lanthanide interactions with humic substances by time resolved laser induced fluorescence, Radiochim. Acta 52/53 (1991) 57.
[22] P. Decambox, P. Mauchien, C. Moulin, V. Moulin, J. Tits, Contribution by CEA, in: J.I. Kim, G. Buckau (Eds.), Effects of Humic Substances on the Migration of Radionuclides: Complexation of Actinides with Humic Substances, Report RCM 00392, TU, München, Germany, 1992.
[23] M. Caceci, The interaction of humic acid with europium(III). Complexation strength as a function of load and pH, Radiochim. Acta. 39 (1994) 51.
[24] W.C. Li, D.M. Victor, C.L. Chakrabarti, Effect of pH and uranium concentration on the interaction of U(VI) and U(IV) with organic ligands in aqueous solution, Anal. Chem. 52 (1980) 520.
[25] L. Carlsen, Radionuclide-soil organic matter interactions, Report: CEC, EUR 9780/I, EN, Brussels, 1985.
[26] J.I. Kim, G. Buckau, G.H. Li, H. Duschner, N. Psarros, Characterization of humic and fulvic acids from Gorleben groundwater, Fresenius J. Anal. Chem. 338 (1990) 245.
[27] J.I. Kim, K.R. Czerwinski, Complexation of metal ions with humic acid: metal ion charge neutralization model, Radiochim. Acta 73 (1996) 5.
[28] C. Tiseanu, M.U. Kumke, F.H. Frimmel, R. Klenze, J.I. Kim, Time-resolved fluorescence spectroscopy of fulvic acid and fulvic acid complexed with Eu^{3+} — a comparative study, J. Photochem. Photobiol. A 117 (3) (1998) 175.
[29] J.C. Brochon, Maximum entropy method of data analysis in time-resolved spectroscopy, in: M.L. Johnson, L. Brand (Eds.), Numerical Computer Methods. Part B. Methods in Enzymology, Vol. 240, Academic Press, New York, 1994, p. 262 (Chapter 13).
[30] J.I. Kim, D.S. Rhee, H. Wimmer, G. Buckau, R. Klenze, Complexation of trivalent actinide ions (Am^{3+}, Cm^{3+}) with humic acid: a comparison of different experimental methods, Radiochim. Acta 62 (1993) 35.
[31] S.A. Huber, F.H. Frimmel, Flow injection analysis for organic and inorganic carbon in the low-ppb range, Anal. Chem. 63 (1991) 2122.
[32] F.H. Frimmel, M.U. Kumke, Fluorescence decay of humic substances, in: G. Davies, E. Ghabbour (Eds.), Humic Substances: Structure, Properties and Uses, Royal Society of Chemistry, Cambridge, 1998, p. 113.
[33] J.M. Monsallier, Influence of humic acid size on actinide complexation, Dissertation, Florida State University, FL, 1998.

Kapitel 3

Aktuelle Arbeiten

Die Komplexierung von Metallionen durch HS ist von zentraler Bedeutung für deren Transport und Immobilisierung. In sensiblen Bereichen, wie z.B. bei der Erschließung und dem Betrieb von End- und Zwischenlagern für radioaktive Abfälle, ist für Sicherheitsanalysen und für die verlässliche Modellierung der Dynamik der Actinidionen[1] (An^{3+}) in den verschiedenen Umweltkompartimenten eine Aufklärung der Bindungsmechanismen an HS sowie die Bestimmung der thermodynamischen und kinetischen Kenngrößen unbedingt erforderlich.
In den z.Z. laufenden Forschungsvorhaben werden vor allem die Lanthanidionen (Ln^{3+}) von Europium (Eu) und Terbium (Tb) und deren Komplexierungsverhalten mit HS untersucht, wobei die Ln^{3+}-Ionen stellvertretend für die An^{3+}-Ionen untersucht werden, die bedingt durch ihre Radioaktivität wesentlich problematischer im Umgang sind. Aufgrund der vergleichbaren Komplexbildungseigenschaften werden die Ln^{3+}-Ionen als Ersatz verwendet. Ferner ermöglichen die spektroskopischen Eigenschaften der Lanthanide, dass die Ln^{3+}-Ionen selbst als Lumineszenzsonden eingesetzt werden und so die HS-Metallkomplexierung untersucht werden kann.

In den aktuellen Forschungsvorhaben werden folgende Ziele verfolgt:

- die Untersuchung von Konformations- und Assoziationseffekten in HS, initiiert durch die Komplexierung von Metallionen,
- die Charakterisierung von Bindungsstellen in HS, speziell deren Abstandsverteilungen,
- die Bestimmung von differenzierten thermodynamischen und kinetischen Parametern zur Beschreibung der HS-Metall-Komplexierung,
- die Weiterentwicklung von Modellen für den Transport und den Verbleib von Metallen in der Umwelt.

Als Untersuchungsmethoden werden stationäre und zeitaufgelöste Fluoreszenztechniken eingesetzt. Die Proben sind nach den Standardvorschriften isolierte FA- und

[1] auch Actinoidionen

HA-Fraktionen von HS verschiedener Ursprungsorte, synthetische HS und einfache Modellverbindungen, die als Bausteine von HS betrachtet werden können. Es wird sowohl die intrinsische Fluoreszenz der HS und der Modellverbindungen wie auch die Lumineszenz der Ln^{3+}-Ionen selbst untersucht. Besonders der Energietransfer zwischen gebundenen Ln^{3+}-Ionen (z.B. Tb^{3+} (Donor) und Nd^{3+} (Akzeptor)) wird genutzt, um Abstandsverteilungen von Bindungsstellen in HS zu bestimmen und das Assoziationsverhalten von HS zu untersuchen.
Die verwendeten HS und Modell-HS sind im Anhang C in Tabelle C.1 zusammengestellt. Bei den untersuchten HS handelt es sich einerseits um Standard- und Referenz-HS der IHSS sowie nach Standardverfahren isolierte HS verschiedener Ursprungsorte. Ergänzend werden Untersuchungen an verschiedenen Hydroxybenzoesäuren durchgeführt.
Im Folgenden sind ausgewählte Ergebnisse der laufenden Arbeiten dargestellt. Da der Lumineszenz der Ln^{3+}-Ionen als Sonden eine besondere Bedeutung in den Untersuchungen zu kommt, sind die grundlegenden photophysikalischen Eigenschaften der Ln^{3+}-Ionen zu Beginn des Kapitels kurz zusammengefasst.

Die in diesem Kapitel dargestellten Ergebnisse sind z.T. in folgenden Veröffentlichungen publiziert bzw. als Tagungsbeiträge präsentiert worden:

15. I. Billard, E. Ansoborlo, K. Apperson, S. Arpigny, M.E. Azehna, D. Birch, P. Bros, H.D. Burrows, G. Choppin, L. Couston, V. Dubois, T. Fanghanel, G. Geipel, S. Hubert, J.I. Kim, T. Kimura, R. Klenze, A. Kronenberg, M. Kumke, G. Lagarde, G. Lamarque, S. Lis, C. Madic, G. Meinrath, C. Moulin, R. Nagaisi, D. Parker, G. Plancque, F. Scherbaum, E. Simoni, S. Sinkov, C. Viallesoubranne
Appl. Spectros., 2002, **57**, 1027-1038.
Aqueous solutions of U(VI) as studied by time-resolved laser-induced fluorescence spectroscopy (TRLFS) : A Round-robin test.

16. C. Tiseanu, R.K. Mehra, R. Kho, M.U. Kumke
Chem.Phys.Lett. 2003, **377**, 131-136.
Optical properties of terbium-doped thiosalicylic-capped CdS nanocrystals.

17. C. Tiseanu, R.K. Mehra, R. Kho, M.U. Kumke
J. Phys. Chem. B, 2003, **107**, 12153-12160.
Comparative study of time-resolved photoluminescence properties of terbium-doped thiosalicylic-capped CdS and ZnS nanocrystals.

18. C. Tiseanu, L. Frunza, M.U. Kumke
Physica B, 2004, **352**, 358-365.
Time-resolved photoluminescence analysis of distribution and migration of terbium ions in zeolites X.

19. M.U. Kumke, S. Eidner
in: Humic substances: molecular details and applications in land and water conservation, E.A. Ghabbour und G. Davies (eds), Taylor and Francis, Inc.,2004 zur Veröffentlichung angenommen.
Fluorescence and energy transfer processes of humic substances and related model compounds in terbium complexes.

* M.U. Kumke, H.-G. Löhmannsröben
6th International Conference on the Biogeochemistry of Trace Elements (ICOBTE), 29. July

- 2 August 2001 in Guelph, Canada.
Binding of metals by natural ligands - What can we learn from fluorescence spectroscopy.

* M.U. Kumke, H.-G. Löhmannsröben, S. Eidner, G. Korshin
11th Meeting of the International Humic Substances Society, 21. -26. July 2002 in Boston, USA.
Inter-Lanthanide luminescence resonance energy transfer in humic substances.

* M.U. Kumke, H.-G. Löhmannsröben, S. Eidner, S. Prenzel
European Young Investors Conference, März 2003 in Slubice, Polen.
Interlanthanide energy transfer in mixed Tb^{3+}/Nd^{3+}-humat complexes.

* M.U. Kumke, S. Eidner
Humic Substances Seminar VII, 17. - 19. März 2004 in Boston, USA.
Investigation of metal ion complexation by humic substances (HS) and related model ligands using lanthanide ion probe spectroscopy (LIPS).

3.1 Lanthanide - Grundlagen

Die Lanthanide[2] (*Seltenen Erdmetalle*, Ln) umfassen die vierzehn auf das Lanthan folgenden Elemente [112–115]. Da allerdings die Chemie des Lanthans der der Lanthanide sehr ähnlich ist, wird diese Element oftmals auch zu den Lanthaniden gezählt. Beginnend mit dem Cer wird die $4f$-Schale nacheinander mit Elektronen aufgefüllt und da die $4f$-Elektronen kaum an der Bindungsbildung teilnehmen, ist das chemische Verhalten der Lanthanide sehr ähnlich. Die vorherrschende Oxidationsstufe der Lanthanide ist +III [112]. Ein Grund dafür ist das höhere Ionisierungspotential der f-Elektronen im Vergleich zu den s- und d-Elektronen der Valenzschale. Unterschiede im chemischen Verhalten sind meistens auf die unterschiedlichen Ionenradien, bedingt durch die sogenannte *Lanthanidenkontraktion*, zurückzuführen. Diese kommt durch die unvollständige Abschirmung der $4f$-Elektronen untereinander zustande, so dass die effektiv wirkende Kernladung mit zunehmender Ordnungszahl wächst. Ausnahmen zur Oxidationsstufe +III bilden Cer, das in der Oxidationsstufe +IV vorkommt, sowie Samarium, Europium und Ytterbium, die in einigen Feststoffen und wässrigen Lösungen die Oxidationsstufe +II bilden können [112, 114, 116]. Als Koordinationszahlen werden für die Oxidationsstufe +III am häufigsten 7, 8 und 9 gefunden. Da die f-Orbitale relativ gut abgeschirmt sind, stehen diese nicht für die Bildung von Hybridorbitalen zur Verfügung. Die stabilsten Komplexe werden mit Liganden, die Sauerstoffatome enthalten, eingegangen [112]. Die Aqua-Ionen ($Ln[H_2O]_n^{3+}$) hydrolysieren in Wasser, wobei die Tendenz mit steigender Ordnungszahl zunimmt. Desweiteren bilden die Ln^{3+}-Ionen mit weiteren anorganischen Liganden wie z.B. Carbonat-Ionen Komplexe. Diese Reaktion ist stark vom pH-Wert abhängig und wird in der Regel für pH-Werte > 7 beobachtet [117]. Aus diesen Gründen sind die Untersuchungen zum Komplexierungsverhalten durch Huminstoffe vorwiegend für einen pH-Wertbereich ≤ 6 durchgeführt worden.
Die Anwendungen von Lanthanid-Ionen bzw. ihren Komplexen sind vielfältig [118–120]. Besonders in Bereich der Entwicklung neuer Lasermaterialien und optischer

[2] auch Lanthanoide

Sensoren werden mit Lanthanid-Ionen dotierte Materialien in zunehmendem Maße eingesetzt [121–127]. Lanthanid-Ionen und ihre Komplexe werden als Sonden für biologische Systeme genutzt [120, 128–134]. Ln^{3+}-Ionen können Ca^{2+} in Proteinen isomorph ersetzen. Dadurch können z.B. Tb^{3+} und Eu^{3+} als Lumineszenzsonden in Untersuchungen von Proteinen bzw. Proteinstrukturen eingesetzt werden [128, 135–138]. Besonders hervorzuheben sind Anwendungen zur Untersuchung von Konformationsänderungen (wie z.B. bei der Muskelkontraktion oder von Proteinen, die die Durchlässigkeit von Ionenkanälen steuern) [139–142]. Lanthanid-Komplexe werden als Donor-Systeme in homogenen Fluoreszenzimmunoassays und in homogenen DNA-Hybridisierungsassays eingesetzt [120, 133, 143, 144]. Diese konkurrieren inzwischen in der Empfindlichkeit mit Radioimmunoassays.

3.1.1 Absorptions- und Lumineszenzeigenschaften von Ln^{3+}

Die Elektronenkonfiguration der Ln^{3+}-Ionen ist in Tabelle B.2 zusammengefasst. Durch elektrostatische Wechselwirkung der f-Elektronen erfolgt eine Aufspaltung der $4f^n$-Elektronenkonfiguration in Terme mit unterschiedlichen Gesamtbahndrehimpuls L. Zusätzlich führt die Austauschwechselwirkung der Elektronen zu unterschiedlichen Gesamtspinquantenzahlen (bei gleicher Gesamtbahndrehimpulsquantenzahl). Durch Spin-Bahn-Wechselwirkung werden die elektronisch entarteten Terme weiter in *spektroskopische Terme* aufgespalten. Die spektroskopischen Terme werden zur Beschreibung der elektronischen Zustände von Lanthanidionen verwendet - im Gegensatz zu der Nomenklatur zur Beschreibung der elektronischen Zustände von organischen Molekülen, bei denen einzig die Spinmultiplizität zur Unterscheidung herangezogen wird. Liganden können dann zu einer weiteren Feinaufspaltung in unterschiedliche Niveaus führen (s. Tabelle B.2). Je nach Anzahl der f-Elektronen wächst die Zahl der möglichen Niveaus sehr schnell an und ist für das Gd^{3+} am größten. Da die $4f$-Orbitale durch die äußeren d- bzw. s-Orbitale weitestgehend von Umgebungseinflüssen abgeschirmt sind, ist die beobachtete Ligandenfeldaufspaltung im Gegensatz zu den d-Blockmetallen klein. Während für die d-Blockmetalle Ligandenfeldaufspaltungen im Bereich von 10000 cm^{-1} bis 30000 cm^{-1} gefunden werden, beobachtet man bei Lanthanidkomplexen gewöhnlich Aufspaltungen < 500 cm^{-1} [120, 145, 146]. In den spektroskopischen Termen erfolgt die Charakterisierung der elektronischen Zustände durch die Quantenzahl L des Gesamtbahndrehimpulses, die Multiplizität M^S, sowie die Quantenzahl J des Gesamtdrehimpulses: ${}^{M^S}L_J$. Bei den elektronischen Übergängen handelt es sich um f-f-Übergänge, d.h. also zwischen Zuständen gleicher Parität. Damit sind die f-f-Übergänge Laport-verboten (Paritätsverbot) und als eine Konsequenz daraus sind die Extinktionskoeffizienten ϵ sehr klein. Das Paritätsverbot wird gelockert durch das Mischen mit Schwingungen von Liganden bzw. elektronischen Übergängen entgegengesetzter Parität [145, 147, 148]. Gewöhnlich liegen die Extinktionskoeffizienten in der Größenordnung von $\epsilon \leq 10^{-2}$ $M^{-1} \cdot cm^{-1}$. Da bei der elektronischen Anregung nur f-Elektronen involviert sind, die nicht an chemischen Bindungen beteiligt sind, ist die Gleichgewichtsgeometrie des elektronischen Grundzustands und des elektronisch-angeregten Zustands nahe-

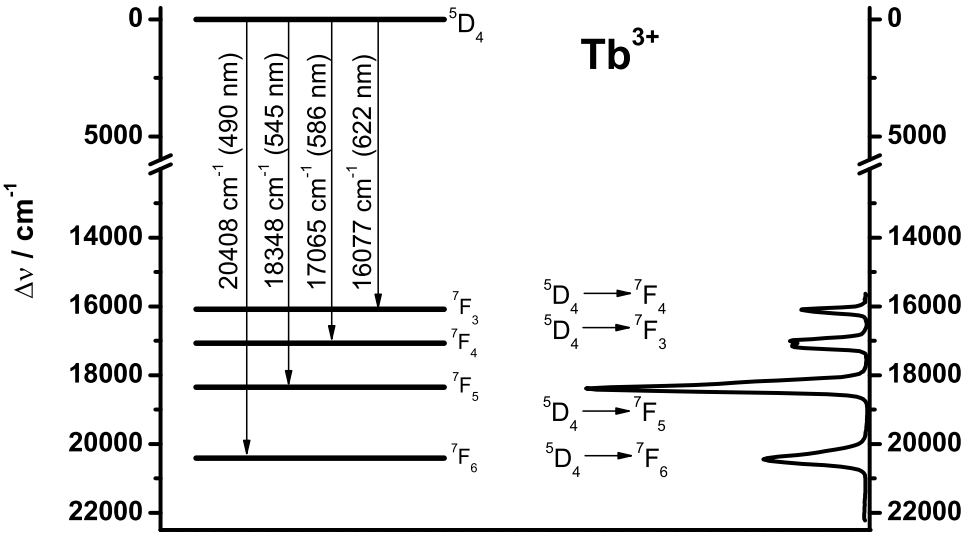

Abbildung 3.1: Energieniveauschema von Tb^{3+}.

zu identisch, so dass Absorptions- und Emissionsbanden der Ln^{3+}-Ionen sehr scharf sind [112, 145, 148, 149]. Selbst bei Raumtemperatur können Linienspektren gemessen werden, die eine Halbwertsbreite von nur wenigen cm^{-1} haben [128].
Von den Ln^{3+}-Ionen zeigen nur das Samarium (Sm), das Europium (Eu), das Terbium (Tb) und das Dysprosium (Dy) bei Raumtemperatur in Lösung nennenswerte Lumineszenz. In Abbildung 3.1 sind das Termschema, die spektroskopischen Terme sowie das Lumineszenzspektrum für Tb^{3+}(aq) gezeigt. Für Tb^{3+} wird in Lösung die Lumineszenz gewöhnlich aus dem $^5D_4$-Zustand beobachtet, Eu^{3+} besitzt im Prinzip zwei lumineszierende Zustände ($^5D_0$ und $^5D_1$) wobei der erste der dominierende ist (siehe auch Abbildung 3.4). Die Lumineszenz des Eu^{3+} erfolgt in das Multiplet des elektronischen Grundzustandes (^7F_J, mit $J = 0 - 6$) [150–152]. Basierend auf den Auswahlregeln für elektronische Dipol-Übergänge sind die Übergänge $^5D_0 \rightarrow {}^7F_{2,4,6}$ erlaubt, ebenso wie der magnetische Dipol-Übergang $^5D_0 \rightarrow {}^7F_1$. Die Übergänge $^5D_0 \rightarrow {}^7F_{0,3,5}$ sollten stark verboten sein. Dass diese dennoch teilweise in Spektren beobachtet werden können, hängt mit der Symmetrie der Komplexe bzw. der Erniedrigung dieser durch Schwingungen zusammen [145, 146].
Obwohl Veränderungen in der Koordinationssphäre der Ln^{3+}-Ionen nur kleine Änderungen in der spektralen Lage der Absorptions- und Emissionsbanden bzw. den relativen Intensitäten bewirkt, sind diese Änderungen sehr spezifisch und können zur Identifikation von Komplexgeometrien oder deren Änderung verwendet werden [145,146,148,151,152]. So sind z.B. für Eu^{3+} der $^7F_0$- und der $^5D_0$-Zustand nicht weiter durch das Ligandenfeld aufgespalten, so dass aus der Anzahl der energetisch-verschiedenen $^5D_0 \rightarrow {}^7F_0$-Übergänge auf die Anzahl der unterschiedlichen Kom-

plexe in einer Probe geschlossen werden kann. Die Fluoreszenzquantenausbeuten von Ln^{3+}-Aquaionen sind gewöhnlich sehr gering, was darauf hindeutet, dass die Desaktivierung der elektronisch-angeregten Zustände überwiegend strahlungslos erfolgt (sieh auch 3.1.2) [129, 145, 151–154].

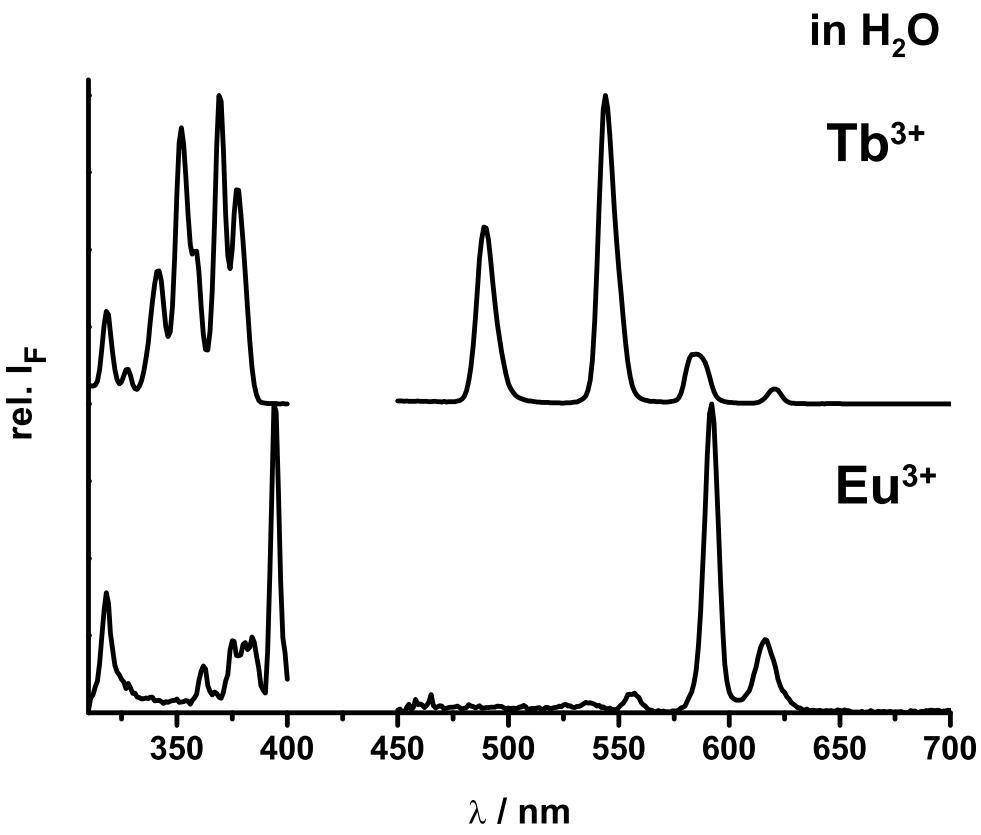

Abbildung 3.2: Lumineszenzanregungs- und Lumineszenzspektren von Tb^{3+} (oben) und Eu^{3+} (unten) in Wasser ($c_{Ln^{3+}} = 10^{-3}$ M; $\lambda_{ex,Tb^{3+}} = 350$ nm und $\lambda_{ex,Eu^{3+}} = 395$ nm; $\lambda_{em,Tb^{3+}} = 545$ nm und $\lambda_{em,Eu^{3+}} = 593$ nm; Fluoromax 3, Yobin Yvonne).

Qualitative und quantitative Untersuchungen von Ln^{3+}-Komplexen in Lösung können mittels Lumineszenz- und Lumineszenzanregungsspektroskopie sehr empfindlich durchgeführt werden (Konzentrationsbereich $\ll 10^{-9}$ M) [155]. Zur Veranschaulichung sind in Abbildung 3.2 die Lumineszenz- und Lumineszenzanregungsspektren von Tb^{3+}(aq) und Eu^{3+}(aq) gezeigt. Da es sich bei der beobachteten Emission von Ln^{3+}-Ionen wie oben beschrieben um elektronische Übergänge zwischen Zuständen mit unterschiedlicher Spinmultiplizität handelt, wird der Begriff *Lumi-*

neszenz verwendet[3]. Die spektral hochaufgelösten Lumineszenz- und Lumineszenzanregungsspektren von Ln^{3+}-Komplexen werden zur qualitativen und quantitativen Charakterisierung eingesetzt [128, 153, 156–158]. So wurden z.B. durch Messen der Lumineszenz- und Lumineszenzanregungsspektren von Eu^{3+} bei 614 nm ($^5D_0 \rightarrow {}^7F_2$-Übergang) und Anregung im Bereich von 578 nm $< \lambda_{ex} <$ 581 nm ($^7F_0 \rightarrow {}^5D_0$-Übergang)) thermodynamische Komplexbildungskonstanten für verschiedene organische Liganden bestimmt. Dabei wurde eine konkurrierende Komplexierung mit einem Liganden mit bekannter Stabilitätskonstante durchgeführt [159, 160].
Besonders für die Speziation von Actiniden ist die zeitaufgelöste laser-induzierte Fluoreszenzspektroskopie (*time-resolved laser-induced fluorescence spectroscopy*, TRLFS) etabliert. Für Eu^{3+}, Tb^{3+}, Am^{3+} und Cm^{3+} wurden Komplexbildungskonstanten verschiedener Huminstoff-, Carbonat- und Hydroxokomplexe mittels TRLFS bestimmt [100, 117, 161–164]. Besonders Eu^{3+} wurde vielfach zur Untersuchung der Metallkomplexierung durch HS eingesetzt [80, 82, 83, 117, 165–167].
Eine weitere Konsequenz des Paritätsverbots der elektronischen f-f-Übergänge ist die außergewöhnlich lange Lumineszenzlebensdauer τ der Ln^{3+}-Ionen und ihrer Komplexe [129, 151–154]. In Abbildung 3.3 sind die Lumineszenzabklingkurven von Tb^{+3}(aq) und Eu^{+3}(aq) dargestellt. Die Angaben in der Literatur für die Lumineszenzlebenszeit τ der Aquaionen schwanken: $\tau_{Eu^{3+}} = 100 \pm 10$ μs und $\tau_{Tb^{3+}} = 400 \pm 10$ μs (s. auch Tabelle B.1) [151,152,154]. Für die Strahlungslebensdauer τ_0 von Tb^{+3} in H_2O und in D_2O wird ein Wert von $\tau_{0,Tb^{3+}} = 4800$ μs bis 8300 μs genannt, die für Eu^{3+} ($\tau_{0,Eu^{3+}} = 9500$ μs) sind sehr ähnlich [150, 168, 169]. Die großen Unterschiede zwischen τ und τ_0 sind ein weiterer Hinweis dafür, dass in den Aquokomplexen der Ln^{3+}-Ionen sehr effektive strahlungslose Desaktivierungsprozesse stattfinden. In Ln^{3+}-Komplexen, die eine gute Abschirmung des Ln^{3+}-Ions gegen äußere Einflüsse gewährleisten, werden wesentlich längere Lumineszenzlebensdauern gefunden (ebenso werden erhöhte Lumineszenzquantenausbeuten bestimmt) [156, 170].

Hypersensitive elektronische Übergänge in Lanthanid-Komplexen Die Intensität der elektronischen Übergänge in Lanthanid-Komplexen wird durch ihre erste und zweite Koordinationsspähre beeinflusst. Wird durch Substitution von Liganden die Symmetrie verändert, so kann sich dies besonders auf die beobachtete Intensitätsverteilung im Absorptions- und Lumineszenzspektrum auswirken. Bei einigen Lanthaniden wird für bestimmte elektronische Übergänge eine wesentlich stärkere Beeinflussung gefunden als für andere Übergänge. Die Intensität der elektronischen Übergänge ist direkt proportional der Oszillatorstärke des betrachteten elektronischen Übergangs. Die beobachtete verstärkte Sensitivität der Oszillatorstärke bestimmter Übergänge relativ zu anderen auf Veränderungen in der Koordinationsspähre des Lanthanidions wird als *Hypersensitivität* bezeichnet [171, 172]. Der prominenteste Vertreter ist das Europium, bei dem der hypersensitive Übergang in Absorption einem $^7F_0 \rightarrow {}^5D_2$-Übergang (bei 464 nm) und in Emission

[3]Genau genommen sollte *Phosphoreszenz* verwendet werden. Diese Nomenklatur ist in der Literatur allerdings für die Emission der Lanthanide selten zu finden.

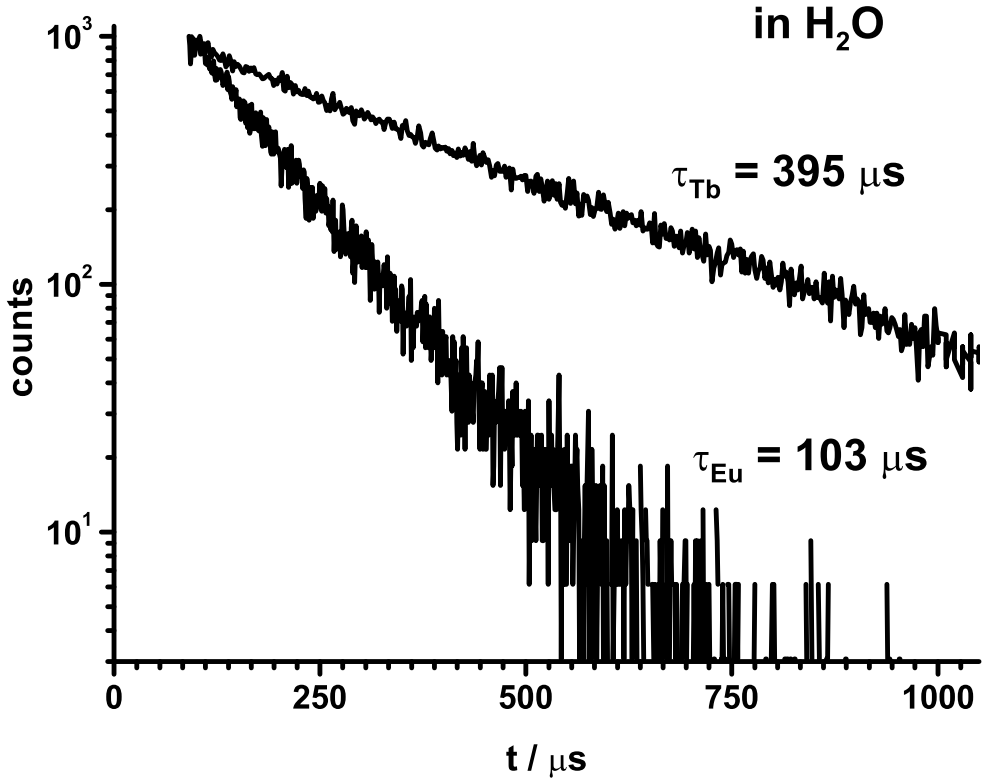

Abbildung 3.3: Lumineszenzabklingkurven von Tb^{3+} und Eu^{3+} in Wasser ($c_{Ln^{3+}} = 10^{-3}$ M; $\lambda_{ex,Ln^{3+}} = 337.1$ nm; $\lambda_{em,Tb^{3+}} = 545$ nm und $\lambda_{em,Eu^{3+}} = 593$ nm; FL920, μs-Modus, Edinburgh Instruments).

einem $^5D_0 \rightarrow {}^7F_2$-Übergang (bei 614 nm) entspricht. Dieser Übergang ist ein magnetischer Dipol-Übergang. Durch Veränderungen der Komplexsymmetrie werden die Übergangswahrscheinlichkeiten der Übergänge mit elektrischem Dipolcharakter des Eu^{3+} verändert, während die magnetischen Dipolübergänge unbeeinflusst bleiben [150,171,173]. Neben Europium werden auch noch für Praseodym (Pr), Neodym (Nd), Samarium (Sm), Dysprosium (Dy), Holmium (Ho), Erbium (Er) und Thulium (Tm) hypersensitive elektronische Übergänge beschrieben [171]. Die beobachtete Hypersensitivität in den Absorptions- aber vor allem in den Lumineszenzspektren dieser Lanthanide hat dazu geführt, dass diese als molekulare Sonden eingesetzt werden, um z.B. Veränderungen in der Komplexierung von Metallionen zu untersuchen. Choppin et al. haben so z.B. eine gute Korrelation zwischen der Basizität der Liganden und der Intensität der hpersensitiven Übergänge in Lanthanid-Komplexen beschrieben, die sowohl in fester Phase wie auch in Lösungen bestätigt wurde [171].

3.1.2 Strahlungslose Desaktivierungsprozesse

Die Lumineszenzquantenausbeute Φ und die Lumineszenzlebensdauer τ von Lanthanidionen in Lösung werden hauptsächlich durch die erste Koordinationsphäre des Ions bestimmt. Einfluß auf die Parameter Φ und τ nehmen neben der Art der Liganden (koordinierten Moleküle) in *gemischten* Komplexen die Anzahl der Liganden sowie deren Anordnung im Komplex [150, 174].
Die wirkungsvollste strahlungslose Desaktivierung der elektronisch-angeregten Lanthanidionen geschieht durch die Kopplung an OH- bzw. CH-Schwingungen von Liganden in der ersten Koordinationssphäre [145, 150]. Es konnte gezeigt werden, dass die beobachtete Geschwindigkeitskonstante proportional zur Anzahl der OH- (bzw. CH-) Bindungen im Komplex ist [128, 150, 175]. Kropp und Windsor haben für Tb^{3+}- und Eu^{3+}-Ionen die Lumineszenzintensität und die Lumineszenzlebensdauer τ in reinem H_2O, D_2O und in verschiedenen Mischungsverhältnissen, sowie in verschiedenen deuterierten Lösungsmitteln untersucht [150, 175, 176]. Es wird ein ausgeprägter Isotopeneffekt beobachtet (s. Tabelle B.1).
Für die Lumineszenz wurde in allen Fällen eine Kinetik erster Ordnung gefunden, was u.a. darauf hindeutet, dass der Austausch zwischen den *freien* Lösungsmittelmolekülen und Lösungsmittelmolekülen aus der Koordinationssphäre sehr schnell ist im Vergleich zu τ. Als Richtgröße wird für Lanthanidionen für den Austausch von Lösungsmittelmolekülen aus der Koordnationssphäre eine Geschwindigkeitskonstante $k_{Austausch}$ von ca. $2 \cdot 10^7$ s^{-1} angegeben. Daher wird bei Messungen der Lumineszenzlebenszeit gewöhnlich eine mittlere Koordinationssphäre beobachtet [150].
In wässrigen Lösungen erfolgt die Desaktivierung der angeregten Zustände dieser Ionen sehr effektiv durch einen strahlungslosen Energietransfer auf die OH-Schwingungen des Wassers. Im Prinzip kann dabei die Energie auf eine einzelne Schwingungsmode, auf verschiedene Schwingungsmoden eines einzelnen Moleküls oder auf verschiedene Schwingungsmoden verschiedener Moleküle übertragen werden. Für die Desaktivierung der Europium- und Terbiumionen in Wasser wird der Energietransfer auf einzelne OH-Schwingungsmoden bzw. deren höher angeregte Zustände als der vorherrschende Mechanismus angesehen [135, 145, 175, 177]. Der Energieabstand zwischen dem Energieniveau, aus dem die Lumineszenz erfolgt und dem höchsten Schwingungsenergieniveau des Grundzustands beträgt für Europium ca. 12200 cm^{-1} und für Terbium ca. 14800 cm^{-1} [152]. Wird für die Energie der fundamentalen OH-Schwingungsmode 3600 cm^{-1} angesetzt, so werden zur Desaktivierung des Europiums $\Delta n = 4$ und für Terbium ein $\Delta n = 5$ benötigt, wobei n die Anzahl der Schwingungsquanten ist, die vom Lanthanidion auf die OH-Schwingung zu Desaktivierung übertragen werden. Dieser Desaktivierungskanal ist in D_2O sehr viel weniger effizient aufgrund der niedrigeren Frequenz der OD-Schwingungen. Mit zunehmender Energielücke zwischen Grund- und emittierendem Zustand in den Ln^{3+}-Ionen nimmt die Effektivität der Löschung durch OH- bzw. CH-Schwingungen ab [128, 168, 175]. Kann die elektronische Anregungsenergie nicht mehr auf eine einzelne Schwingungsmode übertragen werden (bei zu großem Energieabstand zwischen emittierendem Zustand und Grundzustand ist das der Fall), ist ein Isotopeneffekt nicht mehr ef-

fektiv wirksam (*energy gap law*) [168]. Wird die Energielücke andererseits zu klein, können andere Desaktivierungskanäle wirksam werden, wie z.B. über Schwingungen des gesamten Komplexes, auch dann wird kein (oder ein nur sehr kleiner) Isotopeneffekt beobachtet [168].
Aus Messungen der Lumineszenzlebensdauer von Ln^{3+}-Komplexen in H_2O und D_2O kann die Anzahl der koordinativ-gebundenen Wassermoleküle ermittelt werden [128, 135, 150, 175, 178]. Für verschiedene Komplexe von Terbium und Europium mit verschiedenen Liganden (z.B. Acetat, EDTA, Sulfat, Chlorid, Oxalat usw.) konnte so die mittlere Anzahl von Wassermolekülen in der ersten Koordinationssphäre bestimmt werden [128, 178]. Es wurde dabei davon ausgegangen, dass die beobachtete Lumineszenzlebensdauer zusammengesetzt ist aus der strahlungslosen und strahlenden Desaktivierung sowie einem Anteil, der nur von der Anzahl q der OH-Gruppen in der ersten Koordinationsspähre abhängt:

$$\tau_{beob.}^{-1} = \tau_{nat.}^{-1} + \tau_{nr}^{-1} + \tau_{OH}^{-1} \tag{3.1}$$

$$q = A_{Ln^{3+}} \cdot (\tau_{H_2O}^{-1} - \tau_{D_2O}^{-1}) \tag{3.2}$$

Der Parameter $A_{Ln^{3+}}$ ist eine empirische Konstante, die für jedes Ln^{3+}-Ion separat ermittelt werden muss. $A_{Eu^{3+}}$ wird mit 1.05 und $A_{Tb^{3+}}$ mit 4.2 angegeben für den Fall, dass τ_{H_2O} und τ_{D_2O} in ms eingesetzt werden [128, 172, 179]. Daneben gibt es noch eine Reihe weiterer einfacher empirischer Beziehungen, die einen Zusammenhang zwischen der Anzahl an Wassermolekülen in der ersten Hydratationssphäre der Ln^{3+}-Komplexe und der Lumineszenzlebensdauer herstellen [172]. Allerdings werden diese seltener benutzt.
Im Gegensatz zu organischen Molekülen und einer Reihe von d-Elementkomplexen wird die Lumineszenz der Ln^{3+}-Ionen durch Sauerstoff in Lösung nicht gelöscht [150, 175, 180].

3.1.3 Antenneneffekt und Energietransferprozesse

In wässrigen Lösungen wird durch die Komplexierung mit organischen Liganden in der überwiegenden Zahl von Fällen eine deutliche Zunahme der Lumineszenzintensität der Ln^{3+}-Ionen beobachtet. Diese wird einmal durch die Verdrängung von Wassermolekülen aus der ersten Hydratationssphäre und einer damit verbundenen effektiveren Abschirmung gegen die Desaktivierung durch OH-Schwingungen (s.o.) verursacht. Der zweite Grund liegt im sogenannten Antenneneffekt [156, 170]. In den Komplexen wird die Lichtenergie durch die Liganden absorbiert und in einem Energietransferschritt[4] auf das Ln^{3+}-Ion übertragen. Da die Extinktionskoeffizienten der organischen Liganden oft um den Faktor 10^3 bis 10^4 größer sind als die der Ln^{3+}-Ionen selbst, kann so auch bei wenig effizienten Energietransferprozessen zwischen Ligand (D) und Ln^{3+} (A) eine insgesamt deutliche Zunahme

[4]Die theoretischen Hintergründe zu den grundlegenden intra- und intermolekularen Energietransferprozessen sind im Anhang A zusammengestellt.

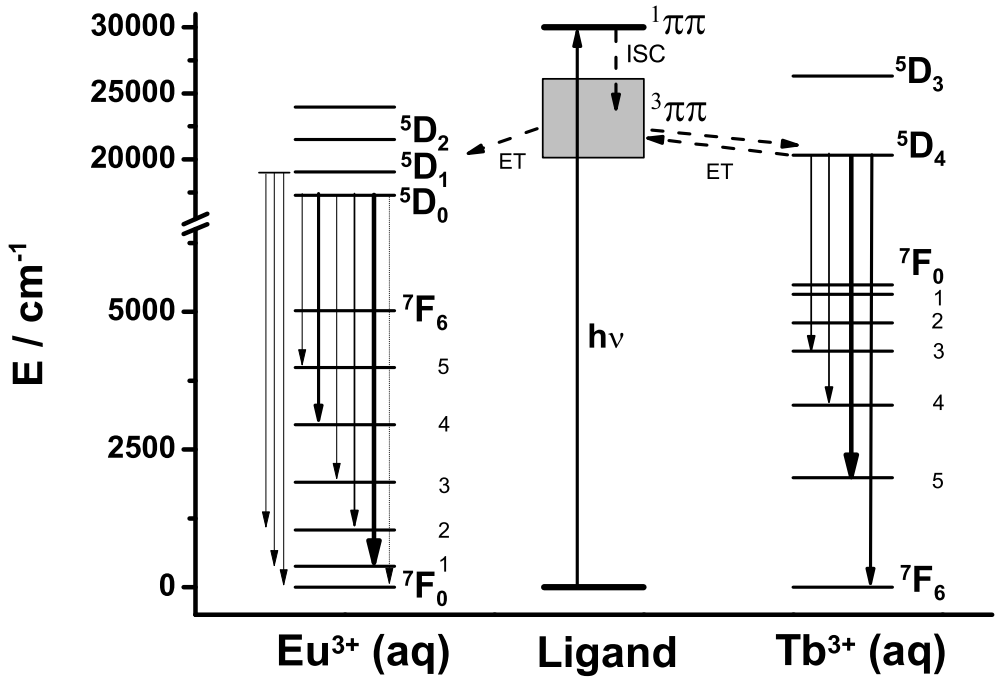

Abbildung 3.4: Energieniveauschema von Eu^{3+} und Tb^{3+} in Wasser (aq). Die Pfeile symbolisieren die als Lumineszenz bei Raumtemperatur sichtbaren Übergänge, wobei die Strichstärke die Intensität des jeweiligen Übergangs repräsentiert (Daten aus [152]). Weiterhin gezeigt sind die Energieniveaus eines hypothetischen Liganden sowie die möglichen Energietransferschritte (ET) vom Liganden auf das Ln^{3+}-Ion bzw. zurück zum Liganden (nach [170]).

der Ln^{3+}-Lumineszenzintensität beobachtet werden. Diese Lumineszenzverstärkung ist für eine sehr große Zahl der verschiedensten Typen von Liganden beschrieben [148, 156, 170, 181–183]. Die Lumineszenz von verschiedenen Europium- und Terbiumkomplexen kann z.B. sehr effektiv durch Carbonylverbindungen sensibilisiert werden [184–187]. In einigen seltenen Fällen wurde auch ein zusätzlicher *intermolekularer* Energietransferschritt beobachtet, bei dem die Energie von freien Ligandmolekülen auf den Komplex übertragen werden kann. Dieser Schritt ist diffusionskontrolliert und wird dementsprechend durch experimentelle Parameter wie Temperatur und Viskosität der Lösung stark beeinflusst [173, 186]. Für einige Kombinationen von Ligand / Ln^{3+} werden Verstärkungsfaktoren von bis zu 1100 berichtet [170, 184, 187, 188]. Auch wenn die Ln^{3+}-Ionen in Proteinen, wie z.B. Parvalbumin und Cadmodulin, gebunden werden (und dort Ca^{2+} isomorph ersetzen) wird ein Energietransfer von Tryptophan auf Eu^{3+} und Tb^{3+} beobachtet [189, 190].
Für einen effektiven Energietransfer zwischen Ligand und Ln^{3+}-Ion ist die relative

energetische Lage des Triplett-Zustands des Liganden und der relevanten Zustände der Ln^{3+}-Ionen (für Tb^{3+} das $^5D_4$-Niveau und für Eu^{3+} die $^5D_1$- bzw. $^5D_0$-Niveaus) entscheidend [148, 173, 186, 187, 191–193]. Dies ist in Abbildung 3.4 zusammenfassend dargestellt [170]. Neben der Energieübertragung auf das Ln^{3+}-Ion sind für Eu^{3+} und Tb^{3+} weiter Prozesse beschrieben, die gesteuert durch die relative energetische Lage von Ligand-Triplett-Zustand und lumineszierendem Niveau des Ln^{3+}-Ions zu einer strahlungslosen Desaktivierung führen können. Zum einen kann es zu einem effizienten Rücktransfer der Energie kommen, wenn die energetische Lage von Triplett-Zustand des Liganden und lumineszierenden Zustand des Ln^{3+}-Ions zu klein wird [148,170]. Für Tb^{3+} konnte gezeigt werden, dass eine Energiedifferenz von mehr als 1850 cm^{-1} zwischen beiden Zuständen notwendig ist, um einen effizienten Energierücktransfer zu verhindern [180, 188]. Daneben kann es in Eu^{3+}-Komplexen auch zu *Ligand-zu-Metall-Ladungsübertragungsreaktionen* (ligand-to-metal charge transfer, LMCT) kommen, in denen der Europiumkomplex im angeregten Zustand in einer f^7-Konfiguration vorliegt [138, 170]. Dies entspricht für Europium formal einer Oxidationsstufe von +II.
Die bereits angesprochene Unempfindlichkeit der Ln^{3+}-Lumineszenz gegenüber O_2 gilt nur für die Aquokomplexe oder Komplexe mit anorganischen Liganden. Ln^{3+}-Komplexe mit organischen Liganden zeigen eine Löschung der Lumineszenz durch O_2. Dabei handelt es sich um eine dynamische Löschung der Triplett-Zustände der Liganden, wie in zeitaufgelösten Messungen gezeigt werden konnte [180].

Interlanthanid-Energietransfer Neben den intramolekularen Energietransferprozessen zwischen Liganden und Ln^{3+}-Ionen wurde in Gläsern und Kristallen, die mit verschiedenen Ln^{3+}-Ionen dotiert waren, auch ein Interlanthanid-Energietransfer beobachtet. Häufig wurden Eu^{3+} und Tb^{3+} als Donatoren und verschiedene andere Ln^{3+}-Ionen (z.B. Nd^{3+}) als Akzeptoren eingesetzt. Als Mechanismus wird ein resonanter Energietransfer durch Quadrupol-Dipol-Wechselwirkung (s. auch Anhang A.2.2) vorgeschlagen[5] [147, 197–199]. Für kleine Abstände zwischen Donor- und Akzeptor-Lanthanidionen wird von Tanaka und Ishibashi allerdings der Austausch-Mechanismus favorisiert [199, 200]. Die bestimmten Geschwindigkeitskonstanten für den Energietransfer in zweikernigen Lanthanidkomplexen waren ca. ein bis zwei Größenordnungen zu hoch, um durch den Coulomb Mechanismus erklärt werden zu können. Der Abstand der Lanthanidionen in den untersuchten Komplexen betrug ca. 4 Å. Neben Festkörpern wurde auch in mehrkernigen Komplexen bzw. in Makromolekülen, die mehr als ein Ln^{3+}-Ion binden können, ein Interlanthanid-Energietransfer beobachtet. Für Komplexe mit Picolin- und Nicotinsäure, verschiedenen Carbonsäuren und Aminosäuren wurde in wässrigen Lösungen ein effektiver *inter*molekularer Energietransfer zwischen Eu^{3+} und Tb^{3+} gefunden. Dieser hängt sehr stark vom pH-Wert der Lösung ab. Je nach verwendetem Liganden können mehrere Disso-

[5] Häufig wird diese Art des Energietransfers auch als *Resonanzenergietransfer* (RET), Förster Resonanzenergietransfer, Fluoreszenz-Resonanzenergietransfer (FRET) bzw. im Falle von Lanthaniden Lumineszenz-Resonanzenergietransfer (LRET) bezeichnet [141, 194–196]. Zu den theoretischen Grundlagen von Energietransferprozessen s. Anhang A.

ziationsstufen des Liganden vorliegen, wodurch die Ausbildung von polynuklearen Komplexen begünstigt wird. In diesen ist der Interlanthanid-Energietransfer dann für den Fall, dass gemischte polynukleare Komplexe vorliegen, möglich [201–205]. In mehrkernigen Komplexen, die Cer und Terbium (oder Europium) enthielten, wurde eine Energieübertragung vom angeregten Cer zum Terbium (Europium) beobachtet [203]. Neben einem reinen Interlanthanid-Energietransfer wurden weitere Metallkationen als Akzeptoren in entsprechenden Komplexen verwendet. So wurde in verschiedenen Proteinen ein Energietransfer zwischen Eu^{3+} und Co^{2+}, beide an Protein gebunden, gefunden. Ebenso wurde Fe^{3+} als Energieakzeptor in Proteinen mit Eu^{3+} als Donor eingesetzt [128]. In diesen Fällen wird das Vorliegen eines Energietransfers nach dem Coulomb Mechanismus angenommen (LRET; s. auch Anhang A.2.2).
Durch die Untersuchung der Effizienz des Energietransfers zwischen Donor und Akzeptor läßt sich der Abstand der beiden auf molekularer Ebene bestimmen und durch Variation des Donor-Akzeptor-Paares kann eine Art *molekulares Lineal* erhalten werden, mit dem Abstände in der Größenordnung von einigen Å bis hin zu ca. 10 nm gemessen werden können [195, 196]. Zwischen der beobachteten Effizienz E des Resonanzenergietransfers und dem mittleren Abstand r zwischen Donor und Akzeptor besteht folgender Zusammenhang (s. auch Anhang A.2):

$$E = 1 - \frac{I_D}{I_{D,0}} = 1 - \frac{\tau_D}{\tau_{D,0}} \tag{3.3}$$

$$E = \left[1 + \left(\frac{r}{R_0}\right)^6\right]^{-1} \tag{3.4}$$

I_D und τ_D sind die Lumineszenzintensität bzw. die Lumineszenzlebensdauer des Donors, wobei der Index 0 die Größen in Abwesenheit eines Energieakzeptors bezeichnet. R_0 ist der sogenannte *Försterradius*, bei dem eine 50 %ige Wahrscheinlichkeit für einen Energietransfer besteht. Die für ein Donor-Akzeptor-Paar charakteristische Größe R_0 wird durch die spektroskopischen Eigenschaften des Paares bestimmt (s. Anhang A.2.2). Im Falle des Interlanthanid-Energietransfers liegen die Werte für R_0 im Bereich 5 Å bis 27 Å (s. Tabelle B.3).
Ein Beispiel für die Anwendung des Interlanthanid-Energietransfers zur Untersuchung von molekularen Strukturen sind Ca^{2+}-bindende Proteine. Durch isomorphe Substitution von Ca^{2+} in den Proteinen durch Eu^{3+} bzw. Tb^{3+} konnten die Abstände und die Struktur der Proteine in Lösung untersucht werden. Ein Untersuchung der funktionsfähigen Proteine mittels anderer Methoden (z.B. mikroskopischer) ist mit vergleichbarer Auflösung nicht möglich, da entweder die Auflösung von optischen Mikroskopen zu gering ist oder im Falle von Rastersonden-basierten Verfahren, die Proben aufwendig präpariert werden müssen und die Proteine dabei ihre Funktionstüchtigkeit einbüßen. Die aus den LRET-Untersuchungen ermittelten mittleren Abstände r der gebundenen Ln^{3+}-Ionen (z.B. an Thermolysin, Parvalbumin und Calmodulin) stimmen sehr gut mit aus Röntgenkristalluntersuchungen ermittelten Abständen der Metallbindungsplätze überein [128, 136, 137, 206].

3.1.4 Komplexierung von Ln^{3+}-Ionen durch HS

Polymaleinsäure-Derivate wurden als Modellpolymere zur Untersuchung der Komplexbildung mit Eu^{3+} verwendet. Aus zeitaufgelösten Lumineszenzmessungen wurde die Anzahl der koordinierten Wassermoleküle und die Komplexstöchiometrie abgeleitet. Es zeigten sich Parallelen zur Komplexierung durch HS [207–209]. Ausserdem wurden verschiedene Carbonsäure-Derivate als Modellsysteme zur Untersuchung der HS-Ln^{3+}-Komplexierung eingesetzt [164, 166, 210].
Für Actinide wie Cm^{3+} und Lanthanide wie Tb^{3+} ist eine Steigerung der Lumineszenzintensität in HS-Komplexen um ein bis zwei Größenordnungen beschrieben [164,211]. Der Energietransfer von HS auf komplexiertes Curium wird zur Speziation von Cm^{3+}-HS-Komplexen in natürlichen Wässern eingesetzt [161–163, 212, 213].
Durch die Wechselwirkung mit HS wird die relative Intensität der hypersensitiven Lumineszenzbande des Eu^{3+} bei 615 nm verändert, was ein direktes Indiz für die Komplexierung ist. Aus der Konzentrationsabhängigkeit des Verhältnisses der Lumineszenzintensitäten bei $\lambda_{em} = 593$ nm zu $\lambda_{em} = 615$ nm wurde die Komplexbildungskonstante für verschiedene HS mit Eu^{3+} bestimmt [82, 83, 165]. Eine Unterscheidung verschiedener Bindungsplätze in HS wurde basierend auf dem nichtentarteten $^7F_0 \rightarrow {}^5D_0$-Übergang des Eu^{3+} gemacht [78, 166]. Durch Peakentfaltung wurden zwei verschiedene Eu^{3+}-HS-Komplexbindungsplätze identifiziert, mit den Maxima bei 17271.1 cm^{-1} und 17265.4 cm^{-1}. Aus der Verschiebung der hypersensitiven Eu^{3+}-Lumineszenzbande und aus zeitaufgelösten Lumineszenzmessungen wurden von Thomason et al. auf mindestens vier verschiedene Bindungsplätze geschlossen - alle mit Carboxylgruppen als Liganden [167].
Die zeitaufgelösten Fluoreszenzspektren von Eu^{3+}-HS Komplexen zeigen eine deutliche Veränderung im Peakverhältnis I_{593nm}/I_{615nm}, was auf eine Veränderung der molekularen Umgebung im Eu^{3+}-HS-Komplex schließen lässt. Allerdings werden von Planque et al. keine Veränderungen in der Lumineszenzlebensdauer des durch HS komplexierten Eu^{3+} gefunden. Mit 110 μs entspricht die Lebenszeit der des Aquoions, woraus sich in der ersten Koordinationssphäre neun Wassermoleküle ableiten lassen und somit das Europium in HS als *outer-sphere* Komplex vorliegen würde [117]. Ebenso wird für Cm^{3+} und Dy^{3+} nur ein geringer Einfluss auf die Lumineszenzlebenszeiten durch HS-Komplexierung beschrieben [214]. In diesen Untersuchungen wurde eine 1:1-Komplexbildung zwischen HS und Ln^{3+} angenommen. Im Gegensatz dazu werden von Choppin et al. und Kim et al. nicht mono-exponentielle Lumineszenzabklingverhalten für Cm^{3+}- und Eu^{3+}-HS-Komplexen beschrieben [78, 213]. Die Heterogenität oder die Anwesenheit von Spuren weitere Metallionen in HS werden als mögliche Erklärungen für die beobachtete komplexe Abklingkinetik angeführt. Aus den Lumineszenzabklingkinetiken wurde die Anzahl der im HS-Eu^{3+}-Komplex an das Ln^{3+} gebundenen Wassermoleküle abgeschätzt. Unter Verwendung der Gl.(3.2) wurden abgeschätzt, dass durch die Komplexierung mit HS vier Wassermoleküle aus der ersten Koordinationssphäre des Eu^{3+} freigesetzt werden [167]. Allerdings wurde bei der Berechnung nur eine der aus einer bi-exponentiellen Anpassung erhaltenen Lumineszenzabklingzeiten berücksichtigt.

3.2 Löschung der intrinsischen Fluoreszenz durch Ln^{3+}-Ionen

In den folgenden Abschnitten 3.2.1 bis 3.2.3 werden eigene Arbeiten zur Charakterisierung der intrinsischen Fluoreszenz von Benzoesäure-Derivaten, Modell-HS und HS verschiedener Ursprungsorte sowie deren Löschung durch Ln^{3+} diskutiert. Bei den Benzoesäure-Derivaten handelt es sich um Hydroxy- und Methoxy-Derivate der Benzoesäure. Diese wurden als Modelle für einfache Strukturbausteine von HS untersucht und sind vor allem aus bekannten Abbauprodukten z.B. des Lignins abgeleitet [1,2,79,215,216]. Lignin selbst stellt einen, wenn nicht sogar den größten, Pool an Substanzen dar, aus dem HS durch biotische und abiotische Reaktionen gebildet werden. Gestützt werden diese Annahmen durch die aus neuen hochauflösenden massenspektrometrischen Untersuchungen abgeleiteten Strukturen von HS [15, 18].

3.2.1 Löschung der intrinsischen Fluoreszenz von Benzoesäure-Derivaten durch Ln^{3+}-Ionen

Die intrinsische Fluoreszenz von verschiedenen Benzoesäure-Derivaten ist in Abbildung 3.5 vergleichend dargestellt. Im Prinzip überstreicht die Fluoreszenz dieser Verbindungsklasse den gesamten Spektralbereich zwischen 300 nm $< \lambda_{em} <$ 600 nm. Zum Vergleich ist in Abbildung 3.5 das Fluoreszenzspektrum einer Braunwasser FA gezeigt. Die spektrale Überlappung und die Übereinstimmung in der Form der Spektren sind groß. Die Quantenausbeuten und die Sensitivität gegenüber pH-Wertänderungen dieser Verbindungsklasse sind sehr unterschiedlich. Besonders für die hydroxysubstituierten Derivate wird eine starke Abhängigkeit der Fluoreszenz vom pH-Wert beobachtet. Dies ist in der Hydroxygruppe begründet, die als so genannte *Photosäure* agieren kann, d.h. die Säurekonstante der OH-Gruppe ist im elektronischen Grundzustand und im elektronisch-angeregten Zustand mitunter um einige Größenordnungen unterschiedlich. Qualitativ läßt sich dieses Phänomen durch den nach Th. Förster benannten Förster-Zyklus beschreiben. Für aromatische Hydroxyverbindungen wird in der Regel eine Verschiebung zu kleineren pK_a-Werten erwartet. In der Praxis hängt das aber vom Verhältnis der Geschwindigkeitskonstanten der Desaktivierung des S_1-Zustands über intramolekulare Prozesse (Fluoreszenz und innere Konversion) zu der der Abspaltung des Protons aus der OH-Gruppe ab. Wie erste stationäre und zeitaufgelöste Fluoreszenzuntersuchungen gezeigt haben, sind beide Fallgruppen bei den hydroxysubstituierten Benzoesäuren vorhanden[6]. Die Fluoreszenzabklingzeiten der Benzoesäure-Derivate überstreichen einen weiten Bereich, von wenigen ps bis zu einigen ns, wobei der pH-Wert einen großen Einfluss hat [217]. Wie in Abbildung 3.6 am Beispiel der Fluoreszenzabklingkurven der 3-Methoxybenzoesäure gezeigt ist, sind die beobachteten Fluoreszenzkinetiken nur bei

[6]Diplomarbeit von Sascha Eidner, *Photodynamik substituierter Benzoesäuren*, Universität Potsdam, November 2004

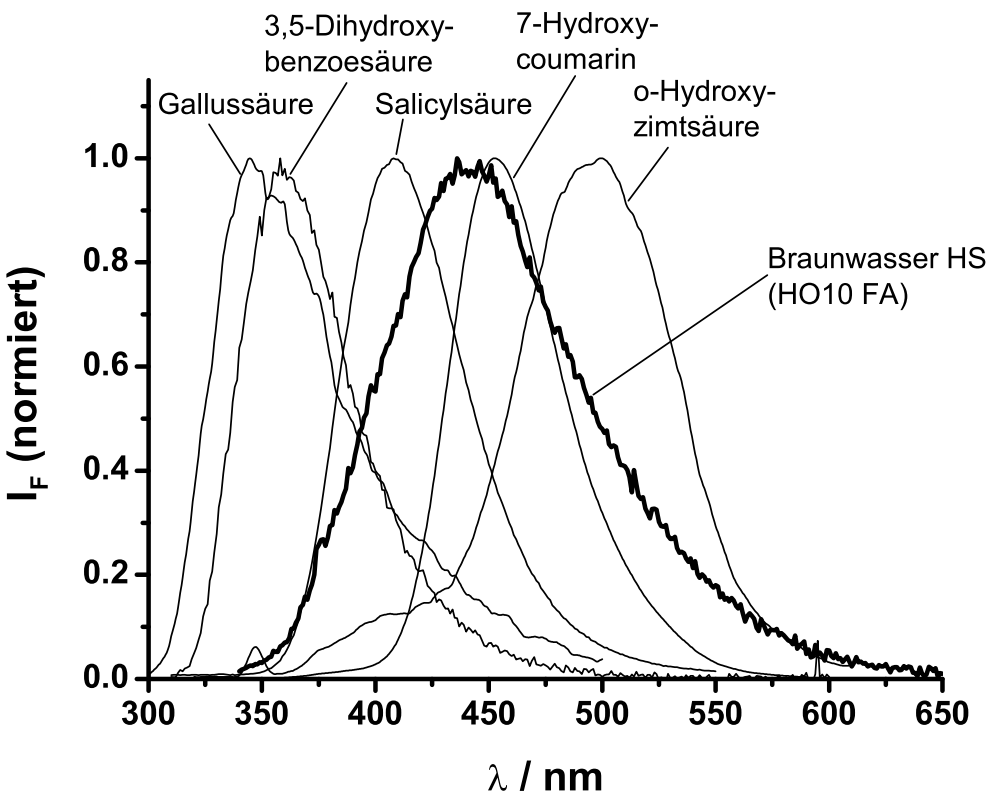

Abbildung 3.5: Fluoreszenzspektren verschiedener Benzoesäuren (c = 10^{-4} M, pH 6, λ_{ex}= 266 nm; Fluoromax, Yobin Yvon).

sehr kleinen pH-Werten bzw. sehr hohen pH-Werten mono-exponentiell, ansonsten werden komplexe Kinetiken höherer Ordnung gefunden, sehr ähnlich zu denen von HS (s. dazu z.B. Abschnitt 2.1.6). Die komplexen Abklingkinetiken werden durch das Vorliegen verschiedener Spezies, die durch Protonierung bzw. Deprotonierung der funktionellen Gruppen entstehen, verursacht. Hierbei sind sowohl Grundzustandsreaktionen wie auch Reaktionen im angeregten Zustand zu berücksichtigen.
Bei der Zugabe von Ln^{3+}-Ionen zu wässrigen Lösungen der Benzoesäure-Derivate wird keine (oder eine nur minimale) Fluoreszenzlöschung beobachtet. In Abbildung 3.7 sind die Fluoreszenzspektren von Gallussäure in Gegenwart verschiedener Tb^{3+}-Konzentrationen gezeigt. Es wird keine Abnahme der Fluoreszenzintensität beobachtet. Zu einem ähnlichen Ergebnis führt die Analyse der Salicylsäurefluoreszenz bei steigender Tb^{3+}-Konzentration (s. Abbildung 3.12) [183, 218]. Eine Fluoreszenzlöschung durch Tb^{3+} aufgrund eines Schweratomeffektes würde eine effektive Spin-Bahn-Kopplung zwischen den f-Elektronen des Ln^{3+} und den Elektronen des Liganden voraussetzen. Dies scheint nicht sonderlich ausgeprägt zu sein, mög-

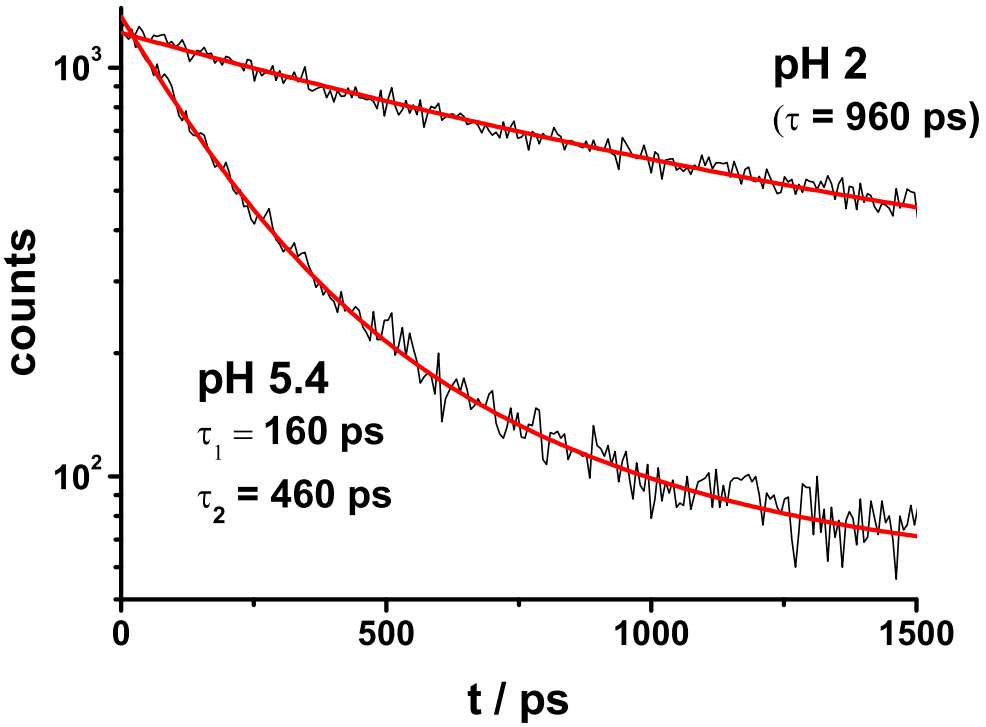

Abbildung 3.6: Fluoreszenzabklingkinetiken von 3-Methoxybenzoesäure (3-MBS) (c(3-MBS)= 10^{-4} M, λ_{ex}= 282 nm; Streak-Kamera, Hamamatsu). Die Fluoreszenzabklingzeiten sind durch eine globale Anpassung über den gesamten spektralen Bereich (340 nm $< \lambda_{em} <$ 420 nm) der 3-MBS Fluoreszenz erhalten worden (Das Streak-Kamera Messsystem wurde mit verschiedenen Fluoreszenzlebenszeitstandards kalibriert - s. dazu Anhang C.3).

licherweise weil die f-Orbitale durch die äußeren s, p und d-Orbitale weitestgehend abgeschirmt sind. Ein ähnliches Ergebnis wird für den Einfluss von Tb^{3+} auf die Fluoreszenz von Anthracen (c(Anthracen) = 1 μM in Methanol) gefunden. Für eine Tb^{3+}-Konzentration bis 10^{-4} M wurde keine Fluoreszenzlöschung beobachtet.

3.2.2 Löschung der intrinsischen Fluoreszenz von Modell-HS durch Ln^{3+}-Ionen

Die Beeinflussung der intrinsischen Fluoreszenz ist vollkommen verschieden von der bei den Benzoesäuren und auch bei den natürlichen HS beobachteten (s.u.). Mit steigender Tb^{3+}-Konzentration wird eine Verschiebung des Fluoreszenzmaximums und eine Fluoreszenzverstärkung beobachtet - ähnlich wie dies für die Komplexierung

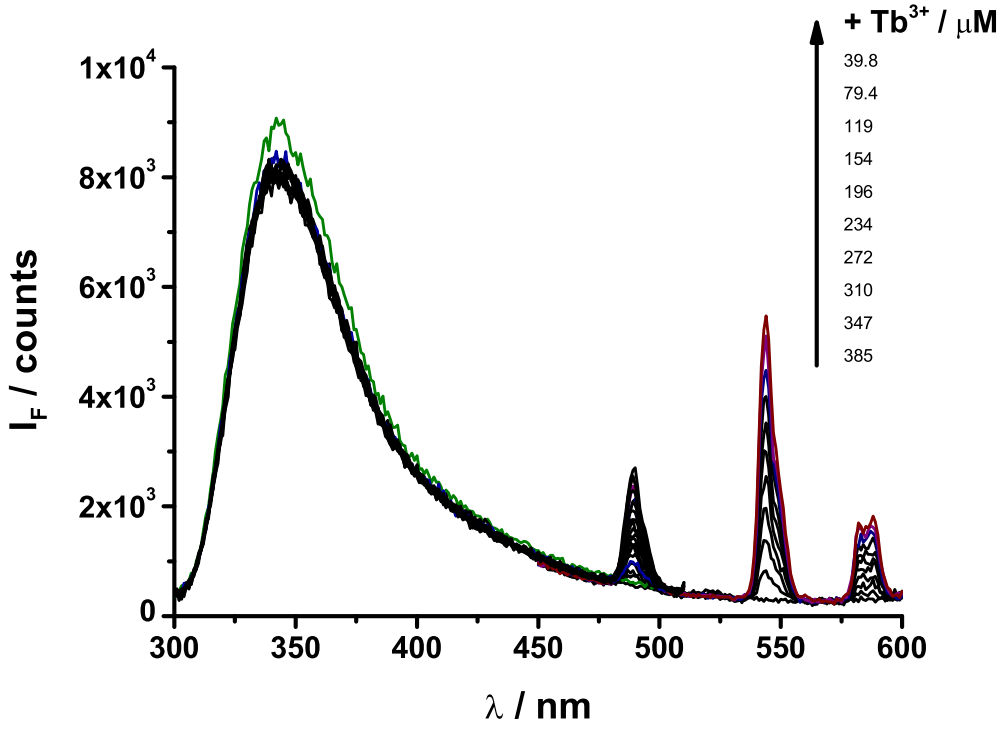

Abbildung 3.7: Löschung von Gallussäure durch Tb^{3+} (c(Gallussäure)= 10^{-4} M, λ_{ex}= 275 nm, pH 4; Fluoromax 3, Yobin Yvonne).

von Al^{3+}durch HS beschrieben wurde[7] [98]. Die spektrale Verschiebung ist besonders stark für die Probe M42 ausgeprägt (s. Abbildung 3.8). Im spektralen Bereich $\lambda_{em}>$ 500 nm wird eine leichte Abnahme der M42-Fluoreszenz gefunden, während bei Wellenlängen $\lambda_{em}<$ 475 nm eine Zunahme zu sehen ist. Insgesamt ist für die Proben M1 und M42 die gefundene Fluoreszenzverstärkung im Spektralbereich 400 nm $< \lambda_{em}<$ 460 nm sehr ähnlich. Die beobachteten Tendenzen sind für Tb^{3+} und Eu^{3+} qualitativ gleich (s. Abbildung 3.9).

3.2.3 Löschung der intrinsischen HS-Fluoreszenz durch Ln^{3+}-Ionen

In Abbildung 3.10 ist der typische Verlauf der Löschung der intrinsischen HS-Fluoreszenz mit steigender Konzentration von Tb^{3+} dargestellt. Im Gegensatz zu den untersuchten Benzoesäuren und den Modell-HS wurde für alle bislang untersuchten

[7] M.U. Kumke, H.-G. Löhmannsröben, S. Eidner, G. Korshin; 11th Meeting of the Inernational Humic Substances Society, 21. -26. July 2002 in Boston, USA. *Inter-Lanthanide luminescence resonance energy transfer in humic substances.*

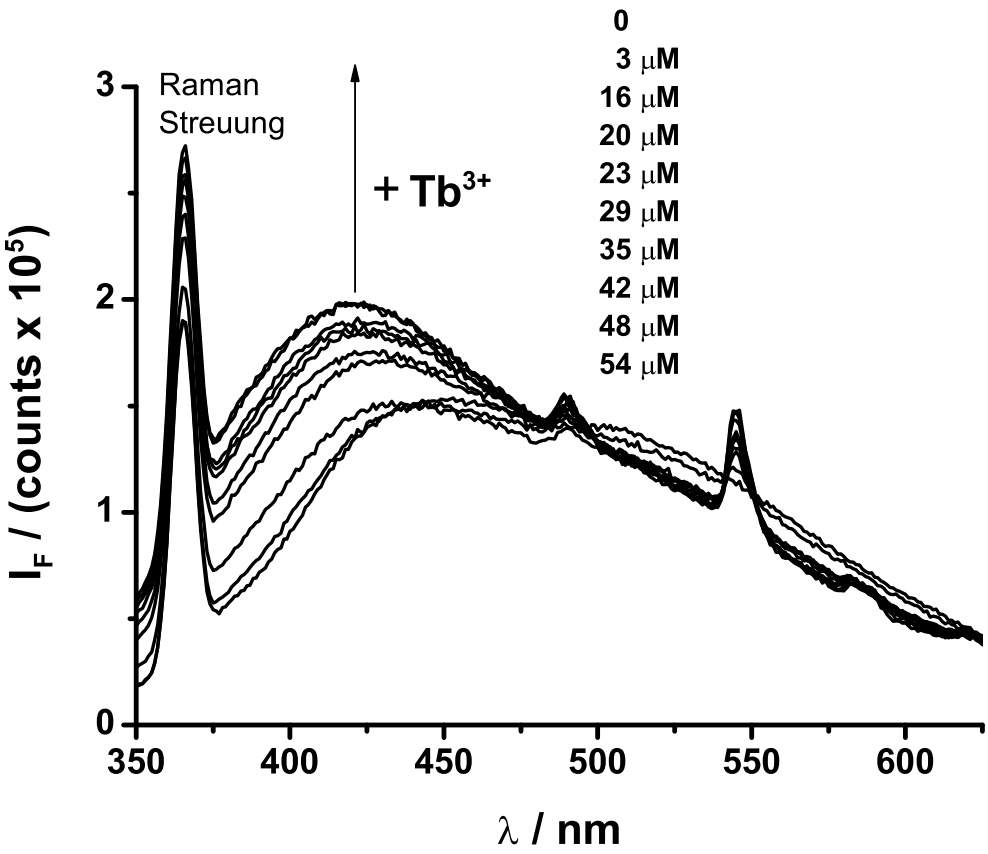

Abbildung 3.8: Löschung der Fluoreszenz des Modellhuminstoffs M42 durch Tb^{3+} (c(M42)= 10 mg/L, λ_{ex}= 325 nm, pH 5, I = 10^{-2} M; Fluoromax 3, Yobin Yvonne).

HS eine mehr oder weniger deutliche Löschung der intrinsischen HS-Fluoreszenz gefunden. In Abhängigkeit vom Ursprungsort der HS bzw. welche Fraktion (FA, HA) betrachtet wird, werden qualitative Unterschiede gefunden. So wird z.B. die Fluoreszenz von Gohy573 FA relativ stark gelöscht, im Fluoreszenzspektrum werden aber keine spektralen Veränderungen analog zu den für die Modell-HS beobachteten gefunden (s. Abbildung 3.10). Im Gegensatz dazu wird für Gohy573 HA quantitativ ebenfalls eine Fluoreszenzlöschung beobachtet, zusätzlich kann eine spektrale Verschiebung beobachtet werden (s. Abbildung 3.11). Die Löschung der intrinsischen HS-Fluoreszenz durch Komplexierung von Tb^{3+} oder Eu^{3+} ist abhängig vom Ursprungsort der HS. In Abbildung 3.12 ist die relative Abnahme der intrinsischen Fluoreszenz von HS verschiedener Ursprungsorte gegenübergestellt. Die eingezeichneten Trendlinien sind nach einem einfachen Modell von Ryan und Weber angepasst

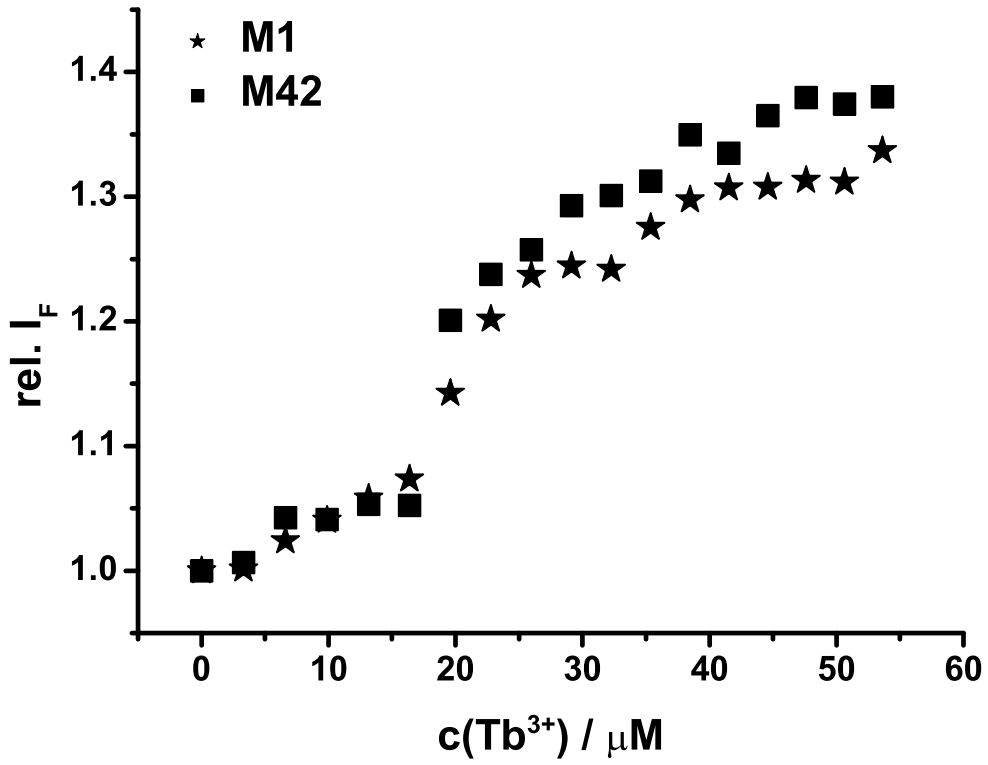

Abbildung 3.9: Einfluss von Tb^{3+} auf die Fluoreszenz von M1 und M42. Ausgewertet wurde die Fluoreszenz im Bereich 400 nm < λ_{em}< 460 nm (c(Modell-HS)= 10 mg/L, λ_{ex}= 325 nm, pH 5, I = 10^{-2} M; Fluoromax 3, Yobin Yvonne).

worden (s. Gl. 3.5) [99].

$$I = \frac{(I_{lim} - I_L)}{(2 \cdot K \cdot c_L)(K \cdot c_L + K \cdot c_M + 1)} - \sqrt{(K \cdot c_L + K \cdot c_M + 1)^2 - 4 \cdot K^2 \cdot c_L \cdot c_M} + I_L \quad (3.5)$$

In diesem wird von einer einfachen 1:1-Komplexierung zwischen HS-Molekülen und Metallionen ausgegangen[8]. Das einfache Modell gibt die experimentellen Daten erstaunlich gut wieder. Allerdings ist die Annahme eines 1:1-Komplexes eine grobe Vereinfachung. Ein spezielles Problem bei der Verwendung von Fluoreszenzlöschexperimenten zur Bestimmung von Komplexbildungskonstanten ist der unbekannte Zusammenhang zwischen Metallbindungsplätzen und Fluorophoren der HS [219, 220]. Ein Vergleich der Löscheffizienz von Tb^{3+} und Eu^{3+} zeigt Unterschiede zwischen den beiden Ln^{3+}-Ionen (s. Abbildung 3.13). Die Differenz in der beobachteten Löschung

[8] I = HS-Fluoreszenzintentsität; I_{lim} = durch weitere Zugabe von $M(= Me^{n+})$ nicht weiter löschbare HS-Restfluoreszenz; I_L = aus Normierung resultierender Faktor (1 oder 100%); K = Gleichgewichtskonstante des 1:1 Komplexes; c_M = Konzentration der Metallionen Me^{n+}

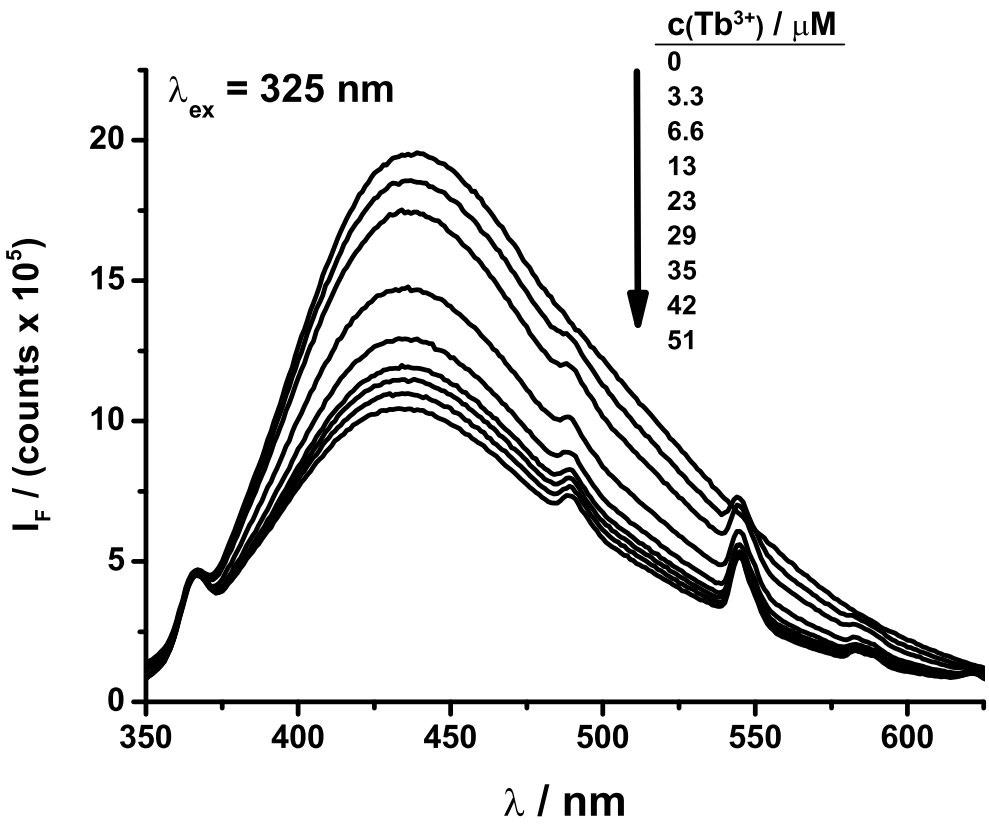

Abbildung 3.10: Löschung der Fluoreszenz einer HS (Gohy573 FA) durch Tb^{3+} (c(HS)=10 mg/L, λ_{ex}=325 nm, pH 5, I = 10^{-2} M; Fluoromax 3, Yobin Yvonne).

durch verschiedene Ln^{3+}-Ionen ist einerseits von den Ln^{3+} selbst abhängig, zusätzlich sind die beobachteten Unterschiede aber noch durch die HS (Ursprungsort, Fraktion) bestimmt. So ist die Differenz zwischen Tb^{3+} und Eu^{3+} für die Probe Gohy573 FA besonders stark ausgeprägt. Für die entsprechende HA-Fraktion der Probe wird eine deutlich kleinere Differenz gefunden. Die Gründe für die beobachteten Differenzen können in kleinen Unterschieden in den physiko-chemischen Eigenschaften der Ln^{3+}-Ionen liegen. So ist z.B. die Differenz in den Ionenradien zwischen Eu^{3+} und Tb^{3+} klein (92,3 pm für Tb^{3+} und 95 pm für Eu^{3+} [112]). Ebenso sind die bekannnten Bindungslängen der Ln-O-Bindung für beide Ln^{3+} sehr ähnlich [221]. Eu^{3+} unterscheidet sich aber von allen anderen Ln^{3+} in seiner Elektronegativität (EN). Der Vergleich zwischen Tb^{3+} und Eu^{3+} ergibt in der EN einen Unterschied von $\Delta EN = 1.716$ (bei einer für Lanthanide typischen Koordinationszahl von 10). Im Gegensatz dazu zeigen Tb^{3+} und Nd^{3+} nur einen Unterschied von $\Delta EN = 0.144$. Nd^{3+} sollte somit in der beobachteten Löscheffizienz dem Tb^{3+} ähnlich sein [221].

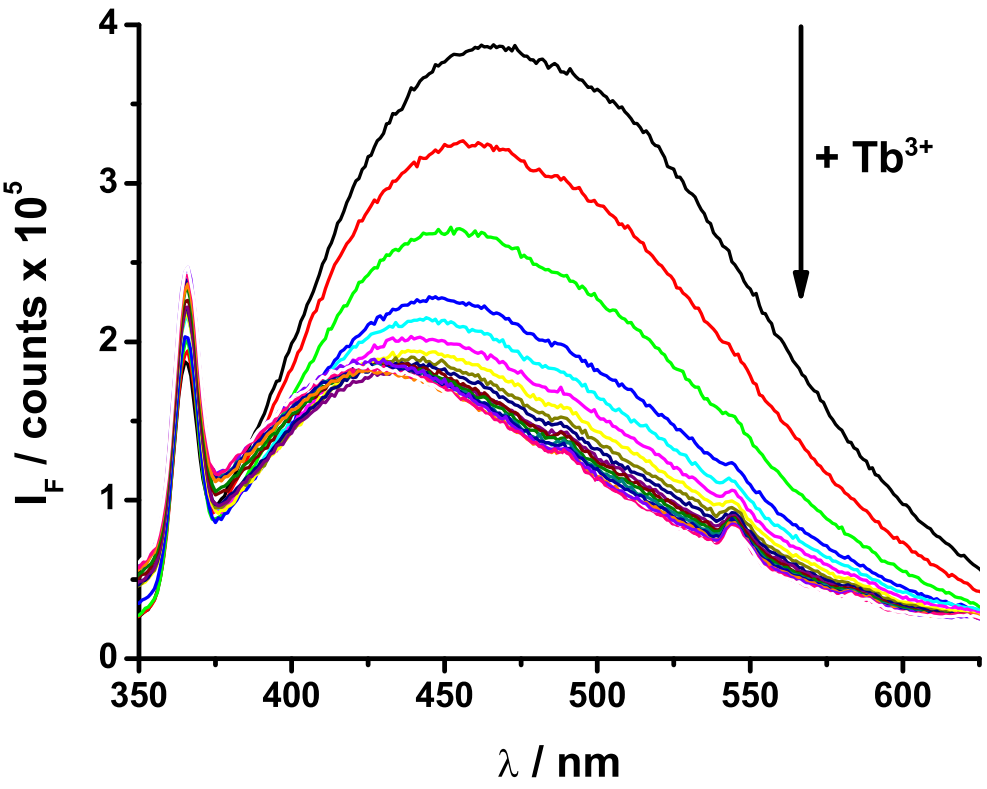

Abbildung 3.11: Löschung der Fluoreszenz einer HS (Gohy573 HA) durch Tb^{3+} (c(HS)=10 mg/L, λ_{ex}=325 nm, $0 < c_{Tb^{3+}} < 54$ μM, pH 5, I = 10^{-2} M; Fluoromax 3, Yobin Yvonne).

Möglicherweise wird ein Teil des komplexierten Eu^{3+} nach Photoanregung der HS zu Eu^{2+} reduziert und zeigt deshalb die größere Löscheffizienz.
Die konditionellen Komplexbildungskonstanten K für Tb^{3+}, Eu^{3+} und Nd^{3+} sind in Tabelle 3.1 zusammengefasst. Aufgrund der geringen Unterschiede in ihrem chemischen Verhalten sind diese für die verschiedenen Ln^{3+}-Ionen sehr ähnlich. Weitere Versuche mit anderen Ln^{3+}-Ionen sind geplant, um die z.T. stark unterschiedlichen Löscheffizienzen weiter zu untersuchen und die (erwarteten) geringen Unterschiede in β zu erhärten.
Der große Unterschied zwischen Benzoesäure-Derivaten und HS in Bezug auf die Löschung der intrinsischen Fluoreszenz deutet im Fall der HS auf eine Beteiligung von intramolekularen Prozessen, die der HS-Fluoreszenz vorgelagert sind, hin. Das können z.B. Prozesse sein, in denen nach erfolgter Lichtabsorption eine Ladungstrennung (*charge transfer*, CT) oder ein Protonentransfer erfolgt, mit dem dann eine Veränderung der HS-Struktur einher geht. Eine Komplexierung verändert in

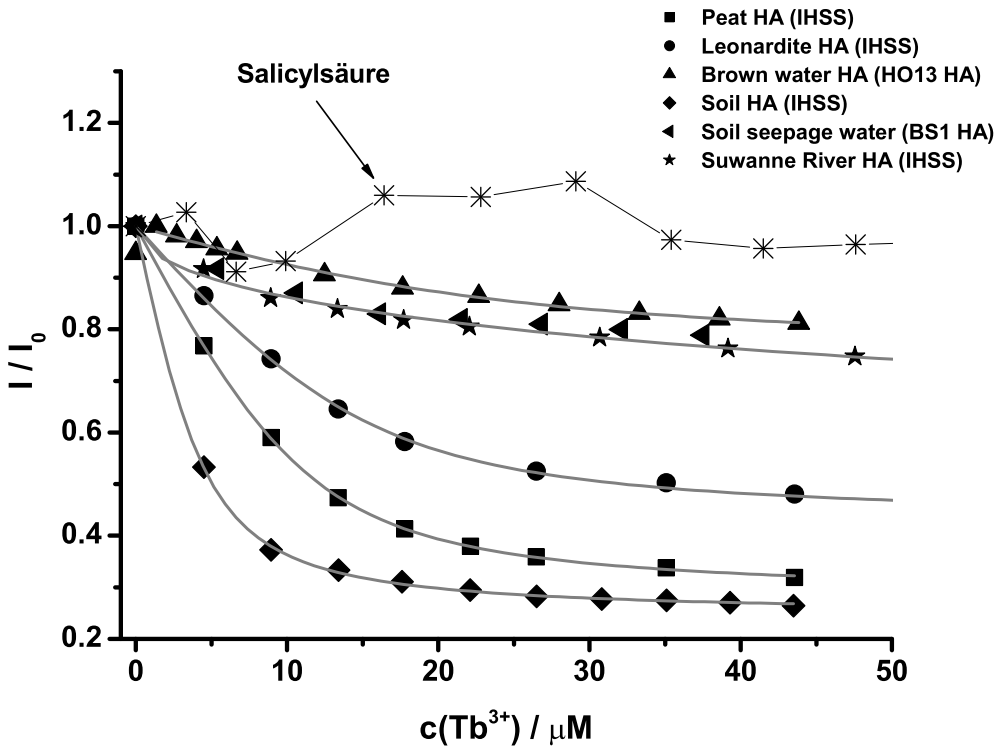

Abbildung 3.12: Übersicht der Löschung der Fluoreszenz verschiedener HS durch Tb^{3+}. Die Trendlinien sind nach dem Modell von Ryan und Weber angepasst worden (s. Gleichung 3.5) [99] (c(HS)=10 mg/L, λ_{ex}= 325 nm, λ_{em}= 425-475 nm, pH 5).

diesem Fall die Reaktionswege, wodurch als Nettoeffekt eine Veränderung der HS-Fluoreszenz beobachtet wird. Ein weiterer möglicher Mechanismus könnte die einschränkende Wirkung von Me^{n+} auf die Beweglichkeit (z.B. die Rotationsfreiheit von Bindungen) in einem HS-Molekül sein [222, 223]. Durch die Komplexierung von Me^{n+}-Ionen werden bestimmte Konformationen *eingefroren*, wodurch wieder eine Abnahme der Fluoreszenz verursacht wird - z.B. würde die Formation von verdrillten CT-Zuständen (*twisted intramolecular charge transfer*, TICT) beeinträchtigt werden. Der Einfluss von strukturbildenden Effekten der Me^{n+}-Ionen in HS wird durch die beobachtete HS-Fluoreszenzverstärkung durch Al^{3+}-Komplexierung sowie einiger anderer Me^{n+}-Ionen unterstrichen [223, 224]. Al^{3+} zeigt keine Spin-Bahn-Kopplung. In der Regel wird die HS-Fluoreszenz durch die Komplexierung von Al^{3+} verstärkt [98, 225, 226]. Eine ähnliche Fluoreszenzverstärkung wird bei der Zugabe von Borat oder Ga^{3+} beobachtet[9]. Daraus folgt, dass die Verwendung der intrinsi-

[9]Nicht veröffentliche Ergebnisse, vorgetragen auf der 44th International Conference on Analytical Sciences and Spectroscopy, 9 - 12 August 1998 in Kingston, Canada.

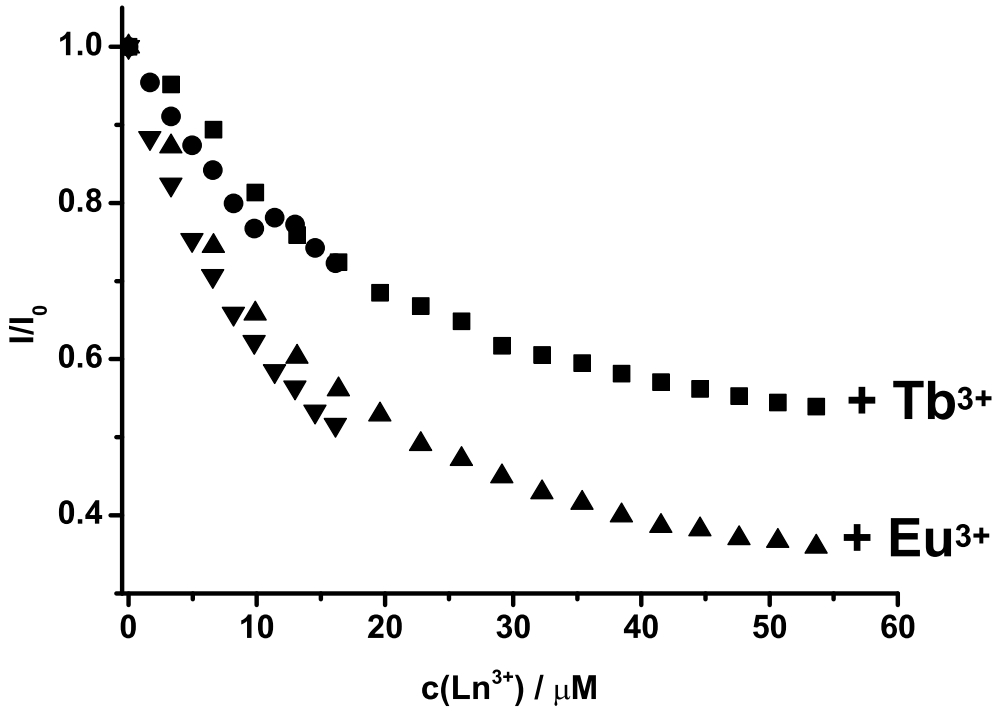

Abbildung 3.13: Vergleich der Löschung der Fluoreszenz einer HS (Gohy573 FA) durch Tb^{3+} und Eu^{3+} (c(HS)= 10 mg/L, λ_{ex}= 325 nm, pH 5, I = 10^{-2} M; Fluoromax 3, Yobin Yvonne). Dargestellt sind je zwei Messreihen. Ausgewertet wurde die Intensität der intrinsischen HS Fluoreszenz im Wellenlängeninterval 400 nm $< \lambda_{em} <$ 460 nm.

schen HS-Fluoreszenz zur Bestimmung von Komplexbildungskonstanten nur eingeschränkt benutzt werden kann. So muss z.B. sichergestellt sein, dass keine spektralen Veränderungen im HS-Fluoreszenzspektrum durch die Komplexierung von Me^{n+}-Ionen induziert werden. Diese große Schwäche wird prinzipiell bei der Auswertung der sensibilisierten Ln^{3+}-Lumineszenz umgangen, weil nur der Anteil der gebundenen Ln^{3+}-Ionen detektiert wird (s.u.) und zwar über die gut definierten, charakteristischen Lumineszenzbanden der Ln^{3+}-Ionen. Allerdings ist einschränkend zu beachten, dass für die Sensibilisierung der Ln^{3+}-Lumineszenz geeignete Chromophore (genauer gesagt Chromophore mit passenden Triplett-Zuständen) der HS vorhanden sein müssen. Außerdem ist der mögliche Rücktransfer der Energie zu einem Triplett-Zustand der HS zu beachten (s. Abbildung 3.4).

	$\log K$ **(in** $\mathbf{M}^{-1}$**)**		
$\mathbf{Ln^{3+}}$	**Aldrich HS**	**Gohy573 HA**	**Gohy573 FA**
Tb^{3+}	5.6	5.7	4.7
Eu^{3+}	5.7	5.1	5.1
Nd^{3+}	5.7	5.6	5

Tabelle 3.1: Bestimmung der konditionellen Komplexbildungskonstanten K aus der Löschung der intrinsischen Fluoreszenz von HS durch verschiedene Ln^{3+}-Ionen. Die Auswertung erfolgte nach Gl.(3.5). Bei den Ergebnissen für Gohy573 HA ist zu beachten, dass in diesem Fall im Fluoreszenzspektrum eine spektrale Verschiebung durch die Metallkomplexierung induziert wird, was die Aussagekraft der Daten einschränkt. Zur Datenauswertung wurde die Protonenaustauschkapazität der HS als Äquivalent für die vorhandenen Metallbindungsplätze verwendet (c(HS) = 10 mg/L, pH 5, I = 10^{-2} M, λ_{ex}= 325 nm, 400 nm < λ_{em}< 460 nm).

3.3 Antenneneffekte in den untersuchten Ln^{3+}-Komplexen

In den Abbildungen 3.7, 3.8 und 3.10 ist neben der Veränderung der intrinsischen Fluoreszenz der untersuchten Liganden die Lumineszenz des Tb^{3+} zu beobachten. Diese steigt mit zunehmender Konzentration immer weiter an. Eine qualitativ entsprechende Zunahme der Lumineszenz wurde auch in den Experimenten mit Eu^{3+} gefunden. Wichtig ist zu beachten, dass unter den gewählten experimentellen Bedingungen in reinem Wasser, keine Lumineszenz der Ln^{3+}-Ionen zu beobachten ist (s. z.B. Abbildung 3.18). In den Fluoreszenzexperimenten wurde die Anregungswellenlänge λ_{ex}= 325 nm bzw. 337 nm gewählt, da bei diesen Wellenlängen nur eine minimale direkte Anregung der untersuchten Ln^{3+}-Ionen erfolgt (s. dazu z.B. die Anregungsspektren der Ln^{3+}-Ionen in Abbildung 3.2) und somit die beobachtete Lumineszenz in erster Linie sensibilisiert ist.

3.3.1 Sensibilisierung der Ln^{3+}-Lumineszenz durch Hydroxy-Benzoesäuren

Obwohl die Fluoreszenz der untersuchten Benzoesäure-Derivate nicht (oder nur sehr gering) gelöscht wird, ist dennoch eine effektive Sensibilisierung der Tb^{3+}-Lumineszenz zu beobachten. Dies ist ein indirekter Beleg für die Komplexierung der Ln^{3+}-Ionen durch die Benzoesäure-Derivate. Die Sensibilisierung wird über einen strahlungslosen Energietransfer aus dem Triplett-Zustand der Benzoesäure-Derivate zum Ln^{3+} induziert[10]. Die Abfolge der Einzelschritte der Sensibilisierung sind in Abbildung 3.4 gezeigt. Allerdings ist zu bedenken, dass ein LRET-Prozess auch für den Fall von freien Liganden möglich ist [173, 186]. Ein Unterscheidung kann über Variation der Viskosität der Lösung gemacht werden, da diese Art des LRET diffusionskontrolliert sein sollte. Entsprechende Experimente stehen noch aus. In Abbildung 3.14 ist die Zunahme der Tb^{3+}-Lumineszenz als Funktion des Verhältnisses zwischen Tb^{3+} und Salicylsäure gezeigt. Bei einem Molverhältnis um eins, ist eine veränderte Steigung der Kurve zu erkennen. Dies kann als Hinweis auf einen Stöchiometriewechsel gedeutet werden, das also neben 1:1-Komplexen auch 1:2-Komplexe zwischen Tb^{3+} und Salicylsäure gebildet werden. Andererseits könnte die fortschreitende Sensibilisierung der Tb^{3+}-Lumineszenz - auch über das Verhältnis von 1:1 hinaus - durch einen Energietransfer zwischen ungebundener Salicylsäure und Tb^{3+}(aq) zustande kommen. Aus den Messungen der Lumineszenzabklingzeiten von Tb^{3+} in Gegenwart verschiedener Benzoesäure-Derivate ist zu sehen, dass abhängig vom Liganden inter- und intramolekulare Energietransferprozesse möglich sind. Während für Benzoesäure in den statischen Lumineszenzmessungen eine deutliche Sensibilisierung der Tb^{3+}-Lumineszenz gefunden wurden, verändert sich die Abklingzeit des Tb^{3+} nicht (s. Abbildung 3.15). Es werden Lumineszenzabklingzeiten τ von 390 μs

[10]Die grundsätzlichen Mechanismen des strahlungslosen Energietransfers sind im Anhang A.2 zusammengefasst.

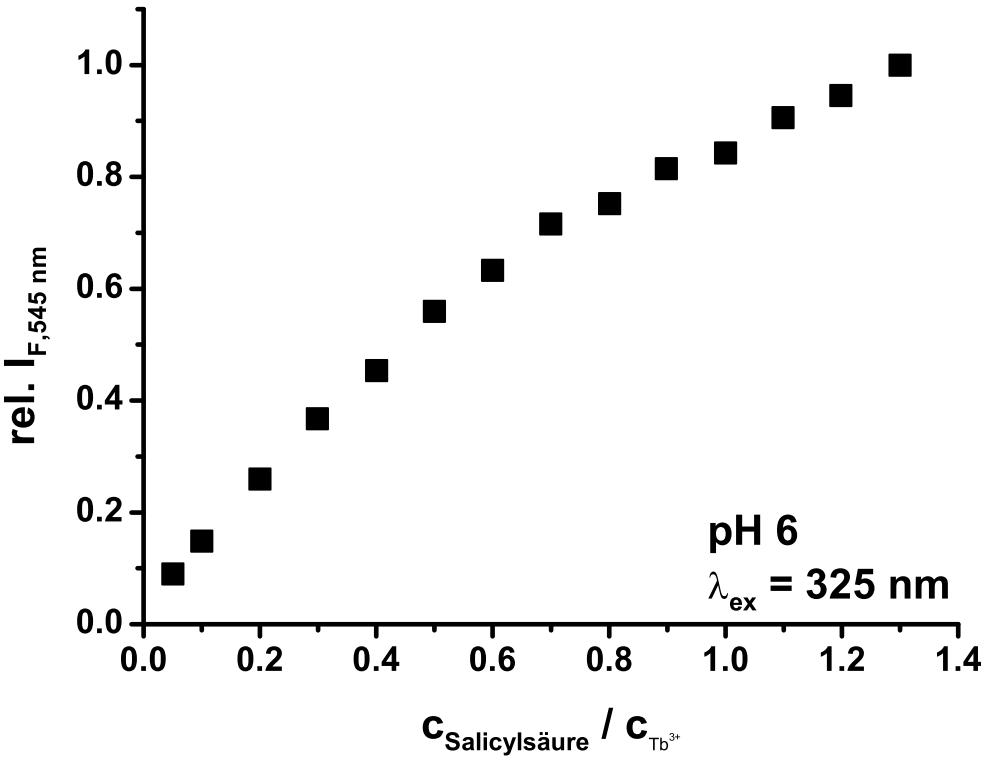

Abbildung 3.14: Verstärkung der Tb^{3+}-Lumineszenz durch Salicylsäure in Abhängigkeit vom Molverhältnis der beiden Partner (Die Signale sind auf den Intensitätswert der höchsten Salicylsäure-Konzentration normiert. Fluoromax 3, Yobin Yvon).

$\pm$ 10 μs gefunden, was den τ-Werten für Tb^{3+} in Wasser entspricht ($\tau_{Tb^{3+}}$(pH 6) = 390 μs). Für andere Liganden werden in Abhängigkeit vom Molverhältnis veränderte Lumineszenzabklingzeiten τ gefunden. Ab einem Molverhältnis von ca. 1 werden konstante Werte für $\tau_{Tb^{3+}}$ gemessen, die signifikant kürzer sind als für Tb^{3+}(aq). Bei zu kleiner werdenden Molverhältnissen von Ligand : Tb^{3+} steigt die beobachtete Lumineszenzabklingzeit an und nähert sich dem Wert für Tb^{3+}(aq). Dafür gibt es zwei mögliche Erklärungen: 1) es liegt immer mehr freies Tb^{3+} vor und experimentell wird ein Mix aus den Lebenszeiten von Tb^{3+}(aq) und Tb^{3+}-Ligand gefunden und 2) die Komplexe sind kinetisch sehr labil und es findet ein rascher Austausch der Liganden statt. Im ersten Fall sollte eine bi-exponentielle Luminezenzabklingkinetik gefunden werden. Dies war nicht der Fall. Das legt die Vermutung nahe, dass die Komplexe kinetisch labil sind, was nicht ungewöhnlich für Komplexe der Ln^{3+}-Ionen ist [120]. Kontrollexperimente, in denen die Viskosität der Lösung und das Lösungsmittel variiert werden, stehen noch aus und sollten Klarheit bringen. Die verkürzten Lumineszenzlebenszeiten in den Komplexen mit Benzoesäure-Derivaten deuten auf

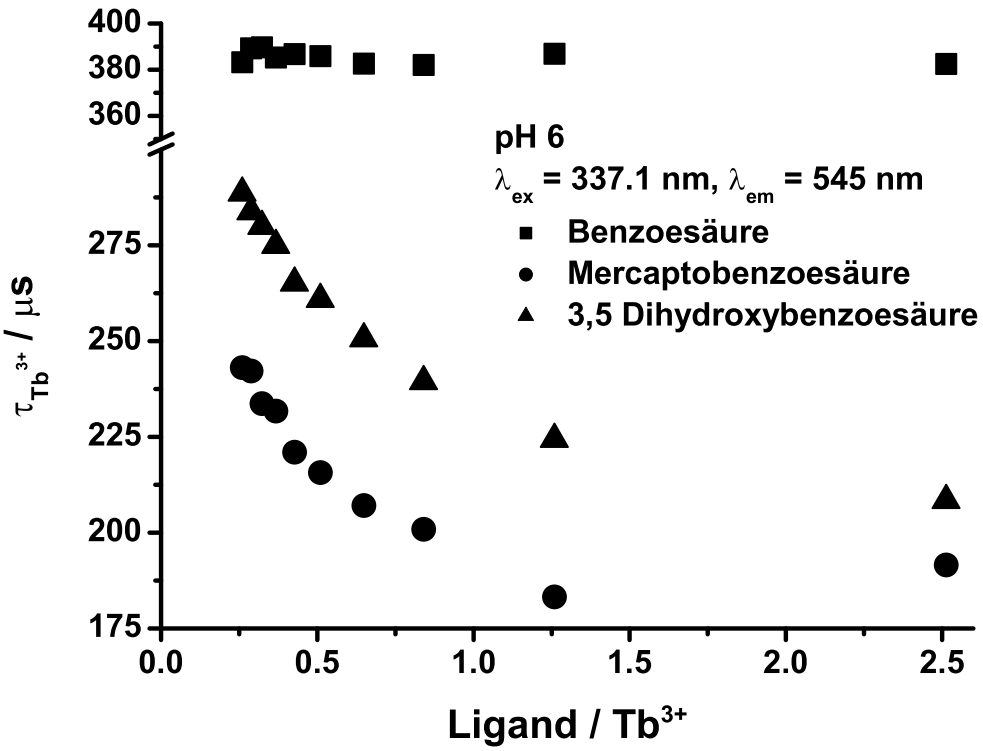

Abbildung 3.15: Abklingzeiten der Tb^{3+}-Lumineszenz in Gegenwart verschiedener Benzoesäure-Derivate in Abhängigkeit vom Molverhältnis der beiden Partner (FL920, μs-Modus).

einen Energierücktransfer zum Triplett-Zustand des Liganden hin. Die energetische Lage der Triplett-Zustände für viele Benzoesäure-Derivate liegt zwischen 20000 cm^{-1} und 25000 cm^{-1} [127, 227, 228] und somit in der Nähe des $^5D_4$-Zustandes von Tb^{3+} (20300 cm^{-1}).

3.3.2 Antenneneffekte in Komplexen zwischen Ln^{3+}-Ionen und Modell-HS

Für die untersuchten Modell-HS M1 und M42 wird eine Zunahme des Tb^{3+}-Signals beobachtet (s. Abbildung 3.8). Für Eu^{3+} wird zwar eine effektive Löschung der intrinsischen Fluoreszenz gefunden, aber in den stationären Spektren ist nur eine sehr schwache sensibilisierte Eu^{3+}-Lumineszenz zu beobachten. Eine Analyse der aus stationären Spektren erhaltenen Daten analog zu Tb^{3+} wurde daher nicht durchgeführt (s. dazu Abbildung 3.16). In zukünftigen Messungen werden zeitaufgelöste Lumineszenzspektren aufgenommen werden, die eine hintergrundfreie De-

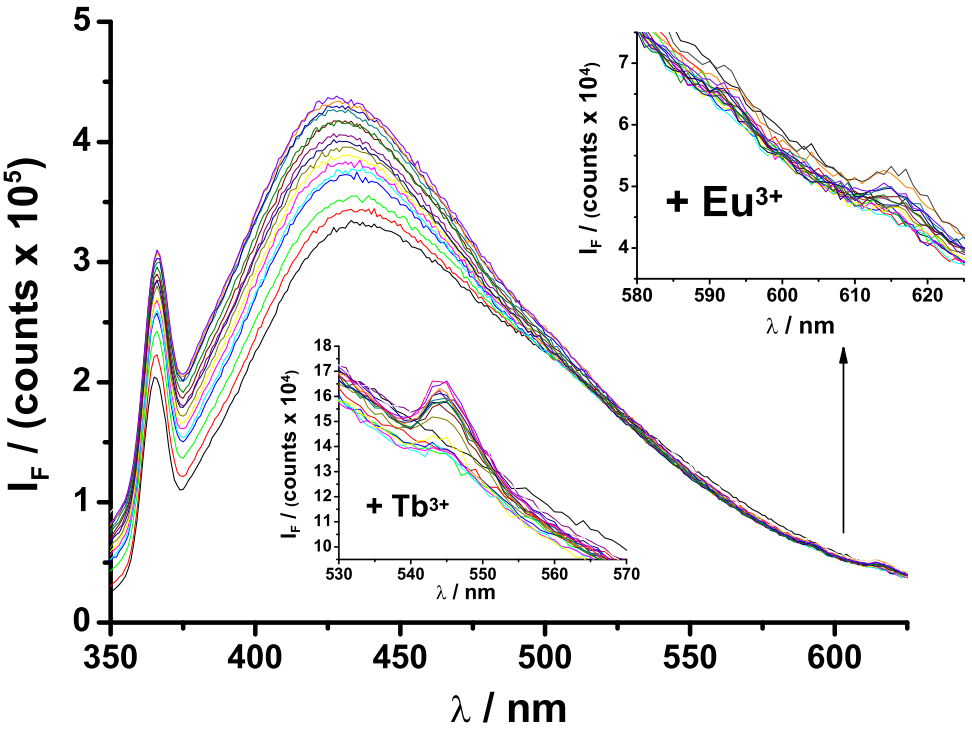

Abbildung 3.16: Fluoreszenzspektren von M1 in Gegenwart von Eu^{3+} (c(M1) = 10 mg/L, pH 5, λ_{ex}= 325 nm; Fluoromax 3, Yobin Yvon). In den Insets sind die jeweiligen Bereiche der Eu^{3+}- und Tb^{3+}-Lumineszenz vergrößert dargestellt.

tektion der sensibilisierten Eu^{3+}-Lumineszenz gestatten (s. dazu als Beispiel Abb. 3.18). Gründe für die schwache Sensibilisierung der Eu^{3+}-Lumineszenz können die Bildung von *charge-transfer*-Komplexen in den Europiumverbindungen und die im Vergleich zum Tb^{3+} niedrigere Energie des lumineszierenden Zustands sein, aufgrund der ein effektiverer Energierücktransfer möglich sein könnte. Ein Vergleich der Tb^{3+}-Lumineszenzsensibilisierung durch die Modell-HS M1 und M42 zeigt, dass der Modell-HS M42 einen deutlich stärkeren Effekt zeigt (s. Abbildung 3.20).
Die Wechselwirkung zwischen Ln^{3+}-Ionen und Modell-HS wird desweiteren in den zeitaufgelösten Lumineszenzmessungen charakterisiert. Für Tb^{3+} und Eu^{3+} werden in Gegenwart von Modell-HS komplexe Abklingkinetiken gefunden, die von einfachen Kinetiken ersten Ordnung abweichen. Die beobachteten Abweichungen im Zeitverhalten deuten auf das Vorhandensein von Energierücktransferprozessen hin, in denen Energie vom elektronisch-angeregten Ln^{3+}-Ion zurück auf den Modell-HS übertragen wird. Dieses Verhalten unterscheidet die Modell-HS von den untersuch-

ten Benzoesäure-Derivaten und entspricht dem bei HS beobachteten Verhalten[11].

3.3.3 Antenneneffekte in Komplexen zwischen Ln^{3+}-Ionen und HS verschiedener Ursprungsorte

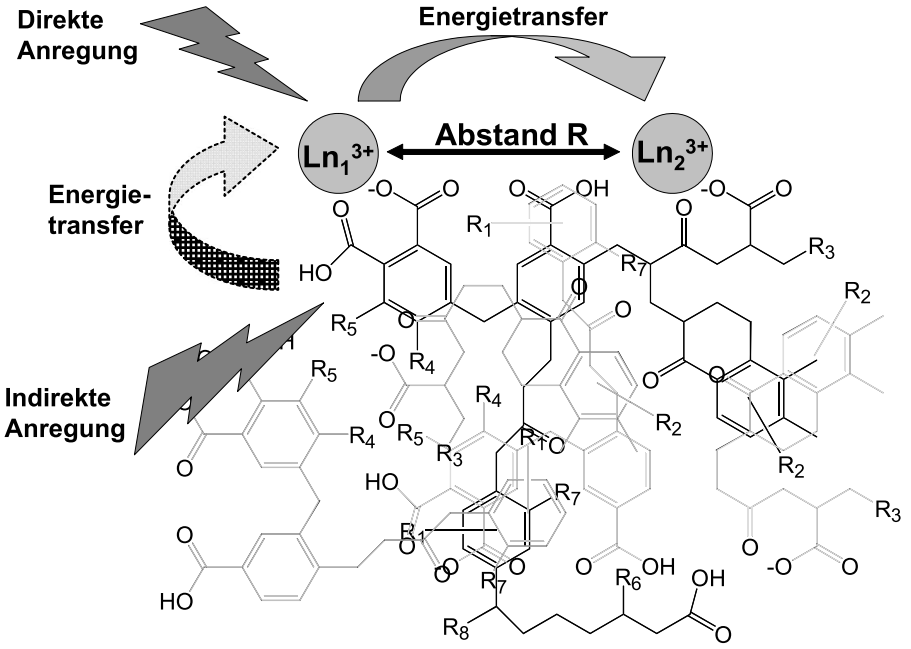

Abbildung 3.17: Energietransfer in HS-Ln^{3+}-Komplexen. Dargestellt ist sowohl der Fall der direkten Anregung, bei dem das Ln_1^{3+}-Ion zunächst direkt angeregt wird und dann in einem Energietransferschritt Energie auf das Ln_2^{3+}-Ion überträgt sowie der Fall der indirekten Anregung, in dem ein Chromophor im HS angeregt wird und dieser dann Energie auf das Ln_1^{3+}-Ion überträgt. Die gezeigte HS-Struktur ist hypothetisch und dient ausschließlich der Illustration.

In Abbildung 3.17 sind die möglichen Energietransferprozesse in HS-Ln^{3+}-Komplexen vereinfacht dargestellt. Da die Extinktionskoeffizienten der HS mit Sicherheit wesentlich größer sind als die der Ln^{3+}-Ionen und HS gewöhnlich ein äußerst breites, wenig strukturiertes - beginnend im UV-Bereich bis in den NIR-Bereich auslaufendes - Aborptionsspektrum[12] besitzen, kann es in HS-Ln^{3+}-Komplexen immer zu

[11] Zur Diskussion dieses Phänomens s. Kapitel 3.3.3, zeitaufgelöste Messungen.

[12] Genau genommen sind die in der Literatur beschriebenen Spektren eine Kombination von echter Absorption und Lichtstreuung, d.h. es handelt sich um Extinktionsspektren. Zur Bestimmung der echten Absorption müsste erst der Anteil der Lichtstreuung bestimmt werden [229].

einer indirekten Anregung der Ln^{3+}-Ionen via strahlungslosen Energietransfer kommen. Wie bereits in Kapitel 3.1.3 beschrieben ist dazu ein in seiner energetischen Lage passender Triplett-Zustand der HS notwendig [156, 170, 181]. Experimentell lässt sich der Energietransfer von HS auf Ln^{3+} in den veränderten Lumineszenzanregungsspektren der Ln^{3+}, im Anstieg der Lumineszenzintensität im Vergleich zu Ln^{3+}(aq) und im geänderten Lumineszenzabklingverhalten nachweisen.
Der Vorteil der indirekten Anregung der Ln^{3+}-Ionen ist, dass nur die komplexierten Ionen zur Lumineszenz beitragen. Da die Lumineszenzabklingzeiten der Ln^{3+}-Ionen und ihrer Komplexe im Mikrosekundenbereich liegen, die Fluoreszenzabklingzeiten der HS aber im Nanosekundenbereich, kann durch Schalten des Detektors die Messung frei von Beiträgen durch HS-Fluoreszenz sehr empfindlich durchgeführt werden (s. Abbildung 3.18) [164, 167, 230].

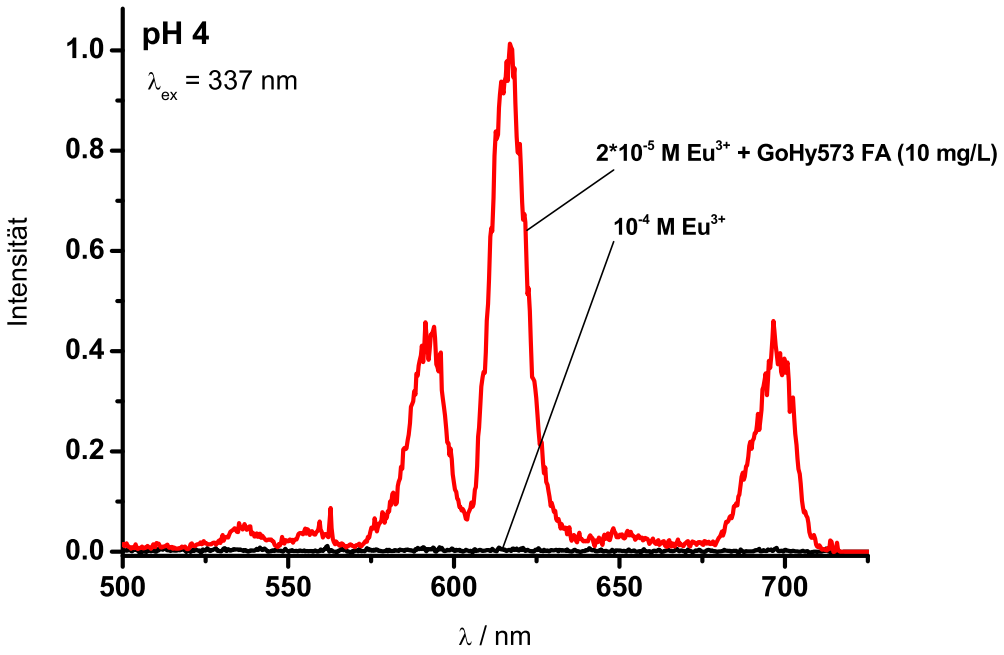

Abbildung 3.18: Zeitaufgelöstes Fluoreszenzspektrum (TRFLS) von Eu^{3+} in An- und Abwesenheit von HS (Verzögerung nach Anregungspuls $\Delta t = 1$ μs; iCCD, LOT).

Stationäre Messungen In Abbildung 3.10 ist neben der Löschung der intrinsischen HS-Fluoreszenz auch die Zunahme der Terbiumlumineszenz zu beobachten. Gleiches Verhalten wird für die Zugabe von Eu^{3+} zu HS-Lösungen gefunden. In Abbildung 3.18 ist das zeitaufgelöste Lumineszenzspektrum von Eu^{3+} in Ab- und Anwesenheit von HS gezeigt. Selbst bei fünffach größerer Konzentration ist unter den gewählten experimentellen Bedingungen keine Lumineszenz des Eu^{3+}(aq) sichtbar.

Erst durch die Sensibilisierung via Energietransfer von HS auf das komplexierte Eu^{3+} wird eine Lumineszenz messbar. Dass es sich um eine Komplexierung und somit um einen intramolekularen Energietransfer handelt, zeigt ein Vergleich des Verhältnisses der Lumineszenzintensitäten I_{595nm} zu I_{615nm} mit dem des $Eu^{3+}(aq)$ [152]. Das Verhältnis ändert sich für den Fall der HS-Komplexierung von 1.57 auf 0.46.

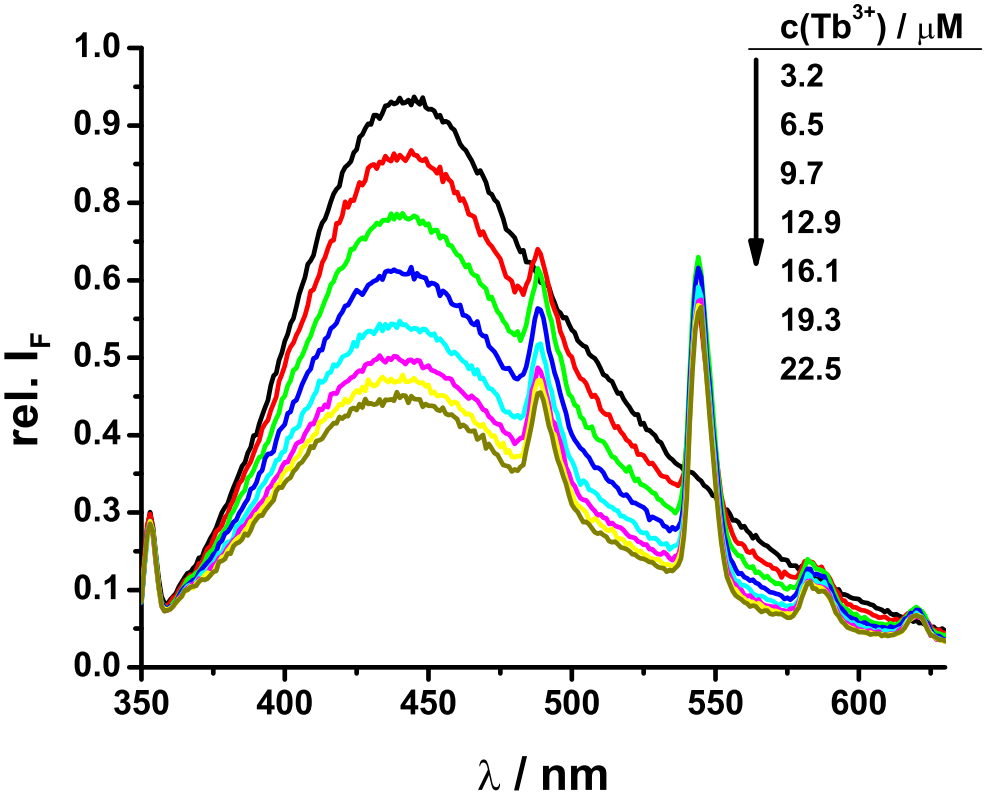

Abbildung 3.19: Löschung der HS-Fluoreszenz und Sensibilisierung der Tb^{3+}-Lumineszenz in D_2O (c(HPOA)=10 mg/L, λ_{ex}= 325 nm; Fluoromax 3, Yobin Yvonne).

Die beobachtete Sensibilisierung der Ln^{3+}-Lumineszenz ist in D_2O noch wesentlich stärker (s. Abbildung 3.19). Der beobachtet Isotopeneffekt ist ein Indiz dafür, dass selbst in Anwesenheit von HS noch Wassermoleküle in der ersten Hydratationssphäre des Ln^{3+}-Ions gebunden sind, die effektiv zur Desaktivierung des Ln^{3+}-Ions beitragen. Aus Messungen der Lumineszenzabklingzeiten in D_2O und H_2O wurde nach Gl.(3.2) die Anzahl der in der ersten Koordinationssphäre gebundenen Wassermoleküle zu 8.5 ± 0.5 bestimmt (s. Abbildung 3.23). Danach handelt es sich bei den Ln^{3+}-HS-Komplexen höchst wahrscheinlich um fast reine *outer-sphere*-Komplexe, möglicherweise sind ein oder zwei H_2O-Molekül aus der ersten Hydratationssphäre

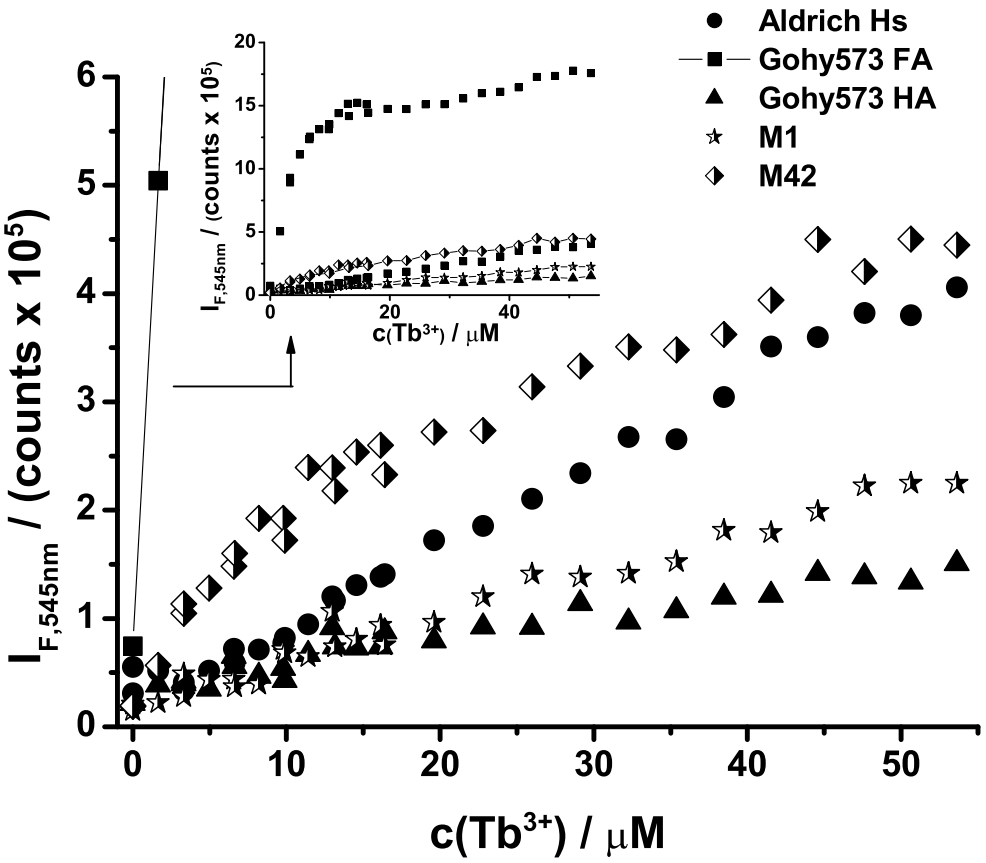

Abbildung 3.20: Übersicht der Tb^{3+}-Lumineszenzverstärkung durch Modell-HS, Gohy573 HS (FA, HA) und Aldrich HS (c(HS)=10 mg/L, λ_{ex}= 325 nm, pH 5, I = 10^{-2} M).

entfernt, je nachdem welche Koordinationszahl zugrunde gelegt wird.
In den Abbildungen 3.20 und 3.21 ist die Verstärkung der Tb^{3+}-Lumineszenz durch Komplexierung mit HS verschiedener Ursprungsorte gezeigt[13]. Im Gegensatz zur Löschung der intrinsischen HS-Fluoreszenz durch Tb^{3+}-Ionen, die für alle untersuchten HS als deutlich ausgeprägt gefunden wurde (s. Abbildung 3.12), wird eine Verstärkung der Tb^{3+}-Lumineszenz in den stationären Emissionsspektren nicht in gleichem Maße für die untersuchten HS verschiedener Ursprungsorte beobachtet. Für zwei IHSS Standardreferenz HS (Soil HA und Peat HA) wurde nur eine sehr geringe Sensibilisierung der Tb^{3+}-Lumineszenz gefunden, während andere HS vergleichbare

[13]Die in Abbildung 3.20 und 3.21 gezeigten Daten für Aldrich HS sind in ihrem Verlauf leicht unterschiedlich, da es sich einmal um eine gereinigte, d.h. im Metallgehalt abgereicherte Probe handelt und im anderen Fall (s. Abbildung 3.21) um die nicht weiter aufgereinigte kommerzielle Aldrich HS.

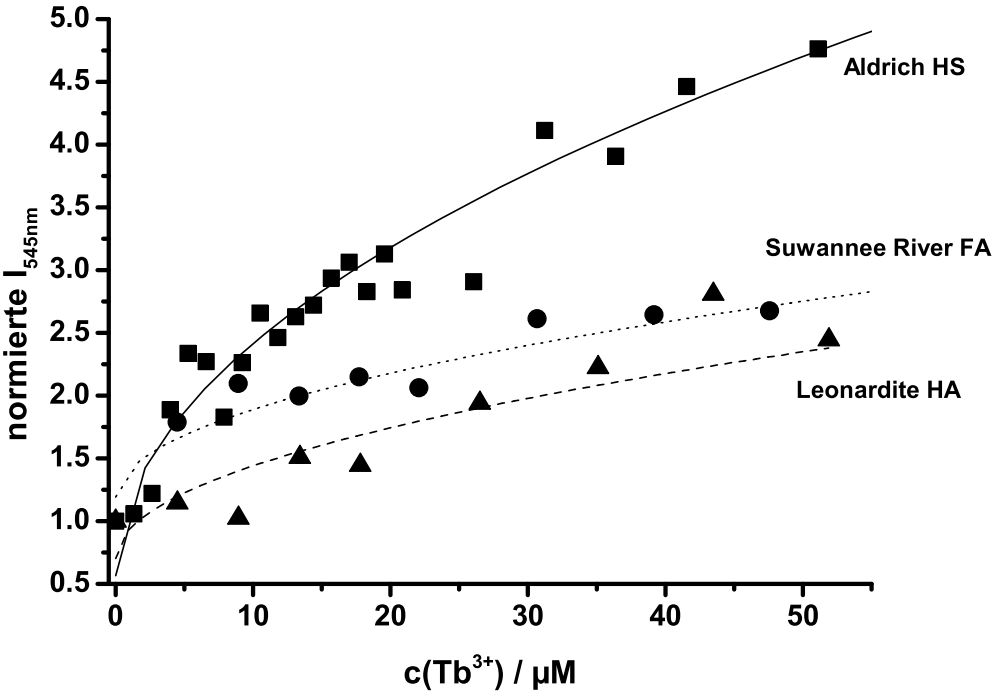

Abbildung 3.21: Übersicht der Tb^{3+}-Lumineszenzverstärkung durch HS von IHSS Referenz-HS (c(HS)=10 mg/L, λ_{ex}= 325 nm, pH 5). Die Daten sind normiert.

Ergebnisse zu den in Abbildungen 3.20 und 3.21 dargestellten lieferten (BS1 HA und HO10 HA). Inwieweit für die IHSS Standardreferenz HS (Soil HA und Peat HA) eine schwache sensibilisierte Lumineszenz in zeitaufgelösten Emissionsspektren gefunden werden kann, wird zurzeit in den laufenden Experimenten untersucht. Die intensive Hintergrundfluoreszenz der HS stellte in der Auswertung der stationären Fluoreszenzspektren ein Problem dar und eine Veränderung der Tb^{3+}-Lumineszenz gegenüber diesem starken Hintergrund der HS-Fluoreszenz war nicht vernünftig quantifizierbar. Das sollte in zeitaufgelösten Lumineszenzmessungen wesentlich zuverlässiger aufgelöst werden. Auffällig ist weiter die außergewöhnlich ausgeprägte Sensibilisierung der Tb^{3+}-Lumineszenz durch Gohy573 FA. In welchen HS-Eigenschaften dieses Ausnahmestellung begründet liegt, ist Gegenstand von zurzeit laufenden Arbeiten, in denen weitere FA-Fraktionen verschiedener HS untersucht werden.
Ebenso wie bei den Modell-HS war die beobachtbare Sensibilisierung der Eu^{3+}-Lumineszenz durch Komplexierung mit HS schwach. Die möglichen Gründe dafür wurden bereits in 3.3.2 diskutiert. Auch hier ist die Messung zeitaufgelöster Emissionsspektren geplant, die eine hintergrundfreie Aufnahme des Eu^{3+}-Signals erlauben werden. Ein Beispiel dafür ist bereits in Abbildung 3.18 gezeigt.

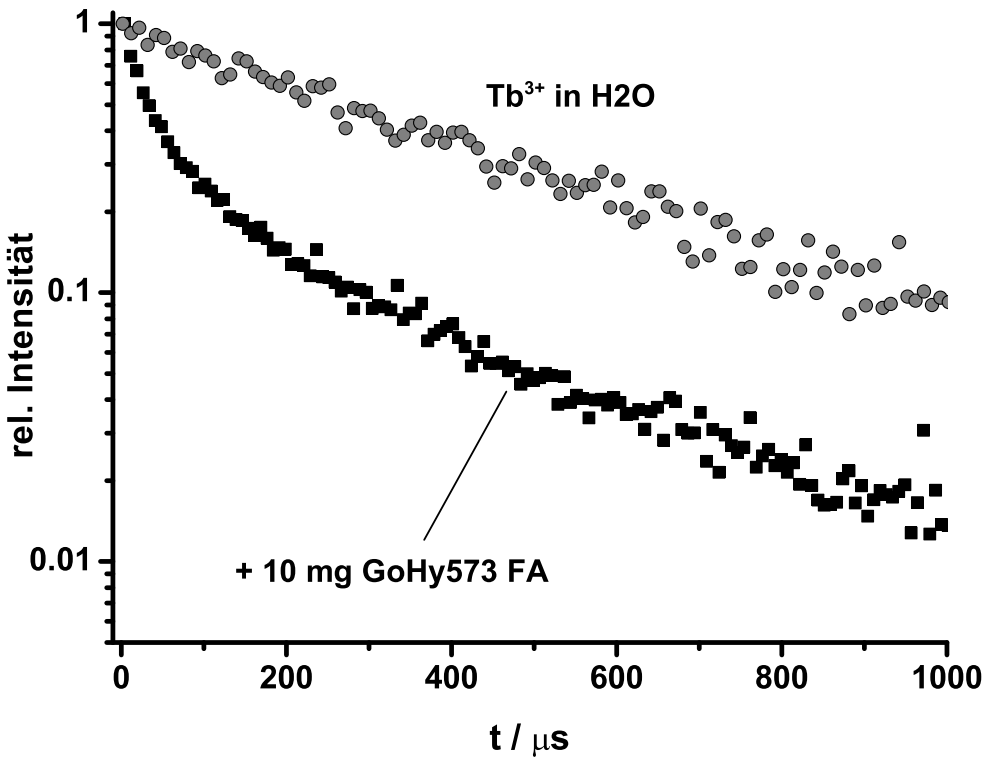

Abbildung 3.22: Lumineszenzabklingkurven von Tb^{3+} in An- und Abwesenheit von HS (λ_{ex}= 337 nm, c(Tb^{3+})=$1 \cdot 10^{-5}$ M, pH 4; iCCD, LOT). Für die Lumineszenzabklingzeit des Tb^{3+} (aq) wurden 401 μs bestimmt.

Zeitaufgelöste Messungen Die Komplexität der Wechselwirkung zwischen HS und Tb^{3+} ist auch im Zeitverhalten der Tb^{3+}-Lumineszenz zu sehen. Während das Tb^{3+}-Ion in Wasser eine monoexponentielle Abklingkinetik der Lumineszenz zeigt, wird das Lumineszenzzeitverhalten in Anwesenheit von HS komplexer. In Abbildung 3.22 sind die Lumineszenzabklingkurven von Tb^{3+} in An- und Abwesenheit von HS gezeigt. Gewöhnlich wird eine deutliche Zunahme der Fluoreszenzabklingzeiten nach Komplexierung mit organischen Liganden beobachtet, da Wassermoleküle aus der ersten Koordinationssphäre verdrängt werden und so die Desaktivierung über Kopplung an OH-Schwingungen verringert wird [156, 170, 188]. In den bislang untersuchten Tb^{3+}-HS-Komplexen ist dies allerdings nicht zu beobachten. Es werden durchweg Tb^{3+}-Lumineszenzabklingkurven gefunden, die deutlich vom monoexponentiellen Verhalten abweichen und insgesamt eine schnellere Lumineszenzabklingkinetik zeigen. Ein vergleichbares Verhalten ist für Eu^{3+} zu beobachten. Ebenso wird eine komplexe Lumineszenzabklingkinetik der Tb^{3+}-HS-Komplexe in D_2O gefunden. Zwar klingt die Lumineszenz auf einer deutlich längeren Zeitbasis ab, wie dies für

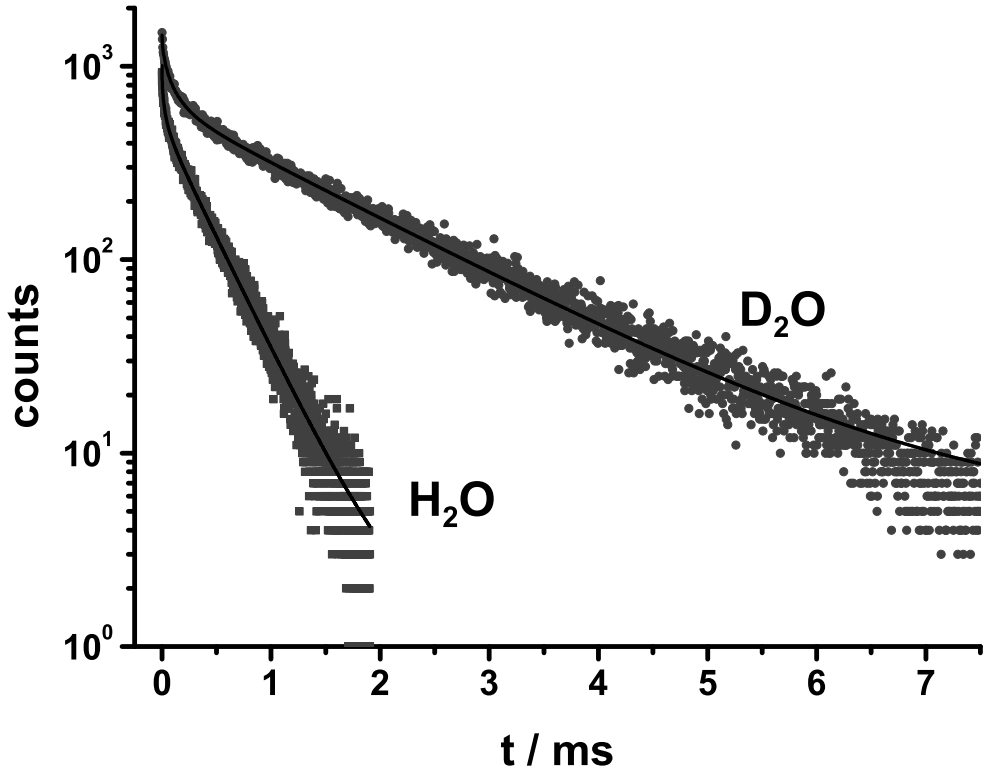

Abbildung 3.23: Lumineszenzabklingverhalten von Tb^{3+} in Gegenwart von HPOA in D_2O und H_2O (c(HPOA)=10 mg/L, λ_{ex}= 337 nm, pH 5). Die experimentellen Daten wurden nach Gleichung (3.7) mit nur einer Lumineszenzabklingzeit angepasst (τ_{D_2O} = 1.57 ms und τ_{H_2O} = 0.373 ms; FL920, μs-Modus).

den Austausch von OH- gegen OD-Schwingungskopplung erwartet wird, allerdings bleibt das nicht-exponentielle Abklingverhalten bestehen. In Abbildung 3.23 sind die Lumineszenzabklingkurven von Tb^{3+} in Gegenwart von HS (HPOA) für D_2O und H_2O gegenübergestellt. Das nicht-exponentielle Zeitverhalten bei kurzen Zeiten legt die Vermutung nahe, dass im Ln^{3+}-HS-Komplex intramolekulare Energietransferprozesse wirksam sind.
Für die Anpassung der kinetischen Daten können verschiedene Modelle herangezogen werden. Eine einigermaßen befriedigende Anpassung der experimentellen Daten kann durch eine biexponentielle Kinetik erhalten werden:

$$I(t) = A + B_1 \cdot e^{-\frac{t}{\tau_1}} + B_2 \cdot e^{-\frac{t}{\tau_2}} \tag{3.6}$$

Für die Komplexierung von Cm^{3+} durch HS ist ebenfalls eine vom monoexponentiellen Verhalten abweichende Lumineszenzabklingkinetik gefunden worden. Es wurde

angenommen, dass zwei verschiedene HS-Cm^{3+}-Komplexe vorliegen, die für die beiden beobachteten kinetischen Komponenten mit den Lumineszenzabklingzeiten τ_1 und τ_2 verantwortlich sind [212]. Gestützt wurde diese Annahme durch die Beobachtung, dass die Amplitudenverhältnisse B_1 zu B_2 mit dem Verhältnis von HS zu Cm^{3+} variieren. Werden experimentellen Abklingkinetiken der sensibilisierten Tb^{3+}-Lumineszenz analog zu Gl.(3.6) ausgewertet und wird bei der Anpassung eine globale Analyse durchgeführt, d.h. die Lumineszenzabklingzeiten τ_1 und τ_2 werden unabhängig vom Verhältnis Tb^{3+} zu HS angepasst und nur die relativen Amplituden B_1 und B_2 werden je Datensatz individuell angepasst. Dann ergibt sich für die beiden Amplituden in Abhängigkeit von der Tb^{3+}-Konzentration der für Sättigungskurven typische Verlauf (s. Abb. 3.24).

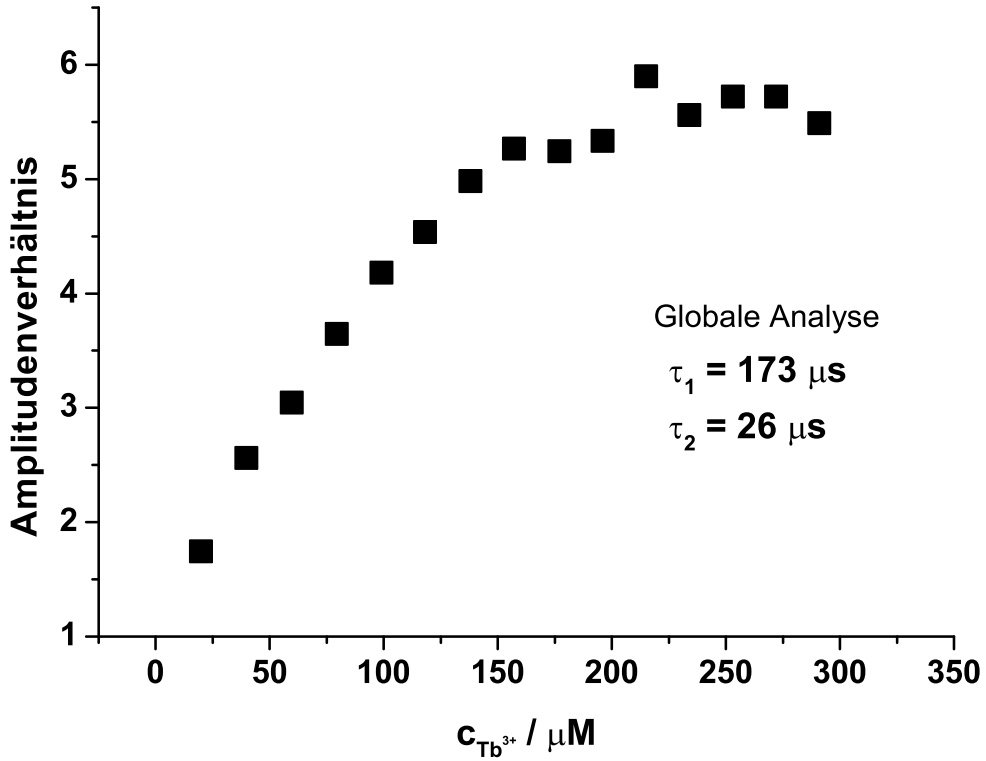

Abbildung 3.24: Amplitudenverhältnis B_2 zu B_1 aus der global bi-exponentiell ausgewerteten Lumineszenzabklingkinetik von Tb^{3+} komplexiert an HS (GoHy573 FA, 10 mg/L, λ_{ex}= 337 nm, pH 4; FL920, Edinburgh Instruments). Als globale Lumineszenzabklingzeiten wurden $\tau_1 = 173$ μs und $\tau_2 = 26$ μs) bestimmt.

Allerdings zeigt sich, dass besonders für kleine Tb^{3+}-Konzentrationen die Anpassung mit Gl.(3.6) nicht wirklich gut ist. In Abbildung 3.25 sind die experimentellen

	Gohy573 FA	**M42**
β	0.406	0.099
τ_D	284 μs	204 μs

Tabelle 3.2: Ergebnisse der Auswertung der Tb^{3+}-Lumineszenzabklingkurven nach Gl.(3.7).

Daten, sowie die durch globale Anpassung von Gl.(3.6) (gestrichelte Linien) erhaltenen Kurven für drei Tb^{3+}-Konzentrationen beispielhaft dargestellt. Markant sind die Abweichungen zwischen experimentellen und angepassten Daten speziell bei langen Zeiten, dort wird der Kurvenverlauf durch eine biexponentielle Abklingkinetik nicht passend wiedergegeben.
Der beobachtete zeitliche Verlauf der Lumineszenzintensität kann auch durch einen Energierücktransfer vom Tb^{3+} auf HS bedingt sein. Ein Phänomen, dass schon für eine Reihe von anderen Tb^{3+}-Komplexen bekannt ist [156,170]. Unter der Annahme, dass es sich um einen Dipol-Dipol-basierten Energietransfer-Mechanismus handelt, wurden die Daten nach Gl.(3.7) ausgewertet.

$$I(t) = A + B_1 \cdot \exp\left(-\frac{t}{\tau_D} - P \cdot \left(\frac{t}{\tau_D}\right)^{\beta}\right) + B_2 \cdot \exp - \left(\frac{t}{\tau_D^{\star}}\right) \tag{3.7}$$

Mit Hilfe dieser gedehnten Exponentialfunktion wurden bereits nicht-exponentielle Lumineszenzabklingkinetiken in verschiedensten heterogenen Systemen analysiert [231–237]. Dabei wurde die Heterogenität der Probe einerseits in der ungleichmäßigen Verteilung von Fluorophoren (oder speziell von Donor und Akzeptor) verursacht oder aber durch geometrische Einschränkungen des Systems, wie sie z.B. in Zeolithen oder anderen porösen Materialien gefunden werden [238–245]. In letzteren sind durch die eingeschränkte Geometrie der Matrix auf molekularer Ebene Wechselwirkungen nicht kontinuierlich über alle Raumwinkel bzw. -entfernungen möglich. Ebenso wird in lichtstreuenden Lösungen oft eine Abweichung der experimentellen Daten von einfachen monoexponentiellen Verhalten gefunden [246]. Formal entspricht Gleichung (3.7) dem Zeitverlauf, der für den Fall einer diffusionskontrollierten Energieübertragung nach Förster für homogene Lösungen gefunden wird, wobei dann $\beta = 0.5$ ist. In Polymeren und Systemen (z.B. Zeolithe, Dendrimere), in denen nur eine eingeschränkte relative Bewegung von Donor und Akzeptor möglich ist, kann $\beta \neq 0.5$ sein. Für diese Fälle wird β der Charakter einer fraktalen Dimension zugeschrieben [239, 240, 247]. Zusätzlich wurde ein weiterer Exponentialterm angefügt, um einem Anteil von komplexiertem Tb^{3+} Rechnung zu tragen, der keinem Energierücktransfer zu HS unterliegt[14].

[14]Die Lumineszenzabklingzeit τ_D und $\tau_D^{\star}$ sind in diesem Fall gleich. Es ist außerdem vernünftig anzunehmen, dass die Lumineszenzabklinzeit τ_D einer mittleren Abklingzeit einer Verteilung entspricht, da höchst wahrscheinlich mehr als zwei diskrete Bindungsplätze in HS vorhanden sind. Der Parameter P skaliert mit dem Abstand zwischen Donor und Akzeptor

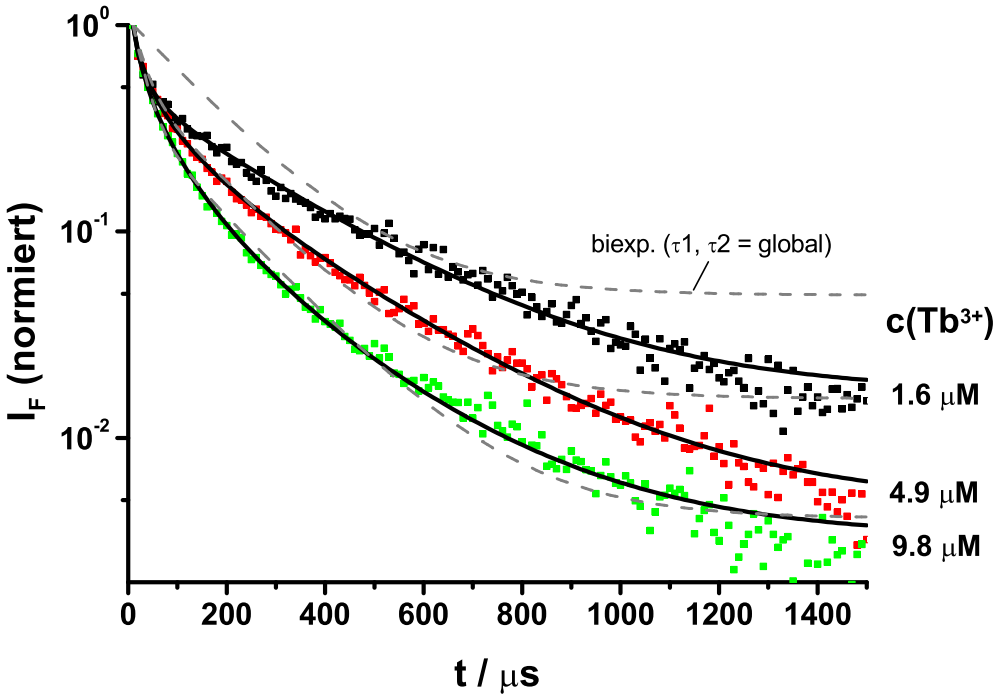

Abbildung 3.25: Anpassung der Tb^{3+}-Abklingkinetik in Anwesenheit von HS für verschiedene Tb^{3+}-Konzentrationen (GoHy573 FA, 10 mg/L, λ_{ex}= 337 nm, pH 5, I = 10^{-2} M; iCCD, LOT). Die experimentellen Daten wurden global bi-exponentiell und mit Gl.(3.7) ausgewertet.

In den Anpassungen der Lumineszenzabklingkinetiken der Tb^{3+}-HS-Komplexe wurde eine gute Übereinstimmung zwischen experimentellen und durch das Model beschriebenen Daten erhalten (s. Abbildung 3.25). In neuesten Experimenten wurden Untersuchungen mit synthetischen HS, die als Reaktionsprodukte verschiedener Aminosäuren und Zucker erhalten wurden, durchgeführt. In den zeitaufgelösten Lumineszenzmessungen wurden auch für diese Systeme nicht-exponentiell abklingendes Zeitverhalten gefunden und eine Auswertung nach Gl. (3.7) lieferte gute Anpassungsergebnisse. Es ist interessant, dass der Wert für β für die beiden bisher untersuchten HS sehr unterschiedlich war (s. Tabelle 3.2). Im laufenden BMWA-Forschungsvorhaben Spektroskopische Bestimmung von thermodynamischen und kinetischen Kenngrößen zur Beschreibung der Huminstoff-Metall-Komplexierung werden diese Arbeiten in Zukunft fortgesetzt und weitere HS untersucht werden.

3.4 Interlanthanid-Energietransfer in Ln^{3+}-HS-Komplexen

Ein fundamentales Problem der Untersuchung von HS ist die Heterogenität der Proben, u.a. ist daher die Angabe *einer* HS-Struktur aussichtslos. Das Assoziationsverhalten, die Bildung von Kolloiden oder die Sorptionseigenschaften von HS sind Eigenschaften, die für die Beurteilung von Mobilität und Verbleib von Xenobiotika in der Umwelt äußerst relevant sind. Diese Parameter hängen direkt mit Strukturen und Größenverteilungen der HS zusammen.
Ergebnisse aus chromatographischen Methoden, die zur Bestimmung der Größenverteilungen der HS bzw. des Einflusses von Solvensbedingungen auf diese eingesetzt werden, sind mit großer Vorsicht zu interpretieren, da die eingestellten Trennbedingungen (Puffergemisch, Ionenstärke) und die gewählten Standards zur Kalibrierung einen beachtlichen Einfluss auf die bestimmten Molekülgrößenverteilungen haben [248]. Andere Methoden, die auf massenspektrometrischen Verfahren basieren, zerstören häufig die Proben und sind anfällig für Artefaktbildungen. Andere Verfahren brauchen sehr hohe, von Realbedingungen weit entfernte Konzentrationen (z.B. NMR-Methoden) [1].
Durch das Einführen von Lumineszenzsonden kann dieses Problem reduziert werden. Zur Untersuchung des Assoziationsverhaltens der HS und zur Bestimmung von mittleren Abständen r der Metallbindungsplätze in HS kann der Interlanthanid-Energietransfer zwischen an HS gebundene Tb^{3+}- und Nd^{3+}-Ionen genutzt werden. Dieser experimentelle Ansatz erlaubt eine Bestimmung von Abständen gebundener Ln^{3+}-Ionen z.B. unter verschiedenen Solvensbedingungen. Die Konzentrationen der HS entsprechen Realbedingungen und eine vorgeschaltete Probenauftrennung ist nicht notwendig, d.h. es ist ein nicht-invasives Verfahren mit minimaler Probenveränderung durch die Messung selbst.
Der Interlanthanid-Energietransfer zwischen Tb^{3+} (Donor) und Nd^{3+} (Akzeptor) ist gut beschrieben und wurde für die Untersuchung von Proteinstrukturen eingesetzt (s. 3.1.3). Die physiko-chemischen Eigenschaften mit Hinblick auf Bindungslängen (speziell der Ln-O-Bindung) und EN sind für die beiden Ln^{3+}-Ionen sehr ähnlich, so dass für das Komplexbildungsverhalten gegenüber HS keine signifikanten Unterschiede zu erwarten sind (im Gegensatz zu Eu^{3+}, s. Tabelle 3.3).
Werden zu einer Lösung, in der durch HS komplexierte Tb^{3+}-Ionen vorliegen, Nd^{3+}-

	La	**Nd**	**Eu**	**Tb**
Ln-O-Bdg. (Å)	2.591	2.534	2.490	2.460
EN	1.053	1.094	2.954	1.238

Tabelle 3.3: Vergleich der Bindungslängen und der Elektronegativitätswerte (EN) für verschiedene Ln^{3+}-Ionen (für den Fall der Koordinationszahl 10, nach [221]).

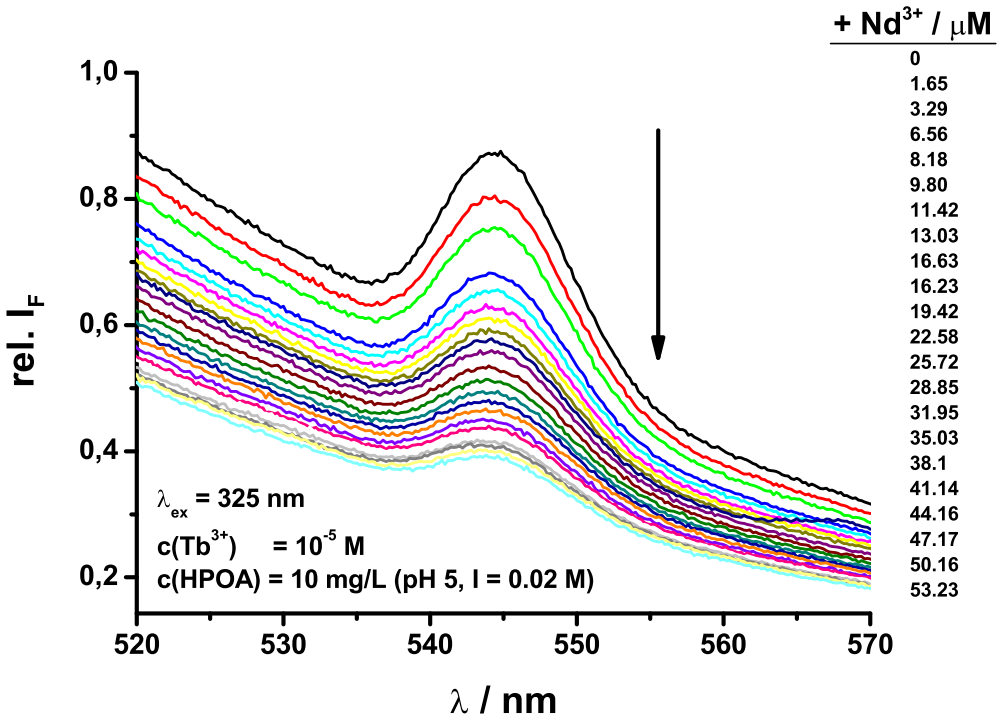

Abbildung 3.26: Löschung der Tb^{3+}-Lumineszenz durch Nd^{3+} (Fluoromax 3, Yobin Yvonne).

Ionen titriert, so wird zweierlei beobachtet: 1) die intrinsische HS-Fluoreszenz wird weiter gelöscht, was ein gutes Indiz dafür ist, dass weitere Ln^{3+}-Ionen (hier: Nd^{3+}) gebunden werden und 2) die sensibilisierte Lumineszenz des Tb^{3+} nimmt ab. In Abbildung 3.26 ist die durch Nd^{3+} induzierte Löschung der Tb^{3+}-Lumineszenz für den Terbiumlumineszenzpeak bei $\lambda_{em} = 545$ nm gezeigt. Weiterhin ist für den Spektralbereich 520 nm $< \lambda_{em} <$ 530 die fortschreitende Löschung der intrinsischen HS-Fluoreszenz zu erkennen, anhand der die Komplexierung von Nd^{3+} durch HS abgelesen werden kann. Dies ist wichtig, da ansonsten die beobachtete Abnahme der Tb^{3+}-Lumineszenz durch eine Verdrängung der Tb^{3+}-Ionen aus HS durch Nd^{3+}-Ionen nicht unterschieden werden könnte. Für den Fall eines schlichten Austausches von an HS gebundenen Tb^{3+}- durch Nd^{3+}-Ionen kann erwartet werden, dass zwar die Tb^{3+}-Lumineszenz auch abnimmt, da unter den gewählten experimentellen Bedingungen in erster Linie sensibilisiert Tb^{3+}-Lumineszenz beobachtet wird, aber die HS-Fluoreszenz sollte dann in erster Näherung erstmal unverändert bleiben.
Zur Überprüfung wurden zusätzlich Experimente mit La^{3+} durchgeführt. La^{3+} ist in seinen Eigenschaften (s. Tabelle 3.3) dem Nd^{3+} sehr ähnlich und sollte in Bezug auf die Komplexierung durch HS gleiche Eigenschaften besitzen, allerdings ist La^{3+}

nicht als Energieakzeptor für LRET-Experimente mit Tb^{3+} geeignet (s. auch Tabelle B.3).

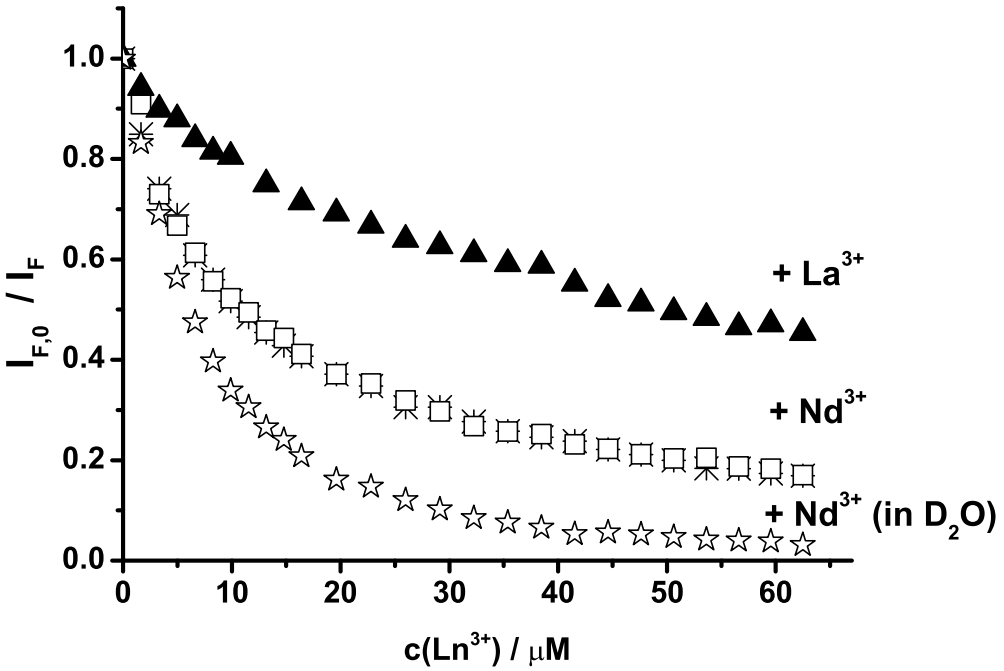

Abbildung 3.27: Einfluss von Nd^{3+} und La^{3+} auf die Tb^{3+}-Lumineszenzintensität (λ_{ex}= 325 nm, λ_{em}= 545 nm, c(Tb^{3+}) = 10^{-5} M, c(HPOA) = 10 mg/L, pH 5, I = 0.02 M; Fluoromax 3, Yobin Yvonne). Für Nd^{3+} sind zwei separate Messreihen in H_2O und eine Messreihe in D_2O gezeigt.

Wie in Abbildung 3.27 zu sehen ist, nimmt die Tb^{3+}-Lumineszenzintensität auch bei steigender Konzentration von La^{3+} ab. Dies muss in der Verdrängung der an HS gebundenen Tb^{3+}-Ionen durch La^{3+}-Ionen liegen. Allerdings ist deutlich zu erkennen, dass der Effekt im Vergleich zur Zugabe von Nd^{3+} viel kleiner ist. D.h. für kleine Konzentrationen von Tb^{3+} bzw. Nd^{3+} spielt dieser Verdrängungseffekt eine untergeordnete Rolle und die beobachtete Abnahme der Tb^{3+}-Lumineszenz ist durch LRET zwischen Tb^{3+} und Nd^{3+} bedingt. Desweiteren ist in Abbildung 3.27 die beobachtete Lumineszenzlöschung in H_2O und D_2O verglichen. Es ist ein deutlicher Isotopeneffekt sichtbar, der zeigt, dass die Ln^{3+} in HS noch eine Reihe von Wassermolekülen in der ersten Koordinationssphäre enthalten (s. auch Abbildung 3.19). Diese Annahme wird durch die zeitaufgelösten Lumineszenzmessungen von an HS gebundenen Tb^{3+}-Ionen gestützt. In diesen werden im Allgemeinen Abklingkinetiken beobachtet, die im Vergleich zu Tb^{3+}(aq) schneller ablaufen (s.o.), was einerseits durch einen effektiven Energierücktransfer auf HS erklärt werden kann und andererseits die Vermutung nahe legt, dass es sich bei der Bindung der Ln^{3+} an

die HS um *outer-sphere*-Komplexe handelt, in denen die erste Koordinationssphäre der Ln^{3+}-Ionen weiterhin durch H_2O besetzt ist.
Der LRET zwischen an HS gebundenen Tb^{3+} und Nd^{3+}-Ionen konnte durch zeitaufgelöste Lumineszenzmessungen untermauert werden. Mit steigender Konzentration an Nd^{3+} wurde eine Abnahme der Lumineszenzlebensdauer des Tb^{3+} beobachtet für den Fall das beide an HS gebunden vorlagen. In homogener wäßriger Lösung ohne HS konnte für ähnliche Ln^{3+}-Konzentrationen keine Abnahme in der Lumineszenzabklingzeit des Tb^{3+} beobachtet werden (s. Abbildung 3.28).

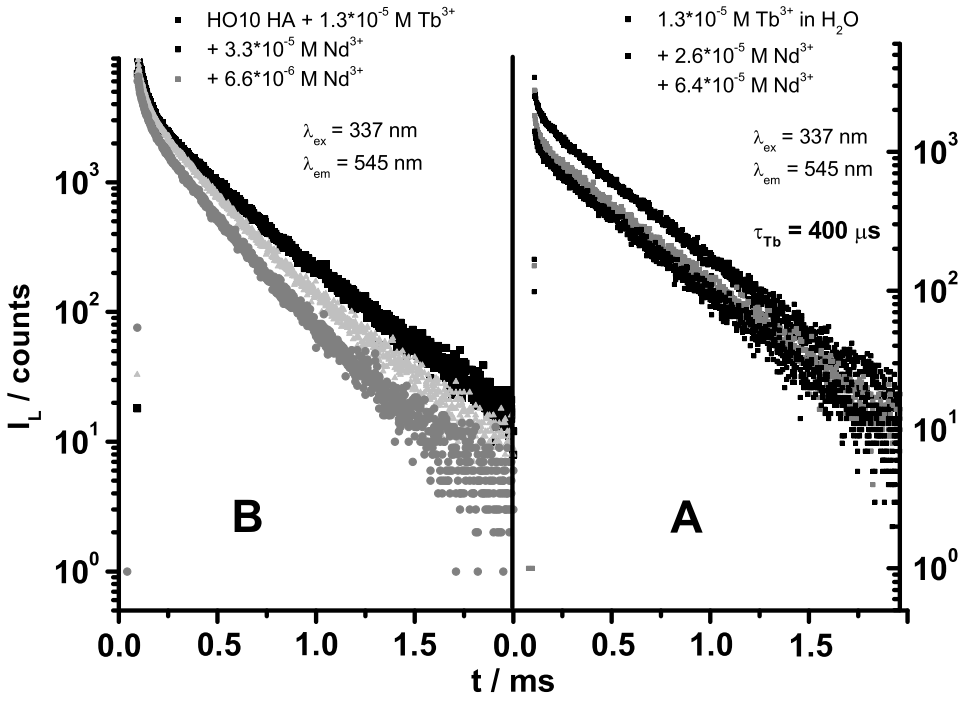

Abbildung 3.28: Einfluss von Nd^{3+} auf die Lumineszenzabklingkurven von Tb^{3+} in An- und Abwesenheit von HS (FL920 im μs-Modus, Edinburgh Instruments).

Ein Auswertung der Lumineszenzabklingzeiten des Tb^{3+} zur Bestimmung des mittleren Abstandes zwischen gebundenen Tb^{3+} und Nd^{3+}-Ionen ist allerdings aufgrund des komplexen Lumineszenzabklingverhaltens des an HS gebundenen Tb^{3+} schwierig und ein Gegenstand der laufenden Forschung. Daher wurde die Auswertung zunächst über die Lumineszenzintensitäten bei λ_{em}= 545 nm nach Gleichung (3.3) und (3.4) durchgeführt und um den Anteil der Löschung, der durch einfache Verdrängung verursacht wird, korrigiert. Dieser wurde in separaten Messungen mit La^{3+} ermittelt.
Die nach Gleichung (3.3) und (3.4) bestimmten mittleren Abstände r sind in Abbildung 3.30 für HS verschiedener Ursprungsorte gegenübergestellt. Erwartungsgemäß sinkt zunächst der mittlere Abstand r mit zunehmender Konzentration an Nd^{3+}

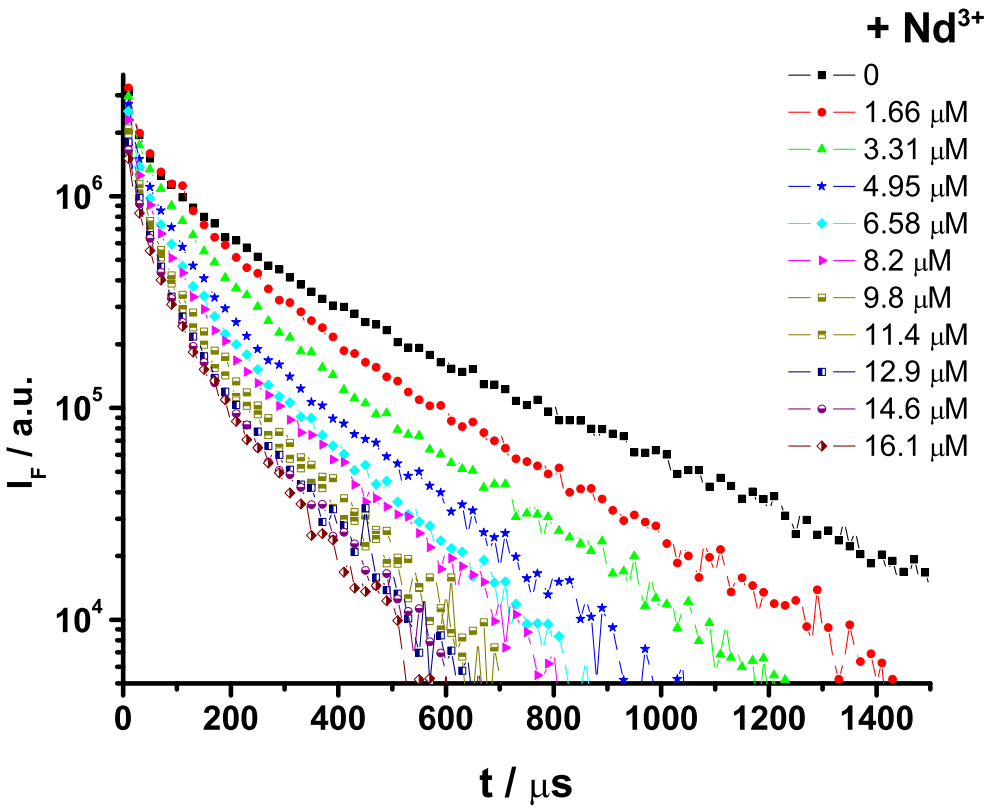

Abbildung 3.29: Einfluss von Nd^{3+} auf das Lumineszenzabklingverhalten von Tb^{3+} (Gohy573 FA, c(HS) = 10 mg/L, c(Tb^{3+}) = 3.3 μM , λ_{ex}= 337 nm, λ_{em}= 545 nm, pH 5; iCCD, LOT).

und nähert sich scheinbar einem minimalen Grenzabstand r_{min} an, welcher für den jeweiligen HS typisch zu sein scheint. Damit liegen die mittleren Abstände zwischen den an HS gebundenen Ln^{3+}-Ionen im Bereich von ca. 7 bis 10 Ionenradien (der Ionenradius beträgt 99.5 pm für Nd^{3+} und 92.3 pm für Tb^{3+} , nach [112]).

Die mittleren Abstände r von an HS gebundenen Ln^{3+}-Ionen verändern sich in Abhängigkeit vom pH-Wert der Lösung. In Abbildung 3.31 ist ein deutlicher Unterschied der mittleren Abstände zwischen den pH-Werten 3 und 6 zu erkennen. Interessanter Weise nimmt der mittlere Abstand zwischen den gebundenen Ln^{3+}-Ionen mit sinkendem Abstand zu (für eine bestimmte Nd^{3+}-Konzentration, z.B. 10 μM) - entgegen der gängigen Erwartung, dass sich HS bei sinkendem pH-Wert der Lösung *verknäulen*. Dies sollte z.B. durch die Ausbildung von intramolekularen Wasserstoffbrückenbindungen und durch die abnehmende Ladungsdichte begünstigt werden. Allerdings stehen mit sinkendem pH-Wert immer mehr Protonen in Konkurrenz zu den Ln^{3+}-Ionen, so dass insgesamt weniger Bindungsplätze zur Verfügung

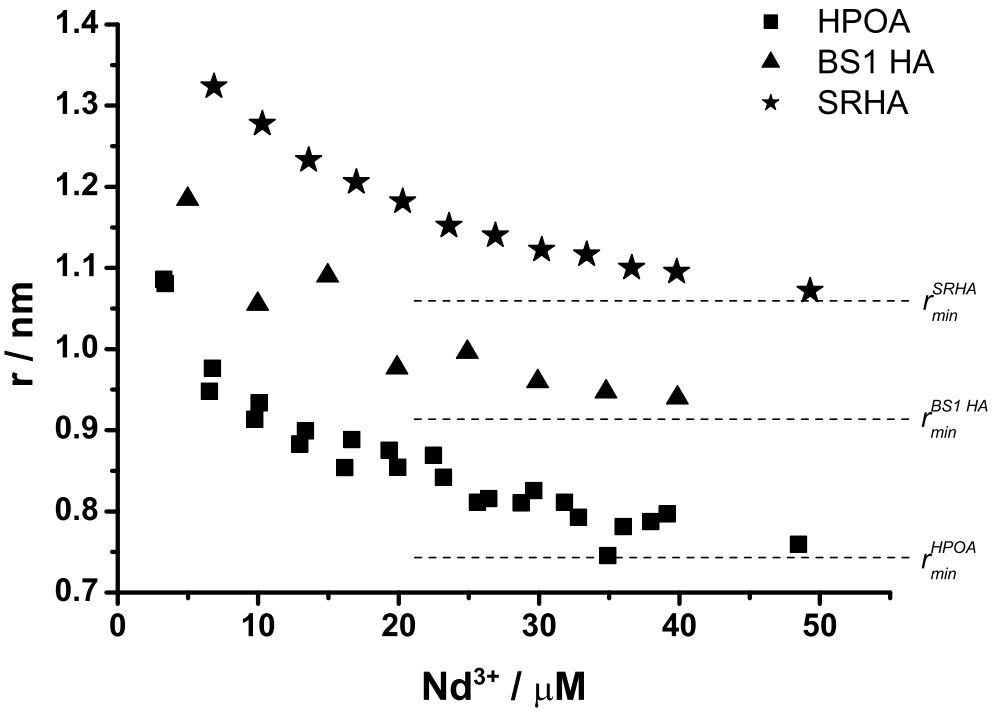

Abbildung 3.30: Mittlere Abstände r zwischen Tb^{3+} und Nd^{3+} gebunden an HS verschiedener Ursprungsorte (c(HS) = 10 mg/L, pH 5, I = 0.02 M).

stehen werden. Zusätzlich könnte eine intermolekulare Aggregation zu einem vergrößerten mittleren Abstand r führen.

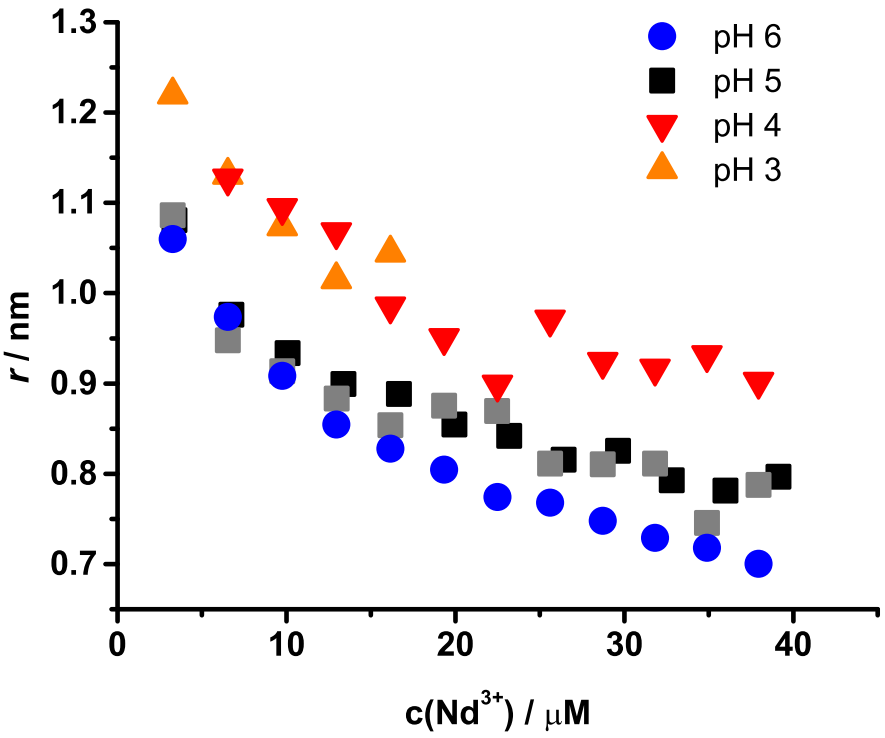

Abbildung 3.31: Mittlere Abstände r zwischen Tb^{3+} und Nd^{3+} gebunden an HS für verschiedene pH-Werte (c(HPOA) = 10 mg/L, I = 0.02 M).

3.5 Ausblick

Spektroskopische Techniken, wie z.B. fluoreszenzbasierte Methoden, mit ihrer großen Sensitivität und Selektivität sind in Kombination mit den spezifischen Eigenschaften von molekularen Sonden, wie z.B. Lanthanide, die geeigneten Werkzeuge, auch außergewöhnlich heterogene Systeme wie Huminstoffe (HS) direkt, ohne das System möglicherweise störende Trennschritte zu untersuchen.
Die Anwendung von Lanthaniden als molekulare Sonden zur Untersuchung von HS setzt ein grundlegendes Verständnis der Wechselwirkungsmechanismen voraus. Dafür ist es notwendig, dass die intrinsischen Fluoreszenzprozesse von HS weiter aufgeklärt werden. Es ist ein Ziel, die Beteiligung von intra- und intermolekularen Desaktivierungskanälen, die konformative Veränderungen der HS beinhalten, in Zukunft weiter zu charakterisieren. Als wichtigste Desaktivierungskänale ist geplant die Beiträge von Konformationsänderungen über TICT-Zustände, photoinduzierten Protonenabspaltungen und Energietransferprozessen charakterisiert werden. In zurzeit laufenden Untersuchungen wird die photoinduzierte Dissoziation von verschiedenen substituierten Benzoesäuren untersucht. Geplant sind dann weiterführende Untersuchungen an Ligninen, Chitosanen und Chitinen, die als Ausgangsstoffe bei der Entstehung von HS angesehen werden. Durch die schrittweise Annäherung von einfachen zu komplexen Verbindungen werden die beteiligten Desaktvierungsprozesse in HS systematisch weiter differenziert und charakterisiert werden. Zusätzlich sind stationäre und zeitaufgelöste Fluoreszenzanisotropieuntersuchungen geplant. Prinzipiell können aus Fluoreszenzanisotropieexperimenten Informationen über Molekül- oder Aggregatgrößen bzw. deren Veränderung bei chemischen Reaktionen abgeleitet werden. Dazu müssen allerdings die zugrundeliegenden Fluoreszenzmechanismen bekannt sein (s.o.). Aus den Veränderungen der Fluoreszenzanisotropie und den Rotationskorrelationszeiten werden Rückschlüsse auf das Aggregationsverhalten von HS zugänglich, die nicht durch Artefakte, wie sie z.B. bei der SEC bedingt durch Zusatz von Puffern (Acetat oder Borat) verursacht werden, verfälscht sind und eine direkte Messung am heterogenen System gestatten.
Ein weiteres Ziel der zukünftigen Arbeiten ist, den Einsatz von Lumineszenzsonden zur Charakterisierung der HS-Metall-Wechselwirkungen weiter auszubauen. Neben den lumineszierenden Lanthaniden Samarium und Dysprosium werden dann auch organische Moleküle als Fluoreszenzsonden in die Experimente eingeflochten. Zur Zeit wird an einem kombinierten Auswerteformalismus für die intrinsische HS-Fluoreszenzlöschung und die sensibilisierte Ln^{3+}-Lumineszenz gearbeitet, der in ein übergreifendes Modell zur Bestimmung von Komplexbildungskonstanten integriert werden soll.
Im Rahmen eines von der Europäischen Union geförderten Wissenschaftleraustausches[15] werden Tieftemperatur-Lumineszenzexperimente ($T < 10$ K; *fluorescence line narrowing*, FLN) mit HS-Eu^{3+}-Komplexen bzw. Komplexen von Eu^{3+} mit organischen Modellliganden durchgeführt werden. In den FLN-Experimenten ist das Ziel, aus der Anzahl der beobachtbaren $^5D_0$-$^7F_0$-Banden die Anzahl von unterschied-

[15] Antrag ist bewilligt.

lichen HS-Eu^{3+}-Komplexen in HS zu bestimmten. Durch die Reduktion der spektralen Bandbreite bei tiefen Temperaturen wird eine erheblich verbesserte Auflösung der Signale von unterschiedlichen Eu^{3+}-Komplexen erreicht. Dabei sind Untersuchungen über einen großen Konzentrationsbereich (für die $Ln^{3+} <$ nM, für HS « 10 mg/L) möglich, wodurch die Experimente unter Realbedingungen durchgeführt werden können. Aus den erhaltenen Ergebnissen ist es dann möglich, detailliertere Aussagen zu den in HS vorliegenden Komplexstöchiometrien zu machen.
Besonders bei den gängigen Methoden zur Strukturuntersuchung muss meist mit hohen Konzentrationen an HS gearbeitet werden. Methoden wie XPS oder EXAFS gestatten dann die Untersuchung der ersten und zweiten Koordinationssphäre der Ln^{3+}-Ionen. Das Ziel ist aus Untersuchungen des Interlanthanid-Energietransfers zwischen an HS-gebundenen Ln^{3+}-Ionen, Informationen auch über größere Abstände in HS-Molekülen bzw. -Aggregaten zu erhalten. Durch entsprechende Variation der Donor-Akzeptor-Paare könnten Distanzen von bis zu 10 nm bestimmbar werden. Auf diese Weise können Konformationsänderungen, wie sie durch die Variation der Ionenstärke, des pH-Wertes oder der Anwesenheit von Metallionen in HS möglicherweise induziert werden, direkt gemessen werden. Es können weiterhin Konformations- und Aggregationsverhalten von HS als Konsequenz der Komplexierung über den Nahbereich der Metallbindung hinaus analysiert werden. Diese Untersuchungen sind komplementär zu den schon erwähnten Fluoreszenzanisotropiemessungen. Als eine weitere Anwendung ist geplant, den Interlanthanid-Energietransfer in *stopped-flow*-Experimenten zu nutzen, um die Kinetik der Aggregation von Huminstoffen und der durch Lösungsmittelparameter bedingte Reorganisation der HS auf einer Mikrosekunden-Zeitskala zu bestimmen. Für die Anwendung des Interlanthanid-Energietransfers ist es allerdings notwendig, die fundamentalen Prozesse weiter zu hinterfragen und zu verstehen. Bei der Verwendung der Lanthanid-Ionen Tb^{3+} und Eu^{3+} sind die komplexen Reaktionswege, in denen die elektronische Energie von HS auf das Ln^{3+}-Ion übertragen wird bzw. der Rücktransfer von HS zum Ln^{3+}-Ion weiter zu untersuchen.

Anhang A

Ausgewählte Aspekte zu theoretischen Grundlagen von bimolekularen Lumineszenzlöschprozessen

A.1 Allgemeine Formulierungen zu Fluoreszenzlöschprozessen: Stern-Volmer-Formalismus

Nach der Wechselwirkung mit Licht geeigneter Energie befinden sich Molekülen in einem elektronisch-angeregten Zustand[1] (s. Gleichung A.1). Die elektronisch-angeregten Moleküle (D^*) können durch Wechselwirkung mit anderen Molekülen (A) desaktiviert werden, wobei die elektronische Energie auf das Molekül A übertragen wird. Das Molekül A kann sich dann seinerseits in einem elektronisch-angeregten Zustand befinden. Es gibt dabei eine Reihe von möglichen intermolekularen Wechselwirkungen, die zu dieser sogenannten „Löschung“ (*Quenching*) der Fluoreszenz führen können. Als ein Beispiel sei hier der Resonanzenergietransfer genannt, der später noch genauer betrachtet werden wird (s. Abschnitt A.2.2). Ganz allgemein werden zwei grundlegende Arten von Löschung unterschieden: statische und dynamische Löschung.

$$D + h\nu \longrightarrow D^* \tag{A.1}$$
$$D^* + A \longrightarrow D + A^* \tag{A.2}$$

Statische Fluoreszenzlöschung Bei der statischen Löschung kommt es zwischen A und D bereits im elektronischen Grundzustand von D zu einer Wechselwirkung (z.B. einer Komplexbildung), so dass D nicht mehr direkt angeregt werden kann. Hierbei handelt es sich also eigentlich um eine Grundzustandsreaktion zwischen D

[1] Dies gilt für den Fall, dass die Resonanzbedingung erfüllt ist.

und A, wobei das Produkt (AD) nicht fluoreszenzfähig ist, d.h. der unter Gleichung A.6 beschriebene Reaktionsschritt läuft nicht ab.

$$\begin{aligned} D + A &\longrightarrow (AD) && \text{(A.3)} \\ (AD) + h\nu &\longrightarrow (AD)^* && \text{(A.4)} \\ (AD)^* &\longrightarrow (AD) + \Delta && \text{(A.5)} \\ (AD)^* &\longrightarrow (AD) + h\nu_F && \text{(A.6)} \end{aligned}$$

Durch das Messen der Fluoreszenzintensität in An- und Abwesenheit der Löschers A (I_0 bzw. I) kann die Löschkonstante K_s bestimmt werden, die in diesem Fall den Charakter einer Gleichgewichtskonstanten für die Bildung von (AD) hat (s. Gleichung A.3). Die Fluoreszenzlebenszeit τ von D bleibt auch in Anwesenheit von A unverändert.

$$\frac{I_0}{I} = 1 + K_s \cdot [A] \quad \text{und} \quad \frac{\tau_0}{\tau} = 1 \tag{A.7}$$

Dynamische Fluoreszenzlöschung In dynamische Fluoreszenzlöschprozessen findet die Wechselwirkung zwischen D und A nur im elektronisch angeregten Zustand von D statt. Diese Prozesse sind gewöhnlich diffusionskontrolliert. Im Gegensatz zur statischen Fluoreszenzlöschung werden sowohl die Fluoreszenzquantenausbeute als auch die Fluoreszenzabklingzeit von D durch den Löschprozess verändert. Es gilt:

$$\frac{I_0}{I} = 1 + K_d \cdot [A] \quad \text{und} \quad \frac{\tau_0}{\tau} = 1 + k_q \cdot \tau_0 \cdot [A] \tag{A.8}$$

Im Fall der dynamischen Löschung entspricht die aus stationären Messungen ermittelte Löschkonstante K_d dem Produkt aus der Fluoreszenzlebenszeit τ_0 von D in Abwesenheit des Löschers und der bimolekularen Löschkonstanten k_q.

A.2 Energietransfer-Prozesse

Die elektronische Anregungsenergie, die von einem Moleküle (Donor, D) durch Absorption eines Lichtquants passender Energie aufgenommen wurde, kann auf ein zweites Molekül (Akzeptor, A) übertragen werden. Es können dabei drei grundlegend verschiedene Mechanismen identifiziert werden.
Von den beiden interessanten Mechanismen (s. Abschnitt A.2.1 und A.2.2) muss grundsätzlich der *triviale* Mechanismus der Energieübertragung unterschieden werden. Bei diesem handelt es sich um einen Zwei-Schritt-Prozeß:

$$\begin{aligned} D^* &\longrightarrow D + h\nu_F && \text{(A.9)} \\ h\nu_F + A &\longrightarrow A^* && \text{(A.10)} \end{aligned}$$

Nachdem das angeregte Donormolekül D^* ein Photon emittiert hat, wird dieses in einem zweiten Schritt vom Akzeptor re-absorbiert. Vorraussetzungen für diesen Prozeß sind eine hohe Fluoreszenzquantenausbeute des Donors, ein intensiver Absorptionsübergang des Akzeptors im spektralen Bereich der Donorfluoreszenz und ein großer Überlapp der Donorfluoreszenz mit der Akzeptoremission. Der Überlapp wird als Überlappungsintegral J quantifiziert. Das Überlappungsintegral J entspricht formal dem integriertem Überlapp zwischen dem experimentellen Absorptionsspektrum des Akzeptors und dem Fluoreszenzspektrum des Donors.

$$J \equiv \int_0^\infty I_D \cdot \epsilon_A \cdot d\,\widetilde{\nu} \tag{A.11}$$

Hierbei entspricht I_D dem experimentellen Fluoreszenzspektrum des Donors und ϵ_A dem Absorptionsspektrum des Akzeptors. Beide sind auf einer Energieskala dargestellt, z.B. als Funktion der Wellenzahl $\widetilde{\nu}$ (in cm^{-1}) und sind normiert, so dass für den maximalen Überlapp $J = 1$ wird. Der *triviale* Mechanismus wird normalerweise erst bei hohen Konzentrationen von Donor und / oder Akzeptor beobachtet.
In der allgemeinen Formulierung kann die Wahrscheinlichkeit P für den strahlungslosen Transfer elektronischer Energie von einem Donor D auf einen Akzeptor A nach der *Golden Regel von Fermi* beschrieben werden (s. Gl. A.12) [199].

$$P(D^* + A \longrightarrow D + A^*) \sim \frac{2\pi}{h} \cdot \rho \cdot \langle \Psi_i \mid H \mid \Psi_f \rangle^2 \tag{A.12}$$

Hierbei sind Ψ_i und Ψ_f die Wellenfunktionen des Anfangs- und Endzustands und ρ ein Maß für die Dichte der beteiligten Zustände. Der Operator H beinhaltet die spezifische Wechselwirkung, die Ausgangs- und Endzustand miteinander wechselwirken läßt. Strahlungsloser Energietransfers kann einmal durch elektronische Wechselwirkungen (s. Abschnitt A.2.1) bewirkt werden und zum Zweiten durch elektrostatische Wechselwirkungen (s. Abschnitt A.2.2) [74, 194, 199, 249, 250]. Bei der elektrostatischen Wechselwirkung ist kein echter Kontakt zwischen Donor und Akzeptor notwendig, da die Wechselwirkung durch ein elektromagnetisches Feld erfolgt. Diese Wechselwirkung wird auch als Coulomb- oder Dipol-Dipol-Wechselwirkung bezeichnet. Bildlich kann angenommen werden, dass die Bewegung der Elektronen im angeregten Donor (= elektromagnetisches Feld) eine Störung der Bewegung der Elektronen im Akzeptor bewirkt und im Falle der Resonanz dann zu einer Energieübertragung führt, ähnlich einem Sender-Empfänger-Paares. Hingegen ist bei der elekronischen Wechselwirkung ein echter Kontakt zwischen Donor und Akzeptor notwendig, damit die beteiligten Orbitale beider überlappen. Es kommt zu einem „echten“ Austausch von Elektronen zwischen Donor und Akzeptor. Der wesentliche Unterschied besteht also darin, dass beim Coulomb-Mechanismus die Wechselwirkung durch den Raum und beim Austausch-Mechanismus durch Kontakt zustande kommt.

A.2.1 Austausch Mechanismus (Dexter-Energietransfer)

Bimolekulare Wechselwirkung, z.B. durch Kollision, zwischen Molekülen können im einfachsten Bild als Zusammenstöße zwischen zwei Molekülen gleicher oder unterschiedlicher Art sein. Im Verlauf der Kollision kommt es zu einer Überlappung der

Elektronenwolken. Oftmals sind für den Ablauf von echten chemischen Reaktionen dabei stereochemische Gesichtspunkte ganz maßgeblich, damit eine chemische Reaktion (z.B. ein Bindungsbruch oder -bildung) abläuft. Werden diese in erster Näherung ersteinmal vernachlässigt, so nimmt die Überlappung der Orbitale zwischen den Molekülen exponentiell mit dem Abstand zwischen ihnen ab. Im Falle der Energieübertragung durch den Austausch-Mechanismus bedeutet das, dass die Geschwindigkeitskonstante k_{ex} exponentiell mit dem Abstand R_{DA} zwischen Donor und Akzeptor abnimmt. Nach *Dexter* gilt für k_{ex}:

$$k_{ex} = K \cdot J \cdot exp\left(-\frac{2R_{DA}}{L}\right) \tag{A.13}$$

Die Konstante K beinhaltet die spezifischen Orbitalwechselwirkungen für das untersuchte Donor-Akzeptor Paar und J ist das spektrale Überlappungsintegral. Anders als für den Fall der Energieübertragung durch elektrostatische Wechselwirkungen (s.u. Abschnitt A.2.2) ist hier das Absorptionsspektrum des Akzeptors auf eins normiert, d.h. die Oszillatorstärke der Übergänge $D \rightleftharpoons D^*$ und $A \rightleftharpoons A^*$ ist unerheblich. Während also die Geschwindigkeitskonstante k_{FRET} stark von der Stärke dieser Übergänge abhängt (s. Abschnitt A.2.2), ist diese für k_{ex} ohne Einfluß. Das ist ein wichtiger Unterschied zwischen beiden Mechanismen.

A.2.2 Coulomb Mechanismus (Resonanz-Energietransfer)

Der Transfer elektronischer Energie durch Dipol-Dipol-Wechselwirkung (Coulomb Mechanismus[2]) zwischen einem elektronisch-angeregten Donor D^* und einem Akzeptor A erfolgt nach:

$$D^* + A \xrightarrow{R_0} D + A^* \tag{A.14}$$

Das Ausmaß der Dipol-Dipol-Wechselwirkung hängt von der Wechselwirkungsenergie E ab. Diese wiederum ist verknüpft mit den Dipolmomenten μ von Donor und Akzeptor und dem Abstand R_{DA} zwischen Donor und Akzeptor (s. Gl. A.15).

$$E(Dipol - Dipol) \sim \frac{\mu_D \cdot \mu_A}{R_{DA}^3} \tag{A.15}$$

Durch die Verknüpfung der Dipolmomente von Donor und Akzeptor mit den experimentell zugänglichen spektroskopischen Parametern der Oszillatorstärke f für die strahlenden Übergänge $D \rightleftharpoons D^*$ und $A \rightleftharpoons A^*$ gilt:

$$\mu_D^2(D \rightleftharpoons D^*) \sim \int \epsilon_D(\widetilde{\nu})\, d\,\widetilde{\nu} \sim k_D^0 \tag{A.16}$$

$$\mu_A^2(A \rightleftharpoons A^*) \sim \int \epsilon_A(\widetilde{\nu})\, d\,\widetilde{\nu} \sim k_A^0 \tag{A.17}$$

[2]Der Coulomb Mechanismus wird oft auch als Resonanzenergietransfer oder Förster-Energietransfer bezeichnet.

Da außerdem noch das Quadrat der Wechselwirkungsenergie E proportional zur Geschwindigkeitskonstante k_{FRET} für einen durch elektrostatische Wechselwirkungen veranlaßten Energietransfer ist, kann ein Ausdruck für k_{FRET} erhalten werden [196, 199, 251]:

$$k_{FRET} \sim \frac{\kappa^2 \cdot k_D^0}{R_{DA}^6} \cdot J \tag{A.18}$$

J stellt dabei das sogenannte Überlappungsintegral dar (s.u.). Der kritische Transferradius (Försterradius) R_0 wird zur Charakterisierung der Stärke der Coulomb-Wechselwirkung verwendet. Er bezeichnet die Entfernung zwischen Donor und Akzeptor, bei der die Effizienz des Energietransfers gerade 50% beträgt und somit die gleiche Wahrscheinlichkeit besitzt wie die Summe der anderen Desaktivierungsmechanismen für den elektronisch-angeregten Donor.

$$k_{FRET} \cdot [A] = k_F + k_{IC} + k_{ISC} = \frac{1}{\tau_D} \tag{A.19}$$

Nach der von Förster entwickelten Theorie zum Resonanzenergietransfer gilt für R_0:

$$R_0^6 = \frac{(9000 \cdot ln10) \cdot \kappa^2 \cdot \Phi_D}{128 \cdot \pi^5 \cdot n^4 \cdot N} \cdot \int_0^\infty \frac{F_D(\widetilde{\nu}) \cdot \epsilon_A(\widetilde{\nu})}{\widetilde{\nu}^4} d\,\widetilde{\nu} \tag{A.20}$$

In Gleichung A.20 und A.18 bezeichnet κ einen Faktor, der berücksichtigt, dass für die Stärke der Wechselwirkung zwischen zwei oszillierenden Dipolen die Orientierung der Übergangsdipolmomente (hier: von Donor und Akzeptor) wichtig ist. Für den Fall der vollständigen Rotationsfreiheit und schneller Rotation im Vergleich zur Fluoreszenzlebenszeit von Donor und Akzeptor wird ein Wert von $\frac{2}{3}$ für κ^2 angenommen. Ganz allgemein kann κ^2 im Bereich $0 < \kappa^2 < 4$ variieren, wobei der Wert 0 bedeutet, dass Donor- und Akzeptor-Übergangsdipolmoment senkrecht zueinander stehen und der Wert 4 im Falle einer vollständig parallelen Orientierung erreicht wird [196]. Werden Donor-Akzeptor-Systeme mit langen Fluoreszenzabklingzeiten eingesetzt, wie z.B. im Falle von Lanthanidionen, so ist der Einfluß der Orientierung der Übergangsdipolmomente herausgemittelt [251]. Φ_D ist die Fluoreszenzquantenausbeute des Donors in Abwesenheit von A, n ist der Brechungsindex des Lösungsmittels und N ist die Avogadrozahl. Im als *Überlappungsintegral* J bezeichneten integralen Ausdruch stehen die spektralen Verteilungen der Donoremission und der Akzeptorabsorption in Form des molaren dekadischen Extinktionskoeffizienten (beide als Funktion der Wellenzahl $\widetilde{\nu}$). Dieser Ausdruck gilt für den Fall, dass der Donor fluoreszenzfähig ist. Ganz allgemein formuliert muss für Dipol-Dipol-Wechselwirkung der equilibrierte S_1-Zustand des Donors und ein Franck-Condon-Zustand des Akzeptors gleiche Energie haben [199,252]. Je größer die Zustandsdichte an isoenergetisch-resonaten Energieniveaus von Donor und Akzeptor, desto größer ist J und damit auch die Geschwindigkeitskonstante k_{FRET}.

Nach Gleichung A.20 und A.18 hängt die Geschwindigkeit und damit auch die Effizienz der Dipol-Dipol-Wechselwirkung stark vom Abstand zwischen Donor und Akzeptor ab und kann im Gegenzug für ein bekanntes, d.h. spektroskopisch gut charakterisiertes, Donor-Akzeptor-Paar zur Abstandsbestimmung zwischen beiden benutzt werden. Denn für einen beliebigen Abstand R zwischen A und D gilt:

$$k_{FRET} = \frac{1}{\tau_D} \cdot \left(\frac{R_0}{R}\right)^6 \tag{A.21}$$

Zusammenfassend kann festgehalten werden, dass der Austausch-Mechanismus nur für relativ kleine Abstände zwischen Donor und Akzeptor wirksam werden kann, während der Coulomb Mechanismus eine wesentlich größere Reichweite hat. Dies ist in Abbildung A.1 nochmal verdeutlicht.

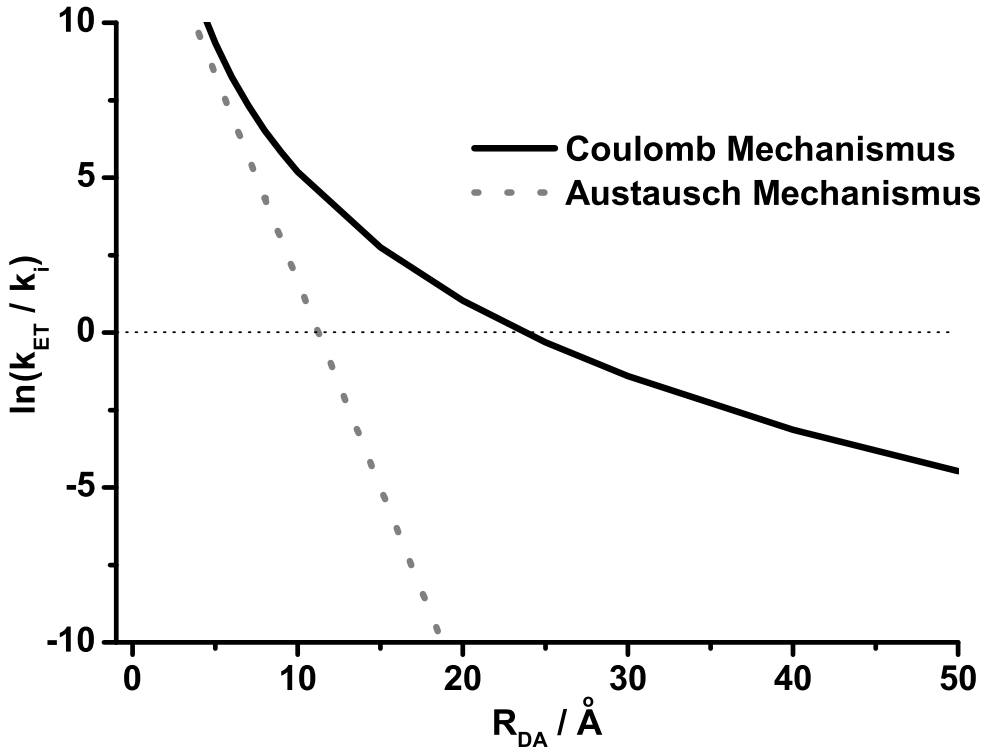

Abbildung A.1: Vergleich der Abstandsabhängigkeit des Coulomb und Austausch Mechanismus als Verhältnis der Geschwindigkeitskonstanten des Energietransfers k_{ET} und der übrigen Desaktivierungsprozesse k_i

Einflüsse auf das Fluoreszenzabklingverhalten von Donor und Akzeptor

$$I_D(t) = I_D(0) \cdot exp\left\{-\frac{t}{\tau_D} + 2 \cdot \gamma \cdot \sqrt{\left(\frac{t}{\tau_D}\right)}\right\} \tag{A.22}$$

Gleichung (A.22) gilt für den 3-dimensionalen Fall und einer gegen Unendlich reichenden Anzahl von Akzeptor-Molekülen in der Umgebung des Donors. Die Größe $\gamma = \frac{c_A}{c_0}$ verknüpft die Akzeptorkonzentration c_A und den Försterradius R_0 ($c_0 = 3000 \cdot (2 \cdot \pi^{2/3} \cdot N \cdot R_0^3)$). In dieser Näherung wird angenommen, dass die Diffusionslänge während des Energietransferprozesses klein gegenüber R_0 ist, was für ausreichend viskose Lösungen erfüllt ist. Dann kann die Verteilung von Donor und Akzeptor als stationär angenommen werden. Stryer und Haugland konnten für Modellverbindungen, in denen Donor (eine Naphthyl-Gruppe) und Akzeptor (eine Dansyl-Gruppe) durch Prolin-Oligomere verschiedener Länge getrennt waren für den intramolekularen Fall, die von Förster geforderte R^{-6}-Abstandsabhängigkeit experimentell bestätigen [195].

$$I_D(t) = I_D(0) \cdot exp\left\{-\frac{t}{\tau_D} + 2 \cdot y(t) \cdot \gamma \cdot \sqrt{\left(\frac{t}{\tau_D}\right)}\right\} \tag{A.23}$$

Für den Fall von endlichen Diffusionslängen während des Energietransferprozesses kann ein zeitabhängiger Korrekturterm ($y(t)$ in Gleichung (A.23)) eingeführt werden. Sind die Akzeptormoleküle nicht homogen um den Donor verteilt, treten durch diese Inhomogenität Abweichungen auf, die durch weitere Korrekturterme in Gleichung (A.22) berücksichtigt werden müssen [252].
Neben Dipol-Dipol-Wechselwirkungen gibt es auch noch Dipol-Quadropol und Quadropol-Quadropol-Wechselwirkungen. Methoden, die auf der Bestimmung des Coulomb Energietransfers beruhen, werden zur Bestimmung von Abständen zwischen Donor-Akzeptor-Molekülen bis zu 100 Å in Polymer- und Biowissenschaften häufig eingesetzt. Unter dem Akronym *FRET* (Fluoreszenz Resonanz Energie Transfer) wurde die Methode zur Untersuchung von Proteinen, Oligopeptiden, DNA, Myosin, Enzymen und synthetischen Polymeren eingesetzt [196]. Hierbei werden nicht nur statisch die Distanz zwischen zwei Punkten im Makromolekül bestimmt, sondern es können auch dynamische Prozesse, wie z.B. Proteinfaltungen, untersucht werden.

Anhang B

Tabellen

$\mathbf{Ln^{3+}}$	τ (μs)	Φ (%)	ϵ (λ_{abs}) ($M^{-1} \cdot cm^{1-}$)	**Ref.**
Eu^{3+} (H_2O)	104 - 110	0.5 - 1.9	0.01 (580)	[146, 168, 179]
$Eu(NO_3)_3$ (H_2O)	100	-	-	[175]
Eu^{3+} (D_2O)	2630 - 4000	78	-	[146, 168, 179]
$Eu(NO_3)_3$ (D_2O)	1900	-	-	[175]
$EuCl_3$ (D_2O)	2270	-	-	[175]
Tb^{3+} (H_2O)	400	8.4	-	[168]
$TbCl_3$ (H_2O)	430 - 470	-	-	[175, 176]
$Tb(NO_3)_3$ (H_2O)	390 - 460	-	-	[175, 176]
Tb^{3+} (D_2O)	3880	-	-	[168]
$TbCl_3$ (D_2O)	1300 - 3300	-	-	[175, 176]
$Tb(NO_3)_3$ (D_2O)	ca. 1200 - 3300	-	-	[175, 176]

Tabelle B.1: Einige photophysikalische Daten von Tb^{3+} und Eu^{3+} in Lösung (τ = Lumineszenzlebensdauer, Φ = Lumineszenzquantenausbeute, ϵ = Extinktionskoeffizient).

Ord.-zahl	**Name**	**Sym-bol**	**Elektronenkonfig. Ln**	**Ln^{3+}**	**Spektrosk. Grundterm**	**N**[1)]
57	*Lanthan*	La	$5d^16s^2$	$[Xe]$	$^1S_0$	1
58	Cer	Ce	$4f^15d^16s^2$	$4f^1$	$^2F_{5/2}$	2
59	Praeseodym	Pr	$4f^36s^2$	$4f^2$	$^3H_4$	13
60	Neodym	Nd	$4f^46s^2$	$4f^3$	$^4I_{9/2}$	41
61	Promethium	Pm	$4f^56s^2$	$4f^4$	$^5I_4$	107
62	Samarium	Sm	$4f^66s^2$	$4f^5$	$^6H_{1/2}$	198
63	Europium	Eu	$4f^76s^2$	$4f^6$	$^7F_0$	295
64	Gadolinium	Gd	$4f^86s^2$	$4f^7$	$^8S_{7/2}$	327
65	Terbium	Tb	$4f^96s^2$	$4f^8$	$^7F_6$	295
66	Dysprosium	Dy	$4f^{10}6s^2$	$4f^9$	$^6H_{15/2}$	198
67	Holmium	Ho	$4f^{11}6s^2$	$4f^{10}$	$^5I_8$	107
68	Erbium	Er	$4f^{12}6s^2$	$4f^{11}$	$^4I_{15/2}$	41
69	Thulium	Tm	$4f^{13}6s^2$	$4f^{12}$	$^3H_6$	13
70	Ytterbium	Yb	$4f^{14}6s^2$	$4f^{13}$	$^2F_{7/2}$	2
71	*Lutetium*	Lu	$4f^{14}5d^16s^2$	$4f^{14}$	$^1S_0$	1

Tabelle B.2: Elektronenkonfiguration von Lanthanidatomen und -ionen nach [112, 151] ([1)]Anzahl der möglichen Niveaus).

Donor	**Akzeptor**	**R_0 in Å**	**Ref.**
Tb^{3+}	Co^{2+}	19.6	[128]
Tb^{3+}	Fe^{3+}	27.1	[128]
Tb^{3+}	La^{3+}	0	[198]^a
Tb^{3+}	Dy^{3+}	5	[198]^a
Tb^{3+}	Eu^{3+}	7	[198]^a
Tb^{3+}	Nd^{3+}	12	[198]^a
Eu^{3+}	La^{3+}	0	[198]^a
Eu^{3+}	Dy^{3+}	7	[198]^a
Eu^{3+}	Nd^{3+}	11	[198]^a

Tabelle B.3: Förster Radien für den Energietransfer verschiedener Donor-Akzeptor-Paare (^{a}in $Ca(PO_3)_2$-Glas).

Anhang C

Geräte und Chemikalien

C.1 Verwendete Spektrometer

In den folgenden zwei Unterkapiteln sind die für die Durchführung der Messungen verwendeten Spektrometer tabellarisch zusammengestellt.

C.1.1 Messung von Fluoreszenz- und Lumineszenzabklingzeiten

	FL 920 (Edinburgh Instruments)		**Streak Kamera**	**iCCD**
	ns-Modus	**μs-Modus**	(Hamamatsu)	(LOT)
Anregungs-	Ti:Sa Laser	N_2-Laser	Ti:Sa Laser	N_2-Laser
lichtquelle	(Tsunami 3960,	(LTB)	(Tsunami 3960,	(LTB)
	Spectra Physics)		Spectra Physics)	
Rep.-rate	1 MHz	20 Hz	80 MHz	20 Hz
Pulsbreite	100 fs	10 ns	100 fs	10 ns
Pulsenergie	nJ	800 mJ	nJ	800 mJ
λ_{ex} (in nm)[6]	$260 < \lambda_{ex} < 300$	337.1	$260 < \lambda_{ex} < 300$	337.1
Detektion	MCP[1]	PMT[2]	MCP + iCCD[3]	iCCD
	ELDY EM1	R928	C5680	iStar
	(Europhoton)	(Hamamatsu)	(Hamamatsu)	(Andor)
Methode	SPC[4]	MCS[5]	SPC	Boxcar
IRF[7]	100 ps		3 ps	
λ_{em} (in nm)	$325 < \lambda_{em} < 500$	545, 593, 615	$325 < \lambda_{em} < 600$	$500 < \lambda_{em} < 700$

[1] Mikrokanalplatte (*micro channel plate*)
[2] Photomuliplier
[3] *intensified charged coupled device*
[4] Einzelphotonenzählung (*single photon counting*)
[5] *multi channel scaling* (Verfahren entspricht im Prinzip der Boxcar-Methode)
[6] THG
[7] Instrument-Antwort-Funktion (*instrument response function*)

C.1.2 Absorptions- und Fluoreszenzspektrometer

Typ	Hersteller
Lambda 2	Perkin Elmer
Cary 500	Varian
Fluoromax 3	Jobin Yvon
FS920	Edinburgh Instruments

In den Absorptionsmessungen wurden im Allgemeinen eine Vorschubgeschwindigkeit von 120 nm/min gewählt. Die spektrale Bandbreite der Detektion betrug standardmäßig 1 nm.
Bei der Aufnahme der stationären Fluoreszenzmessungen wurden die Spaltbreiten am FS920 und am Fluoromax 3 zur Messung der HS-Spektren auf 5 nm (Ex) und 2 nm (Em) eingestellt. Die Integrationszeit pro Datenpunkt war auf 0.5 s gesetzt. Die Fluoreszenzspektren der HS wurden - soweit nicht anders erwähnt - nicht quantenkorrigiert.

C.2 Chemikalien: Huminstoffe

Kurzbezeichung	**Ursprungsort**
Aldrich HS	kommerzielles Produkt (Aldrich)
BS1 FA bzw. HA	Bodensickerwasser [1]
GoHy573 FA bzw. HA	Gorleben-Grundwasser [253]
HO10 FA bzw. HA	Braunwassersee (Holohsee, Nordschwarzwald) [1]
Leonardite HA	IHSS Standard
Peat HA	IHSS Standard
Soil HA	IHSS Standard
Suwannee River (SR) FA und HA	IHSS Standard
HPOA	Suwannee River HS (Georgia, USA)
M42	Modellhuminstoff aus Xylose und Glutaminsäure, FZ Rossendorf [254, 255]
M1	Modellhuminstoff aus Xylose, Phenylalanin und Glycin, FZ Rossendorf [254, 255]

Tabelle C.1: Liste der verwendeten Huminstoffe

C.3 Referenzsubstanzen und -messungen

Die verschiedenen Messungen von Fluoreszenzabklingkinetiken im Nano- und Pikosekundenzeitbereich wurden mit Substanzen, von denen die Fluoreszenzabklingzeiten bekannt sind, überprüft. Im Falle des Nanosekundenzeitbereichs wurden Perylen, Anthracen und Pyren verwendet. Wesentlich aufwendiger waren die Messungen in der Pikosekundenzeitdomäne. Zur Überprüfung wurden Erythrosin, Rose Bengal, POPOP und Xanthion in verschiedenen Lösungsmitteln eingesetzt. Xanthion wurde zu diesem Zweck eigens hergestellt [256]. In den Abbildungen C.1 und C.2 sind das Absorptions- und das Fluoreszenzspektrum sowie die Fluoreszenzabklingkurven von Xanthion in zwei verschiedenen Lösungsmitteln beispielhaft dargestellt. Die weiteren photophysikalischen Daten (Fluoreszenzabklingzeit τ_F und Fluoreszenzquantenausbeute Φ_F) der untersuchten Referenzsubstanzen sind in Tabelle C.2 zusammengefaßt.

	Lösungsmittel		Literatur	Ref.
		τ_F / **ps**		
Xanthion	Benzen		12 ± 3	[257]
	Toluol	15		
	i-Octane		43	[258]
	Methylcyclohexan	28	42⋆	[259]
	Methanol	18	19⋆	[259]
	Perfluorhexan	190	460⋆	[259]
Erythrosin	Wasser	85	66 ± 8	[260]
Rose Bengal	MeOH	450	500 ± 20	[260]
		$\Phi_F \cdot 10^{-2}$		
Xanthion	Methylcyclohexan	0.49	0.36	[259]
	Methanol	0.37	0.15	[259]
	Perfluorhexan	1.23	3.8	[259]

Tabelle C.2: Photophysikalische Parameter der verwendeten Referenzverbindungen bei Streak-Kamera-Messungen. Die mit einem ⋆ gekennzeichneten Fluoreszenzlebenszeiten sind nach Strickler und Berg berechnet worden.

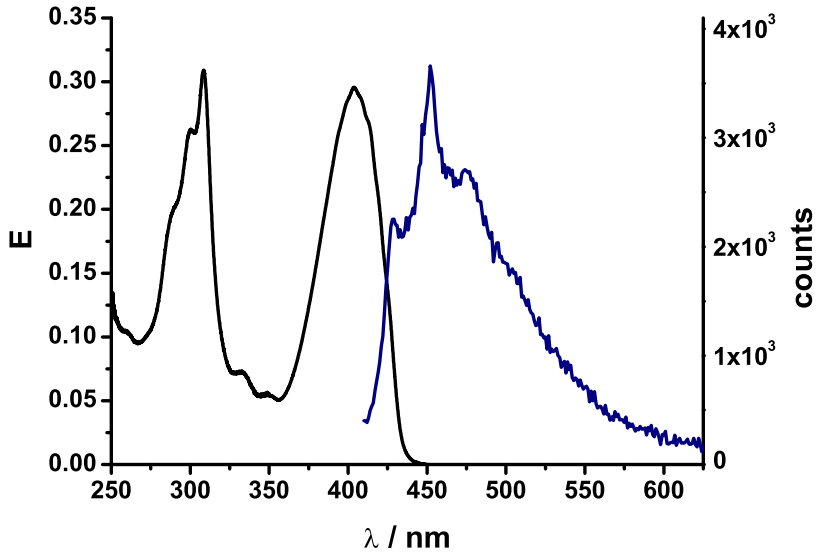

Abbildung C.1: UV/Vis-Absorptions- und Fluoreszenzspektrum von Xanthion in i-Propanol (λ_{ex}= 394 nm, $\Phi_F = 0.38 \cdot 10^{-2}$); Fluoromax, Yobion Yvon).

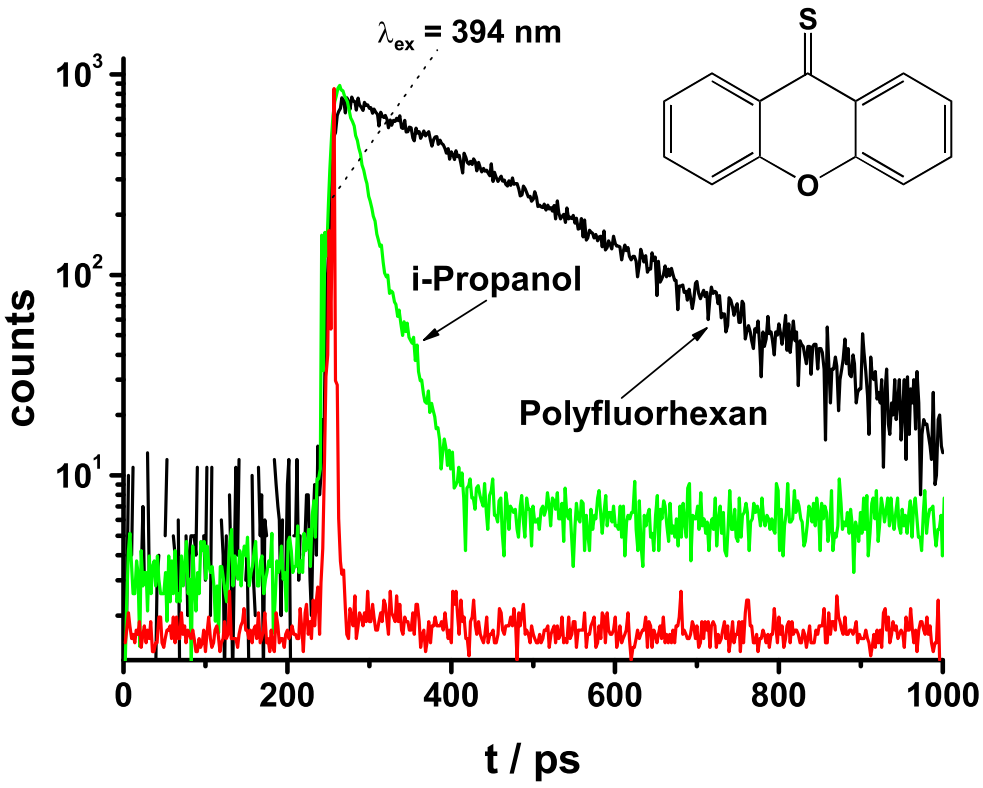

Abbildung C.2: Fluoreszenzabklingkurven von Xanthion in verschiedenen Lösungsmitteln (λ_{ex}= 394 nm, λ_{em}= 450 nm, $\tau_{Polyfluorhex.}$ = 190 ps, $\tau_{i-Prop.}$ = 29 ps); Streak Kamera Messsystem, Hamamatsu).

Anhang D

Veröffentlichungen und Tagungsbeiträge

D.1 Liste der Veröffentlichungen

1. Haberz, R. Müller-Hurtig, F. Wagner, M.U. Kumke, H.-G. Löhmannsröben, Th. Roch
   DECHEMA Biotechnology Conferences, Verlag Chemie, Weinheim, 1992, Band **5B**, S. 1017 - 1021.
   Microbial degradation and luminescence analysis of PAH/alkane mixtures in a stirred reactor with 10% soil content.

2. M.U. Kumke, H.-G. Löhmannsröben, Th. Roch
   in: Polycyclic Aromatic Compounds, P. Garrigues, M. Lamotte (eds.); Gordon and Breach, Amsterdam, 1993, S. 459 - 466.
   Luminescence spectroscopy of polynuclear aromatic hydrocarbons on soil surfaces.

3. M.U. Kumke, H.-G. Löhmannsröben, Th. Roch
   Analyst, 1994, **119**, S. 997 - 1001.
   Fluorescence quenching of polynuclear aromatic compounds by humic acid.

4. M.U. Kumke, H.-G. Löhmannsröben, Th. Roch, K. Czeschka, R. Müller-Hurtig
   Optical Sensing for Environmental Monitoring, Air&Waste Management Association, Pittsburgh, USA, 1994, S. 744 - 750.
   Stationary and time-resolved fluorescence spectroscopy of polynuclear aromatic compounds in environmental monitoring.

5. M.U. Kumke, H.-G. Löhmannsröben, Th. Roch
   J. Fluorescence 1995, **5**, S. 139 - 153.
   Fluorescence spectroscopy in environmental monitoring.

6. H.-G. Löhmannsröben, M.U. Kumke, Th. Roch
   GIT - Fachzeitschrift Labor, 1995, **39**, S. 112 - 116.

Fluoreszenzspektroskopie für die Umweltanalytik.

7. H.-G. Löhmannsräben, M.U. Kumke, Th. Meyer, Th. Roch, U. Zimmermann
Field Screening Methods for Hazardous Wastes and Toxic Chemicals, Proc. AWMA, 1995, **Vol. VIP-47**, 825 - 836.
Laser-induced fluorescence spectroscopy of polynuclear aromatic compounds and model oils in humic acid- and soil-containing compartments.

8. M.U. Kumke, L.B. McGown, T. Walker, P. Linn
Anal. Chem., 1995, **67**, S. 3945 - 3951.
Hybridisation of Fluorescein-labeled DNA oligomers detected by fluorescence anisotropy with protein binding enhancement.

9. J.W. Hofstraat, H.J. Verhey, J.W. Verhoeven, M.U. Kumke, L.B. McGown, E.G. Novikov, A. van Hoek, A.J.W.G. Visser
SPIE, 1996, **2705**, S. 110 - 121.
Time-resolved spectroscopy of charge-transfer fluorescenct molecules in polymer matrices.

10. M.U. Kumke, F.H. Frimmel
in: The Role of Humic Substances in the Ecosystems and in Environmental Protection, J. Drozd, S.S. Gonet, N. Senesi, J. Weber (eds), Proceedings of the 8th Meeting of the IHSS 8, Wroclaw, Poland, September 9-14, 1996, PTSH, Wroclaw, 1997, 525 - 531.
NOM - Experienced by time-resolved spectroscopy.

11. J.W. Hofstraat, H.J. Verhey, J.W. Verhoeven, M.U. Kumke, L.B. McGown, G. Li, S.L. Hemmingsen
Polymer, 1997, **38**, 2987 - 2994.
Fluorescence lifetime studies of labeled polystyrene latices.

12. M.U. Kumke, L.B. McGown, L.Shu, T. Walker, P. Linn, B. Pittner
Anal. Chem., 1997, **69**, 500 - 506.
Temperature and quenching studies of fluorescence polarization detection of DNA hybridization.

13. M.U. Kumke
SpectroLas-News, 1997, **3**, 5.
Anwenderbericht: Lumineszenz-Lebenszeitspektrometer FL900CDT.

14. M.U. Kumke, G. Abbt-Braun, F.H. Frimmel
Acta Hydrochem. Hydrobiol., 1998, **26**, 73 - 81.
Time-resolved fluorescence measurements of aquatic natural organic matter.

15. M.U. Kumke, C. Tiseanu, G. Abbt-Braun, F.H. Frimmel
J. Fluorescence, 1998, **8**, 309 - 318.
Fluorescence decay of natural organic matter (NOM) - Influence of fractionation, oxidation, and metal ion complexation.

16. D. Schmitt, M.U. Kumke, F. Seibel, F.H. Frimmel
Chemosphere, 1999, **38**, 2807 - 2824.
Mobilization experiments of pyrene and naphthalene from quartz in a completely mixed batch reactor.

17. F.H. Frimmel, M.U. Kumke
in: Humic substances: structure, properties, and uses, G. Davies and E. Ghabbour (eds.), Royal Society of Chemistry, Cambridge 1998, p. 113 - 122.
Fluorescence decay of humic substances (HS) - A comparative study.

18. C. Tiseanu, M.U. Kumke, F.H. Frimmel, R. Klenze, J.I. Kim
J. Photochem. Photobiol. A, 1998., **117**(3), 175 - 184.
Time-resolved fluorescence spectroscopy of fulvic acid and fulvic acid complexed with Eu^{3+} - A comparative study.

19. G.V. Korshin, M.U. Kumke, C.-W. Li, M.M. Benjamin, F.H. Frimmel
Environ. Sci. Technol., 1999, **33**, S. 1207 - 1212.
Influence of chlorination on chromophores and fluorophores in humic substances.

20. T.E. Doll, F.H. Frimmel, M.U. Kumke, G. Ohlenbusch
Fres. J. Anal. Chem., 1999, **364**, 313 - 319.
Interaction between natural organic matter (NOM) and polycyclic aromatic compounds (PAC) - comparison of fluorescence quenching and solid phase micro extraction (SPME).

21. C. Zwiener, M.U. Kumke, G. Abbt-Braun, F.H. Frimmel
Acta Hydrochim. Hydrobiol., 1999, **27**, 208 - 213.
Adsorbed and bound residues in fulvic acid fractions of a contaminated ground water: Isolation, chromatographic and spectroscopic characterization.

22. F.H. Frimmel, M.U. Kumke
Wiener Mitteilungen, 1999, **156**, 1 - 24.
Optische Parameter zur Stoffcharakterisierung vom Trinkwasser bis zum Abwasser.

23. M.U. Kumke, C. Zwiener, G. Abbt-Braun, F.H. Frimmel
Acta Hydrochim. Hydrobiol., 2000, **27**, 409 - 415.
Spectroscopic characterization of fulvic acid fractions of a contaminated groundwater.

24. Y.Y. Win, M.U. Kumke, C.H. Specht, A.J. Schindelin, G. Kolliopoulos, G. Ohlenbusch, G. Kleiser, S. Hesse, F.H. Frimmel
Wat. Res., 2000, **34**, 2098 - 2104.
Influence of oxidation of dissolved organic matter (DOM) on subsequent water treatment processes.

25. G. Ohlenbusch, M.U. Kumke, F.H. Frimmel
Sci. Tot. Environ., 2000, **253**, 63 - 74.
Sorption of phenols to dissolved organic matter investigated by solid phase microextraction.

26. C.H. Specht, M.U. Kumke, F.H. Frimmel
Wat. Res., 2000, **34**, 4063 - 4069.
Humic substances - clay minerals interactions investigated by size-exclusion chromatography coupled with online detection of dissolved organic carbon, UV-absorbance and fluorescence.

27. M.U. Kumke, F.H. Frimmel, F. Ariese, C. Gooijer
Environ. Sci. Technol., 2000, **34**, 3818 - 3823.
Fluorescence of humic acids (HA) and pyrene-HA complexes at ultra-low temperature.

28. M.U. Kumke, C.H. Specht, T. Brinkmann, F.H. Frimmel
Chemosphere, 2001, **45**, 1023 - 1031.
Alkaline hydrolysis of humic substances - Spectroscopic and chromatographic investigations.

29. J.-M. Monsalier, F. Scherbaum, G. Buckau, J.I. Kim, M.U. Kumke, C.H. Specht, F.H. Frimmel
J. Photochem. Photobiol. A, 2001, **138**, 55 - 63.
Influence of photochemical reactions on the complexation of humic acid with europium(III).

30. F.H. Frimmel, M. Assenmacher, M.U. Kumke, C.H. Specht, G. Abbt-Braun, G. Gräbe
Chem. Eng. Proc., 2001, **41**, 731 - 736.
Removal of hydrophilic compounds from water with organic polymers. Part II: Adsorption behavior of industrial wastewater.

31. M.U. Kumke, F.H. Frimmel
in: Refractory organic substances in the Environment, F.H. Frimmel, G. Abbt-Braun (eds), Wiley 2002, 215 - 231.
Stationary and time-resolved fluorescence for refractory organic substances characterization.

32. F.-D. Kopinke, A. Georgi, K. Mackenzie, M.U. Kumke
in: Refractory organic substances in the Environment, F.H. Frimmel, G. Abbt-Braun (eds), Wiley 2002, 475 - 515.
Sorption and chemical reactions of PAHs with dissolved humic substances and related model polymers.

33. K. Mackenzie, A. Georgi, M.U. Kumke, F.-D. Kopinke
Environ. Sci. Technol., 2002, **36**, 4403 - 4409.

Sorption of pyrene to dissolved humic substances and related model polymers. 2. Solid-phase microextraction (SPME) and fluorescence quenching technique (FQT) as analytical methods.

34. I. Billard, E. Ansoborlo, K. Apperson, S. Arpigny, M.E. Azehna, D. Birch, P. Bros, H.D. Burrows, G. Choppin, L. Couston, V. Dubois, T. Fanghanel, G. Geipel, S. Hubert, J.I. Kim, T. Kimura, R. Klenze, A. Kronenberg, M. Kumke, G. Lagarde, G. Lamarque, S. Lis, C. Madic, G. Meinrath, C. Moulin, R. Nagaisi, D. Parker, G. Plancque, F. Scherbaum, E. Simoni, S. Sinkov, C. Viallesoubranne
Appl. Spectros., 2002, **57**, 1027 - 1038.
Aqueous solutions of U(VI) as studied by time-resolved laser-induced fluorescence spectroscopy (TRLFS) : A round-robin test.

35. C. Dosche, M.U. Kumke, H.-G. Löhmannsröben, F. Ariese, A.N. Bader, C. Gooijer, K.P.C. Vollhardt
Phys. Chem. Chem. Phys., 2003, **5**, 4563 - 4569.
Shpol'skii spectroscopy and vibrational analysis of [N]phenylenes.

36. C. Tiseanu, R.K. Mehra, R. Kho, M.U. Kumke
Chem.Phys.Lett., 2003, **377**, 131 - 136.
Optical properties of terbium-doped thiosalicylic-capped CdS nanocrystals.

37. C. Tiseanu, R.K. Mehra, R. Kho, M.U. Kumke
J. Phys. Chem. B, 2003, **107**, 12153 - 12160.
Comparative study of time-resolved photoluminescence properties of terbium-doped thiosalicylic-capped CdS and ZnS nanocrystals.

38. T. Kietzke, D. Neher, M.U. Kumke, R. Montenegro, K. Landfester, U. Scherf
Macromolecules, 2004, **37**, 4882 - 4890.
A Nanoparticle approach to control the phase separation in polyfluorene photovoltaic devices.

39. C. Tiseanu, L. Frunza, M.U. Kumke
Physica B, 2004, **352**, 358 - 365.
Time-resolved photoluminescence analysis of distribution and migration of terbium ions in zeolites X.

40. M.U. Kumke, S. Eidner
in: Humic substances: molecular details and applications in land and water conservation, E.A. Ghabbour und G. Davies (eds), Taylor and Francis, Inc., 2004, zur Veröffentlichung angenommen.
Fluorescence and energy transfer processes of humic substances and related model compounds in terbium complexes.

41. C. Dosche, M.U. Kumke, H.-G. Löhmannsröben, F. Ariese, A.N. Bader, C. Gooijer, O.S. Miljanic, M. Iwamoto, K.P.C. Vollhardt, R. Puchta and N.J.R.

van Eikema Hommes
Phys. Chem. Chem. Phys., 2004, **6**, 5476 - 5483.
Deuteration effects on the vibronic structure of the fluorescence spectra and the internal conversion rates of triangular [4]Phenylene.

42. B. Schuler, E.A. Lipman, P.J. Steinbach, M.U. Kumke, W.A. Eaton
Proc. Natl. Acad. Sci., 2004, zur Veröffentlichung angenommen.
Polyproline and the spectroscopic ruler revisited with single molecule fluorescence.

D.2 Vorträge

1. M.U. Kumke, L.B. McGown, T. Walker, P. Linn
PitCon, 1995 in New Orleans, USA.
Hybridisation of fluorescein-labeled DNA oligomers detected by time-resolved fluorescence anisotropy.

2. M.U. Kumke
Wasserchemisches und -technologisches Kolloquium des Lehrstuhls für Wasserchemie am Engler-Bunte-Institut der TH Karlsruhe, 1995 in Karlsruhe, Deutschland.
Fluoreszenzspektroskopische Untersuchungen der Wechselwirkungen zwischen Huminstoffen und polyzyklischen aromatischen Kohlenwasserstoffen.

3. M.U. Kumke, F.H. Frimmel
8th Meeting of the International Humic Substances Society, 9. - 14. September 1996 in Wroclaw, Polen.
NOM - Experienced by time-resolved spectroscopy.

4. M.U. Kumke, G. Abbt-Braun, F.H. Frimmel
Jahrestagung der Fachgruppe Wasserchemie in der Gesellschaft Deutscher Chemiker, 5. - 7. Mai 1997 in Lindau, Deutschland.
Dynamik natürlicher Wasserinhaltsstoffe - Untersuchungen zum Fluoreszenzabklingverhalten von Huminstoffen.

5. M.U. Kumke, F.H. Frimmel
43rd International Conference on Analytical Sciences and Spectroscopy, 10. - 13. August 1997 in Montreal, Canada.
Interactions of metals with natural organic matter (NOM) characterized by time-resolved fluorescence.

6. M.U. Kumke, F.H. Frimmel
24th Meeting of the Federation of Analytical Chemistry and Spectroscopic Sciences, 26. - 30. Oktober 1997 in Providence, USA.
Fluorescence decay of natural organic matter (NOM) - Influence of fractionation, oxidation and metal ion complexation.

7. M.U. Kumke, F.H. Frimmel
   Analytica Conference 98 - Advanced Aquatic Analyses, 24. April 1998 in München, Deutschland.
   Fluorescence, a tool for measuring interactions of water constituents.

8. M.U. Kumke
   Faculty of Chemistry, Department of General and Analytical Chemistry, vrije Universuteit Amsterdam, 12. Mai 1998 in Amsterdam, Niederlande.
   Analysis of humic substances (including sorption reactions) by time-resolved fluorescence techniques.

9. M.U. Kumke, F.H. Frimmel
   44th International Conference on Analytical Sciences and Spectroscopy, 9 - 12 August 1998 in Kingston, Canada.
   Investigation of the complexation dynamics between refractory organic substances (ROS) and metal ions.

10. F.H. Frimmel, M.U. Kumke
    Bildungszentrum für die Entsorgung und Wasserwirtschaft, 9. November 1998 in Duisburg, Deutschland.
    Optische Parameter zur Stoffcharakterisierung vom Trinkwasser bis zum Abwasser.

11. M.U. Kumke
    Faculty of Chemistry, Department of General and Analytical Chemistry, vrije Universuteit Amsterdam, 24. März 1999 in Amsterdam, Niederlande.
    Interaction of humic materials with organic and inorganic contaminants.

12. M.U. Kumke, F.H. Frimmel
    45th International Conference on Analytical Sciences and Spectroscopy, 24. - 29. Oktober 1999 in Vancouver, Canada.
    Conformational changes of natural organic matter - Induced by metal complexation.

13. M.U. Kumke, F.H. Frimmel, C. Gooijer, F. Ariese
    26th Meeting of the Federation of Analytical Chemistry and Spectroscopic Sciences, 24. - 29. Oktober 1999 in Vancouver, Canada.
    Interaction of PAH and humic substances - New aspects.

14. M.U. Kumke
    Wasserchemisches und -technologisches Kolloquium des Lehrstuhls für Wasserchemie der TH Karlsruhe, 21. Januar 2000 in Karlsruhe, Deutschland.
    Fluoreszenzsonden zur Untersuchung der Wechselwirkung von organischen Mikroverunreinigungen und NOM.

15. M.U. Kumke, H.-G. Löhmannsröben
    6th International Conference on the Biogeochemistry of Trace Elements (ICOBTE), 29. July - 2. August 2001 in Guelph, Canada.
    Binding of metals by natural ligands - What can we learn from fluorescence spectroscopy.

16. M.U. Kumke, H.-G. Löhmannsröben, S. Eidner, G. Korshin
    11th Meeting of the Inernational Humic Substances Society, 21. - 26. Juli 2002 in Boston, USA.
    Inter-Lanthanide luminescence resonance energy transfer in humic substances.

17. M.U. Kumke, H.-G. Löhmannsröben, S. Eidner, S. Prenzel
    European Young Investors Conference, März 2003 in Slubice, Polen.
    Interlanthanide energy transfer in mixed Tb^{3+}/Nd^{3+}-humat complexes.

18. M.U. Kumke, C. Dosche, H.-G. Löhmannsröben, R. Puchta, F. Ariese, A. Bader
    19th Meeting of the International Society for Polycyclic Aromatic Compounds, 21. - 25. September 2003 in Amsterdam, Niederlande.
    Shpol'skii spectroscopy of [N]phenylenes.

19. M.U. Kumke, S. Eidner
    Humic Substances Seminar VII, 17. - 19. März 2004 in Boston, USA.
    Investigation of metal ion complexation by humic substances (HS) and related model ligands using lanthanide ion probe spectroscopy (LIPS).

D.3 Posterbeiträge

1. M.U. Kumke, F.H. Frimmel
   Gordon Research Conference on Environmental Sciences: Water - Interaction of Chemical and Biological Processes, 23. - 28. Juni 1996 in New Hampton, USA.
   Molecular probes to investigate the structure-interaction-relationship between biogenic organic matter (BOM) and xenobiotics.

2. Symposium on Refractory Organic Substances in the Environment, 6. - 8. Oktober 1997 in Karlsruhe, Deutschland:

   - M.U. Kumke, G. Abbt-Braun, F.H. Frimmel
     Characterization of natural organic matter (NOM) using time resolved fluorescence spectroscopy.
   - S.R. Göb, S.H. Bossmann, A.M. Braun, M.U. Kumke, G. Abbt-Braun, F.H. Frimmel
     Single-photon counting investigations of the luminescence of humic substances from the Hohlohsee (Germany) in dependence of pH and DOC.

- A.J. Schindelin, S. Hesse, M.U. Kumke, G. Ohlenbusch, F. Seibel, M. Sörensen, F.H. Frimmel
  Influence of irradiation on physical and biological properties of brown water NOM.
- G. Abbt-Braun, A. Dankwardt, F.H. Fimmel, A. Georgi, B. Hock, U. Klaus, F.-D. Kopinke, M.U. Kumke, I. Lebelt, H.-G. Löhmannsröben, M. Spiteller, U. Zimmermann
  Reversible and irreversible interactions between refractory organic substances (ROS) and xenobiotics.
- D. Schmitt, C. Barth, M.U. Kumke, F. Seibel, F.H. Frimmel
  Mobilization of polycyclic aromatic hydrocarbons (PAH) from contaminated model soils in the presence of natural organic matter (NOM).
  Ch. Specht, M.U. Kumke, F.H. Frimmel
  FTIR measurements of natural organic matter adsorption on clay minerals in aqueous phase.

3. Ch. Specht, M.U. Kumke, F.H. Frimmel, G. Abbt-Braun
   Jahrestagung der Fachgruppe Wasserchemie in der Gesellschaft Deutscher Chemiker, 5. - 7. Mai 1997 in Lindau, Deutschland.
   Charakterisierung der Adsorption von NOM an Tonmineralien in Wasser.

4. M.U. Kumke, F.H. Frimmel
   Karlsruhe - Nancy -Twente Meeting 1997, 20. - 22.- Juni 1997 in De Lutte, Niederlande.
   Impact of complexation and oxidation reactions on the dynamic processes in natural organic matter.

5. M.U. Kumke, C. Barth, B. Ebrahimi, F.H. Frimmel
   Jahrestagung der Fachgruppe Wasserchemie in der Gesellschaft Deutscher Chemiker, 18. - 20. Mai 1998 in Lübeck, Deutschland.
   Untersuchung und Modellierung der Ausbreitung von hydrophoben organischen Substanzen (HOS) im Grundwasserleiter.

6. C. Specht, M.U. Kumke, F.H. Frimmel
   GDCh Umwelttagung, 27. - 30. September 1998 in Karlsruhe, Deutschland.
   Transport of contaminants in sediments and ground water - solute vs. suspended particle interaction phenomena.

7. M.U. Kumke, T. Brinkmann, C. Specht, F.H. Frimmel
   Symposium on Refractory Organic Substances in the Environment, 1. - 3. August 2000 in Karlsruhe, Deutschland.
   Alkaline hydrolysis of humic substances - spectroscopic and chromatographic investigations.

8. C. Dosche, M.U. Kumke, H.-G. Löhmannsröben, K.P.C. Vollhardt, A. Bader, F. Ariese, C. Gooijer

Symposium: Crossing Borders - Lasers in Physics, Chemistry and Biology, 30. - 31. Mai 2002 in Amsterdam, Niederlande.
Shpol'skii spectroscopy of zig-zag [N]phenylenes.

9. IUPAC Symposium on Photochemistry, 17. - 22. Juli 2004 in Granada, Spanien.

   - M.U. Kumke, C. Dosche, A. Bader, F. Ariese, R. Puchta
     Spectroscopic characterization of [N]Phenylenes
   - C. Dosche, M.U. Kumke, H.-G. Löhmannsröben, F. Ariese, R. Puchta, N.J.R. van Eikema Hommes
     Ground- and excited state vibrations as probes for bond strength changes in excited starphenylene

Anhang E

Thesen der Habilitationsschrift

Immobilisierung bzw. Mobilisierung und Transport von Xenobiotika in den Umweltkompartimenten Boden und Wasser sind von fundamentaler Bedeutung für unser (Über)Leben auf der Erde. Als einer der Hauptreaktionspartner für organische und anorganische Xenobiotika in der Umwelt sind Huminstoffe (HS) zu nennen, die Abbauprodukte pflanzlichen und tierischen Gewebes. Zur qualitativen und quantitativen Charakterisierung der Wechselwirkungen zwischen HS und Xenobiotika werden analytische Methoden benötigt, die auch bei der Untersuchung von extrem heterogenen Systemen aussagekräftige Daten zu liefern vermögen. HS stellen bedingt durch ihre Genese außerordentlich komplexe Stoffsysteme dar, die höchste Anforderungen an die Untersuchungsmethoden stellen. Spektroskopische Verfahren besitzen neben der hervorragenden Selektivität und Sensitivität, auch eine Multidimensionalität, die es gestattet, heterogene Systeme direkt zu untersuchen. Durch die Multidimensionalität der Fluoreszenz (mit den Observablen Intensität I_F, Anregungswellenlänge λ_{ex}, Emissionswellenlänge λ_{em} und Fluoreszenzabklingzeit τ_F) sind fluoreszenzbasierte Methoden besonders geeignet für die Untersuchung von heterogenen Systemen, wie sie HS darstellen.

Kapitel 2.1:
Zur spektroskopischen Charakterisierung der Huminstoffe (HS) wurden systematisch die intrinsische Fluoreszenz von HS mit stationären und zeitaufgelösten Methoden untersucht. Durch gezielte chemische Modifikationen, wie z.B. enzymatischer Hydrolyse wurde ein zusätzlicher strukturrelevanter Parameter in die Untersuchungen eingebunden.
In den spektroskopischen Untersuchungen der HS konnte in Kombination mit chemischen Verfahren sowie chromatographischen Trennmethoden der Einfluss des Ursprungsortes und damit der Vorläufersubstanzen auf die (spektroskopischen) Eigenschaften der HS gezeigt werden. Am Beispiel von speziellen Standorten, wie z.B. eines alten Gaswerksgeländes, wurde das Fortschreiten der Huminfizierung und der Abbau bzw. Einbau von organischen Xenobiotika (polyzyklischen aromatischen Kohlenwasserstoffen, PAK) in die HS-Matrix gezeigt. Desweiteren konnten substituierte Benzoesäuren als wesentliche Elemente der intrinsischen HS-Fluoreszenz von HS

nachgewiesen werden. Es zeigte sich, dass diese bei einem Großteil der HS verschiedener Ursprungsorte das die Fluoreszenz bestimmende Strukturelement sind. Diese Verbindungen zeichnen sich durch eine z.T. komplexe Photophysik aus, die sich auch im Fluoreszenzverhalten der HS wiederfindet. Es sind vor allem intra- und intermolekulare Energietransferprozesse sowie konformative Reorganisationsprozesse, die die Photophysik der HS prägen.

Kapitel 2.2:
Durch die Kombination von stationären und zeitaufgelösten Fluoreszenzmethoden mit der Mikrofestphasenextraktion wurden die Wechselwirkungen von PAK - als Leitsubstanzen für hydrophobe, organische Xenobiotika - und HS eingehend untersucht und charakterisiert. Besonders die erstmals durchgeführte spektral-hochaufgelöste Charakterisierung von PAK-HS-Komplexen bei Temperaturen < 10 K brachte neue Erkenntnisse über die vorliegenden PAK-HS-Komplexe. Es konnte gezeigt werden, dass ein Teil der PAK-Moleküle sich in einer Mikroumgebung befinden, die in ihrer Polarität der eines kurzkettigen Alkohols analog ist. Durch die Kombination von Fluoreszenzlöschung und Mikrofestphasenextraktion wurden konzentrationsbezogene und aktivitätsbezogene Effekte unterschieden. Es konnten zwei unterschiedlich starke Wechselwirkungen der PAK mit HS identifiziert werden. Durch vergleichende Experimente mit Polymeren, die als Modelle für HS eingesetzt wurden, konnte ebenso wie in den Tieftemperaturexperimenten gezeigt werden, dass im Falle der schwachen Wechselwirkung die molekulare Umgebung, in der sich die hydrophoben Xenobiotika befinden, der von kurzkettigen Alkoholen entspricht. Neben den Wechselwirkungen, die durch den hydrophilen bzw. hydrophoben Charakter von HS und Xenobiotika definiert werden, sind zusätzlich spezifische Wechselwirkungen in Betracht zu ziehen, falls die Xenobiotika auch funktionelle Gruppen enthalten (z.B. OH-Gruppen).

Kapitel 2.3:
Als zweite große Gruppe von Xenobiotika wurden Metallionen (Me^{n+}) und deren Wechselwirkungen mit HS betrachtet. Es wurde einerseits die intrinsische Fluoreszenz der HS und andererseits die Lumineszenz von Lanthanid-Ionen (Ln^{3+}) als Parameter untersucht. Der Mechanismus der Löschung der intrinsischen HS-Fluoreszenz durch Me^{n+} wurde systematisch mit stationären und zeitaufgelösten Fluoreszenztechniken charakterisiert. Es zeigte sich, dass neben der Löschung durch die Komplexierung bestimmter Metalle (z.B. Al^{3+} und Ga^{3+}) die HS-Fluoreszenz auch verstärkt werden kann. Die Verstärkung zeigte sich in spezifischen Spektralbereichen der HS-Fluoreszenz, wie durch die Aufnahme von Totalen Lumineszenzspektren demonstriert werden konnte. In den Fluoreszenzabklingkinetiken der HS wurden durch die Komplexierung von z.B. Eu^{3+}-Ionen Veränderungen in den Abklingzeitenverteilungen induziert. Diese waren abhängig von der Behandlung der HS (z.B. vorhergehende Oxidation) und den experimentellen Bedingungen, vor allem der Emissionswellenlänge. Qualitativ läßt sich die Löschung der intrinsischen Fluoreszenz durch Komplexierung von Metallionen als die Kombination aus äußerem Schweratomeffekt,

Veränderung der konformativen Freiheit der HS und Ladungstransfer-Reaktionen zwischen HS und Metallionen (z.B. Ligand-zu-Metall-Ladungstransfer) verstehen. Besonders die Bedeutung von konformativen Veränderungen, wie sie etwa für eine Reihe von organischen Fluorophoren (z.B. TICT-Zustände, *twisted intramolecular charge transfer*) gut beschrieben sind, war bisher für HS unterbewertet worden.

Kapitel 3:
Komplementär zu den Untersuchungen der intrinsischen HS-Fluoreszenz wurden Lumineszenzsonden, speziell Ln^{3+}-Ionen, eingesetzt, um die Wechselwirkungen zwischen HS und Me^{n+} zu charakterisieren. Die Lumineszenz der Ln^{3+} zeichnet sich durch außergewöhlich scharfe, spektral wohl-charakterisierte Lumineszenzbanden und durch μs-Lumineszenzabklingzeiten aus. Die Intensitätsverteilung im Lumineszenzspektrum verschiedener Ln^{3+} zeigt außerdem eine sogenannte Hypersensitivität, die es erlaubt, direkt auf die molekulare Umgebung der Ln^{3+}-Ionen in ihren jeweiligen Komplexen zu schließen. Da die Lumineszenzabklingkinetiken auf einer μs-Zeitskala stattfinden, können Störungen aufgrund von Matrixfluoreszenz durch entsprechendes Schalten des Detektors (*gaten*) ausgeschlossen werden.
Durch einen Vergleich der Lumineszenz- und Fluoreszenzeigenschaften von Ln^{3+}-Komplexen mit verschiedenen substituierten Benzoesäuren und mit HS konnte gezeigt werden, dass die beobachtete Veränderung der HS-Fluoreszenz nach Komplexierung von Me^{n+} stark durch die Veränderung der konformativen Freiheiten bzw. die Assoziation der HS bedingt ist. In diesen Experimenten wurde neben der Löschung der intrinsischen Fluoreszenz der substituierten Benzoesäuren bzw. der HS auch die sensibilisierte Lumineszenz der Ln^{3+} (Tb^{3+}, Eu^{3+}) untersucht. Auf diese Weise konnte die Komplexbildung über zwei unabhängige Messgrößen charakterisiert werden. Das war besonders im Fall der untersuchten Modellsubstanzen vorteilhaft, da für diese nur eine sehr geringe bzw. überhaupt keine Löschung der intrinsischen Fluoreszenz durch Ln^{3+}-Ionen gefunden wurde. Als Lumineszenzsonden wurden in erster Linie Tb^{3+}- und Eu^{3+}-Ionen verwendet. Die Sensibilisierung der Lumineszenz wird über einen strahlungslosen Energietransfer vom Liganden auf das Ln^{3+}-Ion bewirkt. Da die direkte Anregung bedingt durch die sehr kleinen Extinktionskoeffizienten wenig effizient ist, erlaubt die indirekte Anregung, die auch als Antenneneffekt bezeichnet wird, eine sehr empfindliche Messung der komplexierten Ln^{3+}-Ionen. Die Effizienz der Lumineszenzsensibilisierung war für die beiden Ionen unterschiedlich und hängt von den photophysikalischen Eigenschaften der eingesetzten Modellliganden bzw. der jeweiligen HS ab. Als wichtige Einflussgrößen sind dabei die Triplettenergie der Liganden und deren Redoxeigenschaften zu beachten. Im Fall des Tb^{3+} wird die Desaktivierung durch einen Energierücktransfer zum Liganden bestimmt und im Falle des Eu^{3+} durch die Bildung von nicht-lumineszierenden Ladungsübertragungskomplexen (*charge transfer*-, CT-Komplex). Der Energierücktransfer zeigte sich besonders deutlich in den komplexen Lumineszenzabklingkinetiken der Tb^{3+}-HS-Komplexe. Abweichend vom Lumineszenzverhalten der Tb^{3+}-Komplexe mit den substituierten Benzoesäuren, die erwartungsgemäß monoexponentielles Zeitverhalten zeigten, wurde für die HS-Komplexe ein nicht-exponentielles Lumineszenzab-

klingverhalten gefunden. Die Lumineszenzabklingkinetiken waren von Grad der Beladung der HS mit Tb^{3+} abhängig, wobei mit steigender Beladung die Unterschiede im Zeitverhalten immer geringer wurden. Die Auswertung erfolgte über eine gedehnte Exponentialfunktion (*stretched exponential fit*), aus der die Abklingzeit des ungelöschten Tb^{3+}-Ions im Komplex bestimmt werden konnte. Die Auswertung der Daten ergab u.a., dass in der inneren Koordinationssphäre von Ln^{3+}-HS-Komplexen mindestens noch acht Wassermoleküle gebunden sind, d.h. die gebildeten Komplexe von Ln^{3+} und HS liegen zunächst als Komplexe mit starkem *outer-sphere*-Charakter vor.
Aus der Untersuchung des Interlanthanid-Energietransfers in gemischten HS-Ln^{3+}-Komplexen, in denen Ln^{3+}-Ionen-Paare - vorzugsweise Tb^{3+} und Nd^{3+} - als Energie-Donor und -Akzeptor verwendet wurden, konnte der mittlere Abstand von Metallbindungsstellen in HS bestimmt werden. Dieser hängt einerseits von der HS selbst ab (Ursprungsort, Fulvin- bzw. Huminsäurefraktion) und von den Solvensbedingungen, wie z.B. dem pH-Wert. Mit steigender Beladung verringerte sich erwartungsgemäß der mittlere Abstand zwischen den Ln^{3+}-Ionen und näherte sich aber dann einem für die jeweilige HS charakteristischen Grenzabstand. Bei konstanter Beladung der HS mit Ln^{3+}-Ionen änderte sich der mittlere Abstand der gebundenen Ln^{3+} durch pH-Wertvariation. Mit abnehmendem pH-Wert wurde eine Zunahme des mittleren Abstands gefunden. Dies wird durch die sinkende Anzahl an verfügbaren Bindungsplätzen verursacht, da bei sinkendem pH-Wert eine fortschreitende Neutralisation der Ladung der HS-Moleküle erfolgt und außerdem eine z.B über Wasserstoffbrückenbindungen initiierte Bildung von größeren HS-Aggregaten stattfindet.

Anhang F

Lehre und Lebenslauf

Titel	**Zeitraum**	**Art**	**Umfang**
Engler-Bunte-Institut, TH Karlsruhe			
Untersuchung und Beurteilung	WS 98/99	VL	2 SWS
von Gewässern	WS 99/00		
Institut für Chemie, Universität Potsdam			
Physikalische Chemie I	WS 00/01	Ü	1 SWS
	WS 01/02		
	WS 02/03		
Physikalische Chemie II	SS 01	Ü	2 SWS
	SS 02		
Physikalische Chemie IV	WS 02/03	VL	2 SWS
	WS 03/04		
	WS 04/05		
Physikalische Chemie V	SS 04	VL	2 SWS
Grundpraktikum Physikalische	SS 01	P	6 SWS
Chemie für DC	SS 02		
	SS 03		
	SS 04		
Fortgeschrittenen Praktikum	WS 00/01	P	6 SWS
Physikalische Chemie für DC	WS 01/02		
	WS 02/03		8 SWS
	WS 03/04		
	WS 04/05		8 SWS

Curriculum vitae

Persönliche Daten

Name	Michael U. Kumke
Geburtsdatum	21.9.1963 in Braunschweig
Familienstand	verheiratet, eine Tochter
Staatsangehörigkeit	deutsch
Anschrift	Golmer Fichten 1, 14476 Potsdam-Golm

Ausbildung

1983	Abitur (Humboldt-Gymnasium, Gifhorn)
1984 - 1990	Chemiestudium (TU Braunschweig)
1990 - 1994	Anfertigung der Dissertation
1994	Promotion in der Physikalischen Chemie an der TU Braunschweig

Beruflicher Werdegang

1990 - 1993	wissenschaftl. Angestellter an der TU Braunschweig
1994 - 1995	Research Associate an der Duke University (NC, USA)
1995 - 1998	Angestellter beim Deutschen Verein des Gas- und Wasserfachs
1998 - 2000	wissenschaftl. Angestellter am Engler-Bunte-Institut (TH Karlsruhe)
seit 2000	Abteilungsleiter und stellvertretender Arbeitsgruppenleiter in der Physikalischen Chemie (Institut für Chemie, Universität Potsdam)
seit 2001	Leitung verschiedener F&E-Projekte

Auslandsaufenthalte

1994 - 1995	Postdoc an der Duke University (NC, USA)
seit 1995	mehrere, durch die Europäische Union geförderte, Forschungsaufenthalte an der Faculty of Chemistry, vrije Universiteit Amsterdam, Niederlande

Erklärungen

Hiermit versichere ich, dass zu keinem anderen Zeitpunkt an einer anderen Hochschule ein Habilitationsantrag gestellt worden ist.

Von der Habilitationsordnung der Universität Potsdam habe ich Kenntnis genommen.

Literaturverzeichnis

[1] Frimmel, F.H. ; Abbt-Braun, G. ; Heumann, K.G. ; Hock, B. ; Lüdemann, H.-D. ; Spiteller, M.: *Refractory organic substances in the environment*. Wiley-VCH, 2002

[2] Stevenson, F.J.: *Humus chemistry - genesis, composition, reactions*. Wiley, 1982

[3] Christman, R.F. ; Gjessing, E.T.: *Aquatic and terrestrial humic materials*. Ann Arbor Science, 1983

[4] Aiken, G.R. ; McKnight, D.M. ; Wershaw, R.L. ; MacCarthy, P.: *Humic substances in soil, sediments and water: geochemistry, isolation, and characterization*. Wiley, 1985

[5] Choundhry, G.G.: *Humic Substances: structural, photophysical, photochemical, free radical and interactions with environmental chemicals*. Gordon and Breach, 1984

[6] Frimmel, F.H. ; Christman, R.F.: *Humic Substances and their role in the environment*. Wiley, 1988

[7] Kögelknabner, I. ; Totsche, K.U.: Influence of dissolved and colloidal phase humic substances on the transport of hydrophobic organic contaminants in soils. In: *Phys. Chem. Earth* 23 (1998), S. 179–185

[8] Weigand, H. ; Totsche, K.U. ; Kögelknabner, I.: Effect of fluctuating input of dissolved organic matter on long-term mobility of polycyclic aromatic hydrocarbons in soils. In: *Phys. Chem. Earth* 23 (1998), S. 211–214

[9] Kögel-Knabner, I. ; Totsche, K.U. ; Raber, B.: Desorption of polycyclic aromatic hydrocarbons from soil in the presence of dissolved organic matter: effect of solution composition and aging. In: *J. Environ. Qual.* 29 (2000), S. 906–916

[10] Weigand, H. ; Totsche, K.U. ; Huwe, B. ; Kögel-Knabner, I.: PAH mobility in contaminated industrial soils: a Markov chain approach to the spatial variability of soil properties and PAH levels. In: *Geoderma* 102 (2001), S. 371–389

[11] Mantoura, R.F.C. ; Riley, J.P.: The analytical concentration of humic substances from natural waters. In: *Anal. Chim. Acta* 76 (1975), S. 97–106

[12] Abbt-Braun, G. ; Frimmel, F.H. ; Lipp, P.: Isolation of organic substances from aquatic and terrestrial systems - comparison of some methods. In: *Z. Wasser-Abwasser-Forsch.* 24 (1991), S. 285–292

[13] Hayes, M.H.B. ; MacCarthy, P. ; Malcom, R.L. ; Swift, R.S.: *Humic substances II: in search of structure.* Wiley, 1989

[14] Christl, I. ; Knicker, H. ; Kögel-Knabner, I. ; Kretzschmar, R.: Chemical heterogeneity of humic substances: characterization of size fractions obtained by hollow-fibre ultrafiltration. In: *Eur. J. Soil Sci.* 51 (2000), S. 617–625

[15] Rostad, C.E. ; Leenheer, J.A.: Factors that affect molecular weight distribution of Suwannee river fulvic acid as determined by electrospray ionization/mass spectrometry. In: *Anal. Chim. Acta* 523 (2004), S. 269–278

[16] Nurmi, J.T. ; Tratnyek, P.G.: Electrochemical properties of natural organic matter (NOM), fractions of NOM, and model biogeochemical electron shuttles. In: *Environ. Sci. Technol.* 36 (2002), S. 617–624

[17] Frimmel, F.H.: Development in aquatic humic chemistry. In: *Agronomie* 20 (2000), S. 451–463

[18] Stenson, A.C. ; Marshall, A.G. ; Cooper, W.T.: Exac masses and chemical formulas of individual Suwannee river fulvic acids from ultrahigh resolution electrospray ionization fourier transform ion cyclotron resonance mass spectra. In: *Anal. Chem.* 75 (2003), S. 1275–1284

[19] Abbt-Braun, G. ; Lankes, U. ; Frimmel, F.H.: Structural characterization of aquatic humic substances - The need for a multiple method approach. In: *Aqua. Sci.* 66 (2004), S. 151–170

[20] Lead, J.R. ; Wilkinson, K.J. ; Starchev, K. ; Canonica, S. ; Buffle, J.: Determination of diffusion coefficients of humic substances by fluorescence correlation spectroscopy: Role of solution conditions. In: *Environ. Sci. Technol.* 34 (2000), S. 1365–1369

[21] Lead, J.R. ; Wilkinson, K.J. ; Balnois, E. ; Cutak, B.J. ; Larive, C.K. ; Assemi, S. ; Beckett, R.: Diffusion coefficients and polydispersities of the Suwannee River fulvic acid: Comparison of fluorescence correlation spectroscopy, pulse-field gradient nuclear magnetic resonance, and flow field-flow fractionation. In: *Environ. Sci. Technol.* 34 (2000), S. 3508–3513

[22] Hosse, M. ; Wilkinson, K.J.: Determination of electrophoretic mobilities and hydrodynamic radii of three humic substances as a function of pH and ionic strength. In: *Environ. Sci. Technol.* 35 (2001), S. 4301–4306

[23] Avena, M.J. ; Wilkinson, K.J.: Disaggregation kinetics of a peat humic acid: mechanism and pH effects. In: *Environ. Sci. Technol.* 36 (2002), S. 5100–5105

[24] Lead, J.R. ; Starchev, K. ; Wilkinson, K.J.: Diffusion coefficients of humic substances in aarose gel and in water. In: *Environ. Sci. Technol.* 37 (2003), S. 482–487

[25] Alberts, J.J. ; Takacs, M. ; Egeberg, P.K.: Total luminescence spectral characteristics of natural organic matter (NOM) size fractions as defined by ultrafiltration and high performance size exclusion chromatography (HPSEC). In: *Org. Geochem.* 33 (2002), S. 817–828

[26] Wu, F.C. ; Evans, R.D. ; Dillon, P.J.: Separation and characterization of NOM by high-performance liquid chromatography and on-line three-dimensional excitation emission matrix fluorescence detection. In: *Environ. Sci. Technol.* 37 (2003), S. 3687–3693

[27] Hewitt, J.D. ; McGown, L.B.: On-the-fly fluorescence lifetime detection of humic substances in capillary electrophoresis. In: *Appl. Spectrosc.* 57 (2003), S. 256–265

[28] Her, N. ; Amy, G. ; McKnight, D. ; Sohn, J. ; Yoon, Y.M.: Characterization of DOM as a function of MW by fluorescence EEM and HPLC-SEC using UVA, DOC, and fluorescence detection. In: *Wat. Res.* 37 (2003), S. 4295–4303

[29] Alberts, J.J. ; Takacs, M.: Total luminescence spectra of IHSS standard and reference fulvic acids, humic acids and natural organic matter: comparison of aquatic and terrestrial source terms. In: *Org. Geochem.* 35 (2004), S. 243–256

[30] Esteves, V.I. ; Duarte, A.C.: Differences between humic substances from riverine, estuarine, and marine environments observed by fluorescence spectroscopy. In: *Acta Hydrochim. Hydrobiol.* 28 (2001), S. 359–363

[31] Chen, W. ; Westerhoff, P. ; Leenheer, J.A. ; Booksh, K.: Fluorescence excitation-emission matrix regional integration to quantify spectra for dissolved organic matter. In: *Environ. Sci. Technol.* 37 (2003), S. 5701–5710

[32] Hautala, K. ; Peuravuori, J. ; Pihlaja, K.: Measurement of aquatic humus content by spectroscopic analyses. In: *Wat. Res.* 34 (2000), S. 246–258

[33] Bengraine, K. ; Marhaba, T.F.: Comparison of spectral fluorescent signatures-based models to characterize DOM in treated water samples. In: *J. Hazard. Mat.* 100 (2003), S. 117–130

[34] Goslan, E.H. ; Voros, S. ; Banks, J. ; Wilson, D. ; Hillis, P. ; Campbell, A.T. ; Parsons, S.A.: A model for predicting dissolved organic carbon distribution in a reservoir water using fluorescence spectroscopy. In: *Wat. Res.* 38 (2004), S. 783–791

[35] Kang, K.H. ; Shin, H.S. ; Park, H.: Characterization of humic substances present in landfill leachates with different landfill ages and its implications. In: *Wat. Res.* 36 (2002), S. 4023–4032

[36] Zanardi-Lamardo, E. ; Clark, C.D. ; Moore, C.A. ; Zika, R.G.: Comparison of the molecular mass and optical properties of colored dissolved organic material in two rivers and coastal waters by flow field-flow fractionation. In: *Environ. Sci. Technol.* 36 (2002), S. 2806–2814

[37] Baker, A.: Fluorescence excitation-emission matrix characterization of river waters impacted by a tissue mill effluent. In: *Environ. Sci. Technol.* 36 (2002), S. 1377–1382

[38] Santos, E.B.H. ; Filipe, O.M.S. ; Duarte, R.M.B.O. ; Pinto, H. ; Duarte, A.C.: Fluorescence as a tool for tracing the organic contamination from pulp mill effluents in surface waters. In: *Acta Hydrochim. Hydrobiol.* 28 (2001), S. 364–371

[39] Baker, A. ; Lamont-Black, J.: Fluorescence of dissolved organic matter as a natural tracer of ground water. In: *Ground Wat.* 39 (2001), S. 745–750

[40] Parlanti, E. ; Wörz, K. ; Geoffroy, L. ; Lamotte, M.: Dissolved organic matter fluorescence spectroscopy as a tool to estimate biological activity in a coastal zone submitted to anthropogenic inputs. In: *Org. Geochem.* 31 (2000), S. 1765–1781

[41] Westerhoff, P. ; Chen, W. ; Esparza, M.: Fluorescence analysis of a standard fulvic acid and tertiary treated wastewater. In: *J. Environ. Qual.* 30 (2001), S. 2037–2046

[42] Ahmad, U.K. ; Ujang, Z. ; Yusop, Z. ; Fong, T.L.: Fluorescence technique for the characterization of natural organic matter in river water. In: *Wat. Sci. Technol.* 46 (2002), S. 117–125

[43] Clark, C.D. ; Jimenez-Morais, J. ; Jones, G. ; Zanardi-Lamardo, E. ; Moore, C.A. ; Zika, R.G.: A time-resolved fluorescence study of dissolved organic matter in a riverine to marine transition zone. In: *Mar. Chem.* 78 (2002), S. 121–135

[44] McKnight, D.M. ; Boyer, E.W. ; Westerhoff, P.K. ; Doran, P.T. ; Kulbe, T. ; Anderson, D.T.: Spectrofluorometric characterization of dissolved organic matter for indication of precursor organic material and aromaticity. In: *Limnol. Oceanogra.* 46 (2001), S. 38–48

[45] Kalbitz, K. ; Geyer, S. ; Geyer, W.: A comparative characterization of dissolved organic matter by means of original aqueous samples and isolated humic substances. In: *Chemosphere* 40 (2000), S. 1305–1312

[46] Fiedler, S. ; Kalbitz, K.: Concentrations and properties of dissolved organic matter in forest soils as affected by the redox regime. In: *Soil Sci.* 168 (2003), S. 793–801

[47] Cocozza, C. ; D'Orazio, V. ; Miano, T.M. ; Shotyk, W.: Characterization of solid and aqueous phases of a peat bog profile using molecular fluorescence spectroscopy, ESR and FT-IR, and comparison with physical properties. In: *Org. Geochem.* 34 (2003), S. 49–60

[48] Ohno, T.: Fluorescence inner-filtering correction for determining the humification index of dissolved organic matter. In: *Environ. Sci. Technol.* 36 (2002), S. 742–746

[49] Milori, D.M.B.P. ; Marin-Neto, L. ; Bayer, C. ; Mielniczuk, J. ; Bagnato, V.S.: Humification degree of soil humic acids determined by fluorescence spectroscopy. In: *Soil Sci.* 167 (2002), S. 739–749

[50] Komada, T. ; Schofield, O.M.E. ; Reimers, C.E.: Fluorescence characteristics of organic matter released from coastal sediments during resuspension. In: *Mar. Chem.* 79 (2002), S. 81–97

[51] Patel-Sorrentino, N. ; Mounier, S. ; Benaim, J.Y.: Excitation-emission fluorescence matrix to study pH influence on organic matter fluorescence in the Amazon basin rivers. In: *Wat.Res.* 36 (2002), S. 2571–2581

[52] Peuravuori, J. ; Koivikko, R. ; Pihlaja, K.: Characterization, differentiation and classification of aquatic humic matter separated with different sorbents: synchronous scanning fluorescence spectroscopy. In: *Wat. Res.* 36 (2002), S. 4552–4562

[53] Richard, C. ; Trubetskaya, O. ; Trubetskoj, O. ; Reznikova, O. ; Eva, G. A. ; Aguer, J.-P. ; Guyot, G.: Key role of the low molecular size fraction of soil humic acids for fluorescence and photoinductive activity. In: *Environ. Sci. Technol.* 28 (2004), S. 2052–2057

[54] Fasnacht, M.P. ; Blough, N.V.: Aqueous photodegradation of polycyclic aromatic hydrocarbons. In: *Environ. Sci. Technol.* 36 (2002), S. 4364–4369

[55] Chen, J. ; Gu, B.H. ; LeBoeuf, E.J. ; Pan, H.J. ; Dai, S.: Spectroscopic characterization of the structural and functional properties of natural organic matter fractions. In: *Chemosphere* 48 (2002), S. 59–68

[56] Chen, J. ; LeBoeuf, E.J. ; Dai, S. ; Gu, B.H.: Fluorescence spectroscopic studies of natural organic matter fractions. In: *Chemosphere* 50 (2003), S. 639–647

[57] Filippova, E.M. ; Fadeev, V.V. ; Chubarov, V.V. ; Dolenko, T.A. ; Glushkov, S.M.: Laser fluorescence spectroscopy as a method for studying humic substance. In: *Appl. Spectros. Rev.* 36 (2001), S. 87–117

[58] Ariese, F. ; van Assema, S. ; Gooijer, C. ; Bruccoleri, A.G. ; Langford, C.H.: Comparison of Laurentian fulvic acid luminescence with that of the hydroquinone/quinone model system: evidence from low temperature fluorescence studies and EPR spectroscopy. In: *Aquat. Sci.* 66 (2004), S. 86–94

[59] Klapper, L. ; McKnight, D.M. ; Fulton, J.R. ; Nevin, K.P. ; Lovley, D.R. ; Hatcher, P.G.: Fulvic acid oxidation state detection using fluorescence spectroscopy. In: *Environ. Sci. Technol.* 36 (2002), S. 3170–3175

[60] Vecchio, R. D. ; Blough, N.V.: On the origin of the optical properties of humic substances. In: *Environ. Sci. Technol.* 38 (2004), S. 3885–3891

[61] Haitzer, M. ; Löhmannsröben, H.G. ; Steinberg, C.E.W. ; Zimmermann, U.: In vivo laser-induced fluorescence detection of pyrene in nematodes and determination of pyrene binding constants for humic substances by fluorescence quenching and bioconcentration experiments. In: *J. Environ. Mon.* 2 (2000), S. 145–149

[62] Steinberg, C.E.W. ; Haitzer, M. ; Bruggemann, R. ; Perminova, I.V. ; Yashchenko, N.Y. ; Petrosyan, V.S.: Towards a quantitative structure activity relationship (QSAR) of dissolved humic substances as detoxifying agents in freshwaters. In: *Int. Rev. Hydrobiol.* 85 (2000), S. 253–266

[63] Perminova, I.V. ; Grechishcheva, N.Y. ; Kovalevskii, D.V. ; Kudryavtsev, A.V. ; Petrosyan, V.S. ; Matorin, D.N.: Quantification and prediction of the detoxifying properties of humic substances related to their chemical binding to polycyclic aromatic hydrocarbons. In: *Environ. Sci. Technol.* 35 (2001), S. 3841–3848

[64] Terashima, M. ; Tanaka, S. ; Fukushima, M.: Distribution behavior of pyrene to adsorbed humic acids on kaolin. In: *J. Environ. Qual.* 32 (2003), S. 591–598

[65] Karthikeyan, K.G. ; Chorover, J.: Effects of solution chemistry on the oxidative transformation of 1-naphthol and its complexation with humic acid. In: *Environ. Sci. Technol.* 34 (2000), S. 2939–2946

[66] Karthikeyan, K.G. ; Chorover, J.: Humic acid complexation of basic and neutral polycyclic aromatic compounds. In: *Chemosphere* 48 (2002), S. 955–964

[67] Lee, C.L. ; Kuo, L.J. ; Wang, H.L. ; Hsieh, P.C.: Effects of ionic strength on the binding of phenanthrene and pyrene to humic substances: three-stage variation model. In: *Wat. Res.* 37 (2003), S. 4250–4258

[68] Laor, Y. ; Rebhun, M.: Evidence for nonlinear binding of PAHs to dissolved humic acids. In: *Environ. Sci. Technol.* 36 (2002), S. 955–961

[69] Kopinke, F.D. ; Georgi, A. ; Mackenzie, K.: Sorption and chemical reactions of PAHs with dissolved humic substances and related model polymers. In: *Acta Hydrochim. Hydrobiol.* 28 (2001), S. 385–399

[70] Peuravuori, J.: Partition coefficients of pyrene to lake aquatic humic matter determined by fluorescence quenching and solubility enhancement. In: *Anal. Chim. Acta* 429 (2001), S. 65–73

[71] Backhus, D.A. ; Golini, C. ; Castellanos, E.: Evaluation of fluorescence quenching for assessing the importance of interactions between nonpolar organic pollutants and dissolved organic matter. In: *Environ. Sci. Technol.* 37 (2003), S. 4717–4723

[72] Shane, E.C. ; Price-Everett, M. ; Hanson, T.: Fluorescence measurement of pyrene wall adsorption and pyrene association with humic acids - an experiment for physical chemistry or instrumental methods. In: *J. Chem. Edu.* 77 (2000), S. 1617–1618

[73] Burel, L. ; Giamarchi, P. ; Stephan, L. ; Lijour, Y. ; Bihan, A. L.: Molecular and atomic ultra trace analysis by laser induced fluorescence with OPO systems and ICCD camera. In: *Talanta* 60 (2003), S. 295–302

[74] Valeur, B.: *Molecular fluorescence*. Wiley-VCH, 2002

[75] Zander, M.: *Polycyclische Aromaten*. 1. Auflage. Teubner Studienbücher Chemie, 1995

[76] Moulin, V. ; Moulin, C.: Radionuclide speciation in the environment: a review. In: *Radiochim. Acta* 89 (2001), S. 773–778

[77] Dierckx, A. ; Maes, A. ; Vancluysen, J.: Mixed complex-formation of Eu^{3+} with humic-acid and a competing ligand. In: *Radiochim. Acta* 66 (1994), S. 149–156

[78] Shin, H.S. ; Choppin, G.R.: A study of Eu(III)-humate complexation using Eu(III) luminescence spectroscopy. In: *Radiochim. Acta* 86 (1999), S. 167–174

[79] Sposito, G.: Trace metals in contaminated waters. In: *Environ. Sci. Technol.* 15 (1981), S. 396–403

[80] Lead, J.R. ; Hamilton-Taylor, J. ; Peters, A. ; Reiner, S. ; Tipping, E.: Europium binding by fulvic acids. In: *Anal. Chim. Acta* 369 (1998), S. 171–180

[81] Perdue, E.M. ; C.R.Lytle: Distribution model for binding of protons and metal ions by humic substances. In: *Environ. Sci. Technol.* 17 (1983), S. 654–660

[82] Dobbs, J.C. ; Susetyo, W. ; Knight, F.E. ; Castles, M.A. ; Carreira, L.A. ; Azarraga, L.V.: Characterization of metal binding sites in fulvic acids by lanthanide ion probe spectroscopy. In: *Anal. Chem.* 61 (1989), S. 483–488

[83] Dobbs, J.C. ; Susetyo, W. ; Carreira, L.A. ; Azarraga, L.V.: Competitive binding of protons and metal ions in humic substances by lanthanide ion probe spectroscopy. In: *Anal. Chem.* 61 (1989), S. 1519–1524

[84] Susetyo, W. ; Dobbs, J.C. ; Carreira, L.A. ; Azarraga, L.V. ; Grimm, D.M.: Development of a statistical model for metal-humic interactions. In: *Anal. Chem.* 62 (1990), S. 1215–1221

[85] Milne, C.J. ; Kinniburgh, D.G. ; Tipping, E.: Generic NICA-Donnan model parameters for proton binding by humic substances. In: *Environ. Sci. Technol.* 35 (2001), S. 2049–2059

[86] Gustafsson, J.P.: Modeling the acid-base properties and metal complexation of humic substances wit the Stockholm humic model. In: *J. Coll. Interf. Sci.* 244 (2001), S. 102–112

[87] Hummel, W. ; Glaus, M.A. ; van Loon, L.R.: Trace metal-humate interactions. II. The „conservative roof“model and its application. In: *Appl. Geochem.* 15 (2000), S. 975–1001

[88] Saito, T. ; Nagasaki, S. ; Tanaka, S.: Evaluation of the complexation behavior between humic acid and UO_2^{2+} with fluorescence spectroscopy and its mixture analysis. In: *Radiochim. Acta* 90 (2002), S. 27–33

[89] Saito, T. ; Nagasaki, S. ; Tanaka, S.: Molecular fluorescence spectroscopy and mixture analysis for the evaluation of the complexation between humic acid and UO_2^{2+}. In: *Radiochim. Acta* 90 (2002), S. 545–548

[90] Hays, M.D. ; Ryan, D.K. ; Pennell, S.: A modified multisite Stern-Volmer equation for the determination of conditional stability constants and ligand concentrations of soil fulvic acid with metal ions. In: *Anal. Chem.* 76 (2004), S. 848–854

[91] Schmitt, D. ; Frimmel, F.H.: Ligand exchange rate of metal-NOM complexes by EDTA. In: *Environ. Sci. Pollu. Res.* 10 (2003), S. 9–12

[92] Moulin, C.: On the use of time-resolved laser-induced fluorescence (TRLIF) and electrospray mass spectrometry (ES-MS) for speciation studies. In: *Radiochim. Acta* 91 (2003), S. 651–657

[93] Provenzano, M.R. ; D'Orazio, V. ; Jerzykiewicz, M. ; Senesi, N.: Fluorescence behaviour of Zn and Ni complexes of humic acids from different sources. In: *Chemosphere* 55 (2004), S. 885–892

[94] Lu, X.Q. ; Jaffe, R.: Interaction between Hg(II) and natural dissolved organic matter: A fluorescence spectroscopy based study. In: *Wat. Res.* 35 (2001), S. 1793–1803

[95] Monteil-Rivera, F. ; Dumonceau, J.: Fluorescence spectrometry for quantitative characterization of cobalt(II) complexation by Leonardite humic acid. In: *Anal. Bioanal. Chem.* 374 (2002), S. 1105–1112

[96] da Silva, J.C.G.E. ; Herrero, A.I. ; Machado, A.A.S.C. ; Barrado, E.: Molecular fluorescence analysis of the effect of the pH on the complexation of Cu(II), Ni(II) and Fe(III) ions by the stronger binding sites of a soil fulvic acid. In: *Quimica Anal.* 20 (2002), S. 203–210

[97] Hays, M.D. ; Ryan, D.K. ; Pennell, S.: Multi-wavelength fluorescence-quenching model for determination of Cu^{2+} conditional stabiltiy constants and ligand concentrations of fulvic acid. In: *Appl. Spectrosc.* 57 (2003), S. 454–460

[98] Smith, D.S. ; Kramer, J.R.: Multisite mital binding to fulvic acid determined using multiresponse fluorescence. In: *Anal. Chim. Acta* 416 (2000), S. 211–220

[99] Ryan, D.K. ; Weber, J.H.: Fluorescence quenching titration for determination of complexing capacities and stability constants of fulvic acid. In: *Anal. Chem.* 54 (1982), S. 986–990

[100] Morgenstern, M. ; Klenze, R. ; Kim, J.I.: The formation of mixed-hydroxo complexes of Cm(III) and Am(III) with humic acid in the neutral pH range. In: *Radiochim. Acta* 88 (2000), S. 7–16

[101] Monsallier, J.M. ; Artinger, R. ; Denecke, M.A. ; Scherbaum, F.J. ; Buckau, G. ; Kim, J.I.: Spectroscopic study (TRLFS and EXAFS) of the kinetics of An(III)/Ln(III) humate interaction. In: *Radiochim. Acta* 91 (2003), S. 567–574

[102] Tits, J. ; Stumpf, T. ; Rabung, T. ; Wieland, E. ; Fanghänel, T.: Uptake of Cm(III) and Eu(III) by calcium silicate hydrates: a solution chemistry and

time-resolved laser fluorescence spectroscopy study. In: *Environ. Sci. Technol.* 37 (2003), S. 3568–3573

[103] Stumpf, T. ; Tits, J. ; Walther, C. ; Wieland, E. ; Fanghänel, T.: Uptake of trivalent actinides (curium(III)) by hardened cement paste: a time-resolved laser fluorescence spectroscopy study. In: *J. Coll. Int. Sci.* 276 (2004), S. 118–124

[104] Takahashi, Y. ; Kimura, T. ; Minai, Y.: Direct observation of Cm(III)-fulvate species on fulvic acid-montmorillonite hybrid by laser-induced fluorescence spectroscopy. In: *Geochim. Cosmochim. Acta* 66 (2002), S. 1–12

[105] Kowal-Fouchard, A. ; Drot, R. ; Simoni, E. ; Marmier, N. ; Fromage, F. ; Ehrhardt, J.J.: Structural identification of europium(III) adsorption complexes on montmorillonite. In: *New J. Chem.* 28 (2004), S. 864–869

[106] Moll, H. ; Stumpf, T. ; Merroun, M. ; Rossberg, A. ; Selenska-Pobell, S. ; Bernhard, G.: Time-resolved laser fluorescence spectroscopy study on the interaction of Curium(III) with *Desulfovibrio aspoensis DSM 10631*. In: *Environ. Sci. Technol.* 38 (2004), S. 1455–1459

[107] Shin, H.S. ; Hong, K.H. ; Lee, M.H. ; Cho, Y.H. ; Lee, C.W.: Fluorescence quenching of three molecular weight fractions of a soil fulvic acid by UO_2(II). In: *Talanta* 53 (2001), S. 791–799

[108] Billard, I. ; Ansoborlo, E. ; Apperson, K. ; Arpigny, S. ; Azehna, M. E. ; Birch, D. ; Bros, P. ; Burrows, H. D. ; Choppin, G. ; Couston, L. ; Dubois, V. ; Fanghanel, T. ; Geipel, G. ; Hubert, S. ; Kim, J. I. ; Kimura, T. ; Klenze, R. ; Kronenberg, A. ; Kumke, M. ; Lagarde, G. ; Lamarque, G. ; Lis, S. ; Madic, C. ; Meinrath, G. ; Moulin, C. ; Nagashi, R. ; Parker, D. ; Plancque, G. ; Scherbaum, F. ; Simoni, E. ; Sinkov, S. ; Viallesoubranne, C.: Aqueous Solutions of U(VI) as Studied by Time-Resolved Laser-induced Fluorescence Spectroscopy (TRLFS) : A Round-Robin Test. In: *Appl. Spectros.* 57 (2003), S. 1027–1038

[109] Pompe, S. ; Schmeide, K. ; Bubner, M. ; Geipel, G. ; Heise, K.H. ; Bernhard, G. ; Nitsche, H.: Investigation of humic acid complexation behavior with uranyl ions using modified synthetic and natural humic acids. In: *Radiochim. Acta* 88 (2000), S. 553–558

[110] Brachmann, A. ; Geipel, G. ; Bernhard, G. ; Nitsche, H.: Study of uranyl(VI) malonate complexation by time resolved laser-induced fluorescence spectroscopy (TRLFS). In: *Radiochim. Acta* 90 (2002), S. 147–153

[111] Moll, H. ; Geipel, G. ; Reich, T. ; Bernhard, G. ; Fanghanel, T. ; Grenthe, I.: Uranyl(VI) complexes with alpha-substituted carboxylic acids in aqueous solution. In: *Radiochim. Acta* 91 (2003), S. 11–20

[112] Cotton, F.A. ; Wilkinson, G.: *Anorganische Chemie*. VCH, 1985

[113] Moeller, T. ; Martin, D.F. ; Thompson, L.C. ; Ferrus, R. ; Feistel, G.R. ; Randall, W.J.: The coordination chemistry of yttrium and the rare earth metall ions. In: *Chem. Rev.* 65 (1965), S. 1–49

[114] Morss, L.R.: Thermochemical properties of Yttrium, Lanthanum, and the Lanthanide elements and ions. In: *Chem. Rev.* 76 (1976), S. 827–841

[115] Rard, J.A.: Chemistry and thermodynamics of europium and some of its simpler inorganic compounds and aqueous species. In: *Chem. Rev.* 85 (1985), S. 555–582

[116] Karbach, H.-J.: *Spektroskopischer Nachweis der bimolekularen Annihilation metastabiler angeregter Zustände von Terbium(III)- und Europium(III)-Ionen in flüssiger Lösung*, Universität Göttingen, Diss., 1988

[117] Plancque, G. ; Moulin, V. ; Toulhoat, P. ; Moulin, C.: Europium speciation by time-resolved laser-induced fluorescence. In: *Anal. Chim. Acta* 478 (2003), S. 11–22

[118] Gomez-Hens, A. ; Aguilar-Caballos, M.P.: Terbium-sensitized luminescence: a selective and versatile analytical approach. In: *Trends Anal. Chem.* 21 (2002), S. 131–141

[119] Piguet, C. ; Bünzli, J.C.G.: Lanthanide metal ions as cornerstones in functional self-assembled supramolecular complexes. In: *Chimia* 52 (1998), S. 579–584

[120] Bünzli, J.-C. G.: Luminescent lanthanide probes as diagnostic and therapeutic tools. In: Sigel, A. (Hrsg.) ; Sigel, H. (Hrsg.): *Metal ions in biological systems, Volume 42*, Marcel Dekker, Inc., 2001, S. 39–76

[121] Kido, J. ; Okamoto, Y.: Organo lanthanide metal complexes for electroluminescent materials. In: *Chem. Rev.* 102 (2002), S. 2357–2368

[122] Kuriki, K. ; Koike, Y. ; Okamoto, Y.: Platic optical fiber lasers and amplifiers containing lanthanide complexes. In: *Chem. Rev.* 102 (2002), S. 2347–2356

[123] Parker, D.: Luminescent lanthanide sensors for pH, pO_2 and selected anions. In: *Coord. Chem. Rev.* 205 (2000), S. 109–130

[124] de Sa, G.F. ; Malta, O.L. ; Donega, C.D. ; Simas, A.M. ; Longo, R.L. ; Santa-Cruz, P.A. ; da Silva, E.F.: Spectroscopic properties and design of highly luminescent lanthanide coordination complexes. In: *Coord. Chem. Rev.* 196 (2000), S. 165–195

[125] Woods, M. ; Sherry, A.D.: Synthesis and luminescence studies of aryl substituted tetraamide complexes of europium(III): A new approach to pH responsive luminescent europium probes. In: *Inorg. Chem.* 42 (2003), S. 4401–4408

[126] Seward, C. ; Hu, N.-X. ; Wang, S.: 1-D chain and 3-D grid green luminescent terbium(III) coordination polymers: $(Tb(O_2CPh)_3(CH_3OH)_2(H_2O))_n$ and $(Tb_2(O_2CPh)_6(4,4'\text{-bipy}))_n$. In: *J. Chem. Soc., Dalton Trans.* (2001), S. 134–137

[127] Lam, A. W.-H. ; Wong, W.-T. ; Gao, S. ; Wen, G. ; Zhang, X.-X.: Synthesis, crystal structure, and photophysical and magnetic properties of dimeric and polymeric lanthanide complexes with benzoic acid and its derivatives. In: *Eur. J. Inorg. Chem.* (2003), S. 149–163

[128] Horrocks, W. D. ; Sudnick, D.R.: Lanthanide ion luminescence probes of the structure of biological macromolecules. In: *Acc. Chem. Res.* 14 (1981), S. 384–392

[129] Richardson, F.S.: Terbium(III) and Europium(III) ions as luminescent probes and stains for biomolecular systems. In: *Chem. Rev.* 82 (1982), S. 541–552

[130] Selvin, P.R.: Luminescent lanthanide chelates for improved resonance energy transfer and applications to biology. In: Rettig, W. (Hrsg.) ; Strehmel, B. (Hrsg.) ; Schrader, S. (Hrsg.) ; Seifert, H. (Hrsg.): *Applied fluorescence in chemistry, biology and medicine*, Springer Verlag, 1999, S. 457–490

[131] Blair, S. ; Lowe, M.P. ; Mathieu, C.E. ; Parker, D. ; Senanayake, P.K. ; .Kataky, R: Narrow-range optical pH sensors based on luminescent europium and terbium complexes immobilized in a sol gel glass. In: *Inorg. Chem.* 40 (2001), S. 5860–5867

[132] Connally, R. ; Veal, D. ; Piper, J.: High resolution detection of fluorescently labeled microorganisms in environmental samples using time-resolved fluorescence microscopy. In: *FEMS Microbiol. Ecol.* 41 (2002), S. 239–245

[133] Sueda, S. ; Yuan, J. ; Matsumoto, K.: Homogeneous DNA hybridization assay by using europium luminescence energy transfer. In: *Bioconjugate Chem.* 11 (2000), S. 827–831

[134] Matsumoto, K. ; Nojima, T. ; Sano, H. ; Majima, K.: Fluorescent lanthanide chelates for biological systems. In: *Macromol. Symposia* 186 (2002), S. 117–121

[135] Horrocks, W.DeW. ; Schmidt, G.F. ; Sudnick, D.R. ; Kittrell, C. ; Bernheim, R.A.: Laser-induced lanthanide ion luminescence lifetime measurements by direct excitation of metal ion levels. A new class of structural

probe for calcium binding proteins and nucleic acids. In: *J. Am. Chem. Soc.* 99 (1977), S. 2378–2380

[136] Rhee, M.-J. ; Sudnick, D.R. ; Arkle, V.K. ; Horrocks, W. D.: Lanthanide ion luminescence probes. Characterization of metal ion binding sites and intermetal energy transfer distance measurements in calcium-binding proteins. 1. Parvalbumin. In: *Biochemistry* 20 (1981), S. 3328–3334

[137] Snyder, A.P. ; Sudnick, D.R. ; Arkle, V.K. ; Horrocks, W. D.: Lanthanide ion luminescence probes. Characterization of metal ion binding sites and intermetal energy transfer distance measurements in calcium-binding proteins. 2. Thermolysin. In: *Biochemistry* 20 (1981), S. 3334–3339

[138] Horrocks, W. D. ; W.E.Collier: Lanthanide ion luminescence probes. Measurement of distances between intrinsic protein fluorophores and bound metal ions: quantification of energy transfer between Tryptophan and Terbium(III) or Europium(III) in the Calcium-binding protein Parvalbumin. In: *J. Am. Chem. Soc.* 103 (1981), S. 2856–2862

[139] Selvin, P.R.: Lanthanide-based resonance energy transfer. In: *IEEE J. Selec. Top. Quant. Elec.* 2 (1996), S. 1077–1087

[140] Cha, A. ; Snyder, G.E. ; Selvin, P.R. ; Bezanilla, F.: Atomic scale movement of the voltage-sensing region in a potassium channel measured via spectroscopy. In: *Nature* 402 (1999), S. 809–813

[141] Selvin, P.R.: The renaissance of fluorescence resonance energy transfer. In: *Nat. Struc. Biol.* 7 (2000), S. 730–734

[142] Xiao, M. ; Reifenberger, J.G. ; Wells, A.L. ; Baldacchino, C. ; Chen, L.-Q. ; Ge, P. ; Sweeney, H.L. ; Selvin, P.R.: An actin-dependent conformational change in myosin. In: *Nat. Struc. Biol.* 10 (2003), S. 402–408

[143] Mathis, G.: Rare earth crypthates and homogeneous fluoroimmunoassays with human sera. In: *Clin. Chem.* 39 (1993), S. 1953–1959

[144] Tsourkas, A. ; Behlke, M.A. ; Xu, Y.Q. ; Bao, G.: Spectroscopic features of dual fluorescence/luminescence resonance energy-transfer molecular beacons. In: *Anal. Chem.* 75 (2003), S. 3697–3703

[145] Balzani, V. ; Sabbatini, N. ; Scandola, F.: Second-sphere photochemistry and photophysics of coordination compounds. In: *Chem. Rev.* 86 (1986), S. 319–337

[146] Bünzli, J.-C.G.: Luminescent probes. In: Bünzli, J.-C.G. (Hrsg.) ; Choppin, G.R. (Hrsg.): *Lanthanide probes in life, chemical and earth sciences*, Elsevier, 1989, S. 219–293

[147] Yamase, T. ; Kobayashi, T. ; Sugeta, M. ; Naruke, H.: Europium(III) luminescence and intramolecular energy transfer studies of polyoxometalloeuropates. In: *J. Phys. Chem. A* 101 (1997), S. 5046–5053

[148] Buono-Core, G.E. ; Li, H. ; Marciniak, B.: Quenching of excited states by lanthanide ions and chelates in solution. In: *Coordin. Chem. Rev.* 99 (1990), S. 55–87

[149] Misumi, S. ; Kida, S. ; Aihara, M.: Spectral and potentiometric studies of some lanthanide(III) complexes. In: *Coordin. Chem. Rev.* 3 (1968), S. 189–200

[150] Kropp, J.L. ; Windsor, M.W.: Luminescence and energy transfer in solutions of rare earth complexes. II. Studies of the solvation shell in europium(III) and terbium(III) as a function of acetate concentration. In: *J. Phys. Chem.* 71 (1967), S. 477–482

[151] Carnall, W.T. ; Beitz, J.V. ; Crosswhite, H. ; Rajnak, K. ; Mann, J.B.: Spectroscopic properties of the f-elements in compounds and solutions. In: Sinha, S.P. (Hrsg.): *Systematics and the properties of the lanthanides*, D. Reidel Publishing Company, 1983, S. 389–450

[152] Sinha, S.P.: Fluorescence spectra and lifetimes of the lanthanide aquo ions and their complexes. In: Sinha, S.P. (Hrsg.): *Systematics and the properties of the lanthanides*, D. Reidel Publishing Company, 1983, S. 451–500

[153] Horrocks, W. D. ; Albin, M.: Lanthanide ion luminescence in coordination chemistry and biochemistry. In: Lippard, S.J. (Hrsg.): *Progress in inorganic chemistry*, Wiley, 1984, S. 1–104

[154] Billard, I.: Lanthanide and actinide solutions chemistry as studied by time-resolved emission spectroscopy. In: Gschneider, K.A. (Hrsg.) ; Bünzli, J.-C.G. (Hrsg.) ; Pecharsky, V.K. (Hrsg.): *Handbook on the physics and chemistry of rare earths, volume 33*, Elsevier, 2003, S. 465–514

[155] Jenkins, A.L. ; Murray, G.M.: Ultratrace determination of selected lanthanides by luminescence enhancement. In: *Anal. Chem.* 68 (1996), S. 2974–2980

[156] Sabbatini, N. ; Guardigli, M. ; Lehn, J.-M.: Luminescent lanthanide complexes as photochemical supramolecular devices. In: *Coord. Chem. Rev.* 123 (1993), S. 201–228

[157] Kim, J.I. ; Klenze, R. ; Wimmer, H. ; Runde, W. ; Hauser, W.: A study of the carbonate complexation of Cm^{III} and Eu^{III} by time-resolved laser fluorescence spctroscopy. In: *J. Alloys Comp.* 213/214 (1994), S. 333–340

[158] Selvin, P.R.: Principles and biophysical applications of lanthanide-based probes. In: *Annu. Rev. Biophys. Biomol. Struct.* 31 (2002), S. 275–302

[159] Albin, M. ; Farber, G.K. ; Horrocks, W. D.: Europium(III) luminescence excitation spectroscopy. A species-specific method for the quantification of lanthanide ion binding to chelatin agents. Complexes of (1,2-Ethanediyldioxy)diacetate. In: *Inorg. Chem.* 23 (1984), S. 1648–1651

[160] Wu, S.L. ; Horrocks, W. D.: General method for the determinaiton of stability constants of lanthanide ion chelates by ligand-ligand competition: laser-excited Eu^{3+} luminescence excitation spectroscopy. In: *Anal. Chem.* 68 (1996), S. 394–401

[161] Wimmer, H. ; Kim, J.I. ; Klenze, R.: A direct speciation of Cm(III) in natural aquatic systems by time-resolved laser-induced fluorescence spectroscopy (TRLFS). In: *Radiochim. Acta* 58/59 (1992), S. 165–171

[162] Kim, J.I. ; Rhee, D.S. ; Wimmer, H. ; Buckau, G. ; Klenze, R.: Complexation of trivalent actinide ions (Am^{3+}, Cm^{3+}) with humic acid: A comparison of different experimental methods. In: *Radiochim. Acta* 62 (1993), S. 35–43

[163] Panak, P. ; Klenze, R. ; Kim, J.I.: A study of ternary complexes of Cm(III) with humic acid and hydroxide or carbonate in neutral pH range by time-resolved laser fluorescence spectroscopy. In: *Radiochim. Acta* 74 (1996), S. 141–146

[164] Panak, P.: *Untersuchung von intramolekularen Energietransferprozessen in Cm(III)- und Tb(III)-Komplexen mit organischen Liganden mit Hilfe der zeitaufgelösten Laserfluoreszenzspektroskopie*, TU München, Diss., 1996

[165] Susetyo, W. ; Carreira, L.A. ; Azarraga, L.V. ; Grimm, D.M.: Fluorescence techniques for metal-humic interactions. In: *Fresenius J. Anal. Chem.* 339 (1991), S. 624–635

[166] Yoon, T.H. ; Moon, H. ; Park, Y.J. ; Park, K.K.: Investigation of metal biding sites on soil fulvic acid using Eu(III) luminescence spectroscopy. In: *Environ. Sci. Technol.* 28 (1994), S. 2139–2146

[167] Thomason, J.W. ; Susetyo, W. ; Carreira, L.A.: Fluorescence studies of metal-humic complexes with the use of lanthanide ion probe spectroscopy. In: *Appl. Spectros.* 50 (1996), S. 401–408

[168] Stein, G. ; Würzberg, E.: Energy gap law in the solvent isotope effect on radiationless transitions of rare earth ions. In: *J. Chem. Phys.* 62 (1975), S. 208

[169] Werts, M.H.V. ; Jukes, R.T.F ; Verhoeven, J.W.: The emission spectrum and the radiative lifetime of Eu3+ in luminescent lanthanide complexes. In: *Phys. Chem. Chem. Phys.* 4 (2002), S. 1542–1548

[170] Alpha, B. ; Ballardini, R. ; Balzani, V. ; Lehn, J.-M. ; Perathoner, S. ; Sabbatini, N.: Antenna effect in luminescent lanthanide cryptates: A photophysical study. In: *Photochem. Photobiol.* 52 (1990), S. 299–306

[171] Henrie, D.E. ; Fellows, R.L. ; Choppin, G.R.: Hypersensitivity in the electronic transitions of lanthanide and actinide complexes. In: *Coordin. Chem. Rev.* 18 (1976), S. 199–224

[172] Lis, S.: Luminescence spectroscopy of lanthanide(III) ions in solution. In: *J. Alloys Comp.* 341 (2002), S. 45–50

[173] Tanner, S.P. ; Thomas, D.L.: Fluorescence studies of Europium(III) and o-benzoylbenzoate in ethanol-water solution. In: *J. Chem. Am. Soc.* 96 (1974), S. 706–709

[174] Haas, Y. ; Stein, G.: Pathways of radiative and radiationless transitions in europium(III) solutions: role of solvents and anions. In: *J. Phys. Chem.* 75 (1971), S. 3668–3677

[175] Kropp, J.L. ; Windsor, M.W.: Luminescence and energy transfer in solutions of rare-earth complexes. I. Enhancement of fluorescence by Deuterium substitution. In: *J. Chem. Phys.* 42 (1964), S. 1599–1608

[176] Kropp, J.L. ; Windsor, M.W.: Enhancement of fluorescence yield of rare-earth ions by heavy water. In: *J. Chem. Phys.* 39 (1963), S. 2769–2770

[177] Heller, A.: Formation of hot OH bonds in the radiationless relaxations of excited rare earth ions in aqueous solutions. In: *J. Am. Chem. Soc.* 88 (1966), S. 2058–2059

[178] Horrocks, W. D. ; Sudnick, D.R.: Lanthanide ion probes of structure in biology. Laser-induced lumnescence decay constants provide a direct measure of the number of metal-coordinated water molecules. In: *J. Am. Chem. Soc.* 101 (1979), S. 334–340

[179] Horrocks, W. D. ; Sudnick, D.R.: Time-resolved europium(III) excitation spectroscopy: a luminescence probe of metal binding sites. In: *Science* 206 (1979), S. 1194–1196

[180] Yu, J.A.: An observation of back energy transfer in complex Tb(III) with 2-naphthoate in methanol. In: *J. Luminesc.* 78 (1998), S. 265–270

[181] Lis, S. ; Elbanowski, M. ; Makowska, B. ; Hinatejko, Z.: Energy transfer in solution of lanthanide complexes. In: *J. Photochem. Photobiol. A* 150 (2002), S. 233–247

[182] Parker, D. ; Dickins, R.S. ; Puschmann, H. ; Crossland, C. ; Howard, J.A.K.: Being excited by lanthanide coordination complexes: aqua species, chrality, excited-state chemistry, and exchange dynamics. In: *Chem. Rev.* 102 (2002), S. 1977–2010

[183] Maji, S. ; Sundararajan, K. ; Viswanathan, K.S.: Effect of ligand structure on synergism in Tb^{3+}-aromatic acid complexes: fluorescence lifetime studies. In: *Spectrochim. Acta A* 59 (2003), S. 455–461

[184] El-Sayed, M.A. ; Bhaumik, M.I.: Inter-Intra- (Intera) molecular energy transfer to rare-earth ions in chelates. In: *J. Chem. Phys.* 39 (1963), S. 2391–2393

[185] Matovich, E. ; Suzuki, C.K.: Observation of fluorescence in ketone solutions of Europium and Terbium salts. In: *J. Chem. Phys.* 39 (1963), S. 1442–1444

[186] Heller, A. ; Wasserman, E.: Intermolecular energy transfer from excited organic compounds to rare-earth ions in dilute solutions. In: *J. Chem. Phys.* 42 (1965), S. 949–955

[187] McCarthy, W.J. ; Winefordner, J.D.: Intermolecular energy transfer as a means of chemical analysis. In: *Anal. Chem.* 38 (1966), S. 848–853

[188] Latva, M. ; Takalo, H. ; Mukkala, V.M. ; Matachescu, C. ; Rodriguesz, J.C. ; Kankare, J.: Correlation between the lowest triplet state energy level of the ligand and lanthanide(III) luminescence quantum yield. In: *J. Luminesc.* 75 (1997), S. 149–169

[189] Breen, P.J. ; Hild, E.K. ; Horrocks, W. D.: Spectroscopic studies of metal ion binding to a Tryptophan-containing Parvalbumin. In: *Biochemistry* 24 (1985), S. 4991–4997

[190] Breen, P.J. ; Hild, E.K. ; Horrocks, W. D.: Characterization of lanthanide(III) ion binding to Cadmodulin using luminescence spectroscopy. In: *Biochemistry* 24 (1985), S. 6639–6645

[191] Ying, L. ; Yu, A. ; Zhao, X. ; Q.Li ; Zhou, D. ; Huang, C. ; Umetani, S. ; Matasai, M.: Excited state properties and intramolecular energy transfer of rare-earth Acrylpyrazolone complexes. In: *J. Phys. Chem.* 100 (1996), S. 18387–18391

[192] Voloshin, A.I. ; Shavaleev, N.M. ; Kazakov, V.P.: Luminescence of praseodymium(III) chelates from two excited states ($^3P_0$ and $^1D_2$) and its dependence on ligand triplet state energy. In: *J. Luminesc.* 93 (2001), S. 199–204

[193] Malta, O.L. ; Legendziewicz, J. ; Huskowska, E. ; Turowska-Tyrk, I. ; Albuquerque, R.Q. ; de Mello Donega, C. ; e Silva, F.R.G.: Experimental and theoretical study of ligand field, 4f-4f intensities and emission

quantum yield in the compound $Eu(bpyO_2)_4(ClO_4)_3$. In: *J. Alloys Comp.* 323-324 (2001), S. 654–660

[194] Förster, T.: Intermolecular energy migration and fluorescence. In: *Ann. Phys. Leipzig* 2 (1948), S. 55–75

[195] Stryer, L. ; Haugland, R.P.: Energy transfer: a spectroscopic ruler. In: *Proc. N. A. S.* 58 (1967), S. 719–726

[196] Selvin, P.R.: Fluorescence resonance energy transfer. In: *Meth. Enzymol.* 246 (1995), S. 301–335

[197] Axe, J.D. ; Weller, P.F.: Fluorescence and energy transfer in $Y_2O_3 : Eu^{3+}$. In: *J. Chem. Phys.* 40 (1964), S. 3066–3069

[198] Nakazawa, E. ; Shionoya, S.: Energy transfer between trivalent rare-earth ions in inorganic solids. In: *J. Chem. Phys.* 47 (1967), S. 3211–3219

[199] Turro, N.J.: *Modern molecular photochemistry.* 1. Auflage. The Benjamin / Cummings Publishing Company, Inc., 1978

[200] Tanaka, F. ; Ishibashi, T.: Energy transfer between lanthanide ions in dinuclear complexes. In: *J. Chem. Soc., Faraday Trans.* 92 (1996), S. 1105–1110

[201] Brittain, H.B.: Intermolecular energy transfer between lanthanide complexes in aqueous solution. 1. Transfer from Terbium(III) to Europium(III) complexes of Pyridinecarboxylic acids. In: *Inorg. Chem.* 17 (1978), S. 2762–2766

[202] Brittain, H.G.: Intermolecular energy transfer between lanthanide complexes in aqueous solution. 4. Stereoselectivity in the transfer from Terbium(III) to Europium(III) complexes of Aspartic acid. In: *Inorg. Chem.* 18 (1979), S. 1740–1745

[203] Frey, S.T. ; Horrocks, W. D.: Complexation, luminescence, and energy transfer of Ce^{3+} with a series of multidentate amino phosphonic acids in aqueous solution. In: *Inorg. Chem.* 30 (1991), S. 1073–1079

[204] Latva, M. ; Makinen, P. ; Kulmala, S. ; Haapakka, K.: Self-assembled heterodinuclear europium(III)-lanthanide(III) chelates of 2,6-bis[N,N-bis(carboxymethyl)aminomethyl]-4-benzoylphenol and their radiative $^5D_0 \rightarrow {}^7F_j$ transitions of Eu^{III}. In: *J. Chem. Soc., Faraday Trans.* 92 (1996), S. 3321–3326

[205] Brittain, H.G.: Intermolecular energy transfer between lanthanide complexes. 10. Tb(III) donor and Eu(III) accptor complexes of Triethylenetetraaminehexaacetic acid. In: *J. Coord. Chem.* 21 (1990), S. 295–299

[206] Horrocks, W. D. ; Rhee, M.-J. ; Snyder, A.P. ; Sudnick, D.R.: Laser-induced metal ion luminescence: Interlanthanide ion energy transfer distance measurements in the Calcium-binding proteins, Parvalbumin and Thermolysin. Metalloprotein models adress a photophysical problem. In: *J. Am. Chem. Soc.* 102 (1980), S. 3650–3652

[207] Montavon, G. ; Markai, S. ; Billard, I. ; Nehlig, A. ; Grambow, B.: Complexation and luminescence spectroscopic studies of europium(III) with polymaleic acid. In: *Radiochim. Acta* 90 (2002), S. 289–296

[208] Montavon, G. ; Markai, S. ; Andres, Y. ; Grambow, B.: Complexation studies of Eu(III) with alumina-bound polymaleic acid: effect of organic polymer loading and metal ion concentration. In: *Environ. Sci. Technol.* 36 (2002), S. 3303–3309

[209] Montavon, G. ; Grambow, B.: Study of the reversibility of the interaction between Eu(III) and polyacrylic acids. In: *New J. Chem.* 27 (2003), S. 1344–1352

[210] Klenze, R. ; Panak, P. ; Kim, J.I.: A complexation study of Cm(III) and Tb(III) with chelating aromatic ligands by time-resolved laser fluorescence spectroscopy. In: *J. Alloys Comp.* 271-273 (1998), S. 746–750

[211] Bidoglio, G. ; Omenetto, N. ; Robouch, P.: Kinetic-studies of lantahnide interactions with humic substances by time resolved laser-induced fluorescence. In: *Radiochim. Acta* 52 (1991), S. 57–63

[212] Kim, J.I. ; Wimmer, H. ; Klenze, R.: A study of Curium(III) humate complexation by time-resolved laser fluorescence spectroscopy (TRLFS). In: *Radiochim. Acta* 54 (1991), S. 35–41

[213] Panak, P. ; Klenze, R. ; Kim, J.I. ; Wimmer, H.: A study of intramolecular energy transfer in Cm(III) complexes with aromatic ligands by time-resolved laser fluorescence spectroscopy. In: *J. Alloys Comp.* 225 (1995), S. 261–266

[214] Moulin, V. ; Tits, J. ; Moulin, C. ; Decambox, P. ; Mauchien, P. ; Deruty, O.: Complexation behavior of humic substances towards actinides and lanthanides studied by time-resolved laser-induced spectrofluorometry. In: *Radiochim. Acta* 58 (1992), S. 121–128

[215] Burges, N.A. ; Hurst, H.M. ; Walkden, B.: The phenolic substituents of humic acid and their relation to the lignin of the plant cover. In: *Geochim. Cosmochim. Acta* 28 (1964), S. 1547–1554

[216] Linder, P.W. ; Murray, K.: Statistical determination of the molecular structure and the metal binding sites of fulvic acids. In: *Sci. Tot. Environ.* 64 (1987), S. 149–161

[217] Geipel, G. ; Acker, M. ; Vulpius, D. ; Bernhard, G. ; Nitsche, H. ; Fanghänel, T.: An ultrafast time-resolved fluorescence spectroscopy system for metal ion complexation studies with organic ligands. In: *Spectrochim. Acta A* 60 (2004), S. 417–424

[218] Kumke, M.U. ; Eidner, S.: Fluorescence and Energy Transfer Processes of Humic Substances and Related Model Compounds in Terbium Complexes. In: Davis, G. (Hrsg.) ; Ghabour, E.A. (Hrsg.): *Humic Substance - Molecular details and applications in land and water conservation*, Taylor and Francis, Inc., 2005

[219] Cabaniss, S.E. ; Shuman, M.S.: Fluorescence quenching measurements of copper-fulvic acid binding. In: *Anal. Chem.* 60 (1988), S. 2418–2421

[220] Ryan, D.K. ; Ventry, L.S. ; Cabaniss, S.E. ; Shuman, M.S.: Exchange of comments on fluorescence quenching measurements of Copper-fulvic acid binding. In: *Anal. Chem.* 62 (1990), S. 1523–1528

[221] Xue, D. ; Zuo, S. ; Ratajczak, H.: Electronegativity and structural characteristics of lanthanides. In: *Physica B* in press (2004)

[222] Tiseanu, C. ; Kumke, M.U. ; Frimmel, F.H. ; Klenze, R. ; Kim, J.I.: Time-Resolved Spectroscopy of Fulvic Acid and Fulvic Acid Complexed with Eu^{3+} - A Comparative Study. In: *J. Photochem. Photobiol.* 117 (1998), S. 175–184

[223] Piana, M.J. ; Zahir, K.O.: Investigation of metal ion binding of humic substances using fluorescence emission and synchronous-scan spectroscopy. In: *J. Environ. Sci. Health B* 35 (2000), S. 87–102

[224] Kumke, M.U. ; Tiseanu, C. ; Abbt-Braun, G. ; Frimmel, F.H.: Fluorescence Decay of Natural Organic Matter (NOM) - Influence of Fractionation, Oxidation, and Metal Ion Complexation. In: *J. Fluorescence* 8 (1998), S. 309–318

[225] Elkins, K.M. ; Nelson, D.J.: Fluorescence and FT-IR spectroscopic studies of Suwannee river fulvic acid complexation with aluminum, terbium and calcium. In: *J. Inorg. Biochem.* 87 (2001), S. 81–96

[226] Elkins, K.M. ; Nelson, D.J.: Spectroscopic approaches to the study of the interaction of aluminum with humic substances. In: *Coord. Chem. Rev.* 228 (2002), S. 205–225

[227] Arnaud, N. ; Georges, J.: Influence of pH, surfactant and synergic agent on the luminescent properties of terbium chelated with benzoic acid derivatives in aqueous solutions. In: *Analyst* 125 (2000), S. 1487–1490

[228] Yan, B. ; Zhang, H. ; Wang, S. ; Ni, J.: Intramolecular energy transfer mechanism between ligands in ternary rare earth complexes with aromatic carboxylic acids and 1,10-phenanthroline. In: *J. Photochem. Photobiol. A* 116 (1998), S. 209–214

[229] Srivanek, T.J.A.: *Fluoreszenz- und absorptionsspektroskopische Untersuchung der Struktur-/Wechselwirkungseigenschaften von Huminstoffen und organischen Substanzen*, Universität Erlangen, Diss., 2001

[230] Li, C.-W. ; Korshin, G.V.: Studies of metal-binding sites in natural organic matter and their role in the generation of disinfection by-products using lanthanide ion probes. In: *Chemosphere* 49 (2002), S. 629–636

[231] Klafter, J. ; Blumen, A.: Direct energy transfer in restricted geometries. In: *J. Luminesc.* 34 (1985), S. 77–82

[232] Hirayama, S. ; Sakai, Y. ; Ghiggino, K.P. ; Smith, T.A.: The application of a simple deconvolution method to the analysis of stretched exponential fluorescence decay functions. In: *J. Photochem. Photobiol. A* 52 (1990), S. 27–38

[233] Carey, M.J. ; Phillips, D.: Modelling excimer formation in vinyl aromatic polymers. In: *Chem. Phys.* 185 (1994), S. 75–89

[234] Novikov, E.G. ; van Hoek, A. ; Visser, A.J.W.G. ; Hofstraat, J.W.: Linear algorithms for stretched exponential decay analysis. In: *Opt. Comm.* 166 (1999), S. 189–198

[235] Huber, D.L.: Two-state model for sub-exponential fluorescence. In: *J. Luminesc.* 86 (2000), S. 95–99

[236] Garcia-Adeva, A.J. ; Huber, D.L.: Two-state model for sub-exponential fluorescence revisited. In: *J. Luminesc.* 92 (2001), S. 65–72

[237] Im, C. ; Lupton, J.M. ; Schouwink, P. ; Heun, S. ; Becker, H. ; Bassler, H.: Fluorescence dynamics of phenyl-substituted polyphenylenevinylene-trinitrofluorenone blend systems. In: *J. Chem. Phys.* 117 (2002), S. 1395–1402

[238] Drake, J.M. ; Levitz, P.: Direct energy transfer in restricted geometries as a probe of the pore morphology of silica. In: *Phys. Rev. Lett.* 58 (1987), S. 686–689

[239] Pekcan, O. ; Winnik, M.A. ; Croucher, M.D.: Direct energy transfer studies on doped and labeled polymer latex particles. In: *Phys. Rev. Lett.* 61 (1988), S. 641–644

[240] Pekcan, Ö. ; Egan, L.S. ; Winnik, M.A. ; Croucher, M.D.: Energy transfer in restricted dimensions: a new approach to latex morphology. In: *Macromolecules* 23 (1990), S. 2210–2216

[241] Vanderauweraer, M. ; Ballet, P. ; DeSchryver, F.C. ; Kowalczyk, A.: Parameter recovery and discrimination between different types of fluorescence decays obtained for dipole-dipole energy transfer in low-dimensional systems. In: *Chem. Phys.* 187 (1994), S. 399–416

[242] Metzler, R. ; Klafter, J. ; Jortner, J. ; Volk, M.: Multiple time scales for dispersive kinetics in early events of peptide folding. In: *Chem. Phys. Lett.* 293 (1998), S. 477–484

[243] Zaccaria, S. ; Casarin, M. ; Speghini, A. ; Ajo, D. ; Bettinelli, M.: Optical spectroscopy of trivalent lanthanide ions in strontium metaphosphate glasses. In: *Spectrochim. Acta A* 55 (1999), S. 171–177

[244] Speghini, A. ; Francini, R. ; Martinez, A. ; Tavernese, M. ; Bettinelli, M.: Spectroscopic properties of Er^{3+}, Yb^{3+} and Er^{3+}/Yb^{3+} doped metaphosphate glasses. In: *Spectrochim. Acta A* 57 (2001), S. 2001–2008

[245] Tcherkasskaya, O. ; Gronenborn, A.M. ; Klushin, L.: Excluded volume effect within the continous model for the fluorescence energy transfer. In: *Biophys. J.* 83 (2002), S. 2826–2834

[246] Kuwana, E. ; Sevick-Muraca, E.M.: Fluorescence lifetime spectroscopy in multply scattering media with dyes exhibiting multiexponential decay kinetics. In: *Biophys. J.* 83 (2002), S. 1165–1176

[247] Tcherkasskaya, O. ; Spiro, J.G. ; S.Ni ; Winnik, M.A.: Energy transfer in restricted geometryy: polyisoprene-poly(methyl methacrylate) block copolymer interfaces. In: *J. Phys. Chem.* 100 (1996), S. 7114–7121

[248] Specht, C.: *Wechselwirkungen von organischen Substanzen mit mineralischen Festphasen - Untersuchungen mit Hilfe der Größenausschlusschromatographie und der FTIR-Spektroskopie*, Universität Karlsruhe, Diss., 2002

[249] Dexter, D.L.: A theory of sensitized luminescence in solids. In: *J. Chem. Phys.* 21 (1953), S. 836–850

[250] Dexter, D.L. ; Schulman, J.H.: Theory of concentration quenching in inorganic phosphors. In: *J. Chem. Phys.* 221 (1954), S. 1063–1070

[251] Wu, P. ; Brand, L.: Resonance energy transfer: methods and applications. In: *Anal. Biochem.* 218 (1994), S. 1–13

[252] Brückner, V. ; Feller, K.-H. ; Grummt, U.-W.: *Application of time-resolved optical spectroscopy.* erste. Akademische Verlagsgesellschaft Geest & Portig K.-G, 1990

[253] Buckau, G. ; Wolf, M. ; Geyer, S. ; Artinger, R. ; Kim, J.I.: Origin and mobility of aquatic humic substances from wetland recharge in the Gorleben aquifer system. In: Buckau, G. (Hrsg.): *Humic substances in performance assessment of nuclear wast disposal: actinide and iodine migration in the far field - first technical progress report*, Forschungszentrum Karlsruhe in der Helmholtz-Gemeinschaft, 2003, S. 41–50

[254] Sachs, S. ; Heise, K.H. ; Bernhard, G.: Synthetic humic acid model substances with specific functional properties for the use in complexation and sorption experiments with actinides. In: Buckau, G. (Hrsg.): *Humic substances in performance assessment of nuclear wast disposal: actinide and iodine migration in the far field - first technical progress report*, Forschungszentrum Karlsruhe in der Helmholtz-Gemeinschaft, 2003, S. 51–64

[255] Pompe, S.: *Entwicklung huminsäureähnlicher Melanoidine als Funktionalitätsmodelle für Huminsäuren und ihr Vergleich mit Fluka-Huminsäure hinsichtlich ihres Komplexbildungsverhaltens gegenüber Uran(VI)*, TU Dresden, Diss., 1997

[256] Scheeren, J.W. ; Ooms, P.H.J. ; Nivard, R.J.F.: A general procedure for the conversion of a carbonyl group into a thione group with tetraphosphorus decasulfide. In: *Synthesis* 3 (1973), S. 149–151

[257] Anderson, R.W. ; Hochstrasser, R.M. ; Pownall, H.J.: Picosecond absorption spectra of the second excited singlet state of a molecule in the condensed phase: Xanthione. In: *Chem. Phys. Lett.* 43 (1976), S. 224–227

[258] Boens, N. ; van den Zegel, M. ; Schryver, F.C. D.: Picosecond lifetime determination of the second excited singlet state of xanthione in solution. In: *Chem. Phys. Lett.* 111 (1984), S. 340–345

[259] Mahaney, M. ; Huber, J.R.: Solvent effect on the non-radiative $S_2(\pi\pi^\star)$ decay of xanthione. In: *Chem. Phys. Lett.* 105 (1984), S. 395–399

[260] Eaton, D.F.: Reference materials for fluorescence measurement. In: *J. Photochem. Photobiol., B* 2 (1988), S. 523–531